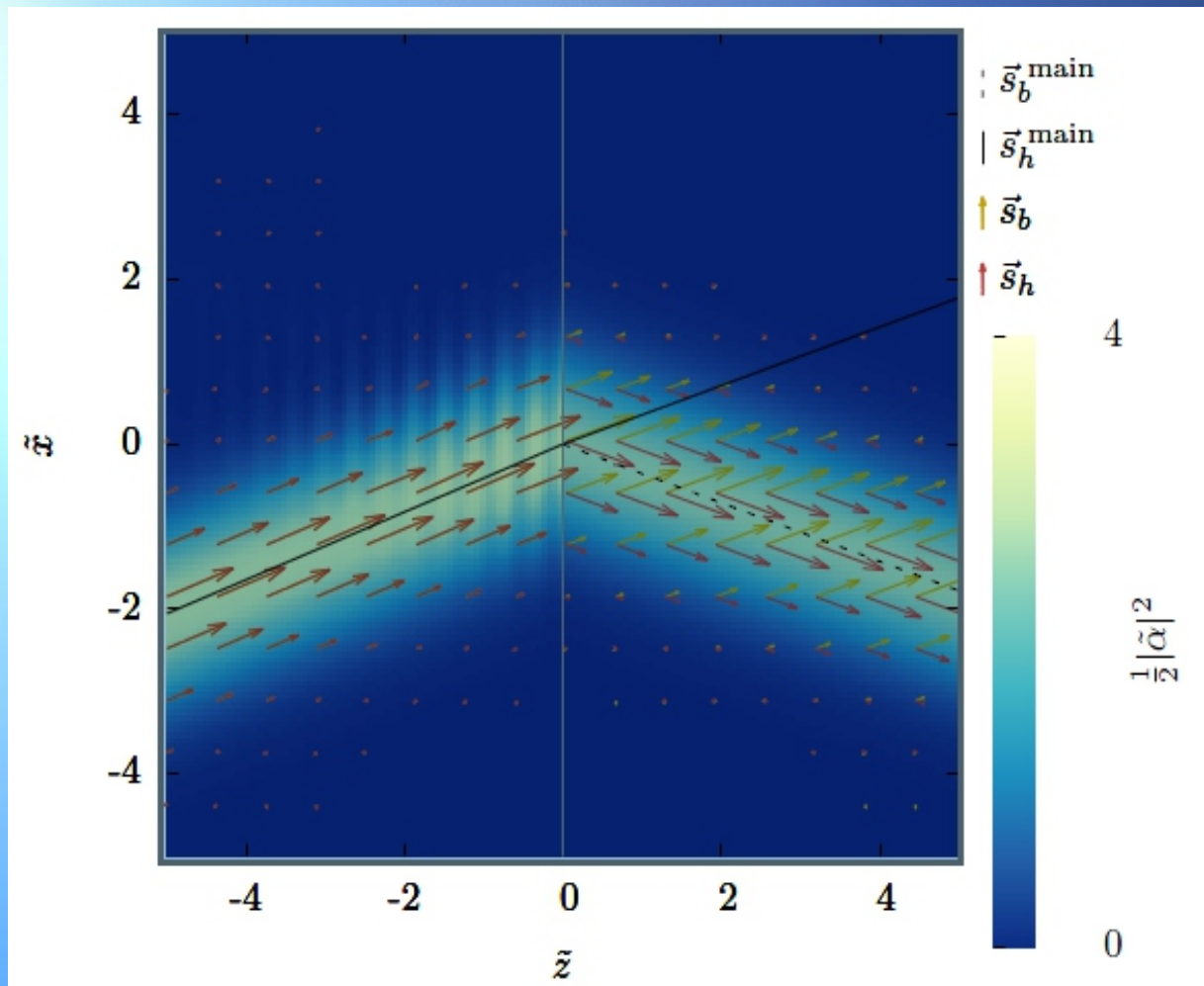


# Journal of Modern Physics



ISSN: 2153-1196



# Journal Editorial Board

ISSN: 2153-1196 (Print) ISSN: 2153-120X (Online)

<http://www.scirp.org/journal/jmp>

---

## Editor-in-Chief

Prof. Yang-Hui He

City University, UK

## Executive Editor-in-Chief

Prof. Marko Markov

Research International, Buffalo Office, USA

## Managing Executive Editor

Prof. Chang Liu

Wuhan University, China

## Editorial Board

Prof. Nikolai A. Sobolev

Universidade de Aveiro, Portugal

Prof. Yohannes Abate

California State University, USA

Dr. Mohamed Abu-Shady

Menoufia University, Egypt

Dr. Hamid Alemohammad

Advanced Test and Automation Inc., Canada

Prof. Changle Chen

University of Science and Technology of China, China

Prof. Stephen Robert Cotanch

NC State University, USA

Prof. Ju Gao

The University of Hong Kong, China

Prof. Sachin Goyal

University of California, USA

Dr. Wei Guo

Florida State University, USA

Prof. Alioscia Hamma

Tsinghua University, China

Prof. Cosmin Ilie

Los Alamos National Laboratory, USA

Prof. Haikel Jelassi

National Center for Nuclear Science and Technology, Tunisia

Prof. Preston B. Landon

The University of California, USA

Prof. Chunlei Liu

Carnegie Mellon University, USA

Prof. Christophe J. Muller

University of Provence, France

Prof. Ambarish Nag

National Renewable Energy Laboratory, USA

Dr. Rada Novakovic

National Research Council, Italy

Prof. Valery Obukhov

Tomsk State Pedagogical University, Russia

Prof. Tongfei Qi

University of Kentucky, USA

Prof. Richard Saurel

University of Aix Marseille I, France

Prof. Alejandro Crespo Sosa

Universidad Nacional Autónoma de México, Mexico

Prof. Bo Sun

Oregon State University, USA

Prof. Mingzhai Sun

Ohio State University, USA

Dr. Sergei K. Suslov

Arizona State University, USA

Dr. A. L. Roy Vellaisamy

City University of Hong Kong, China

Prof. Yuan Wang

University of California, Berkeley, USA

Prof. Fan Yang

Fermi National Accelerator Laboratory, USA

Prof. Peter H. Yoon

University of Maryland, USA

Dr. S. Zerbini

University of Trento, Italy

Prof. Meishan Zhao

University of Chicago, USA

Prof. Pavel Zhuravlev

University of Maryland at College Park, USA

# Table of Contents

Volume 7    Number 12

August 2016

<b>Universe and Matter Conjectured as a 3-Dimensional Lattice with Topological Singularities</b>	
G. Gremaud.....	1389
<b>Surface Wave Echo in a Semi-Bounded Plasma</b>	
H. J. Lee, M.-J. Lee.....	1400
<b>The Influence of Pico-Second Pulse Electron Irradiation on the Electrical-Physical Properties of Silicon Crystals</b>	
H. N. Yeritsyan, A. A. Sahakyan, N. E. Grigoryan, E. A. Hakhverdyan, V. V. Harutyunyan, V. A. Sahakyan, A. A. Khachatryan, B. A. Grigoryan, V. Sh. Avagyan, G. A. Amatuni, A. S. Vardanyan.....	1413
<b>Max Planck Half Quanta as a Natural Explanation for Ordinary and Dark Energy of the Cosmos</b>	
M. S. El Naschie.....	1420
<b>Determination of the Dynamic ITER Energy Confinement Time Scalings</b>	
G. Sonnino, A. Sonnino, J. Evslin, P. Nardone, G. Steinbrecher.....	1429
<b>Joule-Lenz Energy of Quantum Electron Transitions Compared with the Electromagnetic Emission of Energy</b>	
S. Olszewski.....	1440
<b>Success and Incoherence of Orthodox Quantum Mechanics</b>	
M. E. Burgos.....	1449
<b>A Fundamentally Irreversible World as an Opportunity towards a Consistent Understanding of Quantum and Cosmological Contexts</b>	
H. Tributsch.....	1455
<b>S Bosons and Dark Particles of Space Field</b>	
Y. G. Feng.....	1483
<b>Comparing Gravitation in Flat Space-Time with General Relativity</b>	
W. Petry.....	1492
<b>Reexamination of Criticality Accident in JCO</b>	
S. Oshima, M. Hisada, Y. Saito, T. Fujita.....	1500
<b>Complete Destruction of Ag Br Emulsion Nuclei BY<sup>28</sup>Si Ions with 4.5 GeV/Nucleon Energy</b>	
A. Abd EL-Daiem.....	1506

<b>The Investigation Capability of Plasma Focus Device for <math>^{13}\text{N}</math> Radioisotope Production by Means of Deuteron Experimental Spectrum</b>	
M. Saed, M. V. Roshan, A. Banoushi, M. Habibi.....	1512
<b>Electromagnetic-Energy Flow in Anisotropic Metamaterials: The Proper Choice of Poynting's Vector</b>	
C. Prieto-López, R. G. Barrera.....	1519
<b>Complex Systems Are Not Black Boxes but Solvable Systematical Problems; Proven by Simulation and New Conception</b>	
D.-S. Cha.....	1540
<b>Quantum Statistical Theory of Superconductivity in <math>\text{MgB}_2</math></b>	
S. Fujita, A. Suzuki, Y. Takato.....	1546
<b>Diffraction Line Width in Quasicrystals—Sharper than Crystals</b>	
A. J. Bourdillon.....	1558
<b>Towards the Unification of All Interactions (The First Part: The Spinor Wave)</b>	
C. Daviau, J. Bertrand, D. Girardot.....	1568
<b>The Accurate Mass Formulas of Leptons, Quarks, Gauge Bosons, the Higgs Boson, and Cosmic Rays</b>	
D.-Y. Chung.....	1591
<b>The Hubble Field vs Dark Energy</b>	
J. Lartigue.....	1607

## **Journal of Modern Physics (JMP)**

### **Journal Information**

#### **SUBSCRIPTIONS**

The *Journal of Modern Physics* (Online at Scientific Research Publishing, [www.SciRP.org](http://www.SciRP.org)) is published monthly by Scientific Research Publishing, Inc., USA.

#### **Subscription rates:**

Print: \$89 per issue.

To subscribe, please contact Journals Subscriptions Department, E-mail: [sub@scirp.org](mailto:sub@scirp.org)

#### **SERVICES**

##### **Advertisements**

Advertisement Sales Department, E-mail: [service@scirp.org](mailto:service@scirp.org)

##### **Reprints (minimum quantity 100 copies)**

Reprints Co-ordinator, Scientific Research Publishing, Inc., USA.

E-mail: [sub@scirp.org](mailto:sub@scirp.org)

#### **COPYRIGHT**

##### **COPYRIGHT AND REUSE RIGHTS FOR THE FRONT MATTER OF THE JOURNAL:**

Copyright © 2016 by Scientific Research Publishing Inc.

This work is licensed under the Creative Commons Attribution International License (CC BY).

<http://creativecommons.org/licenses/by/4.0/>

##### **COPYRIGHT FOR INDIVIDUAL PAPERS OF THE JOURNAL:**

Copyright © 2016 by author(s) and Scientific Research Publishing Inc.

##### **REUSE RIGHTS FOR INDIVIDUAL PAPERS:**

Note: At SCIRP authors can choose between CC BY and CC BY-NC. Please consult each paper for its reuse rights.

##### **DISCLAIMER OF LIABILITY**

Statements and opinions expressed in the articles and communications are those of the individual contributors and not the statements and opinion of Scientific Research Publishing, Inc. We assume no responsibility or liability for any damage or injury to persons or property arising out of the use of any materials, instructions, methods or ideas contained herein. We expressly disclaim any implied warranties of merchantability or fitness for a particular purpose. If expert assistance is required, the services of a competent professional person should be sought.

#### **PRODUCTION INFORMATION**

For manuscripts that have been accepted for publication, please contact:

E-mail: [jmp@scirp.org](mailto:jmp@scirp.org)

# Universe and Matter Conjectured as a 3-Dimensional Lattice with Topological Singularities

G rard Gremaud

Swiss Federal Institute of Technology, Lausanne, Switzerland

Email: [gerard.gremaud@epfl.ch](mailto:gerard.gremaud@epfl.ch)

Received 30 June 2016; accepted 30 July 2016; published 2 August 2016

Copyright   2016 by author and Scientific Research Publishing Inc.

This work is licensed under the Creative Commons Attribution International License (CC BY).

<http://creativecommons.org/licenses/by/4.0/>



Open Access

---

## Abstract

One fundamental problem of modern physics is the search for a *theory of everything* able to explain the nature of space-time, what matter is and how matter interacts. There are various propositions, as *Grand Unified Theory*, *Quantum Gravity*, *Supersymmetry*, *String and Superstring Theories*, and *M-Theory*. However, none of them is able to consistently explain *at the present and same time* electromagnetism, relativity, gravitation, quantum physics and observed elementary particles. In this paper, one summarizes the content of a new book, published in English [2] and in French [3], in which it is suggested that Universe could be a *massive elastic 3D-lattice*, and that fundamental building blocks of Ordinary Matter could consist of *topological singularities of this lattice*, namely diverse dislocation loops and disclination loops. For an isotropic elastic lattice obeying Newton's law, with specific assumptions on its elastic properties, one obtains the result that the behaviours of this lattice and of its topological defects display "all" known physics, unifying electromagnetism, relativity, gravitation and quantum physics, and resolving some longstanding questions of modern cosmology. Moreover, studying lattices with axial symmetries, represented by "*colored*" *cubic 3D-lattices*, one has identified a lattice structure whose topological defect loops coincide with the complex zoology of elementary particles, which could open a very promising field of research. Here, only main steps and principal results of the new theory are presented and discussed, without showing the mathematical concepts and developments contained in the book.

## Keywords

Massive Deformable 3D-Lattice, Dislocation, Disclination, Electromagnetism, Relativity, Gravitation, Quantum Physics, Cosmology, Standard Model of Particles, Theory of Everything

---

## 1. Introduction

This paper presents a theory recently developed [1] and published in a book [2] [3], which shows that an Eulerian approach of the deformation of a Newtonian lattice in an absolute space can furnish an investigation frame extremely rich and interesting for physics, if judicious elastic and structural properties of the considered lattice are postulated. Indeed, it shows very strong and often perfect analogies with all the modern physics theories of the macrocosm and microcosm, as the Maxwell equations, the special relativity, the Newtonian gravitation, the general relativity, the modern cosmology, the quantum physics and the standard model of elementary particles.

This book does not present a *theory of everything* which would be completely elaborated and usable, but it would and could be extremely fruitful to give simple explanations to the modern physics theories which are very difficult, if not impossible, to deeply understand. It could also and above all be useful to define close links and unifying bridges between the diverse theories of modern physics.

In a first part, one summarizes autonomously a first book published in French during year 2013 [4] (also recently translated in English [5]), which lays methodically the foundations of an original approach of the solid lattices deformation using the Euler coordinates, and which introduces in details the concept of tensor dislocation charges and tensor disclination charges within a lattice. This new concept allows one to quantify the topological singularities, which can appear at the microscopic scale of a solid lattice. On the basis of this original approach of the solid lattices and their topological singularities, one can deduce a set of fundamental and phenomenological equations allowing to treat rigorously the macroscopic spatiotemporal evolution of a Newtonian solid lattice which deforms in the absolute space of an external observer laboratory.

In a second part, one introduces an imaginary lattice, named “*cosmic lattice*”, with quite special elastic and structural properties. The Newton equation of this lattice and its topological singularities present then a set of very surprising properties, which will be progressively developed in the course of the chapters. It will appear strong and amazing analogies with all modern physics theories: Maxwell equations, special relativity, Newtonian gravitation, general relativity, modern cosmology, quantum physics and standard model of elementary particles.

## 2. The Problem of Unified Theories

One fundamental problem of modern physics is the search for a *theory of everything* able to explain the nature of space-time, what matter is and how matter interacts. Since the 19<sup>th</sup> century, physicists have attempted to develop unified field theories [6], which would consist of a single coherent theoretical framework able to account for several fundamental forces of nature. For instance:

- *Grand Unified Theory* [7] merges electromagnetic, weak and strong interaction forces,
- *Quantum Gravity* [8], *Loop Quantum Gravity* [9] and *String Theories* attempt to describe the quantum properties of gravity,
- *Super-symmetry* [10]-[15] proposes an extension of the space-time symmetry relating the two classes of elementary particles, bosons and fermions,
- *String and Superstring Theories* [16]-[23] are theoretical frameworks incorporating gravity in which point-like particles are replaced by one-dimensional strings, whose quantum states describe all types of observed elementary particles,
- *M-Theory* [24]-[32] is a unifying theory of five different versions of string theories, with the surprising property that extra dimensions are required for its consistency.

However, none of them is able to consistently explain *at the present and same time* electromagnetism, relativity, gravitation, quantum physics and observed elementary particles. Many physicists believe now that 11-dimensional *M-theory* is the theory of everything. However, there is no widespread consensus on this issue and, at present, there is no candidate theory able to calculate the fine structure constant or the mass of the electron. Particle physicists expect that the outcome of the ongoing experiments-search for new particles at the large particle accelerators and search for dark matter-are needed to provide further input for a theory of everything.

In the recent theoretical work presented in the book [2] [3], it is suggested that Universe could be a *massive elastic 3D-lattice*, and that fundamental building blocks of Ordinary Matter could consist of *topological singularities of this lattice*, namely diverse dislocation loops and disclination loops. We find, for an isotropic elastic lattice obeying Newton’s law, with specific assumptions on its elastic properties, that the behaviors of this lattice and of its topological defects display “all” known physics, unifying electromagnetism, relativity, gravitation and

quantum physics, and resolving some longstanding questions of modern cosmology. Moreover, studying lattices with axial symmetries, represented by “*colored*” *cubic 3D-lattices*, one can identify a lattice structure whose topological defect loops coincide with the complex zoology of elementary particles, which could open a promising field of research.

In this paper, motivations, main steps and principal results of the new theories presented in the two parts of book [2] [3] are summarized as succinctly as possible, without showing the mathematical concepts and developments contained in the book.

### 3. Motivation of the First Part: Searching for a New Description of the Lattice Deformation

#### 3.1. Eulerian Deformation Theory of Newtonian Lattices

When one desires to study the solid deformation, one generally uses Lagrangian coordinates to describe the evolution of the deformations, and diverse differential geometries to describe the topological defects contained in the solid.

*The use of Lagrangian coordinates* presents a number of inherent difficulties. From the mathematical point of view, the tensors describing the continuous solid deformation are always of order higher than one concerning the spatial derivatives of the displacement field components, which leads to a very complicated mathematical formalism when the solid presents strong distortions (deformations and rotations). To these mathematical difficulties are added physical difficulties when one has to introduce some known properties of solids. Indeed, the Lagrangian coordinates become practically unusable, for example when one has to describe the temporal evolution of the microscopic structure of a solid lattice (phase transitions) and of its structural defects (point defects, dislocations, disclinations, boundaries, etc.), or when it is necessary to introduce some physical properties of the medium (thermal, electrical, magnetic or chemical properties) leading to scalar, vectorial or tensorial fields in the real space.

*The use of differential geometries* in order to introduce topological defects as dislocations in a deformable continuous medium has been initiated by the work of Nye [33] (1953), who showed for the first time the link between the dislocation density tensor and the lattice curvature. On the other hand, Kondo [34] (1952) and Bilby [35] (1954) showed independently that the dislocations can be identified as a crystalline version of the Cartan’s concept [36] of torsion of a continuum. This approach was generalized in details by Kröner [37] (1960). However, the use of differential geometries in order to describe the deformable media leads very quickly to difficulties similar to those of the Lagrangian coordinates system. A first difficulty arises from the complexity of the mathematical formalism which is similar to the formalism of general relativity, what makes very difficult to handle and to interpret the obtained general field equations. A second difficulty arises with the differential geometries when one has to introduce topological defects other than dislocations. For example, Kröner [38] (1980) has proposed that the existence of extrinsic point defects could be considered as extra-matter and introduced in the same manner that matter in general relativity under the form of Einstein equations, which would lead to a pure Riemannian differential geometry in the absence of dislocations. He has also proposed that the intrinsic point defects (vacancies and interstitials) could be approached as a non-metric part of an affine connection. Finally, he has also envisaged introducing other topological defects, as disclinations for example, by using higher order geometries much more complex, as Finsler or Kawaguchi geometries. In fact, the introduction of differential geometries implies generally a heavy mathematical artillery (metric tensor and Christoffel symbols) in order to describe the spatiotemporal evolution in infinitesimal local referentials, as shown for example in the mathematical theory of dislocations of Zorawski [39] (1967).

In view of the complexity of calculations in the case of Lagrangian coordinates as well as in the case of differential geometries, it seemed that it would be better to develop a much simpler approach of deformable solids, but at least equally rigorous, which has been finally published in a first book [4] during year 2013: *la théorie eulérienne des milieux déformables*.

In the first part of book [2] [3], one presents a summary of this new and original Eulerian approach of the deformation of solids through several sections:

*The first section* introduces *the Eulerian deformation theory of Newtonian lattices*. The deformation of a lattice is characterized by *distortions and contortions*. A vectorial representation of the tensors, presenting undeniable advantages over purely tensorial representation thanks the possibility to use the powerful formalism of the

vectorial analysis, allows to obtain *the geometro-compatibility equations* of the lattice which insure its solidity, and *the geometro-kinetics equations* of the lattice, which allow one to describe the deformation kinetics. One introduces then the physics in this topological context, namely *the Newtonian dynamics* and *the Eulerian thermo-kinetics* (based on the first and second principles of thermodynamics). With all these ingredients, it becomes possible to describe the particular behaviors of a solid lattice, as *the elasticity*, *the anelasticity*, *the plasticity* and *the self-diffusion*. This first section ends with the establishment of the complete set of evolution equations of a lattice in the Euler coordinate system.

*The second section* is dedicated to *the applications of the Eulerian theory*. It presents very succinctly some examples of *phenomenologies of everyday solids*. One shows how to obtain the functions and equations of state of an isotropic solid, what are the elastic and thermal properties which can appear, how waves propagate and why there exist thermoelastic relaxations, what are the mass transport phenomena and why it could appear inertial relaxations, what are the common phenomenologies of anelasticity and plasticity, and finally how it can appear structural transitions of first and second order in a solid lattice.

### 3.2. Dislocation and Disclination Charges in Eulerian Lattices

Regarding *the description of defects (topological singularities)* which can appear within a solid, as dislocations and disclinations, it is a domain of physics initiated principally by the idea of macroscopic defects of Volterra [40] (1907). This domain experienced a fulgurant development during the twentieth century, as well illustrated by Hirth [41] (1985). The lattice dislocation theory started up in 1934, when Orowan [42], Polanyi [43] and Taylor [44] published independently papers describing the edge dislocation. In 1939, Burgers [45] described the screw and mixed dislocations. And finally in 1956, Hirsch, Horne et Whelan [46] and Bollmann [47] observed independently dislocations in metals by using electronic microscopes. Concerning the disclinations, it is in 1904 that Lehmann [48] observed them in molecular crystals, and in 1922 that Friedel [49] gave them a physical explanation. From the second part of the century, the physics of lattice defects has grown considerably.

In the first part of the books [2] [3], the dislocations and the disclinations are approached by introducing intuitively the concept of dislocation charges by using the famous Volterra pipes [40] (1907) and an analogy with the electrical charges. With Euler coordinates, the concept of dislocation charge density appears then in an equation of geometro-compatibility of the solid, when the concept of flux of charges is introduced in an equation of geometro-kinetics of the solid.

The *rigorous formulation of the charge concept* in the solids makes the essential originality of this approach of the topological singularities. The detailed development of this concept leads to the appearance of tensorial charges of first order, *the dislocation charges*, associated with *the plastic distortions* of the solid (plastic deformations and rotations), and of tensorial charges of second order, *the disclination charges*, associated with *the plastic contortions* of the solid (plastic flexions and torsions). It appears that these topological singularities are quantified in a solid lattice and that they have to appear as *strings (thin tubes)* which can be modeled as unidimensional lines of dislocation or disclination, or as *membranes (thin sheets)* which can be modeled as two-dimensional boundaries of flexion, torsion or accommodation.

The concept of dislocation and disclination charges allows one to find rigorously the main results obtained by the classical dislocation theory. But it allows above all to define a tensor  $\mathcal{A}_i$  of *linear dislocation charge*, from which one deduces a scalar  $\Lambda$  of *linear rotation charge*, which is associated with the screw part of the dislocation, and a vector  $\mathcal{A}$  of *linear flexion charge*, which is associated with the edge part of the dislocation. For a given dislocation, both charges  $\Lambda$  and  $\mathcal{A}$  are perfectly defined without needing a convention at the contrary of the classical definition of a dislocation with its Burger vector! On the other hand, the description of the dislocations in the Eulerian coordinate system by the concept of dislocation charges allows one to treat exactly the evolution of the charges and the deformations during very strong volumetric contractions and expansions of a solid medium.

The description of this new approach of the topological defects of a lattice is presented in the two following sections of part one of the book:

*The third section* is dedicated to the introduction of *dislocation charges* and *disclination charges* in the Eulerian lattices. After the analytical introduction of the concepts of density and flux of dislocation and disclination charges in the lattices, one presents a detailed review of *the lattice macroscopic and microscopic topological singularities*, which can be associated to the dislocation and disclination charges. Then one discusses the motion of dislocation charges within the lattice by introducing *the dislocation charges flux* and *the Orowan relations*.

Finally, one deduces the Peach and Koehler force, which acts on the dislocations, and one establishes the new set of evolution equations of a lattice in the Euler coordinate system, which takes into account the existence of topological singularities within the lattice.

*The fourth section is dedicated to the applications of the charge concept within the Eulerian solid lattice. It shows the elements of the dislocation theory in the everyday solids. One begins to show that, in the particular case of the deformation of isotropic lattices by pure shears, one can replace the shear strain tensor by the rotation vector, which allows one to find a set of equations, which corresponds strictly to all the Maxwell equations of electromagnetism!* Then one shows how to calculate the fields and energies of the screw and edge dislocations in an isotropic lattice, just as the interactions, which can occur between dislocations. One finishes this section of applications by presenting *the string model* of dislocations, which is the fundamental model allowing one to explain most of the macroscopic behaviors of anelasticity and plasticity of crystalline solids.

#### 4. Motivation of the Second Part: Searching for a “Cosmic Lattice”

In the first part of the book, it is shown that it is possible to calculate the resting energy  $E_0$  of the dislocations, which corresponds to *the elastic energy stored in the lattice* by their presence, and their kinetic energy  $E_{cin}$ , which corresponds to the kinetic energy of the lattice particles mobilized by their movement. This allows to assign to the dislocations *a virtual inertial mass*  $M_0$  which satisfies relations similar to the famous equation  $E_0 = M_0 c^2$  of the Einstein special relativity, but which is obtained here through purely classical calculations, without using relativity principles! Moreover, at high velocity, the dislocation dynamics satisfy also *the special relativity principles and the Lorentz transformations*.

It is also shown in the first part that it appears, in the case of isotropic solid media presenting a constant and homogeneous volumetric expansion, a perfect and complete analogy with the Maxwell equations of electromagnetism when the shear stress tensor is replaced by the rotation vector. The existence of an analogy between the electromagnetism and the theory of incompressible continuous media has already been distinguished very long ago by several authors, as shown by Whittaker [50] (1951). However, this analogy is much more complete in the first book [4], because it is not restricted to one of the two Maxwell equation couples in the vacuum, but it is generalized to the two equation couples as well as to *the diverse phenomenologies of dielectric polarization and magnetization of matter*, just as to *the electrical charges and the electrical currents!* The analogy with the Maxwell equations is very surprising on account of the fact that it is initially postulated a solid lattice satisfying a simple and purely Newtonian dynamics in the absolute reference frame of the external observer laboratory, which is equipped with absolute orthonormal measuring rods and an absolute clock. At the contrary, the topological singularities within the lattice (dislocations and disclinations) with their respective charges, responsible for the plastic distortions and contortions of the lattice, are submitted to a relativistic dynamics within the lattice, due to the Maxwellian equation set governing the shear strains of the massive elastic lattice. From this point of view, the relativistic dynamics of the topological singularities is a direct consequence of the purely classical Newtonian dynamics of the elastic lattice in the absolute frame of the external observer!

Finally, it also appears in the first part that the tensorial aspect of the distortion fields at short distances of a localized topological singularities cluster formed by one or more dislocation or disclination loops can be easily neglected at great distances of the cluster, because the distortion fields can then be completely described by only two vectorial fields, the vectorial field of rotation by torsion and the vectorial field of curvature by flexion, associated respectively to the only two scalar charges of the cluster, its *scalar rotation charge* and its *scalar curvature charge*. The rotation charge becomes the perfect analogue of *the electrical charge* in the Maxwell equations, when the curvature charge presents some analogy with *the gravitational mass* in the gravitation theory.

The existence of analogies between the theories of continuum mechanics and solid defects and the theories of electromagnetism, special relativity and gravitation has already been the subject of several publications, from which the more famous are most certainly those of Kröner [37] [38]. Excellent reviews in this physics field have also been published, in particular by Whittaker [50] (1951) and Unzicker [51] (2000). But none of these publications has gone as far as the approach published in the first book [4] concerning these highlighted analogies.

The numerous analogies which appear in the first part between the Eulerian theory of deformable media and the theories of electromagnetism, gravitation, special relativity, general relativity and even standard model of elementary particles, reinforced by the absence of particles analogue to magnetic monopoles, by a possible solution of the famous paradox of electron field energy and by the existence of a small asymmetry between curvature

charges of vacancy or interstitial type, were sufficiently surprising and remarkable to alert any open and curious scientific spirit! But it was also clear that these analogies were, by far, not perfect. It was then tantalizing to analyze much more carefully these analogies and to try to find how to perfect them. That is the reason of the second part of the book, which is entirely allotted to the deepening, the improvement and the understanding of these analogies.

The second part of book [2] [3] is composed of five sections. Progressively, by introducing several judicious conjectures, one addresses the problem of the analogies existing between 1) the Eulerian theory of lattice deformation described in the first part, and applied to a very particular lattice, *the cosmic lattice*, and 2) the modern physics theories of the macrocosm and the microcosm, as the Maxwell equations, the special relativity, the Newtonian gravitation, the general relativity, the modern cosmology, the quantum mechanics and the standard model of elementary particles.

#### 4.1. The “Cosmic Lattice” and Its Newton’s Equation

*The first section* of part two is dedicated to the introduction of the “*cosmic lattice*”. By introducing an imaginary lattice with very original elastic properties concerning the volumetric expansion, the shear strain and especially the rotation field, and by expressing the distortion free energy *per volume unit of this lattice*, one obtains a lattice, which presents a very particular Newton equation. Indeed, it appears in particular a novel force term directly related to the distortion free energy due to the singularities contained in the lattice, which will play subsequently a very important role for the analogies with the gravitation and the quantum physics.

Then one shows that the propagation of waves in this cosmic lattice presents interesting particularities: propagation of linearly polarized transversal waves is always associated with longitudinal wavelets, and propagation of pure transversal waves can only be obtained with circularly polarized waves (which will be strongly linked with the photons). On the other hand, when the local value of the lattice volumetric expansion becomes less than a given critical value, propagation of longitudinal waves disappears for the benefit of the appearance of localized longitudinal vibrations modes (which will be strongly linked with the quantum physics).

Afterwards, the calculation of *the curvature of wave rays* in the vicinity of a singularity of the lattice volumetric expansion allows one to find the conditions for which this expansion singularity becomes a real capturing trap for the waves, in other words a “*black hole*”!

Finally, one shows that such a cosmic lattice, if finite in the absolute space, can present *dynamical volumetric expansion and/or contraction* if it contains some quantity of expansion kinetics energy. This phenomenon is perfectly similar to the cosmological expansion of the universe! Following the signs and the values of the lattice elastic modules, several cosmological behaviors of the lattice can appear, some of which presenting phenomena as *big-bang, rapid inflation and acceleration of the expansion velocity*, which can be sometimes followed by a *re-contraction of the lattice driving to a big-bounce phenomenon*! One deduces that it is *the expansion elastic energy* contained in the lattice which is responsible for these phenomena, and notably for *an expansion velocity increase*, a phenomenon which has been recently discovered by the astrophysicists in the case of the present universe, and which has been attributed to a hypothetical “*black energy*”.

#### 4.2. Maxwell’s Equations and Special Relativity

*The second section* is dedicated to *the Maxwell equations* and *the special relativity*. One begins to show that the Newton equation of the cosmic lattice can be separated in a curl part and a divergent part, and that the curl part creates a set of equations for the macroscopic rotation field, which is perfectly identical to the set of *the Maxwell equations of the electromagnetism*.

Then one shows that the Newton equation can also be separated in a different manner, in *two partial Newton equations* allowing to calculate on the one hand *the distortion elastic fields* associated with the topological singularities, and on the other hand *the volumetric expansion perturbations* associated with the distortion elastic energies of the topological singularities. By using the first partial Newton equation, one can calculate the fields and energies of elastic distortions generated by topological singularities within the cosmic lattice. One can then find conditions on the elastic modules of this lattice such as it is possible to attribute in a perfectly conventional manner *an inertial mass* to the topological singularities, which always satisfies the famous Einstein relation  $E_0 = M_0 c^2$ .

Then one demonstrates that the topological singularities satisfy a typically relativist dynamics when their

velocity inside the lattice becomes close to the celerity of the transversal waves.

On these foundations, one finishes this section by discussing the analogy between this theory and *the theory of special relativity*. One notices that the cosmic lattice acts in fact as *an aether*, in which the topological singularities satisfy exactly the same properties than those of the special relativity concerning *the length contraction, the time dilatation, the Michelson-Morley experiment and the Doppler-Fizeau effect*. The existence of the cosmic lattice allows then to explain very simply some obscure sides of the special relativity, as for example *the twin paradox!*

### 4.3. Gravitation, General Relativity, Weak Interaction and Cosmology

*The third section* is dedicated to *the gravitation and the cosmology*. Thanks to *the second partial Newton equation*, one begins with the calculation of *the external expansion perturbations*, that is to say *the external scalar gravitation field*, associated with a localized macroscopic topological singularity, knowing either *its distortion elastic energy, or its curvature charge, or its rotation charge*.

Immediately afterwards, one describes also *macroscopic vacancy singularities and macroscopic interstitial singularities*, which can appear within the lattice in the form of a macroscopic hole in the lattice or an interstitial embedment of a piece of lattice. These singularities will become subsequently the ideal candidates to explain respectively *the black holes and the pulsars* of our universe.

By applying the calculations of the external gravitation field of topological singularities to localized microscopic topological singularities, in the form of loops of screw disclination, loops of edge dislocation or loops of mixed dislocation, one deduces the whole of the properties of these loops. It appears then the new concept of *“curvature mass”* of the edge dislocation loops, which corresponds to the equivalent mass associated to the gravitational effects of *the curvature charges of these loops*, and which can be positive (in the case of loops of vacancy type) or negative (in the case of loops of interstitial type). In fact, the curvature charge and the equivalent curvature mass which is associated do not appear in any other physics theory, neither in general relativity, nor in quantum physics, nor in standard model of elementary particles. The appearance of this new curvature charge *is certainly the most important finding of our theory*, because it is precisely that curvature mass which is responsible for *a small asymmetry* between the particles (hypothetically containing edge dislocation loops of interstitial type) and the antiparticles (hypothetically containing edge dislocation loops of vacancy type), which will play a fundamental role concerning the weak interaction and the cosmological evolution of the topological singularities within the universe!

By considering the gravitational interactions existing between the topological singularities composed essentially of screw disclination loops, one can deduce the behaviors of *the measuring rods and clocks of local observers* as a function of the local expansion field, which takes place within the cosmic lattice. One shows that, for any local observer, and whatever is the value of the local volumetric expansion of the lattice, the Maxwell equations remain always perfectly invariant, so that, for this local observer, the transversal wave velocity is a perfect constant, when the transversal wave velocity measured by a hypothetical observer situated outside the lattice in the absolute space depends strongly on the local expansion of the lattice!

One shows that these gravitational interactions present strong analogies with the Newton’s gravitation and with the general relativity, and one discusses in details the perfectly analogue points, as the perfect analogy with the Schwarzschild metric at great distances from massive objects and the curvature of wave rays by massive objects.

But one shows that this Eulerian theory of the cosmic lattice provides also new elements to the gravitation theory, notably modifications of the Schwarzschild metric at very short distances from massive objects, and a better understanding of the critical radii associated with black holes: the radii of the photon perturbation sphere and of the point of no return become both equal to the Schwarzschild radius  $R_{\text{Schwarzschild}} = 2GM/c^2$ , and the limit radius for which the time dilatation of a falling observer would stretch to an infinite value becomes zero, so that our theory is not limited beyond the Schwarzschild sphere for the description of a black hole.

One establishes next a complete table of *all the gravitational interactions* existing between the diverse topological singularities of the cosmic lattice, and one finds that the gravitational interactions between screw disclination loops is largely dominant.

By considering now a topological singularity formed by coupling a screw disclination loop with an edge dislocation loop, called *a dispiration loop*, it appears *an interaction force between the rotation field of the screw*

*loop and the curvature field of the edge loop, which is perfectly similar to a catch potential with a very small range, and which presents an interaction between the two loops perfectly analog to the weak interaction between elementary particles of the standard model.*

On the basis of the cosmological behaviors of a lattice described in the first section, and the gravitational interactions between topological singularities described in the third section, one can imagine *a very plausible scenario for the cosmological evolution of the topological singularities contained in a cosmic lattice*, leading to the present structure of our universe. This scenario allows one to give a very simple explanation of several facts occurring during the universe expansion and still poorly understood, as *the formation of galaxies, the disappearance of antimatter, the formation of gigantic black holes at the heart of the galaxies*, and even *the famous “dark matter”* that the astrophysicists had to concoct for explaining the gravitational behavior of the galaxies.

In our theory, the *dark matter* would be in fact *a sea of repulsive neutrinos* in which the galaxies would have precipitated and would be immersed. Indeed, in the case of the simplest edge dislocation loops, analogically similar to neutrinos, *the “gravitational curvature mass” dominates the inertial mass*, so that the neutrinos should be the only particles gravitationally repulsive, when the antineutrinos should be gravitationally attractive. It is this surprising peculiarity which could explain the formation of a repulsive neutrinos sea playing the role of dark matter for the galaxies, due to the compression force exerted by the repulsive neutrinos sea on the galaxies periphery!

Finally, one shows how can be treated *the Hubble constant, the galaxy redshift and the evolution of the cosmic microwave background* in the frame of our Eulerian theory of cosmic lattice.

#### 4.4. Quantum Physics, Particles Spin and Photons

*The fourth section is dedicated to the quantum physics and the standard model of particles.* One begins by using the second partial Newton equation, in the dynamical case, to show that there exists also *longitudinal gravitational perturbations* associated to moving topological singularities inside the lattice. By conjecturing operators similar to those of the quantum mechanics, one shows then that the second partial Newton equation allows one to deduce the gravitational fluctuations associated to a topological singularity moving quasi-freely with relativistic velocities within the lattice.

In the case of non-relativistic topological singularities bonded to a potential, one shows that the second partial Newton equation applied to the longitudinal gravitational fluctuations associated to these singularities leads to *the Schrödinger equation of the quantum physics*, which allows one *for the first time* to give a simple and realistic physical interpretation to the Schrödinger equation and to the quantum wave function: *the quantum wave function deduced from the Schrödinger equation represents the amplitude and the phase lag of longitudinal gravitational vibrations associated to a topological singularity within the cosmic lattice!*

All the consequences of the Schrödinger equation appear now with a simple physical explanation, as for example *the stationary wave equation* of a topological singularity placed inside a static potential, *the Heisenberg uncertainty principle* and *the probability interpretation* of the square of the wave function.

In the case where the gravitational fluctuations of two topological singularities are coupled, it appears also very simply *the concepts of bosons and fermions*, as well as *the Pauli exclusion principle*.

At the heart of a topological singularity loop, one shows that there cannot exist static solutions to the second partial Newton equation for the longitudinal gravitational fluctuations. It becomes then necessary to find a dynamical solution to this equation. The simplest dynamical solution is to imagine that the loop rotates around one of its diameter. By solving this rotation motion with the second partial Newton equation, which is nothing other than the Schrödinger equation, one obtains a quantified solution for the internal gravitational fluctuations of the loop. This solution is in fact nothing other than *the quantic loop spin*, which can take several different values ( $1/2, 1, 3/2, \dots$ ) and which is perfectly similar to the spin of particles in the standard model! If the loop is composed of a screw disclination loop, it appears also *a magnetic moment of the loop*, proportional to *the famous Bohr magneton*. The notorious argument of the quantum physics pioneers wherein the spin cannot be a real rotation of the particle on itself because the equatorial velocity should become superior to light velocity, is swept out in our theory by the fact that the static expansion at the vicinity of the loop heart is so high that the light velocity becomes much higher than the equatorial rotation velocity of the loop!

In this argumentation about the absolute necessity of a spin of the singularity loops for satisfying the second partial Newton equation, only the exact value of the spin of a loop, namely  $1/2$  or  $1$ , does not find at the moment

a simple explanation!

One finishes by showing how to construct a pure transversal wave packet with a circular polarization *and why it appears a quantification of the energy of these fluctuations*. These waves packets form quasi-particles which have properties perfectly similar to *the quantum properties of photons: circular polarization, zero mass, non-zero momentum, non-locality, wave-particle duality, quantum entanglement and quantum decoherence*.

#### 4.5. Standard Model of Elementary Particles and Strong Interaction

In a second part of *the fourth section*, one searches for the ingredients, which have to be added to the cosmic lattice in order to find an analogy between the loop singularities and the diverse particles of the standard model. One shows that, by introducing a cubic lattice with *three families of planes (imaginary “colored” in red, green and blue)*, satisfying some simple rules concerning their successive arrangement and their mutual rotation, one can find topological loops perfectly analogous to *all the particles, leptons and quarks, of the first family of elementary particles of the standard model*. One finds also topological loops analogous to *the W and Z bosons of the standard model*. It appears spontaneously a *strong force*, in the sense that this force presents an asymptotical behavior, acting between the loops analogous to the quarks of the standard model, and which is due to the formation of a tube of stacking fault linking these loops. This implies that these loops have to group together in *triplets* to form combinations of three loops analogous to *the baryons*, or in doublets to form combinations of loop-anti-loop analogous to *the mesons*. Furthermore, one finds topological bicolor loops which correspond perfectly to *the gluons* associated to the strong force in the standard model!

In order to explain the existence of *three families of quarks and leptons in the standard model*, one shows that the introduction of more complicated topological structures of the edge dislocation loops, based on *assembling of pairs of edge disclination* loops replacing the edge dislocation loops, allows one to explain in a satisfactory way the existence of three, or even four, families of particles with very different energies.

Finally, one discusses the interest of this strong analogy between the topological singularities of a cubic “colored” lattice and the elementary particles of the standard model, as well as the numerous questions still pending concerning this analogy.

#### 4.6. Vacuum Quantum State Fluctuations

*The fifth section* is dedicated to some very hypothetical consequences concerning *the pure gravitational fluctuations* associated to the perfect cosmic lattice. One can imagine the existence of pure longitudinal fluctuations within the cosmic lattice, which are not correlated with the presence of topological singularities, and which can be treated either as *random gravitational fluctuations* that could present some analogy with *the vacuum quantum state fluctuations*, or as *stable gravitational fluctuations* that could lead at the macroscopic scale to *a cosmological theory of multiverse*. At the microscopic scale, stable gravitational fluctuations could also lead to *stable quasiparticles* which could be called *gravitons*, by analogy with the photons, but which have nothing common with the gravitons postulated in the frame of the general relativity.

One finishes the book by a general conclusion in which one shows the central roles played by the Newton equation and by the microscopic structure of the cosmic lattice. One highlights also the numerous positive points, but also the still misunderstood points, which have appeared throughout this essay concerning the analogy between the Newtonian cosmic lattice and all the theories of modern physics.

### 5. Conclusions

It is remarkable that the description, using Euler’s coordinates in an absolute space-time frame, of *a massive elastic “colored” cubic 3D-lattice containing loop topological singularities* and having particular elastic properties allows one to find all observed natural phenomena.

In fact, the theory described in the book [2] [3] and summarized here is not yet completed, as there remain several questions without answers, as for example the exact nature of the “colored” 3D-lattice and its relation with the Higgs field postulated in standard model, the detailed rotation mechanisms of the topological loops and the reason for spin values of 1/2 or 1, and still several other unsolved problems detailed in the book.

However, it appears that this theory is the first and only 1) to combine all known physics in a very simple manner, unifying electromagnetism, relativity, gravitation and quantum physics, 2) to give a simple meaning to

the local space-time and the quantum behavior of topological singularities, 3) to find *a new scalar curvature charge* which allows very simple explanations of the weak asymmetry observed between matter and anti-matter, of the nuclear weak interaction, of the formation of galaxies, of the disappearance of antimatter, of the formation of gigantic black holes in the heart of the galaxies, and of the famous dark matter, 4) to propose simple explanations to well-known problems of modern cosmology, as for example the universe expansion, the big-bang and the dark energy, and 5) to propose a model of “*colored*” *cubic 3D-lattice* whose diverse microscopic loop singularities correspond exactly to each of the elementary particles of the three families of particles of the standard model, and which allows to give a simple structural explanation to the strong force.

## Acknowledgements

I would like to thank Gianfranco D’Anna, Marc Fleury, Daniele Mari and Willy Benoit for providing valuable input and comments, and Marc Fleury for his English translation of the book.

## References

- [1] <http://gerardgremaud.ch/en/>
- [2] Gremaud, G. (2016) Universe and Matter conjectured as a 3-dimensional Lattice with Topological Singularities. 646 p. (Available on [1]) <https://www.createspace.com/6398875>
- [3] Gremaud, G. (2015) Univers et Matière conjecturés comme un Réseau Tridimensionnel avec des Singularités Topologiques. 660 p. (Available on [1]) <https://www.createspace.com/6427358>
- [4] Gremaud, G. (2013) Théorie eulérienne des milieux déformables, charges de dislocation et de désinclinaison dans les solides. Presses polytechniques et universitaires romandes (PPUR), Lausanne, 750 p. (Available on [1]) [http://www.ppur.org/produit/619/9782880749644/Theorie%20eulerienne%20des%20milieux%20deformables%20?search\\_text=g%C3%A9rard%20Gremaud](http://www.ppur.org/produit/619/9782880749644/Theorie%20eulerienne%20des%20milieux%20deformables%20?search_text=g%C3%A9rard%20Gremaud)
- [5] Gremaud, G. (2016) Eulerian Theory of Newtonian Deformable Lattices—Dislocation and Disclination Charges in Solids. 308 p. (Available on [1]) <https://www.createspace.com/6439507>
- [6] Goenner, H.F.M. (2005) On the History of Unified Field Theories. Living Reviews in Relativity. <http://relativity.livingreviews.org/open?pubNo=lrr-2004-2>
- [7] Ross, G. (1984) Grand Unified Theories. Westview 1 Press, Boulder.
- [8] Kiefer, C. (2007) Quantum Gravity. Oxford University Press, Oxford. <http://dx.doi.org/10.1093/acprof:oso/9780199212521.001.0001>
- [9] Rovelli, C. (2011) Zakopane Lectures on Loop Gravity. arXiv:1102.3660.
- [10] Wess, J. and Bagger, J. (1992) Supersymmetry and Supergravity. Princeton University Press, Princeton.
- [11] Junker, G. (1996) Supersymmetric Methods in Quantum and Statistical Physics. Springer-Verlag, Berlin. <http://dx.doi.org/10.1007/978-3-642-61194-0>
- [12] Weinberg, S. (1999) The Quantum Theory of Fields. Volume 3: Supersymmetry. Cambridge University Press, Cambridge.
- [13] Kane, G.L. and Shifman, M. (Eds.) (2000) The Supersymmetric World: The Beginnings of the Theory. World Scientific, Singapore.
- [14] Kane, G.L. (2001) Supersymmetry: Unveiling the Ultimate Laws of Nature. Basic Books, New York
- [15] Duplij, S., Duplij, W. and Siegel, J.B. (Eds.) (2005) Concise Encyclopedia of Supersymmetry. Springer, Berlin/New York. (2nd Printing)
- [16] Green, M., Schwarz, J.H. and Witten, E. (1987) Superstring Theory. Vol. 1, Introduction; Vol. 2, Loop Amplitudes, Anomalies and Phenomenology. Cambridge University Press, Cambridge.
- [17] Polchinski, J. (1998) String Theory. Vol. 1, An Introduction to the Bosonic String; Vol. 2, Superstring Theory and Beyond. Cambridge University Press, Cambridge.
- [18] Johnson, C.V. (2003) D-Branes. Cambridge University Press, Cambridge.
- [19] Zwiebach, B. (2004) A First Course in String Theory. Cambridge University Press, Cambridge. <http://dx.doi.org/10.1017/CBO9780511841682>
- [20] Becker, K., Becker, M. and Schwarz, J. (2007) String Theory and M-Theory: A Modern Introduction. Cambridge University Press, Cambridge.
- [21] Dine, M. (2007) Supersymmetry and String Theory: Beyond the Standard Model. Cambridge University Press, Cam-

- bridge. <http://dx.doi.org/10.1017/CBO9780511618482>
- [22] Kiritsis, E. (2007) *String Theory in a Nutshell*. Princeton University Press, Princeton.
- [23] Szabo, R.J. (2007) *An Introduction to String Theory and D-Brane Dynamics*. Imperial College Press, London.
- [24] Cremmer, E., Bernard, J. and Scherk, J. (1978) *Physics Letters B*, **76**, 409-412.  
[http://dx.doi.org/10.1016/0370-2693\(78\)90894-8](http://dx.doi.org/10.1016/0370-2693(78)90894-8)
- [25] Bergshoeff, E., Sezgin, E. and Townsend, P. (1987) *Physics Letters B*, **189**, 75-78.  
[http://dx.doi.org/10.1016/0370-2693\(87\)91272-X](http://dx.doi.org/10.1016/0370-2693(87)91272-X)
- [26] Duff, M. (1996) *International Journal of Modern Physics A*, **11**, 5623-5641.  
<http://dx.doi.org/10.1142/S0217751X96002583>
- [27] Duff, M. (1998) *Scientific American*, **278**, 64-69. <http://dx.doi.org/10.1038/scientificamerican0298-64>
- [28] Greene, B. (2010) *The Elegant Universe: Superstrings, Hidden Dimensions, and the Quest for the Ultimate Theory*. W. W. Norton & Company, New York.
- [29] Griffiths, D. (2004) *Introduction to Quantum Mechanics*. Prentice Hall, Upper Saddle River.
- [30] Zwiebach, B. (2009) *A First Course in String Theory*. Cambridge University Press, Cambridge.  
<http://dx.doi.org/10.1017/CBO9780511841620>
- [31] Zee, A. (2010) *Quantum Field Theory in a Nutshell*. 2nd Edition, Princeton University Press, Princeton.
- [32] Kaku, M. (2000) *Strings, Conformal Fields, and M-Theory*. 2nd Edition, Springer-Verlag, New York.
- [33] Nye, J.F. (1953) *Acta Metallurgica*, **1**, 153-162. [http://dx.doi.org/10.1016/0001-6160\(53\)90054-6](http://dx.doi.org/10.1016/0001-6160(53)90054-6)
- [34] Kondo, K. (1952) *RAAG Memoirs of the Unifying Study of the Basic Problems in Physics and Engineering Science by Means of Geometry*. Vol. 1, Gakujutsu Bunken Fukyu-Kay, Tokyo.
- [35] Bilby, B.A., Bullough, R. and Smith, E. (1955) *Proceedings of the Royal Society of London A*, **231**, 263-273.  
<http://dx.doi.org/10.1098/rspa.1955.0171>
- [36] Cartan, E. (1922) *C. r. hebd. séances Acad. sci. (CRAS)*, **174**, p. 593 & *C.R. Akad. Sci.*, 174, p. 734.
- [37] Kröner, E. (1960) *Archive for Rational Mechanics and Analysis*, **4**, 273-313. <http://dx.doi.org/10.1007/BF00281393>
- [38] Kröner, E. (1980) *Continuum Theory of Defects*. In: Balian, R., *et al.*, Eds., *Physics of Defects, Les Houches, Session 35*, North Holland, Amsterdam, 215-315.
- [39] Zorawski, M. (1967) *Théorie mathématique des dislocations*. Dunod, Paris.
- [40] Volterra, V. (1907) *L'équilibre des corps élastiques*. *Ann. Ec. Norm.* (3), XXIV, Paris.
- [41] Hirth, J.-P. (1985) *Metallurgical Transactions A*, **16**, 2085-2090. <http://dx.doi.org/10.1007/BF02670413>
- [42] Orowan, E. (1934) *Zeitschrift für Physik*, **89**, 605-613, 614-633, 634-659.
- [43] Polanyi, M. (1934) *Zeitschrift für Physik*, **89**, 660-664. <http://dx.doi.org/10.1007/BF01341481>
- [44] Taylor, G.I. (1934) *Proceedings of the Royal Society of London A*, **145**, 362-387.  
<http://dx.doi.org/10.1098/rspa.1934.0106>
- [45] Burgers, J.M. (1939) *Proceedings of the Koninklijke Nederlandse Akademie van Wetenschappen*, **42**, 293-378.
- [46] Hirsch, P.B., Horne, R.W. and Whelan, M.J. (1956) *Philosophical Magazine*, **1**, 677-684.  
<http://dx.doi.org/10.1080/14786435608244003>
- [47] Bollmann, W. (1956) *Physical Review*, **103**, 1588-1589. <http://dx.doi.org/10.1103/PhysRev.103.1588>
- [48] Lehmann (1904) *Flussige Kristalle*. Engelmann, Leipzig.
- [49] Friedel, G. (1922) *Annales de Physique*, **18**, 273.
- [50] Whittaker, S.E. (1951) *A History of the Theory of Aether and Electricity*. Vol. 1, Dover Reprint, Mineola, 142.
- [51] Unzicker, A. (2000) *What Can Physics Learn from Continuum Mechanics?* ArXiv:gr-qc/0011064.

# Surface Wave Echo in a Semi-Bounded Plasma

Hee J. Lee, Myoung-Jae Lee

Department of Physics, Hanyang University, Seoul, Korea

Email: [hjlee@hanyang.ac.kr](mailto:hjlee@hanyang.ac.kr)

Received 8 June 2016; accepted 5 August 2016; published 8 August 2016

Copyright © 2016 by authors and Scientific Research Publishing Inc.

This work is licensed under the Creative Commons Attribution International License (CC BY).

<http://creativecommons.org/licenses/by/4.0/>



Open Access

---

## Abstract

Plasma echo theory is revisited to apply it to a semi-bounded plasma. Spatial echoes associated with plasma surface wave propagating in a semi-bounded plasma are investigated by calculating the second order electric field produced by external charges and satisfying the boundary conditions at the interface. The boundary conditions are two-fold: the specular reflection condition and the electric boundary condition. The echo spots are determined in terms of the perpendicular coordinate to the interface and the parallel coordinate along which the wave propagates. This improves the earlier works in which only the perpendicular coordinate is determined. In contrast with the echo in an infinite medium, echoes in a bounded plasma can occur at various spots. The diversity of echo occurrence spots is due to the discontinuity of the electric field at the interface that satisfies the specular reflection boundary condition. Physically, the diversity appears to be owing to the reflections of the waves from the interface.

## Keywords

Plasma Echo, Semi-Bounded Plasma, Boundary Condition

---

## 1. Introduction

Plasma echoes in an infinite plasma have long been known theoretically [1] [2] as well as experimentally [3]. Spatial echoes were theoretically investigated in a static situation where the non-propagating electric field is directed perpendicular to the interface of a semi-bounded plasma [4] [5]. If the perpendicular direction is designated as the  $x$  direction, the electric field  $E$  as well as the distribution function  $f$  is spatially one-dimensional:  $E = E(x, t)$  and  $f = f(x, v, t)$ , where  $x > 0$  ( $x < 0$ ) is the plasma (vacuum) region. In this case, the corresponding Vlasov equation takes the form of a first order differential equation, and can be solved by satisfying the specular reflection boundary condition at the interface  $x = 0$ :  $f(v, 0) = f(-v, 0)$  [6]. This

differential equation approach with the specular reflection boundary condition for a semi-bounded plasma has been shown to be entirely equivalent with the Fourier transform (with respect to  $x$ ) under the recipe that the  $E(x)$  is extended into the region  $x < 0$  in an odd function manner,  $E(x) = -E(-x)$  [5]. This odd function extension of  $E(x)$  gives rise to a surface term in the Fourier transform of the Poisson equation, which plays a significant role in the determination of the echo spots. It appears that this surface term, which the earlier authors entirely neglected, gives rise to diversity of echo spots [5]. Physically, the surface term manifests the reflection of the electric field at the boundary.

The echo phenomena is the result of a quadratic interaction of the two primary waves launched by two external charges at different locations (spatial echoes) or different times (temporal echoes). In response to the external charges, the plasma distribution function  $f(x, v, t)$  is modulated with the exponential phase  $e^{ik(x-vt)}$ , which is derived from the singularity at  $\omega = kv$  of the linear response function. This term is called the free streaming term since  $x = vt$  is the characteristic line of the Vlasov equation for a free particle. This rapidly modulating exponential phase makes the  $f(x, v, t)$  more and more oscillatory as  $t$  or  $x$  increases, and consequently,  $\int f dv$  will become vanishingly small due to almost complete *phase mixing*. Therefore, in the first order, the phase mixing obliterates any appreciable effect on the macroscopic variable such as density perturbation. However, the second order distribution function which is a product of two first order distribution functions is not phase-mixed when or where the condition for a constructive interference is met, thereby the second order electric field does not vanish, resulting in an echo. It is evident from the expression for the product of two free-streaming exponentials  $e^{ik_1(x_1-vt_1)}e^{ik_2(x_2-vt_2)}$  that a constructive interference can result in at a certain time (temporal echo) or a certain spot (spatial echo) such that  $k_1x_1 + k_2x_2 = v(k_1t_1 + k_2t_2)$ .

In this work, we investigate spatial echoes in a semi-bounded plasma, taking a full account of the boundary terms which originate from the oddly continuation of the electric field. This work is an extension of the earlier paper by Lee and Lee [5]; the distribution function and the electric field are now spatially two-dimensional, allowing for the  $z$ -dependence. Therefore, the echoes are associated with the surface wave which is propagating in the  $z$ -direction. The second order electric field endowed with the additional  $z$ -dependence can be Fourier-inverted by contour integration with unstraightforward analytic exercise, and delineating the echo condition requires extra complexity. The important boundary term is the discontinuity of the perpendicular electric field at the interface that is necessary to have the specular reflection boundary condition satisfied [5]. The diversity of echo occurrence spots has been experimentally reported [7] and can be explained by this boundary term. The identification of the echo spot associated with surface wave appears to be useful in experimental point of view [7].

## 2. Formulation of the Problem

We consider a plasma consisting of electrons and stationary ions, the latter forming the uniform background. The plasma is assumed to occupy the half-space  $x \geq 0$ . The region  $x < 0$  is assumed to be a vacuum. The perturbed electron distribution function  $f(\mathbf{r}, \mathbf{v}, t)$  and the electric field  $\mathbf{E}(\mathbf{r}, t)$  will depend on  $x$  and  $z$ -coordinates with the  $y$  coordinate ignored since  $y$  direction has a translational invariance. We have the nonlinear Vlasov equation and the Poisson equation to describe the electrostatic perturbation:

$$\frac{\partial}{\partial t} f(\mathbf{v}, \mathbf{r}, t) + \mathbf{v} \cdot \frac{\partial f}{\partial \mathbf{r}} - \frac{e}{m} \mathbf{E}(\mathbf{r}, t) \cdot \frac{\partial f}{\partial \mathbf{v}} = 0 \tag{1}$$

with  $\mathbf{r} = \hat{x}x + \hat{z}z$ ,  $\mathbf{v} = \hat{x}v_x + \hat{z}v_z$ ,  $\mathbf{E} = \hat{x}E_x + \hat{z}E_z$

$$\nabla \cdot \mathbf{E} = \frac{\partial E_x}{\partial x} + \frac{\partial E_z}{\partial z} = 4\pi \left( -e \int d^2v f + \rho_0(x, t) \right) \tag{2}$$

where  $f$  is a two-dimensional distribution function, and  $\rho_0$  represents the external charges:

$$\rho_0(x, z, t) = \left( \rho_1 e^{i\omega t} \delta[k_0(x - L_1)] \delta[k_0(z - S_1)] + 1 \rightarrow 2 \right) \tag{3}$$

$k_0$  is introduced to make the argument of the  $\delta$ -function dimensionless, and  $1 \rightarrow 2$  means the replica of the preceding term with the subscript 1 replaced by subscript 2. We solve the simultaneous Equations (1) and (2) for a given  $\rho_0(x, t)$  as prescribed by Equation (3). In mathematical terms, we have an inhomogeneous system, driven by the source term in Equation (3). The responses  $f$  and  $E$  should be determined by  $\rho_0$ .

The kinetic equation is supplemented by the kinematic boundary condition which we assume to be the specular reflection condition

$$f(v_x, v_z, x=0, z) = f(-v_x, v_z, x=0, z) \quad (4)$$

This specular reflection boundary condition is automatically satisfied by extending the electric field component  $E_x(x)$  in odd function manner into the region  $x < 0$ , i.e.,  $E_x(-x) = -E_x(x)$ . Assuming that the external perturbation is small, we solve Equations (1) and (2) by successive approximation. First, the linear solution of Equation (1) will be obtained for  $f$  with the boundary condition (4). Substituting this solution in Equation (2) yields an integral equation for the electric field which is solved by Fourier transform. Then the linear solution will be used to obtain the higher order solutions. We work only up to the second order. The higher order distribution function should also satisfy the boundary condition (4). The electric field should satisfy the electric boundary conditions: the normal component of the electric displacement  $D_x(x)$  and the tangential electric field  $E_z$  are continuous across the interface. In this work, the Fourier transform is defined by

$$f(k, \omega) = \int_{-\infty}^{\infty} dx \int_{-\infty}^{\infty} dt f(x, t) e^{-ikx + i\omega t}$$

$$f(x, t) = \int_{-\infty}^{\infty} \frac{dk}{2\pi} \int_{-\infty}^{\infty} \frac{d\omega}{2\pi} f(k, \omega) e^{ikx - i\omega t}$$

Let us Fourier transform Equations (1)-(3) with respect to  $t$  and  $z$  to write

$$-i(\omega - \mathbf{k} \cdot \mathbf{v}) f(\mathbf{v}, \mathbf{k}, \omega) - \frac{e}{m} \int \frac{d\omega'}{2\pi} \int \frac{d^2k'}{(2\pi)^2} \mathbf{E}(\mathbf{k} - \mathbf{k}', \omega - \omega') \cdot \frac{\partial}{\partial \mathbf{v}} f(\mathbf{v}, \mathbf{k}', \omega') = 0 \quad (5)$$

$$i\mathbf{k} \cdot \mathbf{E}(\mathbf{k}, \omega) + N(k_z, \omega) = 4\pi \left[ -e \int f(\mathbf{k}, \mathbf{v}, \omega) d^2v + \rho_0(\mathbf{k}, \omega) \right] \quad (6)$$

where

$$N(k_z, \omega) = E_x(0^-, k_z, \omega) - E_x(0^+, k_z, \omega)$$

is derived from the discontinuity of  $E_x$  at  $x=0$ . This N-term is characteristic of a semi-bounded plasma and responsible for the diversity of surface wave echoes, as compared with an infinite plasma. The external charges are Fourier transformed to

$$\rho_0(\mathbf{k}, \omega) = \frac{2\pi}{k_0^2} \left[ \rho_1 \delta(\omega + \omega_1) e^{-ik_x L_1} e^{-ik_z S_1} + 1 \rightarrow 2 \right] \quad (7)$$

Equations (5) and (6) constitute a set of nonlinear simultaneous equations. We solve the set of equations by successive approximations in terms of perturbation series:

$$f(\mathbf{k}, \mathbf{v}, \omega) = f_0(\mathbf{v}) + f^{(1)}(\mathbf{k}, \mathbf{v}, \omega) + f^{(2)}(\mathbf{k}, \mathbf{v}, \omega) + \dots$$

$$\mathbf{E}(\mathbf{k}, \omega) = \mathbf{E}^{(1)}(\mathbf{k}, \omega) + \mathbf{E}^{(2)}(\mathbf{k}, \omega) + \dots$$

Breaking down Equations (5) and (6) order by order, we have

$$-i(\omega - \mathbf{k} \cdot \mathbf{v}) f^{(1)}(\mathbf{k}, \mathbf{v}, \omega) = \frac{e}{m} \mathbf{E}^{(1)}(\mathbf{k}, \omega) \cdot \frac{d f_0}{d \mathbf{v}} \quad (8)$$

$$i\mathbf{k} \cdot \mathbf{E}^{(1)}(\mathbf{k}, \omega) + N(k_z, \omega) = 4\pi \left[ -e \int f^{(1)}(\mathbf{k}, \mathbf{v}, \omega) d^2v + \rho_0(\mathbf{k}, \omega) \right] \quad (9)$$

$$\begin{aligned} & -i(\omega - \mathbf{k} \cdot \mathbf{v}) f^{(2)}(\mathbf{k}, \mathbf{v}, \omega) \\ & = \frac{e}{m} \mathbf{E}^{(2)}(\mathbf{k}, \omega) \cdot \frac{d f_0}{d \mathbf{v}} + \frac{e}{m} \int_{-\infty}^{\infty} \frac{d\omega'}{2\pi} \int_{-\infty}^{\infty} \frac{dk'_x}{2\pi} \int_{-\infty}^{\infty} \frac{dk'_z}{2\pi} \mathbf{E}^{(1)}(\mathbf{k} - \mathbf{k}', \omega - \omega') \cdot \frac{\partial}{\partial \mathbf{v}} f^{(1)}(\mathbf{k}', \omega', \mathbf{v}) \end{aligned} \quad (10)$$

$$i\mathbf{k} \cdot \mathbf{E}^{(2)}(\mathbf{k}, \omega) = -4\pi e \int f^{(2)}(\mathbf{k}, \mathbf{v}, \omega) d^2v \quad (11)$$

The quantity  $N(k_z, \omega)$  in Equation (9) should be determined in terms of the vacuum field from the electric field boundary condition: electric displacement  $D_x(x)$  is continuous across the interface  $x=0$ ,

$$D_x^{(1)}(0^+) = D_x^{(1)}(0^-) \quad (12)$$

where  $D_x^{(1)}(0^-)$  equals to the vacuum electric field  $E_0$ .

### 3. Linear Solution

Equations (8) and (9), and  $\nabla \times \mathbf{E} = 0$  give

$$\mathbf{E}^{(1)}(\mathbf{k}, \omega) = \frac{i\mathbf{k}}{k^2 \varepsilon(\mathbf{k}, \omega)} [N(k_z, \omega) - 4\pi\rho_0(\mathbf{k}, \omega)] \quad (13)$$

$$\varepsilon(\mathbf{k}, \omega) = 1 + \frac{\omega_p^2}{k^2} \int d^2v \frac{\mathbf{k} \cdot \frac{d\mathbf{f}_0}{d\mathbf{v}}}{\omega - \mathbf{k} \cdot \mathbf{v}} \quad (14)$$

is the dielectric function ( $\omega_p$  is the plasma frequency).  $N$  is determined from the electric boundary condition as shown in the following. We need the normal component of electric displacement,  $D_x(x)$  to enforce the boundary condition (12). By definition,  $D_x(\mathbf{k}, \omega) = E_x(\mathbf{k}, \omega) + \frac{4\pi i}{\omega} J_x(\mathbf{k}, \omega)$  where  $J$  is the current:

$J_x(\mathbf{k}, \omega) = -e \int d^2v v_x f(\mathbf{k}, \omega, \mathbf{v})$ . We calculate

$$\frac{4\pi i}{\omega} J_x = \frac{4\pi i}{\omega} (-e) \int v_x f d^2v = \frac{\omega_p^2}{\omega} \int d^2v v_x \frac{E_j \frac{\partial f_0}{\partial v_j}}{\omega - \mathbf{k} \cdot \mathbf{v}}$$

where we used Equation (8). The above quantity equals to  $(\varepsilon - 1)E_x$ . Thus we have  $D_x = \varepsilon E_x$ . This statement can be most easily proved by assuming  $f_0$  a Maxwellian. Use  $\frac{\partial f_0}{\partial v_j} = -\frac{T}{m} v_j f_0$  and  $\mathbf{E} \cdot \mathbf{v} = \frac{E_x}{k_x} \mathbf{k} \cdot \mathbf{v}$  to write for the last term

$$\frac{4\pi i}{\omega} J_x = -E_x \frac{\omega_p^2 T}{\omega m} \int \frac{v_x}{k_x} \frac{\mathbf{k} \cdot \mathbf{v}}{\omega - \mathbf{k} \cdot \mathbf{v}} f_0 d^2v$$

Put  $\frac{\mathbf{k} \cdot \mathbf{v}}{\omega - \mathbf{k} \cdot \mathbf{v}} = -1 + \frac{\omega}{\omega - \mathbf{k} \cdot \mathbf{v}}$ . Then, (-1)-term vanishes upon integration, and we have

$$\begin{aligned} \frac{4\pi i}{\omega} J_x &= -E_x \frac{\omega_p^2 T}{k_x m} \int \frac{v_x f_0}{\omega - \mathbf{k} \cdot \mathbf{v}} d^2v = E_x \frac{\omega_p^2}{k_x} \int \frac{\frac{\partial f_0}{\partial v_x}}{\omega - \mathbf{k} \cdot \mathbf{v}} d^2v \\ &= -E_x \omega_p^2 \int \frac{f_0 d^2v}{(\omega - \mathbf{k} \cdot \mathbf{v})^2} = E_x \frac{\omega_p^2}{k^2} \int d^2v \frac{\mathbf{k} \cdot \frac{\partial f_0}{\partial \mathbf{v}}}{\omega - \mathbf{k} \cdot \mathbf{v}} \quad q.e.d. \end{aligned}$$

Using the above result, we obtain

$$D_x^{(1)}(\mathbf{k}, \omega) = \varepsilon(\mathbf{k}, \omega) E_x^{(1)}(\mathbf{k}, \omega) = \frac{ik_x}{k^2} [N - 4\pi\rho_0(\mathbf{k}, \omega)] \quad (15)$$

To invert Equation (15), we write

$$D_x^{(1)}(x, k_z, \omega) = \int_{-\infty}^{\infty} \frac{dk_x}{2\pi} e^{ik_x x} \frac{ik_x}{k^2} \left[ N - \frac{8\pi^2}{k_0^2} \rho_1 e^{-ik_x L_1} \delta(\omega + \omega_1) e^{-ik_z S_1} + 1 \rightarrow 2 \right] \quad (16)$$

In the above integral, we take the limit  $x \rightarrow 0^+$ . Evaluating the integral by residue theorem gives

$$\lim_{x \rightarrow 0^+} \int_{-\infty}^{\infty} dk_x \frac{k_x e^{ik_x x}}{k_x^2 + k_z^2} = i\pi$$

Note that we set up the contour encircling the upper half plane since  $x > 0$ . When  $Re k_z > 0$  ( $Re k_z < 0$ ), the relevant pole located in the upper  $k_x$ -plane is  $k_x = ik_z$  ( $k_x = -ik_z$ ). In either case, the integral is found to be  $i\pi$ . Then, Equation (16) takes the form

$$D_x^{(1)}(0^+, k_z, \omega) = -\frac{N}{2} - \frac{4\pi}{k_0^2} e^{-ik_z s_1} i I(L_1, k_z) \rho_1 \delta(\omega + \omega_1) + 1 \rightarrow 2 \quad (17)$$

$$\text{where } I(L_1, k_z) = \int_{-\infty}^{\infty} d\xi \frac{\xi e^{-i\xi L_1}}{\xi^2 + k_z^2} = -i\pi e^{\pm k_z L_1} \quad (18)$$

where  $+$  ( $-$ ) sign corresponds to  $Re k_z < 0$  ( $Re k_z > 0$ ). The above equality can be easily proven by using the contour winding the lower half plane. Taking the limit  $k_z \rightarrow 0$  gives the useful identity  $\int_{-\infty}^{\infty} d\xi \frac{e^{-i\xi L_1}}{\xi} = -i\pi$ , independently of  $L_1 (> 0)$ . Clearly, this integral manifests the nature of a step function. By equating the quantity on the right hand side of Equation (17) to the  $x$ -component of the vacuum electric field ( $\equiv E_0$ ), we obtain

$$N = -2E_0 - \frac{8\pi}{k_0^2} \rho_1 \delta(\omega + \omega_1) e^{-ik_z s_1} i I(L_1, k_z) + 1 \rightarrow 2 \quad (19)$$

Using the above equation in Equation (13) gives

$$\mathbf{E}^{(1)}(\mathbf{k}, \omega) = \frac{i\mathbf{k}}{k^2 \varepsilon(\mathbf{k}, \omega)} \left[ -2E_0 - \frac{8\pi^2}{k_0^2} \rho_1 \delta(\omega + \omega_1) e^{-ik_z s_1} \left( \frac{i}{\pi} I(L_1, k_z) + e^{-ik_x L_1} \right) + 1 \rightarrow 2 \right] \quad (20)$$

For an infinite plasma without boundary, we have  $N = 0$  in Equation (13), and the plasma electric field is given by

$$\mathbf{E}^{(1)}(\mathbf{k}, \omega) = \frac{i\mathbf{k}}{k^2 \varepsilon(\mathbf{k}, \omega)} \left[ -\frac{8\pi^2}{k_0^2} \rho_1 \delta(\omega + \omega_1) e^{-ik_z s_1} e^{-ik_x L_1} + 1 \rightarrow 2 \right]$$

Note that in Equation (20), the  $E_0$ -term and  $I(L_1, k_z)$ -term are the boundary terms which are non-existent in an infinite plasma.

In the static situation where the electric field is nonpropagating, we put  $k_z = 0$  in Equation (20), and the electric field reduces to Equation (23) in Lee and Lee [5]:

$$E^{(1)}(k, \omega) = \frac{-2i}{k\varepsilon(k, \omega)} \left[ E_0 + \frac{4\pi^2}{k_0^2} \rho_1 \delta(\omega + \omega_1) (1 + e^{-ikL_1}) + 1 \rightarrow 2 \right]$$

#### 4. Second Order Solution and Echo Occurrence

Next, we deal with the second order equations, Equations (10) and (11). Using Equation (10) in Equation (11) yields, owing to the electrostatic nature of  $\mathbf{E}^{(2)}$ ,

$$\mathbf{E}^{(2)}(\omega, \mathbf{k}) = \frac{4\pi e^2}{m} \frac{\mathbf{k}}{k^2 \varepsilon(\mathbf{k}, \omega)} \int d^2v \frac{\mathbf{k} \cdot \mathbf{Q}}{(\omega - \mathbf{k} \cdot \mathbf{v})^2} \quad (21)$$

where  $\mathbf{Q}$  stands for

$$\mathbf{Q}(\omega, \mathbf{k}, \mathbf{v}) = \int_{-\infty}^{\infty} \frac{d\omega'}{2\pi} \int_{-\infty}^{\infty} \frac{dk'_x}{2\pi} \int_{-\infty}^{\infty} \frac{dk'_z}{2\pi} \mathbf{E}^{(1)}(\omega - \omega', \mathbf{k} - \mathbf{k}') f^{(1)}(\omega', \mathbf{k}', \mathbf{v}) \quad (22)$$

Substituting the first order solutions [Equations (8) and (20)], into the above equations, we can write  $\mathbf{E}^{(2)}$  in the form,

$$\mathbf{E}^{(2)}(\omega, \mathbf{k}) = \frac{e^3}{2\pi^2 m^2} \frac{\mathbf{k}}{k^2 \varepsilon(\mathbf{k}, \omega)} \int \frac{d^2v}{(\omega - \mathbf{k} \cdot \mathbf{v})^2} \int dk'_z \int dk'_x \int d\omega' \times \frac{\mathbf{k} \cdot (\mathbf{k} - \mathbf{k}')}{\varepsilon(\omega - \omega', \mathbf{k} - \mathbf{k}') (\mathbf{k} - \mathbf{k}')^2} \frac{\mathbf{k}' \cdot \frac{d\mathbf{f}_0}{d\mathbf{v}}}{k'^2 \varepsilon(\omega', \mathbf{k}') (\omega' - \mathbf{k}' \cdot \mathbf{v})} AB, \quad (23)$$

$$A = -2E_0 - \frac{8\pi^2}{k_0^2} \rho_1 \delta(\omega' + \omega_1) e^{-ik_z S_1} \left( \frac{i}{\pi} I(L_1, k'_z) + e^{-ik'_x L_1} \right) + 1 \rightarrow 2 \quad (24)$$

$$B = -2E_0 - \frac{8\pi^2}{k_0^2} \rho_1 \delta(\omega - \omega' + \omega_1) e^{-i(k_z - k'_z) S_1} \left( \frac{i}{\pi} I(L_1, k_z - k'_z) + e^{-i(k_x - k'_x) L_1} \right) + 1 \rightarrow 2 \quad (25)$$

where  $I$  stands for the exponential function as given by Equation (18). Since we don't know yet which sign should be chosen, we keep on using the symbol  $I$ . Equation (23) is to be used for investigation of echo occurrence. The various cross terms in the product (AB) are the candidates of echo resonances to see if the condition for vanishing phase can be met.

We choose to investigate a cross term which is 1-term in A multiplied by 2-term in B. With this term, the  $t$ -inversion of Equation (23) can be easily carried out by simply putting  $\omega' \rightarrow -\omega_1$  and  $\omega \rightarrow -\omega_3$ :

$$\begin{aligned} E^{(2)}(t, \mathbf{k}) &= \beta e^{i\omega_3 t} e^{-ik_z S_2} \frac{\mathbf{k}}{k^2 \varepsilon(-\omega_3, \mathbf{k})} \int \frac{d^2 \mathbf{v}}{(\omega_3 + \mathbf{k} \cdot \mathbf{v})^2} \int dk'_z \int dk'_x \\ &\times \frac{\mathbf{k} \cdot (\mathbf{k} - \mathbf{k}')}{(\mathbf{k} - \mathbf{k}')^2 \varepsilon(-\omega_2, \mathbf{k} - \mathbf{k}')} \frac{\mathbf{k}' \cdot \frac{d\mathbf{f}_0}{d\mathbf{v}}}{k'^2 \varepsilon(-\omega_1, \mathbf{k}') (\omega_1 + \mathbf{k}' \cdot \mathbf{v})} e^{ik'_z (S_2 - S_1)} \\ &\times \left( \frac{i}{\pi} I(L_1, k'_z) + e^{-ik'_x L_1} \right) \left( \frac{i}{\pi} I(L_2, k_z - k'_z) + e^{-i(k_x - k'_x) L_2} \right) \end{aligned} \quad (26)$$

where

$$\omega_3 = \omega_1 + \omega_2, \quad \beta = \frac{-16\pi e^3 \rho_1 \rho_2}{k_0^4 m^2} \quad (27)$$

In the above equation, we can assume that the poles associated with the dielectric functions contribute negligibly in the  $\int d\mathbf{k}$  - or  $\int d\mathbf{k}'$  -integral. [The dominant contribution comes from the free-streaming poles.] Also we assume  $f_0$  to be a Maxwellian. Then we have

$$\frac{\mathbf{k}' \cdot \frac{d\mathbf{f}_0}{d\mathbf{v}}}{\omega_1 + \mathbf{k}' \cdot \mathbf{v}} = -\frac{m}{T} f_0 \left( 1 - \frac{\omega_1}{\omega_1 + \mathbf{k}' \cdot \mathbf{v}} \right)$$

where 1 can be assumed to contribute nothing to the inversion integral in the following, due to phase mixing. Thus, Equation (26) can be further simplified as

$$\begin{aligned} E^{(2)}(t, \mathbf{k}) &= \frac{\beta m \omega_1}{T} e^{i\omega_3 t} e^{-ik_z S_2} \frac{\mathbf{k}}{k^2 \varepsilon(-\omega_3, \mathbf{k})} \int \frac{d^2 \mathbf{v} f_0}{(\omega_3 + \mathbf{k} \cdot \mathbf{v})^2} \int dk'_z \int dk'_x \\ &\times \frac{\mathbf{k} \cdot (\mathbf{k} - \mathbf{k}')}{(\mathbf{k} - \mathbf{k}')^2 \varepsilon(-\omega_2, \mathbf{k} - \mathbf{k}') k'^2 \varepsilon(-\omega_1, \mathbf{k}') (\omega_1 + \mathbf{k}' \cdot \mathbf{v})} \\ &\times e^{ik'_z (S_2 - S_1)} \left( \frac{i}{\pi} I(L_1, k'_z) + e^{-ik'_x L_1} \right) \left( \frac{i}{\pi} I(L_2, k_z - k'_z) + e^{-i(k_x - k'_x) L_2} \right) \end{aligned} \quad (28)$$

Let us write explicitly the inversion integral of Equation (28) with respect to  $k$ :

$$\begin{aligned} E^{(2)}(t, x, z) &= \frac{\beta m \omega_1}{4\pi^2 T} e^{i\omega_3 t} \int \frac{d^2 \mathbf{v} f_0}{v_x^2} \int dk_z e^{ik_z (z - S_2)} \int dk_x \frac{\mathbf{k}}{k^2 \varepsilon(-\omega_3, \mathbf{k})} \frac{e^{ik_x x}}{\left( k_x + \frac{k_z v_z + \omega_3}{v_x} \right)^2} \\ &\times \int dk'_z e^{ik'_z (S_2 - S_1)} \int dk'_x \frac{\mathbf{k} \cdot (\mathbf{k} - \mathbf{k}')}{(\mathbf{k} - \mathbf{k}')^2 \varepsilon(-\omega_2, \mathbf{k} - \mathbf{k}') k'^2 \varepsilon(-\omega_1, \mathbf{k}') (\omega_1 + \mathbf{k}' \cdot \mathbf{v})} \\ &\times \left( \frac{i}{\pi} I(L_1, k'_z) + e^{-ik'_x L_1} \right) \left( \frac{i}{\pi} I(L_2, k_z - k'_z) + e^{-i(k_x - k'_x) L_2} \right) \end{aligned} \quad (29)$$

This equation will be examined in view of the possibility of the vanishing phase.

(1) First, we shall consider the interference of two exponential terms in Equation (29):  
 $e^{-ik'_x L_1} e^{-i(k_x - k'_x)L_2} = e^{ik'_x(L_2 - L_1)} e^{-ik_x L_2}$

The important singularities are: the double pole at  $k_x = -(k_z v_z + \omega_3)/v_x$  and the simple poles associated respectively with  $k^2 = 0$  and  $k'^2 = 0$  and  $\omega_1 + k_x v_x + k_z v_z = 0$ . We shall consider only these four poles. Singularities at  $\varepsilon = 0$  are not important. Therefore we can put

$$\frac{\mathbf{k} \cdot (\mathbf{k} - \mathbf{k}')}{(\mathbf{k} - \mathbf{k}')^2} = \frac{1}{2}$$

and all the  $\varepsilon$ 's can be taken out of the integral. The residue at the double pole is obtained by taking  $\partial/\partial k_x$   $\left[ \text{Integrand} \times \left( k_x + \frac{k_z v_z + \omega_3}{v_x} \right)^2 \right]$  and substituting for  $k_x = -(k_z v_z + \omega_3)/v_x$ . Here it is sufficient to differentiate only the exponential functions because they yield asymptotically dominant result. [Or integrate by parts with respect to  $k_x$ .] Thus let us calculate

$$\begin{aligned} \Phi &= \frac{i(x - L_2)}{v_x} \int dk_z e^{ik_z(z - S_2)} \int dk_x \frac{\mathbf{k}}{k^2} \frac{e^{ik_x(x - L_2)}}{k_x + (k_z v_z + \omega_3)/v_x} \\ &\quad \times \int dk'_z \frac{e^{ik'_z(S_2 - S_1)}}{k'^2} \int dk'_x \frac{e^{ik'_x(L_2 - L_1)}}{k'_x + (k'_z v_z + \omega_1)/v_x} \end{aligned} \quad (30)$$

Then  $E^{(2)}$  is obtained by  $e^{i\omega_3 t} \int d^2 v \Phi f_0 / v_x^2$ , suppressing the unessential factor.

Integral  $\int dk'_x$  can be easily done by picking up the pole at

$$k'_x = -\frac{k'_z v_z + \omega_1}{v_x} \quad (31)$$

For definiteness we assume  $L_2 > L_1$ . Then the contour in  $k'_x$ -plane should encircle the upper half  $k'_x$ -plane, and in order for the pole to lie in the upper  $k'_x$ -plane, the imaginary part of  $(k'_z v_z / v_x)$  should be negative. Now  $k'^2$  is only a function of  $k'_z$  per Equation (31), and we can write the second part of Equation (30) as

$$\begin{aligned} J' &\equiv \int dk'_z \frac{e^{ik'_z(S_2 - S_1)}}{k'^2} \int dk'_x \frac{e^{ik'_x(L_2 - L_1)}}{k'_x + (k'_z v_z + \omega_1)/v_x} \\ &= -\frac{\pi v_x}{\omega_1} e^{-i(L_2 - L_1)\omega_1/v_x} \int dk'_z e^{i\theta'} \left( \frac{1}{k'_z - k'_{z+}} - \frac{1}{k'_z - k'_{z-}} \right) H\left(-\frac{v_z}{v_x} \text{Im } k'_z\right) \end{aligned} \quad (32)$$

where

$$k'_{z\pm} = -\frac{\omega_1}{v^2} (v_z \pm i v_x) \quad (33)$$

$$\theta' = S_2 - S_1 + (L_1 - L_2) \frac{v_z}{v_x} \quad (34)$$

and  $H(x)$  is a step function;  $H(x) = 1$  for  $x > 0$  and  $H(x) = 0$  for  $x < 0$ .

The contour in  $\int dk'_z$ -integral depends on the sign of  $\theta'$ : when  $\theta' > 0$  ( $\theta' < 0$ ), the contour must wind the upper (lower)  $k'_z$ -plane. The location of the poles depends upon the sign of  $v_x$ . Sorting out the relevant cases, we carry out the integral for  $J'$ :

$$\theta' > 0: J' = \frac{-2i\pi^2 v_x}{\omega_1} e^{i(L_1 - L_2)\omega_1/v_x} \left[ e^{i\theta' k'_{z+}} H(v_z) H(-v_x) - e^{i\theta' k'_{z-}} H(-v_z) H(v_x) \right] \quad (35)$$

$$\theta' < 0: J' = \frac{2i\pi^2 v_x}{\omega_1} e^{i(L_1 - L_2)\omega_1/v_x} \left[ e^{i\theta' k'_{z+}} H(v_z) H(v_x) - e^{i\theta' k'_{z-}} H(-v_z) H(-v_x) \right] \quad (36)$$

Next, taking on the first part of the integral in Equation (30) ( $\int dk_z (\dots)$ ), we have two cases:

1)  $x < L_2$

In this case, the  $k_x$  contour must encircle the lower half plane and the  $k_x$ -integral does not vanish under the provision  $\text{Im}(k_z v_z / v_x) > 0$ . Then, the integral can be written as

$$\begin{aligned} \mathbf{J} &\equiv \int dk_z e^{ik_z(z-S_2)} \int dk_x \frac{\mathbf{k}}{k^2} \frac{e^{ik_x(x-L_2)}}{k_x + (k_z v_z + \omega_3)/v_x} \\ &= \frac{\pi v_x}{\omega_1} e^{-i(x-L_2)\omega_3/v_x} \int dk_z e^{i\theta} \left( \frac{1}{k_z - k_{z+}} - \frac{1}{k_z - k_{z-}} \right) H\left(\frac{v_z}{v_x} \text{Im} k_z\right) \left[ -\hat{\mathbf{x}} \frac{k_z v_z + \omega_3}{v_x} + z \hat{\mathbf{k}}_z \right] \end{aligned} \quad (37)$$

where

$$k_{z\pm} = -\frac{\omega_3}{v^2} (v_z \pm i v_x) \quad (38)$$

$$\theta = z - S_2 + (L_2 - x) \frac{v_z}{v_x} \quad (39)$$

Analogously to the foregoing calculation in  $\mathbf{J}'$ , the above integral depends on the sign of  $\theta$ :

$$\theta > 0: \mathbf{J} = \frac{2i\pi^2 v_x}{\omega_3} e^{i(L_2-x)\omega_3/v_x} \left[ \mathbf{k}_{z+} e^{i\theta k_{z+}} H(-v_x) H(-v_z) - \mathbf{k}_{z-} e^{i\theta k_{z-}} H(v_x) H(v_z) \right] \quad (40)$$

$$\theta < 0: \mathbf{J} = \frac{-2i\pi^2 v_x}{\omega_3} e^{i(L_2-x)\omega_3/v_x} \left[ \mathbf{k}_{z+} e^{i\theta k_{z+}} H(v_x) H(-v_z) - \mathbf{k}_{z-} e^{i\theta k_{z-}} H(-v_x) H(v_z) \right] \quad (41)$$

2)  $x > L_2$

Repeating a similar analysis, we obtain

$$\theta > 0: \mathbf{J} = \frac{-2i\pi^2 v_x}{\omega_3} e^{i(L_2-x)\omega_3/v_x} \left[ \mathbf{k}_{z+} e^{i\theta k_{z+}} H(-v_x) H(v_z) - \mathbf{k}_{z-} e^{i\theta k_{z-}} H(v_x) H(-v_z) \right] \quad (42)$$

$$\theta < 0: \mathbf{J} = \frac{2i\pi^2 v_x}{\omega_3} e^{i(L_2-x)\omega_3/v_x} \left[ \mathbf{k}_{z+} e^{i\theta k_{z+}} H(v_x) H(v_z) - \mathbf{k}_{z-} e^{i\theta k_{z-}} H(-v_x) H(-v_z) \right] \quad (43)$$

where

$$\mathbf{k}_{z\pm} = k_{z\pm} (\mp i \hat{\mathbf{x}} + \hat{\mathbf{z}}) \quad (44)$$

Now, we have to multiply  $\mathbf{J}$  and  $\mathbf{J}'$ . In doing it, note that  $H(x)H(x) = H(x)$  and  $H(x)H(-x) = 0$ . Nonzero results surviving the velocity integral are obtained in the following four cases:

a)  $x < L_2$ ,  $\theta < 0$ ,  $\theta' > 0$ ; b)  $x < L_2$ ,  $\theta > 0$ ,  $\theta' < 0$ ; c)  $x > L_2$ ,  $\theta > 0$ ,  $\theta' > 0$ ; d)  $x > L_2$ ,  $\theta < 0$ ,  $\theta' < 0$

Let us first consider case a). Using Equations (35) and (41), we obtain

$$\begin{aligned} \Phi &= \frac{(2\pi^2 v_x)^2}{\omega_1 \omega_3} \frac{i(x-L_2)}{v_x} \left[ H(v_x) H(-v_z) k_{z+} \exp(i\theta_0 + i\theta k_{z+} + i\theta' k'_{z-}) \right. \\ &\quad \left. + H(-v_x) H(v_z) k_{z-} \exp(i\theta_0 + i\theta k_{z-} + i\theta' k'_{z+}) \right] \end{aligned} \quad (45)$$

where

$$\theta_0 = (L_2 - x) \frac{\omega_3}{v_x} + (L_1 - L_2) \frac{\omega_1}{v_x} \quad (46)$$

Using Equations (34), (39), and (46), we can obtain the exponential phases:

$$i\theta_0 + i\theta k_{z-} + i\theta' k'_{z+} = \varphi'_r + i\varphi_i \quad (47)$$

$$i\theta_0 + i\theta k_{z_+} + i\theta' k'_{z_-} = -\phi'_r + i\phi_i \quad (48)$$

with

$$\phi'_r = \frac{1}{v^2} [v_x \omega_3 (S_2 - z) + v_x \omega_1 (S_2 - S_1) + v_z \omega_3 (x - L_2) + v_z \omega_1 (L_1 - L_2)] \quad (49)$$

$$\phi_i = \frac{1}{v^2} [v_z \omega_3 (S_2 - z) + v_z \omega_1 (S_1 - S_2) + v_x \omega_3 (L_2 - x) + v_x \omega_1 (L_1 - L_2)] \quad (50)$$

Thus Equation (45) can be written in the form

$$\Phi = \frac{(2\pi^2 v_x)^2}{\omega_1 \omega_3} \frac{i(x - L_2)}{v_x} e^{i\phi_i} [H(v_x) H(-v_z) \mathbf{k}_{z_+} \exp(-\phi'_r) + H(-v_x) H(v_z) \mathbf{k}_{z_-} \exp(\phi'_r)] \quad (51)$$

Therefore the velocity integrals in Equation (29) survive the phase mixing when  $\phi_i = 0$ , that is,

$$\omega_3 (z - S_2) + \omega_1 (S_2 - S_1) = 0, \quad \omega_3 (L_2 - x) + \omega_1 (L_1 - L_2) = 0 \quad (52)$$

$$\text{or } x = \frac{\omega_1 L_1 + \omega_2 L_2}{\omega_1 + \omega_2}, \quad z = \frac{\omega_1 S_1 + \omega_2 S_2}{\omega_1 + \omega_2} \quad (53)$$

where an echo is given rise to. The electric field  $\mathbf{E}^{(2)}$  can be obtained by velocity integral in the form (see Equation (29))

$$\mathbf{E}^{(2)}(t, x, z) = \left[ \int_0^\infty dv_x \int_{-\infty}^0 dv_z \mathbf{k}_{z_+} e^{-\phi'_r} + \int_{-\infty}^0 dv_x \int_0^\infty dv_z \mathbf{k}_{z_-} e^{\phi'_r} \right] (\dots) \quad (54)$$

where  $(\dots)$  denotes the obvious integrand.

Next, let us calculate case (b). Using Equations (36) and (40) gives

$$\Phi = \frac{(2\pi^2 v_x)^2}{\omega_1 \omega_3} \frac{i(x - L_2)}{v_x} \left[ H(-v_x) H(-v_z) \mathbf{k}_{z_+} \exp(i\theta_0 + i\theta k_{z_+} + i\theta' k'_{z_-}) \right. \\ \left. + H(v_x) H(v_z) \mathbf{k}_{z_-} \exp(i\theta_0 + i\theta k_{z_-} + i\theta' k'_{z_+}) \right] \quad (55)$$

This equation is identical with Equation (45) if  $H(v_x)$  and  $H(-v_x)$  are interchanged in the latter. Thus, this case can give rise to an echo at the same spot as predicted by Equation (53). The corresponding electric field is obtained by a similar velocity integral to Equation (54) but over different range of  $v_x$ .

The cases (a) and (b) predict the same echo spot because they yield the same imaginary phase  $\phi_i$ . One more task: the various inequality conditions set forth to specify the contour in the contour integrations need to be checked against the echo coordinate found in Equation (54). Let us consider the inequalities  $\theta < 0$  and  $\theta' > 0$  postulated in the case (a). Using Equation (52), the inequality  $\theta < 0$  can be written in the form

$$S_1 - S_2 + \frac{v_z}{v_x} (L_2 - L_1) < 0$$

which is the condition  $\theta' > 0$ . Therefore the conditions  $\theta < 0$  and  $\theta' > 0$  imply each other. Also we can ascertain that the echo  $x$ -coordinate is in accord with the condition  $x < L_2$ . So in cases (a) and (b), the premise and the result are consistent. For the cases of (c) and (d), we state without repeating a similar algebra that the imaginary part of the phase is still obtained by Equation (50) [the real part of the phase is different]. Although the echo spot is predicted by the same equation as Equation (53), these cases of (c) and (d) are not acceptable because the conditions  $\theta > 0$  and  $\theta' > 0$  or  $\theta < 0$  and  $\theta' < 0$  are contradictory to each other. We have the conclusion: an echo occurs where  $x < L_2$  and the echo coordinates are predicted by Equation (53).

(2) Next, we consider the product of two boundary terms,  $I(L_1, k'_z) I(L_2, k_z - k'_z)$  in Equation (29):

$$\mathbf{E}^{(2)}(t, x, z) = C e^{i\omega_3 t} \int \frac{d^2 v f_0}{v_x^2} \int dk_z \exp[ik_z (z - S_2)] \int dk_x \frac{\mathbf{k}}{k^2} \frac{\exp[ik_x]}{(k_x + (k_z v_z + \omega_3)/v_x)^2} \\ \times \int dk'_z e^{ik'_z (S_2 - S_1)} I(L_1, k'_z) I(L_2, k_z - k'_z) \int \frac{dk'_x}{k'^2 (\omega_1 + \mathbf{k}' \cdot \mathbf{v})} \quad (56)$$

where  $C$  is a nonessential constant factor. For definiteness, we assume  $S_2 - S_1 > 0$ .  $\int dk'_x$ -integral and  $\int dk_x$ -integral can be done easily by picking up the relevant poles, and we can write

$$E^{(2)}(t, x, z) = ix Ce^{i\omega_3 t} \int \frac{d^2 v f_0}{v_x^3} \exp\left[-ix \frac{\omega_3}{v_x}\right] \int dk_z \frac{\mathbf{k}}{k^2} \exp\left[ik_z \left(z - S_2 - x \frac{v_x}{v_z}\right)\right] \times \int \frac{dk'_z}{k'^2} e^{ik'_z(S_2 - S_1)} I(L_1, k'_z) I(L_2, k_z - k'_z) \tag{57}$$

where

$$k'^2 = k_z'^2 + \frac{(\omega_1 + k'_z v_z)^2}{v_x} \tag{58}$$

$$k = -x \frac{k_z v_z + \omega_3}{v_x} + zk_z \tag{59}$$

The contour of  $\int dk'_z$ -integral should encircle the upper  $k'_z$ -plane. Since the relevant singularity should be located in the upper  $k'_z$ -plane, the residue is calculated from  $k'_z = k'_{z+}$  for  $v_x < 0$  and  $k'_z = k'_{z-}$  for  $v_x > 0$ .  $k'_{z\pm}$  are defined in Equation (33). Then the last integral ( $\int dk'_z$ ) in Equation (57) can be carried out in the form

$$\int dk'_z(\dots) = \frac{-\pi v_x}{\omega_1} \left[ \exp[ik'_{z+}(S_2 - S_1)] I(L_1, k'_{z+}) I(L_2, k_z - k'_{z+}) H(-v_x) - \exp[ik'_{z-}(S_2 - S_1)] I(L_1, k'_{z-}) I(L_2, k_z - k'_{z-}) H(v_x) \right] \equiv J(k_z) \tag{60}$$

where

$$I(L_1, k'_{z\pm}) = -i\pi \left( \exp[L_1 k'_{z\pm}] H(v_z) + \exp[-L_1 k'_{z\pm}] H(-v_z) \right) \text{ (see Equation (18))} \tag{61}$$

To carry out  $\int dk_z(\dots)$  in Equation (59), let us assume that  $z - S_2 - x \frac{v_x}{v_z} \equiv \vartheta < 0$ .

Now we are ready to evaluate  $\int dk_z$ -integral in Equation (59):

$$\int dk_z(\dots) = \int dk_z \frac{\mathbf{k} e^{ik_z \vartheta}}{k^2} J(k_z) = \frac{iv_x}{2\omega_3} \int dk_z \mathbf{k} J(k_z) \left[ \frac{e^{ik_z \vartheta}}{k_z - k_{z+}} - \frac{e^{ik_z \vartheta}}{k_z - k_{z-}} \right] = \frac{\pi v_x}{\omega_3} \left[ \mathbf{k}(k_{z+}) e^{ik_{z+} \vartheta} J(k_{z+}) H(v_x) - \mathbf{k}(k_{z-}) e^{ik_{z-} \vartheta} J(k_{z-}) H(-v_x) \right] \tag{62}$$

Using Equation (60) in Equation (62) yields

$$\int dk_z(\dots) = \frac{\pi^2 v_x^2}{\omega_1 \omega_3} \left[ \mathbf{k}(k_{z+}) \exp[ik_{z+} \vartheta] \exp[ik'_{z-}(S_2 - S_1)] I(L_1, k'_{z-}) I(L_2, k_{z+} - k'_{z-}) H(v_x) + \mathbf{k}(k_{z-}) \exp[ik_{z-} \vartheta] \exp[ik'_{z+}(S_2 - S_1)] I(L_1, k'_{z+}) I(L_2, k_{z-} - k'_{z+}) H(-v_x) \right] \tag{63}$$

where we have  $Re(k_{z+} - k'_{z-}) = Re(k_{z-} - k'_{z+}) = -\frac{\omega_2}{v^2} v_z$ . Therefore, we obtain

$$I(L_2, k_{z+} - k'_{z-}) = -i\pi \left( \exp[L_2(k_{z+} - k'_{z-})] H(v_z) + \exp[-L_2(k_{z+} - k'_{z-})] H(-v_z) \right) \tag{64}$$

$$I(L_2, k_{z-} - k'_{z+}) = -i\pi \left( \exp[L_2(k_{z-} - k'_{z+})] H(v_z) + \exp[-L_2(k_{z-} - k'_{z+})] H(-v_z) \right) \tag{65}$$

The above two equations and Equation (61) yield

$$I(L_1, k'_{z-}) I(L_2, k_{z+} - k'_{z-}) = -\pi^2 \left[ \exp[L_2 k_{z+} + (L_1 - L_2) k'_{z-}] H(v_z) + \exp[-L_2 k_{z+} - (L_1 - L_2) k'_{z-}] H(-v_z) \right] \tag{66}$$

$$I(L_1, k'_{z+})I(L_2, k_{z-} - k'_{z+}) = -\pi^2 \left[ \exp[L_2 k_{z-} + (L_1 - L_2) k'_{z+}] H(v_z) + \exp[-L_2 k_{z-} - (L_1 - L_2) k'_{z+}] H(-v_z) \right] \quad (67)$$

Now we are ready to carry out the velocity integral in Equation (59) by substituting Equation (63) into it. Because of the step functions  $H(v_x)$  and  $H(v_z)$ , the velocity integral consists of four parts corresponding to  $H(\pm v_x)H(\pm v_z)$ . Since we are interested in the echo spots, we pay attention only to the exponential phases:

$$H(v_x)H(-v_z)e^{\varphi_1}, H(v_x)H(v_z)e^{\varphi_2}, H(-v_x)H(v_z)e^{\varphi_3}, H(-v_x)H(-v_z)e^{\varphi_4} \quad (68)$$

Straightly we can identify:

$$\varphi_1 = -ix \frac{\omega_3}{v_x} + ik_{z+} \mathcal{G} + ik'_{z-} (S_2 - S_1) - L_2 k_{z+} + (L_2 - L_1) k'_{z-} \quad (69)$$

$$\varphi_2 = -ix \frac{\omega_3}{v_x} + ik_{z+} \mathcal{G} + ik'_{z-} (S_2 - S_1) + L_2 k_{z+} + (L_1 - L_2) k'_{z-} \quad (70)$$

$$\varphi_3 = -ix \frac{\omega_3}{v_x} + ik_{z-} \mathcal{G} + ik'_{z+} (S_2 - S_1) + L_2 k_{z-} + (L_1 - L_2) k'_{z+} \quad (71)$$

$$\varphi_4 = -ix \frac{\omega_3}{v_x} + ik_{z-} \mathcal{G} + ik'_{z+} (S_2 - S_1) - L_2 k_{z-} + (L_2 - L_1) k'_{z+} \quad (72)$$

From above, the imaginary phases are obtained as

$$\text{Im } \varphi_1 = \text{Im } \varphi_3 = \frac{v_z}{v^2} \left[ \omega_1 (S_1 - S_2) - \omega_3 (z - S_2) \right] + \frac{v_x}{v^2} \left[ L_2 (\omega_1 + \omega_3) - L_1 \omega_1 - x \omega_3 \right] \quad (73)$$

$\text{Im } \varphi_2 = \text{Im } \varphi_4$  is obtained from  $\text{Im } \varphi_1$  by replacing  $L_1 \rightarrow -L_1$  and  $L_2 \rightarrow -L_2$ . Putting  $\text{Im } \varphi_{1,2} = 0$ , we obtain the echo spots as

$$z_{echo} = \frac{\omega_1 S_1 + \omega_2 S_2}{\omega_3} \quad (74)$$

$$x_{echo} = \frac{\pm L_2 (2\omega_1 + \omega_2) \mp L_1 \omega_1}{\omega_3} \quad (75)$$

In Equation (75),  $x_{echo}$  corresponding to upper signs and  $x_{echo}$  corresponding to lower signs are mutually exclusive because if one of them is inside the plasma the other is necessarily outside the plasma. We add that the condition  $\mathcal{G} < 0$  amounts to  $\frac{\omega_1}{\omega_3} (S_1 - S_2) < x \frac{v_z}{v_x}$ , which poses no problem in as much as we have ample liberty in choosing the sign of  $v_z/v_x$ .

## 5. Discussion

In Section 3, the plasma electric field was determined in terms of the vacuum electric field. Judicious application of the boundary conditions at the interface enables one to determine the plasma electric field entirely in terms of the external charges without introducing the vacuum electric field  $E_0$ . Inverting Equation (13), we can write

$$D_x(0, \omega) = -\frac{N}{2} - i \frac{4\pi}{k_0^2} \rho_1 \delta(\omega + \omega_1) e^{-ik_z S_1} I(k_z, L_1) \quad (76)$$

$$E_z(0, \omega) = iN \int \frac{k_z}{k^2 \varepsilon} \frac{dk_x}{2\pi} - i \frac{4\pi}{k_0^2} \rho_1 \delta(\omega + \omega_1) e^{-ik_z S_1} I_\varepsilon(k_z, L_1) \quad (77)$$

$$\text{where } I_\varepsilon(k_z, L_1) = \int \frac{k_x dk_x}{k^2 \varepsilon} e^{-ik_x L_1} \quad (78)$$

Next, we turn to the vacuum solution.

$$E_x(x, k_z) = -B' k_z e^{k_z x} \equiv E_0 e^{k_z x} \quad (79)$$

where  $E_0$  is the vacuum electric field, the quantity designated by the same symbol  $E_0$  in Equation (19).

$$E_z(x, k_z) = -iB'k_z e^{k_z x} \quad (80)$$

Continuity of  $E_z$  across the interface  $x=0$  gives that Equation (22) equals to  $-iB'k_z$ . Also continuity of  $D_x$  across  $x=0$  yields that Equation (20) equals to  $-B'k_z$ . Eliminating  $B'$  between these two equations gives N in the form

$$N = \frac{\frac{8\pi}{k_0^2} \rho_1 \delta(\omega + \omega_1) e^{-ik_z S_1} (I_\varepsilon(k_z, L_1) - iI(k_z, L_1)) + 1}{1 + \int \frac{dk_x}{\pi} \frac{k_z}{k^2 \varepsilon}} \rightarrow 2 \quad (81)$$

Substituting the above equation into Equation (13) yields

$$\mathbf{E}(\mathbf{k}, \omega) = \frac{8\pi^2}{k_0^2} \frac{i\mathbf{k}}{k^2 \varepsilon} \rho_1 \delta(\omega + \omega_1) e^{-ik_z S_1} \frac{-iI(k_z, L_1)/\pi - e^{-ik_x L_1}}{1 + \int \frac{dk_x}{\pi} \frac{k_z}{k^2 \varepsilon}} \quad (82)$$

Equation (82) should be compared with Equation (20). Eliminating the vacuum field introduces the denominator  $1 + \int \frac{dk_x}{\pi} \frac{k_z}{k^2 \varepsilon}$  in Equation (82). In fact, the relation

$$1 + \int \frac{dk_x}{\pi} \frac{k_z}{k^2 \varepsilon} = 0 \quad (83)$$

is the electrostatic dispersion relation of the surface wave in a semi-bounded plasma [10].

In the investigation of echo occurrence,  $E_0$  in Equation (20) can be discarded because echoes are given rise to by interference of influences of the external charges. This amounts to saying that the denominator  $\left(1 + \int \frac{dk_x}{\pi} \frac{k_z}{k^2 \varepsilon}\right)$  doesn't play any role in the determination of echo locations.

Equations (53) and (74) and (75) are the main results of this work in locating the echo spots associated with the surface wave in a semi-bounded plasma launched by the oscillating external charges at  $(x, z) = (L_1, S_1)$  and  $(L_2, S_2)$ . In the static situation, the  $z$ -coordinate is irrelevant. The echo spot given by Equation (53) corresponds to  $x_{echo}$  in Equation (45) in Lee and Lee [5]. The echo spot given by Equations (74) and (75) is surface wave-proper. Our search for the echo spots are not exhaustive; we put aside many other product terms in (AB) in Equations (24) and (25). It appears that we have diversity of echoes in a bounded plasma, which was also experimentally reported [7]. The diversity seems to be due to reflections of the wave at the interface.

In reality, bounded plasmas are usual rather than exceptional. Important literatures to get acquainted with this field are References [8] and [9], among others. Surface wave dispersion relation in a plasma slab is derived in Ref. [10]. An exact nonlinear solution of a surface wave excited by external charges is obtained in Ref. [11].

## Acknowledgements

Hee J. Lee thanks Professor L. Stenflo for correspondence. The work of MJL is supported by the National R&D Program through the National Research Foundation of Korea (NRF) funded by the Ministry of Science, ICT & Future Planning (Grant No. 2015M1A7A1A01002786). This support is greatly appreciated.

## References

- [1] Gould, R.W., O'Neil, T.M. and Malmberg, J.H. (1967) *Physical Review Letters*, **19**, 219-222. <http://dx.doi.org/10.1103/physrevlett.19.219>
- [2] Krall, N.A. and Trivelpiece, A.W. (1974) *Principles of Plasma Physics*. McGraw-Hill, New York, p. 547. <http://dx.doi.org/10.1109/tps.1974.4316834>
- [3] Malmberg, J.H., Wharton, C.B., Gould, R.W. and O'Neil, T.M. (1968) *Physical Review Letters*, **20**, 95-98. <http://dx.doi.org/10.1103/physrevlett.20.95>
- [4] Sitenko, A.G., Pavlenko, V.N. and Zasenkov, V.I. (1975) *Physics Letters A*, **53**, 259-260.

- [http://dx.doi.org/10.1016/0375-9601\(75\)90431-4](http://dx.doi.org/10.1016/0375-9601(75)90431-4)
- [5] Lee, H.J. and Lee, M.-J. (2015) *The Open Plasma Physics Journal*, **8**, 1-7.  
<http://dx.doi.org/10.2174/1876534301508010001>
- [6] Landau, L. (1946) *Journal of Physics*, **10**, 25-34.
- [7] Shivarova, A. and Zhelyazkov, I. (1982) Surface Waves in Gas-Discharge Plasmas. In: Boardman, A.D., Ed., *Electromagnetic Surface Modes*, Wiley, New York, p. 516.
- [8] Vukovic, S. (1986) *Surface Waves in Plasmas and Solids*. World Scientific, Hong Kong.
- [9] Gradov, O.M. and Stenflo, L. (1983) *Physics Reports*, **94**, 111-137.  
[http://dx.doi.org/10.1016/0370-1573\(83\)90004-2](http://dx.doi.org/10.1016/0370-1573(83)90004-2)
- [10] Lee, H.J. and Lim, Y.K. (2007) *Journal of the Korean Physical Society*, **50**, 1056-1061.  
<http://dx.doi.org/10.3938/jkps.50.1056>
- [11] Stenflo, L. and Yu, M.Y. (2002) *Physics of Plasmas*, **9**, 5129-5130. <http://dx.doi.org/10.1063/1.1521715>



Scientific Research Publishing

---

**Submit or recommend next manuscript to SCIRP and we will provide best service for you:**

Accepting pre-submission inquiries through Email, Facebook, LinkedIn, Twitter, etc.

A wide selection of journals (inclusive of 9 subjects, more than 200 journals)

Providing 24-hour high-quality service

User-friendly online submission system

Fair and swift peer-review system

Efficient typesetting and proofreading procedure

Display of the result of downloads and visits, as well as the number of cited articles

Maximum dissemination of your research work

Submit your manuscript at: <http://papersubmission.scirp.org/>

# The Influence of Pico-Second Pulse Electron Irradiation on the Electrical-Physical Properties of Silicon Crystals

Hrant N. Yeritsyan<sup>1\*</sup>, Aram A. Sahakyan<sup>1</sup>, Norair E. Grigoryan<sup>1</sup>, Eleonora A. Hakhverdyan<sup>1</sup>, Vachagan V. Harutyunyan<sup>1</sup>, Vahan A. Sahakyan<sup>2</sup>, Armenuhi A. Khachatryan<sup>2</sup>, Bagrat A. Grigoryan<sup>3</sup>, Vardan Sh. Avagyan<sup>3</sup>, Gayane A. Amatuni<sup>3</sup>, Ashot S. Vardanyan<sup>3</sup>

<sup>1</sup>A.I. Alikhanyan National Science Laboratory (Yerevan Physics Institute), Yerevan, Armenia

<sup>2</sup>National Institute of metrology, Yerevan, Armenia

<sup>3</sup>CANDLE Synchrotron Research Institute, Yerevan, Armenia

Email: \*grant@yerphi.am

Received 20 June 2016; accepted 5 August 2016; published 8 August 2016

Copyright © 2016 by authors and Scientific Research Publishing Inc.

This work is licensed under the Creative Commons Attribution International License (CC BY).

<http://creativecommons.org/licenses/by/4.0/>



Open Access

---

## Abstract

The studies of the influence of pico-second ( $4 \times 10^{-13}$  sec.) pulse electron irradiation with energy of 3.5 MeV on the electrical-physical properties of silicon crystals (n-Si) are presented. It is shown that in spite of relatively low electron irradiation energy, induced radiation defects are of cluster type. The behavior of main carrier mobility depending on temperature and irradiation dose is analyzed and charge carriers' scattering mechanisms are clarified: on ionized impurities, on point radiation defects with transition into cluster formation. Dose dependencies of electrical conductivity and carrier mobility for samples of various specific resistivities are given.

## Keywords

Silicon Crystal, Electron Irradiation, Pico-Second Pulse Beam, Conductivity, Carriers' Mobility

---

## 1. Introduction

There are numerous publications devoted to the influence of irradiations, in particular high energy electron irradiation, on the properties of silicon crystal. One can present an extensive bibliography, however it is better to refer to reviews and monographs presenting more informative data about findings on this subject [1]-[5]. The irradiation sources used in these works are conventional sources based on micro-second pulse beams (accelerators,

---

\*Corresponding author.

nuclear reactors and so on) allowing to accumulate a large amount of irradiation doses in a short time and, consequently, quickly affect properties of irradiated materials. Not into details of discussing the type and energy of irradiation, it is important to note, though, that at the same irradiation dose, the irradiation intensity (amount of particles per 1 sec. on 1 cm<sup>2</sup> cross-section of beam) was proved to play an important role in affecting the properties of semiconductors [6]-[8].

The case, when the irradiation source has a beam with a pulse shorter than “microsecond”, is important, because it is scientific and practice interest (pulse nuclear reactors, space particle interactions, atmospheric processes, etc.). For the first time very short pulses with pico-second duration ( $4 \times 10^{-13}$  sec.) and electron beam with 3.5 MeV energy was applied which also has scientific meaning for the study of very fast processes in-situ, e.g. interaction of irradiation with material, different chemical and biological reactions. For understanding the pico-second pulse beam influence on the materials, it is better to describe known steps and time intervals of radiation interactions which take place at common “microsecond” irradiation with materials.

## 2. Problem Formulation and Time Characteristics of Radiation Interaction with Matter

The processes which take place in materials under irradiation can be roughly presented as a raw of consequent stages. The precise duration of each stage depends on initial energy and mass of high energy particle or gamma-quanta, potential of interaction between particles, and can vary an order of magnitude, hence, it is important to estimate the time intervals separating these steps.

The first stage of radiation influence is ionization and excitation of atomic orbital electrons or elastic transfer of irradiation energy to the atoms; the collision time with atoms is estimated to be  $10^{-16}$  -  $10^{-15}$  second [2]. Atoms and electrons with excessive energy and impulse come into interaction with other atoms and electrons of matter, losing energy through this action. This stage is called “energy exchange” from primary exciting particle and transition of the system to quasi-equilibrium state. The energy exchange corresponds to the value of coupling energy of atoms in matter, *i.e.* a few eV, and takes place very quickly. At the inter-atomic distances this time is about  $10^{-14}$  -  $10^{-13}$  second.

The next process, relaxation of excessive energy received by atoms and electrons in crystal, takes place at time which is typical for the period of atomic oscillations, *i.e.*,  $10^{-13}$  -  $10^{-12}$  second in solid states. In fact, at this stage relaxation leads the system to the initial state with minimum free energy and to formation of different meta-stable primary radiation defects; the role of thermal movement of atoms in solids becomes significant.

Further consideration relates to processes at average-statistic kinetic energy in order of  $kT$  ( $k$ -Boltzman’s constant,  $T$ -absolute temperature). The system which is excited by irradiation passes through different quasi-equilibrium states and reconstruction of primary radiation defects occur. The speed of the latter exponentially depends on temperature and can extend over time. Secondary radiation defects are formed which are stable at room temperatures. In their formation both primary radiation defects (vacancies and interstitial atoms) and chemical impurities which were present in samples before irradiation, participate. Diffusion processes and distribution of the components of primary defects over distances play essential role at this stage; this relaxation time duration is estimated by seconds and hours. The formed secondary radiation defects can be “annealed” at high temperatures, but it is not within the scope of present work. Note, that at given pico-second pulse beam irradiation “radiation annealing” which is typical to conventional microsecond pulse beam irradiation, doesn’t take place, because the thermal processes (duration  $10^{-6}$  -  $10^{-7}$  second) don’t have enough time to develop.

## 3. Experimental Procedure and Results

Irradiation of samples was carried out at room temperatures in linear accelerator of CANDLE Synchrotron Radiation Institute (Armenia) by electrons with 3.5 MeV energy,  $4 \times 10^{-13}$  second pulse duration, 12 Hz frequency, charge in impulse was 30 pico-Coulomb. The samples of n-Si were cut out in double-cross shape having 6 Ohmic contacts for electrical measurements, at 0.8 - 1.0 mm thickness, and  $3 \times 10$  mm<sup>2</sup> size.

Irradiation dose was defined:

$$D = 6.25 \times 10^{12} \times \frac{It}{S} \frac{eI}{\text{cm}^2}, \quad (1)$$

where  $I$  is the mean current in  $\mu\text{A}$ ,  $t$  is exposition time in seconds and  $S$  is the cross-section of the beam in cm<sup>2</sup>.

The beam current was measured by accumulated charge in Faraday cup. Electrical conductivity and charge carriers' mobility were measured applying known Hall effect method at different temperatures. Electrical conductivity was calculated by  $\sigma = \mu n e$ , where  $\mu$ —charge carriers' (Hall) mobility,  $n$ —concentration of main charge carriers',  $e$ —charge of electron. The charge carriers' mobility was defined by Hall effect measurements:

$$\mu = \frac{U_H \cdot l}{U_\rho \cdot b \cdot B}, \quad (2)$$

where  $U_H$  is the potential difference between Hall contacts,  $U_\rho$  is the potential difference between conductivity contacts,  $B$ —magnetic field induction,  $l$ —sample's length,  $b$ —sample's width.

The measurement results are presented in **Figures 1-7** as a graphics of dose and temperature dependencies of electrical conductivity and charge carriers' mobility for samples of different specific resistivity. An obvious "critical dose" is seen on **Figure 1**, after which the electrical conductivity of samples smoothly decreases and then sharply falls down. This effect depends on their initial specific resistivity, *i.e.* when the specific resistivity is high the "critical dose" is reached rapidly, so the dependence is inverse to specific resistivity. The charge carrier mobility has similar dependence (**Figure 2**). Note that for samples with specific resistivity 100  $\Omega\cdot\text{cm}$  and 700  $\Omega\cdot\text{cm}$  this dependence is almost the same; even in numerical values this dependence is only slightly different, in spite of significant difference in initial carrier concentrations. For samples with specific resistivity 950  $\Omega\cdot\text{cm}$  and 700  $\Omega\cdot\text{cm}$  the difference in carrier concentration is not so high but there is a significant difference in dose dependences. From comparison of **Figure 1** and **Figure 2** it is obvious that point radiation defects accumulation kinetics has a marked influence on the mechanism of charge carriers scattering. Note that these measurements were carried out at room temperatures.

Temperature dependencies of electrical conductivity and carrier mobility were studied to clarify the physical nature of their variations after irradiation (**Figures 3-7**). The carrier mobility measurement results at the 120 - 300 K temperatures for samples with specific resistivity 100  $\Omega\cdot\text{cm}$  are presented in **Figure 3**. It is obvious that the behavior of carriers' mobility temperature dependence before and after irradiation is almost the same up to maximum applied irradiation dose of  $6 \times 10^{13}$   $\text{el}/\text{cm}^2$ .

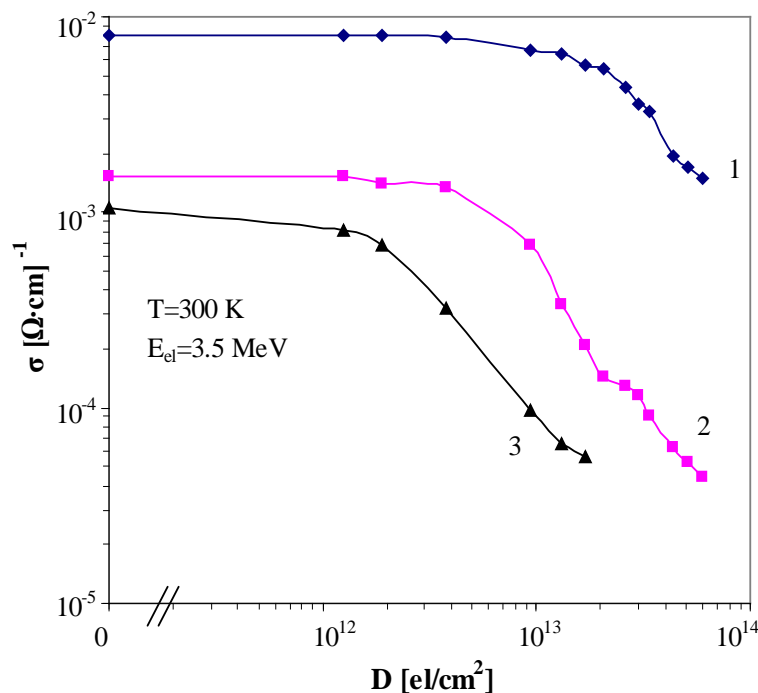


**Figure 1.** Silicon crystal (n-Si) electrical conductivity dose dependence by electron pico-second beam irradiation (energy 3.5 MeV). Samples specific resistivity: 1—100  $\Omega\cdot\text{cm}$ , 2—700  $\Omega\cdot\text{cm}$ , 3—950  $\Omega\cdot\text{cm}$ . Maximum irradiation dose was  $6 \times 10^{13}$   $\text{el}/\text{cm}^2$ .

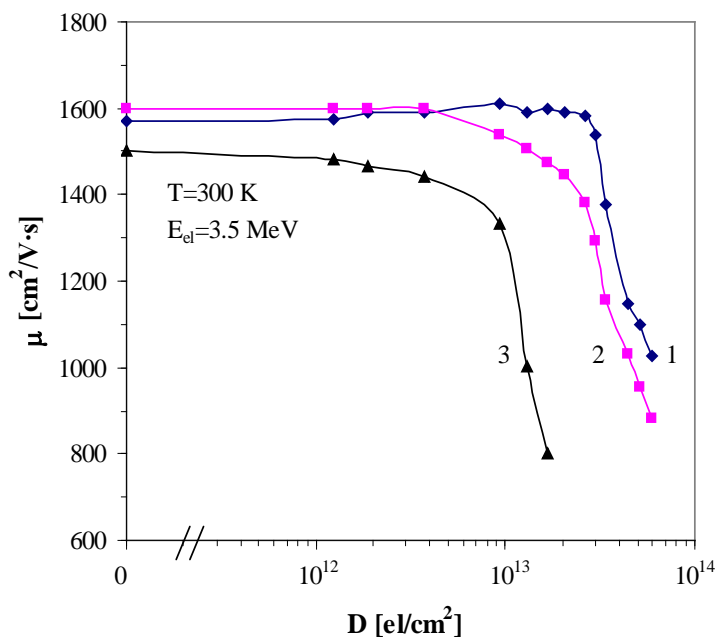


**Figure 2.** Silicon crystal (n-Si) charge carrier's mobility dose dependence by electron pico-second beam irradiation (energy 3.5 MeV). Samples specific resistivity: 1—100 Ω·cm, 2—700 Ω·cm, 3—950 Ω·cm. Maximum irradiation dose was  $6 \times 10^{13}$  el/cm<sup>2</sup>.

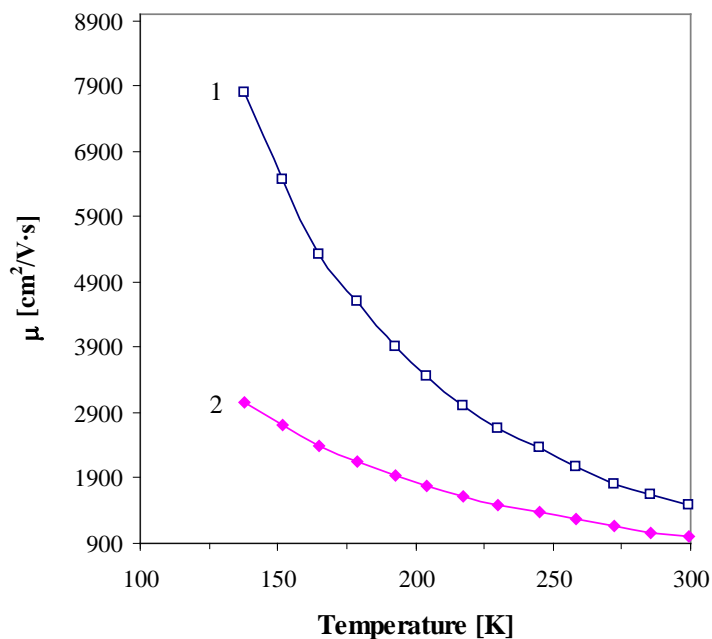


**Figure 3.** Silicon crystal (n-Si) charge carriers' mobility temperature dependence after electron pico-second beam irradiation (energy 3.5 MeV). Sample specific resistivity 100 Ω·cm: 1—before irradiation, 2—after irradiation by dose  $6 \times 10^{13}$  el/cm<sup>2</sup>.

However, detailed study of carriers' mobility temperature dependence in log-log scale points to a difference between these dependences (**Figure 4**). Almost a straight line over entire temperature interval (line 1) before irradiation indicates the existence of uniform mechanism for carriers' scattering-scattering on the ionized impurity

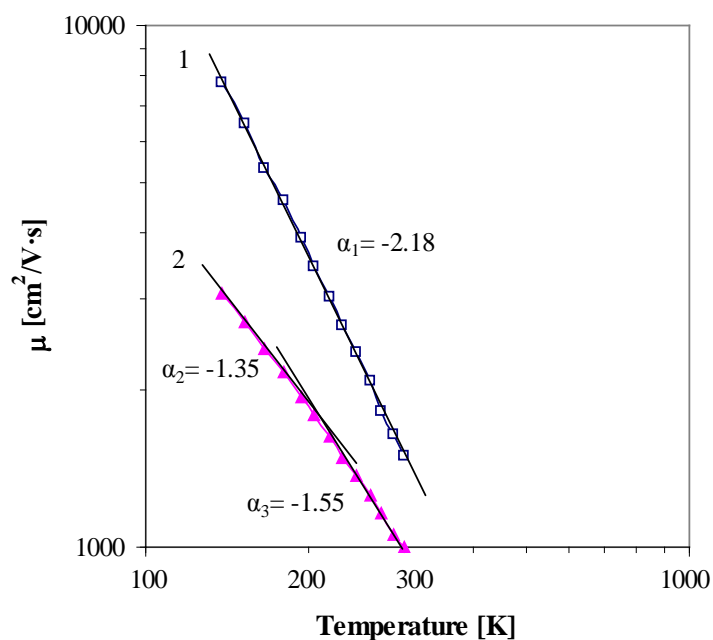


**Figure 4.** Silicon crystal (n-Si) charge carriers' mobility temperature dependence after electron pico-second beam irradiation (energy 3.5 MeV). Sample specific resistivity  $100 \Omega \cdot \text{cm}$ : 1—before irradiation, 2—after irradiation by dose  $6 \times 10^{13} \text{ e/cm}^2$ . The graphs are in log-log scale for better demonstration. The mathematical expression  $\mu \sim T^\alpha$  gives possibility to explain charge carriers scattering mechanism for  $\alpha_1 = -2.18$  before irradiation and  $\alpha_2 = -1.55$ ;  $\alpha_3 = -1.35$  after irradiation. Such behavior of carriers' mobility (line 2) is explained by carriers' scattering on the lattice defects.

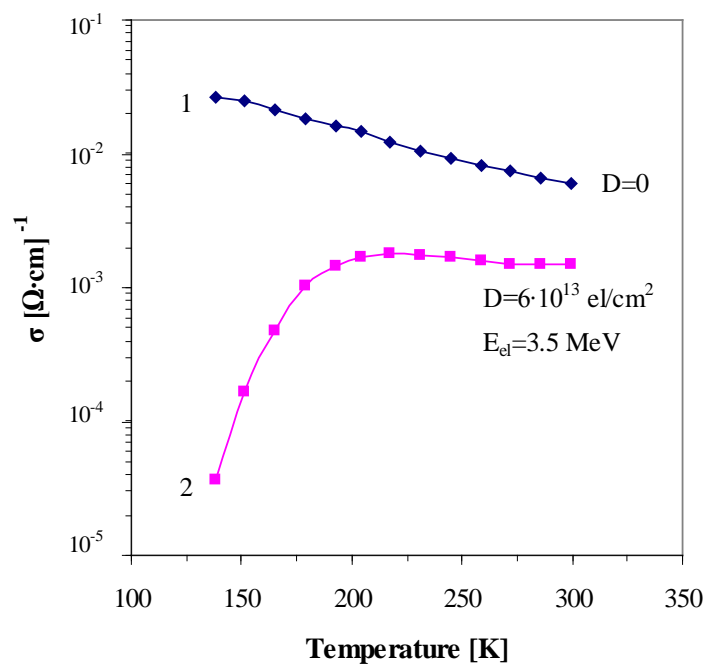


**Figure 5.** Silicon crystal (n-Si) electrical conductivity temperature dependence after electron pico-second beam irradiation (energy 3.5 MeV). Sample specific resistivity is  $100 \Omega \cdot \text{cm}$ : 1—before irradiation, 2—after irradiation by  $6 \times 10^{13} \text{ e/cm}^2$  dose.

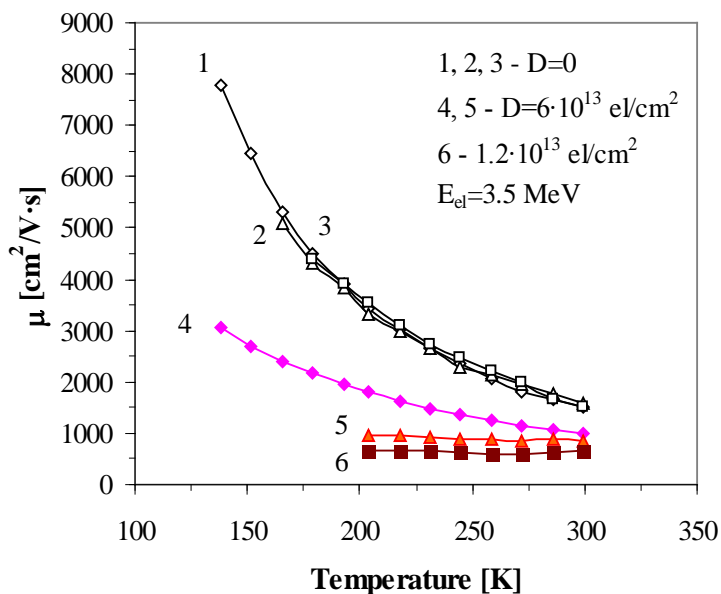


**Figure 6.** Silicon crystal (n-Si) charge carriers' mobility temperature dependence after electron pico-second beam irradiation (energy 3.5 MeV). Samples specific resistivity: 100 Ω·cm, 1—before irradiation, 4—after irradiation by dose  $6 \times 10^{13}$  el/cm<sup>2</sup>; 700 Ω·cm, 2—before irradiation, 5—after irradiation by dose  $6 \times 10^{13}$  el/cm<sup>2</sup>; 950 Ω·cm, 3—before irradiation, 6—after irradiation by dose  $1.2 \times 10^{13}$  el/cm<sup>2</sup>.

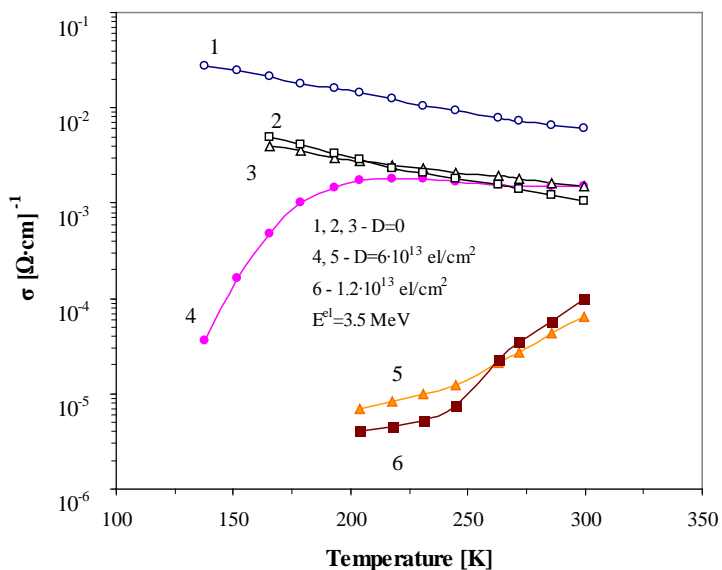


**Figure 7.** Silicon crystal (n-Si) electrical conductivity temperature dependence after electron pico-second beam irradiation (energy 3.5 MeV). Samples specific resistivity: 100 Ω·cm, 1—before irradiation, 4—after irradiation by  $6 \times 10^{13}$  el/cm<sup>2</sup> dose; 700 Ω·cm, 2—before irradiation, 5—after irradiation by dose  $6 \times 10^{13}$  el/cm<sup>2</sup>; 950 Ω·cm, 3—before irradiation, 6—after irradiation by  $1.2 \times 10^{13}$  el/cm<sup>2</sup> dose.

of phosphorus in n-Si. After irradiation there are two mechanisms for carrier scattering (line 2). The mathematical expression for the mentioned cases is as follows:  $\mu \sim T^{\alpha}$ ,  $\alpha_1 = -2.18$  before irradiation and  $\alpha_2 = -1.55$ ;  $\alpha_3 = -1.35$  after irradiation. Such behavior of carriers' mobility (line 2) is explained by carriers' scattering on the lattice

defects [5]; in the given case, scattering on the radiation defects created by pico-second pulse irradiation with 3.5 MeV energy. Evidence for this statement is temperature dependencies of electrical conductivity and carrier mobility for different samples with specific resistivity of 100  $\Omega\cdot\text{cm}$ , 700  $\Omega\cdot\text{cm}$ , 950  $\Omega\cdot\text{cm}$  (Figure 5 and Figure 6). Samples with specific resistivity of 700  $\Omega\cdot\text{cm}$  and 950  $\Omega\cdot\text{cm}$  (curves 5 and 6; Figure 6) have an interesting behavior: the constancy of mobility with temperature variation and different temperature dependence of electrical conductivity (Figure 7). This point requires additional comprehensive study.

It is worth mentioning that the behavior of samples with low specific resistivity (*i.e.* having high impurity concentration) is significantly different from others at low temperatures, where the region of scattering on ionized impurities seen; whereas in samples with high specific resistivity, this region is not observed, although the measurements are difficult at these temperatures because the conductivity is near intrinsic (Figure 7). The primary defect capture by different centers, that were present in samples before irradiation play an important role during these processes [8]. However, at sufficiently high doses (“critical dose”) these channels may be exhausted, *i.e.* the centers saturated, but, on the other hand, concurrent radiation defects are accumulated, acting as channels for new reactions, leading to the changes of secondary radiation defects spectrum with irradiation dose, other conditions being equal. Along with this, the charge state of formed radiation defects changes, consequently the electrical-physical properties of the crystal also change.

## 4. Conclusions

From the above given results, the following conclusions can be drawn:

- 1) In spite of low intensity, pico-second electron irradiation has a significant effect on the electrical-physical properties of silicon crystal.
- 2) The analysis of measurements shows that stable at room temperatures radiation defect formation in silicon crystal takes place in stages; at first phase defects are formed as vacancy and interstitial atoms which subsequently gather into clusters, although cluster formation is difficult in Si crystal at 3.5 MeV electron energy.
- 3) Study of temperature dependence of charge carrier mobility helped to reveal their scattering mechanism: scattering on the ionized impurities and on the radiation defects. At the same time it became possible to observe formation of point defects, followed by their cluster formation.
- 4) The influence of pico-second electron beam irradiation on the silicon crystal with different specific resistivity was studied. It was shown that the “critical dose” corresponding to sharp changes of electrical-physical properties depends on specific resistivity. In these cases it is found to be more appropriate to use an expression “dose threshold” of cluster formation instead of the more commonly used “energy threshold”.

## Acknowledgements

This work was supported by the State Committee of Science MES Republic of Armenia in frame of the research project grant NO. 14AR-1c02.

## References

- [1] Vavilov, V.S. (1963) Radiation Influence on the Semiconductors. Phys.-Mat. Edition, Moscow, 264 p. (In Russian)
- [2] Vinetskij, V.L. and Kholodar, G.A. (1979) Radiation Physics of Semiconductors. “Naukova Dumka” Edition, Kiev, 333 p. (In Russian)
- [3] Leroy, C. and Rancoita, P.G. (2007) *Reports on Progress in Physics*, **70**, 493-625. <http://dx.doi.org/10.1088/0034-4885/70/4/R01>
- [4] Duzellier, S. (2005) *Aerospace Science and Technology*, **9**, 93-99. <http://dx.doi.org/10.1016/j.ast.2004.08.006>
- [5] Coleman, P.G., Edwardson, C.J., Knights, A.P. and Gwilliam, R.M. (2012) *New Journal of Physics*, **14**, Article ID: 025007. <http://dx.doi.org/10.1088/1367-2630/14/2/025007>
- [6] Emtsev, V.V., Ivanov, A.M., *et al.* (2012) *Physics and Technics of Semiconductors*, **46**, 473-481.
- [7] Yeritsyan, H.N., Sahakyan, A.A., Harutyunyan, V.V., *et al.* (2011) *Journal of Spacecraft and Rockets*, **48**, 34-37. <http://dx.doi.org/10.2514/1.49303>
- [8] Emtsev, V.V., Ehrhart, P., Poloskin, D.S. and Emtsev, K.V. (2007) *Journal of Material Science: Materials in Electronics*, **18**, 711-714. <http://dx.doi.org/10.1007/s10854-006-9103-6>

# Max Planck Half Quanta as a Natural Explanation for Ordinary and Dark Energy of the Cosmos

**Mohamed S. El Naschie**

Department of Physics, Faculty of Science, University of Alexandria, Alexandria, Egypt

Email: Chaossf@aol.com

Received 25 July 2016; accepted 5 August 2016; published 8 August 2016

Copyright © 2016 by author and Scientific Research Publishing Inc.

This work is licensed under the Creative Commons Attribution International License (CC BY).

<http://creativecommons.org/licenses/by/4.0/>



Open Access

---

## Abstract

The work gives a natural explanation for the ordinary and dark energy density of the cosmos based on conventional quantum mechanical considerations which dates back as far as the early days of the quantum theory and specifically the work of Max Planck who seems to be the first to propose the possibility of a half quanta corresponding to the ground state, *i.e.* the energy zero point of the vacuum. Combining these old insights with the relatively new results of Hardy's quantum entanglement and Witten's topological quantum field theory as well as the fractal version of M-theory, we find a remarkably simple general theory for dark energy and the Casimir effect.

## Keywords

Half Quanta, Dark Energy, Hardy's Entanglement, Casimir Energy, Topological Quantum Field, Witten's Theory, Pointless Geometry, Non-Commutative Geometry, Fractal Spacetime, Dark Matter, tHooft Renormalization, E-Infinity Theory, Cantor Sets

---

## 1. Introduction

The true nature and origin of dividing energy into two main categories namely ordinary energy which we are able to measure and dark energy which should be there but could not be found or measured in any direct way is one, if not the most puzzling questions of modern science [1]-[6]. In a large number of papers, this question was answered and we think satisfactorily solved by the Author and his associates using mainly advanced mathematics and novel theories about spacetime [7]-[14]. However, and in all fairness to the readers as well as to ourselves, it seems that in the heat of the battle of resolving the mystery of dark energy which came upon all of us

as a sudden shock, we seem to have overlooked more conventional elements which may have helped us and others in understanding the main problems within a more conventional framework.

The present work sprang out of such a realization and our final result and explanation of Casimir energy [15]-[17], ordinary energy and dark energy [18]-[20] is basically a synthesis of an old well known proposal by Max Planck [21] [22], conventional quantum mechanics [23], Witten's topological quantum field theory and M-theories [24]-[27] and last but not least, Hardy's marvellous result of his gedanken experiment on quantum entanglement [28] [29]. How this is actually done will be shown in what follows. We should also add that we divided the references in the present paper into two parts where Refs. [1]-[76] are the main readings while Refs. [77]-[119] are additional readings which we think deepen and enhance understanding of the subject.

## 2. Max Planck Half Quanta

We know very well, at least since J. von Neumann's pointless continuous geometry [30] [31] and A. Connes' noncommutative geometry [32] [33] that the definition of a point in classical geometry is totally inadequate on both the philosophical and the pure mathematical level [34] [35]. Thus apart of the Heisenberg uncertainty principle, the statement that energy could be zero within a theory based entirely on probability like quantum mechanics cannot be right [23]. Luckily we all know the quantization recipe in quantum mechanics whether found algebraically or using any other method leads to the following famous energy levels equation [23]

$$E_n = (n + 1/2) \hbar w \quad (1)$$

where  $\hbar$  is the Planck reduced constant and  $w$  is the frequency. In the above formula  $n$  can take only integer values, namely 1, 2, 3, ... because there can be no half  $\hbar w$  in quantum mechanics since a photon is an elementary particle, in fact the most fundamental elementary messenger particle of them all and  $\hbar w$  has the same physical meaning as a photon [23]. The more surprising it must be for the uninitiated to see that even when we have no photon at all, meaning when  $n = 0$ , then  $E_n \equiv E_o \neq 0$ , *i.e.* is not zero but a most recognized value given by [23]

$$E_o = (1/2) \hbar w \quad (2)$$

The innocent conclusion of the above half quanta is that our postulate gained mainly from experiments that quanta are indivisible cannot be as straight forward as one could naively have thought and who knows, it may open the door to unsuspected connections related to fractional-Hall effects and similar things [119]. Historically speaking this (1/2) which ought to be quite famous because it gives a clear justification for the Casimir effect, goes back to the pioneering efforts of Max Planck to make sense out of his own discovery of the quantization of energy [21]-[23]. In the present work we hope that the reader will also see in the same way that this half is the first step on the road to understand ordinary energy and dark energy [15]-[20].

## 3. Hardy's Amazing Quantum Entanglement Result

As far as the present Author is concerned there are few modern results in quantum physics that can rival Hardy's magnificent gedanken experiment regarding the maximal quantum entanglement probability for two quantum particles [28] [29]. The exact answer is found by Hardy using Dirac's formalism to be [29].

$$P(\text{Hardy}) = \phi^5 \quad (3)$$

where  $\phi = (\sqrt{5} - 1)/2$  in full agreement with experiments [4]-[6]. The implications and ramifications of this exact result for physics and quantum cosmology are tremendous and are amply documented by the hundreds of papers published in the last ten years on this subject by many authors all over the world [2]-[6]. In the next section we will see how  $P(\text{Hardy}) = \phi^5$  could be interpreted as a dimensionless, topological Planck constant and how it relates to the zero point energy.

## 4. The Topological Quantum Field Theory and the Fractal Version of Witten's M-Theory

Quantum field theory is primarily concerned with investigating the topological invariants of a theory and is the result of pioneering efforts of Schwartz, Attya, Donaldson and Witten [24]-[26] [36]. It is not possible to

overestimate the importance of the work done on this subject. It is equally impossible that the work of the present Author could have seen the light without the work of L. Hardy and Witten’s work, particularly his M-theory as well as his five D-branes in eleven dimensional spacetime model [37]. In fact looking at our own work in the last ten years it appears as if it was a realization of Koester’s sleep-waking hypothesis [38] where our mind was working almost subconsciously at night and consciously during the day on finding hidden connections and links between Witten’s theory, hardy’s result and our own efforts to formulate an exact non-classical spacetime theory guided by Ord-Nottale’s fractal spacetime theory [9]-[13]. At the end it becomes evident that  $P = \phi^5$  may be seen as a topological Planck energy while the inverse  $1/P = 11 + \phi^5$  is a topological cosmic distance also playing the role of the dimensionality of the fractal counterpart of Witten’s M-theory as developed by the present Author [27]. We discuss all of that in the next section.

### 5. The Unifying Power of a Bird’s Eye Topological View

We all have a pretty reasonable understanding and intuitive feel for what a topological dimension means. However what exactly is a Hausdorff dimension [39]? In nonlinear dynamics the word fractal dimension is used to mean more or less the same as the Hausdorff dimension [39]. Consequently we may see the Hausdorff-fractal dimension not as a normal dimension but as a measure for the irregularity of a fractal shape, its ruggedness or smoothness. This understanding of the Hausdorff dimension brings into it the meaning of entropy which measures the degree of disorder in a system [5] [54]. Proceeding in the same direction it is reasonable to associate the Hausdorff dimension via entropy with energy which is not a stretch [40]. Remembering that our random triadic Cantor set used to model space and time had a Hausdorff dimension equal  $\phi$  as per a theorem due to American mathematicians Mauldin and Williams [7] [41] and remembering also that the result  $P(\text{Hardy}) = \phi^5$  was found using this “Cantorian” theory, then due to what we said earlier on  $P = \phi^5$  could be seen not only as a probability but also as energy, albeit a “topological” energy [7] [14] [42]. Our reasoning is based on the following: First quantum entanglement may be loosely likened to a force acting instantly at a distance and second the probability of finding a point in a Cantor set was fixed not combinatorically because we have infinitely many points, nor geometrically because we have a zero measure [43] but topologically because the Hausdorff dimension is a finite positive value equal  $\phi$  so that we may write:

$$P_{(x)} = (\phi)/(1) = \phi \tag{4}$$

where the length of the unit interval within which the random Cantor set lives is unity. That way we see that  $P = \phi^5$  may indeed be seen as a maximal topological energy unit similar to  $\hbar w$  being our minimal Planck energy unit. By contrast smaller topological probabilities are possible so that for infinitely many entangled points we have [28]

$$P = \phi^\infty \rightarrow \text{zero} \tag{5}$$

which is what we find in our classical world where we are dealing with almost infinitely many particles and that is why in classical mechanics we do not have measurable entanglement of any kind. From the preceding discussion we see clearly that we could replace  $\hbar w$  by  $\phi^5$  and we assure the reader that this is a sound and bold move which will pay off dividend as we will see in the next section.

### 6. From Planck’s Half Quantum to Dark Energy via Ordinary and Casimir Energy

Let us now synthesize and fuse together the preceding result and discussion into a single coherent unity. We start with stating the final result. This is first that the vacuum zero point energy is found from replacing  $\hbar w$  by  $\phi^5$  and is consequently equal to the ordinary energy density of the cosmos [44]-[57]

$$E_o = \hbar w/2 \rightarrow \gamma(O) = \phi^5/2 \tag{6}$$

Second this energy is clearly the cause behind the Casimir effect which is observed via a change of the boundary condition created by the two uncharged but conducting Casimir plates brought at nano distance of each other [15]-[17] [22]. Third, since the boundary condition is the crucial element in the Casimir effect experiment, it follows that at the hyperbolic horizon of our universe we have a one sided boundary condition akin to a one sided Möbius strip but in higher dimensions [65] converting the “local” Casimir effect “energy” into a global dark energy “effect” pushing the boundary of the holographic boundary of the universe and causing the ob-

served accelerated expansion of the cosmos [58]-[62]. Seen that way we may rewrite  $E_o$  in terms of Einstein's maximal energy density but using  $\gamma(O) = \phi^5/2$  instead of  $\gamma(\text{Einstein}) = 1$ . Proceeding this way one finds [1]-[3] [66].

$$E_o = \hbar\omega/2 \rightarrow E_o = mc^2 (\phi^5/2) \quad (7)$$

This clearly means that  $E_o$  is in this case equivalent to the ordinary energy density of the cosmos  $E(O)$ :

$$E_o = mc^2 (\phi^5/2) = E(O) \quad (8)$$

Consequently it follows that the dark energy density is simply [1]-[3] [66]

$$E(D) = 1 - E_o = 1 - E(O) = mc^2 (5\phi^2/2) \quad (9)$$

Comparing these results with the actual cosmic measurements of WMAP, Planck and type 1a supernova [50]-[57] we find that they are in excellent agreement as well as being identical to the result obtained previously using many different methods and models [1]-[6].

## 7. Deriving Einstein's $E = mc^2$ from Quantum Mechanics and Planck's Half Quanta

The result that  $E_o = mc^2 (\phi^5/2)$  leads us to ponder if we could retrieve Einstein's celebrated formula, namely  $E = mc^2$ , from it [1]-[6]. That could be seen as a brand new derivation of  $E = mc^2$  using ironically quantum mechanics which Einstein was not able to bring himself to embrace without many reservations to say the least [67]. There are at least two ways to derive  $E = mc^2$  from the above. First we have to admit that  $E = mc^2$  is already included in  $E_o = mc^2 (\phi^5/2)$ . However  $E_o$  was not found by appealing to any spacetime. It is simply the vacuum energy density so that to find the entire energy density of our spacetime it should be multiplied with the topological "volume" of our spacetime [1]-[14]. We could argue now that a Hausdorff dimension is partially dimension and partially volume because it is based on a covering procedure. So we could multiple  $E_o$  with the Hausdorff dimension of our spacetime and expect to find a reasonable answer. However what is the Hausdorff dimension of our universe? One could be tempted to answer hastily that it is our  $4 + \phi^3$  Cantorian spacetime expectation value for the Hausdorff dimension of spacetime. However this is not correct. The correct answer is to use the topological rectangular "volume" resulting from multiplying the "Bosonic" dimension  $4 + \phi^3$  with the spin 1/2 fermionic dimension [7] [63] [64]  $1 + 4 + \phi^3 = 5 + \phi^3$  and finding a practically super symmetric volume [52]-[62]

$$V = (4 + \phi^3)(5 + \phi^3) = 22 + k = (2)(11 + \phi^5) \quad (10)$$

This is twice the dimension of the fractal version of Witten's M-theory. Proceeding this way one finds [27]

$$2(11 + \phi^5)(E_o) = mc^2 (22 + 2\phi^5) (\phi^5/2) = mc^2 = E(\text{Einstein}) \quad (11)$$

The second possibility is far more straight forward and is nothing more than adding  $E_o = E(O)$  and  $E(D)$  together and finding that [27] [35] [39]

$$E(O) + E(D) = mc^2 \left[ (\phi^5/2) + (5\phi^2/2) \right] = mc^2 \quad (12)$$

Either way we see that  $E = mc^2$  consists of two quasi quantum components well hidden inside the deceptively simple Einstein's beauty  $E = mc^2$  [119]. We could touch upon trisecting  $E = mc^2$  not only into two parts  $E(O)$  and  $E(D)$  but into three parts making a distinction between dark matter energy  $E(DM)$  and pure dark energy  $E(DE)$  where  $E(DM) + E(DE) = E(D)$ . The situation in this case is not straight forward because  $E(DM)$  and  $E(DE)$  are at least mathematically coupled. To show what we mean we recall our earlier published results that [68]

$$E(O) = (\phi^5/2)mc^2 = mc^2/(22 + k) \quad (13)$$

while

$$E(D) = (5\phi^2/2)mc^2 = mc^2/(21 + k/22 + k) \quad (14)$$

In the case of writing  $E$  in three parts, we cannot escape the coupling term  $\Delta$  which cancels out at the end in

the following fashion [68]

$$E = mc^2 \left[ \frac{1}{22+k} + \frac{5-\Delta}{22+k} + \frac{16+k+\Delta}{22+k} \right] \quad (15)$$

where  $k = 2\phi^5$  is 'tHooft's renormalon [118] and the coupling  $\Delta$  is given by

$$\Delta = (8+k^2)/100 \quad (16)$$

This coupling could be taken to be approximately  $k_o = \phi^5 (1-\phi^5)$ . At the end  $\Delta$  cancels out and we find [68]

$$E(D) = \left( \frac{5-\Delta+16+k+\Delta}{22+k} \right) (mc^2) = \frac{21+k}{22+k} mc^2 = (5\phi^2/2) mc^2 \quad (17)$$

exactly as should be.

## 8. Conclusion

We gave a derivation for the ordinary energy density and the dark energy density of the universe starting from and based upon conventional and generally accepted quantum mechanical principles. In particular we relied upon a fact introduced probably for the first time by Max Planck, which shows that even in the absence of any real photon, completely empty spacetime has a non-zero energy. From there we went on to show that using this half quanta of Planck which is in the meantime part of most text books on quantum mechanics, we can explain not only the Casimir effect but could also explain the division of energy into ordinary measurable energy as well as dark energy which we cannot measure directly. Thus unlike our previous publications, we did not need to invoke new advanced mathematics nor really any new concepts beyond what one is taught in an advanced course or two in a good university undergraduate program in physics.

## References

- [1] El Naschie, M.S. (2013) *Journal of Quantum Information Science*, **3**, 23-26. <http://dx.doi.org/10.4236/jqis.2013.31006>
- [2] El Naschie, M.S. (2013) *Journal of Modern Physics*, **4**, 591-596. <http://dx.doi.org/10.4236/jmp.2013.45084>
- [3] El Naschie, M.S. (2013) *International Journal of Modern Nonlinear Theory & Application*, **2**, 43-54. <http://dx.doi.org/10.4236/ijmnta.2013.21005>
- [4] El Naschie, M.S. (2014) *Journal of Quantum Information Science*, **4**, 83-91. <http://dx.doi.org/10.4236/jqis.2014.42008>
- [5] Marek-Crnjac, L., El Naschie, M.S. and He, J.H. (2013) *International Journal of Modern Nonlinear Theory and Application*, **2**, 78-88. <http://dx.doi.org/10.4236/ijmnta.2013.21A010>
- [6] Marek-Crnjac, L. and El Naschie, M.S. (2013) *Journal of Modern Physics*, **4**, 31-38. <http://dx.doi.org/10.4236/jmp.2013.411A1005>
- [7] El Naschie, M.S. (2004) *Chaos, Solitons & Fractals*, **19**, 209-236. [http://dx.doi.org/10.1016/S0960-0779\(03\)00278-9](http://dx.doi.org/10.1016/S0960-0779(03)00278-9)
- [8] El Naschie, M.S. (2005) *International Journal of Nonlinear Sciences and Numerical Simulation*, **6**, 95-98. <http://dx.doi.org/10.1515/IJNSNS.2005.6.2.95>
- [9] Ord, G.N. (1983) *Journal of Physics A: Mathematical and General*, **16**. <http://dx.doi.org/10.1088/0305-4470/16/9/012>
- [10] Ord, G.N. (1996) *Chaos, Solitons & Fractals*, **7**, 821-843. [http://dx.doi.org/10.1016/0960-0779\(95\)00100-X](http://dx.doi.org/10.1016/0960-0779(95)00100-X)
- [11] McKeon, D.G.C. and Ord, G.N. (1992) *Physical Review Letters*, **69**. <http://dx.doi.org/10.1103/physrevlett.69.3>
- [12] Nottale, L. (1998) *Fractal Spacetime and Microphysics. Towards a Theory of Scale Relativity*. World Scientific, Singapore.
- [13] Nottale, L. (1989) *International Journal of Modern Physics A*, **4**, 5047. <http://dx.doi.org/10.1142/S0217751X89002156>
- [14] El Naschie, M.S. (2004) *Chaos, Solitons & Fractals*, **22**, 495-511. <http://dx.doi.org/10.1016/j.chaos.2004.02.028>
- [15] Plunien, G., Muller, B. and Greiner, W. (1986) *Physics Reports*, **134**, 87-193. [http://dx.doi.org/10.1016/0370-1573\(86\)90020-7](http://dx.doi.org/10.1016/0370-1573(86)90020-7)
- [16] Bordag, M., Mohideen, U. and Mostepanenko, V.M. (2001) *Physics Reports*, **353**, 1-205. [http://dx.doi.org/10.1016/S0370-1573\(01\)00015-1](http://dx.doi.org/10.1016/S0370-1573(01)00015-1)
- [17] Milton, K.A. (2001) *The Casimir Effect: Physical Manifestations of Zero-Point Energy*. World Scientific Publishing,

Singapore.

- [18] Marek-Crnjac, L. (2009) *Chaos, Solitons & Fractals*, **41**, 2697-2705. <http://dx.doi.org/10.1016/j.chaos.2008.10.007>
- [19] Helal, M., Marek-Crnjac, L. and He, J.-H. (2013) *Open Journal of Microphysics*, **3**, 141-145. <http://dx.doi.org/10.4236/ojm.2013.34020>
- [20] Marek-Crnjac, L. and He, J.-H. (2013) *International Journal of Astronomy and Astrophysics*, **3**, 464-471. <http://dx.doi.org/10.4236/ijaa.2013.34053>
- [21] Mehra, J. and Rechenberg, H. (1999) *Foundations of Physics*, **29**, 91-132. <http://dx.doi.org/10.1023/A:1018869221019>
- [22] El Naschie, M.S. (2007) *International Journal of Nonlinear Sciences and Numerical Simulation*, **8**, 195-198. <http://dx.doi.org/10.1515/IJNSNS.2007.8.2.195>
- [23] Griffiths, D.J. (2005) *Introduction to Quantum Mechanics*. 2nd Edition, Pearson Education International, Prentice Hall, London.
- [24] Witten, E. (1988) *Communications in Mathematical Physics*, **117**, 353-386. <http://dx.doi.org/10.1007/BF01223371>
- [25] Atiyah, M.F. (1988) *Publications Mathématiques de l'IHÉS*, **68**, 175-186. <http://dx.doi.org/10.1007/BF02698547>
- [26] Schwarz, A. (2000) Topological Quantum Field Theories. arXiv preprint hep-th/0011260
- [27] El Naschie, M.S. (2016) *Journal of Astronomy & Astrophysics*, **6**, 135-144. <http://dx.doi.org/10.4236/ijaa.2016.62011>
- [28] El Naschie, M.S. (2011) *Journal of Quantum Information Science*, **1**, 50-53. <http://dx.doi.org/10.4236/jqis.2011.12007>
- [29] Hardy, L. (1993) *Physics Review Letters*, **71**, 1665-1668. <http://dx.doi.org/10.1103/PhysRevLett.71.1665>
- [30] Von Neumann, J. (1960) *Continuous Geometry*. Vol. 25, Princeton University Press, Princeton.
- [31] Von Neumann, J. (1981) *Continuous Geometries with a Transition Probability*. Volume 34, Number 252, American Mathematical Society, Providence.
- [32] Connes, A. (2000) *Noncommutative Geometry*. In: Alon, N., Bourgain, J., Connes, A., Gromov, M. and Milman, V., Eds., *Visions in Mathematics*, Birkhäuser, Basel, 481-559. [http://dx.doi.org/10.1007/978-3-0346-0425-3\\_3](http://dx.doi.org/10.1007/978-3-0346-0425-3_3)
- [33] Connes, A. (2008) *Noncommutative Geometry, Quantum Fields and Motives*. Vol. 55, American Mathematical Society, Colloquium Publications, Providence.
- [34] El Naschie, M.S. (2016) *Advances in Pure Mathematics*, **6**, 446-454. <http://dx.doi.org/10.4236/apm.2016.66032>
- [35] El Naschie, M.S. (2016) *Journal of Modern Physics*, **7**, 729-736. <http://dx.doi.org/10.4236/jmp.2016.78069>
- [36] Seiberg, M. and Witten, E. (1999) *Journal of High Energy Physics*, **09**, 032. <http://dx.doi.org/10.1088/1126-6708/1999/09/032>
- [37] El Naschie, M.S. (2008) *Chaos, Solitons & Fractals*, **38**, 1349-1354. <http://dx.doi.org/10.1016/j.chaos.2008.07.002>
- [38] Koestler, A. (1968) *The Sleep Walkers*. Penguin Books, London.
- [39] El Naschie, M.S. (2016) *International Journal of Astronomy & Astrophysics*, **6**, 56-81. <http://dx.doi.org/10.4236/ijaa.2016.61005>
- [40] El Naschie, M.S., Olsen, S., He, J.H., Nada, S., Marek-Crnjac, L. and Helal, A. (2012) *International Journal of Modern Nonlinear Theory and Application*, **1**, 84-92. <http://dx.doi.org/10.4236/ijmnta.2012.13012>
- [41] El Naschie, M.S. (2006) *Chaos, Solitons & Fractals*, **30**, 579-605. <http://dx.doi.org/10.1016/j.chaos.2006.03.030>
- [42] El Naschie, M.S. (2006) *Chaos, Solitons & Fractals*, **27**, 297-330. <http://dx.doi.org/10.1016/j.chaos.2005.04.116>
- [43] He, J.-H. (2014) *International Journal of Theoretical Physics*, **53**, 3698-3718. <http://dx.doi.org/10.1007/s10773-014-2123-8>
- [44] El Naschie, M.S. (2013) *International Journal of Astronomy & Astrophysics*, **3**, 205-211. <http://dx.doi.org/10.4236/ijaa.2013.33024>
- [45] El Naschie, M.S. (2013) *Journal of Quantum Information Science*, **3**, 57-77. <http://dx.doi.org/10.4236/jqis.2013.32011>
- [46] El Naschie, M.S. (2013) *International Journal of Astronomy and Astrophysics*, **3**, 483-493. <http://dx.doi.org/10.4236/ijaa.2013.34056>
- [47] El Naschie, M.S. and Marek-Crnjac, L. (2012) *International Journal of Modern Nonlinear Theory and Applications*, **1**, 118-124. <http://dx.doi.org/10.4236/ijmnta.2012.14018>
- [48] El Naschie, M.S. and Helal, A. (2013) *International Journal of Astronomy and Astrophysics*, **3**, 318-343.

- <http://dx.doi.org/10.4236/ijaa.2013.33037>
- [49] El Naschie, M.S. (2013) *Journal of Modern Physics*, **4**, 757-760. <http://dx.doi.org/10.4236/jmp.2013.46103>
- [50] El Naschie, M.S. (2013) *Journal of Modern Physics*, **4**, 354-356. <http://dx.doi.org/10.4236/jmp.2013.43049>
- [51] El Naschie, M.S. (2013) *Journal of Modern Physics*, **4**, 1417-1428. <http://dx.doi.org/10.4236/jmp.2013.410170>
- [52] El Naschie, M.S. (2013) *Open Journal of Microphysics*, **3**, 64-70. <http://dx.doi.org/10.4236/ojm.2013.33012>
- [53] El Naschie, M.S. (2013) *Journal of Quantum Information Science*, **3**, 121-126. <http://dx.doi.org/10.4236/jqis.2013.34016>
- [54] El Naschie, M.S. (2013) *International Journal of Modern Nonlinear Theory & Applications*, **2**, 107-121. <http://dx.doi.org/10.4236/ijmnta.2013.22014>
- [55] El Naschie, M.S. (2014) *Journal Modern Physics and Applications*, **2**, 1-7.
- [56] El Naschie, M.S. (2015) *International Journal of High Energy Physics*, **2**, 13-21. <http://dx.doi.org/10.11648/j.ijhep.20150201.12>
- [57] El Naschie, M.S. (2014) *American Journal of Astronomy & Astrophysics*, **2**, 72-77. <http://dx.doi.org/10.11648/j.ajaa.20140206.13>
- [58] El Naschie, M.S. (1992) Physics-Like Mathematics in Four Dimensions—Implication for Classical and Quantum Mechanics. Computational and Applied Mechanics II, Differential Equations, Elsevier Publisher, North Holland, 15-23. (Selected and Revised Papers from the IMACS 13th World Congress, Edited by Ames, W.F. and Van der Houwen, P.J., Dublin, July 1991)
- [59] El Naschie, M.S. (2016) *Journal of Quantum Information Science*, **6**, 57-61. <http://dx.doi.org/10.4236/jqis.2016.62007>
- [60] El Naschie, M.S. (2016) Einstein-Rosen bridge (ER), *Journal of Quantum Information Science*, **6**, 1-9. <http://dx.doi.org/10.4236/jqis.2016.61001>
- [61] El Naschie, M.S. (2016) *Natural Science*, **8**, 152-159. <http://dx.doi.org/10.4236/ns.2016.83018>
- [62] El Naschie, M.S. (2016) *World Journal of Condensed Matter Physics*, **6**, 63-67. <http://dx.doi.org/10.4236/wjcmp.2016.62009>
- [63] El Naschie, M.S. (2006) *Chaos, Solitons & Fractals*, **30**, 656-663. <http://dx.doi.org/10.1016/j.chaos.2006.04.043>
- [64] El Naschie, M.S. (2007) *International Journal of Nonlinear Science and Numerical Simulation*, **8**, 11-20. <http://dx.doi.org/10.1515/IJNSNS.2007.8.1.11>
- [65] El Naschie, M.S. (2015) *World Journal of Nano Science and Engineering*, **5**, 49-56. <http://dx.doi.org/10.4236/wjnse.2015.52007>
- [66] Susskind, L. and Friedman, A. (2014) *Quantum Mechanics—The Theoretical Minimum*. Allen Lane-Penguin Books, London.
- [67] Penrose, R. (2004) *The Road to Reality*. J. Cape, London.
- [68] El Naschie, M.S. (2014) *Journal of Quantum Information Science*, **4**, 284-291. <http://dx.doi.org/10.4236/jqis.2014.44023>
- [69] El Naschie, M.S. (2006) *Chaos, Solitons & Fractals*, **30**, 636-641. <http://dx.doi.org/10.1016/j.chaos.2006.04.044>
- [70] El Naschie, M.S. (2006) *Chaos, Solitons & Fractals*, **30**, 622-628. <http://dx.doi.org/10.1016/j.chaos.2006.04.042>
- [71] El Naschie, M.S. (2007) *Chaos, Solitons & Fractals*, **32**, 911-915. <http://dx.doi.org/10.1016/j.chaos.2006.08.014>
- [72] El Naschie, M.S. (2006) *Chaos, Solitons & Fractals*, **30**, 1025-1033. <http://dx.doi.org/10.1016/j.chaos.2006.05.088>
- [73] El Naschie, M.S. (2006) *International Journal Nonlinear Science & Numerical Simulation*, **7**, 407-409.
- [74] El Naschie, M.S. (2006) *Chaos, Solitons & Fractals*, **29**, 816-822. <http://dx.doi.org/10.1016/j.chaos.2006.01.013>
- [75] El Naschie, M.S. (2008) *Chaos, Solitons & Fractals*, **35**, 202-211. <http://dx.doi.org/10.1016/j.chaos.2007.05.006>
- [76] El Naschie, M.S. (2007) *Chaos, Solitons & Fractals*, **32**, 468-470. <http://dx.doi.org/10.1016/j.chaos.2006.08.011>
- [77] El Naschie, M.S. (2007) *Chaos, Solitons & Fractals*, **32**, 927-936. <http://dx.doi.org/10.1016/j.chaos.2006.08.017>  
El Naschie, M.S. (2006) *Chaos, Solitons & Fractals*, **29**, 845-853. <http://dx.doi.org/10.1016/j.chaos.2006.01.073>
- [78] El Naschie, M.S. (2006) *International Journal of Nonlinear Science & Numerical Simulation*, **7**, 129-132. <http://dx.doi.org/10.1515/IJNSNS.2006.7.2.129>
- [79] El Naschie, M.S. (2016) *Quantum Matter*, **5**, 1-4. <http://dx.doi.org/10.1166/qm.2016.1247>
- [80] El Naschie, M.S. (2016) *Journal of Modern Physics*, **17**, 156-161.
- [81] Marek-Crnjac, L. (2003) *Chaos, Solitons & Fractals*, **15**, 611-618. [http://dx.doi.org/10.1016/S0960-0779\(02\)00174-1](http://dx.doi.org/10.1016/S0960-0779(02)00174-1)

- [82] Marek-Crnjac, L. (2004) *Chaos, Solitons & Fractals*, **20**, 669-682. <http://dx.doi.org/10.1016/j.chaos.2003.10.013>
- [83] He, J.-H., Marek-Crnjac, L., Helal, M.A., Nada, S.I. and Rössler, O.E. (2011) *Nonlinear Science Letters B*, **1**, 45-50.
- [84] Marek-Crnjac, L. (2003) *Chaos, Solitons & Fractals*, **18**, 125-133. [http://dx.doi.org/10.1016/S0960-0779\(02\)00587-8](http://dx.doi.org/10.1016/S0960-0779(02)00587-8)
- [85] El Naschie, M.S., Marek-Crnjac, L. (2013) *International Journal of Modern Nonlinear Theory and Application*, **1**, 118-124. <http://dx.doi.org/10.4236/ijmnta.2012.14018>
- [86] El Naschie, M.S. (2006) *International Journal of Nonlinear Sciences and Numerical Simulations*, **7**, 477-481.
- [87] El Naschie, M.S. (1997) *Chaos, Solitons & Fractals*, **8**, 753-759. [http://dx.doi.org/10.1016/S0960-0779\(96\)00139-7](http://dx.doi.org/10.1016/S0960-0779(96)00139-7)
- [88] El Naschie, M.S. (1997) *Chaos, Solitons & Fractals*, **8**, 1865-1872. [http://dx.doi.org/10.1016/S0960-0779\(97\)00039-8](http://dx.doi.org/10.1016/S0960-0779(97)00039-8)
- [89] He, J.-H. (2006) *Chaos, Solitons & Fractals*, **28**, 285-289. <http://dx.doi.org/10.1016/j.chaos.2005.08.001>
- [90] He, J.-H., Xu, L., Zhang, L.-N. and Wu, X.-H. (2007) *Chaos, Solitons & Fractals*, **33**, 5-13. <http://dx.doi.org/10.1016/j.chaos.2006.10.048>
- [91] He, J.-H., Ren, Z.F., Fan, J. and Xu, L. (2009) *Chaos, Solitons & Fractals*, **41**, 1839-1841. <http://dx.doi.org/10.1016/j.chaos.2008.07.035>
- [92] He, J.-H. (2006) *Chaos, Solitons & Fractals*, **30**, 506-511. <http://dx.doi.org/10.1016/j.chaos.2005.11.033>
- [93] El Naschie, M.S. and He, J.-H. (2012) *Fractal Spacetime, Non-Commutative Geometry in High Energy Physics*, **2**, 41-49.
- [94] He, J.-H. (2005) *International Journal Nonlinear Science & Numerical Simulation*, **6**, 343-346.
- [95] Nottale, L. (1996) *Chaos, Solitons & Fractals*, **7**, 877-938. [http://dx.doi.org/10.1016/0960-0779\(96\)00002-1](http://dx.doi.org/10.1016/0960-0779(96)00002-1)
- [96] Nottale, L. (1997) *Astronomy and Astrophysics*, **327**, 867-889.
- [97] Nottale, L. (1992) *International Journal of Modern Physics A*, **7**, 4899-4936. <http://dx.doi.org/10.1142/S0217751X92002222>
- [98] Nottale, L. (1999) *Chaos, Solitons & Fractals*, **10**, 459-468. [http://dx.doi.org/10.1016/S0960-0779\(98\)00195-7](http://dx.doi.org/10.1016/S0960-0779(98)00195-7)
- [99] Alexandrov, M., Schwarz, A. and Zabronsky, O. (1997) *Journal of Modern Physics A*, **12**, 1405-1430. <http://dx.doi.org/10.1142/S0217751X97001031>
- [100] Witten, E. (1989) *Communications in Mathematical Physics*, **121**, 351-399. <http://dx.doi.org/10.1007/BF01217730>
- [101] Baez, J.C. and Dolan, J. (1995) *Journal of Mathematical Physics*, **36**, 6073-6105. <http://dx.doi.org/10.1063/1.531236>
- [102] Crane, L. and Frenkel, I.B. (1994) *Journal of Mathematical Physics*, **35**, 5136-5154. <http://dx.doi.org/10.1063/1.530746>
- [103] Lapidus, M.L. and van Frankenhuysen, M. (2000) *Fractal Geometry and Number Theory: Complex dimensions of Fractal Strings and Zeros of Zeta Functions*. Cambridge University Press, Cambridge. <http://dx.doi.org/10.1007/978-1-4612-5314-3>
- [104] Connes, A., Douglas, M.R. and Schwarz, A. (1998) *Journal of High Energy Physics*, **02**, 003. <http://dx.doi.org/10.1088/1126-6708/1998/02/003>
- [105] Varilly, J.C. and Gracia-Bondia, J.M. (1993) *Journal of Geometry and Physics*, **12**, 223-301. [http://dx.doi.org/10.1016/0393-0440\(93\)90038-G](http://dx.doi.org/10.1016/0393-0440(93)90038-G)
- [106] Connes, A. (1995) *Journal of Mathematical Physics*, **36**, 6194-6231. <http://dx.doi.org/10.1063/1.531241>
- [107] Chamseddine, A.H. and Connes, A. (1996) *Physical Review Letters*, **77**, 4868-4871. <http://dx.doi.org/10.1103/PhysRevLett.77.4868>
- [108] Birkhoff, G. and Von Neumann, J. (1936) *Annals of Mathematics*, **37**, 823-843. <http://dx.doi.org/10.2307/1968621>
- [109] Von Neumann, J. (2012) *The Computer and the Brain*. 3rd Edition, Yale University Press, New Haven.
- [110] Von Neumann, J. (1936) *Proceedings of the National Academy of Sciences of the United States of America*, **22**, 101-108. <http://dx.doi.org/10.1073/pnas.22.2.101>
- [111] Von Neumann, J. (1955) *Mathematical Foundations of Quantum Mechanics*. Princeton University Press, Princeton.
- [112] El Naschie, M.S. (2015) *American Journal of Nano Research and Applications*, **3**, 33-40.
- [113] El Naschie, M.S. (2015) *Natural Science*, **7**, 287-298. <http://dx.doi.org/10.4236/ns.2015.76032>
- [114] El Naschie, M.S. (2015) *World Journal of Nano Science & Engineering*, **5**, 26-33. <http://dx.doi.org/10.4236/wjnse.2015.51004>
- [115] El Naschie, M.S. (2015) *Natural Science*, **7**, 210-225. <http://dx.doi.org/10.4236/ns.2015.74024>
- [116] El Naschie, M.S. (2014) *Journal of Modern Physics*, **5**, 743-750. <http://dx.doi.org/10.4236/jmp.2014.59084>

- [117] El Naschie, M.S. (2016) *American Journal of Computational Mathematics*, **6**, 185-199. <http://dx.doi.org/10.4236/ajcm.2016.63020>
- [118] Babchin, A.J. and El Naschie, M.S. (2015) *World Journal of Condensed Matter Physics*, **7**, 581-598.
- [119] Da Cruz, W. (2004) *Chaos, Solitons & Fractals*, **23**, 373-378. <http://dx.doi.org/10.1016/j.chaos.2004.05.031>



Scientific Research Publishing

**Submit or recommend next manuscript to SCIRP and we will provide best service for you:**

Accepting pre-submission inquiries through Email, Facebook, LinkedIn, Twitter, etc.

A wide selection of journals (inclusive of 9 subjects, more than 200 journals)

Providing 24-hour high-quality service

User-friendly online submission system

Fair and swift peer-review system

Efficient typesetting and proofreading procedure

Display of the result of downloads and visits, as well as the number of cited articles

Maximum dissemination of your research work

Submit your manuscript at: <http://papersubmission.scirp.org/>

# Determination of the Dynamic ITER Energy Confinement Time Scalings

Giorgio Sonnino<sup>1,2</sup>, Alberto Sonnino<sup>3</sup>, Jarah Evslin<sup>4</sup>, Pasquale Nardone<sup>1</sup>, György Steinbrecher<sup>5</sup>

<sup>1</sup>Department of Theoretical Physics and Mathematics, Université Libre de Bruxelles (U.L.B.), Campus Plaine, Brussels, Belgium

<sup>2</sup>Royal Military School (RMS), Brussels, Belgium

<sup>3</sup>Ecole Polytechnique de Louvain (EPL), Université Catholique de Louvain (UCL), Louvain-la-Neuve, Belgium

<sup>4</sup>High Energy Nuclear Physics Group, Institute of Modern Physics, Chinese Academy of Sciences, Lanzhou, China

<sup>5</sup>Physics Department, University of Craiova, Craiova, Romania

Email: gsonnino@ulb.ac.be, alberto.sonnino@gmail.com, jarah@ihep.ac.cn, pnardon@ulb.ac.be, gyorgy.steinbrecher@gmail.com

Received 19 June 2016; accepted 8 August 2016; published 11 August 2016

Copyright © 2016 by authors and Scientific Research Publishing Inc.

This work is licensed under the Creative Commons Attribution International License (CC BY).

<http://creativecommons.org/licenses/by/4.0/>



Open Access

---

## Abstract

We derive the differential equation, which is satisfied by the ITER scalings for the dynamic energy confinement time. We show that this differential equation can also be obtained from the differential equation for the energy confinement time, derived from the energy balance equation, when the plasma is near the steady state. We find that the values of the scaling parameters are linked to the second derivative of the power loss, estimated at the steady state. As an example of an application, the solution of the differential equation for the energy confinement time is compared with the profile obtained by solving numerically the balance equations (closed by a transport model) for a concrete Tokamak-plasma.

## Keywords

Fusion Reactors, Theory, Design, and Computerized Simulation

---

## 1. Introduction

Global scaling expressions for the energy confinement time,  $\tau_E$ , or the stored energy,  $W$ , are powerful tools for predicting the confinement performance of burning plasmas [1]-[3]. The fusion performance of ITER is predicted using three different techniques: statistical analysis of the global energy confinement data in the

**How to cite this paper:** Sonnino, G., Sonnino, A., Evslin, J., Nardone, P. and Steinbrecher, G. (2016) Determination of the Dynamic ITER Energy Confinement Time Scalings. *Journal of Modern Physics*, 7, 1429-1439.

<http://dx.doi.org/10.4236/jmp.2016.712130>

parameters (simple (multivariate) linear regression tools can be used to determine the parameters from a set of data) [4] [5], a dimensionless scaling analysis, based on dimensionless physics parameters [5]-[7], and theory-based on transport models and modelling the plasma profiles [8]-[10]. Although the three methods give overlapping predictions for the performance of ITER, the confidence interval of all of the techniques is still quite wide [11]. The Confinement Database and Modelling Expert Group recommended for ITER design the so-called *ITERH-98P*( $y, 2$ ) confinement scaling [5] [12]:

$$\tau_E^{H98(y,2)} = 0.0562 I_p^{0.93} R^{1.97} \epsilon^{0.58} \kappa^{0.78} B_{0\phi}^{0.15} \bar{n}_e^{-0.41} P^{-0.69} M^{0.19} \quad (1)$$

Here, the parameters are the plasma current  $I_p$ , the major radius  $R$ , the inverse aspect ratio  $\epsilon = a/R$  (with  $a$  denoting the minor radius of the Tokamak), the elongation  $\kappa$ , the toroidal magnetic field (at the major radius  $R$ )  $B_{0\phi}$ , the central line averaged electron density  $\bar{n}_e$ , the loss power  $P$ , and the ion mass number  $M$ , respectively. The expression (1) is valid for the ELMy H-mode thermal energy confinement time. The 2log-linear interval was determined to be 20%. By recent analyzing the enlarged *ITERH.DB3* dataset, the practical reliability of the *ITERH-98P*( $y, 2$ ) scaling was confirmed and 2log-linear interval was reduced to 14% [13]. Tables showing some of the most generally used sets of scaling parameters for the ELMy H-mode and L-mode can be found in Refs [5] [14]-[16].

For stellarators, a similar scaling has been obtained [17] [18]

$$\tau_E = 0.148 R^{0.64} a^{2.33} \bar{n}_e^{-0.55} B_{0\phi}^{0.85} l^{0.41} P^{-0.61} \quad (2)$$

where  $l/2\pi$  is the rotational transform (or the field line pitch).

The confinement time is defined as

$$\tau_E = \frac{W_e}{P_{tot} - \dot{W}_e} = \frac{W_e}{P_Q} \quad (3)$$

where  $W_e$ ,  $P_Q$  and  $P_{tot}$  are the internal energy, the power loss and the power source, respectively. From Equation (3) results that when the tokamak is not in the steady state the quantity  $\tau_E$  is a time dependent quantity. Hence,  $\tau_E$ , given by Equations (1) and (2), is viewed as a time-dependent variable, which depends on a collection of variables dependent on time (e.g.,  $\bar{n}$ ,  $P$ , etc.). The value of  $\tau_E$  at the steady state condition  $\dot{\tau}_E = 0$ , attained at some time moment  $t_0$ , corresponds to the numerical value provided by the database. For example, the point prediction for the thermal energy confinement time in ITER is  $(\tau_E, \dot{\tau}_E) = (3.6 \text{ sec}, 0)$ .

The main objective of this work is to estimate the energy confinement time, close to the steady state.  $\tau_E$  at the steady state condition is calculated by using the expression

$$\tau_E^0 = \frac{W_{estat.}}{P_{Qstat.}} \quad (4)$$

where  $W_{estat.}$  and  $P_{Qstat.}$  are obtained by solving the stationary balance equations. An example of calculation can be found in Ref. [19]. To estimate the dynamic confinement time we should solve the evolutive balance equations. However, this is a very complex task. An alternative strategy (which is the one that we shall adopt here) consists in deriving the time differential equation for the energy confinement time, with  $\tau_E^0$ , estimated by using Equation (4), playing the role of the initial condition. We show that  $\tau_E$  is the solution of a nonlinear differential equation of second order in time, obtained by combining Equation (3) with the (dynamic) balance equations. The critical fact which makes our approach useful is that in the vicinity of the stationary state, this differential equation depends only on one coefficient which varies very slowly in time

$$\begin{cases} \tau_E \ddot{\tau}_E - \dot{\tau}_E^2 = \chi(t) \tau_E^2 \\ \tau_E^0 = \frac{W_{estat.}}{P_{Qstat.}}; \quad \dot{\tau}_E = 0 \end{cases} \quad (5)$$

where  $\chi(t) = \chi_0(t - t_0)$ , and  $\chi_0$  is a numerical coefficient estimated at the steady state. Hence, at the ‘‘leading order’’, all of the dependence on the machine is reduced to just a number,  $\chi_0$ , which can be determined. This is the real advantage of this approach. As an example of calculation, we have considered the simplest case of IGNITOR-plasmas. In this case, we solved the time differential equation for  $\tau_E$  where the parameters (*i.e.*,

the initial condition as well as the coefficient appearing in the differential equation) have been estimated at the steady state. The solution of this equation is in agreement with the one obtained by solving numerically the dynamic balance equations, with the aid of a transport model [20].

In this work, we shall also justify the dynamic scaling laws, like

$$\tau_E = CI_p^{\alpha_1} \bar{n}_e^{\alpha_2} P^{\alpha_3} M^{\alpha_4}, \quad (6)$$

where  $C$  is a constant and  $M$  is the effective mass, respectively (note that when the plasma is a mixture, due to the dependence of particle transport properties on particle mass and charge,  $M$  is also time dependent). In particular, we shall prove that the dynamic expression for the energy confinement time, like Equation (6), is solution of the differential equation for  $\tau_E$ , which can be obtained by combining Equation (3) with the energy balance equation.

The paper is organized as follows. In Section (2), we show that Equation (6) satisfies a nonlinear differential equation of the second order in time, tacking into account the (experimentally established) slow variation in time of the coefficient entering in this equation. Successively, we show that this equation can also be derived from the energy balance equation, combined with definition (3). This will allow a linking of the scaling coefficients with the (measurable) second time derivatives of the heat power loss, which at the leading order may also be estimated at the stationary state. These tasks will be accomplished in the Section (3). As an example of an application, in the Section (4), we compare the solution obtained by solving the differential equation for the energy confinement time with the numerical simulations obtained using the code JETTO [20], for the specific case of IGNITOR-plasmas. Concluding remarks can be found in Section (5).

## 2. Differential Equation Satisfied by the ITER Scalings

The expression for the energy confinement time, obtained by scaling laws, raises several questions. Firstly, Equation (1) applies quite well to a large number of Tokamaks (ASDEX, JET, DIII-D, ALCATOR C-Mod, COMPASS, etc.) and it is currently used for predicting the energy confinement time for Tokamaks, which are presently in construction (ITER) or will be constructed in the future (DEMO). Hence, the first objective of this work is to understand the main reason for such a “universal” validity. Secondly, it is legitimate to ask “where does this expression originate from?”. More concretely, “Is it possible to determine the (minimal) differential equation which is satisfied by expression (6)?”. In case of a positive answer, “Is it possible to re-obtain this (minimal) differential equation from the balance equations and, in particular, from the energy balance equations?”. Finally, “How can we estimate the values of the scaling coefficients  $\alpha_i$ ?”. In this Section, we shall determine the (minimal) differential equation satisfied by Equation (6). In the next Section we shall prove that, near the stationary state, this differential equation can be re-obtained from the energy balance equation.

The equations of one-dimensional plasma dynamics, in toroidal geometry, assuming the validity of the standard model, can be brought into the form (see, for example, [21])

$$\begin{aligned} \frac{\partial n_e}{\partial t} &= -\frac{1}{r} \frac{\partial}{\partial r} (r \langle \gamma_r^e \rangle) \\ \frac{3}{2} \frac{\partial p}{\partial t} + \frac{1}{r} \frac{\partial}{\partial r} \left[ r \left( \langle q_e \rangle + \langle q_i \rangle + \frac{5}{2} (1+Z^{-1}) T_e \langle \gamma_r^e \rangle \right) \right] \\ &= \frac{c}{4\pi} \frac{E_0 B_{0\phi}}{Rr} \frac{\partial}{\partial r} \left( \frac{r^2}{q(r)} \right) + S_{\text{gain-loss}} \end{aligned} \quad (7)$$

with  $r$  and  $q(r)$  denoting the radial coordinate and the safety factor, respectively.  $p$ ,  $n_e$ ,  $T_e$  and  $Z$  are the total plasma pressure, the electron density, the electron temperature and the ion charge number, respectively. Here,  $\langle \dots \rangle$  denotes the surface-average operation.  $\langle q_\zeta \rangle$  and  $\langle \gamma_r^e \rangle$  are the averaged radial heat flux of species  $\zeta$  ( $\zeta = e$  for electrons and  $\zeta = i$  for ions) and the averaged electron flux, respectively.  $c$  and  $E_0$  are light speed and the external electric field, respectively, and  $S_{\text{gain-loss}}$  is the source term, *i.e.* the loss and energy gain. Equation (7) must be completed with the transport equations, *i.e.* with the thermodynamic flux-force relations, in order to close the plasma dynamical equations. The  $0-D$  power balance equation is now derived as follows. Equation (7) is integrated over the volume of the plasma and then divided by the plasma

volume  $V$ . We obtain

$$\begin{cases} \dot{N}_e = -\Gamma \\ \dot{W}_e + P_Q = P_{tot} \end{cases} \quad (8)$$

with

$$\begin{aligned} N_e &\equiv V^{-1} \int n_e dV; \quad \Gamma \equiv V^{-1} \int \frac{1}{r} \frac{\partial}{\partial r} (r \langle \gamma_r^e \rangle) dV \\ W_e &\equiv \frac{3}{2} V^{-1} \int p dV; \quad P_{tot} \equiv V^{-1} \int \left[ \frac{c}{4\pi} \frac{E_0 B_{0\phi}}{Rr} \frac{\partial}{\partial r} \left( \frac{r^2}{q(r)} \right) + S_{\text{gain-loss}} \right] dV \\ P_Q &\equiv V^{-1} \int \left( \frac{1}{r} \frac{\partial}{\partial r} \left[ r \left( \langle q_e \rangle + \langle q_i \rangle + \frac{5}{2} (1 + Z^{-1}) T_e \langle \gamma_r^e \rangle \right) \right] \right) dV \end{aligned} \quad (9)$$

where the “dot” over the variables stands for the (total) time derivative ( $d/dt$ ).

The energy confinement time is defined as

$$\tau_E = \frac{W_e}{P_{tot} - \dot{W}_e} = \frac{W_e}{P_Q} \quad (10)$$

From definition (10), we find

$$\dot{\tau}_E P_Q + \tau_E \dot{P}_Q - \dot{W}_e = 0 \quad (11)$$

Note that the stationary state is reached when  $P_Q = P_{tot}$ . Hence, at the steady state (corresponding to  $t = t_0$ ) we have

$$\dot{W}_e \Big|_{t=t_0} \equiv \dot{W}_e^0 = 0 \quad (12)$$

At the steady state, we find

$$\tau_E(t_0) \equiv \tau_E^0 = \frac{W_e^0}{P_{tot}^0}; \quad \frac{d\tau_E}{dt} \Big|_{t=t_0} \equiv \dot{\tau}_E^0 = 0 \quad (13)$$

where  $W_e^0$  and  $P_{tot}^0$  indicate the values of  $W_e$  and  $P_{tot}$ , estimated at the steady state, respectively.

Equation (6) may be re-written in the generic form:

$$\tau_E = C X_1^{\alpha_1} X_2^{\alpha_2} \dots X_n^{\alpha_n} \quad (14)$$

where  $X_1, X_2, \dots$  are a positive and independent system of variables  $X_i$ , and  $\alpha_i$  the *scaling parameters*, respectively. For simplicity, we firstly suppose that in Equation (14) all the variables  $X_i$  are time-dependent. The case whereby  $X_i$  is a collection of variables dependent on time, as well as variables not-dependent on time, will be treated in the following sub-Section *Analysis in the Physics Variables*. Note that  $C$  is a (dimensional) constant satisfying the condition

$$C = \tau_E^0 X_1(t_0)^{-\alpha_1} X_2(t_0)^{-\alpha_2} \dots X_n(t_0)^{-\alpha_n} \quad (15)$$

Unless stated otherwise, in the sequel we shall adopt the summation convention on the repeated indexes. By taking the logarithm of Equation (14) we find

$$y = \log C + \alpha_1 \xi_1 + \alpha_2 \xi_2 + \dots + \alpha_n \xi_n \quad (16)$$

with  $y \equiv \log \tau_E$  and  $\xi_i \equiv \log X_i$  (with  $i = 1, \dots, n$ ). The first and the second derivatives of  $y$ , with respect to variable  $\xi_i$ , read respectively

$$\frac{\partial y}{\partial \xi_i} = \alpha_i; \quad \frac{\partial^2 y}{\partial \xi_i \partial \xi_j} = 0 \quad (17)$$

In terms of variable  $\tau_E$ , instead of  $y$ , we get

$$\frac{\partial \tau_E}{\partial \xi_i} = \tau_E \alpha_i; \quad \tau_E \frac{\partial^2 \tau_E}{\partial \xi_i \partial \xi_j} - \frac{\partial \tau_E}{\partial \xi_i} \frac{\partial \tau_E}{\partial \xi_j} = 0 \quad (18)$$

The differential equation with respect to time is easily obtained by tacking into account the identities

$$\dot{\tau}_E = \frac{\partial \tau_E}{\partial \xi_i} \dot{\xi}_i = \tau_E \alpha_i \dot{\xi}_i; \quad \frac{\partial^2 \tau_E}{\partial \xi_i \partial \xi_j} \dot{\xi}_i \dot{\xi}_j = \ddot{\tau}_E - \frac{\partial \tau_E}{\partial \xi_i} \ddot{\xi}_i = \ddot{\tau}_E - \tau_E \alpha_i \ddot{\xi}_i \quad (19)$$

By multiplying the second equation of Equation (18) by  $\dot{\xi}_i \dot{\xi}_j$  and by summing over indexes, we finally obtain the differential equation satisfied by the ITER scaling laws

$$\tau_E \ddot{\tau}_E - \dot{\tau}_E^2 = \left( \sum_{i=1}^n \alpha_i \ddot{\xi}_i(t) \right) \tau_E^2 \quad (20)$$

Equation (20) should be solved with the initial conditions (13):

$$\begin{cases} \tau_E \ddot{\tau}_E - \dot{\tau}_E^2 = \chi(t) \tau_E^2 \\ \tau_E^0 = \frac{W_e^0}{P_{tot}^0}; \quad \dot{\tau}_E^0 = 0 \end{cases} \quad (21)$$

with  $\chi(t) \equiv \left( \sum_{i=1}^n \alpha_i \ddot{\xi}_i(t) \right)$ . We have derived two differential equations for the time derivatives of  $\tau$ , the first equation of Equation (19) which is first order and also Equation (20) which is second order. It may appear hopeless to solve these equations, as they depend on  $\alpha_i \dot{\xi}_i(t)$  and  $\chi(t) = \alpha_i \ddot{\xi}_i(t)$  respectively, which in turn depend on the full dynamics of the system. The critical fact which makes our approach useful is that the second time derivatives of the logarithm of  $X_i$  are generally weakly dependent on time. As a result, one may approximate  $\chi(t)$  to be a constant,  $\chi_0$ . In this sense, all of the dependence on the machine is reduced to just a number, which can be determined. The evolution of  $\tau_E$  can then be obtained uniquely by integrating Equation (20) with the initial conditions (13). Such an approach would not work for the first equation of Equation (19) as  $\alpha_i \dot{\xi}_i(t)$  depends strongly on time, indeed it vanishes at the initial stationary state and then becomes nonzero as the state evolves.

It is not difficult to check that the nonlinear Equation (21) is the “minimal” differential equation, in the sense that Equation (21) admits one, and only one, solution (*i.e.*, the nonlinear differential Equation (21) *does not generate* additional solutions).

It may appear hopeless to solve Equation (21), as it depends on the coefficient  $\chi = \left( \sum_{i=1}^n \alpha_i \ddot{\log X}_i \right)$ , which in turn depend on the full dynamics of the system. The critical fact which makes our approach useful is that the second time derivatives of the logarithm of  $X_i$  are generally weakly time-dependent. In all the cases examined by the authors,  $\chi(t)$  is very well approximated (numerically) by a linear function in time

$$\chi(t) \approx \chi_0 (t - t_0) \quad \text{with} \quad \chi_0 = -\frac{1}{t_0} \sum_{i=1}^n \alpha_i \ddot{\xi}_i(t_0) \quad (22)$$

Hence, all of the dependence on the machine is reduced to just a number,  $\chi_0$ , which can be *estimated at the steady state*.

### 3. Differential Equation for the Energy Confinement Time

The aim of this Section is to obtain the differential equation for the energy confinement time from the balance equations. In analogy with Equation (21), the coefficients of this differential equation should be expressed only in terms of the internal energy  $W_e$  and the total power  $P_{tot}$ . To this end, let us reconsider the energy balance equation Equation (8) and the definition of the energy confinement time, Equation (10). Taking the derivative of Equation (11) with respect to time, after a little algebra, we get

$$\tau_E \ddot{\tau}_E - \dot{\tau}_E^2 = -f(t) \tau_E^2 - g(t) \tau_E \dot{\tau}_E \quad (23)$$

with

$$\begin{aligned}
 f(t) &\equiv \frac{\ddot{P}_{tot} - \ddot{W}_e}{P_{tot} - \dot{W}_e} - \frac{\ddot{W}_e}{W_e} = -\chi(t) \\
 g(t) &\equiv \frac{\dot{P}_{tot} - \dot{W}_e}{P_{tot} - \dot{W}_e} + \frac{\dot{W}_e}{W_e}
 \end{aligned}
 \tag{24}$$

Note that the dimensions of  $f(t)$  and  $g(t)$  are  $[t]^{-2}$  and  $[t]^{-1}$ , respectively. Finally, the *differential equation for the energy confinement time* reads

$$\begin{cases}
 \tau_E \ddot{\tau}_E - \dot{\tau}_E^2 + f(t) \tau_E^2 + g(t) \tau_E \dot{\tau}_E = 0 \\
 \tau_E^0 = \frac{W_e^0}{P_{tot}^0}; \quad \dot{\tau}_E^0 = 0
 \end{cases}
 \tag{25}$$

We might object that the previous equation has the same degree of difficulty as the initial expression, Equation (10). However, as we shall see more in detail in the next Subsection, the coefficients  $g(t)$  and  $f(t)$  possess special properties: close to the steady state  $g(t)$  tends to vanish and  $f(t)$  is a function varying very slowly in time. So, at the leading order,  $g(t) \approx 0$  and  $f(t)$  may be estimated at the stationary state [see Equation (22) and the discussion after Equation (21)]. This is the real advantage of Equation (25) with respect to Equation (10): Equation (25) allows determining the dynamic behaviour of the energy confinement time when the system is close to the steady state, solely by the knowledge of one coefficient estimated at the stationary state. Moreover, from the previous Section we know that this equation admits one (and only one) solution corresponding to the ITER scalings. A concrete application of Equation (25) can be found in the Section (4). Note that Equation (25) may be re-written in the more convenient form

$$\begin{cases}
 \dot{\tau}_E = \tau_E y \\
 \dot{y} + g(t) y + f(t) = 0 \\
 \tau_E(t_0) = \frac{W_e^0}{P_{tot}^0}; \quad y(t_0) = 0
 \end{cases}
 \tag{26}$$

showing that the differential equation for the energy confinement time may be expressed as two *quasi-decoupled* differential equations of first order in time derivative. The general solution of Equations (26) may be brought into the form

$$\tau_E(t) = \tau_E^0 \exp \left[ - \int_{t_0}^t dx^n \left( \exp \left( - \int_{t_0}^{x^*} dx g(x) \right) \left[ \int_{t_0}^{x^*} dx' f(x') \exp \left( \int_{t_0}^{x'} dx g(x) \right) \right] \right) \right]
 \tag{27}$$

By taking into account that  $f(t) = -\sum_{i=1}^n \alpha_i \dot{\xi}_i$  (with  $\xi_i = \log X_i$ ), solution (27) generalizes the ITER scaling laws out of the steady state, reducing to Equation (14) close to the stationary state. Equation (27) shows that close to the steady state, the leading contribution to the mathematical expression for the energy confinement time is provided by the power laws. However, when we deviate from the steady state, supplementary contributions, which are different from the power ones, may modify the mathematical form of the power laws significantly. Generally, for ITER, these contributions tend to lower the numerical value of the energy confinement time. This can be easily checked by setting in Equation (27)  $g(x) \approx \hat{\alpha} \epsilon_1$ , with  $\epsilon_1$  and  $\hat{\alpha}$  denoting a very small parameter and a positive constant having dimension  $[t]^{-1}$ , respectively. By developing expression (27) up to the first order in  $\epsilon_1$ , we find the power laws at the leading order, corrected by a (small) negative expression at the first order in  $\epsilon_1$ .

- **Differential Equation for the Energy Confinement Time Near the Steady State**

The term  $P_{tot}$  is specified as follows

$$P_{tot} = P_\alpha(T) - P_b(T) + P_{aux}(r, t)
 \tag{28}$$

where  $P_\alpha(T)$  is the alpha power,  $P_b(T)$  is the power radiation loss (Bremsstrahlung) and  $P_{aux}$  is the external heating power density supplied to the system (*e.g.* ohmic heating power or external RF), respectively. The alpha power and the Bremsstrahlung power loss depend explicitly on the temperature of the plasma. The auxiliary heating power is operational during both the transient and steady states. This is the dominant source of

external heating power, and it is assumed to be deposited in the plasma with a known profile, independent of  $p$  and  $T$ . Hence,  $P_{Aux} = P_{Aux}(r, t)$ . The time derivative of  $P_{tot}$  reads

$$\dot{P}_{tot} = \frac{\partial P_a}{\partial T} \dot{T} - \frac{\partial P_b}{\partial T} \dot{T} + \dot{P}_{Aux} \quad (29)$$

At the steady state  $\dot{T}(t_0) = 0$  and  $\dot{P}_Q(t_0) = \dot{P}_{Aux}(t_0) = 0$ . Consequently, from the energy balance equation we find that also  $\dot{W}_e(t_0) = 0$ . By taking into account Equations (12) and (24), we get  $g(t) \rightarrow 0$  as the system approaches the steady state. Hence, near the stationary state, we find

$$\begin{cases} \tau_E \ddot{\tau}_E - \dot{\tau}_E^2 \approx \chi(t) \tau_E^2 \\ \tau_E^0 = \frac{W_e^0}{P_{tot}^0}; \quad \dot{\tau}_E^0 = 0 \end{cases} \quad (30)$$

with

$$\chi(t) = -\frac{\ddot{P}_{tot} - \ddot{W}_e}{P_{tot}} = \sum_{i=1}^n \alpha_i \ddot{\xi}_i(t) \approx \chi_0(t - t_0) \quad (31)$$

where Equation (22) has been used. As shown in the Section (2), Equation (30) admits one (and only one) solution, corresponding to the ITER scalings Equation (6). Note that Equation (31) provides the desired relation between the exponent coefficients  $\alpha_i$  and the macroscopic quantities  $P_{tot}$  and  $W_e$ . If we have  $n$  free exponent coefficients  $\alpha_i$ , we can set the following  $n$  relations

$$\sum_{i=1}^n \alpha_i \ddot{\xi}_i(t_k) = -\frac{\ddot{P}_{tot}(t_k) - \ddot{W}_e(t_k)}{P_{tot}(t_k)} \quad \text{with } k = 0, 1, \dots, n-1 \quad (32)$$

Equation (32) link the exponent coefficients with variables which, at least in principle, are under the control of the experimental physicist.

- Analysis in the “Physics” Variables

As mentioned, Equations (1) and (2) are composed by several variables independent of time (*e.g.*, major and minor radii, elongation etc.). In this case, it is more convenient to express the energy confinement time only in terms of the time-dependent variables. Let us suppose that  $m$  variables are time-dependent and the remaining  $n - m$  not. In this case, the energy confinement time takes the form [see Equation (15)]

$$\tau_E = \tau_E^0 \left( \frac{X_1^{\alpha_1}}{X_1^{\alpha_1}(t_0)} \right) \left( \frac{X_2^{\alpha_2}}{X_2^{\alpha_2}(t_0)} \right) \dots \left( \frac{X_n^{\alpha_n}}{X_n^{\alpha_n}(t_0)} \right) \quad (33)$$

where, now, the independent variables  $X_i^{\alpha_i}(t)/X_i^{\alpha_i}(t_0)$  are dimensionless. Note that in this case variables  $\xi_i$  are defined as  $\xi_i = \log(X_i/X_i(t_0))$  (no summation convention over the repeated indexes). Of course, this operation reduces the number of independent variables. However, this number may be reduced further if, instead of “engineering variables”, the confinement time is expressed in terms of “physics” parameters such as  $\rho^*$  (normalized Larmor radius),  $\beta$  (normalized pressure),  $\nu^*$  (collisionality), etc. Indeed, according to the observation of Kadomtsev, the transport in the plasma core should be fundamentally governed by three physical dimensionless plasma parameters  $\rho^*$ ,  $\beta$  and  $\nu^*$  [22]. In this respect, an interesting paper is Ref. [23]. In [23] the authors show that, due to the Kadomtsev constraint, the final expression for the ELMy H-mode thermal confinement time has only one free exponent coefficient, according to the law:

$$\tau_E^{best} = 2\pi \times 10^{-3} I_p \epsilon^{-1} n_e^{\alpha_{n_e}} P^{*(6+8\alpha_n)/15} \quad (34)$$

with  $P^*$  denoting the density of the power loss (*i.e.*,  $P^* \equiv P/V$ ). With the choice  $\alpha_{n_e} = 1/2$ , in “physics” variables, scaling (34) goes as  $\alpha_{\rho^*} = -1$  (*i.e.* a gyro-Bohm-like scaling),  $\alpha_\beta = -0.5$  and  $\alpha_{\nu^*} = 0$ . This choice may be tested by using Equation (32) which, in this particular case, reads

$$15\alpha_{n_e} \ddot{\log} n_{0e} - (6 + 8\alpha_{n_e}) \ddot{\log} P_0^* = -15 \frac{\ddot{P}_{tot} - \ddot{W}_{0e}}{P_{tot}^0} \quad (35)$$

where Equation (33) has been taken into account. We find

$$\alpha_{n_e} = \frac{6P_{tot}^0 \ddot{\log} P_0^* - 15(\ddot{P}_{0tot} - \ddot{W}_{0e})}{P_{tot}^0 \left( 15 \ddot{\log} n_{0e} - 8 \ddot{\log} P_0^* \right)} \quad (36)$$

#### 4. Comparison with the Numerical Simulation of the Balance Equations for an L-Mode Tokamak-Plasma

As an example application, we consider in this Section the case of one of the simplest L-mode Tokamak-plasma where the evolution of the energy confinement time has been estimated by solving numerically the balance equations, completed with a transport model. In [20] we find the profile of  $\tau_E$  against time for Ignitor-plasma. The numerical solution has been obtained by using the code JETTO. To compare this profile with the numerical solution of Equation (21), we should firstly estimate  $t_0$ ,  $\tau_E^0$  and  $\chi_0 = \frac{1}{t_0} \ddot{P}_Q(t_0)/P_{tot}(t_0)$  [see Equation (22)

and (24)]. In [19], we have estimated the values of these parameters for Ignitor subject to ICRH power (*i.e.*,  $P_{Aux} = P_{ICRH}$ ). The scenario is considered where IGNITOR is led to operate in a slightly sub-critical regime by adding a small fraction of  $^3\text{He}$  to the nominal 50 - 50 Deuterium-Tritium mixture. The difference between power lost and alpha heating is compensated by an additional ICRH power equal to 1.46 MW, which should be able to increase the global plasma temperature via collisions between  $^3\text{He}$  minority and the background  $D-T$  ions. The analytical expression for the ICRH power profiles inside the plasma has been deduced by fitting the numerical results giving an expression for  $P_{Aux} = P_{ICRH}(r)$ , which is essentially independent of the bulk temperature. Denoting the ICRH power-density as  $P_{ICRH}^*$ , we have

$$P_{ICRH}^*(r) = P_{0ICRH}^* \exp\left[\tilde{\alpha}_2 B(r_{ICRH})/B_{0\phi}\right] \exp\left[-(r-r_{ICRH})^2/\Delta\right] \quad (37)$$

with  $P_{0ICRH}^* = 6.59126 \times 10^{-6} \text{ MW/m}^3$ ,  $\tilde{\alpha}_2 = 15.3478$  and  $\Delta = 0.0477032$ , respectively.

The value of  $\tau_E^0$  has been estimated by the expression [19]

$$\tau_E^0 = \frac{12n_e T}{E_\alpha n_e^2 \langle \sigma v \rangle_{D-T} - 4C_B n_e^2 T^{1/2} + 4P_{ICRH}^*} \quad (38)$$

with  $E_\alpha$  and  $C_B$  denoting the energy at which the alpha particles are created (3.5 MeV), and the Bremsstrahlung constant, respectively.  $\sigma$  is the reaction cross section giving a measure of the probability of a fusion reaction as a function of the relative velocity of the two reactant nuclei.  $\langle \sigma v \rangle_{D-T}$  provides an average over the distributions of the product of cross section and velocity  $v$ . In the core of the plasma we found [19]  $\tau_E^0 = 0.43 \text{ sec}$ ,  $t_0 = 3.5 \text{ sec}$  and  $\chi_0 = 0.171429 \text{ sec}^{-3}$ . **Figure 1** reports on the energy confinement time,  $\tau_E$ , against time for Ignitor-plasmas in the above mentioned conditions. The profiles have been obtained by solving (with the code JETTO) the balance equations and refer to the ITER scalings ITER97L (full dots), ITER97L\* (open dots) and ITER97L [20]. **Figure 2** shows the solutions of the differential equation for the ITER scalings, Equation (21), at the three values of  $(t_0, \tau_E^0)$ :  $(t_0, \tau_E^0) = (0.35 \text{ sec}, 0.43 \text{ sec})$  (ITER97L-blue line),  $(t_0, \tau_E^0) = (0.35 \text{ sec}, 0.625 \text{ sec})$  (ITER97L\* -green line) and  $(t_0, \tau_E^0) = (0.35 \text{ sec}, 0.825 \text{ sec}) =$  (ITER97L(P\_red)-brown line).

Note that in [20] the authors evaluate the ITER scalings by using the reduced power  $P_{red} = P_{tot} - P_{RadTot}$ , whereas in our work we use  $P_{tot}$ , which includes the Bremsstrahlung radiation loss. This may explain the little difference between the numerical [20] and the analytical slopes.

#### 5. Conclusions

A large database on plasma energy confinement in Tokamaks can be summarized in single empirical value of  $\tau_E$ , referred to as the ITER-scalings. These expressions are ‘‘Universal’’, in the sense that they apply to a large number of Tokamaks. Scalings are expressed in terms of product of powers of independent variables [see Equation (14)] and correspond to the L-mode as well as the H-mode confinements. The recommended scaling for ITER operation remains the IPB98 scaling law, while this issue is further investigated. In this work we have shown that the ITER scalings satisfy a general non-linear differential equation of second order in time. The

value provided by the database for ITER scaling laws, coincides with  $\tau_E^0$ , estimated by Equation (4), with  $W_{estat.}$  and  $P_{Qstat.}$  evaluated by solving the stationary balance equations. To estimate the dynamic confinement

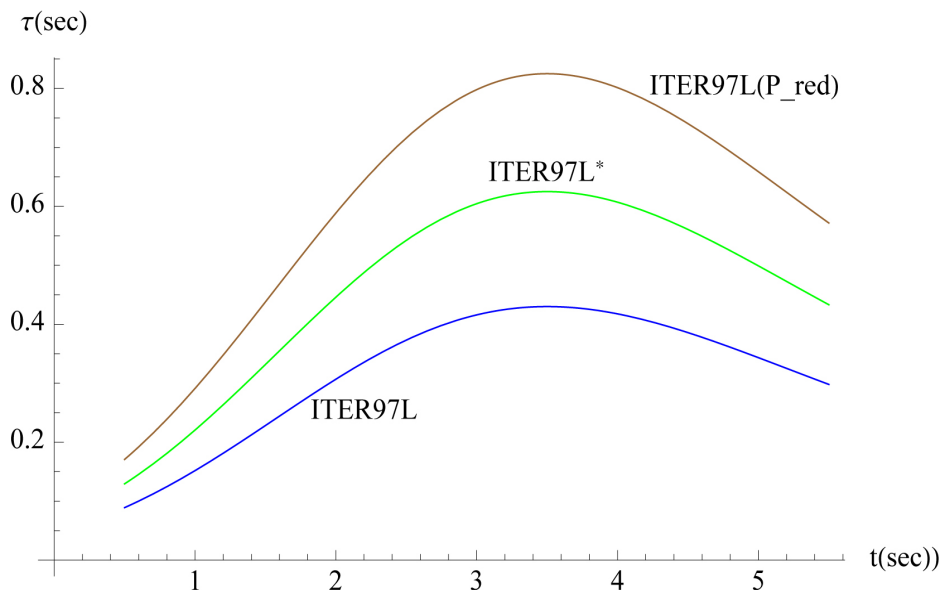


**Figure 1.** Solutions of Equation (21) at the three values of  $(\tau_E^0, t_0)$ . Blue line:  $(t_0, \tau_E^0) = (0.35 \text{ sec}, 0.43 \text{ sec})$  (ITER97L), green line:  $(t_0, \tau_E^0) = (0.35 \text{ sec}, 0.625 \text{ sec})$  (ITER97L\*) and Brown line:  $(t_0, \tau_E^0) = (0.35 \text{ sec}, 0.825 \text{ sec})$  (ITER97L(P\_red)).

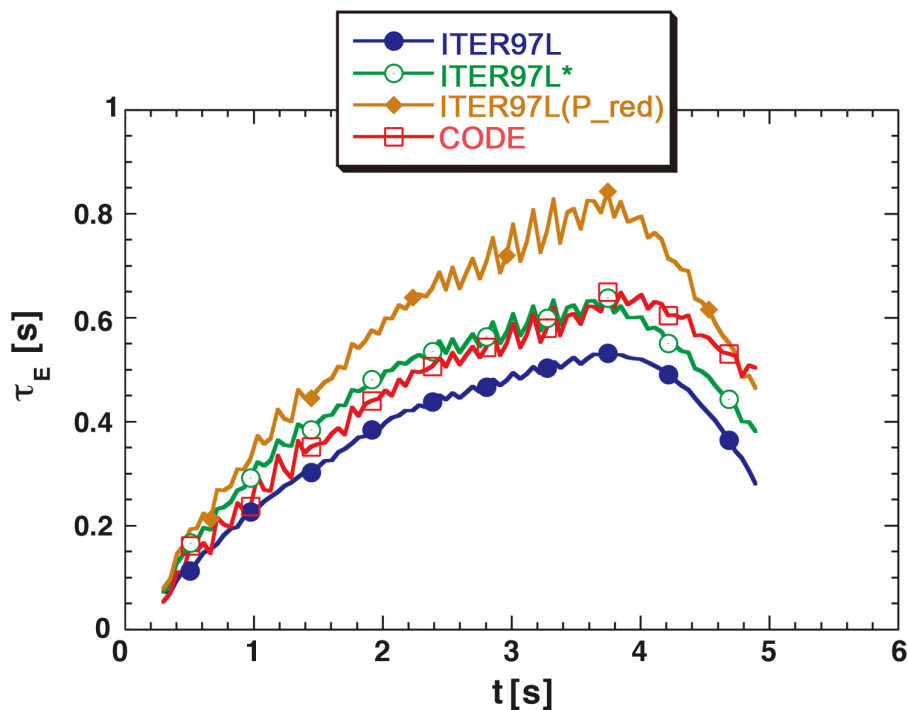


**Figure 2.** Energy confinement time evolution estimated in [20] by solving with JETTO the balance equations (completed with a transport model): ITER97L scaling (full dots-blue line), ITER97L\* scaling (open dots-green line) and ITER97L(P\_red) scaling (brown line).

time, we determined the differential equation for  $\tau_E$  by combining the energy balance equation with definition (3). We found Equations (25). We have solved this equation by taking into account that, in vicinity of the steady state, the coefficient  $g(t)$  tends to vanish and, at the leading order,  $f(t)$  is (almost) a constant independent of time, which may be evaluated at the stationary state. This is the real advantage of the proposed approach: *close to the steady state, the differential equation for the energy confinement time  $\tau_E$  reduces to*

$$\begin{cases} \tau_E \ddot{\tau}_E - \dot{\tau}_E^2 = \chi(t) \tau_E^2 \\ \tau_E^0 = \frac{W_e^0}{P_{tot}^0}; \quad \dot{\tau}_E = 0 \end{cases}$$

where “at the leading order”  $\chi(t)$  is a numerical constant, which may be estimated at the stationary state. As a result, one may approximate  $\chi(t)$  to be a constant,  $\chi_0$  or better, by a linear function  $\chi(t) = \chi_0(t - t_0)$ . In this sense, all of the dependence on the machine is reduced to just a number,  $\chi_0$ , which can be estimated at the steady state. Far from the stationary state the differential equation for  $\tau_E$  contains a nonlinear extra term, which behaves as  $\sim \tau_E \dot{\tau}_E$ . This extra term tends to modify the mathematical form of the power laws. For ITER, the main effect of this nonlinear extra term is to lower the numerical value of the energy confinement time. The general solution is given by Equation (27), which reduces to the one admitting the ITER scaling power laws as the system approaches the steady state. We have also seen that the scaling coefficients may be linked to the variables which, at least in principle, are under the control of the experimental physicist. The validity of our approach has been tested by analyzing a concrete example of Tokamak-plasma where the profile of the energy confinement time has been previously determined by solving the balance equations (with the *auxilium* of a transport model). The solution of the differential equation for the ITER scaling is in a fairly agreement with the numerical finding.

## Acknowledgements

Giorgio Sonnino is very grateful to Dr Philippe Peeters for his useful suggestions. Jarah Evslin is supported by NSFC MianShang grant 11375201. The reproduction of Figure 2, reported in Ref. [20], has been authorized by the review Nuclear Fusion (IoP).

## References

- [1] Kardaun, O.J.W.F. (2005) *Classical Methods of Statistics: With Applications in Fusion-Oriented Plasma Physics*. Springer Science & Business, Heidelberg.
- [2] Tsunematsu, T. (1991) *Fusion Engineering and Design*, **15**, 309. [http://dx.doi.org/10.1016/0920-3796\(92\)90016-W](http://dx.doi.org/10.1016/0920-3796(92)90016-W)
- [3] Doyle, E.J., Houlberg, W.A., Kamada, Y., Mukhovatov, V., Osborne, T.H., Polevoi, A., Bateman, G., Connor, J.W., Cordey, J.G., Fujita, T., Garbet, X., Hahn, T.S., Horton, L.D., Hubbard, A.E., Imbeaux, F., Jenko, F., Kinsey, J.E., Kishimoto, Y., Li, J., Luce, T.C., Martin, Y., Ossipenko, M., Parail, V., Peeters, A., Rhodes, T.L., Rice, J.E., Roach, C.M., Rozhansky, V., Ryter, F., Saibene, G., Sartori, R., Sips, A.C.C., Snipes, J.A., Sugihara, M., Synakowski, E.J., Takenaga, H., Takizuka, T., Thomsen, K., Wade, M.R. and Wilson, H.R., ITPA Pedestal (2007) *Nuclear Fusion*, **47**, S18.
- [4] Wagner, F. (2009) The Physics Basis of ITER Confinement. 2nd ITER Int. Summer School (Kyushu University, Japan, 2009) (New York: AIP) *AIP Conf. Proc.*, **31**, 1095. <http://dx.doi.org/10.1063/1.3097319>
- [5] ITER Physics Expert Groups on Confinement and Transport and Confinement Modelling and Database, ITER Physics Basis Editors and ITER EDA, Naka Joint Work Site, Mukouyama, Naka-machi, Naka-gun, Ibaraki-Ken, Japan (1999) *Nuclear Fusion*, **39**, 2137.
- [6] Luce, T.C., Petty, C.C. and Cordey, J.G. (2008) *Plasma Physics and Controlled Fusion*, **50**, 043001.
- [7] Kadomtsev, B.B. (1975) *Soviet Journal of Plasma Physics*, **1**, 295.
- [8] Kritz, A.H., Kinsey, J., Onjun, T., Voitsekhovich, I., Bateman, G., Waltz, R. and Staebler, G. (2001) Burning Plasma Projections with Internal Transport Barriers. *ITPA Meeting on Burning Plasma Transport, NIFS*, Tokio, 10-12 September 2001, 964-974.
- [9] Weiland, J. (2001) Predictive Simulations of ITER-FEAT Performance. *28th EPS Conference*, Madeira, 18-22 June 2001, P2.039.
- [10] Bateman, G., Kritz, A.H., Onjun, T. and Pankin, A. (2001) Private Communication, 7 Dec.

- [11] Cordey, J.-G. (1997) *Plasma Physics and Controlled Fusion*, **39**, B115. <http://dx.doi.org/10.1088/0741-3335/39/12B/009>
- [12] Scaling Law, FusionWiki, jointly hosted by LNF and FuseNet. It is associated with two domains: fusionwiki.ciemat.es ([http://fusionwiki.ciemat.es/wiki/Scaling\\_law](http://fusionwiki.ciemat.es/wiki/Scaling_law)) and wiki.fusetnet.eu.
- [13] Kardaun, O. (2002) *Nuclear Fusion*, **42**, 841. <http://dx.doi.org/10.1088/0029-5515/42/7/307>
- [14] Cordey, J.G., Snipes, J.A., Greenwald, M., Sugiyama, L., Kardaun, O.J.W.F., Ryter, F., Kus, A., Stober, J., DeBoo, J.C., Petty, C.C., Bracco, G., Romanelli, M., Cui, Z., Liu, Y., Cordey, J.G., Thomsen, K., McDonald, D.C., Miura, Y., Shinohara, K., Tsuzuki, K., Kamada, Y., Takizuka, T., Urano, H., Valovic, M., Akers, R., Brickley, C., Sykes, A., Walsh, M.J., Kaye, S.M., Bush, C., Hogewei, D., Martin, Y., Cote, A., Pacher, G., Ongena, J., Imbeaux, F., Hoang, G.T., Lebedev, S., Chudnovskiy, A. and Leonov, V. (2004) *IAEA 20th Fusion Energy Conference*, Vilamoura, paper IAEA-CN-116/IT/P3-32.
- [15] Yushmanov, P.N., Takizuka, T., Riedel, K.S., Kardaun, O.J.W.F., Cordey, J.G., Kaye, S.M. and Post, D.E. (1990) *Nuclear Fusion*, **30**, 1999. <http://dx.doi.org/10.1088/0029-5515/30/10/001>
- [16] Kaye, S.M., Greenwald, M., Stroth, U., Kardaun, O., Kus, A., Schissel, D., DeBoo, J., Bracco, G., Thomsen, K., Cordey, J.G., Miura, Y., Matsuda, T., Tamai, H., Takizuda, T., Hirayama, T., Kikuchi, H., Naito, O., Chudnovskij, A., Ongena, J. and Hoang, G. (1997) *Nuclear Fusion*, **37**, 1303. <http://dx.doi.org/10.1088/0029-5515/37/9/110>
- [17] Dinklage, A., Maaßberg, H., Preuss, R., Turkin, Yu.A., Yamada, H., Ascasibar, E., Beidler, C.D., Funaba, H., Harris, J.H., Kus, A., Murakami, S., Okamura, S., Sano, F., Stroth, U., Suzuki, Y., Talmadge, J., Tribaldos, V., Watanabe, K.Y., Werner, A., Weller, A. and Yokoyama, M. (2007) *Nuclear Fusion*, **47**, 1265.
- [18] Yamada, H., Harris, J.H., Dinklage, A., Ascasibar, E., Sano, F., Okamura, S., Stroth, U., Kus, A., Talmadge, J., Murakami, S., Yokoyama, M., Beidler, C.D., Tribaldos, V. and Watanabe, K.Y. (2004) *31st EPS Conference on Plasma Physics*, London, 28 June-2 July 2004, ECA Vol. 28G, 5.099.
- [19] Cardinali, A. and Sonnino, G. (2014) Analysis of the Thermonuclear Instability Including Low-Power ICRH Minority Heating in IGNITOR. Submitted for publication in *EPJD*.
- [20] Airoidi, A. and Cenacchi, G. (2001) *Nuclear Fusion*, **41**, 687. <http://dx.doi.org/10.1088/0029-5515/41/6/303>
- [21] Balescu, R. (1988) *Transport Process in Plasmas—Vol. II*. Elsevier Science Publication, North-Holland.
- [22] Kadomtsev, B.B. (1975) *Soviet Journal of Plasma Physics*, **1**, 295.
- [23] Sauter, O. and Martin, Y. (2000) *Nuclear Fusion*, **40**, 955. <http://dx.doi.org/10.1088/0029-5515/40/5/308>



**Submit or recommend next manuscript to SCIRP and we will provide best service for you:**

Accepting pre-submission inquiries through Email, Facebook, LinkedIn, Twitter, etc.

A wide selection of journals (inclusive of 9 subjects, more than 200 journals)

Providing 24-hour high-quality service

User-friendly online submission system

Fair and swift peer-review system

Efficient typesetting and proofreading procedure

Display of the result of downloads and visits, as well as the number of cited articles

Maximum dissemination of your research work

Submit your manuscript at: <http://papersubmission.scirp.org/>

# Joule-Lenz Energy of Quantum Electron Transitions Compared with the Electromagnetic Emission of Energy

Stanisław Olszewski

Institute of Physical Chemistry, Polish Academy of Sciences Kasprzaka, Warsaw, Poland  
Email: [olsz@ichf.edu.pl](mailto:olsz@ichf.edu.pl)

Received 4 July 2016; accepted 19 August 2016; published 22 August 2016

Copyright © 2016 by author and Scientific Research Publishing Inc.  
This work is licensed under the Creative Commons Attribution International License (CC BY).  
<http://creativecommons.org/licenses/by/4.0/>



Open Access

---

## Abstract

In the first step, the Joule-Lenz dissipation energy specified for the electron transitions between two neighbouring quantum levels in the hydrogen atom has been compared with the electromagnetic energy of emission from a single level. Both the electric and magnetic vectors entering the Poynting vector of the electromagnetic field are referred to the one-electron motion performed along an orbit in the atom. In the next step, a similar comparison of emission rates is performed for the harmonic oscillator. Formally a full agreement of the Joule-Lenz and electromagnetic expressions for the energy emission rates has been attained.

## Keywords

Joule-Lenz Energy, Quantum Electron Transitions, Hydrogen Atom, Electromagnetic Energy Emission

---

## 1. Introduction

Usually any calculation of the emission rate of energy in the atom has as its background a rather complicated statistical-and-probabilistic theory. This situation seems to be not changed much since the very end of the nineteenth and beginning of twentieth century [1]-[3]. In practice an individual atomic system has been never considered, but instead of it an ensemble of the oscillating atoms known as the black body was examined. Rather automatically the temperature parameter—important for comparing the theoretical results with experiment—has been involved in such many-atomic calculations. Next the probabilistic approach to the emission intensity found its justification, and a rather extended though complicated application, in quantum mechanics [4] [5].

More recently an approach to the treatment of the energy emission in a single atomic object could be based on

the Joule-Lenz law [6]-[10]. For, when the Bohr theory of the hydrogen atom is taken as an example, any atom has its electron placed on a definite orbit which can be approximated by a circle. Electrically such a circular motion can be represented by a current having a known intensity. For example, for the quantum states  $n$  and  $n+1$  the current intensity is respectively

$$i_n = \frac{e}{T_n} \quad \text{and} \quad i_{n+1} = \frac{e}{T_{n+1}}, \quad (1)$$

where  $T_n$  and  $T_{n+1}$  are the time periods of the electron circulation about the proton nucleus. In the next step, the energy difference between levels  $n+1$  and  $n$ , namely

$$\Delta E = E_{n+1} - E_n, \quad (2)$$

provides us with the electric potential

$$V = \frac{\Delta E}{e}. \quad (3)$$

This leads to the electric resistance

$$R = \frac{V}{i} \approx \frac{V}{i_n} \approx \frac{V}{i_{n+1}} \quad (4)$$

where the approximate relations in (4) hold in virtue of

$$i \approx i_n \approx i_{n+1} \quad (5)$$

valid for large  $n$ . The validity of (5) becomes evident if we apply Formula (7) in (1).

For such large  $n$  we have [11] the energy change

$$\Delta E = -\frac{me^4}{2\hbar^2} \left[ \frac{1}{(n+1)^2} - \frac{1}{n^2} \right] = \frac{me^4}{2\hbar^2} \frac{(n+1)^2 - n^2}{(n+1)^2 n^2} \approx \frac{me^4}{\hbar^2 n^3}; \quad (6)$$

in the last step of (6) the approximation of large  $n$  is considered.

Since [11]

$$T_n = \frac{2\pi n^3 \hbar^3}{e^4 m}, \quad (7)$$

we obtain

$$R = \frac{V}{i_n} = \frac{\Delta E}{ei_n} = \frac{\Delta E T_n}{e^2} \approx \frac{me^4}{\hbar^2 n^3} \frac{1}{e^2} \frac{2\pi n^3 \hbar^3}{e^4 m} = \frac{2\pi \hbar}{e^2} = \frac{h}{e^2}; \quad (8)$$

this is a constant independent of  $n$ . The same value of  $R$  can be calculated also for other quantum systems than the hydrogen atom, see [6] [7] [10]. A characteristic point is that  $R$  is equal to a well-known result of experiments done on the integer quantum Hall effect [12].

The Joule-Lenz law is represented by the well-known relation

$$\frac{\Delta E}{\Delta t} = Ri^2 \quad (9)$$

where  $\Delta t$  is the time interval necessary to produce the emitted energy  $\Delta E$ . In fact (9) implies that for  $i = i_n$  we have

$$\Delta t = \frac{\Delta E}{Ri_n^2} = \frac{me^4}{\hbar^2 n^3} \frac{e^2}{h} \left( \frac{T_n}{e} \right)^2 = \frac{me^4}{\hbar^2 n^3} \frac{e^2}{h} \frac{1}{e^2} \left( \frac{2\pi n^3 \hbar^3}{e^4 m} \right)^2 = \frac{2\pi}{me^4} \frac{2\pi}{h} n^3 \hbar^4 = \frac{2\pi n^3 \hbar^3}{me^4} = T_n. \quad (10)$$

Moreover from (6) and (10) we obtain

$$\Delta E \Delta t = \frac{me^4}{\hbar^2 n^3} \frac{2\pi n^3 \hbar^3}{me^4} = 2\pi \hbar = h \quad (11)$$

or

$$\Delta t = \frac{h}{\Delta E}. \quad (12)$$

Therefore the ratio (9) becomes

$$\frac{\Delta E}{\Delta t} = \frac{(\Delta E)^2}{h} = \left( \frac{me^4}{\hbar^2 n^3} \right)^2 \frac{1}{h} = \frac{m^2 e^8}{2\pi n^6 \hbar^5}. \quad (13)$$

Results similar to (10)-(12) can be obtained also for other quantum systems than the hydrogen atom [6] [7] [10].

The principal aim of the paper is, in the first step, to compare the ratio calculated in (13) with the rate of energy emission obtained in terms of the electromagnetic theory. Next, in order to compare the quantum emission with the classical emission rate, the properties of the harmonic oscillator emission are also studied.

## 2. Fields Induced by the Electron Motion in the Hydrogen Atom

The electric field value  $|\mathbf{E}_n|$  acting on the electron in the Bohr atom is well known:

$$|\mathbf{E}| = |\mathbf{E}_n| = \frac{e}{r_n^2} = \frac{e^5 m^2}{\hbar^4 n^4}. \quad (14)$$

The last step in (14) is attained because of the radius of the orbit  $n$  which is [11]

$$r_n = \frac{\hbar^2 n^2}{me^2}. \quad (15)$$

A less-known magnetic field omitted in the Bohr atomic model [10] is induced in the hydrogen atom due to the circular electron motion done with the frequency

$$\Omega_n = \frac{2\pi}{T_n}. \quad (16)$$

Because of the formula (see e.g. [13])

$$\Omega_n = \frac{eH_n}{mc}, \quad (17)$$

the identity between (16) and (17) combined with (7) gives

$$|\mathbf{H}_n| = H_n = \frac{e^3 m^2 c}{\hbar^3 n^3}. \quad (18)$$

A characteristic point is that when expressions for  $E_n$  and  $H_n$  are substituted to the Lorentz force

$$\mathbf{F}_n = e\mathbf{E}_n + \frac{e}{c}[\mathbf{v}_n \times \mathbf{H}_n], \quad (19)$$

we obtain for the electric component of (19)

$$e|\mathbf{E}_n| = \frac{e^2}{r_n^2} = \frac{e^2}{n^4 \hbar^4} m^2 e^4 = \frac{m^2 e^6}{n^4 \hbar^4} \quad (20)$$

and the same value is obtained for the magnetic component of (19)

$$\frac{e}{c}|\mathbf{v}_n \times \mathbf{H}_n| = \frac{e}{c}v_n H_n = \frac{e e^2}{c n \hbar} \frac{e^3 m^2 c}{n^3 \hbar^3} = \frac{m^2 e^6}{n^4 \hbar^4}, \quad (21)$$

on condition the vector of the electron velocity having the value [11]

$$v_n = \frac{e^2}{n\hbar} \quad (22)$$

is normal to  $H_n$ .

### 3. Field Values Specific for the One-Electron Current Present in the Atom and the Electromagnetic Rate of the Energy Emission

Our aim is to construct the Poynting vector which provides us with the electromagnetic dispense of energy. The vectors  $\mathbf{E}$  and  $\mathbf{H}$  become slightly different than in Section 2 because they refer to the current behaviour of the electron which is circulating along its orbit. With the potential  $V$  given in (3) and (6) and equal to

$$V = \frac{me^3}{\hbar^2 n^3}, \quad (23)$$

the electric field on the orbit having the length

$$l_n = 2\pi r_n \quad (24)$$

attains the value [16]

$$|\mathbf{E}_{\text{orbit } n}| = \frac{V}{2\pi r_n} = \frac{1}{2\pi} \frac{me^3}{\hbar^2 n^3} \frac{me^2}{n^2 \hbar^2} = \frac{1}{2\pi n^5} \frac{m^2 e^5}{\hbar^4}. \quad (25)$$

This gives an electric vector directed along the current.

On the other hand the magnetic field directed normally to the current attains the value [14] [16]

$$|\mathbf{H}_{\text{orbit } n}| = \frac{2i_n}{cr_e} = \frac{2e}{T_n cr_e} = \frac{2e}{2\pi n^3} \frac{e^4 m mc^2}{\hbar^3 e^2} = \frac{e^3 m^2 c}{\pi \hbar^3 n^3}. \quad (26)$$

This field differs from that given in (18) solely by the factor equal to  $1/\pi$ .

It should be noted that parameter  $r_e$  entering (26) is the radius of the circular cross-section area of the orbit assumed to be equal to the cross-section of the electron microparticle considered as a sphere [15] [17]:

$$r_e \cong \frac{e^2}{mc^2}. \quad (27)$$

The value of the Poynting vector emanating the energy from the orbit is calculated according to the formula [14]

$$\begin{aligned} |\mathbf{S}_n^p| &= \frac{c}{4\pi} |\mathbf{E}_{\text{orbit } n} \times \mathbf{H}_{\text{orbit } n}| S_{\text{orbit}} = \frac{c}{4\pi} |\mathbf{E}_{\text{orbit } n}| |\mathbf{H}_{\text{orbit } n}| S_{\text{orbit}} \\ &= \frac{c}{4\pi} \frac{1}{2\pi n^5} \frac{m^2 e^5}{\hbar^4} \frac{1}{\pi} \frac{e^3 m^2 c}{\hbar^3 n^3} 2\pi \frac{n^2 \hbar^2}{m e^2} 2\pi \frac{e^2}{m c^2} = \frac{m^2 e^8}{2\pi n^6 \hbar^5} \end{aligned} \quad (28)$$

where

$$S_{\text{orbit}} = 2\pi r_n 2\pi r_e = 4\pi^2 r_n r_e \quad (29)$$

is the toroidal surface of the orbit having the length (24) and the length of the cross-section circumference of the orbit is equal to

$$2\pi r_e. \quad (30)$$

In effect we obtain from (23), (26) and (28) the result precisely equal to Formula (13) calculated from the Joule-Lenz theory. Since (13) assumed the electron transitions solely between the levels

$$n+1 \rightarrow n, \quad (31)$$

the identity between (13) and (28) implies that the limitation to transition (31) applies also to the electromagnetic result calculated in (28).

A problem may arise to what extent the energy rate (13), or (28), can be radiated as an electromagnetic wave. An alternative behaviour is that the energy  $\Delta E$  is spent for a mechanical rearrangement of the electron position due to the transition process. An argument for that is the presence of the electric force

$$e |\mathbf{E}_{\text{orbit } n}| = \frac{1}{2\pi n^5} \frac{m^2 e^6}{\hbar^4} \quad (32)$$

along the orbit. The force (32) multiplied by the orbit length calculated in (24) gives

$$l_n e |E_{\text{orbit } n}| = 2\pi \frac{n^2 \hbar^2}{m e^2} \frac{1}{2\pi n^5} \frac{m^2 e^6}{\hbar^4} = \frac{m e^4}{\hbar^2 n^3} \quad (33)$$

which is precisely the energy  $\Delta E$  of the electron transition obtained in (6).

#### 4. Quantum and Classical Emission Rate Calculated for the Harmonic Oscillator

A natural tendency is to compare the quantum rate of the energy emission with the classical emission rate. To this purpose the one-dimensional harmonic oscillator has been chosen as a suitable object of examination.

The classical energy of the oscillator is

$$E_{\text{osc}} = \frac{k a^2}{2}, \quad (34)$$

$a$  is the oscillator amplitude;  $m$  is the oscillator mass which together with the force constant  $k$  refers to the circular frequency of the oscillator

$$\omega = \left( \frac{k}{m} \right)^{1/2} = \frac{2\pi}{T}; \quad (35)$$

$T$  is the oscillation period [18].

The quantum oscillator energy is

$$E_n = \left( n + \frac{1}{2} \right) \hbar \omega \cong n \hbar \omega \quad (36)$$

(the last step holds for large  $n$ ) and the change of energy due to transition between the levels  $n+1$  and  $n$  is

$$\Delta E = \hbar \omega. \quad (37)$$

According to the Joule-Lenz approach to the quanta [6]-[10] the emission rate between the levels  $n+1$  and  $n$  is

$$\frac{\Delta E}{\Delta t} = \frac{(\Delta E)^2}{h} = \frac{(\hbar \omega)^2}{h}. \quad (38)$$

This gives

$$\frac{1}{\Delta t} = \frac{\Delta E}{h} = \frac{\hbar \omega}{h} = \frac{h\nu}{h} = \nu = \frac{1}{T}, \quad (39)$$

so

$$\Delta t = T, \quad (40)$$

because the reference between  $\omega$  and  $\nu$  is

$$\omega = 2\pi\nu. \quad (41)$$

The potential  $V$  connected with the energy change  $\Delta E$  is

$$V = \frac{\Delta E}{e} = \frac{\hbar \omega}{e}. \quad (42)$$

If we note that a maximal distance travelled by the electron oscillator in one direction is

$$l = 2a, \quad (43)$$

the electric field connected with the oscillator parallel to its motion is

$$|E| = \frac{V}{l} = \frac{V}{2a} = \frac{\hbar \omega}{2ae}. \quad (44)$$

The electric current let be considered as remaining approximately constant in course of the oscillation. In this case the magnetic field which is normal to the current [see (26)] is

$$|\mathbf{H}| = \frac{2i}{cr_e} = \frac{2e}{Tcr_e} = \frac{2e}{Tc} \frac{mc^2}{e^2} = \frac{2mc}{Te} = \frac{2mcv}{e}, \quad (45)$$

since the cross-section of the electron current is assumed to be identical with the cross-section area of the electron microparticle, see (27).

The surface area of the sample containing the oscillator is

$$S = 2\pi r_e l = 4\pi r_e a = 4\pi \frac{e^2}{mc^2} a, \quad (46)$$

on condition the contribution of the end areas of the sample surface equal to

$$2\pi r_e^2 = 2\pi \left( \frac{e^2}{mc^2} \right)^2 \ll 4\pi \frac{e^2}{mc^2} a \quad (47)$$

has been neglected because (47) is a small number in comparison with  $S$  in (46).

In consequence, for the vector  $\mathbf{H}$  normal to vector  $\mathbf{E}$  the value of the Poynting vector becomes

$$|\mathbf{S}^p| = \frac{c}{4\pi} |\mathbf{E}| |\mathbf{H}| S = \frac{c}{4\pi} \frac{\hbar\omega}{2ae} \frac{2mc}{Te} 4\pi \frac{e^2}{mc^2} a = \frac{4\pi\hbar\omega}{4\pi T} = \frac{\Delta E}{T}. \quad (48)$$

This is a result identical with (38) on condition Formula (39) is taken into account.

According to the classical electrodynamics [19] the emission rate of energy from a classical oscillator is

$$\frac{dE}{dt} = \frac{2}{3} \frac{\omega^4}{c^3} |p|^2 = \frac{2}{3} \left( \frac{2\pi}{T} \right)^4 \frac{e^2 a^2}{c^3} \quad (49)$$

since

$$p = ea \quad (50)$$

is the dipole moment of the classical harmonic oscillator. Formula (49) can be compared with the quantum approach to the Joule-Lenz emission rate of energy [see (38)]:

$$\frac{\Delta E}{\Delta t} = \frac{(\hbar\omega)^2}{h} = \left( \frac{h}{T} \right)^2 \frac{1}{h} = \frac{h}{T^2}. \quad (51)$$

In the case of very small quantum systems the amplitude  $a$  in (49) can be close to its minimal length [10]

$$a \cong \frac{\hbar}{mc} \quad (52)$$

and the time period  $T$  can approach its minimal size [10]

$$T \cong \frac{\hbar}{mc^2}. \quad (53)$$

The equality required between (49) and (51) leads to the relation

$$\frac{2}{3} \left( \frac{2\pi}{T} \right)^4 \frac{e^2 a^2}{c^3} = \frac{h}{T^2}. \quad (54)$$

When  $a$  and  $T$  are taken respectively from (52) and (53), Formula (54) becomes

$$\frac{2}{3} \frac{(2\pi)^4}{\left( \frac{\hbar}{mc^2} \right)^2} \cdot \frac{e^2 \left( \frac{\hbar}{mc} \right)^2}{c^3} = \frac{2}{3} \frac{(2\pi)^4 e^2}{c^{-2} c^3} = \frac{2}{3} \frac{(2\pi)^4 e^2}{c} = h \quad (55)$$

from which we have the relation

$$\frac{2}{3} (2\pi)^3 \approx 165 = \frac{\hbar c}{e^2} = \frac{1}{\alpha}. \quad (56)$$

The result obtained in (56) differs by only 20 percent from the reciprocal value of the atomic constant equal to 137.

## 5. Ratio of the Classical and Quantum Emission Rate Defined by the Damping Coefficient of the Classical Radiation

An attempt of this Section is to demonstrate that the classical emission can be considered as a damped quantum emission rate. The classical damping coefficient of the oscillator is [19]

$$\gamma = \frac{2}{3} \frac{e^2}{mc^3} \omega^2. \quad (57)$$

On the other hand, the classical emission rate given in (49) can be modified when the amplitude  $a$  entering (49) is expressed in terms of the oscillator energy  $E$  [18]:

$$a^2 = \frac{2E}{k} = \frac{2E}{m\omega^2} = \frac{2n\hbar\omega}{m\omega^2} = \frac{2n\hbar}{m\omega}. \quad (58)$$

Here, at the end of (58), the energy  $E$  is replaced by the approximate quantum formula for the oscillator energy given in (36). In effect the classical emission rate in (49) becomes

$$\eta^{\text{class}} = \frac{2}{3c^3} \omega^4 e^2 a^2 = \frac{2}{3c^3} \omega^4 e^2 \frac{2n\hbar}{m\omega} = \frac{4e^2}{3c^3} \frac{\omega^3}{m} n\hbar. \quad (59)$$

Another transformation may concern the quantum emission rate in (51):

$$\eta^{\text{quant}} = \frac{\Delta E}{\Delta t} = \frac{h}{T^2} = \left(\frac{2\pi}{T}\right)^2 \frac{h}{(2\pi)^2} = \frac{\omega^2 \hbar}{2\pi}. \quad (60)$$

As a result of (59) and (60) we obtain the ratio

$$\frac{\eta^{\text{class}}}{\eta^{\text{quant}}} = \frac{4}{3} \frac{e^2}{c^3} \frac{\omega^3}{m} n\hbar : \frac{\omega^2 \hbar}{2\pi} = \frac{8\pi}{3} \frac{e^2}{c^3} \frac{\omega}{m} n = 4\pi \frac{2}{3} \frac{e^2 \omega^2}{c^3 m} \frac{n}{\omega} = 4\pi \gamma \frac{n}{\omega} = 2nT\gamma \quad (61)$$

which is proportional to  $\gamma$  in (57). A multiple of the oscillation time period  $T$  is the proportionality coefficient representing (61) in terms of  $\gamma$ . Therefore another way to write (61) can be

$$\eta^{\text{class}} = 2nT\gamma\eta^{\text{quant}}. \quad (62)$$

Let us note that  $E_n$  entering (36) and (58) is proportional to  $n$ .

It is worth to note that the Einstein coefficient  $A_n^{n-\alpha}$  of the emission probability can be coupled with  $\gamma$  by the relation [20]

$$A_n^{n-\alpha} h\nu = \gamma f_{n,n-\alpha} h\nu \quad (63)$$

so

$$A_n^{n-\alpha} = \gamma f_{n,n-\alpha}. \quad (64)$$

According to Heisenberg [20] [21] we have

$$\left| a(n, n-1) \right|^2 \nu(n, n-1) = \frac{n\hbar}{\pi m \omega_0} \nu(n, n-1) = \frac{h}{8\pi^2 m} f_{n,n-1} \quad (65)$$

where  $a$  is the quantum-theoretical amplitude of the expansion of the coordinate  $x = x(t)$  of an anharmonic oscillator;  $\omega_0$  is the circular frequency of the harmonic oscillator.

For small perturbation  $\lambda$  of the oscillator we have [21]

$$\omega = 2\pi \nu(n, n-1) \approx \omega_0, \quad (66)$$

so Formula (65) gives

$$\frac{n\hbar\omega}{2\pi^2 m \omega_0} \cong \frac{n\hbar\omega_0}{2\pi^2 m \omega_0} = \frac{n\hbar}{2\pi^2 m} = \frac{h}{8\pi^2 m} f_{n,n-1} \quad (67)$$

or

$$4n = f_{n,n-1}. \quad (68)$$

In effect for  $\alpha = 1$  taken in (63) we obtain from (64) and (68):

$$A_n^{n-1} = \gamma f_{n,n-1} = 4n\gamma. \quad (69)$$

If  $\gamma$  is presented, according to (61), in terms of the ratio of  $\eta^{\text{class}}$  and  $\eta^{\text{quant}}$ , we obtain

$$A_n^{n-1} = \frac{4n}{2nT} \frac{\eta^{\text{class}}}{\eta^{\text{quant}}} = \frac{2}{T} \frac{\eta^{\text{class}}}{\eta^{\text{quant}}}, \quad (70)$$

where  $T$  is the oscillation time period of the harmonic oscillator.

## 6. Reciprocal Value of the Atomic Constant and the Electron Spin

The reciprocal value  $\alpha^{-1}$  of the atomic constant ( $\sim 137$ ) approached in (56) is important in the treatment of the electron spin [10] [22] [23]. We show below that the magnetic field intensity necessary to produce the electron spin can be obtained approximately as a result of a coupling of  $\alpha^{-2}$  with the radius  $r_e$  of the electron microparticle, see (27).

According to the classical electrodynamics [14] the magnetic field  $H$  at a distant  $r$  from the center of the linear wire carrying a current  $i$  is coupled with  $i$  and  $r$  by the formula

$$H = \frac{2i}{cr}. \quad (71)$$

If the current  $i$  is flowing on a surface of the conductor which is the electron orbit, we can assume that  $r = r_e$  which is both the radius of the electron microparticle and cross-section of the orbit. The field  $H$  becomes in this case [14]

$$H = \frac{2e}{Tcr_e} = \frac{2e}{c} \frac{e^4 m}{2\pi\hbar^3} \frac{mc^2}{e^2} = \frac{e^3 m^2 c}{\pi\hbar^3}, \quad (72)$$

where the time period  $T$  of the electron circulation along the orbit is taken from Formula (7) for  $n = 1$ :

$$T = T_1 = \frac{2\pi\hbar^3}{e^4 m} \quad (73)$$

The essence of the spin effect is that the path of the spinning electron circumvents the electron orbit about

$$\frac{1}{\alpha^2} = \left( \frac{\hbar c}{e^2} \right)^2 \cong 137^2 \quad (74)$$

times during the time period  $T$  indicated in (73). In classical electrodynamics this means that the magnetic field produced in this way is  $\alpha^{-2}$  times stronger than that obtained in (72):

$$H_{\text{spin}} = \frac{1}{\alpha^2} H = \frac{\hbar^2 c^2}{e^4} \frac{e^3 m^2 c}{\pi\hbar^3} = \frac{m^2 c^3}{\pi e \hbar}. \quad (75)$$

The result in (75) differs solely by the factor of  $\frac{1}{\pi}$  from the magnetic field assumed to produce a spinning electron particle in [10] [22] [23]:

$$H_{\text{spin}} = \frac{m^2 c^3}{e \hbar}. \quad (76)$$

A discrepancy between (75) and (76) can be ascribed to some uncertainty connected with the calculation of the radius  $r_e$ , see [24].

## 7. Conclusions

The aim of the paper was to get more insight into a non-probabilistic description of the transfer of energy

between two quantum levels. A suitable situation for discussion is the case when the levels are neighbouring in their mutual position of the energy states. Then the energy change ( $\Delta E$ ) between the levels, and the time interval  $\Delta t$  necessary to attain  $\Delta E$ , satisfy a very simple formula

$$\Delta E \Delta t = h; \quad (77)$$

see [6]-[10].

In the paper, Formula (77) finds its counterparts supplied by the electromagnetic theory of emission. Two physical objects, namely the hydrogen atom and electron harmonic oscillator, were studied. The case of the electron oscillator allowed us to perform a more direct comparison of the quantum approach to the emission rate with the classical electromagnetic theory. It occurs that the classical rate is equal to the quantum rate multiplied by the Born damping coefficient and an interval of time, see (62).

## References

- [1] Planck, M. (1910) *Acht Vorlesungen ueber Theoretische Physik*. S. Hirzel, Leipzig.
- [2] Einstein, A. (1917) *Physikalische Zeitschrift*, **18**, 121.
- [3] Bohr, N. (1967) On the Quantum Theory of Line Spectra. In: Van der Waerden, B.L., Ed., *Sources of Quantum Mechanics*, Dover Publications, New York, 95-137.
- [4] Bethe, H. (1933) *Quantenmechanik der Ein- und Zwei-Elektronenprobleme*. In: Geiger, H. and Scheeel, K., Eds., *Handbuch der Physik*, Vol. 24, Part 1, Springer, Berlin, 273-560.
- [5] Condon, E.U. and Shortley, G.H. (1970) *The Theory of Atomic Spectra*. Cambridge University Press, Cambridge, UK.
- [6] Olszewski, S. (2015) *Journal of Modern Physics*, **6**, 1277-1288. <http://dx.doi.org/10.4236/jmp.2015.69133>
- [7] Olszewski, S. (2016) *Journal of Modern Physics*, **7**, 162-174. <http://dx.doi.org/10.4236/jmp.2016.71018>
- [8] Olszewski, S. (2016) *Journal of Modern Physics*, **7**, 827-851. <http://dx.doi.org/10.4236/jmp.2016.78076>
- [9] Olszewski, S. (2016) *Journal of Modern Physics*, **7**, 1004-1020. <http://dx.doi.org/10.4236/jmp.2016.79091>
- [10] Olszewski, S. (2016) *Reviews in Theoretical Science*, **4**, 336-352. <http://dx.doi.org/10.1166/rits.2016.1066>
- [11] Sommerfeld, A. (1931) *Atombau und Spektrallinien*. 5th Edition, Vol. 1, Vieweg, Braunschweig.
- [12] MacDonald, A.H. (1989) *Quantum Hall Effect. A Perspective*. Kluwer, Milano.
- [13] Slater, J.C. (1967) *Quantum Theory of Molecules and Solids*. Vol. 3, McGraw-Hill, New York.
- [14] Lass, H. (1950) *Vector and Tensor Analysis*. McGraw-Hill, New York.
- [15] Matveev, A.N. (1964) *Electrodynamics and the Theory of Relativity*. Izd. Wyzszaja Szkola, Moscow. (In Russian)
- [16] Greiner, W. (1998) *Classical Electrodynamics*. Springer, New York. <http://dx.doi.org/10.1007/978-1-4612-0587-6>
- [17] Landau, L.D. and Lifshits, E.M. (1969) *Mechanics. Electrodynamics*. Izd. Nauka, Moscow. (In Russian)
- [18] Sommerfeld, A. (1943) *Mechanik*. Akademische Verlagsgesellschaft, Leipzig.
- [19] Born, M. (1933) *Optik*. Springer, Berlin. <http://dx.doi.org/10.1007/978-3-642-99599-6>
- [20] Van der Waerden, B.L. (1967) Introduction. In: Van der Waerden, B.L., Ed., *Sources of Quantum Mechanics*, Dover Publications, New York. [http://dx.doi.org/10.1007/978-3-662-42424-7\\_1](http://dx.doi.org/10.1007/978-3-662-42424-7_1)
- [21] Heisenberg, W. (1925) *Zeitschrift fuer Physik*, **33**, 879-893. <http://dx.doi.org/10.1007/BF01328377>
- [22] Olszewski, S. (2014) *Journal of Modern Physics*, **5**, 2022-2029. <http://dx.doi.org/10.4236/jmp.2014.518198>
- [23] Olszewski, S. (2014) *Journal of Modern Physics*, **5**, 2030-2040. <http://dx.doi.org/10.4236/jmp.2014.518199>
- [24] Olszewski, S. (2016) *Journal of Modern Physics*, **7**, 1297-1303. <http://dx.doi.org/10.4236/jmp.2016.711114>

# Success and Incoherence of Orthodox Quantum Mechanics

M. E. Burgos

Departamento de Física, Universidad de Los Andes, Mérida, Venezuela  
Email: mburgos25@gmail.com

Received 23 June 2016; accepted 19 August 2016; published 22 August 2016

Copyright © 2016 by author and Scientific Research Publishing Inc.  
This work is licensed under the Creative Commons Attribution International License (CC BY).

<http://creativecommons.org/licenses/by/4.0/>



Open Access

---

## Abstract

**Orthodox quantum mechanics is a highly successful theory despite its serious conceptual flaws. It renounces realism, implies a kind of action-at-a-distance and is incompatible with determinism. Orthodox quantum mechanics states that Schrödinger's equation (a deterministic law) governs spontaneous processes while measurement processes are ruled by probability laws. It is well established that time dependent perturbation theory must be used for solving problems involving time. In order to account for spontaneous processes, this last theory makes use of laws *valid only when measurements are performed*. This incoherence seems absent from the literature.**

## Keywords

**Quantum Measurements—Time Dependent Perturbation Theory**

---

## 1. Introduction

The first formulation of quantum mechanics is due to P. A. M. Dirac from 1930 [1]. J. von Neumann asserted that Dirac's formalism could scarcely be surpassed in brevity and elegance, but it was deficient in mathematical rigor ([2], p. 7). A couple of years later von Neumann published his *Mathematische Grundlagen der Quantenmechanik* [3]. Many other versions of the theory followed these pioneer contributions, most of them motivated by the desire to solve the *measurement problem*. Von Neumann's formulation continues, however, to be preferred to other approaches and, at present, it is frequently the only one taught at the academy. It is known as orthodox (ordinary or standard) quantum mechanics (OQM), although it is sometime referred to as the *Copenhagen interpretation*.

OQM refers to individual systems and consists of five axioms, two of them concerning measurements ([2], p. 5). One is a generalization of Born's postulate and fixes the possible results of a measurement and their corresponding probabilities. The other is the projection postulate. It determines the final state to which the initial state

collapses (is projected, is reduced, jumps) as a result of measurement.

Since the beginning OQM, and in particular its projection postulate, was the target of merciless criticism. Many and very conspicuous scientists denounced what they considered its flaws. For instance, A. Einstein pointed out that

1) There is a conflict between determinism and OQM. He stressed this issue frequently, as evidenced in his letters to M. Born of December 12, 1926, and of September 7, 1944 [4].

2) OQM implies a kind of action-at-a-distance. In 1927, during the Fifth Solvay Congress, he showed that a peculiar kind of action-at-a-distance is inherent to the hypothesis that the state vector  $|\psi\rangle$  completely describes the state of an individual system (as established in OQM) ([2], p. 116) [5] [6].

3) OQM introduces a subjective element into the theory through the projection postulate. This is an unacceptable procedure to account for processes happening in a world which objectively exists. Einstein insisted on this point repeatedly. For instance, referring to Maxwell's influence on the evolution of the idea of physical reality he asserted: "The belief in an external world independent of the perceiving subject is the basis of all natural science" [7].

In addition to these issues, OQM presents a conflict with conservation laws which has been largely ignored. We dealt with this subject some years ago and concluded that in the framework of OQM conservation laws are strictly valid in spontaneous processes (in fact they are theorems which can be derived from the axioms) but have only a statistical sense in measurement processes [8]-[12].

Another source of problems is that OQM imposes two laws of change of the state vector  $|\psi\rangle$  [13]. Since it seems there is no way to reduce to one another, it would be desirable for OQM to unambiguously determine the precise conditions under which each of these laws would apply. Unfortunately this is not the case. J. S. Bell complains: "during 'measurement' the linear Schrödinger evolution is suspended and an ill-defined 'wave-function collapse' takes over. There is nothing in the mathematics to tell what is 'system' and what is 'apparatus', nothing to tell which natural processes have the special status of 'measurements'. Discretion and good taste, born from experience, allows us to use quantum theory with marvelous success, despite the ambiguity of the concepts named above in quotation marks. But it seems clear that in a serious fundamental formulation such concepts must be excluded" ([14], p. 160).

The absence of a rule to determine which law must be applied is the worst flaw that OQM confronts [12] [15].

## 2. Orthodox Quantum Mechanics: A Very Successful Theory

Quoting M. Jammer [2], M. Bunge says that "there can be no doubt that quantum theory is a good approximation to the truth-which is not to say that it is perfect. Thousands upon thousands of observations and experiments have confirmed its predictions in an amazing range of fields, from particle and atomic physics to solid state physics and astrophysics, usually with an astounding accuracy" ([16], p. 167). While J. S. Bell emphatically asserts: "ORDINARY QUANTUM MECHANICS (as far as I know) IS JUST FINE FOR ALL PRACTICAL PURPOSES" (capital letters in the original) [17].

M. Tegmar and J. A. Wheeler detail: "The Copenhagen interpretation [in the present paper named OQM] provided a strikingly successful recipe for doing calculations that accurately described the outcomes of experiments, but the suspicion lingered that some equation ought to describe when and how this collapse occurred. Many physicists took this lack of an equation to mean that something was intrinsically wrong with quantum mechanics and that it would soon be replaced by a more fundamental theory that would provide such an equation. So rather than dwell on ontological implications of the equations, most physicists forged ahead to work out their many exciting applications..." [18].

They continue: "This pragmatic approach proved stunningly successful. Quantum mechanics was instrumental in predicting antimatter, understanding radioactivity (leading to nuclear power), accounting for the behavior of materials such as semiconductors, explaining superconductivity and describing interactions such as those between light and matter (leading to the invention of the laser) and of radio waves and nuclei (leading to magnetic resonance imaging). Many successes of quantum mechanics involve its extension, quantum field theory, which forms the foundations of elementary particle physics..." [18].

At this point we should perhaps listen to R. P. Feynman declaring: "I can safely say that nobody understands quantum mechanics" [19]. So, even if everybody recognizes that quantum mechanics is fine for all practical purposes, nobody understands it. What strange a situation!

The majority of processes involved in the phenomena mentioned by Tegmar and Wheeler *are not measurement but spontaneous processes*. On the one hand, OQM ensures that the Schrödinger equation gives an account for them. On the other hand, *most of these processes depend on time*. According to Dirac, their analyses require the application of the method provided by time dependent perturbation theory (TDPT). In his words, “[this] method must... be used for solving all problems involving a consideration of time... or more generally problems in which the perturbation varies with the time in any way...” ([1], p. 168; emphases added). A similar idea is expressed by W. Heitler in his study of radiation problems ([20], p. 137-138).

In the next section we shall see that TDPT involves not only the Schrödinger equation (a deterministic law governing spontaneous processes) but also laws which are valid only when measurements are performed.

### 3. A Critical Review of Time Dependent Perturbation Theory

In the following we sketch the essential features of TDPT. For more details see for instance: D. R. Bes ([21], Chapter IX); C. Cohen-Tannoudji *et al.* ([22], Chapter XIII); P. A. M. Dirac ([1], Chapter VII); W. Heitler ([20], Chapter IV); E. Merzbacher ([23], Chapter XIX); and/or A. Messiah ([24], Chapitre XVII). *Note: Symbols used by these authors may have been changed for homogeneity.*

The aim of TDPT is to calculate the transition probability between stationary states (*i.e.* eigenstates of a Hamiltonian  $\mathfrak{E}$  which does not depend explicitly on time) induced by a time dependent perturbation  $\mathfrak{W}(t)$ . The theory deals with processes having two clearly different stages. The first governed by the Schrödinger equation. The second ruled by probability laws. According to OQM formalism, Schrödinger equation governs spontaneous processes; Born’s postulate and/or the projection postulate apply only when measurements are performed. *The fact that TDPT requires the application of postulates concerning measurements to give an account for processes supposedly spontaneous is at the very heart of OQM incoherence.*

Let us work out separately the two stages mentioned. We start with a physical system with Hamiltonian  $\mathfrak{E}$ , called the *non-perturbed* Hamiltonian. Its eigenvalue equations are

$$\mathfrak{E}|\varphi_n\rangle = E_n|\varphi_n\rangle \quad (1)$$

where  $E_n$  ( $n = 1, 2, \dots, N$ ) are the eigenvalues of  $\mathfrak{E}$  and  $|\varphi_n\rangle$  the corresponding eigenvectors. For the sake of simplicity we shall consider  $\mathfrak{E}$  spectrum to be entirely discrete and non-degenerate. All the  $E_n$  and  $|\varphi_n\rangle$  are supposed to be known.

**First stage:** Let  $|\psi(t)\rangle$  be the system’s state at time  $t$ . We assume that at the initial time  $t = 0$ , the system is in the stationary state  $|\varphi_i\rangle$ , which is the eigenvector of the non-perturbed Hamiltonian  $\mathfrak{E}$  corresponding to the eigenvalue  $E_i$ . At this instant the *time dependent perturbation*  $\mathfrak{W}(t)$  is applied. So for  $t \geq 0$  the total, *perturbed Hamiltonian* is

$$\mathfrak{H}(t) = \mathfrak{E} + \mathfrak{W}(t) \quad (2)$$

*As long as no measurements are performed*, the process is spontaneous and ruled by the Schrödinger equation

$$i\hbar d|\psi(t)\rangle/dt = \mathfrak{H}(t)|\psi(t)\rangle \quad (3)$$

where  $\hbar$  is Planck’s constant divided by  $2\pi$  and  $i$  is the imaginary unity. The solution  $|\psi(t)\rangle$  of this equation which corresponds to the initial condition  $|\psi(0)\rangle = |\varphi_i\rangle$  is *unique*. This means that  $|\psi(t)\rangle$  is *completely determined* by the initial state  $|\psi(0)\rangle$  and the total Hamiltonian  $\mathfrak{H}(t)$ , which includes the perturbation  $\mathfrak{W}(t)$ . The state  $|\psi(t)\rangle$  can be written

$$|\psi(t)\rangle = \mathcal{U}_{\mathfrak{H}}(t, 0)|\psi(0)\rangle = \mathcal{U}_{\mathfrak{H}}(t, 0)|\varphi_i\rangle \quad (4)$$

where  $\mathcal{U}_{\mathfrak{H}}(t, 0)$  is the evolution operator corresponding to the total Hamiltonian  $\mathfrak{H}(t)$  which acts during the time interval  $0 \rightarrow t$ . To stress that  $|\psi(t)\rangle$  depends on the initial state  $|\varphi_i\rangle$  and on the total Hamiltonian  $\mathfrak{H}(t)$ , or if preferred on the perturbation  $\mathfrak{W}(t)$ , we write

$$|\psi_{i, \mathfrak{H}}(t)\rangle \equiv |\psi(t)\rangle = \mathcal{U}_{\mathfrak{H}}(t, 0)|\varphi_i\rangle \quad (5)$$

**Second stage:** At  $t_f$  the system’s state is  $|\psi_{i, \mathfrak{H}}(t_f)\rangle$ . Then, it is said, *the probability the system has to be*

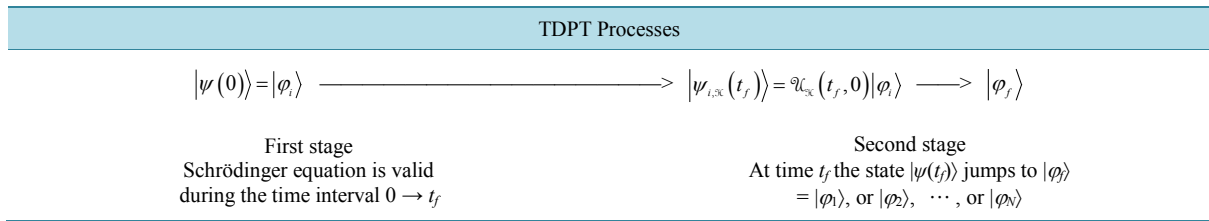
found in the state  $|\varphi_j\rangle$  is  $\left| \langle \varphi_j | \psi_{i,\mathfrak{E}}(t_f) \rangle \right|^2$ .

We sum up: In the first stage the system, initially in the stationary state  $|\psi(0)\rangle = |\varphi_i\rangle$ , follows a Schrödinger evolution which leads it to the state  $|\psi_{i,\mathfrak{E}}(t_f)\rangle = \mathcal{U}_{\mathfrak{E}}(t_f, 0)|\varphi_i\rangle$ ; note that, in general, the state  $|\psi_{i,\mathfrak{E}}(t_f)\rangle$  does not coincide with any stationary state  $|\varphi_n\rangle$  ( $n = 1, 2, \dots, N$ ). In the second stage the system jumps from  $|\psi_{i,\mathfrak{E}}(t_f)\rangle$  to one of the stationary states  $|\varphi_n\rangle$ . The whole process leads the system from the stationary state  $|\varphi_i\rangle$  to the stationary  $|\varphi_j\rangle$  (in particular it can result  $|\varphi_j\rangle = |\varphi_i\rangle$ ).

The evolution during the first stage is an *automatic change*; at time  $t_f$  the system state cannot be different from  $|\psi_{i,\mathfrak{E}}(t_f)\rangle = \mathcal{U}_{\mathfrak{E}}(t_f, 0)|\varphi_i\rangle$ . By contrast, the jump from  $|\psi_{i,\mathfrak{E}}(t_f)\rangle$  to one of the stationary states  $|\varphi_n\rangle$  is ruled by probability laws. The associated probability  $\mathcal{P}_{if}(t_f)$  is by definition *the transition probability* between the initial stationary state  $|\varphi_i\rangle$  and the final stationary state  $|\varphi_j\rangle$  induced by the perturbation  $\mathfrak{W}(t)$  during the time interval  $0 \rightarrow t_f$  and has the expression

$$\mathcal{P}_{if}(t_f) = \left| \langle \varphi_j | \psi_{i,\mathfrak{E}}(t_f) \rangle \right|^2 = \left| \langle \varphi_j | \mathcal{U}_{\mathfrak{E}}(t_f, 0) | \varphi_i \rangle \right|^2 \quad (6)$$

In the following diagram we show the complete process leading the system from the initial  $|\varphi_i\rangle$  to one of the possible final states  $|\varphi_j\rangle$ .



Everything happens as if at time  $t_f$  a *measurement of the non-perturbed energy*, represented by the operator  $\mathfrak{E}$ , has been performed. According to Born’s postulate the possible results are the eigenvalues  $E_n$  ( $n = 1, 2, \dots, N$ ) with probabilities given by  $\left| \langle \varphi_j | \psi_{i,\mathfrak{E}}(t_f) \rangle \right|^2$ . If the measurement yields the result  $E_j$ , the projection postulate ensures that the system jumps from the state  $|\psi_{i,\mathfrak{E}}(t_f)\rangle$  to the eigenstate  $|\varphi_j\rangle$ .

Messiah expresses this idea in the following terms: “Supposons qu’à l’instant initial  $t = 0$  le système se trouve dans l’un des états propres de  $\mathfrak{E}$ , l’état  $|\varphi_i\rangle$  par exemple. Nous nous proposons de calculer la probabilité de le trouver à l’instant  $t_f$  dans un autre état propre de  $\mathfrak{E}$ , l’état  $|\varphi_j\rangle$  par exemple, *dans l’éventualité d’une mesure à cet instant*. Soit  $\mathcal{P}_{if}(t_f)$  cette quantité, c’est par définition la probabilité de transition de  $|\varphi_i\rangle$  en  $|\varphi_j\rangle$ ” ([24], p. 621; emphases added).

Assuming that the initial state is  $|\psi(0)\rangle = |\varphi_i\rangle$ , Dirac asserts: “If there were no perturbation, *i.e.* if the Hamiltonian were  $\mathfrak{E}$ , [the state  $|\psi(t)\rangle$ ] would be stationary. The perturbation causes the state to change” ([1], p. 172). Supposing the deterministic law valid, the state  $|\psi_{i,\mathfrak{E}}(t_f)\rangle = \mathcal{U}_{\mathfrak{E}}(t_f, 0)|\varphi_i\rangle$  results ([1], p. 109). Then, he says: “ $\mathcal{P}_{if}(t_f)$  is the probability of a transition taking place from state  $|\varphi_i\rangle$  to state  $|\varphi_j\rangle$  during the time interval  $0 \rightarrow t_f$ ...” ([1], p. 172). Even though Dirac does not mention measurements, it is quite clear that he applies here a law valid only when measurements are performed.

Other authors proceed in a similar way. When introducing TDPT they do not mention measurements. Instead they make assertions such as: “Our objective is to calculate transition amplitudes between the relevant unperturbed eigenstates, owing to the presence of the perturbation...” ([23], p. 483); or “We want to study the transitions which can be induced by the perturbation...” ([22], p. 1285); or “The transition probability between the initial state  $|\varphi_i\rangle$  and the final state  $|\varphi_j\rangle$  is induced by the perturbation...” ([21], p. 142); etc.

There is a difference between Messiah’s and other authors’ statement of the problem worth mentioning. According to Messiah transitions to particular outcomes (either  $|\varphi_1\rangle$ , or  $|\varphi_2\rangle$ , ... or  $|\varphi_N\rangle$ ) are the result of a measurement of the unperturbed Hamiltonian  $\mathfrak{E}$ . Other authors suggest that these transitions are not the result of a measurement of  $\mathfrak{E}$ , but of a perturbation of  $\mathfrak{E}$ . A *perturbation* of  $\mathfrak{E}$  is completely different from a *measurement* of  $\mathfrak{E}$ . When the perturbation  $\mathfrak{W}(t)$  is applied, the Hamiltonian changes from  $\mathfrak{E}$  to  $\mathfrak{E} + \mathfrak{W}(t)$ , but the Schrödinger

evolution is not suspended. By contrast, a measurement does suspend the Schrödinger evolution.

Paraphrasing Bell, even if nothing has been measured, discretion and good taste allow us to assume that a (virtual?) measurement of the physical quantity represented by the non-perturbed Hamiltonian  $\hat{C}$  is performed at time  $t_f$ . “There is a long tradition of using the textbooks postulate of wave-function collapse as a pragmatic ‘shut up and calculate’ recipe” [18]. We have just shown how it works!

## 4. Conclusions

OQM marvelous success in the area of experimental predictions is mostly based on TDPT. It is agreed that the method provided by this last theory must be used for solving all problems involving a consideration of time, including *spontaneous* time dependent processes. This is, for instance, the case of absorption and emission of light and of processes occurring in semiconductors. *To give an account for such spontaneous processes*, however, *TDPT requires the application of a law which is not valid in spontaneous processes*. This is a flagrant incoherence we have not noticed in the literature.

Quantum weirdness has been traditionally associated with the *measurement problem*. To solve it, different authors have suggested several strategies. Among them are *Statistical interpretation of quantum mechanics* [25], *Many worlds interpretation* [26], *Decoherence* [18] and *Continuous spontaneous localization theory* [27]. We have addressed these and other proposed solutions of the measurement problem in previous papers [6] [9] [12]. Even if valuable, these contributions do not solve the measurement problem, let alone OQM incoherence pointed out in the present study.

We maintain that OQM weirdness is not limited to the *measurement problem*. It is much more serious and justifies a radical revision of the theory.

## Acknowledgements

I am indebted to Professor J. C. Centeno for many fruitful discussions.

## References

- [1] Dirac, P.A.M. (1958) *The Principles of Quantum Mechanics*. Clarendon Press, Oxford.
- [2] Jammer, M. (1974) *The Philosophy of Quantum Mechanics*. John Wiley & Sons, New York.
- [3] Von Neumann, J. (1932) *Mathematische Grundlagen der Quantenmechanik*. Springer, Berlin.
- [4] Born, M. (1971) *The Born Einstein Letters*. The Macmillan Press Ltd., London.
- [5] Burgos, M.E. (2015) *JMP*, **6**, 1663-1670. <http://dx.doi.org/10.4236/jmp.2015.611168>
- [6] Burgos, M.E. (2015) In: Pahlavani, M., Ed., *Selected Topics in Applications of Quantum Mechanics*, INTECH, Croatia, 137-173. <http://dx.doi.org/10.5772/59209>
- [7] Einstein, A. (1931) *James Clerk Maxwell: A Commemoration Volume*. Cambridge University Press, Cambridge.
- [8] Burgos, M.E. (2010) *JMP*, **1**, 137-142. <http://dx.doi.org/10.4236/jmp.2010.12019>
- [9] Burgos, M.E. (2008) *Foundations of Physics*, **38**, 883-907. <http://dx.doi.org/10.1007/s10701-008-9213-5>
- [10] Criscuolo, F.G. and Burgos, M.E. (2000) *Physics Essays*, **13**, 80-84. <http://dx.doi.org/10.4006/1.3025430>
- [11] Burgos, M.E., Criscuolo, F.G. and Etter, T. (1999) *Speculations in Science and Technology*, **21**, 227-233. <http://dx.doi.org/10.1023/A:1005552504638>
- [12] Burgos, M.E. (1998) *Foundations of Physics*, **28**, 1323-1346. <http://dx.doi.org/10.1023/A:1018826910348>
- [13] Laloë, F. (2001) *American Journal of Physics*, **69**, 655-701. <http://dx.doi.org/10.1119/1.1356698>
- [14] Bell, M., Gottfried, K. and Veltman, M. (2001) *John S. Bell on the Foundations of Quantum Mechanics*. World Scientific, Singapore.
- [15] Burgos, M.E. (1990) *Studies on Mario Bunge's Treatise*. Rodopi, Amsterdam, 365-375.
- [16] Bunge, M. (1985) *Treatise on Basic Philosophy, Vol. 7, Philosophy of Science & Technology*. D. Reidel Publishing Company, Dordrecht-Boston-Lancaster.
- [17] Bell, J.S. (1990) *Physics World*, **8**, 33-40.
- [18] Tegmar, M. and Wheeler, J. (2001) *Scientific American*, **284**, 54-61.
- [19] Feynman, R.P. (1964) MIT. <http://bouman.chem.georgetown.edu/general/feynman.html>

- [20] Heitler, W. (1984) *The Quantum Theory of Radiation*. Dover Publications Inc., New York.
- [21] Bes, D.R. (2004) *Quantum Mechanics*. Springer-Verlag, Berlin-Heidelberg.  
<http://dx.doi.org/10.1007/978-3-662-05384-3>
- [22] Cohen-Tannoudji, C., Diu, B. and Laloë, F. (1977) *Quantum Mechanics*. John Wiley & Sons, New York-London-Sydney-Toronto.
- [23] Merzbacher, E. (1961) *Quantum Mechanics*. John Wiley & Sons, New York.
- [24] Messiah, A. (1965) *Mécanique Quantique*. Dunod, Paris.
- [25] Ballentine, L.E. (1970) *Reviews of Modern Physics*, **42**, 358-381. <http://dx.doi.org/10.1103/RevModPhys.42.358>
- [26] Wikipedia. The Free Encyclopedia: Many-Worlds Interpretation.  
[https://en.wikipedia.org/wiki/Many-worlds\\_interpretation](https://en.wikipedia.org/wiki/Many-worlds_interpretation)
- [27] Ghirardi, G.C., Rimini, A. and Weber, T. (1986) *Physical Review D*, **34**, 470-490.



Scientific Research Publishing

---

**Submit or recommend next manuscript to SCIRP and we will provide best service for you:**

Accepting pre-submission inquiries through Email, Facebook, LinkedIn, Twitter, etc.

A wide selection of journals (inclusive of 9 subjects, more than 200 journals)

Providing 24-hour high-quality service

User-friendly online submission system

Fair and swift peer-review system

Efficient typesetting and proofreading procedure

Display of the result of downloads and visits, as well as the number of cited articles

Maximum dissemination of your research work

Submit your manuscript at: <http://papersubmission.scirp.org/>

# A Fundamentally Irreversible World as an Opportunity towards a Consistent Understanding of Quantum and Cosmological Contexts

**Helmut Tributsch**

Bio-Mimetics in Energy Systems Program, Carinthia University for Applied Sciences, Villach, Austria  
Email: [helmut.tributsch@alice.it](mailto:helmut.tributsch@alice.it), [www.helmut-tributsch.it](http://www.helmut-tributsch.it)

Received 20 June 2016; accepted 21 August 2016; published 24 August 2016

Copyright © 2016 by author and Scientific Research Publishing Inc.

This work is licensed under the Creative Commons Attribution International License (CC BY).

<http://creativecommons.org/licenses/by/4.0/>



Open Access

---

## Abstract

In a preceding publication a fundamentally oriented and irreversible world was shown to be derivable from the important principle of least action. A consequence of such a paradigm change is avoidance of paradoxes within a “dynamic” quantum physics. This becomes essentially possible because fundamental irreversibility allows consideration of the “entropy” concept in elementary processes. For this reason, and for a compensation of entropy in the spread out energy of the wave, the duality of particle and wave has to be mediated via an information self-image of matter. In this publication considerations are extended to irreversible thermodynamics, to gravitation and cosmology with its dependence on quantum interpretations. The information self-image of matter around particles could be identified with gravitation. Because information can also impose an always constant light velocity there is no need any more to attribute such a property to empty space, as done in relativity theory. In addition, the possibility is recognized to consider entropy generation by expanding photon fields in the universe. Via a continuous activation of information on matter photons can generate entropy and release small energy packages without interacting with matter. This facilitates a new interpretation of galactic redshift, emphasizes an information link between quantum- and cosmological phenomena, and evidences an information-triggered origin of the universe. Self-organized processes approach maximum entropy production within their constraints. In a far from equilibrium world also information, with its energy content, can self-organize to a higher hierarchy of computation. It is here identified with consciousness. This appears to explain evolution of spirit and intelligence on a materialistic basis. Also gravitation, here identified as information on matter, could, under special conditions, self-organize to act as a super-gravitation, offering an alternative to dark matter. Time is not an illusion, but has to be un-

**How to cite this paper:** Tributsch, H. (2016) A Fundamentally Irreversible World as an Opportunity towards a Consistent Understanding of Quantum and Cosmological Contexts. *Journal of Modern Physics*, 7, 1455-1482.

<http://dx.doi.org/10.4236/jmp.2016.712133>

derstood as flux of action, which is the ultimate reality of change. The concept of an irreversible physical world opens a route towards a rational understanding of complex contexts in nature.

## Keywords

**Fundamental Irreversibility, Gravitation as Information, Redshift as Entropy Phenomenon, Constancy of Light Velocity, Time, Information Driven Universe**

## 1. Introduction

Conventional physics is based on time invertible natural laws. A recent re-examination of the important and much applied principle of least action however led to the conclusion that the world is fundamentally oriented and irreversible [1]:

“Free energy aims at decreasing its presence per state, within the constraints of the system concerned” (1)

Action, energy times time, is thereby produced and minimized. This is the relevant phenomenon linked to the passage of time. Entropy generation is a fundamental, rate controlling process and has also to be considered in elementary mechanisms. One consequence is that the particle-wave duality had to be formulated differently. Particle (energy  $E_p$ ) and wave are not equivalent, but the energy in the distributed wave ( $E_w$ ) is less valuable, because it is highly diluted. Its energy has inferior working ability and is partially present in form of entropy, as non-useful energy ( $E_e$ ). As a consequence, when a particle is converted into a wave, information (energy  $E_n$ ) has to be simultaneously provided for the back conversion of the wave into the particle [1]:

$$hv = E_p \leftrightarrow \sum_w E_w + E_e + E_n \quad (2)$$

The particle-wave duality thus becomes a dynamic process, which involves information on matter (symbolically depicted in the center of **Figure 1**, where arrows indicate energy in form of entropy and the dot pattern energy in form of information on matter, besides of energy in form of the wave).

It could be shown that this concept gives rational explanations for quantization, the double slit experiment, and for quantum correlation. Quantization of electron orbits around a nucleus arises because the energy for information also minimizes and selects the simplest patterns (schematically shown in **Figure 1**, bottom left)). The recognition of a second slit by a particle proceeding through the first slit works, because the particle dynamically changes into the wave and the information on matter brings this information back to the particle after the slits. Quantum correlation can simply be understood as a consequence of splitting up the information self-image of matter, when particles split up. When information is present, which remains relevant for both separating particles (e.g. conservation of spin), this information cannot split up and remains linking the two separating particles (schematically shown in **Figure 1**, top left).

Since information on matter (dot pattern in **Figure 1** center) has an energy content and should always be around elementary particles with the program to decrease energy per state, it must be detectable and measurable. It could be identified with the phenomenon of gravitation. Obviously this would then be the link between elementary processes and cosmology (indicated in **Figure 1**, top). Since a fundamentally oriented and irreversible world, with energy tending to decrease its presence per state, also explains the second law of thermodynamics, this is sufficient motivation to explore additional important phenomena in physics. Here the role of entropy for radiation, the law governing self-organization processes, the meaning of time, of gravitation, the interpretation of relativity, and cosmological phenomena will be considered in the light of the proposed paradigm change.

## 2. Results

### 2.1. Entropy in Quantum Processes and Cosmology

The new proposed particle wave duality (**Figure 1**, center) involves a fundamental consideration of the entropy concept due to spreading of energy into space. This is a nano-scale concession for what is macroscopically known as entropy and dealt with in thermodynamics. Traditional quantum physics has a long history of conflict

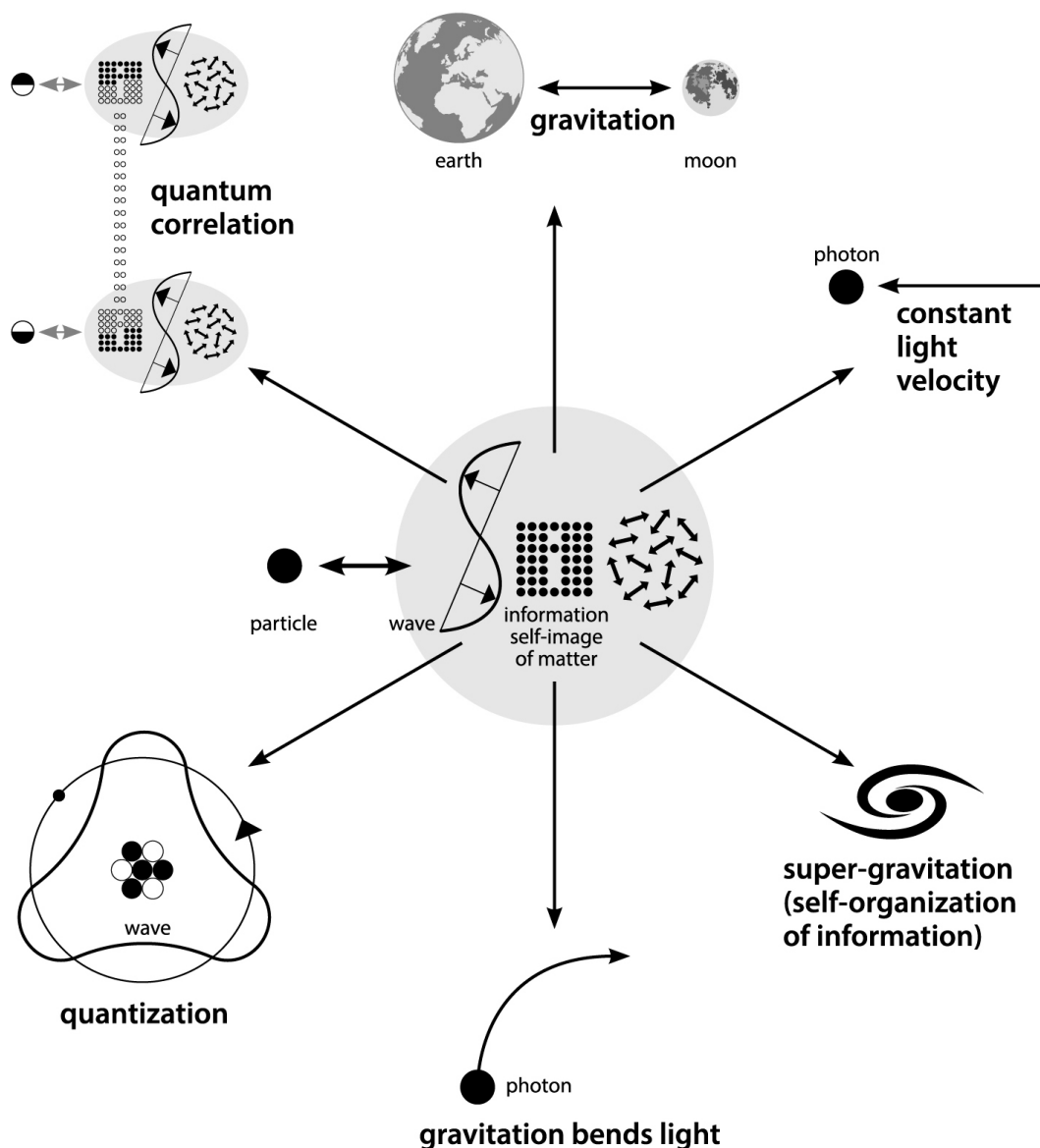


**Figure 1.** The particle-wave duality in “dynamic” quantum physics (shown in center) considers a fundamental generation of entropy due to spreading energy into space, but needs information on matter (dot pattern in center) to recover the particle. This information self-image of matter is found to be gravitation and to be the key for rationally understanding quantum physics, the always constant light velocity, the link to cosmology and diverse additional natural phenomena.

with thermodynamic interpretations. This was not yet the case at the start of quantum physics. Einstein, for example, used Wien’s considerations and his law to argue that the entropy change  $\Delta S$  of a radiation field, when its volume is expanded (**Figure 2(b)**), acts like known for an ideal gas with  $E/h\nu$  as particle number  $n$  [2]. The formula he dealt with reads ( $E$  = radiation energy,  $\nu$  = frequency,  $\beta$  = constant,  $V_0$  = original volume,  $V$  = expanded volume):

$$\Delta S = \frac{E}{\beta\nu} \log \frac{V}{V_0} \tag{3}$$

as compared to the well known formula for entropy generation by an expanding ideal gas ( $n$  = mole number,  $R$  = gas constant):

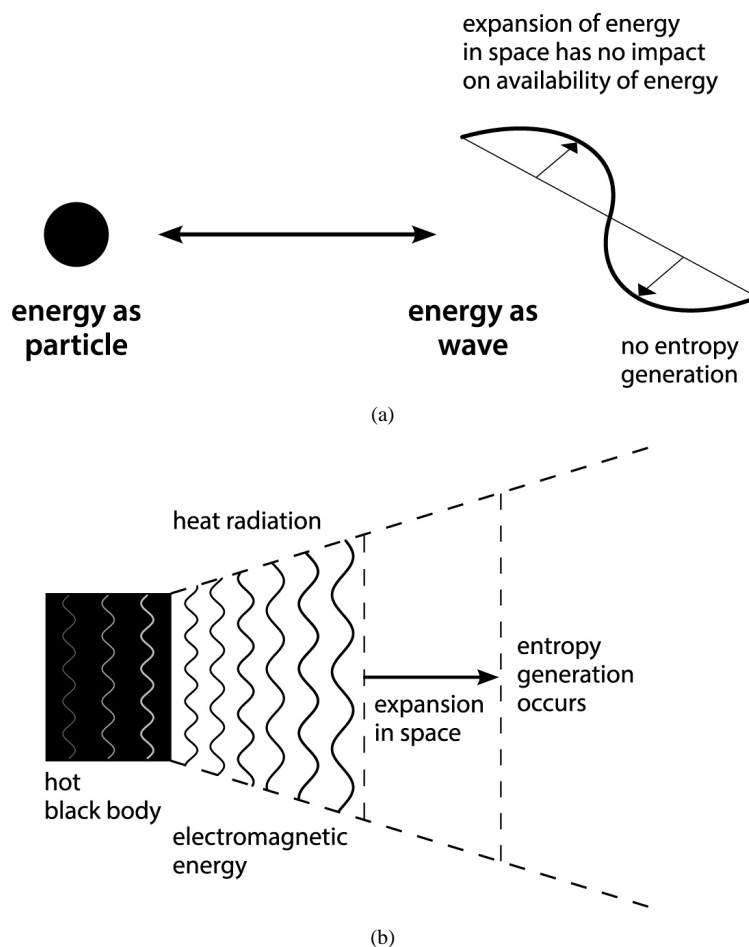


**Figure 2.** (a) By stating a dualism of particle and wave (energy concentrated and distributed respectively) classical quantum physics has eliminated the relevance of space for energy (compare the proposed new interpretation in [Figure 1](#) centre); (b) From classical physics it is however known that when radiation expands from a hot black body, less valuable energy in the form of entropy is generated. A shift of frequency and radiation temperature is the consequence (b).

$$\Delta S = nR \ln \frac{V}{V_0} = 2,302nR \log \frac{V}{V_0} \tag{4}$$

The formulas show, that, when radiation or a gas is spreading into an infinite volume, the entropy gain also tends towards infinity. This means that all energy involved in a radiation field (or a compressed gas) should finally be dissipated and converted into non useful, small, chaotic energy quantities of  $T\Delta S$ . Einstein wrote: “this Equation (3) shows, that the entropy of monochromatic radiation of sufficiently low density varies according to the same law as the entropy of an ideal gas (Equation (4)) or that a diluted solution”.

It is well known that Einstein was awarded the Nobel prize for this finding on the particle nature of photons and its application to electron emission from solids. It is a remarkable science philosophical circumstance that he used an irreversible phenomenon of spreading radiation, entropy generation, to establish a quantum property (later called photon) which then turned out not to tolerate irreversibility and entropy production during its existence. Indeed, in conventional quantum mechanics photons, once emitted into space and spreading cannot generate entropy along their long way by changing frequency and radiation temperature, until they finally interact with matter. During this latter process photon energy is still fully available, as immediately after generation of the photon. In contrast, relation (3) requires, that radiation spreading into space gradually converts its energy in-

to “chaotic”, non useful energy in the form of entropy, radiation of much lower frequency.

An energy loss, observed as a redshift of frequency, is actually observed when photons from characteristic light emission (e.g. from hydrogen) are arriving from deep space. Since a photon without impact can quantum mechanically not lose energy this phenomenon is actually not attributed to entropy turnover, but to a claimed cosmological expansion of free space itself. This (invented) expansion of empty space, as an alternative to not considered and quantum mechanically not tolerated entropy generation by single photons, is expected to stretch the wavelength and is matched to explain the observed redshift.

Here it is stated that fundamental irreversibility requires that photons lose energy during the process of spreading into space. A mechanism must consequently exist, that allows that.

The fundamental irreversibility of radiation processes became already established during a discussion between Planck and Boltzmann from 1897 [3]. The involved thermodynamics of radiation has since been intensively assessed (for a review see e.g. [4]).

For an adiabatic expansion of radiation the following relation is known to be applicable ( $\nu$  = frequency,  $V$  = volume):

$$\nu^3 V = \text{constant} \quad (5)$$

The frequency of radiation is changing with the volume (a property finally not tolerated for photons in free space by quantum theory). Using Wien’s law which states how the frequency  $\nu$  in the maximum of black body radiation is changing with temperature ( $T/\nu = \text{constant}$ ) one obtains the complementary relation

$$VT^3 = \text{constant} \quad (6)$$

Expansion of radiation into space thus changes radiation temperature (6) and radiation frequency (5). Relation (5) has actually been used to interpret the origin of the 2.72°K microwave background radiation from space as a relic of Big Bang explosion, when the universe was assumed to be much smaller. But radiation itself was not understood to expand adiabatically in a given static space to produce entropy (for which the formula was originally calculated), changing radiation’s temperature and frequency, and giving rise to microwave radiation as entropy product. In contrast empty space itself was assumed to expand to a large volume, respecting adiabatic conditions, and stretching the wavelength of photons to microwave dimensions [5].

In order to respect quantum theory, which does not allow a photon to generate entropy without collision with matter, and which claims to be complete and not improvable, entropy phenomena are obviously ignored. The observed or expected frequency shift is presently explained via a new and daring theory: that of an exploding universe, which stretches and expands its void [6]. How can a void, originally defined to contain nothing, develop such properties, and where does the abandoned photon energy go?

The problem with conventional quantum theory is fundamental. It cannot deal properly with the role of space for energy and especially with radiation energy spreading out in space (Figure 2(b)). A photon in an expanding radiation field around a light emitting star cannot engage in energy loss through entropy generation.

After emission it simply maintains its energy and can only change it when interacting with matter or with gravitation fields. This already should have indicated that conventional quantum theory is not complete. Such a conclusion is however, as well known, severely contradicted by quantum physicists [7] [8]. The author is convinced that a theory can never be proved to be correct and complete within one and the same system (such as a time-invertible world) (compare the considerations of the mathematician Kurt Gödel [9]). For a discussion of this claim of completeness of quantum theory from a hierarchy above, the choice between a time-invertible and a fundamentally oriented “dynamic” world, compare [10].

The claim, that quantum physics cannot be improved or extended, has thus crucially shaped the present understanding of cosmological processes. In actual cosmology the increasing redshift of starlight from increasingly distant stars is now mostly attributed to the postulated expansion of empty space (and to a smaller extent to the Doppler effect). Doing this astrophysicists essentially ignore entropy generation as described by relation (3). This relation requires that entropy generation by radiation fields expanding into a vast universe exists and is not limited by distance and only restricted by the final turnover and consumption of the available radiation energy. The consequences for the interpretation of the universe are, of course, dramatically different for the two approaches.

Let us use macroscopic, empirical thermodynamics as an approximation to understand photons in a fundamentally irreversible universe. We look at the energy  $T\Delta S$  turned over in entropy related processes for individual photons by multiplying relations (3) and (4) with the temperature  $T$  and substituting  $R$  for  $k$ , the Boltzmann con-

stant, in (4). Then  $kT$  is the appropriate scaling factor for energy which is relevant for entropy formation. For a typical temperature in space of  $2.72^\circ\text{K}$  it can be calculated to amount to  $0.240 \times 10^{-3}$  eV. This is microwave radiation. When one takes the maximum from the microwave background radiation in space one determines a microwave energy of  $0.6 \times 10^{-3}$  eV. A first conclusion is that in an irreversible universe the actually observed background radiation is simply entropy dumped by spreading radiation (what relation (3) requires). A black body distribution of this radiation is actually to be expected when thermodynamic mechanisms of entropy generation are involved. And entropy generation by starlight over billions of years should actually make microwave radiation the dominant radiation in space [11].

In astrophysics the ratio between the frequency of emitted and observed light is described via  $z$ , a dimensionless constant. For the microwave background radiation a  $z$ -value of  $z = 1089$  has been determined. This means that the change in frequency (energy) from the original photon is 1089 times bigger than the energy of the microwave photon. The highest confirmed redshift of a very distant galaxy appears to be  $z = 8.55$ . This means that the arriving photon has only conserved 11.6% of its original energy. This is entirely consistent with a thermodynamic interpretation of an expanding radiation field. Radiation is emitted and generating entropy according to relation (3). A frequency shift is occurring (relation (5)). But since very far galaxies are still visible only part of their radiation energy has been converted into microwave radiation in form of entropy. Or alternatively: they are still visible, but red-shifted, because not all visible radiation has been converted for entropy.

However in the present picture of an increasingly expanding universe the concerned galaxy is seen to flee at an extremely high speed. There already seems to be a serious problem with transgression of the speed of light, especially when considering galaxies at opposite ends of an exploding universe. However the well known (but not easily comprehensible) explanation of present cosmological physics is that this is not the case since the empty space itself is being stretched and expanding so fast so that the galaxies are just (passively) moved that way.

The here discussed “dynamic” quantum physics derived for a fundamentally oriented world can consider energy turnover for entropy production, when radiation is expanding into space. This is possible for two reasons. First because “a system tends to decrease its energy per state”, a conclusion drawn from the principle of least action (statement (1)). And second it is possible, because the information self-image of matter is continuously mediating the interchange between the particle and the wave ( $E_n$  in relation (2)). Thereby it already considers the entropy of the expanded energy of the wave and may also consider the entropy requirements of a photon in an expanding radiation field.

The photon is consistently reassembled from the wave state and thermodynamic law may be imposed via information, which could then release not any more available, entropic energy in form of low energy radiation. This is graphically shown in **Figure 1**, center, where the equivalence between particle and wave within “dynamic” quantum physics is explained. Information on matter is mediating between a wave plus the entropy involved in spreading energy out into space. This information on matter could be programed in such a way as to consider thermodynamic law, which demands that the radiation itself, when spreading into space, generates entropy. How could this happen? How could distribution into space be monitored by a photon? It could happen via gravitation, because information on matter, as involved in the dynamic particle-wave duality, can be identified with gravitation (see **Figure 1**, center and top, and later in more detail) and because this gravitation is equally a determining cosmological factor.

In “dynamic” quantum processes photons can consequently lose energy via generation of entropy. They are behaving as required by thermodynamics and expressed by relation (3), which Einstein used to argue for the existence of photons [2]. This way, in principle, Einstein also pointed at an irreversible nature of photons. The emitted, not any more useful energy for entropy is, as above estimated, very low (lower approximately by a factor of 1089). Because of the fundamentally claimed minimization of free energy content for the photon (1), because of the small amount of energy for entropy turned over, and because of conservation of momentum, an (entropic) energy release without change of photon direction is to be expected. This way the here proposed thermodynamic process of entropy generation has nothing to do with the already long ago rejected idea on “tired” light, caused by hypothetic collisions of photons with dust in space [12] [13]. No blurring of starlight would be seen and the light particles from the outmost detected galaxies would already have lost 88,4% of their energy for entropy production, for the liberation of low-energy microwave quanta. This is compatible with thermodynamic law for entropy production of spreading radiation (3) which allows in principle all radiation energy finally converted into non useful, chaotic energy,  $T\Delta S$ , if the space covered by spreading radiation approaches very large

values (since the logarithm in (3) tends to infinity).

The irreversibility of expanding radiation is here a very important argument. It should therefore also be derived from additional evidence. It is well known that from an expanding gas energy can be recovered via a piston in a gas motor. The same can be imagined to occur with an expanding radiation field, if energy is harvested via a sun sail (Figure 3). This also characterizes the expansion of light into empty space as an irreversible, entropy producing process. Part of the energy of expanding photons (the energy which could have been harvested by the solar sail) is not any more available.

The information on matter, dealing with the dynamic particle-wave duality ( $E_n$  in (2)) considers and deals with the entropy production due to the expanded wave. And it could also consider entropy generation due to radiation expansion from a star or a galaxy. A key for this is the identity of gravitation, information on matter, on quantum level and cosmological level. An interaction of a photon's information on matter (identified with gravitation) with gravitation in space towards implementing a fundamental empirically confirmed law is to be expected. The increasing redshift of starlight from increasingly distant light sources in space may thus be considered to be essentially the result of entropy loss and the microwave background is simply the expected entropy dump. Unexplained redshift patterns, such as different redshifts from quasars within galaxies, or periodical redshifts, have now to be considered to be essentially a problem of information handling in nature. In this context also the question, whether light from individual galactic objects is beamed in certain directions or evenly distributed will have to be considered (it affects  $V$  in relation (5) and may explain why light sources in similar position show different redshifts). Significant research efforts will, of course, be needed to learn much more about this natural information technology. In conclusion: before speaking about an exploding universe, an inflating space by stretching the void, and a dramatic flight movement of galaxies, entropy loss by spreading photons has to be understood and considered.

Basing on such conclusions we should interpret Hubble's empirical law accordingly and differently. Mathematically, this law describes the supposed increase of the escape velocity of galaxies (in kilometers per second) with respect to our earth and is presently the key for describing the dynamics of the universe including the so-called dark energy. It describes the galaxy velocity  $v$  via the Hubble constant  $H_0$  times the distance  $D$  of the galaxy from earth in light years ( $H_0$  expressed in kilometers per second per megaparsec, which is 3.26 million light years. Its value is estimated to be between 50 and 100, mostly at 70):

$$\text{Galaxy velocity: } v = H_0 D \quad (7)$$

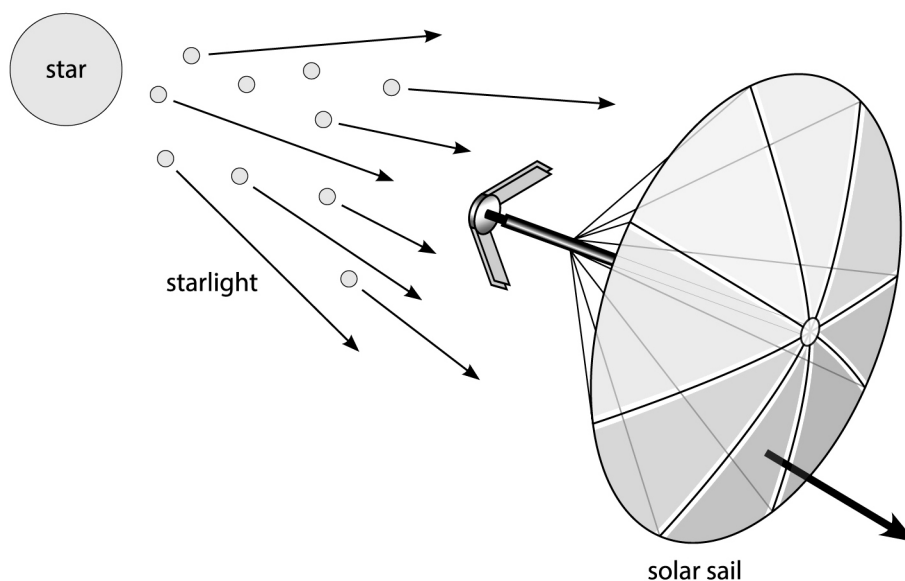


**Figure 3.** When starlight spreads into empty space, entropy is generated. A solar sail accelerated by starlight could harvest part of this spread-out energy. But when this energy is not harvested, it is converted into a non-useful, “entropic” form. “Dynamic” quantum physics allows interpretation of entropy generation as red-shift, conventional quantum physics adopts an inflation process of empty space as alternative explanation.

This empirical formula can, just by mathematical transformation, be converted into a formula expressing the new interpretation of the redshift. If we divide the formula left and right by a distance (kilometers), which is mathematically allowed, we arrive at a statement on the frequency  $\nu$  (1 divided by seconds) of light from galaxies in dependence on their distance from earth  $D$ . This way the formula is still valid but allows an entirely different interpretation. The new proportionality factor should now be named  $F_o$  and has the dimension of frequency shift per mega-parsec (3.26 million light years):

$$\text{Photon frequency: } \nu = F_o D \tag{8}$$

The energy contained in a photon is proportional to the frequency  $\nu$  and a frequency shift per distance (in mega-parsec) consequently reflects energy loss via entropy turnover  $\Delta S$ . The proportionality factor would be related to the entropy turnover:  $F_o \approx \Delta S$ . This means that the frequency shift of light from galaxies changes with their distance  $D$  from earth and is dependent on the rate of photon energy loss  $F_o$  via entropy production.

The latter, entropy production, is not a constant but would be expected to change logarithmically with the distance from the light source and would also be affected by the geometry of light spreading. This simple adapted formula explains, without assuming an inflation of space, why our earth appears to be the center of space. In fact it is of course not the center, but we are seeing from all directions incoming light, which has lost valuable energy on the long journey from galaxies in space for entropy production. We are seeing entropic energy loss corresponding to the distance covered. And we understand why the microwave background radiation is quantitatively the most important radiation source in the universe. It accumulated over billions of years (in contrast to being considered a short snapshot of Big Bangs optical echo).

## 2.2. Are Uncertainty and Zero Point Energy Fundamental?

There is an important quantum phenomenon, which has changed the present way of recognizing and understanding nature, since it is now accepted as fundamental. It is described by the uncertainty relation, which was first proposed by Werner Heisenberg. It cannot directly be derived from fundamental principles but results from the empirically grown considerations on quantum physics. The uncertainty relation states that position and momentum as well as energy and time of a quantum object cannot be measured exactly, but only with an uncertainty, which is proportional to Planck’s constant of action ( $h$ ). Concerning the energy-time uncertainty an interpretation is that when the time interval is too short, energy cannot exactly be determined. For a measurement of frequency (energy) several cycles have to pass. The average energy of an outgoing photon shows a certain distribution, a line width. Fast decaying states have a broad line width, slow decaying states have a sharp line width. Since energy and mass is related, the mass of the photon is accordingly more or less accurately defined. Why can the mass (energy) of a photon,  $E_p$ , vary?

It turned out that the uncertainty is not merely a simple observer effect, but a fundamental property of quantum systems. Uncertainty became a mysterious basis of quantum theory, which thus adopted an element of unpredictability. Not the reality of particles is described in quantum mechanics, but our statistical observation and measurement of these particles. It is known that Einstein was not amused by such a perspective and is known to have commented: “God does not play dice”. But the uncertainty relation has influenced our present view of the universe: The zero point energy and the possibility that energy and particles are popping out from nothing are consequences drawn from the uncertainty principle. Such concepts have been applied to Big Bang scenarios and to Black Hole interpretations.

How can a game with dice be understood within the “dynamic” quantum understanding? Does this empirically deduced quantum phenomenon really mean a departure from causality and rationality? Let us start with the “dynamic” interpretation of the particle-wave duality from (2) and find out whether we can rearrange the relation to understand uncertainty. One can bring the time from the frequency  $\nu = 1/t$  to the right side and multiply the result with the particle energy  $E_p$  in the numerator and denominator to get a relation with the formal structure of the energy-time uncertainty:

$$h = E_p t \leftrightarrow \left( \sum_w E_w + E_e + E_n \right) t \frac{E_p}{E_p} = E_p t \frac{\sum_w E_w + E_e + E_n}{E_p} \tag{9}$$

$E = E_p$ , the total energy of a photon, multiplied by  $t$ , the time of its existence in a given state, is proportional to  $h$ , the Planck constant of action. What is interesting now is the proportionality constant, which shows up on the

right side of Equation (9). It is the ratio between the energy of the particle and the energy of the wave (made up here of distributed energy, entropic energy, energy of information). Considering the dynamic nature of the particle-wave duality in a fundamentally oriented world this is not really a constant equally to one. The magnitude of the proportionality constant will simply vary and depend on whether, during the instance of measurement, the energy is more present in the particle or in the wave. This suggests that the uncertainty is related to the intermediate presence of energy in form of a wave (which also conventional quantum theory assumes) and more specifically, in the form of information on matter for the reconstruction of the particle from the wave. It may be that, depending on the snapshot of inter-conversion between particle and wave captured during the measurement act and related to the presence of information, fluctuating and partial particle properties are reconstructed from a wave. Here, the information self-image of the particle ( $E_n$ ) enters and plays an important role. Under given conditions of measurement only part of the photon mass may be reconstructed.  $E_p$  in relation (9) is simply affected by the ratio between wave and particle state. An uncertainty is to be expected. But there is no reason at all to assume a fundamental origin of uncertainty and unpredictability. There is a complex mechanism involved, which is determining quantum phenomena. The origin of uncertainty is here entirely understandable. It is linked to the structure of the dynamic particle-wave duality. The proposed process of inter-conversion between particle and wave is responsible for a statistically determined reconstruction of the particle's properties. It is true that a detailed theory for our interpretation of the particle-wave dualism still has to be developed. A deterministic statistical chaotic mechanism as a reason for the observed uncertainty is to be expected, since matter in an irreversible world is interpreted as self-organized energy (see below and [10]). Self-organized energy and matter can be subject to deterministic chaos, especially when given structures are decaying or being transformed. And, which is most important, deterministic chaotic statistics cannot, when experimentally observed, be distinguished from arbitrary statistics [14].

Within a “dynamic” quantum physics there is consequently no reason to assume a deviation from causality and determinism. The uncertainty phenomenon is merely shaped by a complex natural process including information turnover. With its complexity it is veiling a logical physics behind.

It is well known that the uncertainty relation predicted that a zero-point energy remains when all other energy is removed from the system. An absurdly large amount of such zero-point energy should consequently be available all over the universe.

The particle-wave duality introduced for a time-oriented physics (2) has shown the information self-image of matter  $E_n$  to be the relevant factor for eliminating paradoxes from quantum physics. The difference in lowest energy between quantum and classical system, which zero point energy appears to be, should therefore also be related to the information self-image of matter. And indeed, when the energy of the wave ( $E_w$  and  $E_e$  in (9), middle) is set zero, the information self-image remains in the formula. The zero-point energy or vacuum energy (in quantum field theory) may not be pure energy itself, but information on energy (and matter). It can be identified with gravitation (see later for more details), which indeed has a cosmological significance. The zero point energy has actually been related to the cosmological constant [15]. Information on matter (gravitation) appears to be the key for understanding the interrelation between (here deterministic) quantum uncertainty behavior and cosmological parameters.

### 2.3. The Law Governing Irreversible Thermodynamics

It has already been mentioned, that the second law of thermodynamics, the observation that entropy maximizes in a closed system, can directly be derived from the basic statement of irreversibility (1) [1]. Traditional physics, basing on time-invertible fundamental processes, cannot do that, which is a significant drawback.

Far from equilibrium self-organization occurs, which requires the involvement of feedback processes, which need a “before” and an “after”. In a fundamentally irreversible, time oriented world self-organization is a straightforward phenomenon. It is the domain where life or hurricanes are functioning. Here, a maximum entropy production is to be expected. Such energy systems, powered by a through-flux of energy, will transform all available energy by decreasing its presence per state (relation (1)) and generating entropy. Entropy production will be rate controlling and only be limited by the constraints of the system.

On the basis of empirical observations a similar result, maximum entropy production for self-organized systems, was already obtained by other scientists. But they could not derive it from more fundamental considerations and prove it. A maximum entropy production rate in the atmosphere, as a state determining the climate, has

been proposed by Paltridge [16] and later others [17]. Pioneering work on maximization of the entropy production rate in relation to human ecology came also from Swenson starting from 1988 [18].

This principle of maximum entropy production, derivable from empirical observations, and following here from the “dynamic” energy postulate, has, however, found strong opposition. It was argued by John Ross from Stanford University that the rates of chemical reactions are controlled by (non-vectorial, non-oriented) thermodynamic quantities such as Gibbs free energy and activation energy and not by the rate of entropy production [19]. And in consequence, he speaks of the “invalidity of the principle of maximum entropy production”. The criticism expressed by John Ross is perfectly reasonable, but it is reasonable only on the basis of reversible thermodynamics, its non-dynamic quantities of state and its traditional understanding of kinetic mechanisms. This situation is entirely changed with the here advanced proposal to introduce a dynamic property of energy via a paradigm change (relation (1)). When energy is given the property or tendency to decrease and minimize its presence per state, then it simultaneously drives the rate of entropy production and controls it. This leads directly to maximum entropy production far from equilibrium within the constraints of a given system. The criticism forwarded by J. Ross [19] no longer applies and, in fact, the requirement mentioned by him exactly matches the introduced paradigm change. The free, available energy no longer “sleeps” but drives entropy production. The law:

$$\text{“Self-organized processes develop maximum entropy production within the constraints of the system involved”} \quad (10)$$

for the non-linear range of irreversible thermodynamics is a straightforward consequence of the “dynamic” energy proposal. It is supported by a great deal of empirical evidence [16]-[18]. It explains, for example, the destructive potential of atmospheric storms, which can rise to dramatic proportions of hurricanes within one day or two. Since biological systems and societies are self-organized, this finding has also significant consequences for understanding biological evolution and the future of human civilization (for a more detailed discussion of this complex subject see [10]).

## 2.4. Gravitation: Information Self-Image of Matter

Within the here presented new understanding of the particle-wave dualism (relation (1) and **Figure 1**, center) energy in the form of particles tends to dilute itself in space, forming a wave and generating some entropy. But information (with energy  $E_n$ ) is activated to keep this process in balance. All together should have the ability to act towards a decrease of energy per state. Compared with the classical picture of matter, there is a difference. To understand matter rationally, it is now not sufficient to describe matter, particle or wave. One also has to consider information on this matter. And this information should be real and somehow present and observable. What is it? This information self-image has an energy value and should therefore somehow be measurable around matter. What energy-related phenomenon is found around matter, increases with matter and penetrates matter? The answer is obvious. It must be gravitation. Can macroscopic gravitational energy indeed be related to this information-mediated balance between concentrated and diluted energy within a dynamic particle-wave duality?

There is an obvious analogy to be seen in our information system, based on television, cell phones and navigation systems. Here the information is contained in the electromagnetic waves, which are transmitted to be present in the environment and to function via digital signals. As with gravitation, the distribution is not even. The communication-mediating electromagnetic waves provide energy, and transmit information. The information, which is considered as mediating activity between the particle and wave nature of matter must also be measurable via the energy, which it involves. Gravitation, the mysterious force around matter, indeed involves energy, gravitational energy. It is therefore concluded that it is actually gravity, which is equivalent to the energy of information  $E_n$  (**Figure 1**, top).

The dynamic energy initiative has yielded a new interpretation of gravitation! It is not a force in the classical sense, but information with a well-determined aim, namely the aim of decreasing the energy per state. But it acts like a force, but unlike other forces (electrostatic, magnetic) only in direction of attraction (and a decrease of energy per state). This deserves being explored more in detail, since gravitation is known to be something very special and a very weak “force”. It also offers an interpretation of gravitation, alternative to that generated by the four dimensional space-time in the general theory of relativity.

When the information self-image of matter, besides of reconstructing the particle from the wave, aims at de-

creasing the presence of energy per state, what happens when one attempts the opposite, to increase the energy per state, for example via acceleration of the same mass? One would expect a “counterforce”, a force that attempts to prevent an increase of energy per state. It can only be inertia. Gravity and inertial forces are determined to be proportional to the same mass or energy. They are forces active towards a decrease of energy per state or are activated in the case of violation of such a situation. The equivalence principle, the observation that inertial and gravitational mass are identical, appears to follow in a straightforward way. The information self-image of matter, interacting with mass and energy, is doing the job. It is gravitation and acts on the particle while the particle decreases its energy per state. It is equally gravitation, which should matter, when the particle’s energy per state is forced to increase during acceleration and thereby generates inertia, a counterforce. This conclusion results from the identification of the information self-image of matter with gravitation. The gravitation on the location concerned should, in fact, be the collective gravitation from the mass of the universe. It is also responsible for inertia. This supports quite a vague idea by Ernst Mach on the origin of inertia, which was later discussed by Einstein, but only partially applied in the general relativity theory.

In the general theory of relativity the phenomenon of gravitation is explained differently and is much more complicated. The mass of a body generates a curvature of space-time. When moving along such a curved space-time, gravity and inertia are expected to become identical for a mass. The experimentally verified equivalence principle is a basic claim, which had been introduced into the general relativity theory. Space was adapted to act in such a way that the equivalence principle is fulfilled.

What is, in fact, gravitation and what speaks for its identification with the information self-image of matter in the model presented here? In science today gravitation is still a poorly understood phenomenon and is discussed in a conflicting way, both physically and philosophically [20]. The “Grand Unifying Theory”, GUT, for elementary particles cannot adequately assign it, because it seems to be something special [21]. It will therefore be all the more interesting to find out what the dynamic energy theory has to say in particular about gravitation as an information self-image of matter.

Gravitation works for large masses of matter, but equally for elementary particles. But the difference in magnitude is large. Between two neutrons and between two weights of one kilogram the ratio of attractive gravitational forces is estimated to be of the order of  $10^{54}$ . Gravitation is nevertheless present everywhere. Gravity indeed supports the tendency to decrease the energy per state (relation (1)). It attracts matter and thereby decreases its potential energy and generates non-useful, chaotic energy, for example, heat. When a rocket accelerates at 9.81 meters per square second, an astronaut feels gravitation like on the earth’s surface. He feels inertia, the resistance against an increase of energy per state. He feels it like a person on the earth’s surface feels gravitation, the pressure to decrease energy’s presence per state. When the rocket engine stops, the inertial force disappears. The energy per state does not increase any more. But if this pressure towards a reduction of energy per state exists why are atoms then not totally compressed? Why are the negatively charged electrons and the positively charged cores of atoms maintaining a large empty space between them? There is an obvious reason why gravitation does not compress atoms and eliminate the enclosed empty space [1]. Quantization results from this attempt, since also energy for information (gravitation) gets minimized. This way electrons are forced into well-defined diffuse orbits of standing waves, which correspond to minimum energy-information conditions. Equation (2), by the way, would then describe the relation of gravity to quantum theory (it occurs via  $E_n$ , the energy involved in information). It would describe a straightforward interrelation between the gravitation phenomena in space and the function of atoms and elementary particles (compare **Figure 1**). Such a relation has been intensively searched for in conventional physics but has never been found. The field of quantum gravity deals with that problem, aiming at a “theory of everything”. String theory is an example of approaches, which have been followed. They seem to have basically failed up to now, and from my point of view the reasons are obvious: quantum theory has to be modified to become “dynamic” and the gravitation concept of the general theory of relativity has to be challenged (see later). This appears to be a harsh statement, but is a necessary consequence of the paradigm change discussed here.

Within the model analyzed here the unification of gravitation with quantum physics is a side product, however with an important new insight: the energy of information,  $E_n$ , identified with the energy contained in gravity causes quantization to occur [1], but is itself not quantized. Also the mysterious phenomenon of quantum correlation would be related to properties of gravitation and would suddenly become more transparent. Since the particle-wave duality involves an information self-image, this self-image has to be dealt with when the particle is split up (**Figure 1**, top left). Due to conservation laws only part of the original self-image can be split up and the

rest will maintain joint information for the separating particles. Lacking a detailed theory it can presently, however, not be said up to which distance such information contact will be supported. However, for energetic reasons, I predict the reach of quantum correlation will not be infinite, as quantum physicists today claim, for quantum theoretical reasons. All together the interpretation given here for quantum correlation would not contradict logics. Correlated particles are acting like couples which maintain a reasonable contact via a cellular phone even when temporarily separated locally. One just has to be prepared to accept that information on matter is part of quantum reality, and information (gravitation) also involves the possibility of communication between separating particles.

The fact that this very special phenomenon of quantum correlation can readily be explained is considered to be strong support for the discussed dynamic energy approach. Indeed, the very circumstance that quantum correlation exists also justifies the existence of an information self-image of matter for the original, undivided particle (**Figure 1**, center). And this information on matter is exactly what makes up the hitherto mysterious gravitation phenomenon.

In contrast to other forces in nature gravitation penetrates all matter. A material body can also not be extracted from a gravitational field nor can it be shielded from it and gravity cannot be neutralized. It can, however, be partially or totally overcome by inertia. A high flying airplane in a sharp curve downwards leaves its passengers temporarily without gravitation. Within the model presented here this means that the drive to decrease the energy per state, and to give by to the attraction of gravitation, is just compensated by the drive resisting against an increase of energy per state, within the phenomenon of inertia. These two opposite drives are felt as forces, which in the described situation just compensate. In fact, however, these are two different communications of information, which are just compensating and neutralizing each other.

Gravitation itself is caused by mass. Gravitation is, therefore, not the consequence of interaction of masses and it could until now not be explained on a more fundamental basis, which however the present effort claims. Gravitation needs mass, but it is not a consequence of action. Since action is the consequence of a cause, which requires time, gravitation should not be exposed to the flow of time. This is, in fact, also in agreement with the new model provided, which identifies gravitation with information. During the information-mediated particle-wave interchange no energy is converted and consequently no action is generated. Therefore, no time flows. In contrast, matter and energy themselves are exposed to changes and time. It is information and the energetic aspect of information which aims at decreasing the energy per state. In a gravitation field this is equivalent to an attracting force and explains why there is no repulsive counterpart of gravitation. It gives weight to objects, attracts them and causes them to fall towards the ground. From the time of Newton we know that when two particles with the mass  $m$  interact, the gravitational force between is proportional to the square of the mass divided by the square of their distance. According to Newton it is a force at a distance, but nobody understands how such a far-reaching force may fundamentally work.

For Einstein, in his theory of relativity, gravity is not a typical force, but the consequence of the movement of objects through a curved space-time. It is an interaction at close distances. In fact, within such a picture, acceleration arises from a “curved” time. This is a time, which changes its flow in such a way as to simulate acceleration. One should reflect here for a moment and try to imagine how a void with nothing in it can have such an elaborate property of manipulating time, which not even the most sophisticated technology can do. Nevertheless, the reasons for planets cycling around the sun are consequently not attractive forces, but a curved space-time structure around the sun and the planets. The energetically permitted orbit for a planet is then its essentially elliptical planetary orbit. Photons, light particles, are also characterized by a mass and momentum and consequently deviated by gravitation. Einstein has simply transformed all the mystery about gravitation into a sophisticated four-dimensional space-time. All moving objects should be exposed to the same natural laws, including a constant light velocity. But Einstein’s theory of general relativity cannot explain the fundamental character and mechanism of gravitation. Empty space is just manipulated to impose the phenomenon of gravitation when masses are present. However, nobody can explain why and how empty space can implement such very special properties and this is a significant weakness. From the point of view of understanding nature, it is a clear setback. No detailed rational theory is imaginable that can explain such complicated behavior of empty space. As mentioned, it is so complicated that Einstein himself, years after publication of the general relativity theory, was again speaking of an “ether” with special properties that should be able to do the job [22].

The dynamic energy approach discussed here which has already helped to eliminate diverse paradoxes and irrationalities offers a much simpler alternative theory for gravitation: the energy related to information,  $E_n$ , in-

volved in the interplay between particle and wave with the aim of decreasing energy per state. Information tells masses how to act. They act like systems guided by remote control. The mechanism is not action at a distance like Newton's gravitation, and not action at a close distance like Einstein's gravitation. It works as long as information is around and this means here gravitation. The technology works as when information is used to operate a system via remote control. An information signal (gravitation) must reach the moving object. Planets around the sun or satellites around the earth would thus follow the natural "remote control" mechanism operating via gravitation, forcing them to always fulfill the condition of minimum energy per state or, equivalent, of least action. They are exposed to gravitation and, accordingly, select their specific orbit. Wherever a planet or a satellite goes, the condition of a minimum of energy per state is fulfilled. It is ultimately the "dynamic nature" of energy, and its implementation, which is the secret of gravitation. Gravitation is neither a force, nor an interaction. It is information implementing a fundamental natural law, which dictates a decrease of energy per state. Looking at the example of a stone rolling down a hill, it can be said that gravitation forces the stone to always fulfill the condition of minimizing the presence of energy per state via its information content. We know now that we can also say that the stone follows the principle of least action in a dynamic way. The same happens with a satellite circulating around a star or a planet.

Since understanding gravitation is so important let us use an additional check-list of properties of gravitation to verify in more detail whether these can reasonably support the claim raised that we are dealing with an information self-image of matter.

1) "Matter and gravity cannot be separated". This is evident from relation (2) since energy of information mediates between particle and wave form of matter

2) "Shielding matter from gravity is not possible. It penetrates all matter". There is no contradiction to be expected to this finding.

3) "Gravity effects can accumulate to large phenomena". There is no reason why energy of information should not accumulate in the presence of large quantities of matter. Information is additive or, if oriented into the opposite direction, subtractive.

4) "Gravity only attracts, it does not repel". This is evident since only attraction of matter can lead to a decrease of energy per state (relation (1)). Such a property makes gravity different from typical forces.

5) Gravity and inertial forces correspond to each other, but are opposite in direction. They reflect the action of masses from the universe. A mass feels all the gravitational forces of the universe. If a mass is accelerated, it acts against the gravitational forces of the universe. This is what the Mach principle claims and thereby rejects an absolute, empty space. In our picture, the following phenomenon would happen: when matter accelerates, the energy per state would increase, so that the energy of information,  $E_{in}$ , would counteract. This would be experienced as inertia. The effect would be supported by all masses from the universe felt via gravitation. Inertia would thus simply be a counteraction to a violation of gravity, which (here) implements the claimed tendency of energy to decrease its presence per state (relation (1)).

6) If gravitation is not the consequence of a cause, then it is not exposed to a flow of time. Indeed, the dynamic particle-wave duality expressed in (2) does not involve a time flux, since energy only spreads and contracts in space, but is not turned over. It is an on-going, eternal phenomenon and will be present as long as matter exists. As a consequence, there cannot be a spreading of gravitation when mass is localized, since spreading would involve time.

7) The general theory of relativity predicts gravitational waves. Lately scientists claim to have detected them [23]. The identification of gravity with information mediating the particle wave duality allows a clear conclusion: information, and the energy related to it, is not expected to be able to generate waves itself. However, self-organized information, expected in a region of exceptionally high gravity and additional energy, could, in principle, induce oscillating phenomena (see next subchapter). But also bursts of information on matter could be liberated via nonlinear mechanisms from cosmic areas with intense gravitation and energy. It should be emphasized here that in order to really confirm an oscillation of space-time according to the general theory of relativity, a parallel oscillation of "time" should be observed. It should actually be detectable since, according to Einstein, time is what the watch shows.

8) In a given gravitation field all bodies, whether as light as a feather or as heavy as a hammer, are exposed to the same acceleration ("g" on the earth surface). They approach the ground at identical speed if air is not present to exert different friction. One can rationally understand that the information self-image imposes such behavior, an identical acceleration. The information given in the same gravitation field towards a decrease of energy per

state is simply identical for different mass objects. The force experienced (and the weight of a body) is, of course, different because acceleration has to be multiplied by the mass, which is accelerated, to obtain the force. The acceleration due to gravity on the surface of the moon is only 0.16 g. Correspondingly less information on matter is active there towards a decrease of energy per state. The acceleration towards a decrease of energy per state is apparently changing proportional to the density of information.

The information self-image of matter could thus indeed be the origin of what is called gravity. It is not a force and not an interaction. It is information on the state and dynamics of matter, energy, and implements a fundamental dynamic law. This turns simultaneously out to be a reasonable and interesting explanation of gravitation. One understands why it had to become a relevant property of nature.

If we, for example, want to understand the deviation of light in a gravity field we would have to explore interaction possibilities of the particle-wave relation (2) with the perturbing systems. Tentatively I would say that, when gravitation (information) from a photon superposes gravitation (information) from a larger mass, a corresponding additive superposition of information should be expected. Light will consequently react in response to external gravitation (information on matter). A quantitative theory remains to be developed.

Gravitation also plays a fundamental role in determining the dynamics of the universe. It may consequently be expected that the information involved in gravitation acts in a similar way in large scale dimensions. It is information, which should consequently control generation, evolution and fate of the universe. Within some kind of fractal similarity, which could be assumed, there should consequently also exist an information self-image of the universe (**Figure 4**). It is information, an information self-image of the primordial world, which activates useful energy at the start of a re-born universe, which then again aims at generating non-useful, chaotic energy in the form of entropy, by allowing energy to decrease its presence per state.

A fractal link between quantum processes and cosmic events (**Figure 4**) implies a joint fundamental (mathematical) basis, which may also help explaining how spreading photons can adequately consider space for entropy generation. This way it is possible to confront the Big Bang theory, which is characterized by extreme and partially irrational assumptions and many contradictions [24], with a fractal model for the evolution of the universe, which emphasizes the role of information. This SI-universe (Self-Image universe) is based on a (periodical) recreation of the primordial universe through an information self-image (**Figure 4**) (for more discussion of this subject compare [10]). The idea that information should be active at the beginning of cosmic development is not alien to the human intellect and human imagination. The Bible, for example, says: "In the beginning was the word" [25]. And such an information induced start of a free energy rich universe with subsequent increase of entropy and local growth of order at the expense of entropy production is entirely in agreement with our understanding of thermodynamic laws. And from the impressive function of 3D printers we understand how information can indeed create structural and dynamic reality. The information based self-image universe is a high-tech scenario compatible with presently recognized and understandable natural laws and with working information technology.

This is in marked contrast to the Big Bang scenario where the universe starts from nothing to chaos and maximum disorder. Here a creation of energy and time-flow from nothing has to be postulated, as well as an explosively fast expanding, inflating void. The latter incredible postulate is in fact needed to explain the reasonably high uniformity in space. But it is also needed to increase the potential for additional disorder (for the purpose of allowing entropy formation during energy conversion processes) via a huge added abstract volume (created through inflation of the void, the empty space). This should enable the energy conversion processes that generate the observed structures and function. The Big Bang theory describes a low-tech model, on the basis of very speculative additional assumptions.

## 2.5. Consciousness, Spirit and Super-Gravitation

Natural science has recently been criticized for not being able to explain evolution and function of consciousness and human spirit. Philosopher Thomas Nagel [26] claimed, that the preconditions for evolution of spirit, in terms of physical laws, must have been there in nature before humans developed. His argument has to be taken seriously. Humans have developed consciousness and there may be innumerable living beings in the universe with similar abilities.

In a fundamentally oriented and irreversible world there is a straightforward answer to this important question: consciousness can be explained on purely materialistic, scientific basis. It can be understood in the following way:

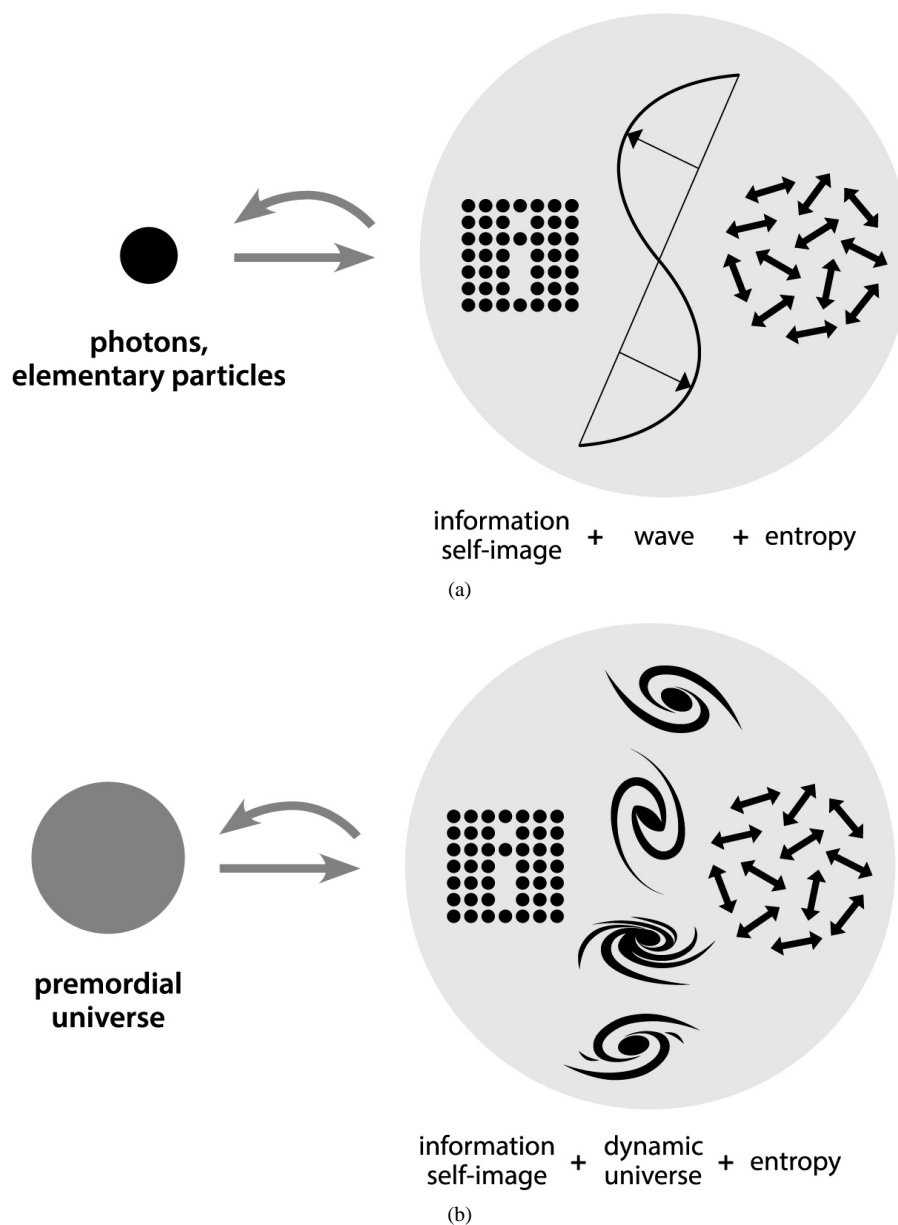


**Figure 4.** Within a fundamentally oriented reality the universe has apparently a fractal, self-similar structure and function: the gigantic space seems to work as a “Self-Image Universe” (b), essentially analogue to the proposed sub-microscopic “dynamic” particle-wave dynamics (a). In both cases information is set aside for the final recovery of the worn-out or spread-out product of energy activity.

In a fundamentally irreversible world in which time is proceeding (via a flow of action) there is a “before” and an “after”. Feedback processes are possible. Therefore self-organization of matter will be a straightforward consequence, as long as energy is flowing through the system, and the system is pushed sufficiently far from equilibrium.

When looking at biological life-forms, one, of course, recognizes that self-organization,  $SO$ , can occur with matter. Self organization of matter is consequently a function of matter  $m_i$ , which can be formulated as follows:

$$SO = f(m_i) \quad (11a)$$

Mathematically, matter can consequently be handled in such a nonlinear way that self-organization works and

can be calculated and demonstrated. Matter is something that occupies space and has mass. Matter is consequently a function of mass  $m$ . Self organization,  $SO$ , therefore proceeds with mass:

$$SO = f(m, (m)) \tag{11b}$$

Mass is, as well known, mathematically linked to energy via  $E = mc^2$ . Consequently, energy can, in a fundamentally irreversible world, also self-organize, when appropriate conditions exist.

$$SO = f(m, (m(E))) \tag{11c}$$

What can be the consequence of self-organization of energy? It is proposed, that the large family of elementary particles is the product of self organization of energy (in more detail discussed in [10]). Their formation and interaction, in nature, and their generation, during high energy experiments, would have to be described and discussed accordingly. Mechanisms and properties of self-organized processes would have to be considered. The conversion of structure and function of one particle into other particles or from a photon particle into a wave could, for example, be triggered just by a small parameter change.

How can now information be considered for self-organization?

Since information,  $I$ , has an energy content and is a function of energy, energy can be expressed as a function of information. This can be considered in (11c), so that information should also be able to self-organize, when appropriate conditions prevail:

$$SO = f(m, (m(E(I)))) \tag{11d}$$

Therefore information itself will also be able to self-organize, provided the system supplies essential material properties and is pushed sufficiently far from equilibrium. In addition adequate structures must exist and adequate feedback processes between information modes have to occur. This important conclusion follows from these simple mathematical considerations. They show, that from the fact, that self-organization of matter exists, self-organization of information can be deduced mathematically.

As matter (energy), which brought about life, can self-organize, information, which is also based on energy turnover, can, in principle, do the same (Figure 5). The preconditions only are that some degree of order in information structures has to evolve before and that the information system has to be pushed sufficiently far away

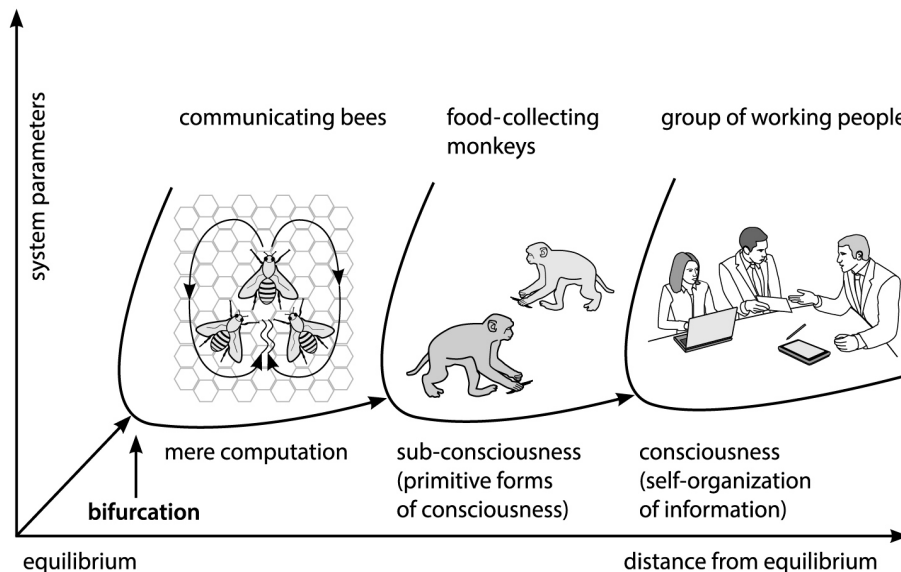


**Figure 5.** The diagram shows the influence of the distance from equilibrium for information systems, which is controlled by the through-flow of energy. During evolution more and more energy became available to the brain and shifted information activity from mere computation to self-organized computation, which initially corresponded to more primitive forms of sub-consciousness, and finally yielded consciousness.

from equilibrium. Also a flexible, variable hardware seems to be required. The information storage elements involved in self-organization could be chemical, as implemented in the genetic code, or electrochemical, as functioning in our brain. The result would be a much higher hierarchy of computation. This higher hierarchy of consciousness is a fact. In addition it is clear that we are actually dealing with an information system, and that consciousness has gone through evolutionary steps (sub-consciousness, collective consciousness, personal consciousness). Furthermore it is known that there is high energy consumption going on in the brain. An additional evidence for such an interpretation of consciousness is the above calculated relation between information and self-organization (11d). All this speaks for a really functioning mechanism of self-organization of information. A science based on equilibrium, time-invertible laws and a time-neutral energy phenomenon could not support such a process, and has for that reason been criticized [26]. The implementation, within the dynamic energy concept in an oriented world, of a fundamental energy-time drive is decisive for the shift of a system away from equilibrium and for the necessary feedback processes.

Consciousness, as humans evolved it, is a very sophisticated information program. It gives a person a personality and active control over his situation. The theory that consciousness controls our computing brain via self-organization of information is also supported by additional arguments: Kurt Gödel [9] developed a theorem in 1931, the incompleteness theorem, which became one of the most important statements of modern logic. It can be interpreted to state that a machine controlling another one has to be associated with a more superior hierarchy. The comparison of self-organization of information in relation to information itself with a living bacterium and its chemical components in water gives the adequate answer: a living bacterium functioning via its self-organization structure represents a hierarchy clearly above that of an aqueous solution of all chemical substances, which make up the bacterium. Its living activities also clearly demonstrate that it can control chemical activities.

Self-organized information could therefore in principle well control pure information. It is hierarchically definitively placed above pure computation. It can, therefore, be understood as the mechanism of consciousness. It makes man conscious and helps him to organize his life in a complex environment in a more creative and competent way. It also shapes his intentions and determination. The “dynamic energy” approach allows a purely materialistic interpretation of consciousness.

An interesting additional subject for further thinking on self-organization of information is also gravitation. In present physics gravitation is, as above mentioned, still a mystery and has been discussed as a very strange force. But in this study gravitation is found to be information, mediating the particle-wave duality (relation (2)) and implementing a decrease of free energy per state. This kind of information, gravitation, should also be able to self-organize, provided enough energy is turned over to push the gravitation system far from equilibrium and feedback processes can develop. A significantly higher and more elaborated gravitation, a kind of super-gravitation may be the consequence (indicated in [Figure 1](#), right, bottom). And super-gravitation should also have the potential to become spatially structured like living organisms. This phenomenon may, for example, take place in the center of galaxies where high concentrations of matter and energy are present and interact. But it may also occur more widely distributed over the space, structuring it via gravitation patterns. Astrophysicists know a phenomenon called “great attractor”. It attracts galaxies, including our own. This may be the result of self-organization and structuring of gravitation. The resulting super-gravitation will have much more sophisticated properties with respect to the interaction of matter than ordinary gravitation. Above all it is to be expected that the capacity to decrease the energy per state, which this information—gravitation—should implement, will be much more effective. There should be a much higher attraction between matter, and it is perfectly understandable why light can penetrate a super-gravitation zone, though with deviations due to the mirage effect, which is actually observed. This happens like an ordinary mirage on earth develops under a special weather condition, a condition of the atmosphere, which itself is a self-organized phenomenon. Self-organized gravitation in space could indeed be compared to special weather conditions on earth. Both self-organization phenomena may generate optical mirages.

Obviously self-organized gravitation is an alternative theory to dark matter since it would explain a high and spatially structured gravitation, which is not balanced by sufficient visible matter. But no additional matter would be needed in this case. There would not be a need to search for invisible new particles, but there must be sources for energy turnover in the environment to push the gravitation system far from equilibrium for self-organization. It is obvious that such an explanation, together with the above, alternative interpretation of galactic redshift as entropy phenomenon, requires a corresponding new evaluation of cosmologic dynamics.

### 2.6. Relativity Theory and Four-Dimensional Space-Time: Do We Need Them?

The information self-image of matter ( $E_n$  in (2) and dot pattern in **Figure 1**, center) provides a straightforward and rational explanation for gravitation on quantum and cosmological level in an irreversible natural environment (see above). The same information self-image of matter could also guarantee an always constant light velocity in any reference system. The generation of a constant light velocity of a photon particle could simply be part of the program executed for recreating the particle from the wave. The program should be the same for every reference system. That this is indeed possible regardless of varying velocities of different reference frames is visualized in **Figure 6**. Imagine an airplane in full flight receiving digital information from a distant television station. A perfect television picture would be seen. In fact, if a corresponding information would be transmitted to the plane for driving a three dimensional printer, this would also be possible irrespective the relative velocity. The printer could produce a toy-car, which is able to drive at a constant velocity. In the same way information could also be used to regenerate a photon from the wave (relation (2)) with always the same constant light velocity in the given reference frame. Information would have been used to produce an object able to propagate

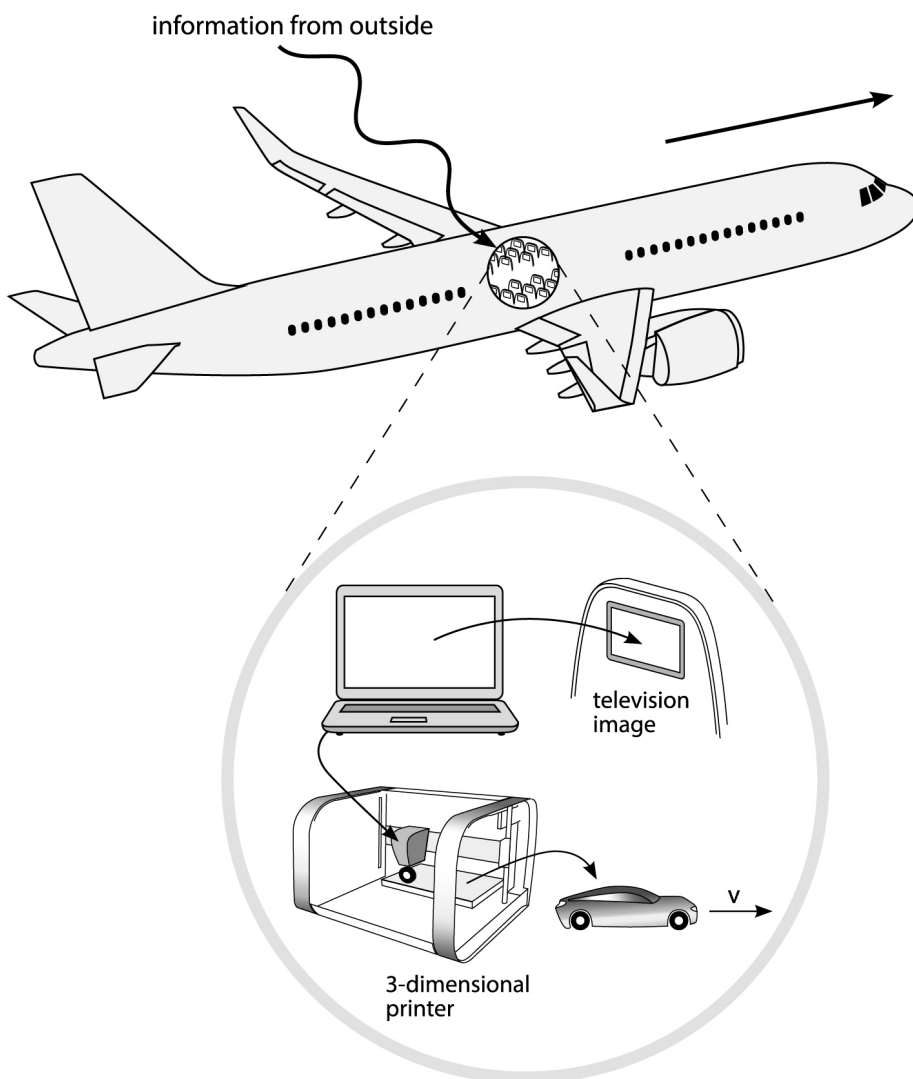


**Figure 6.** Why can the information self-image of matter reconstruct light particles with an always identical velocity? It is like transmitting a television program or the information for a three-dimensional printer to a flying airplane. The printer could produce a toy car, which then drives with a given velocity. The outcome is fixed and will be identical irrespective of the airplane’s flight direction and speed. Information transfer is the key for rationally understanding constant light velocity.

with constant velocity, regardless the flight direction and velocity of the plane or a reference system. This would be a rationally understandable, working mechanism for the fundamental implementation of an always constant light velocity.

The information self-image of matter can indeed explain both gravitation itself (as shown above) and the always constant light velocity (indicated in **Figure 1** right and top). Can this route of explanations replace relativity theory?

The special and general theory of relativity has originally been designed to explain these two natural phenomena: the always constant light velocity and the strange force, called gravitation. The empty space was mathematically manipulated in such a way that gravitation, inertia and the always constant light velocity are adjusted and function as experimentally observed. A complicated four dimensional space-time resulted which around matter shows a dramatic curving of space and time. The general relativity theory has, even though it is based on time invertible basic laws and does not consider energy conservation, become the standard for explaining highly dynamic space phenomena, ranging from the assumed Big Bang event to space inflation and black holes. Why has the general theory of relativity become so important in explaining gravitation and the dynamics of our universe? First, nobody had an idea of how to explain an always constant light velocity differently, besides of suggesting a special “ether”, which was the model preceding Einstein’s special relativity theory [27]. In addition, the mathematics of general relativity turned out to be so complex, that it was only gradually understood [28].

Many of its solutions turned out to be irrelevant, others difficult to interpret. Then new circumstances entered. Since the availability of modern computers, physicists can more easily play with the complicated formula for general relativity and space-time involving ten parameters [29]. Via these many parameters and the singularities, which the general theory of relativity yields, such as extreme peaks and deep valleys, an incredible amount of possible scenarios can be described. Only few solutions seem to make sense. There is presently no indication as to why the relatively inaccurate predictions of the general theory of relativity cannot be explained by other, less farfetched and less complex theories. But what about the famous relation  $E = mc^2$  derived by Einstein from the relativity theory, which describes the energy of a mass  $m$  at zero velocity. It may be necessary to say here that it has been shown that the derivation of this formula was not really based on logic reasoning but already presupposed in the derivation of the result [30]. Classical derivations of analogue formulas have also been cited [31]. Einstein speculated that the energy formula he derived for light (and which included arbitrary choices) may also be valid for any energy in general. Two years before Einstein an Italian geologist, Olinto de Pretto, published the same relation between energy and mass deriving it from other non-relativistic considerations [32].

The point here is that we want to understand what this formula actually means within the relativity theory. In fact the formula  $E = mc^2$  has nothing to do with relativity. It would be still valid if the four-dimensional space did not exist. Einstein had neglected relativistic considerations prior to obtaining the famous energy-mass formula. It can be derived with classic arguments only. The energy-mass relation can therefore not be used in support of the four-dimensional space-time concept. This is here an important argument.

In addition, the reasoning developed here within a time-oriented physics, requires that mass is self-organized energy (see discussion above and relation (11c)). When this is accepted to be true, then mass is accordingly also in this picture proportional to energy. The proportionality constant ( $1/c^2$ ) is, however, not evident and is expected to be much more complicated. The fact that the energy-mass relation also follows from the dynamic energy approach via the interpretation of mass as selforganized energy is an additional support for its consistency.

The concept of a fundamentally irreversible world has thus yielded an entirely new and unexpected explanation for gravitation and the always constant light velocity. Explaining gravitation, inertia and constant light velocity via information is rational, in contrast to giving such properties to a manipulated empty space itself. What incredible properties of empty space must be imagined to control constant light velocity or to adjust the time flow around masses to mimic inertial movements! Relativistic changes in length and time, which are predicted by the relativity theory, can be considered to be simply measurement phenomena caused because of the finite light velocity. Measurements from different orientations and velocity frames would produce different values of length and time. A really shrinking rocket would simple dismantle, but theory predicts it could later land regaining its full dimension.

Also the energy measured from different orientations and velocity frames would produce different values. Can an individual energy system simultaneously have different energy values? What about experimental “proofs”

for relativity theory? Presumed gravitation waves measurements and gyroscopic measurements involve tiny experimental effects (stretching the space by one part in  $10^{21}$ , or by the width of an atomic nucleus for detection of gravitation waves; gyroscope spinning angle change of 1.8 thousands of one degree per year). The here discussed physics of a fundamentally irreversible world could provide alternative explanations. The focus of attention should be the action of information on matter (and gravitation respectively). It explains light velocity, gravitation and inertia in a different way and could consequently also explain phenomena attributed to them differently and rationally.

The here advanced concept of information involved in elementary particle properties and gravitation has the potential to make quantitative predictions, provided a more detailed quantitative theory is elaborated along the line of thoughts presented here. To give an example: In the case of photons deviated by gravitation it is the information self-image of matter, which interacts with information in form of gravitation from other sources, while reassembling of the photon from the wave occurs. This superposition of information on matter will generate the observed change in the flight trajectory of the photon. It is expected that a four-dimensional space-time is not needed for explaining the phenomena observed. Information could much better interpret them than claimed irrational properties of free space (for a short summary of presently favored concepts on space, time and gravitation see for example [33]). And it would be intuitive understanding, like we understand a remote controlled device responding to an external signal.

## 2.7. The Flow of Action and the Phenomenon of Time

For science today time is an illusion. What time should one take, if time flow for systems in relative movement is variable? Historically numerous personalities have reflected about the meaning of time and contributed interesting information and ideas without really fully answering the question: what is time? [34]-[41]. On the basis of an analysis of the principle of least action it was found that this principle describes a fundamentally oriented world and a fundamental, rate controlling flow of action during energy turnover [1]. This required a paradigm change from a time invertible world to an irreversible one. It means that the free energy of physical systems tends to decrease its presence per state. Consequently production of action, energy times time, is the essential basis of changes. Around us many flows of action are proceeding wherever energy is being converted. This is what causes the observed “time flow” in nature. It is what we see happening in the environment and this is what occurs in our brain. But time itself, as described by “ $t$ ”, is only an ordering parameter. It has no material or energetic substance at all and can therefore not directly be measured. Clocks determine it nevertheless by measuring the flow of action resulting from an energy converting mechanism. They basically divide it by the energy turned over and calibrate it with a selected periodical astronomical event in days, hours, minutes and seconds.

Time flow, as determined by action, energy times time, itself is not an illusion. When action is transferred to frames with different velocity it stays actually invariant, even within the theory of relativity. In order to determine real time flow in an irreversible world, action has to be transformed to another frame in relative motion, and the time ( $t$ ), the ordering parameter, has to be determined there by dividing action by the energy turned over locally. Since action stays invariant during transformation, time for energy converting systems would then be the same in frames with different velocities.

This is of course different with time in the theory of relativity. It is separated from energy and transformed independently like energy itself. Here time is relative in frames with different velocities and special phenomena such as time dilation and time travel become possible, which can lead to well known irrational contradictions with physical laws and with thermodynamics. The time “ $t$ ” in the theory of relativity, which is already separated from substance and energy, is thus a theoretically manipulated time and refers to systems, which do not turn over energy, such as quantum states and elementary particles in such situations. Time delays in systems at different velocities are actually measured (such as with muons) and can be considered real, since they are actually determined. But my interpretation is that it is the measurement process, it is the finite light velocity, which is signaling a distortion of reality. This can be recognized, when several observers at different positions and velocities are measuring the time on an identical reference object. It will be different for each one and only be seen in direction of the relative movement. An observed object cannot simultaneously have different times. Another example is the change of length of an object seen on frames with different velocity. If it would be real and if the object would be a rocket, it would be dismantled during the change of dimension. However, when the rocket is landing, its original size appears re-established. The relativistic phenomenon here is just an illusion of measure-

ment, based on transmission of information by light. Time in its naked form,  $t$ , time which the clock shows (according to Einstein) and which is not characterized by substance, matter or energy, is just an ordering parameter in combination with the constant light velocity. In this combination, with the dimension of distance, it evidences the distance across which action can travel in time. But itself this naked time “ $t$ ” is not able to express action, energy times time, which is the origin of real time flow, as it is expected to drive real phenomena like the Big Bang or Black Holes, which are calculated, using the general theory of relativity. Already for this reason the predictions of the general theory of relativity therefore appear not to express the reality of an energy converting universe. But they can, of course, support imaginative theories due to extreme singularities and many adjustable parameters.

In conclusion: the flow of action, as considered in the principle of least action, is the real, energetic basis of time flow. If we select a machine (e.g. an hourglass), which is providing a constant flow of action, a flow of “least” action in the form of trickling sand, and if we calibrate this flow with an astronomical flow of action (e.g. the movement of the earth around the sun) then we get a “time”, which is not an illusion. But the basis of time flow is always the flow of action, and only action, energy times time, should be transformed to another reference with different velocity, if “time” should stay relevant for energy converting systems. However, for exactly such reasons time travel, which is predicted by the theory of relativity, will remain an illusion. “Time” in form of a flow of action is not an illusion and existed and will exist as long as energy conversion occurred and will occur.

## 2.8. Black Holes and Quasars: Understanding Space Objects in an Irreversible Universe

A fundamentally oriented and irreversible world will follow its special laws. Since a time arrow, based on the flow of action, exists, self organization processes will proceed and systems will develop and compete towards maximum entropy production.

Here, an example should be discussed to understand such behavior in relation to the expected dynamics of black holes, in contrast to traditional understanding.

Within the general theory of relativity contracted masses can drastically deform space-time to generate a black hole with an event horizon, beyond which there is no escape for matter and energy. But close to the event horizon virtual fluctuations may cause particle-antiparticle matter to appear and liberate a radiation called “Hawking radiation”, which can gradually lower the mass of the black hole [42]. Time invertible physics of relativity and quantum theory are thus presently used to “understand” the dramatic dynamics of black holes [43].

The approach of fundamental irreversibility draws a different picture since self-organization of matter and energy, as well as maximization of entropy production will become corner stones of understanding. Black holes themselves, which compact and convert large masses through gravitation (here information towards decreasing the presence of energy per state) run gradually into a problem. On one hand they develop to become self-organized systems, but because of the high gravitation, they cannot get easily rid of entropy in the form of chaotic waste energy. The black hole will temporarily serve as a grave for entropy, because gravitation is too high. It would be like if a vegetarian dinosaur could not get rid of digested food any more. How can a black hole deal with such a situation? In this context quasars are especially interesting objects and are typically found associated with a black hole in the center of galaxies with a bulge. This combination could explain how a black hole finally gets rid of its entropy, which becomes confined by massive gravitation. The black holes collect matter and star fragments and rotate them in a so-called accretion disc (Figure 7). From there matter can fall into the black hole or be radiated away with total intensity amounting to between one million to one billion times our solar radiation. In fact, radiation intensities equivalent to that of one hundred Milky Way galaxies have been estimated [44].

Such radiation emitting systems are called quasars. They belong to the most brilliant objects in the universe.

In our view quasars somehow originate from black holes, which have drifted further and further away from equilibrium because of the problem they have in getting rid of entropy due to high gravitation. The quasar black hole assemblies seem to have reached an evolution state where maximum energy turnover and, correspondingly, maximum entropy turnover is approached by a self-organized inorganic system. A black hole alone would, because of extremely high gravity, have difficulties in emitting radiation and matter. But evolution within an irreversible universe has facilitated a way out by modifying the self-organized system while increasing its distance from equilibrium. This way it is probing new “bifurcations” and gradually changing the black hole into a system, which can be understood to be an association with a quasar. The result, a self-organized system with much

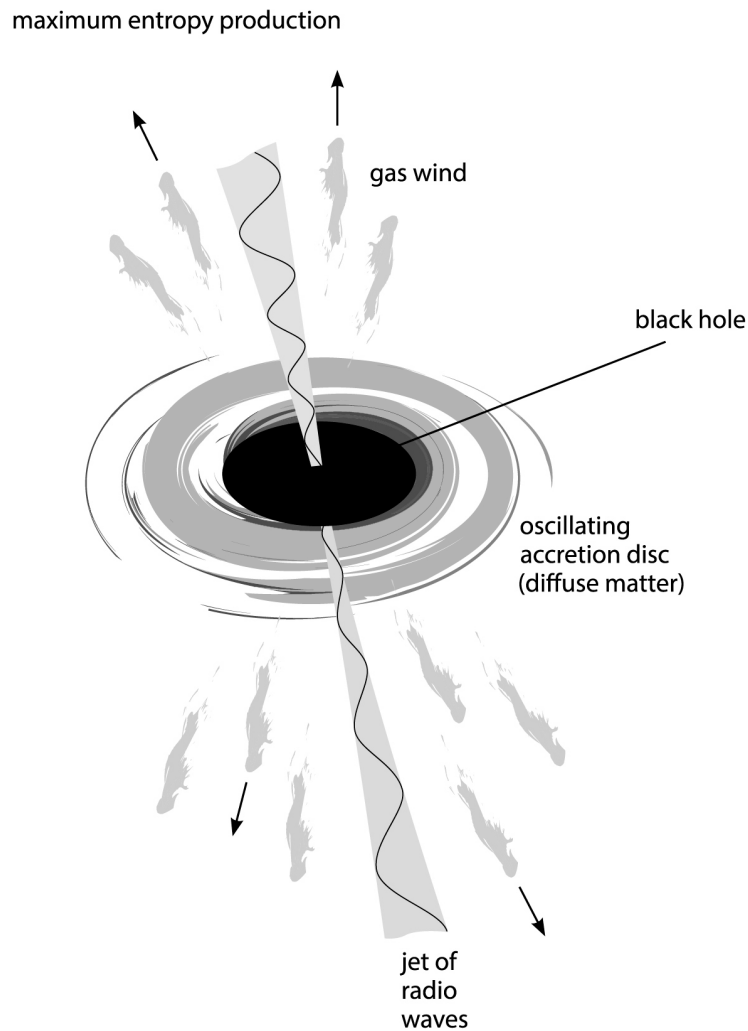


**Figure 7.** Association of black hole and quasar facilitating maximum entropy production. Both are dynamically self-organized systems, which, depending on the energy turned over, vary their distance from equilibrium and their parameter constellations. Maximum entropy emission occurs through the accretion disc, which appears to serve as a kind of logistic platform for the collection of useful matter and emission of waste energy. Self-organized and spatially structured gravitation (information) may be part of the mechanism.

improved ability for entropy production and emission, is convincing. Also self-organization of gravitation (information, as discussed above) may occur leading to structural patterns with gravitation-free channels for entropy emission into space. Jets of electromagnetic waves are actually seen to leave quasars as well as gases.

Quasar-black hole associations change in light intensity within weeks or months. They are inorganic systems essentially behaving like living animals. I compared them with vegetarian dinosaurs. Their activities depend on the existing constraints. Dinosaurs also generated less entropy when finding and digesting less food.

In this way quasars appear to be associated with black holes to which they donate matter and from which they subtract “degraded, chaotic” energy in the form of radiation and dust. The association between a black hole and a quasar thus testifies for maximum entropy production during conversion of solid matter into liberated waste energy.

The “evaporation” of matter from quasar-black hole aggregates via nuclear processes aims at generating a maximum distribution of “chaotic” energy in space and time. They are basically executing, to a maximum performance, because of optimized constraints, what I claim to be a fundamental law: energy’s tendency to decrease its presence per state in space and time (relation (1)).

In conventional cosmology the role of the quasar is interpreted differently: it is just a secondary phenomenon. Its enormous light emission is expected to result from the accretion disc, where matter rotates while waiting to be accepted by the black hole. Energy is essentially thought to be liberated through friction. In contrast, our interpretation here is that evolution of an inorganic self-organized quasar-black hole system has optimized energy turnover for maximum entropy production within the constraints of the system. It is more or less behaving like a storm that grows into a super-hurricane, distributing its entropy over a wide area. Energy and matter is simply following a natural law, maximum entropy production far from equilibrium (statement (10)). And there is an evolution of energy conversion activity: The developing self-organized black hole system dynamically restructures and “searches” for a way to get rid of entropy. This search is simply the consequence of the recognized fundamental energy property. Entropy confined into a limited space has a higher value of energy per state so that black holes grow. Larger black holes finally find a way to get rid of energy in the form of entropy, chaotic waste energy. They do it by restructuring in such a way that entropy, non-useful energy, can be ejected. This apparently happens via the so-called accretion disc, which forms around the black hole and handles the transport of matter-energy to the black hole and of entropy, non-useful matter and energy, from the black hole (Figure 7).

That the accretion disc is a product of dynamic self-organization is not only evident from its spiral structure, but also from quasi-periodic oscillations, which have been observed to occur in these.

Processes far from equilibrium are expected to control many aspects of space structures, ranging from galaxies of different shapes to aggregations of them showing complex order in form of clusters and lines, but also respecting voids. Gravitation has long been recognized to be a very important parameter for structure and function of space. Here identified to represent information on matter and able to self-organize it plays an even more important role in determining evolution, structure and dynamics of the universe. A remarkable result is that one is dealing with information, which is not only responsible for quantum phenomena, but also for cosmological contexts (Figure 1). This opens new ways for asking questions and reflecting about the origin and destination of the universe and its structures. An information based alternative to the presently favored Big Bang scenario of cosmic evolution becomes evident, as discussed in context with gravitation (subchapter 2.4, for more details see [10]).

### 3. Discussion

This effort to explore natural phenomena from the viewpoint of a fundamentally oriented, irreversible world, motivated by a re-evaluation of the meaning of the principle of least action [1], has yielded quite remarkable results. Without additional assumptions, besides of the claim that free energy decreases its presence per state (relation (1)), which led to a dynamic interpretation of the particle-wave dualism, rational explanations for relevant natural phenomena could be obtained. Important is the finding that perturbing counterintuitive assumptions, paradoxes and consequences of presently favored theories based on time-invertible physics, can essentially be avoided. This may be not only because the world is really irreversible, but also because the introduced paradigm change opens the opportunity to consider entropy formation on a fundamental basis. It is possible in form of a reduced energy value when energy is diluted in space. It is for this reason that a wave is not equivalent to a particle within the particle-wave dualism, but information has to be provided to concentrate the energy again in a particle (Figure 1, center). The particle-wave duality is therefore mediated by information on matter. This information has an energy value, is located around matter and penetrates matter. It was identified to be the phenomenon of gravitation. This concept not only allows avoiding quantum paradoxes [1], but also facilitates new quantum interpretations when applied to cosmic contexts. While conventional quantum theory does not allow photons in a spreading radiation field to lose energy for entropy without interaction with matter, this is possible within the dynamic quantum interpretation. The information self-image of matter continuously reassembles the photon from the wave and may adjust the energy balance for entropy generation fulfilling a fundamental law. Since a fractal interrelation is seen between information handling in quantum processes and in cosmological context (Figure 4), a joint functional (mathematical) basis may be assumed, which enables a photon to “sense” the space for considering the entropy law (3). A Hubble-type of equation for the galactic redshift is provided (relation (8)), which explains the redshift phenomenon via entropy production, avoiding the presently favored assumption of a universe inflated by an expanding void. The microwave background is interpreted as entropy dump. Because entropy turnover is a thermodynamic necessity for expanding radiation fields, a quantum physics that can comply with it brings a definitive advantage compared with the established theory postulating an ex-

pansion of empty space and a stretching of wavelengths as explanation for a cosmological redshift.

Another aspect is thermodynamics itself. The second law of thermodynamics, which claims attainment of a maximum entropy situation in a closed system, immediately follows from the dynamic energy claim (statement (1)) or, equivalent, from the identified meaning of the principle of least action [1]. Since entropy production is rate controlling, and feedback processes are facilitated in a time oriented world, self-organized systems far from equilibrium will aim at maximum entropy production within the restraints of the systems. This is the reason why quasars, in association with black holes, are reaching such a high energy turnover. Terrestrial examples are hurricanes, which, under appropriate conditions, can also approach maximum entropy production and can grow from simple storms to super-hurricanes within days. Since living systems are also self-organized, biological evolution and evolution of human civilization have to be looked at in an unconventional new way (this subject is discussed in some detail in [10]).

A remarkable additional finding is that the information self-image of matter, needed for the dynamic particle-wave duality, can be identified with gravitation. In this way quantum phenomena and cosmological phenomena are linked in a straightforward way. It became clear why gravitation is a special “force”. It is actually not a force, but information, aimed at decreasing energy’s presence per state.

Because information has an energy content and energy is related to mass and matter, information can also self-organize under appropriate conditions and create a higher hierarchy of information handling. Information, associated with life, when sufficiently pushed away from equilibrium, may therefore self-organize to yield consciousness and spirit on purely materialistic foundation. Consciousness within human personality actually exists. But a time-invertible physics, which defines the flow of time via statistical probability, could never explain such a phenomenon. When information can self-organize, gravitation can also do it, since it is understood as information on matter within the dynamic energy approach. A precondition is that additional energy is turned over and the system is shifted sufficiently far from equilibrium. This may yield a kind of super-gravitation, a gravitation, which is occupying a hierarchy above normal gravitation. It could explain, what is now attributed to black matter, much more intensive and also structurally patterned gravitation, without the need to postulate invisible matter.

An intriguing possibility is the straightforward explanation of an always constant light velocity via the information self-image of matter. Such an explanation is entirely rational, as **Figure 6** visualizes. Information could control photons towards always constant light velocity. On the other hand imagining how empty space around a moving object could adjust light velocity of an arriving photon for constancy within the general theory of relativity is nearly impossible. Since information on matter is simultaneously identified as the phenomenon of gravitation this opens obviously an alternative to the theory of relativity. In fact, when searching for an explanation for an always constant light velocity more than one century ago, a natural information technology should have been taken in consideration. Information can communicate a constant velocity (**Figure 6**). However, at that time the foundations of information were still unclear with the consequence that they practically do not enter into our understanding of physical laws. Today however the benefits and achievements of artificial information technology are dramatically expanding, and they are working on the basis of existing natural laws. Why should nature itself not use information technology on the basis of gravitation? Of course much has still to be learned and the concept of an information self-image of matter with its consequences, introduced here, may make a beginning.

Even though general relativity theory is now entirely established the author claims that the here suggested approach, to understand gravitation and constant light velocity via the information self-image of matter is much simpler, entirely logic and intuitively understandable. Relativity theory will remain an admirable product of human creativity, but with two significant drawbacks: 1) all crucial physical properties, constant light velocity, gravitation and inertia are designed to be properties of space. However nobody can explain how this works in an environment, the space, originally claimed to contain nothing. The adopted counterintuitive four-dimensional space-time is the consequence; 2) the time in its “crude” form, as the clock shows (in the words of Einstein), is used to describe space-time and its impressive phenomena. It is however only a parameter for monitoring change without energy or substance as basis for measurement. The crude parameter time cannot be used to describe action. In fact, action has to be activated to measure time on the reference system. Properties of energy converting systems have actually to be described by the flow of action, energy times time, as the principle of least action requires. If this is done, if action is transformed and time then locally extracted from action, time dilation and time travel however simply disappear. Action is invariant against transformation.

Gravitation has been recognized as information on matter. Since gravitation is decisive for the dynamics of

the universe, it may be concluded that it is information, which determines its origin and fate. New cosmological concepts are imaginable, such as the Self-Image universe (**Figure 4(b)**), which is proposed as a counterpart to the Big Bang scenario (compare also a discussion in [10]). It avoids irrationalities such as creation of energy and time from nothing in a tiny seed, inflation of empty space, an accelerated expansion of the universe and its final end in darkness.

The self-image universe (**Figure 4(b)**) is created like an object in a 3D printer, energy is conserved, time flow, which here has to be deduced from action, is not interrupted, and the age of the present universe may remain the same when counted from its information mediated recreation.

A remarkable consequence of the proposed paradigm change towards irreversibility in fundamental physics is that many areas of our present physical understanding are affected. A simplified picture of changes, which the irreversibility approach to physical understanding would introduce, is given with the scheme shown in **Figure 8**. In the center of this figure it is indicated how a study of the meaning of the principle of least action (area with dotted border) led to the concept of a fundamentally dynamic energy and, considering the role of space for energy as a necessary concession for entropy formation, to the consideration of the information self-image of matter for the dynamic particle-wave dualism. They (three darker areas in **Figure 8**) became the new “symbolic form” (intellectual aid or logical tool), for understanding physical contexts, according to philosopher Ernst Cassirer [45].

As already shown [1] quantization, the double slit experiment and quantum correlation can rationally be understood with the help of the information self-image of matter (left side of **Figure 8**). In addition it explains gravitation and the constant light velocity with consequences in eliminating relativistic paradoxes and emphasizing the role of information for understanding cosmology (right side and bottom of **Figure 8**).

With the new understanding of gravitation as a natural form of information another quantum phenomenon can rationally be understood, the tunneling phenomenon (left side of **Figure 8**). Gravitation is known to penetrate matter and it corresponds to the information self-image of matter in relation (2). It should therefore be able to penetrate barriers with the possibility of resynthesizing the particle with certain probability again on the opposite site. The identification of information on matter with gravitation thus rationally explains the tunneling effect.

In **Figure 8**, top left, it is indicated how dynamic energy and thus dynamic time allows self-organization of matter, energy and information. Also the information self-image of matter, gravitation, can self-organize under appropriate conditions. The resulting super-gravitation could replace the hypothetical dark matter without need to identify non-visible matter. On the right side of **Figure 8** it is visualized that in a dynamic energy world photons can tolerate entropy generation while spreading out in space and generating the microwave background. The Big Bang concept, inflation, the redshift via space expansion, and dark energy concepts are consequently challenged. This concerns also relativity theory, which has been adapted to describe part of these phenomena. The here proposed alternative explanation, deducible for a fundamentally oriented world, basically involves information, a natural phenomenon of information. It is information on matter, which is around matter and could be identified with gravitation.

Up to the present time information is not handled on the basis of recognized fundamental physical laws. However science has learned to deal with information mathematically and in the field of applications we are now witnessing a real revolution of information technology. Since we are using natural laws when dealing with modern information technology, it is claimed here that nature can deal with information and applies it herself because of its incredibly elegant possibilities. The paradigm change towards a fundamentally irreversible world has automatically conduced us to a natural environment controlled and dominated by information, information on matter. This is credible because we are presently learning about the amazing practical possibilities of information for technology.

Science philosopher Karl Popper [46] insisted that a new hypothesis has to suggest the conditions, under which it can be falsified, proven to be incorrect, before being named a new theory. Three falsification conditions can immediately be named for the here advanced arguments for a fundamentally irreversible world: The here proposed concept of a fundamentally irreversible world is incorrect,

- 1) if it can be shown that a natural process, how simple it may be, can entirely be reversed in time;
- 2) if it can be shown that significantly diluted energy maintains an identical working ability as concentrated energy;
- 3) if the presently used statistical time arrow can be derived from time invertible physics without mathematically throwing away information (energy).

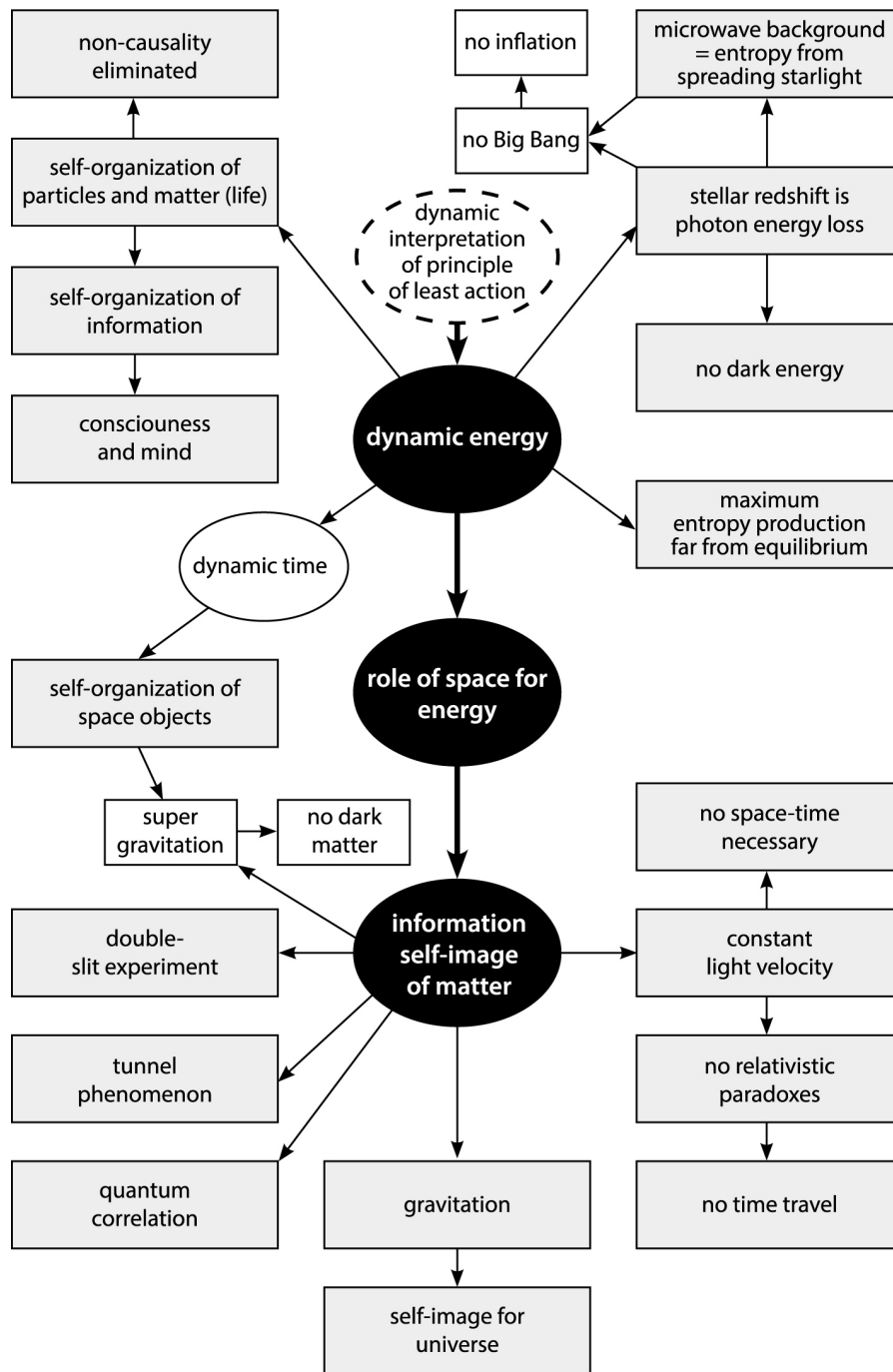


**Figure 8.** The new “symbolic form”, the intellectual program for understanding physics is a fundamentally dynamic energy-time world, a world of action. It is respecting the role of space for energy and considering an information self-image of matter (three basic claims on dark background in diagram). It is shown how from these derived three basic postulates essential conclusions could be deduced for quantum and space phenomena and contexts.

Under such conditions one can talk of a new theory, the theory of a fundamental oriented and irreversible world. In turn, when above conditions 1) to 3) cannot be fulfilled, this is strong evidence against a fundamentally time-invertible world, as it is presently sustained in physics.

The fact that essentially one single paradigm change, the claim of fundamental orientation and irreversibility

in nature, even derivable from the principle of least action [1], can eliminate well known and perturbing paradoxes of physics, deserves attention. And the finding that such a small (but significant) change can yield a remarkably different view of the universe should induce modesty with respect to our present scientific understanding of nature. It is anyway remarkable that the concept of a fundamentally time invertible physics with all its resulting paradoxes and irrationalities could become so powerful over such a long time, even though everything is changing in the universe and nothing actually proved to be entirely time invertible.

After all, it is well known that the Franciscan friar William of Ockham from the 14th century suggested that “one should not admit more causes of natural things than is sufficient to explain them”. This rule of thumb for scientists, also known as Ockham’s razor, would clearly favour the “dynamic” energy approach presented here since it is essentially based on a single paradigm change with the consequence that essential paradoxes, irrationalities and deficiencies can be eliminated or questioned (quantum paradoxes, action without cause, fundamental uncertainty, four-dimensional space-time concept, time travel, inflation of empty space, dark matter, dark energy, inability to explain consciousness and spirit materialistically). Also entropy laws for reversible and irreversible thermodynamics can be logically derived. The inability to do that is a significant drawback for present physical understanding within a time–invertible fundamental physical nature.

The concept proposed here is a working frame, which, of course, has to be deepened in nearly every respect. Only time (flow of action) can facilitate that. It promises a drastically simplified and rational understanding of nature, though with significant new challenges. The natural matter-related information system, looked upon as gravitation, which links quantum processes with cosmological phenomena, needs to be deciphered and self-organization of information explored. We may learn, that also nature around us has grown via a revolution of information technology and that an information based, much more logic and intelligent universe, the “Self-Image universe”, may replace the Big Bang scenario (compare also [10]).

And we may finally answer a question, which, beginning with Heraklitus of Ephesus in the 6<sup>th</sup> century BC, ancient natural philosophers have already been asking. They saw that everything in their environment was changing and were wondered what may be conserved (and still be related to the observed changes) [47] [48]. Now we could answer saying: it is energy with its tendency to decrease its presence per state (relation (1)). Energy is conserved but simultaneously deeply involved in changes. In contrast, the conventional, presently applied energy concept, energy as a scalar quantity, with the ability but no interest to do work, did not conserve an obvious relation to change. It somehow forgot the point of departure, from where the search for the energy concept originally started. It became therefore, in some way, a dead end road, facing more and more paradoxes and irrationalities. The here presented concept of a fundamentally oriented world offers an alternative open road to be explored.

## References

- [1] Tributsch, H. (2016) *Journal of Modern Physics*, **7**, 365-374. <http://dx.doi.org/10.4236/jmp.2016.74037>
- [2] Einstein, A. (1905) *Annalen der Physik*, **17**, 132-148. <http://dx.doi.org/10.1002/andp.19053220607>
- [3] Darrigol, O. (1897) Planck’s Radiation Theory. Chapter III, on Irreversible Radiation Processes. UC Press, Berkeley. <http://publishing.cdlib.org/ucpressebooks/view?docId=ft4t1nb2gv&chunk.id=d0e2674&toc.depth=1&brand=ucpress>
- [4] Kelly, R.E. (1980) *American Journal of Physics*, **49**, 714-719. <http://dx.doi.org/10.1119/1.12416>
- [5] Smoot, G.F. (2006) Cosmic Microwave Background Radiation Anisotropies: Their Discovery and Utilization. *Nobel Lecture*, Nobel Foundation.
- [6] Guth, A.H. (1998) *The Inflationary Universe: The Quest for a New Theory of Cosmic Origins*. Basic Books, New York.
- [7] Bell, J.S. (1964) *Physics*, **1**, 195-200.
- [8] Clauser, J.F. and Shimony, A. (1978) *Reports on Progress in Physics*, **41**, 1881. <http://dx.doi.org/10.1088/0034-4885/41/12/002>
- [9] Gödel, K. (2016). <https://en.wikipedia.org/wiki>
- [10] Tributsch, H. (2015) *Irrationality in Nature or in Science? Probing a Rational Energy and Mind World*. CreateSpace, a Company of Amazon.  
Tributsch, H. (2016) *Der logische Schlüssel zum Universum: Zeit, Information und die Dynamik von Energie, Quanten und Geist*. CreateSpace, a Company of Amazon. (To Be Published)
- [11] *Microwave Background Radiation* (2016).

- [https://en.wikipedia.org/wiki/Cosmic\\_microwave\\_background](https://en.wikipedia.org/wiki/Cosmic_microwave_background)
- [12] Ritz, W. (1908) *Annales de Chimie et de Physique*, **8**, 145.
- [13] Zwicky, F. (1929) *Proceedings of the National Academy of Sciences*, **15**, 773-779.  
<http://dx.doi.org/10.1073/pnas.15.10.773>
- [14] Berliner, L.M. (1992) *Statistical Science*, **7**, 69-90. <http://dx.doi.org/10.1214/ss/1177011444>
- [15] Rugh, S.E. and Zinkernagel, H. (2000) The Quantum Vacuum and the Cosmological Constant Problem.  
<http://arxiv.org/pdf/hep-th/0012253.pdf>
- [16] Paltridge, G.W. (1979) *Nature*, **279**, 630-631. <http://dx.doi.org/10.1038/279630a0>
- [17] Liu, Y., Liu, C. and Wang, D. (2011) *Entropy*, **13**, 211-240. <http://dx.doi.org/10.3390/e13010211>
- [18] Swenson, R. (1997) *Advances in Human Ecology*, **6**, 1-47. <http://rodswenson.com/humaneco.pdf>
- [19] Ross, J. (2008) *Thermodynamics and Fluctuations Far From Equilibrium (12.5: Invalidity of the Principle of Maximum Entropy Production)*. Springer, Berlin, 119.
- [20] Kohaut, E. and Weiss, W. (2007) *Das Rätsel Gravitation*. Edition Va Bene.
- [21] GUT (2016). [https://en.wikipedia.org/wiki/Grand\\_Unified\\_Theory](https://en.wikipedia.org/wiki/Grand_Unified_Theory)
- [22] Einstein, A. (1920) *Ether and Theory of Relativity*. Lecture Given at the University of Leiden on 5th May, 1920.
- [23] *Gravitational Waves Detected* (2016).  
<http://www.sciencealert.com/live-update-big-gravitational-wave-announcement-is-happening-right-now>
- [24] *Big Bang Criticism* (2016). <http://thetechreader.com/top-ten/top-ten-scientific-flaws-in-the-big-bang-theory>
- [25] Bible (Old Testament) (2nd to 1st Millennium BC, Compiled 450 BC) John 1:1.
- [26] Nagel, T. (2012) *Mind and Cosmos, Why the Materialist Neo-Darwinian Conception of Nature Is Almost Certainly False*. Oxford University Press, Oxford. <http://dx.doi.org/10.1093/acprof:oso/9780199919758.001.0001>
- [27] Aether (2016). [https://en.wikipedia.org/wiki/Aether\\_theories](https://en.wikipedia.org/wiki/Aether_theories)
- [28] Lichnerowicz, A. (1955) *Theories relativistes de la gravitation et de l'électromagnetisme*. Masson et Cie, Paris.
- [29] *General Relativity* (2016). [http://en.wikipedia.org/wiki/Mathematics\\_of\\_general\\_relativity](http://en.wikipedia.org/wiki/Mathematics_of_general_relativity)
- [30] Ives, H.E. (1952) *Journal of the Optical Society of America*, **42**, 540-543. <http://dx.doi.org/10.1364/josa.42.000540>
- [31] Gut, B.J. (1981) *Immanent-logische Kritik der Relativitätstheorie*. Oberwil b. Kugler, Zug, 151 S.
- [32] De Pretto, O. (1903). [http://en.wikipedia.org/wiki/Olinto\\_De\\_Pretto](http://en.wikipedia.org/wiki/Olinto_De_Pretto)
- [33] Hawking, S. (2016) *Space and Time Warps*. <http://www.hawking.org.uk/space-and-time-warps.html>
- [34] Augustine, S. (2012) *Confessions*. Simon & Brown, Los Angeles.
- [35] Reichenbach, H. (1999) *The Direction of Time*. Dover, New York.
- [36] Whitrow, G.J. (1988) *Time in History. The Evolution of Our General Awareness of Time and Temporal Perspective*. Oxford University Press, Oxford.
- [37] Rovelli, C. (2006) *What Is Time? What Is Space?* Di Renzo Editore, Rome.
- [38] Heidegger, M. (1962) "V". *Being and Time*. Blackwell, Oxford, UK & Cambridge, USA, 425.
- [39] Davies, P. (1996) *About Time: Einstein's Unfinished Revolution*. Simon & Schuster Paperbacks, New York.
- [40] Tributsch, H. (2008) *Energy, Time and Consciousness*. Shaker Media, Aachen.
- [41] Time (2016) Wikipedia. <https://en.wikipedia.org/wiki/Time>
- [42] *Hawking Radiation* (2016). [https://en.wikipedia.org/wiki/Hawking\\_radiation](https://en.wikipedia.org/wiki/Hawking_radiation)
- [43] *Black Hole* (2016). [https://en.wikipedia.org/wiki/Black\\_hole](https://en.wikipedia.org/wiki/Black_hole)
- [44] *Quasars* (2016) <https://en.wikipedia.org/wiki/Quasar>
- [45] Cassirer, E. (1923) *Philosophie der symbolischen Formen, Die Sprache*, Bd. 1; *Das mythische Denken* (1924), Bd. 2; *Phänomenologie der Erkenntnis* (1929), Bd. 3; Darmstadt (1997).
- [46] Popper, K.R. (1979) *Die beiden Grundprobleme der Erkenntnistheorie* (Herausgeber: Troels Eggers Hansen), J.C.B. Mohr (Paul Siebeck) Tübingen, 426-427.
- [47] Lindsay, R.B. (1971) *Foundations of Physics*, **1**, 383-393. <http://dx.doi.org/10.1007/BF00708586>
- [48] Lindsay, R.B., Ed. (1975) *Energy: Historical Development of the Concept*. Benchmark Papers on Energy, v. 1, Dowden, Hutchinsons & Ross, Inc., Stroudsburg.

# S Bosons and Dark Particles of Space Field

**Youngang Feng**

College of Physics, Guizhou University, Guiyang, China

Email: ygfeng45@aliyun.com

Received 19 July 2016; accepted 21 August 2016; published 24 August 2016

Copyright © 2016 by author and Scientific Research Publishing Inc.

This work is licensed under the Creative Commons Attribution International License (CC BY).

<http://creativecommons.org/licenses/by/4.0/>



Open Access

---

## Abstract

The spacetime lattice model involves time lattice (static lattice) model and space lattice (dynamic lattice) model, both of which have the same lattices' domains and the same fractal structures. The behaviors of the space field obey the uncertainty relations, which gauge invariance shows the space field is a gauge field, making the electromagnetic field, gravitomagnetic field and the fermion field be gauged, and the Lorentz condition and Lorentz gauge are the intrinsic attributes of the spacetime. The quantization of the classical space field produces S bosons of spin-1, which stimulated states by charges and masses are respectively photons and gravitons. The S bosons in thermal excitation are immeasurable and their energies may be dark. The principle of partition of independent freedom degrees regularizes the degrees for all particles including neutrino, which must have mass. By the S bosons, we interpret newly the virtual photons. Using the spacetime lattice model, we investigate the breaking of the symmetry of the gradient fields and the symmetry of the curl fields for the potential functions of the space field, and the creations and the annihilations of the dark photons and the dark gravitons. The complexity requires us to rename the electroweak phase transition as electro-gravito-weak phase transition. Finally, antiparticles are discussed. Our approach for the lattice models is a kind of renormalization group theory, signifying the breaking of symmetries can be renormalized.

## Keywords

Space, S Boson, Dark, Lorentz, Freedom Degree, Higgs

---

## 1. Introduction

In February 2016 scientists announced that they detected gravitational waves by observation of a binary black hole merger [1]. Einstein general relativistic theory and the quantization of the waves become once more hot topic. How should we think about the geometry of spacetime? In our opinion, the framework of Newton's mechanics refers two basic concepts: 1) Absolute space and absolute time; 2) For an object, we can know its accurate mechanical parameters such as position, momentum, and moment by solving motion equation, *i.e.*, any

one metric space can provide us infinitely accurate observed information about these parameters. Einstein's special relativistic theory denied Newton's first concept: there is no such thing as either absolute space or absolute time, and there exists only the mixture of the space and the time. However, his general relativistic theory coincides exactly with Newton's second concept. He imagined that if two persons fell downward freely, they wouldn't feel their own weights, and couldn't discern whether they were falling together toward, as if they were in a stationary state, and their freely falling reference frame was in a universe without gravity. Such equivalence description neglects the interaction of the individualities, thus all quantum effects of particles have been abandoned as the mass of a person is far greater than a particle's. There is now a logical paradox: on one hand, the interaction between particles arising from their masses is absolutely eliminated by theorists; on the other hand the gravitons as a type of particle relating to the masses and coming from the quantization of the general relativistic theory are invariably examined by experiments. Yet, on contrary to Einstein's theory, Maxwell theory can represent the electromagnetic field produced by charged particles, in favor of its quantization.

Weak interaction doesn't mean no interaction. To omit weak gravity will thwart our investigation of the interacting forms originated from masses. Einstein argued that spacetime should be warped out of gravity before the establishment of Maxwell laws of electromagnetism, and he spent most of his last 25 years to unify vainly his theory with Maxwell's. It can be understood that the evolution of universe was not well enough known in the 1900s and early 1905s. According to the standard model of today [2]-[5], mass has no priority to determine the property of spacetime, which is also proved in this paper. We may treat the spacetime as flat like what Maxwell did. To accept this point of view doesn't say we must turn back to the framework of Newton's mechanics. We notice that there exists unique space field together with unique spacetime. No matter whether for electromagnetic force or for gravity, their corresponding ground states are commonly the ground states of the space field. In this sense, the electromagnetic field and the gravitational field all are the stimulated states of the space field. Furthermore, mass not only evokes gravitational field, but also generates magnetic field. A moving object with mass will be exerted by Lorentz-force-like in the magnetic field [6].

The discovery of 3 K microwave background radiation makes us realize there was an early universe as explained by the standard model [7] [8]. The model indicates that the universe has undergone a thermal equilibrium state, which allows us to determine a list of elements. In fact, no one was able by himself to watch such natural scene of the early universe. It is impossible that there is an ideal model to illustrate completely universe, and applicable simplification should be done. For this reason, the standard model has been believed to be an excellent approach to nature so far.

Based on the model, we set up time lattice model and studied on time phase transition, the quanta of the time field are just Higgs with masses, they and the net charges occur simultaneously after the time phase transition [9]. There are two kinds of spacetime, one is mathematical, including nothing. Another is of physics, having its dual space: momentum-energy. We cannot mention the time phase transition for the mathematical one, where time direction is globally and locally allowed to be symmetry. Born out of the universe expansion, a physical space itself, even more than the mathematical one, have to be full of energies, heat diffusion, and temperature distribution. We proved the uncertainty relations are the intrinsic attributes of the spacetime [10]. The relations arise from the duality of the natural bases of the relevant spaces. In terms of mathematics, the inner product of the dual bases is always constant, no matter for which coordinate system.

A stable physical space should have a constant density of energies. This is in fact a dynamic stability as the energies fluctuations, which were proved by the detection of microwave radiation background [11]-[13]. Considering this situation, we construct a physical space lattice model making up of infinite minimal spaces with nonzero volumes due to the uncertainty principle. We put a lattice in each minimal space to represent it. The alternation of the energies can be thought of as the change in the space volume keeping constant density. Such change is equivalent to that the fluctuation force drives the lattices to wiggle around their equilibrium positions, while the space is rigid. Namely, all of the minimal spaces have the identical volumes, and the lattices are successively oscillating. Their equilibrium sites can serve as the coordinate lattices, which determine the fractal structure of the spacetime [14]. When time is in global ordered state, the lattices states cooperate to form harmonic waves, called space fields, and its quantization gives massless bosons, called S bosons. There are four types of S bosons, corresponding respectively to the four types of Higgs particles [9]. The formula  $c^2 dt^2 - dx^2 - dy^2 - dz^2 = 0$  itself shows the spacetime gauge property, and the light speed  $c$  should be essential attributes for the physical spacetime, which can be understood from two hands: On one hand, the motion trail of a stationary spacetime point in the general relativistic theory is the world line with  $ct$ . On the other hand, the re-

levant space point is just the equilibrium position of the lattices of the space lattice model. The two descriptions should be equivalent. This implies that if there is no photon, the real moving object is the waves of the space field, producing the S bosons that propagate at light speed. In other word, the velocity of the S bosons is the light speed. Furthermore, the wave rate does be the rate with respect to the lattice equilibrium sites, which are also the coordinate positions for all inertial reference frames, such that the space field waves velocity, *i.e.* the light speed, is constant for all inertial system.

In Section 2, we prove at first that the Lorentz transformation can't change the uncertainty relations, then introduce classical space field, which quantization leads to S bosons. By the S bosons, we explain newly the virtual photons of the quantum electromagnetics. In Section 3, we propose the principle of partition of independent freedom degrees, it regularizes the degrees for all particles. We reveal the space field makes the conventional electromagnetic field and the fermion field be gauged, and the Lorentz condition and the Lorentz gauge are the intrinsic attributes of the spacetime. Combining the time field, we discuss the creations and the annihilations of some quantum fields, there exists dark photons and dark gravitons. Finally, antiparticles are discussed. Section 4 is conclusion remark.

The parameters applied in this paper have the same meanings and definitions as that of the conventional quantum field theory, if there is no particular expatiation.

## 2. Theory

### 2.1. The Gauge Invariance of Uncertainty Relations

Suppose: 1. The Cartesian coordinate systems used by the observes K and K' are such that the axes of one are to parallel to the relevant axes of the others, and 2. Their relative motion is confined in the direction of one of the axes, notate the x-(or x')-axis, the velocity of K' with respect to K being equal  $u$ . By Lorentz transformation

$$x = (x' + ut') / \sqrt{1 - u^2/c^2}, \quad t = [t' + (u/c^2)x'] / \sqrt{1 - u^2/c^2}, \text{ and}$$

operators' transformation  $\partial/\partial x = (\partial/\partial x') dx'/dx + (\partial/\partial t') dt'/dx$ , we get differential expressions

$$dx = \frac{1}{\sqrt{1 - u^2/c^2}} (dx' + u dt'), \quad \frac{\partial}{\partial x} = \frac{1}{\sqrt{1 - u^2/c^2}} \left( \frac{\partial}{\partial x'} - \frac{u}{c^2} \frac{\partial}{\partial t'} \right) \quad (1)$$

Similarly,

$$dt = \frac{1}{\sqrt{1 - u^2/c^2}} \left( dt' + \frac{u}{c^2} dx' \right), \quad \frac{\partial}{\partial t} = \frac{1}{\sqrt{1 - u^2/c^2}} \left( \frac{\partial}{\partial t'} - u \frac{\partial}{\partial x'} \right) \quad (2)$$

From (1) and (2), we have

$$\frac{\partial}{\partial x} dx = \frac{1}{1 - u^2/c^2} \left( \frac{\partial}{\partial x'} dx' - \frac{u}{c^2} \frac{\partial}{\partial t'} dx' + u \frac{\partial}{\partial x'} dt' - \frac{u^2}{c^2} \frac{\partial}{\partial t'} dt' \right) \quad (3)$$

In terms of mathematics, the duality and the orthogonality of the natural bases are

$$\frac{\partial}{\partial x'} dx' = \frac{\partial}{\partial t'} dt' = 1, \quad \frac{\partial}{\partial x'} dt' = \frac{\partial}{\partial t'} dx' = 0 \quad (4)$$

By Equation (4), Equation (3) turns into

$$\frac{\partial}{\partial x} dx = \frac{1}{1 - u^2/c^2} (1 - u^2/c^2) = 1 \quad (5)$$

Namely,

$$\frac{\partial}{\partial x} dx = \frac{\partial}{\partial x'} dx' = 1 \quad (6)$$

With the same reason, we obtain

$$\frac{\partial}{\partial t} dt = \frac{\partial}{\partial t'} dt' = 1 \quad (7)$$

We can also get the same proof, exchanging  $u$ ,  $x'$ , and  $t'$  for  $-u$ ,  $x$ , and  $t$ , respectively in the above equations due to the relativity. According to reference [10], the uncertainty relation depends on the duality of the natural bases, Equations (6) and (7) show that Lorentz transformation can't change the uncertainty relations, *i.e.*, the behavior of the space field obeys the same law in different inertial reference frames. In a word, Lorentz gauge is the intrinsic attribute of the spacetime.

## 2.2. Classical Space Field

The gradient fields of the potential functions of the space field are symmetric,  $\pm\varphi \pm \partial\mathcal{A}/\partial t$ ; the curl fields are also symmetric,  $\pm\nabla \times \mathcal{A}$ ; where  $\varphi$  is the scalar potential, and  $\mathcal{A}$  the vector potential. It seems as if there were symmetric potential functions  $\pm\varphi$  and  $\pm\mathcal{A}$  [6], that is not true at all! The potential functions are unique,  $\varphi$  and  $\mathcal{A}$ . The total intensity of each kind of the fields is zero because of the symmetry. As the following expressed, the potential functions satisfy wave equations, which solutions are traveling waves at light speed. Let  $\mathbf{\Omega} = \mathbf{\Omega}_1 + \mathbf{\Omega}_2$  denote the gradient field,  $\mathbf{\Theta} = \mathbf{\Theta}_1 + \mathbf{\Theta}_2$  the curl field. The symmetric fields are successively

$$\mathbf{\Omega}_1 = -\nabla\varphi - \frac{1}{c}\frac{\partial\mathcal{A}}{\partial t}, \quad \mathbf{\Omega}_2 = \nabla\varphi + \frac{1}{c}\frac{\partial\mathcal{A}}{\partial t} \quad (8)$$

$$\mathbf{\Theta}_1 = \nabla \times \mathcal{A}, \quad \nabla \times \mathbf{\Theta}_1 = \frac{1}{c}\frac{\partial\mathbf{\Omega}_1}{\partial t} + \frac{4\pi}{c}\mathbf{j}_1 \quad (9)$$

$$\mathbf{\Theta}_2 = -\nabla \times \mathcal{A}, \quad \nabla \times \mathbf{\Theta}_2 = \frac{1}{c}\frac{\partial\mathbf{\Omega}_2}{\partial t} + \frac{4\pi}{c}\mathbf{j}_2 \quad (10)$$

$$\nabla \times \mathbf{\Omega}_1 = -\frac{1}{c}\frac{\partial\mathbf{\Theta}_1}{\partial t}, \quad \nabla \times \mathbf{\Omega}_2 = -\frac{1}{c}\frac{\partial\mathbf{\Theta}_2}{\partial t} \quad (11)$$

$$\nabla \cdot \mathbf{\Omega}_1 = \nabla \cdot \mathbf{\Omega}_2 = 0 \quad (\text{passive fields}) \quad (12)$$

Since there is neither charge nor mass, so  $\mathbf{j}_1 = \mathbf{j}_2 = 0$ . By (8) and (12), we get

$$\nabla^2\varphi - \frac{1}{c^2}\frac{\partial^2\varphi}{\partial t^2} + \frac{1}{c}\frac{\partial}{\partial t}\left(\nabla \cdot \mathcal{A} + \frac{1}{c}\frac{\partial\varphi}{\partial t}\right) = 0 \quad (13.1)$$

For the space field

$$\nabla^2\varphi - \frac{1}{c^2}\frac{\partial^2\varphi}{\partial t^2} = 0 \quad (13.2)$$

Equation (13.2) is a hyperbolic differential equation, describing the wave of the space field. Equations (13.1) and (13.2) result in Lorentz condition

$$\nabla \cdot \mathcal{A} + \frac{1}{c}\frac{\partial\varphi}{\partial t} = 0 \quad (14)$$

Equation (14) manifests the Lorentz condition is the intrinsic attribute of the spacetime. From (9)

$$\nabla \times (\nabla \times \mathcal{A}) = \frac{1}{c}\frac{\partial\mathbf{\Omega}_1}{\partial t} \quad (15)$$

Using the algebraic transformation, the left hand of (15) becomes  $-\nabla^2\mathcal{A} + \nabla(\nabla \cdot \mathcal{A})$ , combining (10), we change (8) into

$$-\nabla^2\mathcal{A} + \frac{1}{c^2}\frac{\partial^2\mathcal{A}}{\partial t^2} + \nabla\left(\nabla \cdot \mathcal{A} + \frac{1}{c}\frac{\partial\varphi}{\partial t}\right) = 0 \quad (16.1)$$

Using (14) and (16.1), we obtain

$$\nabla^2\mathcal{A} - \frac{1}{c^2}\frac{\partial^2\mathcal{A}}{\partial t^2} = 0 \quad (16.2)$$

The meaning of (16.2) is analogue to that of (13.2). For  $\mathbf{\Omega}_2$  and  $\mathbf{\Theta}_2$ , we can derive the same consequences

as (13.2) and (16.2).

### 2.3. The Quantization of the Space Field

There is no current since there is neither electricity charge nor mass such that the equation of the space field behaves as

$$\partial_\mu \partial^\mu A_\nu = 0 \quad (17)$$

where the derivative operator  $\partial_\mu = \partial/\partial x^\mu = (\partial/\partial x^0, \nabla)$ ,  $\hbar = c = 1$ ,  $E = P^0 = P_0$ ,  $P_\mu = i\partial/\partial x^\mu$ ,  $A^\mu = (\varphi, \mathbf{A})$ ,  $\mu = 0, 1, 2, 3$ , corresponding to  $t, x, y, z$ , respectively. Since the wave propagates at light speed there is no inertial mass, the equation is like in form Klein-Gorden (K-G) field equation with mass  $m = 0$ . Applying mechanically the solution of the K-G equation, we express  $A_\mu$  as

$$A_\mu = \int d^3k \frac{1}{\sqrt{(2\pi)^3 2k}} [a_\mu(\mathbf{k}) e^{-ikx} + a_\mu^+(\mathbf{k}) e^{ikx}] \quad (18)$$

where the wave vector is  $k_0 = \omega_k = k$ . The commutation relations for the creators and the annihilators are

$$\begin{aligned} [a_j(\mathbf{k}), a_j^+(\mathbf{k}')] &= \delta_{jj} \delta^3(\mathbf{k} - \mathbf{k}'), \\ [a_0(\mathbf{k}), a_0^+(\mathbf{k}')] &= -\delta^3(\mathbf{k} - \mathbf{k}'), \\ [a_j(\mathbf{k}), a_0^+(\mathbf{k}')] &= [a, a] = [a^+, a^+] = 0 \end{aligned} \quad (19)$$

Adjusting the coordinates, we introduce new operators:  $a^\mu(\mathbf{k}) = \varepsilon^\mu(\mathbf{k}, \lambda) a(\mathbf{k}, \lambda)$ , ( $\lambda = 0, 1, 2, 3$ ), where  $\varepsilon^\mu(\mathbf{k}, \lambda)$  is unit vector,  $\mathbf{k}$  is parallel to the  $z$ -axis and perpendicular to the  $x$ -,  $y$ -axes. Since the Lorentz condition and the field action are invariant for the special relativistic theory, we have

$$\begin{aligned} [a(\mathbf{k}, j), a^+(\mathbf{k}', j)] &= \delta^3(\mathbf{k} - \mathbf{k}'), \quad j = 1, 2, 3 \\ [a(\mathbf{k}, 0), a^+(\mathbf{k}', 0)] &= -\delta^3(\mathbf{k} - \mathbf{k}') \end{aligned} \quad (20)$$

Other commuting operators go away. Equation (18) then translates into

$$A_\mu(x) = \sum_\lambda A_\mu^\lambda(x) = \sum_\lambda \int d^3k \frac{1}{\sqrt{(2\pi)^3 2k}} \varepsilon_\mu(\mathbf{k}, \lambda) [a(\mathbf{k}, \lambda) e^{-ikx} + a^+(\mathbf{k}, \lambda) e^{ikx}] \quad (21)$$

If  $\lambda = 1$  or  $2$ ,  $A_\mu^\lambda(x)$  obeys Lorentz condition,  $\partial^\mu A_\mu^\lambda = 0$ , and  $k^\mu \varepsilon_\mu(\mathbf{k}, \lambda) = 0$ . If  $\lambda = 0$  or  $3$ ,  $A_\mu^\lambda(x)$  violates the condition, so the S bosons are transversal particles of spin-1.

### 2.4. Stimulated States and Virtual Photons

The properties of the stimulated fields are described by reference [6]: Electricity charges stimulate the space field to produce electromagnetic field, which quanta are photons carrying electromagnetic forces. Masses evoke gravitowagnetic field, which quanta are gravitons carrying the gravitowagnetic forces. Besides the charges and masses, heat also can make S bosons be in the states of higher energies than the ground states'. The intensities of the total gradient field and the total curl field of the potential functions vanish still, if there is only the thermal excitation. The S bosons, except photons and gravitons, therefore, even though being the thermal stimulated states, don't observably carry force such as the electromagnetic force or the gravitowagnetic force. In this sense, the S bosons can't be directly measured, and their energies maybe dark. The total energy  $E$  of the field is

$$E = \sum_\omega (n_\omega + 1/2) \hbar \omega \quad (22)$$

where  $\hbar$  is Plank constant,  $\omega$  angle frequency,  $n_\omega$  the number of S bosons with frequency  $\omega$ ,  $(1/2)\hbar\omega$  the ground state energy. The average number of the  $n_\omega$ ,  $\langle n_\omega \rangle$ , is determined by Plank distribution function

$$\langle n_\omega \rangle = 1 / [\exp(\hbar\omega/k_B T) - 1] \quad (23)$$

Introducing the concept of S bosons, the interaction between electrons can be newly interpreted as the fol-

lowing: The first electron  $e_1$  stimulates a S boson making it become the first photon  $q_1$ , the  $e_1$  then loses its partial energy, denoted by  $e_1(-)$

$$e_1 + S \rightarrow q_1 + e_1(-) \quad (24)$$

Similarly, for the second electron  $e_2$  and the second photon  $q_2$ ,

$$e_2 + S \rightarrow q_2 + e_2(-) \quad (25)$$

The  $e_1(-)$  and the  $q_2$  exchange energy, the  $q_2$  loses energy and turns back to be S boson again. The  $e_1(-)$  obtains energy to become  $e_1'$ ,

$$e_1(-) + q_2 \rightarrow S + e_1' \quad (26)$$

For the  $e_2(-)$ , the same process is

$$e_2(-) + q_1 \rightarrow S + e_2' \quad (27)$$

where the  $q_1$  and  $q_2$  are just the virtual photons.

### 3. Discussion

#### 3.1. The Principle of Partition of Independent Freedom Degrees

The world we are living in is a global ordered-time spacetime after the electroweak phase transition, while the fractal structures disappear. Different from those spaces of extra dimensions [15] [16], the fractal structures of higher dimensions can return to the 4-dimensional spacetime by the scaling law [14]. The fractal dimensions used in the lattice models are called box-counting dimensions, generally defined as [17]

$$D = \lim_{\delta \rightarrow 0} \frac{\log N_\delta(F)}{-\log \delta} \quad (28)$$

where  $F$  is any non-empty bounded subset of  $R^n$  and  $N_\delta(F)$  is the smallest number of sets of diameter at most  $\delta$ , which can cover  $F$ . For a lattice model the  $N_\delta(F)$  is the total number of the lattices' domains in a sub-block [14]. For the self-similar transformations the  $D$  is just the similarity dimension. The scaling law regularizes a lattice domain to be an open set of one unit length diameter. These regularities are still effective after the electroweak phase transition. There are two types of lattices in each domain: dynamic lattice and static lattice, the latter positions at the former equilibrium site. The static lattice model is insisted of the static lattices, the dynamic lattice model is made up of the dynamic lattices. The dynamic lattice model can draw the space field, which acts as a background field for the other fields being applicable to the static lattice model. For this reason, we also call the dynamic lattice model as the space lattice model. The two kinds of models correspond to the same spacetime because of the dimension definition. Let coordinates  $x'$  denote the dynamic lattices,  $x$  do the static lattices. When there is not any other field, the potential functions  $A(x')$  and  $A(x)$  are identical for the space field (see subsection 2.2).

The principle of partition of independent freedom degrees is that there are  $(D + 2)$  freedom degrees to be partitioned in the  $(D + 1)$ -dimensional spacetime:  $D$ 's space's, one time's, one spin's,  $(D + 1)$  of which each particle must own. The Higgs particle always occupies independently the time's degree. After the electroweak phase transition the spacetime becomes 4-dimensions ( $D = 3$ ), the Higgs has three spatial degrees for the propagation of its waves. Hence, the Higgs is a scalar boson. The space field lies in the dynamical lattice model different from the static lattice model, in which the time field is set. Because of this, a S boson is independent of the time's degree and has one spin's degree, besides three spatial degrees. Other particles are accommodated to the static lattice model, and each of them has three spatial degrees and one spin degree. Each of them is forced to couple with the Higgs particles to share (not independently) the time's degree, which causes masses. According to this principle a neutrino or an antineutrino must have mass, no matter how weak their coupling with the Higgs may be. Photons and gravitons as the stimulated states of the S bosons have the same degrees as the S bosons'.

#### 3.2. The Nature of the Lorentz Gauge

The so-called conventional electromagnetic field is the field stimulated by charges, which can be describe by

Maxwell theory. When the space field isn't omitted the potential function of the electromagnetic field is assigned as  $A_\mu(x')$ , and the potential function of the conventional electromagnetic field as  $A_\mu(x)$ , while the thermal stimulated state of space field is neglected. It should be emphasized that only the  $A_\mu(x)$  relates to the electricity current. As the field stimulated by charge is far stronger than the thermal stimulated space field, we expand the  $A_\mu(x')$  in a series around the  $x$ , taking its linear term,

$$A_\mu(x') = A_\mu(x) + \left[ \partial^\mu A_\mu(x') \right]_{x'=x} \cdot (x' - x) \tag{29}$$

Only the second expansion term relates to the thermal stimulated space field independent of the current. Recall the definition of the derivative of function  $f(x)$  at the  $x$

$$\frac{df(x)}{dx} = \lim_{\Delta x \rightarrow 0} \frac{f(x + \Delta x) - f(x)}{\Delta x} \tag{30}$$

Clearly, the points  $x + \Delta x$  and  $x$  are in the same domain if  $\Delta x \rightarrow 0$  but zero. This admits  $\left[ \partial^\mu A_\mu(x') \right]_{x'=x} = \partial^\mu A_\mu(x)$ . Since the scaling law defines the distance of nearest neighbors as one unit length [14], thus  $0 < |x' - x| < 1/2$ . We make the domain be so small that the following approximate expression holds

$$A_\mu(x') \cong A_\mu(x) + \partial^\mu A_\mu(x) \cdot \alpha = A_\mu(x) + \partial^\mu \left[ \alpha \cdot A_\mu(x) \right] \tag{31}$$

where  $\alpha$  is constant and  $0 < |\alpha| < 1/2$ . For the conventional electromagnetic field, the Lorentz gauge transformation is

$$A'_\mu(x) = A_\mu(x) + \partial^\mu \theta(x) \tag{32}$$

Equations (31) and (32) say the same field, hence, we have

$$A'_\mu(x) = A_\mu(x') \tag{33}$$

Here  $A'_\mu(x)$  is the potential function including the conventional electromagnetic field and the thermal stimulated space field. Moreover, from (31) and (32):

$$\partial^\mu \theta(x) = \partial^\mu \left[ \alpha \cdot A_\mu(x) \right] = \alpha \cdot \partial^\mu A_\mu(x) \tag{34}$$

where  $\partial^\mu A_\mu(x)$  is the derivative of the  $A_\mu(x')$  with respect to the  $x'$  at the point  $x' = x$ . The second derivative of the  $A_\mu(x')$  at the  $x$  is

$$\left[ \partial_\mu \partial^\mu A_\mu(x') \right]_{x'=x} = \partial_\mu \partial^\mu A_\mu(x) \tag{35}$$

Since only the  $A_\mu(x)$  of the first term of Equation (32), which is the potential function of the conventional electromagnetic field, refers to the current, the  $A_\mu(x)$  in this derivative term should be regarded as the potential function of the thermal stimulated space field (the  $x$  is the equilibrium position of the  $x'$ , so the  $x$  can be viewed as a special point of the  $x'$  system; inversely, the  $x'$  can't belong to the  $x$  system relating only to the equilibrium sites), so Equation (35) is the wave equation of the space field similar to Equations (13.2) and (16.2). From Equations (34) and (35), we get

$$\partial_\mu \partial^\mu \theta(x) = 0 \tag{36}$$

This is just the Lorentz gauge transformation for the conventional electromagnetic field. Equations (32) and (36) result in the Lorentz condition

$$\partial^\mu A'_\mu(x) = \partial^\mu A_\mu(x) = 0 \tag{37}$$

We understand now that the Lorentz gauge is just the intrinsic attribute of the spacetime rather than an artificial additional condition. In addition, the  $\theta(x)$  can also describe the space field because of its linear relation with the  $A_\mu(x)$ .

The space field behaves in the way of the symmetry U(1), and its action on a fermion field  $\Psi$  is represented as

$$\Psi' = e^{-iQe\theta(x)} \Psi \tag{38}$$

where  $Qe$  is the electricity charge of the fermion, Equation (38) is called the gauge transformation of the fermion field. The space field guarantees that the interaction form remains the same when the fermion field takes different phase factors at different spacetime positions. Hence, we should consider the space field as Lorentz gauge field. It is the space field that makes the conventional electromagnetic field and the fermion field become gauge fields. With the same reason, the gravitowagnetic field is also a gauge field.

### 3.3. Dark Photons and Dark Gravitons

The critical temperature  $T_c$  of the time phase transition is given by reference [9], which shows if the temperature  $T$  is higher than  $T_c$ , the particles number equals the antiparticles number, the total charge is neutral, so there is no stimulated field by the charges. When time becomes global ordered, in the temperature region  $T_{ew} < T \leq T_c$ ,  $T_{ew}$  is the turning point of the electroweak phase transition, the particles number attains ascendant and four types of time fields (Higgs particles) emerge, accompanying four types of space fields with the same fractal structures as the time fields'. Thus, the symmetry of the gradient fields and the symmetry of the curl fields are together broken, the net charges and the masses stimulate simultaneously and separately four types electromagnetic fields and four types of gravitowagnetic fields [6]. The photons born in the inner space of a sub-block or a block, concern only short-range interactions, they may be the dark photons [18] [19]. The gravitons produced in the same inner spaces have only limited interacting range, and may be called dark gravitons. The  $D$ -dimensional ( $2 < D < 3$ ) inner space of a sub-block and the  $D^4$ -dimensional ( $16 < D^4 < 81$ ) inner space of a block defer from the 4-dimensional spacetime, corresponding separately to the spacetime of  $(D+1)$  dimensions and the spacetime of  $(D^4+1)$  dimensions, while the Lorentz gauge aren't available. The subsequent symmetries may acquire new gauge fields bring about new particles. At the same time, the symmetry SU(2) in the fractal structures generates particles  $W^+$ ,  $W^-$ , and  $Z$ . All fields are of localities due to the sizes of the sub-blocks and the blocks are confined. We don't exclude the dark photons and the dark gravitons participate in the interactions among the particles such as  $W^+$ ,  $W^-$ ,  $Z$ ,  $e^+$ , and  $e^-$  or other unknown particles. When  $T \leq T_{ew}$  there are no fractal structures with the disappearing of the sub-blocks and the blocks, the correlation lengths of the lattices states become infinity. Three types of Higgs particles, three types of photons (dark photons), and three types of gravitons (dark gravitons) are annihilated, the rest, the fourth types of them become new types: the Higgs particles lead to masses [9], the gravitowagnetic field together with the electromagnetic field form in the 4-dimensional spacetime. Their quanta, the gravitons and the photons, possess infinite forces ranges, the dark photons and the dark gravitons turn possibly into electrons and positrons in their annihilation process. In this sense, we may rename the transition as electro-gravito-weak phase transition.

### 3.4. Antiparticles

For the time field, the p-time state relates to particles, the n-time state to antiparticles [9]. Since the space field is independent of the time field, a S boson is just its antiparticle, so do the photon and the graviton. Conversely, an antineutrino and a neutrino can be distinguishable from one another as they rely on the time field.

## 4. Conclusion

We persist that the solutions for all of phenomena can be found in the spacetime. The quantization of the spacetime gives rise to the Higgs particles and the S bosons, which excitation states relate to dark photons, photons, dark gravitons, and gravitons. The symmetric characteristics of the spacetime lead to a series of gauge fields, illustrating the intrinsic attributes of the spacetime. The spacetime lattice model contains the time lattice model and the space lattice model, and its fractal structures provide us a chance to discover new symmetries, introducing new gauge fields and chasing new particles.

## References

- [1] Abbott, B.P., *et al.* (2016) *Physical Review Letters*, **116**, Article ID: 061102. <http://dx.doi.org/10.1103/PhysRevLett.116.061102>
- [2] Glashow, S.L. (1961) *Nuclear Physics*, **22**, 579-588. [http://dx.doi.org/10.1016/0029-5582\(61\)90469-2](http://dx.doi.org/10.1016/0029-5582(61)90469-2)
- [3] Weinberg, S. (1967) *Physical Review Letters*, **19**, 1264-1266. <http://dx.doi.org/10.1103/PhysRevLett.19.1264>
- [4] Salam, A. (1979) *Nobel Lecture Physics*, 513-538.

- [http://www.nobelprize.org/nobel\\_prizes/physics/laureates/1979/salam-lecture.pdf](http://www.nobelprize.org/nobel_prizes/physics/laureates/1979/salam-lecture.pdf)
- [5] Higgs, P.W. (1964) *Physical Review Letters*, **13**, 508-509. <http://dx.doi.org/10.1103/PhysRevLett.13.508>
- [6] Feng, Y.G. (2015) *Journal of Modern Physics*, **6**, 573-577. <http://dx.doi.org/10.4236/jmp.2015.65062>
- [7] Penzias, A.A. (1978) *Nobel Lecture*, 444-457.  
[http://www.nobelprize.org/nobel\\_prizes/physics/laureates/1978/penzias-lecture.pdf](http://www.nobelprize.org/nobel_prizes/physics/laureates/1978/penzias-lecture.pdf)
- [8] Wilson, R.W. (1978) *Nobel Lecture*, 463-483.  
[http://www.nobelprize.org/nobel\\_prizes/physics/laureates/1978/wilson-lecture.pdf](http://www.nobelprize.org/nobel_prizes/physics/laureates/1978/wilson-lecture.pdf)
- [9] Feng, Y.G. (2016) *Journal of Modern Physics*, **7**, 536-542. <http://dx.doi.org/10.4236/jmp.2016.76056>
- [10] Feng, Y.G. (2014) *Natural Science*, **6**, 1149-1158. <http://dx.doi.org/10.4236/ns.2014.614103>
- [11] Subrahmanyam, R. (1997) *Journal of Astrophysics & Astronomy*, **18**, 251-255. <http://dx.doi.org/10.1007/BF02709314>
- [12] Mather, J.C. (2006) *Nobel Lecture*, 64-96.  
[www.nobelprize.org/nobel\\_prizes/physics/laureates/2006/mather\\_lecture.pdf](http://www.nobelprize.org/nobel_prizes/physics/laureates/2006/mather_lecture.pdf)
- [13] Smoot, G.F. (2006) *Nobel Lecture*, 113-166.  
[http://www.nobelprize.org/nobel\\_prizes/physics/laureates/2006/smoot\\_lecture.pdf](http://www.nobelprize.org/nobel_prizes/physics/laureates/2006/smoot_lecture.pdf)
- [14] Feng, Y.-G. (2014) *American Journal of Modern Physics*, **3**, 184-194. <http://dx.doi.org/10.11648/j.ajmp.20140304.16>
- [15] Hewett, J. and Spiropulu, M. (2002) *Annual Review of Nuclear and Particle Science*, **52**, 397-424.  
<http://dx.doi.org/10.1146/annurev.nucl.52.050102.090706>
- [16] Holman, M. (2012) Physical Degrees of Freedom in Higgs Models. <http://arxiv.org/abs/0910.4054>
- [17] Falconer, K. (2003) *Fractal Geometry*. 2nd Edition, John Wiley & Sons, London.
- [18] Krasznahorkay, A.J., *et al.* (2016) *Physical Review Letters*, **116**, Article ID: 042501,  
<http://dx.doi.org/10.1103/PhysRevLett.116.042501>
- [19] Feng, J.L., *et al.* (2016) Evidence for a Protophobic Fifth Force from  $^8\text{Be}$  Nuclear Transitions.  
<http://arxiv.org/abs/1604.07411>



**Submit or recommend next manuscript to SCIRP and we will provide best service for you:**

Accepting pre-submission inquiries through Email, Facebook, LinkedIn, Twitter, etc.

A wide selection of journals (inclusive of 9 subjects, more than 200 journals)

Providing 24-hour high-quality service

User-friendly online submission system

Fair and swift peer-review system

Efficient typesetting and proofreading procedure

Display of the result of downloads and visits, as well as the number of cited articles

Maximum dissemination of your research work

Submit your manuscript at: <http://papersubmission.scirp.org/>

# Comparing Gravitation in Flat Space-Time with General Relativity

**Walter Petry**

Mathematical Institute, University of Düsseldorf, Düsseldorf, Germany

Email: [wpetry@meduse.de](mailto:wpetry@meduse.de)

Received 18 July 2016; accepted 21 August 2016; published 24 August 2016

Copyright © 2016 by author and Scientific Research Publishing Inc.

This work is licensed under the Creative Commons Attribution International License (CC BY).

<http://creativecommons.org/licenses/by/4.0/>



Open Access

---

## Abstract

General relativity (GR) and gravitation in flat space-time (GFST) are covariant theories to describe gravitation. The metric of GR is given by the form of proper-time and the metric of GFST is the flat space-time form different from that of proper-time. GR has as source the matter tensor and the Einstein tensor describes the gravitational field whereas the source of GFST is the total energy-momentum including gravitation and the field is described by a non-linear differential operator of order two in divergence form. The results of the two theories agree for weak gravitational fields to the order of measurable accuracy. It is well-known that homogeneous, isotropic, cosmological models of GR start from a point singularity of the universe, the so called big bang. The density of matter is infinite. Therefore, our observable universe implies an expansion of space, in particular an inflationary expansion in the beginning. This is the presently most accepted model of the universe although doubts exist because infinities don't exist in physics. GFST starts in the beginning from a homogeneous, isotropic universe with uniformly distributed energy and no matter. In the course of time, matter is created out of energy where the total energy is conserved. There is no singularity. The space is flat and the space may be non-expanding.

## Keywords

Gravitation, Cosmology, Flat Space, No Singularity, Non-Expanding Universe

---

## 1. Introduction

Einstein's general theory of relativity is at present the most accepted theory of gravitation. The theory gives for weak gravitational fields' agreement with the corresponding experimental results. But the results for homogeneous, isotropic, cosmological models imply difficulties. So, the universe starts from a point singularity, *i.e.* the universe starts from a point with infinite density of matter. The observed universe is very big. Hence, the space

of the universe must expand very quickly which implies the introduction of an inflationary universe in the beginning.

GFST has a pseudo-Euclidean geometry and the proper time is defined similar to that of general relativity, *i.e.* space-time and proper time are different from one another. GFST starts from an invariant Lagrangian which gives by standard methods the field equations of gravitation. The source is the total energy-momentum tensor including gravitation. The energy-momentum of gravitation is a tensor. The field is described by non-linear differential equations of order two in divergence form. The theory is generally covariant. The gravitational equations together with the conservation law of the total energy-momentum give the equations of motion for matter. The application of the theory implies for weak gravitational fields the same results as GR to experimental accuracy, e.g. gravitational redshift, deflection of light, perihelion precession, radar time delay, post-Newtonian approximation, gravitational radiation of a two-body system and the precession of the spin axis of a gyroscope in the orbit of a rotation body. But there are also differences of the results of these two theories. GFST gives non-singular, cosmological models and Birkhoff's theorem doesn't hold. GFST may e.g. be found in the book [1] and in the cited references. Additionally, non-singular, cosmological models are e.g. given in the articles [2]-[6].

Subsequently, homogeneous, isotropic, cosmological models will be summarized. Let us use the pseudo-Euclidean geometry. The received universe is non-singular under the assumption that the sum of the density parameters is greater than one, e.g. a little bit greater than one. This implies that the universe may become hot in the course of time. It starts without matter and without radiation and all the energy is gravitational energy. Matter and radiation emerge from this energy by virtue of the conservation of the total energy. The space is flat and the interpretation of a non-expanding space is natural. But it is also possible to state an expansion of space by a suitable transformation as consequence of general covariance of the equations. For a zero cosmological constant matter increases for all times whereas radiation increases and the universe becomes hot. After that radiation decreases to zero as time goes to infinity. Short time after the universe has reached the maximal temperature the production of matter is finished, *i.e.* the universe appears nearly stationary. Under the assumption of a positive cosmological constant, a certain time after the beginning, matter goes to zero and the universe converges to dark energy as time goes to infinity. Hence, a universe given by GFST appears more natural than that received by GR which gives singular solution with infinite densities. The universe starts from a point and therefore space must expand to be in agreement with the observed big universe. The geometry is in general non-Euclidean but the observed universe implies a flat space.

Section 2 contains GFST; Section 3 contains cosmological models and Section 4 contains the comparison of GFST and GR.

## 2. GFST

The theory of GFST is shortly summarized. The metric is the flat space-time given by

$$(ds)^2 = -\eta_{ij} dx^i \quad (1)$$

where  $(\eta_{ij})$  is a symmetric tensor. Pseudo-Euclidean geometry has the form

$$(\eta_{ij}) = (1, 1, 1, -1). \quad (2)$$

Here,  $(x^i) = (x^1, x^2, x^3)$  are the Cartesian coordinates and  $x^4 = ct$ . Let

$$\eta = \det(\eta_{ij}). \quad (3)$$

The gravitational field is described by a symmetric tensor  $(g_{ij})$ . Let  $(g^{ij})$  be defined by

$$g_{ik} g^{kj} = \delta_i^j \quad (4)$$

and put similar to (3)

$$G = \det(g_{ij}). \quad (5)$$

The proper time  $\tau$  is defined by

$$(cd\tau)^2 = -g_{ij} dx^i dx^j. \quad (6)$$

The Lagrangian of the gravitational field is given by

$$L(G) = - \left( \frac{-G}{-\eta} \right)^{1/2} g_{ij} g_{kl} g^{mn} \left( g_{/m}^{ik} g_{/n}^{jl} - \frac{1}{2} g_{/m}^{ij} g_{/n}^{kl} \right) \quad (7)$$

where the bar/ denotes the covariant derivative relative to the flat space-time metric (1).

The Lagrangian of dark energy (given by the cosmological constant  $\Lambda$ ) has the form

$$L(\Lambda) = -8\Lambda \left( \frac{-G}{-\eta} \right)^{1/2}. \quad (8)$$

Let

$$\kappa = 4\pi k/c^4 \quad (9)$$

where  $\kappa$  is the gravitational constant. Then, the mixed energy-momentum tensor of gravitation, of dark energy and of matter of a perfect fluid are

$$T(G)_j^i = \frac{1}{8\kappa} \left[ \left( \frac{-G}{-\eta} \right)^{1/2} g_{kl} g_{mn} g^{ir} \left( g_{/j}^{km} g_{/r}^{ln} - \frac{1}{2} g_{/j}^{kl} g_{/r}^{mn} \right) + \frac{1}{2} \delta_j^i L(G) \right] \quad (10a)$$

$$T(\Lambda)_j^i = \frac{1}{16\kappa} \delta_j^i L(\Lambda) \quad (10b)$$

$$T(M)_j^i = (\rho + p) g_{jk} u^k u^i + \delta_j^i p c^2. \quad (10c)$$

Here,  $\rho$ ,  $p$  and  $u^i$  denote density, pressure and four-velocity of matter. It holds by (6)

$$c^2 = -g_{ij} u^i u^j. \quad (11)$$

Define the covariant differential operator

$$D_j^i = \left[ \left( \frac{-G}{-\eta} \right)^{1/2} g^{kl} g_{jm} g_{/l}^{mi} \right]_{/k} \quad (12)$$

of order two. Then, the field equations for the potentials ( $g_{ij}$ ) have the form

$$D_j^i - \frac{1}{2} \delta_j^i D_k^k = 4\kappa T_j^i \quad (13)$$

where

$$T_j^i = T(G)_j^i + T(M)_j^i + T(\Lambda)_j^i. \quad (14)$$

Define the symmetric energy-momentum tensor

$$T(M)^{ij} = g^{ik} T(M)_k^j \quad (15)$$

Then the equations of motion in covariant form are

$$T(M)_{i/k}^k = \frac{1}{2} g_{kl/i} T(M)^{kl}. \quad (16)$$

In addition to the field Equation (13) and the equations of motion (16) the conservation law of the total energy-momentum holds, *i.e.*

$$T_{i/k}^k = 0. \quad (17)$$

The field equations of gravitation are formally similar to those of GR where  $T_j^i$  is the energy-momentum without that of gravitation since the energy-momentum of gravitation is not a tensor for GR. Therefore, the differential operator is the Einstein tensor which may give a non-Euclidean geometry

The results of this chapter may be found in the book [1] and in many other articles of the author, as e.g. in [5].

### 3. Homogeneous, Isotropic, Cosmological Models

In this chapter GFST is applied to homogeneous, isotropic, cosmological models. The pseudo-Euclidean geometry (1) with (2) is used. The matter tensor is given by perfect fluid with velocity

$$u^i = 0 \quad (i=1,2,3) \tag{18}$$

and pressure  $p$  and density  $\rho$  with

$$p = p_m + p_r, \rho = \rho_m + \rho_r \tag{19}$$

where the indices  $m$  and  $r$  denote matter and radiation. The equations of state for matter (dust) and radiation are

$$p_m = 0, p_r = \frac{1}{3}\rho_r. \tag{20}$$

The potential are by virtue of (18) and the homogeneity and isotropy

$$g_{ij} = \begin{cases} a^2(t) & (i = j = 1,2,3) \\ -1/h(t) & (i = j = 4) \\ 0 & (i \neq j) \end{cases}. \tag{21}$$

The four-velocity is by Equation (18) and Equation (6)

$$(u^i) = (0, 0, 0, ch^{1/2}). \tag{22}$$

Let  $t_0 = 0$  be the present time and assume as initial conditions at present

$$a(0) = h(0) = 1, \dot{a}(0) = H_0, \dot{h}(0) = \dot{h}_0, \rho_m(0) = \rho_{m0}, \rho_r(0) = \rho_{r0} \tag{23}$$

where the dot denotes the time derivative;  $H_0$  is the Hubble constant and  $\dot{h}_0$  is a further constant;  $\rho_{m0}$  and  $\rho_{r0}$  denote the present densities of matter and radiation. It follows from (16) under the assumption that matter and radiation do not interact

$$\rho_m = \rho_{m0}/h^{1/2}, \rho_r = 3p_r = \rho_{r0}/(ah^{1/2}). \tag{24}$$

The field Equation (13) implies by the use of (21) the two nonlinear differential equations

$$\frac{d}{dt} \left( a^3 h^{1/2} \frac{\dot{a}}{a} \right) = 2\kappa c^4 \left( \frac{1}{2}\rho_m + \frac{1}{3}\rho_r + \frac{\Lambda}{2\kappa c^2} \frac{a^3}{h^{1/2}} \right), \tag{25a}$$

$$\frac{d}{dt} \left( a^3 h^{1/2} \frac{\dot{h}}{h} \right) = 4\kappa c^4 \left( \frac{1}{2}\rho_m + \rho_r + \frac{1}{8\kappa c^2} L(G) - \frac{\Lambda}{2\kappa c^2} \frac{a^3}{h^{1/2}} \right) \tag{25b}$$

where

$$L(G) = \frac{1}{c^2} a^3 h^{1/2} \left( -6 \left( \frac{\dot{a}}{a} \right)^2 + 6 \frac{\dot{a}}{a} \frac{\dot{h}}{h} + \frac{1}{2} \left( \frac{\dot{h}}{h} \right)^2 \right). \tag{26}$$

The expression  $\frac{1}{16\kappa} L(G)$  is the density of gravitation. The conservation law of the total energy is

$$(\rho_m + \rho_r) c^2 + \frac{1}{16\kappa} L(G) + \frac{\Lambda}{2\kappa} \frac{a^3}{h^{1/2}} = \lambda c^2 \tag{27}$$

where  $\lambda$  is a constant of integration. The Equations (25), (26) and (27) give by the use of the initial conditions (23)

$$\frac{\dot{h}}{h} = -6 \frac{\dot{a}}{a} + 2 \frac{4\kappa c^4 \lambda t + \varphi_0}{2\kappa c^4 \lambda t^2 + \varphi_0 t + 1} \tag{28}$$

with

$$\varphi_0 = 3H_0 \left( 1 + \frac{1}{6} \frac{\dot{h}_0}{H_0} \right). \quad (29)$$

Integration of (28) yields

$$a^3 h^{\frac{1}{2}} = 2\kappa c^4 \lambda t^2 + \varphi_0 t + 1. \quad (30)$$

Equation (27) gives for the present time  $t_0 = 0$  by the use of the initial conditions (23)

$$\frac{1}{3} (8\kappa c^4 \lambda - \varphi_0^2) = 4 \left[ \frac{8}{3} \pi k \left( \rho_{m0} + \rho_{r0} + \frac{\Lambda c^2}{8\pi k} \right) - H_0^2 \right]. \quad (31)$$

It follows from (27) by the use of the standard definition of the density parameters of matter, radiation and the cosmological constant with the abbreviation

$$K_0 = (\Omega_m + \Omega_r + \Omega_\Lambda) / \Omega_m \quad (32)$$

the differential equation

$$\left( \frac{\dot{a}}{a} \right)^2 = \frac{H_0^2}{(2\kappa c^4 \lambda t^2 + \varphi_0 t + 1)^2} \left[ -\Omega_m K_0 + \Omega_r a^2 + \Omega_m a^3 + \Omega_\Lambda a^6 \right]. \quad (33a)$$

The initial condition is by (23)

$$a(0) = 1. \quad (33b)$$

The solution of (33) with (30) describes a homogeneous, isotropic, cosmological model by GFST. Relation (31) can be rewritten in the form

$$\frac{8\kappa c^4 \lambda}{H_0^2} - \left( \frac{\varphi_0}{H_0} \right)^2 = 12\Omega_m K_0. \quad (34)$$

A necessary and sufficient condition to avoid singular solutions of (33) is

$$K_0 > 0 \quad (35)$$

which yields

$$2\kappa c^4 \lambda t^2 + \varphi_0 t + 1 > 0 \quad (36)$$

for all  $t \in \mathbb{R}$ . Hence, condition (35) implies a non-singular solution for all  $t \in \mathbb{R}$ , *i.e.* we get a non-singular cosmological model. It exists a  $t_1 < t_0 = 0$  such that

$$\dot{a}(t_1) = 0. \quad (37)$$

Put  $a_1 = a(t_1)$  then it follows from (33a) with  $t = t_1$

$$\Omega_r a_1^2 + \Omega_m a_1^3 + \Omega_m a_1^6 = \Omega_m K_0. \quad (38)$$

It holds for all  $t \in \mathbb{R}$

$$a(t) \geq a_1 > 0. \quad (39)$$

Subsequently assume

$$a_1 \ll a(0) = 1. \quad (40)$$

Then we get by virtue of (38)

$$K_0 \ll 1. \quad (41)$$

It follows from (32) by virtue of (41)

$$\Omega_r + \Omega_m + \Omega_\Lambda = 1 + \Omega_m K_0, \quad (42)$$

*i.e.* the sum of the density parameters is a little bit greater than one. Hence,  $a(t)$  starts from a positive value, decreases to a small positive value, and then increases for all  $t \in \mathbb{R}$ .

The proper time from the beginning of the universe till time  $t$  is

$$\tilde{\tau}(t) = \int_{-\infty}^t 1/h^{1/2}(t) dt. \tag{43}$$

The differential Equation (33a) is rewritten by the use of (30) in the form

$$\left(\frac{\dot{a}}{a}\right)^2 = H_0^2 \frac{1}{h} \left( -\frac{\Omega_m K_0}{a^6} + \frac{\Omega_r}{a^4} + \frac{\Omega_m}{a^3} + \Omega_\Lambda \right). \tag{44}$$

Hence, the differential equation for the function  $a$  by the use of the proper time is

$$\left(\frac{1}{a} \frac{da}{d\tilde{\tau}}\right)^2 = H_0^2 \left( -\frac{\Omega_m K_0}{a^6} + \frac{\Omega_r}{a^4} + \frac{\Omega_m}{a^3} + \Omega_\Lambda \right). \tag{45}$$

This differential equation is by virtue of (41) and a not too small function  $a(t)$  identical with that of GR for a flat homogeneous, isotropic universe. Therefore, away from the beginning of the universe, the result for the universe agrees for GFST with that of GR.

These results may be found in the book [1] and in the article [5].

The subsequent considerations can be found in the book [1].

We introduce in addition to the proper time  $\tilde{\tau}$  the absolute time  $t'$  by

$$dt' = \frac{1}{a(t)h^{1/2}(t)} dt = \frac{1}{a(t)} d\tilde{\tau}. \tag{46}$$

This gives for the proper time in the universe

$$(cd\tau)^2 = -a(t)^2 \left[ |dx|^2 - (dct')^2 \right] \tag{47}$$

where  $|dx|$  denotes the Euclidean norm of the vector  $dx = (dx_1, dx_2, dx_3)$ .

Relation (47) implies that the absolute value of the light-velocity is equal to vacuum light-velocity  $c$  for all times  $t'$ .

The introduction of the absolute time  $t'$  in the differential Equation (45) gives

$$\left(\frac{da}{dt'}\right)^2 = \frac{H_0^2}{a^2} \left( -\Omega_m K_0 + \Omega_r a^2 + \Omega_m a^3 + \Omega_\Lambda a^6 \right). \tag{48}$$

Assume that a light ray is emitted at distance  $r$  at time  $t'_e$  resp. at time  $t'_e + dt'_e$  and it is received by the observer at time  $t'$  resp. at time  $t' + dt'$ . Then, it follows

$$r = \int_{t'_e}^{t'} c dt' = c(t' - t'_e), \quad r = \int_{t'_e + dt'_e}^{t' + dt'} c dt' = c(t' + dt' - t'_e - dt'_e).$$

These two equations imply

$$dt' = dt'_e.$$

The age of the universe since the minimal value of  $a(t)$  measured with absolute time  $t'$  till now

$$\begin{aligned} \Delta t' &= \int_{t'_1}^{t'_0} dt' = \int_{a_1}^1 \frac{1}{\left(\frac{da}{dt'}\right)} da = \frac{1}{H_0} \int_{a_1}^1 a da / \left( -\Omega_m K_0 + \Omega_r a^2 + \Omega_m a^3 + \Omega_\Lambda a^6 \right)^{1/2} \\ &\geq \frac{1}{H_0} \int_{a_1}^1 a da / \left( -\Omega_m K_0 + (\Omega_r + \Omega_m + \Omega_\Lambda) a^2 \right)^{1/2} \approx \frac{1}{H_0}. \end{aligned}$$

Therefore, the age of the universe measured with absolute time is greater than  $\frac{1}{H_0}$  independent of the density parameters, *i.e.* there is no age problem.

We will now calculate the redshift of light emitted from a distant object at rest and received by the observer at present time. It is useful to introduce the absolute time. Assume that an atom at a distant object emits a photon at

time  $t'_e$ . It follows from relation (46)

$$d\tilde{\tau} = a(t'_e) dt' \tag{49}$$

Therefore, the energy of the emitted photon is

$$E \sim -g_{44} \frac{dt'}{d\tilde{\tau}} \sim a(t'_e) E_0.$$

The energy of the photon moving to the observer in the universe is constant by virtue of (47), *i.e.* by the constant light velocity. Then, the corresponding received frequency is

$$\nu = a(t'_e) \nu_0 \tag{50}$$

where  $\nu_0$  is the frequency emitted at the observer from the same atom. The redshift is given by

$$z = \nu_0/\nu - 1 = 1/a(t'_e) - 1. \tag{51}$$

Light emitted at distance  $r$  at time  $t'_e$  and received at  $r = 0$  at time  $t'_0$  has by the constant velocity of light the relation

$$r = c(t'_0 - t'_e).$$

This gives by Taylor expansion of  $a(t'_e)$  in relation (51)

$$z = H_0 \frac{r}{c} + \left( 1 - \frac{1}{2} \frac{1}{H_0^2} \frac{d^2 a(t'_0)}{dt'^2_0} \right) \left( H_0 \frac{r}{c} \right)^2$$

Differentiation of Equation (48) yields by neglecting small expressions

$$\frac{d^2 a(t'_e)}{dt'^2_e} \approx H_0^2 \left( 1 - \frac{1}{2} \Omega_m + \Omega_\Lambda \right).$$

This gives the redshift formula

$$z = H_0 \frac{r}{c} + \frac{3}{4} \Omega_m \left( H_0 \frac{r}{c} \right)^2. \tag{52}$$

The detailed calculations of Formula (52) can be found in the book [1]. Higher order Taylor expansion gives higher order redshift approximations.

#### 4. Differences of Theory and Results of GFST and GR

1) It is worth to mention that the space of the universe by GFST is also flat by the use of (6) with (21). This is important because the experiment implying flatness of space of GR uses Formula (6). This is the result of the flat space-time geometry of GFRS. The results for the universe of GFST and GR away from the beginning of the universe agree for a flat space.

2) The metric of GFST is a flat space-time and the space of GFST is flat by the use of (1) and (2). The gravitational field is a tensor of rank two and it is described in flat space-time. The left hand side is a non-linear differential operator of order two and the right hand side is the total energy-momentum tensor including that of gravitation which is a tensor in GFST. Proper time is defined by the use of the gravitational field. The metric of GR is identical with the definition of the proper time which is formally identical with that of GFST. The energy-momentum of gravitation by GR is not a tensor. The left hand side of the field equations is a linear combination of the Ricci tensor and the right hand side of the differential equations is the matter tensor. Both gravitational theories are covariant. The theory of GR implies in general a non-Euclidean geometry. Experimental results indicate that our universe is flat

3) The space of the universe by GFST is by (1) and (2) non-expanding. Experimental results of Lerner [7] also yield a non-expanding universe. The space of the universe by GR is singular in the beginning, *i.e.* it starts from a point. The observed universe is very big. Therefore, the space must expand and perhaps it implies an inflationary universe.

4) The universe received by GFST is non-singular, *i.e.* all the physical quantities are defined in contrast to those of GR where the universe starts with a singularity in the beginning, *i.e.* the space consists of a point with infinite density of matter.

5) The redshift is an intrinsic gravitational effect by GFST whereas GR explains the redshift as Doppler effect of an expanding universe.

6) Linear perturbation theory of cosmological models by GFST can give in the matter dominated universe a quick increase of the inhomogeneity (see [1], chapter 9.4) which may explain the galaxies whereas by the use of GR the increase of the inhomogeneity is much too slow.

7) The theory of GFST gives non-expanding, cosmological models. Hence, gravitational waves cannot be generated in the beginning. In the beginning of the universe by GR, it can imply gravitational waves by virtue of inflation. Signals from the birth of the universe were measured by BICEP2. But shortly after this announcement the result was retracted.

8) Studies of supernovae are used to measure distances in space. It seems that the ancient supernovae aren't as distant as believed. This means that the cosmological constant is smaller than till now assumed. A vanishing cosmological constant (no dark energy) is perhaps not excluded if a modified Hubble law is used where it is assumed that every object is surrounded by a medium (see [1] chapter 12.4 and article [8]). This gives a new redshift formula.

9) A non-singular, non-expanding universe with vanishing cosmological constant is already studied in article [9].

## References

- [1] Petry, W. (2014) A Theory of Gravitation in Flat Space-Time. Science PG.
- [2] Petry, W. (1981) *General Relativity Gravitation*, **13**, 1057-1071. <http://dx.doi.org/10.1007/BF00756365>
- [3] Petry, W. (1990) *General Relativity Gravitation*, **22**, 1045-1965. <http://dx.doi.org/10.1007/BF00757815>
- [4] Petry, W. (1997) *Astrophysics Space Science*, **254**, 305-317. <http://dx.doi.org/10.1023/A:1000938931517>
- [5] Petry, W. (2013) *Journal Modern Physics*, **4**, 20-25. <http://dx.doi.org/10.4236/jmp.2013.47A1003>
- [6] Petry, W. (2014) *Journal Applied Mathematics Physics*, **2**, 50-54. <http://dx.doi.org/10.4236/jamp.2014.25007>
- [7] Lerner, E. (2005) arXiv: astro-ph/0509611.
- [8] Petry, W. (2013) *Physics Essays*, **26**, 315-320. <http://dx.doi.org/10.4006/0836-1398-26.2.315>
- [9] Petry, W. (2015) *Journal Modern Physics*, **6**, 1085-1094. <http://dx.doi.org/10.4236/jmp.2015.68113>



**Submit or recommend next manuscript to SCIRP and we will provide best service for you:**

Accepting pre-submission inquiries through Email, Facebook, LinkedIn, Twitter, etc.

A wide selection of journals (inclusive of 9 subjects, more than 200 journals)

Providing 24-hour high-quality service

User-friendly online submission system

Fair and swift peer-review system

Efficient typesetting and proofreading procedure

Display of the result of downloads and visits, as well as the number of cited articles

Maximum dissemination of your research work

Submit your manuscript at: <http://papersubmission.scirp.org/>

# Reexamination of Criticality Accident in JCO

Sachiko Oshima<sup>1</sup>, Miri Hisada<sup>2</sup>, Yusuke Saito<sup>2</sup>, Takehisa Fujita<sup>2</sup>

<sup>1</sup>College of Industrial Technology, Nihon University, Narashino, Chiba, Japan

<sup>2</sup>Department of Physics, Faculty of Science and Technology, Nihon University, Tokyo, Japan

Email: oshima.sachiko@nihon-u.ac.jp, fffujita@phys.cst.nihon-u.ac.jp

Received 22 June 2016; accepted 22 August 2016; published 25 August 2016

Copyright © 2016 by authors and Scientific Research Publishing Inc.

This work is licensed under the Creative Commons Attribution International License (CC BY).

<http://creativecommons.org/licenses/by/4.0/>



Open Access

---

## Abstract

Nuclear chain reactions are, by now, commonly used in the nuclear reactors, and thus it seems that there is no basic problem in fission processes from the scientific point of view. However, the criticality accident that occurred in JCO in 1999 suggests that one should carefully examine this accident from the nuclear physics point of view. Indeed the chain nuclear reactions should have taken place in the small area of space with 45 cm diameter disk times 30 cm height tank. In fact, when people carry the uranium nitrate solution into sedimentation tank, then this solution with uranium should get into the critical state at the 45ℓ of uranium nitrate solution. The root cause of the accident should not be very simple from the nuclear physics point, and it should be quite important to examine why the uranium nitrate solution with 45ℓ could have become critical.

## Keywords

Nuclear Fission, Criticality, Mean Free Path

---

## 1. Introduction

The criticality accident that occurred in JCO in 1999 must be most serious, and it should not be very easy to understand why the nuclear chain reactions could proceed in a small area of space for a finite period of time. In this sense, it should be quite important to carry out the careful examination of criticality accidents from the nuclear physics point of view. It should be, of course, difficult to claim that the JCO accident can be a target of the scientific study since one cannot make the experimental study of the JCO type accidents. However, we believe that the basic mechanism of the criticality accident should be clarified why it could naturally occur in the small area of space.

This criticality accident occurred when workers in JCO company were carrying the uranium nitrate solution (18.8% enriched uranium) into sedimentation tank [1]-[3]. Here, we should explain the working procedure

which is taken by the workers in JCO. First, they make the uranium nitrate solution which is composed of 2.4 kg  $U_3O_8$  with the nitric acid of 1.7ℓ in the stainless vessel. In addition, they add water to the uranium nitrate solution until the total volume becomes 6.5ℓ. Then, they carry the 6.5ℓ solution into the sedimentation tank, and this working procedure is called one batch.

The criticality accident should have occurred in the middle of the seventh batch since the workers noticed blue lights that should be due to the Cherenkov radiation. In fact, two of the workers suffered from the neutron radiation.

A question should arise as to how the nuclear chain reactions could proceed within the small sedimentation tank (45 cm diameter, 60 cm high). There are, of course, some analyses of this criticality accident [4] [5]. However, these studies are mainly carried out for the computer simulation such that the total energy emitted via radiations can be reproduced in some way or the other. These investigations are, of course, very important in order to understand the accident cause. However, it is also important to carry out the study of the criticality accident from the nuclear physics point of view.

In this paper, we carry out careful calculations of the criticality accident in terms of the multiple scattering theory. Here, we want to understand why the nuclear chain reactions can proceed in the small area of space. In particular, we trace the nuclear fission reactions (nucleon-nucleon collision together with nuclear fission) each by each, and we clarify the microscopic processes why and how the criticality accident occurred. As a result, we should understand some specific reasons why the chain reactions can proceed, and this can be done by making use of the mean free path which is the result of the nuclear multiple scattering theory.

However, when we clarify how the criticality accident occurs, we face to the most difficult question as to why the criticality could stop. In this study, we find an answer for this question, though not necessarily sufficient. This mechanism of stopping criticality may be related to the quick settle of the uranium compound.

As a result of our calculation, we find a possible dangerous situation which was thought to be due to the 8th batch, if it were carried into the sedimentation tank. We see that the estimated energy release after the virtual 8th batch should become the same order of magnitude as the Chernobyl nuclear accident.

## 2. Nuclear Chain Reactions

Nuclear fission reaction by incident neutrons can be written as [6]



where  $A_1$ ,  $A_2$  are new nuclei which are produced in the reactions. In this reaction, there are two important points. The first one is concerned with two or three neutrons which are produced in the reactions. The second point is that the probability of this nuclear reactions is strongly based on the incident neutron energy, and the biggest cross section is for the incident neutron with almost zero energy (thermal energy).

The chain reactions indicate that the produced neutrons should be absorbed by another  ${}^{235}\text{U}$  such that the nuclear fission can proceed further on. In addition, if the chain reactions continue to proceed without the aid of other external neutron sources, then this situation is called a criticality stage. In reactors, this criticality must be kept by controlling the number of neutrons involved in the chain reactions.

In normal reactors, a few % enriched uranium should be commonly used, but in this JCO accident, 18.8% enriched uranium were used, and this high enrichment should be one of the strong reasons why the nuclear reactions run wild.

## 3. Why Criticality?

Now, a question is as to why the criticality is realized in the small area of the sedimentation tank with 50ℓ of the uranium nitrate solution. That is, why nuclear chain reactions continue to occur in this small area. Here we clarify the basic mechanism of the criticality accident.

### 3.1. Neutron Source

The nuclear chain reactions should require thermal neutrons to start for the initial fission reactions. Since neutrons should decay within 15 minutes, they do not exist as a natural source. Neutrons should be produced in some way or the other. Here in this accident, the neutron source should be the decay of  ${}^{238}\text{U}$  spontaneous

fissions. The life time of  $^{238}\text{U}$  is about 4.5 billion years and, in addition, the rate of the spontaneous fission to the total width is around  $5.45 \times 10^{-7}$ . Therefore, 1 g of  $^{238}\text{U}$  make the spontaneous fission of 0.01 times per second. Since one batch contains 1.6 kg of  $^{238}\text{U}$ , we should find about 20 neutrons per second in the one batch solution.

### 3.2. Mean Free Path of $n$ - $^{235}\text{U}$ Fission (Fast Neutrons)

The probability of nuclear fission of  $^{235}\text{U}$  induced by neutrons should be evaluated in terms of mean free path of  $\lambda$  inside the uranium nitrate solution. This mean free path of nuclear reactions can be obtained from the multiple scattering theory as

$$\lambda = \frac{1}{\rho\sigma_f} \quad (2)$$

This derivation of the mean free path (2) is based on the Glauber theory [7], and this theoretical frame work is well examined in atomic and nuclear reactions [8] [9]. Here,  $\rho$  denotes the number density of  $^{235}\text{U}$  in solution and  $\sigma_f$  corresponds to the nuclear fission cross section of  $^{235}\text{U}$  induced by neutrons. In fact, the number density of  $^{235}\text{U}$  in one batch solution is  $\rho \approx 1.5 \times 10^{20} \text{ cm}^{-3}$  which is a constant. On the other hand, the nuclear fission cross section  $\sigma_f$  of  $^{235}\text{U}$  induced by neutrons crucially depends on the incident energy of neutrons. The incident energy dependence of the observed cross sections  $\sigma_f$  can be written as [10]

$$\sigma_f \approx \begin{cases} 585 \text{ b} : E_n \approx 0.025 \text{ eV} \\ 1 \text{ b} : E_n \approx 1 \text{ MeV} \end{cases} \quad (3)$$

where  $1 \text{ b} = 10^{-24} \text{ cm}^2$ .

#### Mean Free Path of Prompt neutrons in Nuclear Fission

In fission process, the average energy of prompt neutrons is around 1 MeV, and therefore the average mean free path of the prompt neutrons after fissions becomes

$$\lambda_f = \frac{1}{\rho\sigma_f} \approx 67 \text{ m}. \quad (4)$$

This is quite long in comparison with the scale of the tank, and therefore this prompt neutrons by themselves cannot induce subsequent fissions in corresponding solution in the tank. In this respect, we ask a question as to why the criticality should take place within the small sedimentation tank.

## 4. Collision between Neutrons and Water Molecule

In reality, the prompt neutrons may collide with protons in water molecule, and they should lose their energy by nucleon-nucleon collisions. Since the nuclear fission cross sections become largest for the thermal neutrons, the fission processes should start in case the prompt neutrons lose most of their energy inside the uranium nitrate solution.

### 4.1. Energy Loss after the Collision of Prompt Neutrons with Protons in Water

When the prompt neutron scatters with protons in water, this neutron should lose a half of its energy. This can be easily understood in the following way. First, we denote the incident momentum and energy of the neutron by  $p, E_n$  with  $E_n = \frac{p^2}{2M}$ , and the final momentum and energy by  $k, E'_n$  with  $E'_n = \frac{k^2}{2M}$ . In this case, we find an equation from the conservation law of momentum and energy as

$$\frac{p^2}{2M} = \frac{k^2}{2M} + \frac{(p-k)^2}{2M} \quad (5)$$

which can be solved and its solution becomes

$$k = p \cos \theta. \quad (6)$$

Since the observed scattering cross section does not depend on the scattering angles, we can make an average

over the angles, and we obtain the average energy after the scattering

$$E'_n = \frac{1}{\pi} \int_0^\pi \frac{k^2}{2M} d\theta = \frac{1}{\pi} \int_0^\pi \frac{P^2}{2M} \cos^2 \theta d\theta = \frac{1}{2} E_n. \quad (7)$$

This means that a neutron should lose a half of its energy in each scattering process.

#### 4.2. The Mean Free Path of Neutrons Inside Water

Now we calculate the mean free path of neutrons after the scattering with protons in one batch solution. The number density of protons in one batch solution is  $\rho_p \approx 4.9 \times 10^{22} \text{ cm}^{-3}$ . The neutron-proton cross section at low energy is observed as  $\sigma_{np} \approx 20 \text{ b}$  [11], and thus the mean free path of neutron in one batch solution becomes

$$\lambda_p = \frac{1}{\rho_p \sigma_{np}} \approx 1 \text{ cm}. \quad (8)$$

Therefore, a prompt neutron with 1 MeV energy should have its energy after it travels around 25 cm,

$$E'_n = 1 \text{ MeV} \times \left(\frac{1}{2}\right)^{25} \approx 0.03 \text{ eV}. \quad (9)$$

This neutron does not have to travel linearly, but in any case, it should become a thermal neutron.

#### 4.3. Mean Free Path of Thermal Neutron in the $n$ - $^{235}\text{U}$ Fission Process

We can easily calculate the mean free path of the thermal neutron before the nuclear fission in one batch solution. Since  $\sigma_f = 585 \text{ b}$ , we find

$$\lambda_f = \frac{1}{\rho \sigma_f} \approx 11 \text{ cm} \quad (10)$$

From these considerations, we see that prompt neutrons with 1 MeV should travel around 25 cm, and then they become thermal neutrons. Further, after they travel 11 cm, they can induce nuclear fissions. Thus, if one carries 50ℓ of the uranium nitrate solution into the sedimentation tank with 45 cm diameter and 25 cm height, then nuclear chain reactions may well start quickly and proceed further on.

#### 4.4. Reaction Time of Neutrons

Now we see that when prompt neutrons travel 36 cm, then they can induce nuclear fissions. Therefore, we should estimate the duration time that is necessary to travel this 36 cm. Since the nuclear reaction time must be smaller than  $10^{-15}$  second, we can ignore this time duration. Since the prompt neutron with 1 MeV should spend  $\tau_0 \approx 7.6 \times 10^{-10}$  second to proceed 1 cm, its energy becomes a half of the previous energy after 1 cm walk. Therefore, the time to proceed the next 1 cm becomes larger by a factor of  $\sqrt{2}$ . In this way, if the prompt neutron proceed 25 cm, then the total time to spend must be

$$T_0 = \left(1 + \sqrt{2} + \dots + 2^{25/2}\right) \tau_0 \approx 15 \mu\text{s}. \quad (11)$$

After that, this neutron becomes thermal, and it should proceed 11 cm before the nuclear fission. Since the thermal neutron may have the energy of 0.03 MeV, it should take  $\tau_{th} \approx 46 \mu\text{s}$ . Thus, the total time that is necessary for the prompt neutron to induce a fission reaction should be  $T_{tot} \approx 61 \mu\text{s}$ .

### 5. Total Energy of Fission with Criticality

Here, we should estimate the total amount of energy which is released from this accident. This evaluation must be very difficult, but we want to calculate it in an approximate way and obtain an order of magnitude of the total energy.

First, the number of neutrons which is required for the criticality reactions should be taken as  $n_r = 1.001$ , which is assumed to be consistent with the total energy released as calculated from the computer simulation. In

nuclear reactors, one should make use of all the possible techniques to keep the number as  $n_r = 1$ .

In addition, we assume that the number of nuclear fissions should be  $N = 40000$ . This number is chosen so that the total nuclear energy release should be consistent with the computer simulation which can reproduce all the observed radiation energies. In this case, the total reaction time of fission becomes  $T_f \approx 2.4$  s, and the total number of fissions becomes

$$N_{tot} = 1.001^{40000} \approx 2.3 \times 10^{17}. \quad (12)$$

Further, we evaluate the neutron number at the beginning, and this neutron should come from the spontaneous fission of  $^{238}\text{U}$ . The number of neutrons in one batch solution must be around 20, and we take a half of this number. The energy release from the nuclear fission must be around 200 MeV in each reaction, and therefore the total energy becomes

$$E_{tot} \approx 4.6 \times 10^{26} \text{ eV} \quad (13)$$

which is just similar to the result of the computer simulation.

## 6. Why Does the Criticality Stop?

It is true that the criticality accident produced a huge amount of energy by the nuclear chain reactions, and the accident is indeed quite serious. In this sense, we here clarify as to how the chain reactions started and continued by reaching the critical stage. However, we face to the more serious problem at this point. That is, *why the criticality accident could stop?* We should understand any reason why the criticality could stop, namely there were only one burst and not any more burst, but why?

### 6.1. Nuclear Fission in the Seventh Batch

Here, we try to answer for this question, though it should be extremely difficult. In order to find a possible mechanism for the stopping of the criticality, we assume that the uranium compound should settle faster than any other compounds in the solution. Further, we assume that uranium should be settled within 20% height from the bottom of the sedimentation tank.

In this case, after the sixth batch, the uranium should be settled up to the 4.9 cm from the bottom. Thus, water should be found for 19.7 cm long in the sedimentation tank. By taking into account this fact, we can calculate the total energy release by nuclear fission as

$$E_{tot} \approx 4.6 \times 10^{26} \text{ eV} \approx 7.4 \times 10^7 \text{ J}. \quad (14)$$

The duration time of this nuclear reactions can be estimated and should be around  $T_f \approx 2.4$  s, which should correspond to the time that the uranium compound is coming down to the bottom.

### 6.2. Nuclear Fission in the Sixth Batch

The same calculation can be carried out for the sixth batch case. In this case, we see that the total energy must be 1000 times smaller than that of the seventh batch case. This is not very large, but at the sixth batch, the nuclear chain reactions already started, and indeed there were a small burst.

From this calculation, we now understand the reason why the criticality stopped. In case the uranium were settled at the bottom of the tank, then the nuclear chain reaction cannot proceed further since the prompt neutrons cannot lose their energy because of the lack of water.

### 6.3. Nuclear Fission in the Eighth Batch

From now on, we only present a possible scenario of nuclear accident, if the 8th batch were carried into the tank. In this case, the number of uranium involved in the nuclear fission must be proportional to the height of water, and thus it should be  $\frac{22.9}{19.7}$  more than the seventh batch. Thus, the number becomes

$$N = 40000 \times \frac{22.9}{19.7} \approx 46500. \quad (15)$$

This means that the number of nuclear fissions should be also increased and the total number becomes

$$N_{tot} = 1.001^{46500} \approx 1.5 \times 10^{20}. \quad (16)$$

Therefore, the total energy becomes

$$E_{tot} \approx 3 \times 10^{29} \text{ eV} \approx 4.8 \times 10^{10} \text{ J}. \quad (17)$$

This energy  $4.8 \times 10^{10}$  J corresponds to 11 ton of TNT powder which is quite a serious explosion. The accident of Chernobyl nuclear power plant is believed to correspond to around 100 ton of TNT powder, and therefore, if the 8th batch were thrown away, then the accident would have been more than serious.

## 7. Summary

We have discussed the basic mechanism of the JCO accident in terms of the nuclear multiple scattering theory. In this paper, we have clarified how the nuclear chain reactions could proceed in the small area of the sedimentation tank. The JCO accident should be studied from the point of view science, even though there must be no serious technical problems in nuclear reactors. In this respect, one may say that the JCO accident is rather similar to scientific phenomena, and it is essentially different from problems found in the nuclear power plants.

## Acknowledgements

We are grateful to N. Yoshinaga for interesting discussions and useful comments.

## References

- [1] (2005) Nihon Genshiryoku Gakkai JCO Jiko-Chosa Inkai, JCO Rinkaijiko; Sonozenbou no kaimei jijitsu youin taiou (Criticality Accident in JCO; Its Solution, Fact, Cause and Study). Tokai University Press, Kanagawa. [In Japanese]
- [2] Yamane, Y., Nakajima, K., Abe, H., Hayashi, Y., Arisawa, J. and Hayami, S. (2010) Kakunenryo-shisetsu no Jiko-eikyohou-hyokashuhou ni kansuru chosa (V) Rinkaijiko-eikyo no hyouka-shuhou to Shikaiseki (Research on Consequence Analysis Method for Probabilistic Safety Assessment of Nuclear Fuel Facilities (V): Evaluation Method and Trial Evaluation of Criticality Accident). Atomic Energy Society of Japan, Tokyo, Vol. 9, No. 1, 96-107. [In Japanese]
- [3] Tateno, J., Noguchi, K. and Aoyagi, N. (2000) Tetteikaimeit Tokaimura Rinkaijiko (Criticality Accident in Tokaimura; Complete analysis). Shin-nihon Shuppan-sha, Tokyo. [In Japanese]
- [4] Tonoike, K., Nakamura, T., Yamane, Y. and Miyoshi, Y. (2003) Power Profile Evaluation of the JCO Precipitation Vessel Based on the Record of the Gamma-Ray Monitor. *Nuclear Technology*, **143**, 364.
- [5] Yamane, Y., Nakajima, K., Yamamoto, T. and Miyoshi, Y. (2003) JAERI-Conf 2003-019, 740-745. Development of Criticality Accident Analysis Code AGNES.  
<http://www.iaea.org/inis/collection/NCLCollectionStore/Public/36/116/36116549.pdf>  
<http://jolissrch-inter.tokai-sc.jaea.go.jp/pdfdata/JAERI-Conf-2003-019-Part2.pdf>
- [6] Bohr, A. and Mottelson, B.R. (1998) *Nuclear Structure*, **1**.
- [7] Glauber, R.J. (1959) In: Brittin, W.E. and Dunham, L.G., Eds., *Lectures in Theoretical Physics*, Vol. 1, Interscience, New York, p. 315.
- [8] Fujita, T. and Hüfner, J. (1979) *Physics Letters*, **87B**, 327-331. [http://dx.doi.org/10.1016/0370-2693\(79\)90546-X](http://dx.doi.org/10.1016/0370-2693(79)90546-X)
- [9] Fujita, T. and Hüfner, J. (1980) *Nuclear Physics A*, **343**, 493-510. [http://dx.doi.org/10.1016/0375-9474\(80\)90666-1](http://dx.doi.org/10.1016/0375-9474(80)90666-1)
- [10] Okajima, S., Kugo, T. and Mori, T. (2012) Genshiro Butsurigaku (Reactor Physics). Ohmsha, Tokyo. [In Japanese]
- [11] Nuclear Data Center. [http://www.ndc.jaea.go.jp/j40fig/jpeg/h001\\_fl.jpg](http://www.ndc.jaea.go.jp/j40fig/jpeg/h001_fl.jpg)

# Complete Destruction of Ag Br Emulsion Nuclei BY<sup>28</sup>Si Ions with 4.5 GeV/Nucleon Energy

**A. Abd EL-Daiem**

Physics Department, Faculty of Science, Sohag University, Sohag, Egypt  
Email: Ahmedalbiomy@yahoo.com

Received 4 July 2016; accepted 22 August 2016; published 25 August 2016

Copyright © 2016 by author and Scientific Research Publishing Inc.  
This work is licensed under the Creative Commons Attribution International License (CC BY).  
<http://creativecommons.org/licenses/by/4.0/>



Open Access

---

## Abstract

The main experimental characteristics (multiplicity characteristics) of secondary particles have been investigated in interactions of <sup>28</sup>Si with emulsion at 4.5 GeV/c per nucleon at rest of emulsion, nuclei. The complete destruction of the heavy target nuclei (Ag, Br) has been studied. The average of shower particles  $\langle n_s \rangle$  is weakly dependent on the target mass whereas the average multiplicity of grey particles  $\langle n_g \rangle$  is strongly dependent on it. The correlations between the multiplicities of the charged secondaries at different mass number of the projectile and center-of-mass-available energy are investigated.

## Keywords

Multiplicity Characteristics, Probability and Energy Available

---

## 1. Introduction

The study of the phenomena of complete destruction of heavy target nuclei is very interesting. This interest stems from the fact that most of these interactions are due to central collisions. The central collisions provide a unique opportunity to investigate the consequences of nuclear compression, such as hydrodynamic effects [1]-[4]. In addition, there is a good possibility to obtain valuable information on the excitation and consequent decay of residual target nucleus. A detailed and systematic study of this phenomenon was carried out in [5]. In this work the criterion  $n_h \geq 28$ , since  $[n_h = (n_g + n_b)$  gray particles and black particles] was used to select events of complete destruction of (Ag, Br) nuclei. Nowadays, there are huge amounts of data concerning the study of this phenomenon. Different beam nuclei at various energies have been used in the experiments. There are two main directions for the interpretation of the experimental results of complete destructions. The first direction

considers such events as a tail in the multiplicity distribution which can be accounted for by the cascade evaporation process inside the target nucleus. The second one implies a one-step like process which occurs due to the collectivity of the target nucleons together. In the present work, we study complete destruction  $n_h \geq 28$  of (Ag, Br) emulsion nuclei induced by 4.5 A GeV/c  $^{28}\text{Si}$  nuclei. The average multiplicities of the different emitted charged particles have been compared with the corresponding experimental values obtained from the interactions of different types of nuclei with emulsion at the same incident momentum per nucleon. The energy available in the centre of mass system for the complete destruction of the target nucleus has been studied for different projectiles. The multiplicity correlations between the charged secondaries produced in these interactions and both the mass number of the projectile and the available energy have also been analyzed. The previous detailed analysis [6] has shown that the selection criterion  $n_h \geq 28$  corresponds to the complete destruction of the target nucleus, nearly, into individual nucleons and light fragments leaving no measurable residual nucleus.

## 2. Experimental Techniques

Nuclear emulsions of the type BR-2 were exposed to 4.5 A GeV/c  $^{28}\text{Si}$  beams at the Dubnasynchrotron. The pellicles of emulsion have the dimensions of 20 cm  $\times$  10 cm  $\times$  600  $\mu\text{m}$  (undeveloped emulsion). The intensity of the beam was  $\sim 10^4$  particles/cm<sup>2</sup> and the beam diameter was approximately 1 cm. Along the track, a double scanning has been carried out fast in the forward direction and slow in the backward one. In the measured interactions, all the charged secondary particles have been classified according to the range L in the emulsion and the relative ionization  $g^* = g/g_0$ , where g is the particle track ionization and  $g_0$  is the ionization of a relativistic shower track in the narrow forward cone of a polar angle  $\theta \leq 3^\circ$ , (the polar angle  $\theta$  of each track, *i.e.* the space angle between the direction of the beam and that of the given tracks) into the following groups:

1) Shower tracks of produced particles, “s-particles”; have a relative ionization  $g^* \leq 1.4$ ; these tracks have an emission angle  $\theta \leq 3^\circ$ ; they have been further subjected to multiple scattering measurements for momentum determination in order to separate the produced pions from the single charged projectile fragments. 2) Grey tracks of produced particles, “g-particles”, having a relative ionization ( $1.4 \leq g^* < 10$ ) and  $L > 3$  mm. 3) Black tracks of produced particles, “b-particles”, having  $L \leq 3$  mm. 4) The b and g tracks, taking together, are both called heavily ionizing particles, “h-particles”.

## 3. The Multiplicity Characteristics

To investigate the dependence of the average multiplicity  $\langle n_s \rangle$  and  $\langle n_g \rangle$  on the mass number of the beam nucleus  $A_p$ , we consider the reactions listed in **Table 1**.

In these reactions, the momentum per incident nucleon is constant and it equals 4.5 GeV/c. The experiments were carried out under the same conditions. **Figure 1(a)** and **Figure 1(b)** show the dependence of the average multiplicities  $\langle n_s \rangle$  and  $\langle n_g \rangle$  on the mass number of the beam nucleus  $A_p$ . The points are the experimental data while the continuous lines are the result of fitting by the relation

$$\langle n_i \rangle = a_i A_p^{\alpha_i} \quad (1)$$

where  $i = s$  or  $g$ . The values of the coefficients  $\alpha_i$  are  $0.39 \pm 0.05$  and  $0.18 \pm 0.01$  and  $a_i$  are  $2.21 \pm 0.66$  and

**Table 1.** The average multiplicities  $\langle n_s \rangle$  and  $\langle n_g \rangle$  of shower and grey tracks produced in the reactions of different projectiles with emulsion at 4.5 A GeV/c.

Projectile	$\langle n_s \rangle$	$\langle n_g \rangle$	Ref
$^1\text{H}$	$1.6 \pm 0.1$	$2.8 \pm 0.1$	[7]
$^2\text{H}$	$2.5 \pm 0.1$	$3.9 \pm 0.1$	[8]
$^3\text{H}$	$3.6 \pm 0.1$	$3.1 \pm 0.1$	[9]
$^4\text{He}$	$3.8 \pm 0.1$	$4.4 \pm 0.1$	[7]
$^{12}\text{C}$	$7.6 \pm 0.2$	$5.9 \pm 0.3$	[7]
$^{16}\text{O}$	$10.5 \pm 0.6$	$7.6 \pm 0.6$	[10]
$^{28}\text{Si}$	$11.9 \pm 0.5$	$7.3 \pm 0.3$	Present work

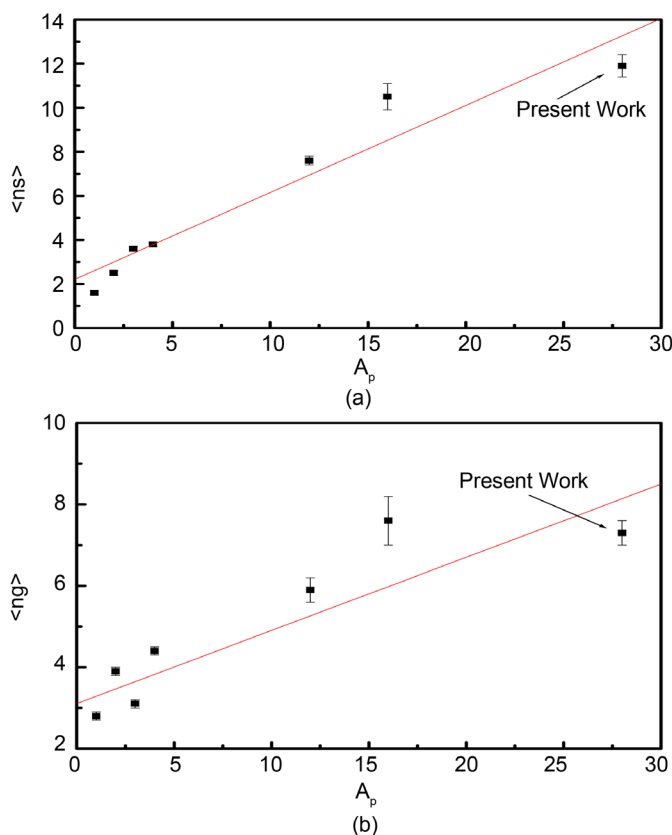


**Figure 1.** Projectile mass number for different elements at 4.5 GeV/c per Nucleon: (a) versus  $\langle n_s \rangle$  and (b) versus  $\langle n_g \rangle$  plots.

$3.11 \pm 0.06$  for shower and grey particles respectively. This result agrees with the fact that the interaction cross section is proportional to  $A_p^{2/3}$  and is proportional to  $A_p^{1/3}$  from  $\langle n_s \rangle$  and  $\langle n_g \rangle$ .

#### 4. Probability of Complete Destruction of Target Nuclei

In the present work, the probability of complete destruction of (Ag, Br) emulsion nuclei  $p$  is defined as the ratio between the number of events of  $n_h \geq 28$  to the total number of inelastic interactions of the incident particle with (Ag, Br) nuclei. **Figure 2** illustrates the dependence of the probability  $p$  on  $A_p$  for various projectile nuclei, all at 4.5 A GeV/c. It is seen that the probability  $p$  increases linearly with  $A_p^{2/3}$  up to the carbon nucleus. The values of the probability  $p$ , predicted by the cascade evaporation model [8], are larger than the corresponding experimental values. Moreover, the behavior of probability  $p$  versus  $A_p$  in the present experiment does not agree with the calculations of the cascade evaporation model.

#### 5. Energy Available

For the events having  $n_h \geq 28$ , and implying the complete destruction of the target nuclei, the relation between  $\langle n_s \rangle$  and the energy available  $E_{av}$  in the centre of mass system is shown in **Figure 3**. The value of  $E_{av}$  is given by:

$$E_{av} = \left( M_p^2 + M_t^2 + 2M_t E_p \right)^{1/2} - (M_t + M_p), \quad (2)$$

where  $M_p$ , is the projectile rest mass in GeV and  $E_p = \left( p_0^2 + M_p^2 \right)^{1/2}$  where  $p_0$  is the projectile momentum in GeV/c. The effective target mass  $M_t$  is equal to  $\frac{3}{2} \left( A_p^{2/3} A_t^{1/3} \right) m$ , where  $m = 0.931$  GeV. The relation between  $\langle n_s \rangle$

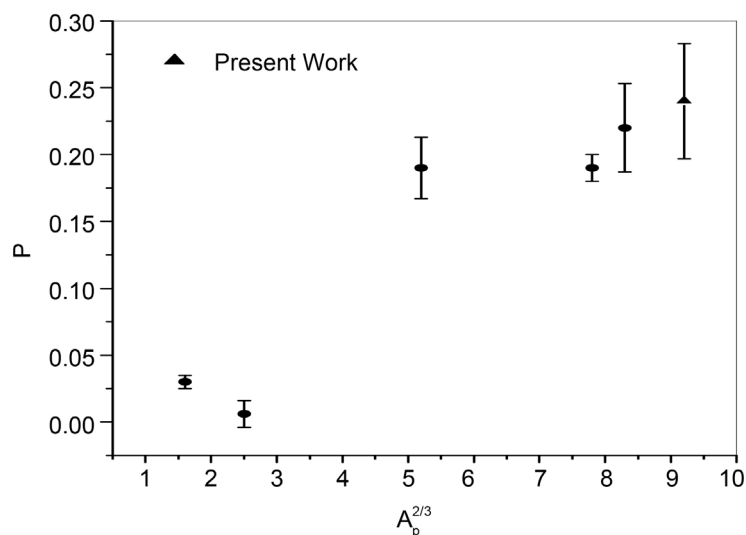


**Figure 2.** The probability,  $p$ , of complete destruction of (Ag, Br) nuclei due to the interactions of different projectile at 4.5 GeV/c per nucleon.

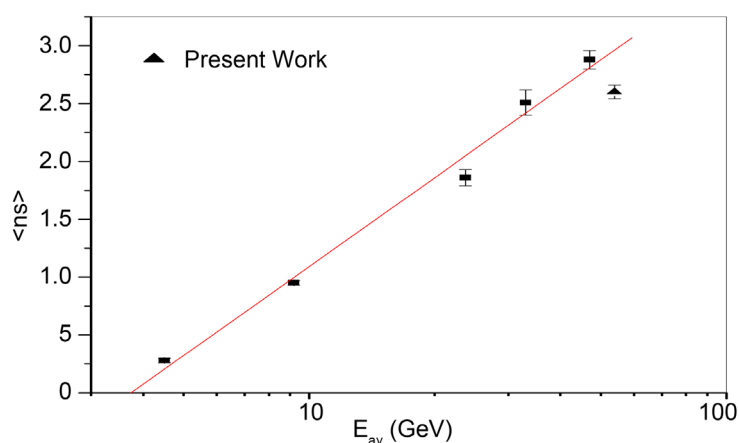


**Figure 3.** The average multiplicity of shower particles  $\langle n_s \rangle$  versus the energy in available c.m.s. for different projectile mass numbers having momentum 4.5 GeV/c per nucleon . for the collisions characterized by  $n_h \geq 28$ .

and the energy available in the centre of mass system,  $E_{av}$ , for different projectiles at the same incident momentum, which shows that as the projectile mass number increases,  $E_{av}$  increases and consequently  $\langle n_s \rangle$  increases. The dependence of  $\langle n_s \rangle$  on  $E_{av}$ , shown in **Figure 3**, can be fitted by the universal relation:

$$\langle n_s \rangle = A + B \ln(E_{av}) \quad (3)$$

with  $A = -13.09$  and  $B = 11.46$ .

## 6. Multiplicity Correlation in Complete Destruction of $^{28}\text{Si}$ Ions

In the present work, we studied the correlation of complete destruction ( $n_h \geq 28$ ) of (Ag, Br) emulsion nuclei induced by 4.5 A GeV/c  $^{28}\text{Si}$  nuclei. The probability of complete destruction of AgBr nuclei different projectile at various energies is shown in [11]. The correlation in complete destruction dependencies between the charge particle multiplicities allows us to discuss the mechanism of nucleus-nucleus interactions. The dependencies  $\langle n_g \rangle = f(n_s)$  and  $\langle n_s \rangle = f(n_g)$  for the event with  $n_h \geq 28$  accompanied by total target disintegration are presented in **Figure 4** and **Table 2**. In this case there is no strong dependence of  $\langle n_g \rangle$  on the value of  $n_s$  or of  $\langle n_s \rangle$  on the value of  $n_g$ . This can be seen from the value of  $\chi^2$  for each type of particle. This means that the degree of

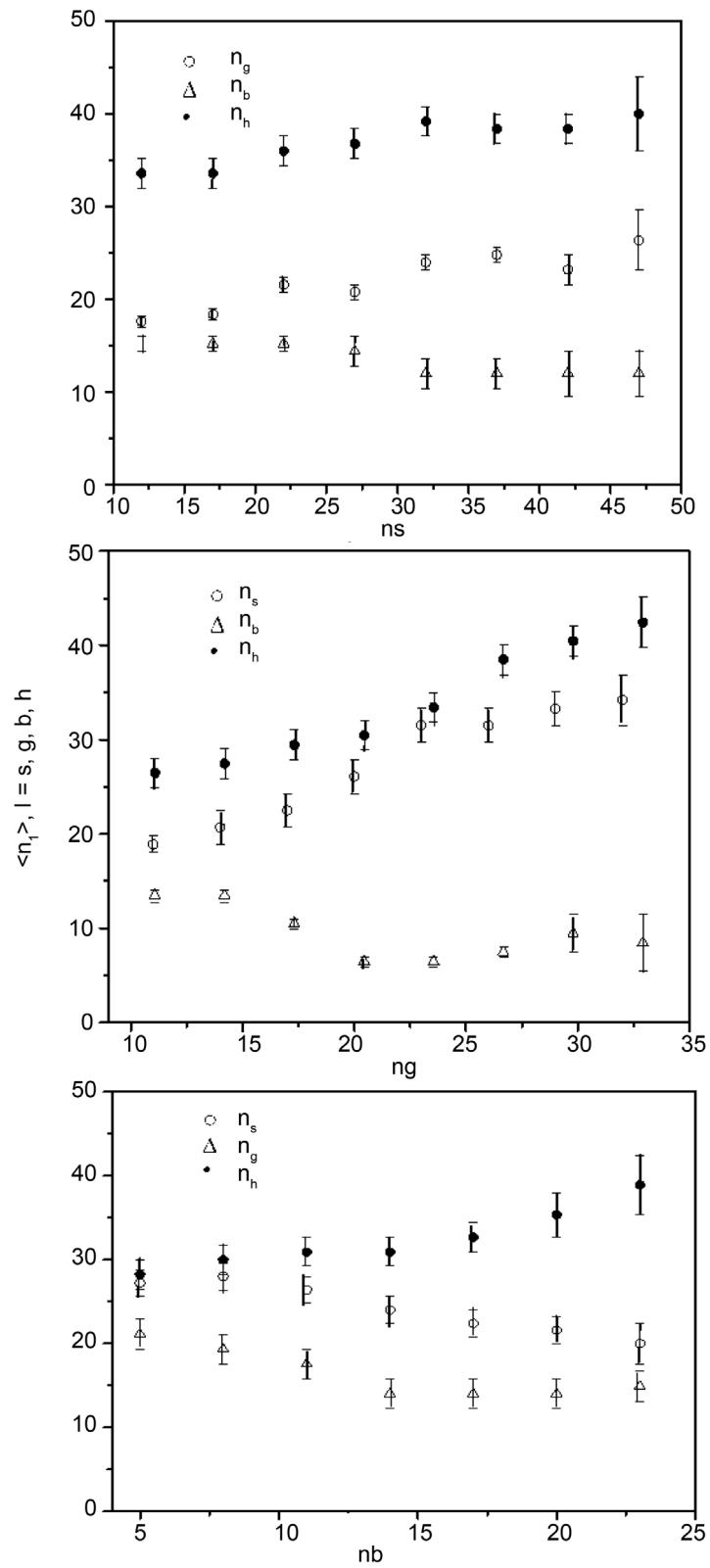


**Figure 4.** The correlations between the secondary particles multiplicities for complete destructions (events with  $n_h > 28$ ) in  $\text{Si}^{28}$  interactions with emulsions.

**Table 2.** Results of approximate fit of the experimental data for the multiplicity correlation from complete destruction in  $^{28}\text{Si}$  ions interactions with emulsion using the dependence  $\langle n_i \rangle = a + kn_j$ .

	$\langle n_s \rangle$	$x^2$	$\langle n_g \rangle$	$x^2$	$\langle n_b \rangle$	$x^2$	$\langle n_h \rangle$	$x^2$
$n_s$	...	...	$14.02 \pm 0.23$	0.87	$-15.60 \pm 0.07$	0.56	$29.65 \pm 0.16$	0.95
$n_g$	$10.42 \pm 0.76$	0.96	...	...	$19.60 \pm 0.25$	0.65	$20.30 \pm 0.69$	0.95
$n_b$	$-33.10 \pm 0.54$	0.94	$14.02 \pm 0.23$	0.84	...	...	$27.09 \pm 0.58$	0.87

disintegration of the target does not depend strongly on the number of shower particles. One can observe the correlation between the fast and the slow stages of the inelastic interactions of tow nuclei by studying the dependencies  $\langle n_b \rangle = f(n_s)$ ,  $\langle n_b \rangle = f(n_g)$  and  $(n_s)$ ,  $(n_g)$  on the  $(n_b)$ . From **Figure 4**, one can see that the correlations have a different character. This can be seen from the fast that the  $\langle n_b \rangle$  dependencies on  $n_s$  and  $n_g$  have negative slopes. Also, from the correlation dependencies of  $\langle n_s \rangle$ ,  $\langle n_g \rangle$  and  $\langle n_h \rangle$  on  $n_b$ , one can see that the slope of  $\langle n_h \rangle$  is positive while the slopes of others are negative. From the above results, one can see that  $\langle n_b \rangle$  has a negative correlation with  $n_s$  and  $n_g$  and the correlation of  $\langle n_s \rangle$  and  $\langle n_g \rangle$  with the  $n_b$  is negative. This may be due to increase the number of interacting projectile nucleons as the impact parameter decreases.

## 7. Conclusion

From the present study, one may concluded that the average number of the shower particles is proportional to  $A_p^{2/3}$  and the average number of grey particles is proportional to  $A_p^{1/3}$ . While that the probability of the complete destruction increases with increasing projectile mass number  $A_p$ , and the average multiplicity of the emitted shower particles depends strongly on the projectile mass number, while does not for the grey and black can be particles. A good correlation between the energy available at the center of mass system,  $E_{av}$ , and the average multiplicity of the shower particles emitted in the complete destruction is found.

## References

- [1] Beavis, D., *et al.* (1985) *Physical Review Letters*, **54**, 1652. <http://dx.doi.org/10.1103/PhysRevLett.54.1652>
- [2] Beckmann, P., *et al.* (1987) *Modern Physics Letters A*, **2**, 163. <http://dx.doi.org/10.1142/S0217732387000215>
- [3] Csernai, L.P., *et al.* (1986) *Physical Reviews*, **34**, 1270-1273.
- [4] Beavis, D., *et al.* (1986) *Phys.*, **34**, 757-760.
- [5] Ameeva, B.U., *et al.* (1987) Preprint No. 87-09 of the Institute of High Energy Physics. Academy of Science of Kazakhsahoi SSR, Alma-Ata.
- [6] Tolstov, R.A. and Krashmukhamedov, R.A. (1995) Complete Destruction of Ag Br Nuclei. Communication of JINR pI6897, Dubna.
- [7] Barashnikov, V.S. and Belyakov, V.A. (1959) Van-shu-fen: Communication of JINR pI-331, Dubna.
- [8] Bogdanov, V.G., *et al.* (1983) *Soviet Journal of Nuclear Physics*, **38**, 909.
- [9] Sherif, M.M. and Mohery, M. (1991) *Egyptian Journal of Physics*, **22**, 125.
- [10] Antonchik, V.A., *et al.* (1984) *Soviet Journal of Nuclear Physics*, **39**, 774.
- [11] Abd-Allah, N.N. (1993) *Physica Scripta*, **47**, 501-504.

# The Investigation Capability of Plasma Focus Device for $^{13}\text{N}$ Radioisotope Production by Means of Deuteron Experimental Spectrum

Maryam Saed<sup>1</sup>, Mahmud Vahdat Roshan<sup>2</sup>, Ayoub Banoushi<sup>3</sup>, Morteza Habibi<sup>4</sup>

<sup>1</sup>Islamic Azad University Tehran Central Branch, Tehran, Iran

<sup>2</sup>School of Particles and Accelerators, Institute for Research in Fundamental Sciences (IPM), Tehran, Iran

<sup>3</sup>Research Institute of Nuclear Science and Technology of Iran, Tehran, Iran

<sup>4</sup>AmirKabir University of Technology, Tehran, Iran

Email: saed.ms1987@yahoo.com, mroshan20@ipm.ir, abanoushi@aeoi.org.ir, mortezahabibi@aut.ac.ir

Received 13 June 2016; accepted 23 August 2016; published 26 August 2016

Copyright © 2016 by authors and Scientific Research Publishing Inc.

This work is licensed under the Creative Commons Attribution International License (CC BY).

<http://creativecommons.org/licenses/by/4.0/>



Open Access

---

## Abstract

Optimal condition for  $^{13}\text{N}$  radioisotope production through  $^{12}\text{C}(\text{d},\text{n})^{13}\text{N}$  within plasma focus device is investigated. As the deuteron spectrum follows the empirical power law of the form  $E^{-m}$ , it is shown that the activity decreases by increasing the value of  $m$ . Unlike the fact that the repetition rate increases the activity, it is possible to achieve higher activities by increasing the bombardment time at a fixed repetition rate.

## Keywords

Positron Emission Tomography (PET), Plasma Focus, Deuteron Spectrum, Activation, Repetition Rate

---

## 1. Introduction

Short-lived radioisotopes (SLR) such as  $^{11}\text{C}$ ,  $^{13}\text{N}$ ,  $^{15}\text{O}$ ,  $^{18}\text{F}$  usually have medical applications, particularly in positron emission tomography (PET). These radioisotopes are obtained through bombarding appropriate targets by ion beams produced in accelerators. Due to the short half-life of such radioisotopes, which is one of the advantages of this method over others, they must be produced in a place where they are expected to be used. To this end, accelerators have to be used in hospitals. PET radioisotopes production by means of cyclotron is an expensive method, therefore it is suitable to consider pulsed plasma devices to produce PET radioisotope.

Plasma focus devices are one of the appropriate systems in producing short lived radioisotopes because they

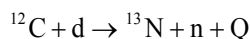
are low cost and easy to use and maintain.

As a switch is closed in a plasma focus device, a voltage of several tens kV is quickly applied to the electrodes. Due to gas electrical breakdown, free electrons move toward the insulation surface, afterward a current layer is formed. Because of the effect of Lorentz force ( $J \times B$ ) on the current layer, the layer is accelerated towards the end of electrodes at a high speed. By the radial Lorentz force, a part of the current layer symmetrically moves towards the center of anode and a very short-lived, dense, hot plasma column is formed which is the source of ion, electron, X-ray and neutron production.

The voltage of capacitor bank for a plasma focus device is usually 10 - 30 kV, but the results of a lot of experiments [1] have shown that deuteron beams emitted from the pinch have a wide range of energy (up to several MeV). Ion acceleration with such high energy is one of the most unexpected aspects of the plasma focus device. Several models have been suggested for acceleration of ions [1] such as instabilities, anomalous resistivity, plasma wave, and shock wave. However, the ion acceleration mechanism in the plasma focus pinch is not understood well. The most important factor in ions acceleration is the  $m = 0$  instability (sausage instability). This instability is often attributed to the acceleration of ions at high energy. The growth of such instabilities is due to radially symmetric disturbances in certain points. At these points, the cross sectional area is reduced, and then azimuthal magnetic field strength at the surface of the plasma will be extended. The magnetic pressure will be increased. As a result, the plasma column at these points compared to other points constricts at a faster rate. Rapid changes of magnetic field at each constriction induce a large longitudinal electric field that accelerates ions within the plasma column at higher energies [2].

A good candidate for studying radioisotope production within the plasma focus is the nuclear reaction of  $^{12}\text{C}$  (d,n)  $^{13}\text{N}$ . The advantages of this reaction are high cross section, low threshold energy, short half-life, and the availability of target materials [3].

Through bombarding the graphite target by high energy deuterons, Nitrogen-13 is produced via the following reaction:



The threshold energy of this reaction is 328 keV. Nitrogen-13 is a SLR and it decays with the half-life of 9.96 minutes and produces a positron ( $\beta^+$ ). The positrons are stopped in the graphite (positron speed is slowed down) and is annihilated with an electron. Two oppositely directed 511 keV gamma-rays are produced by the annihilation of every electron-positron pair.

Radioisotope production within plasma focus has been taken into consideration for a long time. Brzosko group [4] in the U.S., Angeli [5] in Italy, Roshan [6] in Singapore can be named. The amount of activity produced in Singapore group has remarkably increased. Roshan *et al.* [6] have carried out their experiments on a plasma focus device NX2. They placed the target graphite ( $15 \times 15 \times 0.7$ ) to a distance of 100 mm in front of deuteron beam within NX2 device so that the solid angle between deuterons and target graphite was  $O = 1.26$  sr.

The activity reported by Roshan *et al.* within NX2 device with repetition rate of 1 Hz after 30 seconds of graphite bombardment was equal to 5.2 kBq [6]. This amount in this small device (1.7 kJ) is better than the reported activity of bigger devices. However, it is not very important for medical applications.

In this study, first the activity of a set of experimental spectra of deuteron produced by NX2 plasma focus device which has been measured by magnetic spectrometer [7] is calculated and then the optimizing conditions of  $^{13}\text{N}$  production is investigated.

## 2. $^{13}\text{N}$ Activity Calculation Phases

Thick target yield shows the reaction probability or reaction rate [6]:

$$y_{tt} = N \int_0^{E_d} \frac{\sigma(E)}{|dE/dx|} dE \quad (1)$$

where  $N$  is the number of nitrogen 13 nuclei per cubic centimeter;  $\sigma(E)$  is the cross section of reaction  $^{12}\text{C}$  (d,n)  $^{13}\text{N}$ ;  $\frac{dE}{dx}$  is stopping power of deuterons on graphite target, and  $E_d$  is the incident energy of deuterons.

The data of cross section of the reaction  $^{12}\text{C}$  (d,n)  $^{13}\text{N}$  is obtained from EXFOR data base [8] and SRIM code [9] is used to calculate reaction stopping power (Figure 1). In Figure 1, the blue points are experimental data

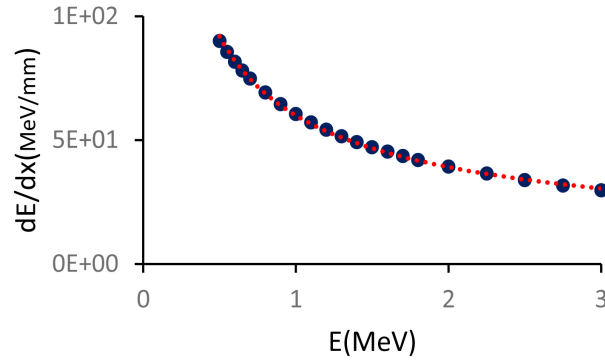


**Figure 1.** Deuteron stopping power in the graphite target.

(by means SRIM code) and the red curve is the fitted diagram on experimental data.

The total number of activated nitrogen 13 nuclei in the target estimated from [6]:

$$N_{13N} = K \int_{E_{min}}^{E_{max}} E^{-m} \times y_{it} dE \quad (2)$$

According to the conducted experiments, deuteron spectrum follows the empirical power law of the form [6] [10] [11]:

$$\frac{dN_d}{dE} = KE^{-m} \quad (3)$$

In this paper, we fit the generated deuteron spectra in plasma focus device NX2 (1.7 kJ energy) by Equation (3). One of deuteron spectra has been given as an instance in **Figure 2**. We have fitted this deuteron spectrum by the exponential function in Equation (3) and it fits with Equation (4) spectrum. In **Figure 2**, the blue points are experimental data and the red curve is the fitted diagram according to Equation (4) on experimental data.

$$\frac{dN}{dE} = 10^{11} \times E^{-3.802} \quad (4)$$

The number of  $^{13}\text{N}$  nuclei can be calculated by replacing Equation (4) in Formula 2. Then, the activity is calculated.

$^{13}\text{N}$  activity, resulting from deuteron collision (**Figure 2**) to graphite target has been calculated,  $A = 0.616$  kBq.

### 3. The Investigation Capability of Plasma Focus Device for $^{13}\text{N}$ Radioisotope Production

$^{13}\text{N}$  radioisotope is achieved based on  $^{12}\text{C}(d,n)^{13}\text{N}$  process. The amount of  $^{13}\text{N}$  activity is dependent on the whole deuteron spectrum descended upon  $^{12}\text{C}$  solid target. As illustrated in **Figure 2**, deuteron energy spectrum follows the power law  $\left(\frac{dN_d}{dE} \propto E^{-m}\right)$ , with the investigations conducted on three sets of deuteron spectra (within pressures of 4, 6, 8 mbar [7]), we realized that the number of incident deuterons and the energy of these deuterons will be reduced with an increase of the amount of  $m$  in the exponential function  $\left(\frac{dN_d}{dE} \propto E^{-m}\right)$ .

**Figure 3** depicts  $m$  changes based on maximum energy of deuterons spectra. As it is clear in the figure, the energy of these deuterons will be reduced with an increase of the amount of  $m$  and with the calculation of  $^{13}\text{N}$  activity (as a consequence of the collision of these deuteron spectra with  $^{12}\text{C}$  target) it was found that in the spectra with higher  $m$ , we would have less activity.

Moreover, the investigation of experimental spectra [7] shows that as the number of incident deuterons increase, the value of  $m$  decreases and the activity increases.

For a better description of deuterons dependence on  $^{13}\text{N}$  activity, we have calculated the number of  $^{13}\text{N}$  nuclei

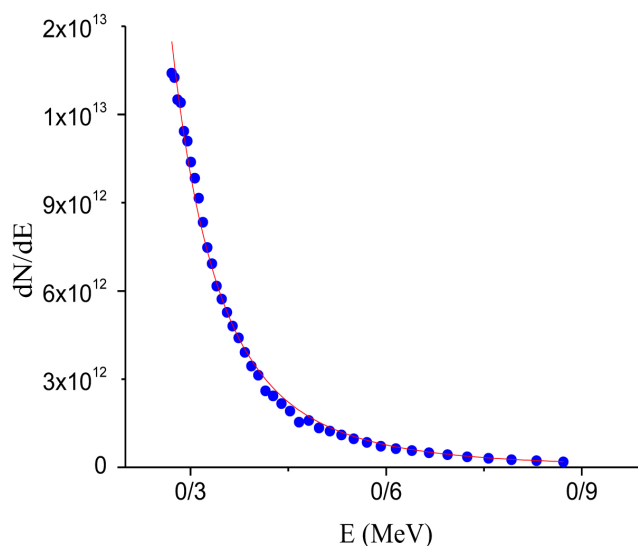


Figure 2. Spectrum of deuteron produced in NX2 plasma focus device [7].

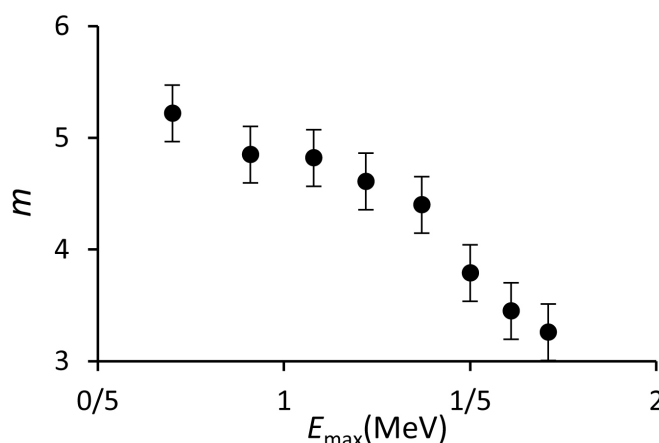


Figure 3. Maximum energy of experimental spectra of deuteron and its corresponding  $m$ .

for three series of deuteron spectra [11].

The relationship between  $m$  and  $A$  is obtained from the following formula [12].

$$N_{13N} = N_d \frac{1 - m}{E_{\max}^{1-m} - E_{\min}^{1-m}} \times \frac{\alpha}{\Omega} \times \int_{E_{\min}}^{E_{\max}} E^{-m} \times y_{it} dE \tag{5}$$

where  $N_d$  is the number of deuterons ejected from the pinch in a solid angle  $\Omega$ . In order to consider the probability of collision between all deuterons and graphite target, the value of the angle was chosen to be  $80^\circ$  [10]-[12],  $\alpha$  is the solid angle subtended by the target of graphite.

In order to calculate  $\alpha$  the same laboratory conditions [6], (a graphite target with dimensions  $(15 \times 15 \times 0.7)$  100 mm away from the pinch) are considered. Figure 4 shows activity changes in terms of  $m$  (exponential function power in Equation (3)). As is apparent from Figure 4 and it was mentioned earlier, deuteron spectra with less  $m$  value as a consequence of the collision with  $^{12}\text{C}$  target would have produced more  $^{13}\text{N}$  nuclei. Therefore, the activity will increase.

Device energy [13] [14] and repetition rate are factors affecting the rate of activity. As the device energy and the repetition rate increases, the number of incident deuterons will increase as well. Consequently, the rate of

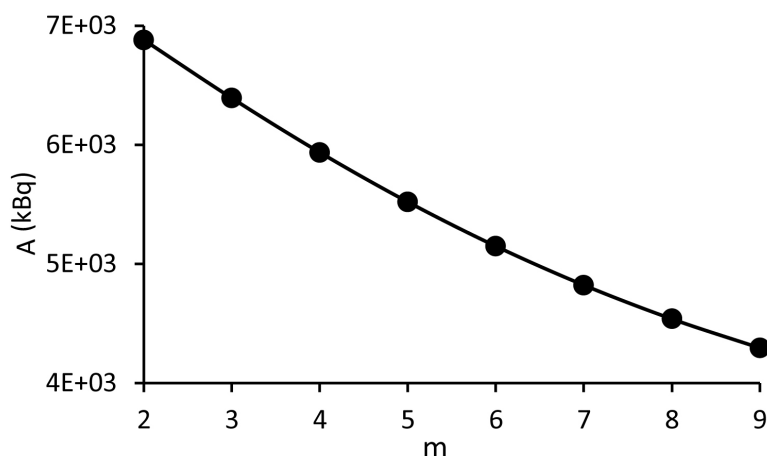


Figure 4. Relationship between  $m$  and  $A$ .

activity will increase remarkably.

In this research, for optimizing Nitrogen 13 radioisotope, the repetition rate is selected as an influential factor in increasing activity.

The activity after  $k$  successive shot [15]:

$$A(k) = A_0 \frac{(1 - e^{-\lambda k T})}{(1 - e^{-\lambda T})} \quad (6)$$

The effect of repetition rate on the amount of activity at frequencies of 1 Hz, 5 Hz, 10 Hz and 16 Hz during the bombardment time of 30 s (the time considered in the lab [6]), 300 s (1/2 of radioisotope half-life), 600 s (1 half-life), 1200 s (2 half-life) 1800 s (3 half-life) is investigated and its diagram is drawn.

As shown in Figure 5, as the repetition rate increases, the activity will also increase in such a way that at repetition rate of 1 Hz after one half-life (600 s), target bombardment is 0.2 MBq, while at the same bombardment time (one half-life) the activity at repetition rate of 16 Hz is 4 MBq. As a result, repetition rate is a very effective factor in increasing the activity.

The required activity for PET is more than 1 GBq. The calculated activity for one of the experimental spectra of deuteron at repetition rate of 16 Hz and bombardment time of 600 s ( $A_{\text{cal}} = 8$  MBq) is less than the required activity for imaging. In order to investigate the ability of plasma focus device for producing the required activity for imaging, by increasing the repetition rate, the activity is calculated at higher frequencies. Therefore, activity at frequencies of 50 Hz, 100 Hz, 500 Hz, and 1 kHz was examined. As shown in Figure 5, activity at repetition rate of 1 kHz after 1800 s is 0.9 GBq. Due to technical restrictions within the available plasma focus devices, achieving such a high repetition rate is difficult. For this reason, instead of increasing the repetition rate, we can increase the bombardment time at a fixed repetition rate. Figure 6 shows the activity at a fixed repetition rate with different bombardment time.

The activity could be increased by increasing the device energy, too [13]. It was shown that there is a linear relationship between device energy and the activity. In order to reach to the required activity for PET imaging, the plasma focus energy should be in the order of kilo joules.

#### 4. Conclusions

A series of experimental deuteron spectra was used to show that the activity is highly dependent on the power of  $m$  in the empirical power law distribution of the deuterons. By decreasing the value of  $m$ , the energy and the number of incident deuterons will increase which will lead to the increment of the activity. Since the repetition rate of the device is a straight forward factor for increasing the number of incident deuterons, the activity is optimized by repetition rate.

In order to produce the practical activity for PET imaging, the repetition rate should be around 1 kHz which is

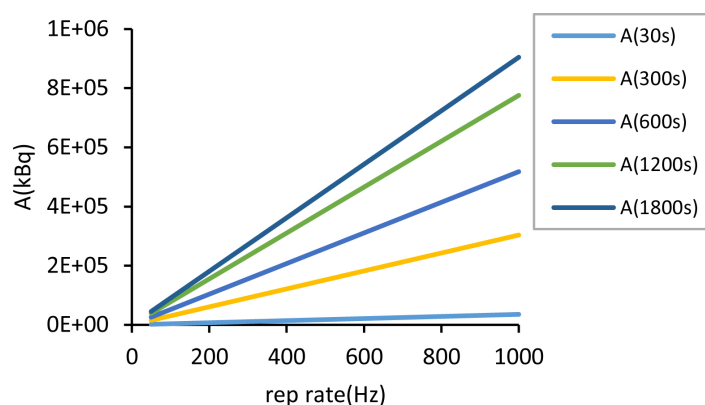


Figure 5. Activity in terms of repetition rate.

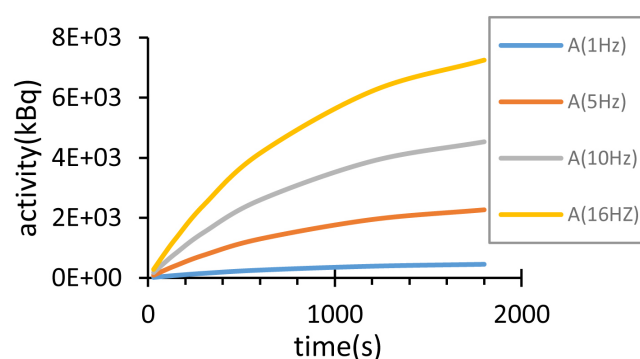


Figure 6. Activity in terms of bombardment time.

technically difficult to achieve. Therefore, the bombardment time is increased at a fixed repetition rate.

## References

- [1] Bernstein, M.J. and Comisar, G.G. (1972) *Physics of Fluids*, **15**, 700. <http://dx.doi.org/10.1063/1.1693966>
- [2] Kruskal, M. and Schwarzschild, M. (1954) *Proceedings of the Royal Society A*, **223**, 348. <http://dx.doi.org/10.1098/rspa.1954.0120>
- [3] Gulickson, R.L., Pickles, W.L., Price, D.F., Sallin, H.L. and Wainwright, T.E. (1978) Ion Beam Production in the Plasma Focus. *The Second International Conference on Energy Storage, Compression, and Switching*, Venice, 5-8 December 1978.
- [4] Brzosko, J.S., Melzacki, K., Powell, C. and Gai, M. (2001) Application of Accelerators in Research and Industry. Sixteenth International Conference of the American Institute of Physics, 277-280.
- [5] Angeli, E., Tartaria, A., Frignanic, M., Mostaccib, D., Rocchic, F. and Sumini, M. (2005) *Nuclear Technology & Radiation Protection*, **1**, 33-37.
- [6] Roshan, M.V., Springham, S.V., Rawat, R.S. and Lee, P. (2010) *IEEE Transactions on Plasma Sciences*, **38**, 3393-3397. <http://dx.doi.org/10.1109/TPS.2010.2083699>
- [7] Roshan, M.V., Springham, S.V., Talebitaher, A., Rawat, R.S. and Lee, P. (2010) *Plasma Physics and Controlled Fusion*, **52**, Article ID: 085007. <http://dx.doi.org/10.1088/0741-3335/52/8/085007>
- [8] Zerkov, V. (2014) Experimental Nuclear Reaction Data (EXFOR). <https://www-nds.iaea.org/exfor/exfor.htm>
- [9] Ziegler, J.F. (2013) SRIM—The Stopping and Range of Ions in Matter. <http://www.srim.org/>
- [10] Sadowski, M., Szydowski, A., Scholz, M., Kelly, H., Marquez, A. and Lepone, A. (1999) *Radiation Measurements*, **31**, 185-190. [http://dx.doi.org/10.1016/S1350-4487\(99\)00083-9](http://dx.doi.org/10.1016/S1350-4487(99)00083-9)
- [11] Sadowski, M., Ese, M., Moroso, R. and Pouzo, J. (2000) *Nukleonika*, **45**, 179-184.
- [12] Bienkowska, B., Jednorog, S., Ivanova-Stanik, I.M., Scholz, M. and Szydowski, A. (2004) *Acta Physica Slovaca*, **54**,

401-407.

- [13] Roshan, M.V., Razaghi, S., Asghari, F., Rawat, R.S., Springham, S.V., Lee, P., Lee, S. and Tan, T.L. (2014) *Physics Letters A*, **3**, 78.
- [14] Lee, S. and Saw, S.H. (2012) *Physics of Plasmas*, **19**, Article ID: 112703. <http://dx.doi.org/10.1063/1.4766744>
- [15] Shirani, B., Abbasi, F. and Fusion, J. (2012) Prospects for  $^{13}\text{N}$  Production in a Small Plasma Focus Device. *Journal of Fusion Energy*, **32**, 235-241. <http://dx.doi.org/10.1007/s10894-012-9558-9>



Scientific Research Publishing

**Submit or recommend next manuscript to SCIRP and we will provide best service for you:**

Accepting pre-submission inquiries through Email, Facebook, LinkedIn, Twitter, etc.

A wide selection of journals (inclusive of 9 subjects, more than 200 journals)

Providing 24-hour high-quality service

User-friendly online submission system

Fair and swift peer-review system

Efficient typesetting and proofreading procedure

Display of the result of downloads and visits, as well as the number of cited articles

Maximum dissemination of your research work

Submit your manuscript at: <http://papersubmission.scirp.org/>

# Electromagnetic-Energy Flow in Anisotropic Metamaterials: The Proper Choice of Poynting's Vector

Carlos Prieto-López, Rubén G. Barrera

Instituto de Física, Universidad Nacional Autónoma de México, México  
Email: [cpl@fisica.unam.mx](mailto:cpl@fisica.unam.mx), [rbarrera@fisica.unam.mx](mailto:rbarrera@fisica.unam.mx)

Received 22 June 2016; accepted 23 August 2016; published 26 August 2016

Copyright © 2016 by authors and Scientific Research Publishing Inc.  
This work is licensed under the Creative Commons Attribution International License (CC BY).  
<http://creativecommons.org/licenses/by/4.0/>



Open Access

---

## Abstract

We study the controversy about the proper determination of the electromagnetic energy-flux field in anisotropic materials, which has been revived due to the relatively recent experiments on negative refraction in metamaterials. Rather than analyzing energy-balance arguments, we use a pragmatic approach inspired by geometrical optics, and compare the predictions on angles of refraction at a flat interface of two possible choices on the energy flux:  $E \times H$  and  $E \times B/\mu_0$ . We carry out this comparison for a monochromatic Gaussian beam propagating in an anisotropic non-dissipative anisotropic metamaterial, in which the spatial localization of the electromagnetic field allows a more natural assignment of directions, in contrast to the usual study of plane waves. We compare our approach with the formalism of geometrical optics, which we generalize and analyze numerically the consequences of either choice.

## Keywords

Poynting Vector, Eikonal, Electromagnetic-Energy Flux, Anisotropic Metamaterials, Geometrical Optics

---

## 1. Introduction

The location of electromagnetic energy is an elusive subject that has been under discussion since the beginning of electrodynamics [1]. Even in the case of electrostatics, one can write at least two different expressions for the energy density of a fixed distribution of charges ([2], p. 21). In one of them, the energy density is proportional to the charge density itself, thus located wherever the charge density is different from zero; in the other one, it is proportional to the square of the electric field generated by the charge distribution, thus located in all space, both

inside and outside the volume occupied by the charge distribution. On the side of electrodynamics, the ambiguity is even greater. The energy-balance equation in vacuum involves the time derivative of energy density of the electromagnetic field, given in terms of the squares of the electric and magnetic fields and the divergence of the Poynting vector; this vector is defined as proportional to the cross product of the electric and magnetic field and it gives the magnitude and direction of the energy flux ([3], sec. 61). Since the balance equation for energy conservation requires only the divergence of the Poynting vector, this vector field is not uniquely defined and it is always possible to add to it an arbitrary vector field with zero divergence. Furthermore, it is also possible to redefine both the Poynting vector and the expression for the energy density, in such a way as to fulfill correctly the balance equation [4]-[10] ([11], ch. 27.5). This freedom leads to an unsurmountable ambiguity about the location of electromagnetic energy and direction of the electromagnetic-energy flux. Nevertheless, it has been argued that the law of conservation of energy does not stand by itself, that there are also conservation laws for linear and angular momentum, and they have to be examined together. For example, in vacuum, the relationship between the Poynting vector (energy-flux field) and the electromagnetic linear-momentum density, together with the conservation of angular momentum, restricts the freedom of choice for the mathematical expression of the Poynting vector, and it has been even claimed that these restrictions remove the ambiguity altogether [12] [13].

The problem of the location of energy and the correct expression for the energy flux in the presence of materials acquires additional intricate subtleties related to the description of the energy-exchange mechanism between fields and matter [14] [15]. First, let us recall that the formulation of macroscopic electromagnetic phenomena is commonly achieved by the introduction, besides the macroscopic electric field  $\mathbf{E}$  and magnetic induction field  $\mathbf{B}$ , of two other fields: the displacement field  $\mathbf{D}$  and the magnetic intensity  $\mathbf{H}$ , or, equivalently, the polarization and magnetization fields:  $\mathbf{P}$  and  $\mathbf{M}$ . In relation to the physical interpretation of these fields, a problem arises about an issue that has been discussed for more than a century: how to establish if  $\mathbf{B}$  or  $\mathbf{H}$  represents the “real” magnetic field, that is, the one that comes after an averaging process of the magnetic field generated by the microscopic components of a given material. There are even carefully argued assertions by W. Thomson that the magnetic field inside the material is not even properly defined ([16] and references therein). The choice in this issue has definite consequences in the energy-balance equation—also known as Poynting’s theorem—when extended to the case where materials are present. As we will discuss briefly in Section 2, this is specially important if we want to separate the total energy density into a component stored in the fields and a component stored or dissipated within the material.

Furthermore, in the more general case when the electromagnetic response is linear but not instantaneous, it necessarily depends on frequency and it is dissipative. In this case it is not possible to separate the energy density into material, field and absorption contributions. But even in low-dissipation frequency bands, the correct expression for the Poynting vector (energy flux) depends on the explicit form of the energy-balance equation. Also, in relation to the freedom of choice of Poynting’s vector and the restrictions imposed by other conservation laws: linear and angular momentum, one has to recall that unlike in vacuum, in the presence of material media the relation between Poynting’s vector and the linear-momentum density of the electromagnetic field is still controversial [17]. There have been at least two proposals for the correct mathematical expression for the linear-momentum density: one given originally by M. Abraham ( $\mathbf{E} \times \mathbf{H}$ ) [18] and the other one given originally by H. Minkowski ( $\mathbf{D} \times \mathbf{B}$ ) [19], being these two choices the source of a persisting debate about either their correctness or their physical interpretation ([20], and references therein). There are also more drastic claims assuring that the macroscopic electromagnetic field within a material is actually a non-physical quantity, and that real measurement devices do not really measure the energy flux given by the Poynting vector [21].

Here we will not analyze all different aspects of these longstanding and sometimes subtle questions. We will rather concentrate only in two different proposals for the mathematical expression of the Poynting vector  $\mathbf{S}$ , whose choice has created controversy even in recent years [22]-[30]. One given by  $\mathbf{S} = \mathbf{E} \times \mathbf{H}$ , which is the commonly used in literature and the one that appears in most textbooks and the other by  $\mathbf{S} = \mathbf{E} \times \mathbf{B}/\mu_0$ , where we use SI units and  $\mu_0$  is the so-called magnetic permeability of vacuum. On the one hand, the first expression is proposed by arguing that with this choice the boundary conditions on  $\mathbf{E}$  and  $\mathbf{H}$  assure no accumulation of energy at any interface between two materials ([3], sec. 61). On the other hand, some authors state that a correct analysis of the energy-balance equation in materials should lead to an expression for the energy flux given, not by  $\mathbf{E} \times \mathbf{H}$ , but rather by  $\mathbf{E} \times \mathbf{B}/\mu_0$ , and that the accumulation of energy at the interface causes no conceptual problem because in magnetic materials the source of energy dissipation at the interface are the induced surface

currents [22] [28] [31]. It is appropriate to recall that these proposals have been recently re-examined, due somewhat to the current work done around the phenomenon of negative refraction in metamaterials [32]-[38].

In this paper, rather than discussing the energetic balance in the material, we propose to look at the controversy from the perspective of geometrical optics in an extremely pragmatic approach, based on the fact that the energy flux is not only used to calculate energy balances, but also to quantify light intensity and its direction of propagation. To watch the refraction of a laser beam on a transparent prism is a very common and intuitive experience, in which one could very naturally speak about the “location” of the energy and the direction and “bending” of the energy flux. In contrast, in the idealized case of a plane wave the energy is on the average evenly distributed over all space, and it is therefore unlocalized, making it impossible to use such “intuitive” arguments as above.

For the two fields  $\mathbf{S}_H = \mathbf{E} \times \mathbf{H}$  and  $\mathbf{S}_B = \mathbf{E} \times \mathbf{B}/\mu_0$  in discussion, however, a comparison in these terms is not illuminating in usual isotropic materials, since their directions coincide. But for anisotropic materials, their directions need not to coincide, and this effect can be particularly important in anisotropic metamaterials, that can exhibit negative refraction, in which this difference becomes critical. Although negative refraction can be obtained also in isotropic metamaterials, anisotropic metamaterials have an important advantage: the conditions for obtaining negative refraction in them are much less restrictive.

Having all this in mind, we tackle the problem by constructing a “ray” of light in order to *see* how does it refract at an interface between vacuum and an anisotropic metamaterial. One can find different definitions of ray in geometrical optics, for example, one, as a line in the direction of the gradient of the eikonal [3] [39], another, simply as a continuous line along the direction of the energy flow [40], and still another one that defines ray merely as a beam [41]. Here we will adopt a rather intuitive picture of a ray by regarding it as a very narrow beam. Then we use continuum electrodynamics to calculate the spatial location of the reflected and refracted beams, together with the energy flow according to the two proposals in question. Then we compare—among other things—their directions with the direction of the beam.

The structure of the paper is as follows: in Section 2 we compare, for each energy-flux proposal, possible interpretations of the energy-balance equations and the terms involved in them; then in Section 3 we present a brief introduction of the electromagnetic properties of anisotropic uniaxial metamaterials with emphasis on the refraction of plane waves at a flat interface; we later state in Section 4 some basic properties of 2D monochromatic electromagnetic fields, on which we build our analysis, and make a comparison with the formalism of geometrical optics, which we extend in Section 5. In Section 5.1 we particularize the results and concepts of these two previous sections to a Gaussian beam; we study some its main characteristics, and sketch how to calculate its refraction, to finally display and analyze the corresponding results of the numerical simulations. Section 6 is devoted to our conclusions.

## 2. Poynting's Theorem

In this section we present briefly the energy-balance equations for the two energy-flux proposals to establish the differences in interpretation of the terms appearing in them. We start with the macroscopic Maxwell's equations and regard the presence of the material as given by the charge and current densities induced by an external electromagnetic field produced by external sources. Maxwell's equations, in SI units, can be then written as

$$\nabla \cdot \epsilon_0 \mathbf{E} = \rho_{ext} + \rho_{ind} \quad (1)$$

$$\nabla \cdot \mathbf{B} = 0 \quad (2)$$

$$\nabla \times \mathbf{E} = -\frac{\partial \mathbf{B}}{\partial t} \quad (3)$$

$$\nabla \times \frac{\mathbf{B}}{\mu_0} = \mathbf{J}_{ext} + \mathbf{J}_{ind} + \epsilon_0 \frac{\partial \mathbf{E}}{\partial t} \quad (4)$$

where  $\rho_{ext}$  and  $\mathbf{J}_{ext}$  are the charge and current densities that are sources of the external field that excites the material, while  $\rho_{ind}$  and  $\mathbf{J}_{ind}$  denote the macroscopic averages of the charge and current densities that are induced within the material. Here  $\mathbf{E}$  denotes the macroscopic electric field while  $\mathbf{B}$  denotes the macroscopic magnetic field obtained as the macroscopic average of the microscopic magnetic field. Let us recall that regrettably  $\mathbf{B}$  is also called magnetic induction. Then we divide  $\mathbf{J}_{ind}$  into two terms,

$$\mathbf{J}_{ind} = \mathbf{J}_P + \mathbf{J}_M = \frac{\partial \mathbf{P}}{\partial t} + \nabla \times \mathbf{M} \quad (5)$$

where 1)  $\mathbf{J}_P$  denotes the induced conduction (“free”) plus polarization current densities and 2)  $\mathbf{J}_M$  denotes a divergence-free current density that behaves as the source of magnetization. Here  $\mathbf{P}$  and  $\mathbf{M}$  are the usual polarization and magnetization material fields. Induced-charge conservation is also assumed, that is,

$$\nabla \cdot \mathbf{J}_{ind} + \frac{\partial \rho_{ind}}{\partial t} = 0 \quad (6)$$

By substituting Equation (5) into Ampère-Maxwell’s law (4) and using the induced charge conservation (6), one can write Equations (1) and (4) as

$$\nabla \cdot \mathbf{D} = \rho_{ext} \quad (7)$$

$$\nabla \times \mathbf{H} = \mathbf{J}_{ext} + \frac{\partial \mathbf{D}}{\partial t} \quad (8)$$

which together with Equations (2) and (3) form the complete set of the four macroscopic Maxwell’s equations. Here

$$\mathbf{D} = \epsilon_0 \mathbf{E} + \mathbf{P} \quad (9)$$

is called the displacement field, while

$$\mathbf{H} = \frac{\mathbf{B}}{\mu_0} - \mathbf{M} \quad (10)$$

is called the magnetic intensity or simply the H field.

If one now calculates  $\nabla \cdot (\mathbf{E} \times \mathbf{H})$  and uses the macroscopic Maxwell’s equations together with the definitions of  $\mathbf{D}$  and  $\mathbf{H}$ , as given by Equations (9) and (10), one can write

$$\nabla \cdot (\mathbf{E} \times \mathbf{H}) + \frac{\partial}{\partial t} \frac{1}{2} \epsilon_0 E^2 + \frac{B^2}{\mu_0} = -\mathbf{E} \cdot \mathbf{J}_{ext} - \left( \mathbf{E} \cdot \frac{\partial \mathbf{P}}{\partial t} - \mathbf{M} \cdot \frac{\partial \mathbf{B}}{\partial t} \right), \quad (11)$$

that takes the mathematical form of a conservation law for the energy, and one can interpret  $\mathbf{E} \times \mathbf{H}$  as an energy flux and  $(1/2)\epsilon_0 E^2 + B^2/\mu_0$  as the energy density stored in the electromagnetic field. Notice that we write the expression of the energy density in terms of  $\mathbf{E}$  and  $\mathbf{B}$ , because we regard them as the fundamental “bare” fields. Nevertheless, since in our calculations below we deal with time averages of monochromatic fields in lossless materials, this choice will have no consequences in the final result. Here  $\mathbf{E} \cdot \mathbf{J}_{ext}$  denotes the power supplied by the external current, while the last term in the right hand side should correspond to the temporal rate of change of the electric and magnetic energy density either stored or dissipated within the material. It is appropriate to point out that in the presence of dissipation the stored energy density within a material is not a well-defined concept since it cannot be written as a time derivative ([3], sec. 61).

Following the same procedure as above, one can also write the following equation:

$$\nabla \cdot \left( \mathbf{E} \times \frac{\mathbf{B}}{\mu_0} \right) + \frac{\partial}{\partial t} \frac{1}{2} \left( \epsilon_0 E^2 + \frac{B^2}{\mu_0} \right) = -\mathbf{E} \cdot \mathbf{J}_{ext} - \mathbf{E} \cdot \left( \frac{\partial \mathbf{P}}{\partial t} + \nabla \times \mathbf{M} \right). \quad (12)$$

In this expression one identifies  $\mathbf{E} \times \mathbf{B}/\mu_0$  as the energy flux, and although the last term in the right hand side can be written as  $-\mathbf{E} \cdot \mathbf{J}_{ind}$ , and it could be naturally identified as the power dissipated by the induced currents, such identification contradicts the one given in Equation (11). Furthermore, the difference between  $\mathbf{E} \times \mathbf{H}$  and  $\mathbf{E} \times \mathbf{B}/\mu_0$  is  $-\mathbf{E} \times \mathbf{M}$ , and let us recall that  $-\mathbf{E} \times \mathbf{M}/c^2$  has been identified in certain circumstances, as a “hidden” momentum, that is, a mechanical momentum conveyed by and within the magnetic material. Here  $c$  denotes the speed of light.

We will not discuss further the physical interpretation of the terms that appear in the energy-conservation laws given in Equations (11) and (12); we now rather construct the conceptual and mathematical framework to analyze the energy transport in the refraction of a beam of light at the interface between vacuum and an anisotropic metamaterial. The advantage of dealing with anisotropic metamaterials rather than with crystals, is that in crystals the anisotropy of the electromagnetic response is fixed by the crystalline structure and cannot be

changed, while in metamaterials this degree of anisotropy, as well as the signs of the response, can be tailored through the fabrication process.

### 3. Uniaxial Metamaterials

As discussed above, we will be dealing with anisotropic uniaxial metamaterials. These are characterized by electric and magnetic response tensors  $\bar{\epsilon}$  and  $\bar{\mu}$ , respectively. We will assume that they have a common anisotropy axis (the  $z$ -axis) thus they are simultaneously diagonalizable, with components  $\epsilon_{xx} = \epsilon_{yy} = \epsilon_{\parallel}$ ,  $\epsilon_{zz} = \epsilon_{\perp}$ , and analogously with the components of  $\bar{\mu}$ . We also assume that we will be working on a frequency band in which the material is transparent, that is, at frequencies where all the components of these response tensors can be regarded as real (*i.e.*, negligible absorption). Furthermore, the premise that we are dealing with metamaterials allows us to choose not only over a wide spread of values for the tensorial components, but also their sign.

We will now introduce notation and summarize some of the properties that we will use in this paper; their derivation can be found, for example, in [42]. First we recall that an uniaxial metamaterial sustains two electromagnetic plane-wave modes, which we will call  $e$  and  $m$ , and refer to them generically as  $\gamma$ . Each mode is characterized by a given frequency  $\omega$  and a corresponding wavevector  $\mathbf{k}$ . In the  $m$ -mode, the electric field  $\mathbf{E}$  is orthogonal to  $\mathbf{k}$  while in the  $e$ -mode the  $\mathbf{H}$  field is orthogonal to  $\mathbf{k}$ . We will also refer generically to the diagonal components of either  $\bar{\mu}$  or  $\bar{\epsilon}$  as  $\gamma_{\parallel}$  and  $\gamma_{\perp}$ , when referring to the  $m$  or to the  $e$  mode, respectively; and in terms of these we define the anisotropy factor  $a_{\gamma} = \gamma_{\parallel}/\gamma_{\perp}$ , that is,  $a_m = \mu_{\parallel}/\mu_{\perp}$  and  $a_e = \epsilon_{\parallel}/\epsilon_{\perp}$ . The anisotropy factor quantifies the degree of anisotropy of the response; its deviation from unity gives us an idea of how anisotropic the response of the medium is.

The dispersion relations of these modes can be put in terms of  $n_{\parallel} = \sqrt{\epsilon_{\parallel}\mu_{\parallel}/\epsilon_0\mu_0}$ , the magnitude of the wavevector of  $\gamma$  mode,  $k_{\gamma}$ , and the wavenumber in vacuum  $k_0 = \omega/c$ . Assuming the wavevector lies in the  $xz$  plane, these can be written as

$$k_{\gamma}^2 = k_0^2 n_{\parallel}^2 + (1 - a_{\gamma}) k_x^2. \tag{13}$$

Note that  $n_{\parallel}$  would be the index of refraction of the system in the absence of anisotropy ( $a_{\gamma} = 1$ ).

Finally, it is important to say that, in this medium, the field  $\mathbf{S}_H = \mathbf{E} \times \mathbf{H}$  is not, in general, parallel to  $\mathbf{k}$  for a monochromatic plane wave. Let us call  $F_{\gamma}$  the amplitude of the  $\mathbf{H}$  field for  $\gamma = e$  and the amplitude of the electric field for  $\gamma = m$ , and the subscripts  $i, r$  and  $t$  will denote the incident, reflected and transmitted fields, respectively. Then, the field  $\mathbf{S}_H$  is, in average,

$$\langle \mathbf{E}_{\gamma} \times \mathbf{H}_{\gamma} \rangle = \frac{F_{\gamma}^2}{2\omega} \left( \frac{k_x}{\gamma_{\perp}}, 0, \frac{k_z}{\gamma_{\parallel}} \right), \tag{14}$$

so both vectors will only be parallel when there is no anisotropy of the corresponding mode ( $a_{\gamma} = 1$ ).

### Refraction of Plane Waves

Let us consider a plane interface between vacuum and the uniaxial metamaterial, set this interface perpendicular to the optical axis of the metamaterial and fix the  $z$ -axis along this direction. Then assume that a plane wave, with its wavevector in the  $xz$  plane, impinges from vacuum into the metamaterial. One can immediately see that if the incident wave is  $p$ -polarized ( $\mathbf{H}$  perpendicular to  $\mathbf{k}$ ) only the  $e$  mode is excited, while if it is  $s$ -polarized ( $\mathbf{E}$  perpendicular to  $\mathbf{k}$ ) only the  $m$  mode is excited; while  $\mathbf{k}$  remains in the  $xz$  plane, and thus, there are separate “refraction laws” for  $\mathbf{S}_H$  and  $\mathbf{k}$ .

Now we look at the reflection and transmission of plane waves in the presence of uniaxial metamaterials, defined as  $t_{\gamma} = F_{\gamma_t}/F_{\gamma_i}$  and  $r_{\gamma} = F_{\gamma_r}/F_{\gamma_i}$ ;  $\gamma_0$  as  $\mu_0$  for  $\gamma = e$  ( $p$ -polarization) and  $\gamma_0 = \epsilon_0$  for  $\gamma = m$  ( $s$ -polarization); and using boundary conditions at the interface, we can write

$$\begin{aligned} t_{\gamma} &= \frac{2}{1 + \delta_{\gamma}} \\ r_{\gamma} &= \frac{1 - \delta_{\gamma}}{1 + \delta_{\gamma}}, \end{aligned} \tag{15}$$

where  $\delta_\gamma = \gamma_0 k_{z_i} / \gamma_\parallel k_{z_i}$ .

In terms of these definitions and basic concepts, we now summarize some interesting features of the refraction of plane waves on uniaxial metamaterials. A derivation of all these results can be found in [42]

- 1) The angle  $\Theta_\gamma$  formed by  $\mathbf{k}$  and  $\hat{e}_z$ , in terms of the incidence angle  $\theta_i$ , is

$$\sin(\Theta_\gamma) = \frac{\sin(\theta_i)}{\sqrt{n_\parallel^2 + (1 - a_\gamma) \sin^2(\theta_i)}} \quad (16)$$

- 2) The angle  $\theta_\gamma$  formed by  $\mathbf{S}_H$  and  $\hat{e}_z$ , again in terms of the incidence angle  $\theta_i$ , is given by

$$\sin(\theta_\gamma) = \frac{\gamma_\perp \sin(\theta_i)}{|\gamma_\parallel| \sqrt{n_\parallel^2 + a_\gamma (a_\gamma - 1) \sin^2(\theta_i)}}, \quad (17)$$

and we call this the *refraction angle*.

- 3) The refraction of  $\mathbf{k}_\gamma$  is towards the interface if  $\gamma_\parallel < 0$  and away the interface if  $\gamma_\parallel > 0$ . The projection of  $\mathbf{S}_{H_\gamma}$  over  $\mathbf{k}_\gamma$  also has the sign of  $\gamma_\parallel$ .

- 4) The sign of refraction is determined by the sign of  $\gamma_\perp$ .

- 5) The refraction angle, as a function of the incidence angle, is an increasing function if  $n_\parallel^2 > 0$  and decreasing if  $n_\parallel^2 < 0$ .

- 6) Whenever  $a_\gamma \geq n_\parallel^2$ , there exists a critical angle (equal for  $\theta_\gamma$  and  $\Theta_\gamma$ ), given by  $\arcsin(n_\parallel / \sqrt{a_\gamma})$ .

- 7) The critical angle has an inverse behavior in the case  $n_\parallel^2 < 0$ , in the sense that, for angles lower than the critical, there is no propagating wave transmitted, but for all angles higher that the critical, there is propagating transmission.

- 8) There exist critical angles for both polarizations.

- 9) There is low variation of the refraction angle for  $a_\gamma \ll 0$ .

- 10) In the particular case when  $a_\gamma = n_\parallel^2$ , the reflectance is constant for all angles.

Note especially, on relation with negative refraction, some less restrictive features of these materials due to their anisotropy, for example, the sign of the projection of  $\mathbf{S}$  over  $\mathbf{k}$  is no longer tied to the sign of the refraction angle, since it is determined by only one parameter; also, there can be propagating transmitted waves even if the “refractive index” is purely imaginary.

With respect to point 3, it is important to note that this refraction problem has a mathematical ambiguity arising from the fact that the dispersion relation (13) is quadratic, and thus two possibilities for  $k_z$  are admitted (while  $k_x$  is fixed by boundary conditions). This is solved by noting that, independently of the physical interpretation of the field  $\mathbf{S}_H$ , the continuity of the parallel components of  $\mathbf{E}$  and  $\mathbf{H}$  lead to the continuity of its normal ( $z$ ) component across the interface. Besides, since  $\mathbf{S}_H \cdot \hat{e}_z$  is, by construction, positive on the incidence medium, it has to be positive on the refraction medium, which together with Equation (14), tells us that  $k_z$  and  $\gamma_\parallel$  should have the same sign. Here  $\hat{e}_z$  is a unit vector along the  $z$  axis.

## 4. 2D Monochromatic Fields

In this work we will be dealing, for simplicity, with the refraction of monochromatic two-dimensional beams, that nevertheless keep most of the physics behind the phenomenon of refraction of actual three-dimensional beams. We consider first an arbitrary two-dimensional monochromatic electric field, defined as a superposition of plane waves in the  $xz$  plane,

$$\mathbf{E}(x, z) = \text{re} \left[ \int_{-\infty}^{\infty} \mathbf{A}(k_x) e^{i(k_x x + k_z z - \omega t)} dk_x \right], \quad (18)$$

where re denotes real part. In a given medium, this will be a solution to Maxwell's equations if  $k_z$  as a function of  $k_x$  is given by the dispersion relation of the electromagnetic waves in this medium. For example, for an isotropic medium with refractive index  $n$ , this relation is:  $k_x^2 + k_z^2 = k_0^2 n^2$ . As it can be seen, this field does not depend on the  $y$  coordinate implying translational invariance along this direction. A plot of the magnitude of this field in the  $xz$  plane will mimic a projection of a three-dimensional monochromatic field.

We can view this superposition as a series of plane waves traveling along different directions and with

different amplitudes, these determined by the function  $A(k_x)$ . In general, this superposition includes not only propagating waves, but also inhomogeneous waves, that is, plane waves with a complex wavevector  $\mathbf{k} = \mathbf{k}' + i\mathbf{k}''$  whose amplitudes decay along  $\mathbf{k}''$  and propagate with its planes of constant phase perpendicular to  $\mathbf{k}'$ .

Recalling now that the magnetic, displacement, and  $\mathbf{H}$  fields linked to the electric field  $\mathbf{E} = \text{re} \left[ \mathbf{E}_0 e^{i(\mathbf{k} \cdot \mathbf{r} - \omega t)} \right]$  of a plane wave of wavevector  $\mathbf{k}$  and frequency  $\omega$ , can be written as

$$\begin{aligned} \mathbf{B} &= \text{re} \left[ \frac{\mathbf{k}}{\omega} \times \mathbf{E}_0 e^{i(\mathbf{k} \cdot \mathbf{r} - \omega t)} \right] \\ \mathbf{D} &= \text{re} \left[ \bar{\bar{\epsilon}} \cdot \mathbf{E}_0 e^{i(\mathbf{k} \cdot \mathbf{r} - \omega t)} \right] \\ \mathbf{H} &= \text{re} \left[ \bar{\bar{\mu}}^{-1} \cdot \frac{\mathbf{k}}{\omega} \times \mathbf{E}_0 e^{i(\mathbf{k} \cdot \mathbf{r} - \omega t)} \right], \end{aligned} \quad (19)$$

it is immediate to write the corresponding monochromatic fields associated to the electric field given in Equation (18), as

$$\begin{aligned} \mathbf{B} &= \text{re} \left[ \int_{-\infty}^{\infty} \frac{\mathbf{k}}{\omega} \times \mathbf{A}(k_x) e^{i(k_x x + k_z z - \omega t)} dk_x \right] \\ \mathbf{D} &= \text{re} \left[ \int_{-\infty}^{\infty} \bar{\bar{\epsilon}} \cdot \mathbf{A}(k_x) e^{i(k_x x + k_z z - \omega t)} dk_x \right] \\ \mathbf{H} &= \text{re} \left[ \bar{\bar{\mu}}^{-1} \cdot \int_{-\infty}^{\infty} \frac{\mathbf{k}}{\omega} \times \mathbf{A}(k_x) e^{i(k_x x + k_z z - \omega t)} dk_x \right]. \end{aligned} \quad (20)$$

For  $s$ -polarization, the amplitudes  $\mathbf{A}(k_x)$  in (18) can be written as  $\mathbf{A}(k_x) = A_e(k_x) \hat{e}_y$ . It is then convenient to define

$$\alpha(x, z) \equiv \int_{-\infty}^{\infty} A_e(k_x) e^{i(k_x x + k_z z)} dk_x, \quad (21)$$

thus in terms of  $\alpha$  the electric field in (18) becomes

$$\mathbf{E}(\mathbf{r}, t) = \text{re} \left[ \alpha(\mathbf{r}) e^{-i\omega t} \right] \hat{e}_y. \quad (22)$$

Note that if we denote  $\alpha_x \equiv \partial \alpha / \partial x$ ,  $\alpha_z \equiv \partial \alpha / \partial z$ , then

$$\int_{-\infty}^{\infty} A_e(k_x) k_x e^{i(k_x x + k_z z)} dk_x = -i\alpha_x, \quad (23)$$

and the same is valid for  $\alpha_z$  replacing  $k_x$  with  $k_z$  in the integrand. Now, since  $\mathbf{k} = (k_x, 0, k_z)$  and  $\mathbf{k} \times \hat{e}_y = (-k_z, 0, k_x)$  one can write, for  $s$ -polarization, the magnetic, displacement, and  $\mathbf{H}$  fields in Equation (20) in a most convenient and succinct way:

$$\begin{aligned} \mathbf{B} &= \text{re} \left[ -i(-\alpha_z, 0, \alpha_x) e^{-i\omega t} / \omega \right] \\ \mathbf{D} &= \text{re} \left[ \epsilon_{\parallel} \hat{e}_y \alpha e^{-i\omega t} \right] \\ \mathbf{H} &= \text{re} \left[ \frac{-i}{\omega} \left( \frac{-\alpha_z}{\mu_{\parallel}}, 0, \frac{\alpha_x}{\mu_{\perp}} \right) e^{-i\omega t} \right]. \end{aligned} \quad (24)$$

For  $p$  polarization, one can write an expression for the  $\mathbf{H}$  field, analogous to the one for the electric field in Equation (18), as

$$\mathbf{H}(\mathbf{r}, t) = \text{re} \left[ \beta(\mathbf{r}) e^{-i\omega t} \right] \hat{e}_y, \quad (25)$$

where

$$\beta(x, z) \equiv \int_{-\infty}^{\infty} A_m(k_x) e^{i(k_x x + k_z z)} dk_x, \quad (26)$$

with the following corresponding expressions for the displacement, electric and magnetic fields,

$$\begin{aligned}
 \mathbf{D} &= \text{re} \left[ -i(\beta_z, 0, -\beta_x) e^{-i\omega t} / \omega \right] \\
 \mathbf{E} &= \text{re} \left[ \frac{-i}{\omega} \begin{pmatrix} -\beta_z & & \\ & \epsilon_{\parallel} & \\ & & \epsilon_{\perp} \end{pmatrix} e^{-i\omega t} \right] \\
 \mathbf{B} &= \text{re} \left[ \mu_{\parallel} \hat{e}_y \beta e^{-i\omega t} \right].
 \end{aligned} \tag{27}$$

It is important to note that the linear superposition of plane waves, as the one given in Equation (18) can be also written as  $\text{re} \left[ e^{-i\omega t} \int_{-\infty}^{\infty} \mathbf{A}(k_x) e^{ik \cdot \mathbf{r}} dk_x \right]$ , where the exponent  $e^{-i\omega t}$  has been pulled out of the integral leaving a factor that is a function only of position. Since in the calculation of the energy densities and energy flux we will be dealing with bilinear products of the form  $\text{re} \left[ e^{-i\omega t} f(\mathbf{r}) \right] \text{re} \left[ e^{-i\omega t} g(\mathbf{r}) \right]$  it is convenient to introduce time averages of these bilinear quantities, because the measuring devices cannot simply follow time variations of the order of  $2\pi/\omega$ . Since the factor multiplying  $e^{-i\omega t}$  is only a function of the position, we will frequently deal with products of this type. If we denote with a ' the real part of a complex numbers and with " its imaginary part, the product above is written as  $(\cos \omega t f'(\mathbf{r}) + \sin \omega t f''(\mathbf{r}))(\cos \omega t g'(\mathbf{r}) + \sin \omega t g''(\mathbf{r}))$ . Now, if one takes the time average over periods much longer than  $2\pi/\omega$  one gets,

$$\langle \text{re} \left[ e^{-i\omega t} f(\mathbf{r}) \right] \text{re} \left[ e^{-i\omega t} g(\mathbf{r}) \right] \rangle = \frac{1}{2} \text{re} \left[ f^*(\mathbf{r}) g(\mathbf{r}) \right], \tag{28}$$

where we have used  $\langle \dots \rangle$  to indicate time average and the \* denotes complex conjugate.

For example, using Equations (22) and (28), the time average of  $E^2$  for s-polarization is

$$\langle E^2 \rangle = \langle \mathbf{E} \cdot \mathbf{E} \rangle = \frac{1}{2} \text{re} \left[ \alpha \alpha^* \right] = \frac{1}{2} |\alpha|^2. \tag{29}$$

Also, from Equations (22) and (24) one can easily calculate  $\mathbf{S}_B$ , and its time average by using again equation (28). One gets, for s-polarization,

$$\langle \mathbf{S}_B \rangle = \frac{1}{2\mu_0\omega} \text{re} \left[ -i\alpha^* (\alpha_x, 0, \alpha_z) \right] = \frac{1}{2\mu_0\omega} \text{im} \left[ \alpha^* \nabla \alpha \right]. \tag{30}$$

Note that this result is general and does not depend on the constitutive relations. On the other hand, for  $\mathbf{S}_H$  we do not have any such general expression, but we can calculate one for the special case of anisotropic metamaterials; using Equations (22) and (24), one gets, again for s-polarization,

$$\langle \mathbf{S}_H \rangle = \frac{1}{2\omega} \text{im} \left[ \alpha^* \begin{pmatrix} \alpha_x & & \\ \mu_{\perp} & & \\ & & \alpha_z \end{pmatrix} \right], \tag{31}$$

which clearly differs in direction from  $\mathbf{S}_B$ .

Finally, regarding to the energetic consequences of the choice of energy flux, note that, taking the divergence of  $\mathbf{S}_B$  and calling  $\alpha_{xx}$  to the second partial derivatives of  $\alpha$ , we get

$$\begin{aligned}
 \nabla \cdot \langle \mathbf{S}_B \rangle &= \frac{1}{2\mu_0\omega} \text{im} \left[ \alpha_x^* \alpha_x + \alpha^* \alpha_{xx} + \alpha_z^* \alpha_z + \alpha^* \alpha_{zz} \right] \\
 &= \frac{1}{2\mu_0\omega} \text{im} \left[ \alpha^* (\alpha_{xx} + \alpha_{zz}) \right].
 \end{aligned} \tag{32}$$

Since  $\alpha_{xx} + \alpha_{zz} = -\int_{-\infty}^{\infty} A(k_x) (k_x^2 + k_z^2) e^{ik \cdot \mathbf{r}} dk_x$ , in isotropic media with real refractive index  $n$ , this quantity has the value  $-k_0^2 n^2 \alpha$  and, therefore, the divergence will be zero. But in a medium with a different dispersion relation-for instance, an anisotropic one-this will be nonzero. Since we don't have a general expression in terms of  $\alpha$  for  $\mathbf{S}_H$ , it is not possible to calculate its divergence in an arbitrary case, but it is possible to do it in the special case of the anisotropic metamaterials, for which we get, with analogous calculations in s-polarization,

$$\nabla \cdot \langle \mathbf{S}_H \rangle = \frac{1}{2\omega} \text{im} \left[ \alpha^* \begin{pmatrix} \alpha_{xx} & & \\ \mu_{\perp} & & \\ & & \alpha_{zz} \end{pmatrix} \right] \tag{33}$$

which, in view of the dispersion relation (13), and following the same reasoning as before with  $\mathbf{S}_B$ , is identically zero in mediums where  $n_{\parallel}^2$  is real. Thus, in the cases of isotropic and anisotropic media for an  $s$ -polarized monochromatic field, we have that  $\nabla \cdot \mathbf{S}_H$  does not predict any local loss or gain of energy within the material, while  $\nabla \cdot \mathbf{S}_B$  does predict it in the anisotropic metamaterial.

### 5. Geometrical Optics and Light Beams

As we already mentioned in the introduction and in the section concerning the refraction of plane waves, the energy-flux vector (Poynting’s vector) is used, besides the calculation of electromagnetic-energy transport, in determining the “detectable” direction of refraction of plane waves, over the direction given by the angle of refraction of the wavevector. Although in many cases they do coincide, their difference in direction is specially critical in the phenomenon of negative refraction. In our pragmatic approach we will look at the refraction of rays—defined as narrow beams—and then calculate the two expressions for the energy flux:  $\mathbf{E} \times \mathbf{B}/\mu_0$  and  $\mathbf{E} \times \mathbf{H}$ , and compare their direction with the actual direction of the beam.

The first question is how to define the location of the beam in order to visualize it. The first idea could be perhaps to identify it with the transmitted energy flux and visualize it by plotting the transmittance, which is what one usually associates as the measurable quantity in optics experiments. The problem with such definition is that the value of the transmittance depends on the definition of the energy flux, which would lead us to a circular argument. Also, let us recall that the transmittance is proportional to the energy flux perpendicular to the interface, as if the detection of the transmitted power would be accomplished only along the perpendicular direction and not along the direction of the beam. Thus, we choose to look instead at the energy density, which in the absence of dissipation is proportional to  $E^2$ , and then take the direction of the beam as the direction of the energy flux.

In the search of a criterion to determine how a monochromatic *field* refracts, one may require to define the direction of propagation of the field. At this respect, we derived the following result which we find interesting, and, to our knowledge, unnoticed yet. Let us start considering the simplest case of an isotropic, homogeneous, non-magnetic medium in which  $\mathbf{S}_B = \mathbf{E} \times \mathbf{B}/\mu_0$  ( $= \mathbf{E} \times \mathbf{H}$ ), and assume that the monochromatic field is  $s$ -polarized. Note that the average of this field given in (30) is proportional to  $\text{im}[\alpha^* \nabla \alpha] = \alpha \nabla \alpha'' - \alpha'' \nabla \alpha'$ , and also that

$$\nabla \arctan\left(\frac{\alpha''}{\alpha'}\right) = \frac{1}{1 + (\alpha''/\alpha')^2} \frac{\alpha \nabla \alpha'' - \alpha'' \nabla \alpha'}{\alpha'^2} = \frac{\text{im}[\alpha^* \nabla \alpha]}{|\alpha|^2}. \tag{34}$$

We recognize in  $\arctan(\alpha''/\alpha')$  the phase  $\phi_\alpha$  of the complex function  $\alpha = |\alpha| e^{i\phi_\alpha}$ ; therefore, by combining Equations (34), (30) and (29), one can write

$$\langle \mathbf{S}_B \rangle = \frac{\langle E^2 \rangle}{\mu_0 \omega} \nabla \phi_\alpha. \tag{35}$$

Since the electric field in Equation (22) can be also written as  $\mathbf{E} = \text{re}\left[|\alpha| \hat{e}_y e^{i(\phi_\alpha - \omega t)}\right]$ , we conclude that in a homogeneous, isotropic, non-magnetic medium, the time average of the field  $\mathbf{S}_B$  of a monochromatic,  $s$ -polarized field, points in the direction of the maximum change of the phase of the electric field. This exact result establishes a connection between the propagation of an arbitrary monochromatic field (which can be, in particular, a localized one) and the formalism of geometrical optics, by generalizing the concept of *eikonal* to such field, in the sense of a function whose gradient yields the direction of the “ray”. Notice that the concept of *eikonal* is usually introduced when there is slow spatial variation of the amplitude function of the electric field ([3], sec. 85), ([39], ch. 8), but here we impose *no restriction* on the spatial part.

Going a little bit further, note that the dependence on the material in the expressions for the electric field  $\mathbf{E}$  in Equation (22) and the magnetic field  $\mathbf{B}$  in Equation (24) comes only through the specific form of  $\alpha$ , that requires the dispersion relation of the specific material in the performance of the integral in Equation (21). Therefore, Equation (35) is valid regardless the optical properties of the material, simply because its derivation is independent of the particular structure of  $\alpha$  (see Equations (30) and (34)). This means that in *any material*, the field  $\mathbf{E} \times \mathbf{B}/\mu_0$  of an *arbitrary s-polarized monochromatic field*, points in the direction of the gradient of phase of the corresponding electric field.

This same result does not hold for all materials while regarding the energy flux as given by  $\mathbf{S}_H = \mathbf{E} \times \mathbf{H}$ . For instance, for an uniaxial magnetic medium excited with  $s$ -polarized light, the average of  $\mathbf{S}_H$  is given by (31) which differs markedly from the expression for the average of  $\mathbf{S}_B$  given in Equation (30). But even if the material is isotropic but has magnetic absorption,  $\langle \mathbf{S}_B \rangle$  and  $\langle \mathbf{S}_H \rangle$  will also differ in direction: one can see this by replacing  $\mu_{\parallel}$  and  $\mu_{\perp}$  in Equation (31) by  $\mu = \mu' + i\mu''$  and recalling that  $1/\mu = \mu^*/|\mu|^2$ ,

$$\langle \mathbf{S}_H \rangle = \frac{1}{2\omega|\mu|^2} \text{im}[\mu^* \alpha^* \nabla \alpha] = \frac{\mu' \text{im}[\alpha^* \nabla \alpha] + \mu'' \text{re}[\alpha^* \nabla \alpha]}{2\omega|\mu|^2}. \quad (36)$$

The real part of  $\alpha^* \nabla \alpha$  is  $\alpha' \nabla \alpha' + \alpha'' \nabla \alpha''$ , which can be expressed as  $\frac{1}{2} \nabla(\alpha'^2 + \alpha''^2) = \frac{1}{2} \nabla|\alpha|^2$ , so one can write

$$\langle \mathbf{S}_H \rangle = \frac{2\mu' E^2 \nabla \phi_{\alpha} + \mu'' \nabla \langle E^2 \rangle}{2\omega|\mu|^2}. \quad (37)$$

One can see that the first term in the right hand side points along the direction of the gradient of phase of the electric field as in the case of a homogeneous nonmagnetic material, but now, due to absorption, the field  $\mathbf{S}_H$  acquires a component in the direction of the maximum change of intensity. One can see this result as a generalization to arbitrary monochromatic fields in  $s$ -polarization, of the characteristics of propagation of inhomogeneous plane waves in absorbing media. In this latter case the inhomogeneous wave is proportional to  $\exp[i(\mathbf{k}' \cdot \mathbf{r} - \omega t) - \mathbf{k}'' \cdot \mathbf{r}]$  where the planes of constant phase travel along  $\mathbf{k}'$  while the planes of constant amplitude decay along  $\mathbf{k}''$ .

Nevertheless, the very general result that for any monochromatic electromagnetic field and for any material the direction of  $\mathbf{S}_B$  coincides with the gradient of the phase of the electric field, makes  $\mathbf{E} \times \mathbf{B}/\mu_0$  a very tempting choice for the energy flux. Note that the result is true even for absorbing media.

The analogous result for  $p$  polarized light might not be as obvious, but is also quite interesting. Using the expressions for the fields given in Equations (25) and (27) one can write,

$$\begin{aligned} \langle \mathbf{S}_B \rangle &= \text{im} \left[ \frac{\mu_{\parallel}^*}{\mu_0} \frac{1}{2\omega} \beta^* \left( \frac{\beta_x}{\epsilon_{\perp}}, 0, \frac{\beta_z}{\epsilon_{\parallel}} \right) \right] \\ \langle \mathbf{S}_H \rangle &= \text{im} \left[ \frac{1}{2\omega} \beta^* \left( \frac{\beta_x}{\epsilon_{\perp}}, 0, \frac{\beta_z}{\epsilon_{\parallel}} \right) \right]. \end{aligned} \quad (38)$$

Without magnetic absorption, both fields are parallel, even in anisotropic media. Moreover, none of them has the property of pointing in the direction of maximum change of the phase of  $\mathbf{H}$ . The field that has this property for  $p$ -polarization is the field  $\mathbf{D}/\epsilon_0 \times \mathbf{H}$ :

$$\frac{\mathbf{D}}{\epsilon_0} \times \mathbf{H} = \text{im} \left[ \frac{1}{2\omega\epsilon_0} \beta^* (\beta_x, 0, \beta_z) \right] = \frac{1}{2\epsilon_0} H^2 \nabla \phi_{\beta} \quad (39)$$

where we have written  $\mathbf{H} = \text{re} \left[ |\beta| e^{i(\phi_{\beta} - \omega t)} \right] \hat{e}_y$ . These results may be in principle unexpected, but perhaps it can be mathematically clarified by the fact that Maxwell's equations in regions free of external sources together with the constitutive relations are invariant under the interchange of  $\mathbf{D} \leftrightarrow \mathbf{B}$  and  $\mathbf{E} \leftrightarrow -\mathbf{H}$  and  $\bar{\epsilon} \leftrightarrow -\bar{\mu}$ . One might think that this third field should be added to the other two options under consideration, however, in view of the equivalence of the  $\mathbf{E} \times \mathbf{B}/\mu_0$  in  $s$ -polarization and  $\mathbf{D}/\epsilon_0 \times \mathbf{H}$  in  $p$ -polarization, we only need to take care of the two first-mentioned cases, fortunately. In the next subsection we adopt our definition of ray as a narrow Gaussian beam.

## Gaussian Beam

We now use the results for 2D monochromatic fields to construct a localized beam. We start by regarding an  $s$ -polarized beam localized along the  $z$ -axis, and impose a boundary condition over the magnitude  $E$  of the

electric field at  $t = 0$ , that defines its shape. This boundary condition requests that in the plane  $z = 0$ ,  $E$  has a Gaussian profile of width  $w$ , that is,

$$E(x, y, 0) = E_0 e^{-\frac{x^2}{2w^2}}. \tag{40}$$

From Equation (22) we get that  $E(x, y, 0) = \text{re} \left[ \int_{-\infty}^{\infty} A(k_x) e^{ik_x x} dk_x \right]$ . This means that  $A(k_x)$  can be identified as the spatial Fourier transform of  $E(x, y, 0)$ , and the condition of  $E$  being real only means that  $A(k_x) = A^*(-k_x)$ . Then

$$A(k_x) = \frac{1}{2\pi} \int_{-\infty}^{\infty} E_0 e^{-\frac{x^2}{2w^2}} e^{ik_x x} dx = \frac{E_0 w}{\sqrt{2\pi}} e^{-\frac{w^2 k_x^2}{2}}. \tag{41}$$

Thus, the electric field in any point at any time is given by

$$E = \text{re} \left[ \frac{E_0 w}{\sqrt{2\pi}} \hat{e}_y \int_{-\infty}^{\infty} e^{-\frac{w^2 k_x^2}{2}} e^{i(k_x x + k_z z - \omega t)} dk_x \right]. \tag{42}$$

This is a 2D Gaussian beam, confined in the  $x$  direction and extended along the  $z$  direction. Regarding its composition as a superposition of plane waves, note that the plane wave corresponding to wavevector  $(0, 0, k_0)$  has the dominant amplitude; we call this wave the *main* mode, and its corresponding vector the main wavevector. Now, given any other plain-wave component with wavevector  $(k_x, 0, k_z)$ , there is a corresponding plane wave component with the same amplitude and opposite  $x$  component, and therefore a wavevector  $(-k_x, 0, k_z)$ ; their sum always “points” in the direction of the main wavevector. This gives the  $z$  axis a special geometrical role of symmetry, and thus we find natural to call it the *axis of the beam* and to say that the beam is propagating in the  $z$  direction. Naturally, the profile of  $E^2$  is also Gaussian, and in it this symmetry is traduced on an invariance under the change of  $z$  by  $-z$  or  $x$  by  $-x$ . This also gives the point  $(x, z) = (0, 0)$  a special geometrical location (exactly at the center of the beam’s waist), and we call it the *center of the beam*.

We will be plotting  $E^2$ , which is given exclusively in terms of the function  $\alpha$  defined in Equation (45), so, from now on, we will abuse lightly from the notation and refer to the function  $\alpha$  as “the beam”.

We are interested in the refraction of an incident beam from vacuum to an anisotropic metamaterial, but with an arbitrary angle of incidence  $\theta_i$ . We assume the interface is located at the plane  $z = 0$  and then we write down the expression of the beam in Equation (42), in a rotated system of coordinates  $(x_i, y, z_i)$  that we will call the incidence system, in which the  $x_i z_i$  plane is rotated an angle  $\theta_i$  with respect to the  $xz$  plane, leaving  $y$  invariant. Then

$$\alpha(x_i, z_i) = \frac{E_0 w}{\sqrt{2\pi}} \int_{-\infty}^{\infty} e^{-\frac{w^2 k_{x_i}^2}{2}} e^{i(k_{x_i} x_i + k_{z_i} z_i)} dk_{x_i}, \tag{43}$$

and the relationship between these two coordinate systems is given by

$$\begin{aligned} z_i &= z \cos \theta_i + x \sin \theta_i \\ x_i &= x \cos \theta_i - z \sin \theta_i. \end{aligned} \tag{44}$$

Replacing these rotated variables in Equation (43) we get the following expression for the incident beam on the  $(x, z)$  system,

$$\alpha_i(x, z) = \frac{E_0 w}{\sqrt{2\pi}} \int_{-\infty}^{\infty} e^{-\frac{w^2 k_{x_i}^2}{2}} e^{i(k_{x_i} \cos \theta_i + k_{z_i} \sin \theta_i)x} e^{i(k_{z_i} \cos \theta_i - k_{x_i} \sin \theta_i)z} dk_{x_i}, \tag{45}$$

where the axis of the beam lies along the line  $x = z \tan \theta_i$ . We can recognize  $k_x$  and  $k_z$  as the quantities in the exponent, that are in parenthesis multiplying  $x$  and  $z$ , respectively. So we can think of this Gaussian beam as a superposition of plane waves with wavevectors  $(k_x, 0, k_z)$  (on the unrotated system)—where  $k_z$  and  $k_x$  are related through the dispersion relation—and amplitudes given by  $e^{-w^2 k_{x_i}^2 / 2}$  (given in the rotated system). Note that the center of the beam remains in the same position.

Given the incident field in Equation (45) and setting the location of the uniaxial metamaterial in  $z > 0$ , we now describe the computation of the electric field of the refracted and reflected beams. The axis of the incident beam subtends an angle  $\theta_i$  with the  $z$  axis. We then refract the beam by refracting mode by mode, understanding that by refraction of the mode we only mean using Maxwell's equations to propagate the plane-wave mode towards the anisotropic metamaterial, without any consideration about the direction of energy flow. This means that a transmitted mode with wave vector  $\mathbf{k}$ , obeys the dispersion relation in the metamaterial keeping its  $x$  component continuous at the interface.

To this purpose, we follow the next steps to refract and reflect a given mode of the incident beam:

1) For a given mode-characterized in the integral by  $k_{x_i}$ -calculate the corresponding  $k_{z_i}$  component using the dispersion relation in vacuum:  $k_{z_i} = \sqrt{k_0^2 - k_{x_i}^2}$ .

2) From the resultant wave vector  $(k_{x_i}, 0, k_{z_i}(k_{x_i}))$ , obtain its component parallel to the interface  $z = 0$  by rotating it as required in Equation (44).

3) Calculate the  $z$ -component of this mode by using the dispersion relation in the corresponding medium (vacuum or metamaterial), and assigning

a) a negative sign for the reflected mode.

b) the sign of  $\mu_{\parallel}$  ( $\text{sgn}(\mu_{\parallel})$ ) for the transmitted mode, as explained above.

4) Multiply the amplitude of this mode by the transmission or reflection coefficient in Equation (15), as a function of the parallel ( $x$ -component) of the wavevector.

To summarize this, we have, in terms of

$$\begin{aligned} k_{z_i}(k_{x_i}) &= \sqrt{k_0^2 - k_{x_i}^2} \\ k_x(k_{x_i}) &= k_{x_i} \cos \theta_i + k_{z_i}(k_{x_i}) \sin \theta_i \\ k_{z_r}(k_{x_i}) &= \sqrt{k_0^2 - k_x^2(k_{x_i})} \\ k_{z_t}(k_{x_i}) &= \sqrt{k_0^2 n_{\parallel}^2 - k_x(k_{x_i})^2}, \end{aligned} \quad (46)$$

the expressions for the reflected and transmitted fields:

$$\begin{aligned} \alpha_r(x, z) &= \frac{E_0 w}{\sqrt{2\pi}} \int_{-\infty}^{\infty} r(k_x(k_{x_i})) e^{-\frac{w^2 k_{x_i}^2}{2}} e^{i[k_x(k_{x_i})x - k_{z_r}(k_{x_i})z]} dk_{x_i} \\ \alpha_t(x, z) &= \frac{E_0 w}{\sqrt{2\pi}} \int_{-\infty}^{\infty} t(k_x(k_{x_i})) e^{-\frac{w^2 k_{x_i}^2}{2}} e^{i[k_x(k_{x_i})x + \text{sgn}(\mu_{\parallel})k_{z_t}(k_{x_i})z]} dk_{x_i}. \end{aligned} \quad (47)$$

It is worth to note that the reflected and transmitted beams are—due to the presence of the transmission and reflection amplitudes inside these integrals—not Gaussian beams any more. This makes them no longer have the symmetries of the incident beam. Thus, we need a criterion to define the direction of propagation of the transmitted and reflected beams. It seems plausible to define this direction tracing a circle of radius  $r$  from the center of the beam, and, for each  $r$ , look for the local maximum of  $|\alpha|^2$ . The curve formed of all this points will serve for terms of this specific beam as the “geometrical ray”. Perhaps this will be more clear when we show the beam in the following subsection.

It is convenient for both, calculations and analysis, to express the above relations regarding the composition of the beam in terms of dimensionless quantities. For this, we define  $\tilde{w} = k_0 w$  which is a measure of the waist of the beam relative to the wavelength of the modes in vacuum;  $(\tilde{k}_x, \tilde{k}_z) = (k_x, k_z)/k_0$ , a dimensionless version of the wave vector, relative to the wavenumber in vacuum;  $(\tilde{x}, \tilde{z}) = (x, z)/w$ , a measure of the position in units of the waist of the beam; and  $\tilde{\alpha} = \sqrt{2\pi}\alpha/E_0$ , the dimensionless complex amplitude.

In terms of these quantities, Equation (43) can be expressed equivalently as,

$$\tilde{\alpha}(\tilde{x}, \tilde{z}) = \int_{-\infty}^{\infty} e^{-\tilde{w}^2 \tilde{k}_{x_i}^2 / 2} e^{i\tilde{w}(\tilde{k}_x \tilde{x} + \tilde{k}_z \tilde{z})} d\tilde{k}_{x_i}. \quad (48)$$

Naturally, there are analogous dimensionless quantities for the reflected and transmitted beams (47). In terms

of  $\tilde{\alpha}$  and of the dimensionless version of the components of  $\overline{\tilde{\mu}}$ :  $\tilde{\mu}_{\parallel} = \mu_{\parallel}/\mu_0$  and  $\tilde{\mu}_{\perp} = \mu_{\perp}/\mu_0$  relative to vacuum, we also define

$$\begin{aligned} s_h &= \text{im} \left[ \left( \tilde{\alpha}_{\tilde{x}}/\tilde{\mu}_{\perp}, 0, \tilde{\alpha}_{\tilde{z}}/\tilde{\mu}_{\parallel} \right) \right] \\ s_b &= \text{im} \left[ \left( \tilde{\alpha}_{\tilde{x}}, 0, \tilde{\alpha}_{\tilde{z}} \right) \right], \end{aligned} \quad (49)$$

which are dimensionless measures of the averages of  $\mathcal{S}_H$  and  $\mathcal{S}_B$ , respectively.

We will now take a look at the results of numerical simulations of the refraction of the Gaussian beam. These computations were obtained through a custom c program and plotted in gnuplot with a little help of bash. The source code can be freely downloaded from our page<sup>1</sup>. For the plotting, we present here some numerical results with effective-medium anisotropic parameters from actual metamaterial experimental reports [43] and [44].

The first material is a laminate metamaterial (LM) made up of a succession of sheets of silver and silica. We took the effective properties at 400 nm of the seven-layered version. This material does not respond magnetically but has an electrical anisotropic permittivity. Its parallel component for this wavelength is  $\epsilon_{\parallel} = -3\epsilon_0$  while the orthogonal component is  $\epsilon_{\perp} = -17\epsilon_0$ . We ignored the imaginary components of the tensor in agreement with the main assumptions presented above. The results should be presented for  $p$ -polarization, but, in order to make a more straight comparison with the second material described below, we switch to  $s$  polarization and interchange  $\overline{\epsilon}$  for  $\overline{\mu}$ .

The second metamaterial is a split ring resonator (SRR). SRR's were the first constructed metamaterials in which negative refraction was observed. In order to obtain an isotropic response they were built by placing equal resonators on the cells of a cubic lattice. This SSR omitted the isotropization process, placing the resonators in parallel sheets, thus obtaining an uniaxial anisotropic metamaterial. At a microwave frequency of 1.8 GHz the effective properties (again, ignoring the imaginary part) are  $\mu_{\parallel} = \mu_0$  and  $\mu_{\perp} = 2.1\mu_0$ , while at 2.0 GHz we have  $\mu_{\parallel} = \mu_0$  and  $\mu_{\perp} = -\mu_0$ . Note that for both, the SRR and the LM we have  $n_{\parallel} = 1$ .

Some points to take into account when looking at the results of the simulations are:

1) Due to the dimensionless representation we are using, the units of length in the plots are the width of the beam. Therefore, a same plot with larger larger units of length is equivalent to a thinner beam and vice-versa. In all the figures presented here, we use a parameter  $\tilde{w} = k_0 w = 300$ . This means that the actual beam waist depends on the beam frequency; for example, for yellow light with a wavelength of 600 nm in vacuum, the waist would be of approximately 28  $\mu\text{m}$ , a really slim beam. Of course, we suppose that assume the beam is sufficiently wide with respect to the metamaterial components so as to retain the validity of the effective-medium theory and—of course—macroscopic electrodynamics.

2) The fields  $s_b$  and  $s_h$  are scaled differently. The use of large values of  $\tilde{\mu}_{\parallel}$  implies very different sizes of  $s_h$  and  $s_b$ , which makes it difficult to visualize them, so, for each given plot, they are rescaled in a way such that their maximum sizes are equal.

First of all and in order to clarify the idea we have been discussing about the refraction of a light beam, we show in **Figure 1** the plot of a beam seen from “far away”. This is the picture of a beam impinging from vacuum at an angle  $\theta_i = 5\pi/16$  over an isotropic material with the refractive index of diamond (2.4). We can see the incident, reflected and transmitted beams. And, as we said, the concentration of the field in this beam allows a natural definition of a direction.

The symmetry of the beam described in the preceding section makes us expect that in some approximation the propagation of the beam is represented by the propagation of the main mode. Thus, we also indicate the direction of  $s_b$  and  $s_h$  for the main mode; since for a plane wave this directions are constant, we plot lines in such directions passing through the center of the beam.

We present the results for the refraction of the beam at a vacuum-LM interface in **Figure 2** and **Figure 4**; and at a vacuum-SRR interface in **Figure 5** and **Figure 6**. The plots include the energy-density patterns, the field lines of  $s_h$  and  $s_b$  and the directions of these two fields for the main mode. For the same setup as in **Figure 2** we display in **Figure 3** the divergence of  $s_b$  given by Equation (32); we omitted to show the divergence of  $s_h$  since, as proved before, it is identically zero, and decided not to include the divergence corresponding to the other figures since they turn out to be very similar to **Figure 4**.

There are some features of these results that we would like to remark:

1) Unlike **Figure 1**, all the figures show an interference pattern between the incident and the reflected beam.

<sup>1</sup><http://www.fisica.unam.mx/personales/rbarrera/gaussian-beam>.

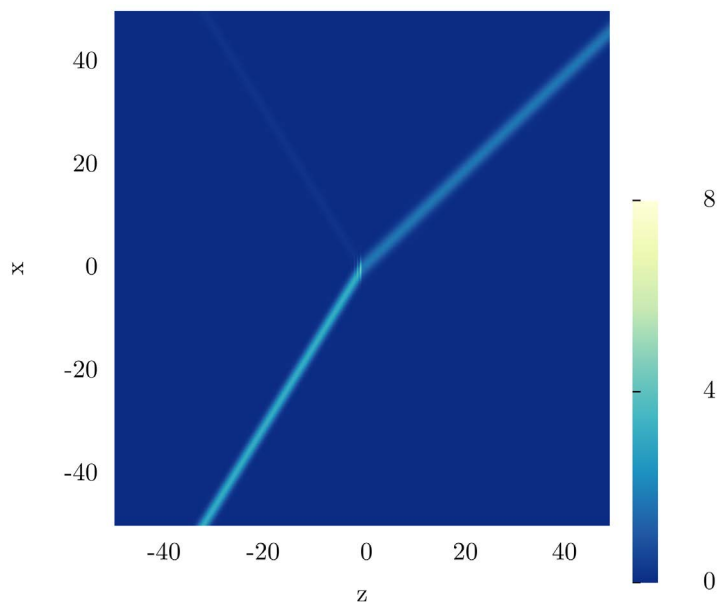


**Figure 1.** Gaussian beam refraction and reflection from vacuum into diamond, when viewed from far away.

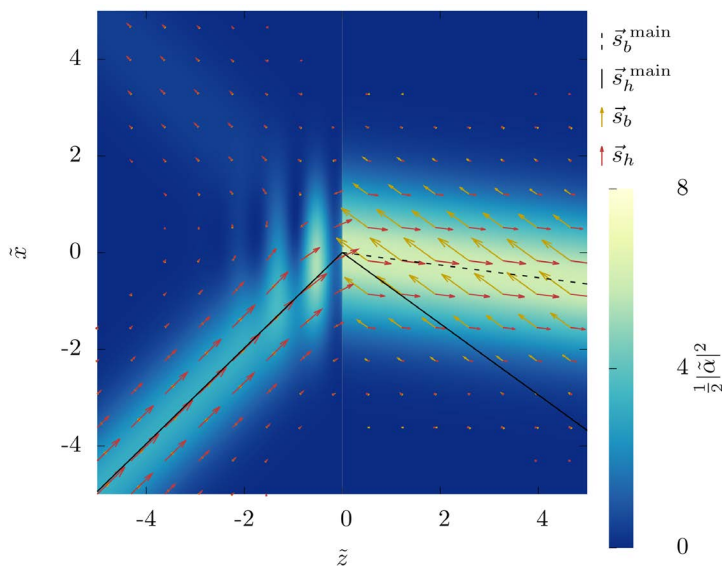


**Figure 2.** Refraction of the Gaussian beam from vacuum towards the LM for  $\lambda_0 = 400 \text{ nm}$  and  $\theta_i = 4\pi/16$ . We plot a measure of the energy density (in the color map), the  $s_b$  and  $s_h$  fields (as vector fields), and the direction of the  $s_h$  and  $s_b$  for the main mode of the beam (as lines).

A stationary field is established by this interference, just as it happens in the interference between incident and reflected plane waves on an interface, case in which the interference term is a function exclusively of  $z$ . This characteristic is somewhat preserved in the beam although it is highly localized (these plots are just windows of  $10 \times 10$  widths of the beam).

2) Away from the interference zone, the direction of both  $s_h$  and  $s_b$  fields does not vary appreciably. In particular in the transmitted beam, both fields seem to preserve their direction over all the plotted region. In the interference zone they bend continuously from the direction of incidence to the direction of reflection. When

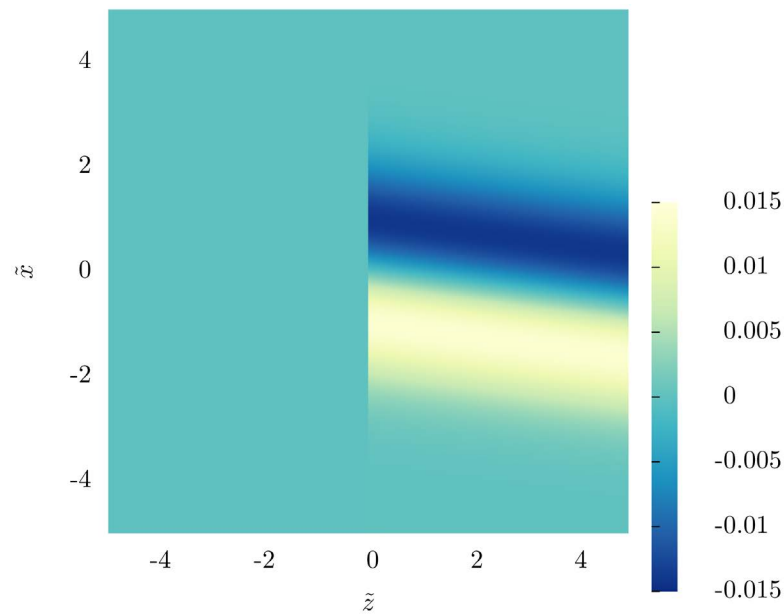


Figure 3. Divergence of  $s_b$  for the Gaussian beam of Figure 2.

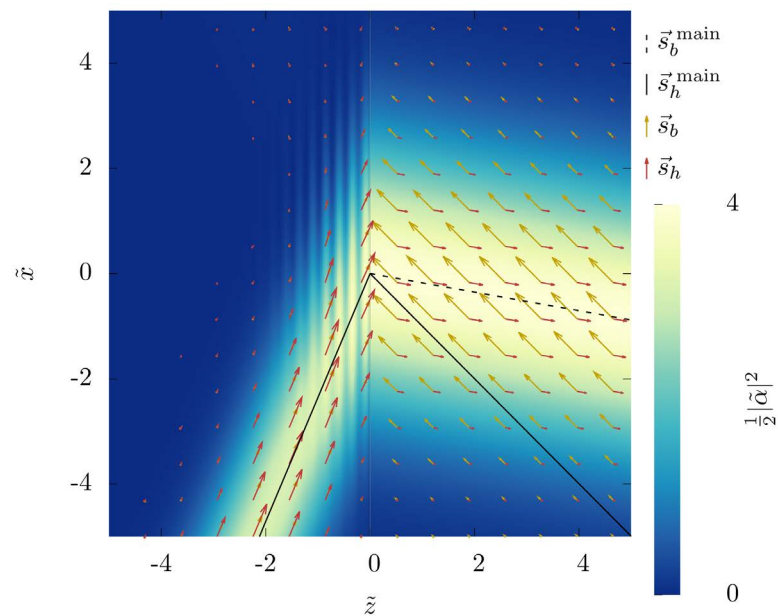


Figure 4. Refraction of the Gaussian beam from vacuum towards the LM for  $\lambda_0 = 400 \text{ nm}$  and  $\theta_i = 6\pi/16$ . We plot a measure of the energy density (in the color map), the  $s_b$  and  $s_h$  fields (as vector fields), and the direction of the  $s_h$  and  $s_b$  for the main mode of the beam (as lines).

viewed from far away, we would only notice an abrupt change in direction from the incidence to the refraction angle.

3) As expected, both  $s_h$  and  $s_b$  coincide in direction in vacuum. Their size is numerically the same, but, as explained before, we used a different scale for the magnitude of each field.

4) The “rays” of  $s_h^{\text{main}}$  and  $s_b^{\text{main}}$  are—with the exception of the interference zone—parallel to the  $s_h$  and  $s_b$  fields, respectively. If there is any deviation, it cannot be appreciated by only looking at the figure.

5) In all the simulations that we displayed, the line traced by the local maxima of  $|\tilde{\alpha}|^2$  described before coincided—without noticeable difference—with the line corresponding to  $\vec{s}_h^{\text{main}}$ .

6) The magnitude of both  $\vec{s}_b$  and  $\vec{s}_h$  is larger on the more “intense” parts of the beam, and decreases when getting away from it.

7) In **Figure 2** and **Figure 4** the transmitted beam seems more intense than the incident beam.

And last, perhaps the most important observations:

8) For all cases,  $\vec{s}_b$  has a small but quantifiable divergence along the transmitted beam. In all cases, it is negative in some regions and positive in others. A plot of this is displayed in **Figure 3**. This means that if  $\vec{s}_b$  is interpreted as an energy flux, there is energy flowing out in some regions of the beam, and energy flowing in in other regions of the beam, which requires a justification in physical terms.

9) Some of the basic refraction properties of the propagation of plane waves in uniaxial metamaterials referred in Section 3 are preserved in the case of the beam: a) Negative refraction is obtained when  $\tilde{\mu}_\perp$  is negative, as in **Figure 2**, **Figure 4** and **Figure 6**. b) The projection of  $\vec{s}_h$  over  $\vec{s}_b$  (the analogous of the projection of  $\mathcal{S}$  over  $\mathbf{k}$  for a plane wave) has the sign of  $\tilde{\mu}_\parallel$ —positive only for **Figure 5**—and is not tied to the sign of refraction.

10) In the metamaterial, the field  $\vec{s}_b$  is not parallel with  $\vec{s}_h$  in any of the cases presented here. And while  $\vec{s}_h$  follows the direction of the beam (whether in visual terms, or more quantitatively in terms of the line of maxima),  $\vec{s}_b$  clearly and distinctively does not point in the direction of the beam. It can even point in directions towards the interface, as in **Figure 2**, **Figure 4** and **Figure 6**.

This results reveal that for this beam the main wave represents an astonishingly good approximation to the beam in geometrical terms. In general, it is important to remark that such agreement is by no means obvious, since the energy and energy flux are not linear quantities; in fact, it does not happen in other less symmetrical beams, which we do not treat here for the sake of brevity.

The point labeled 6 about  $\vec{s}_b$  and  $\vec{s}_h$  having a larger magnitude within the beam is important, since in optics the intensity is defined as the magnitude of the energy flux. It could be thought that the choice of plotting

$i_u = \frac{1}{2}|\tilde{\alpha}|^2$  was in some way biased and that another choice would have lead to different results about the

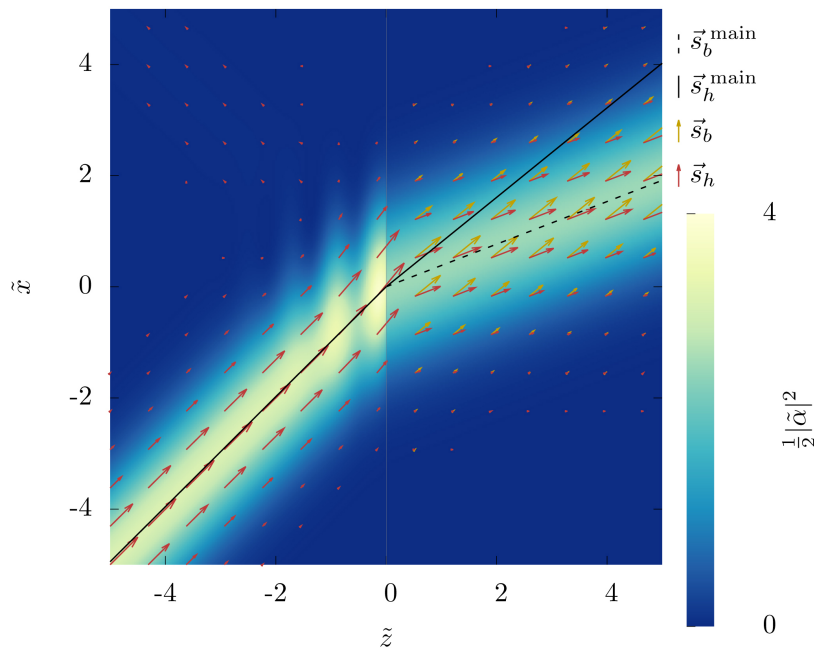


**Figure 5.** Refraction of the Gaussian beam from vacuum towards the SRR for  $\omega_0 = 1.8$  GHz and  $\theta_i = 4\pi/16$ . We plot a measure of the energy density (in the color map), the  $\vec{s}_b$  and  $\vec{s}_h$  fields (as vector fields), and the direction of the  $\vec{s}_h$  and  $\vec{s}_b$  for the main mode of the beam (as lines).

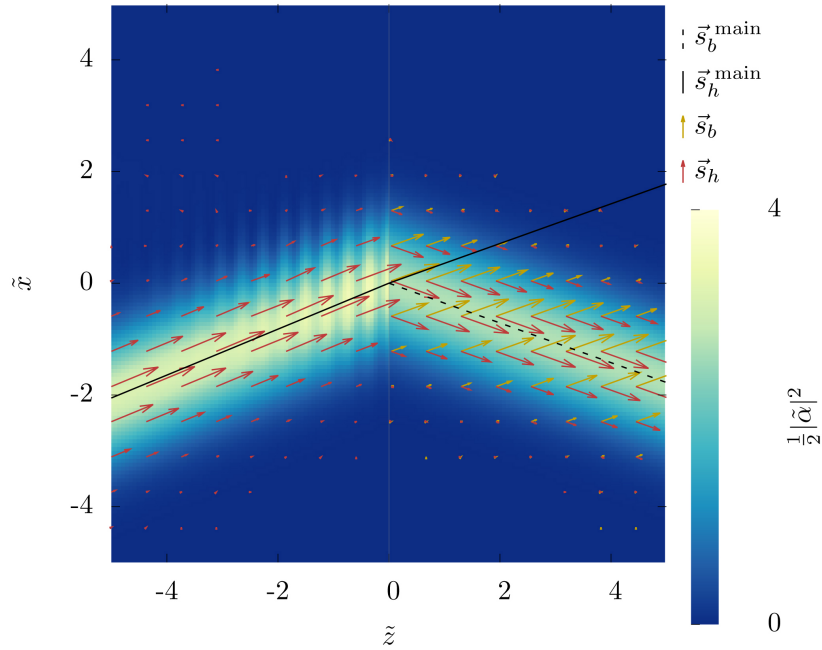


**Figure 6.** Refraction of the Gaussian beam from vacuum towards the SRR for  $\omega_0 = 2.0$  GHz and  $\theta_i = 2\pi/16$ . We plot a measure of the energy density (in the color map), the  $s_b$  and  $s_h$  fields (as vector fields), and the direction of the  $s_h$  and  $s_b$  for the main mode of the beam (as lines).

direction of  $s_b$ . But actually this is not the case, and we wish to quantify and elaborate briefly on this.

Let us define  $i_b = \|s_b\|$  and  $i_h = \|s_h\|$ . An important question is, taken this as intensities, how would the beam profile vary from the one obtained with the mean energy density  $i_u$ ? It should be clear that the quotient  $i_b/i_s$  is exactly 1 on vacuum; on the other side, within the metamaterial we calculated it numerically for the same setups presented in **Figure 2**, **Figures 4-6**; it is practically constant, with a slow variation in the  $x$  direction. For example, for the SRR and parameter values as in **Figure 6**, this ratio is about 1.2. The slow spatial variation in this proportion can be understood in terms of Equation (49), which allows us to write

$$\begin{aligned} \frac{i_b}{i_s} &= \frac{i_b}{\sqrt{\text{im}^2(\alpha^* \alpha_x)/\mu_\perp^2 + \text{im}^2(\alpha^* \alpha_z)/\mu_\parallel^2}} \\ &= \left[ \frac{1}{\mu_\perp^2} + \left( \frac{1}{\mu_\parallel^2} - \frac{1}{\mu_\perp^2} \right) \frac{\text{im}^2(\alpha^* \alpha_z)}{i_b^2} \right]^{-1/2}. \end{aligned} \tag{50}$$

Written in this way, we can recognize the term  $\text{im}^2(\alpha^* \alpha_z)/i_b^2$  as the square cosine of the angle formed between  $s_b$  and the  $z$  axis. As we observed in point 6b of the list above, this directions do not seem to vary along space. All this tells us that the beam profiles (the “shapes”) predicted by  $i_s$  and  $i_b$  are essentially the same, that they only vary in the prediction of the *intensity* of the transmitted beam.

On the other hand, note, from Equation (35) that the essential difference between  $i_u$  and  $i_b$  (or  $i_h$ , in view of the former conclusion) is the magnitude of the gradient of the phase of the electric field  $\|\nabla\phi_\alpha\|$  (which is clearly not constant). In **Figure 7** we can see the quotient  $i_u/i_h$ . This is essentially the magnitude of the gradient of phase, and, as it can be seen, except in the interference zone, it seems “constant”. The quotes here are because the value of that constant is one in the vacuum side and a different one on the metamaterial side.

The numerical analysis of these two quantities  $i_h/i_b$  and  $i_u/i_h$  show two important things: first, that the profile given by  $i_u$ ,  $i_b$  and  $i_s$  are essentially the same (and thus there is no bias with respect to this two fields in the choice of plotting  $\langle E^2 \rangle$ ); and second, that there is a difference with respect to the predictions of the intensities of the transmitted beams, which manifest in the abrupt change of  $i_h/i_b$  when passing from vacuum

to the metamaterial. This last observation is expected, since, for the polarization we are analyzing,  $E^2$  is continuous, while  $\mathbf{H}$  is not. The effect of this discontinuity is—at least for the cases we analyze—desirable from the point of view of experience, because, as **Figure 8** and **Figure 9** show, the profiles of  $i_h$  no longer have a more intense transmitted beam than the incident one, as it does happen in the corresponding **Figure 2** and **Figure 4**.

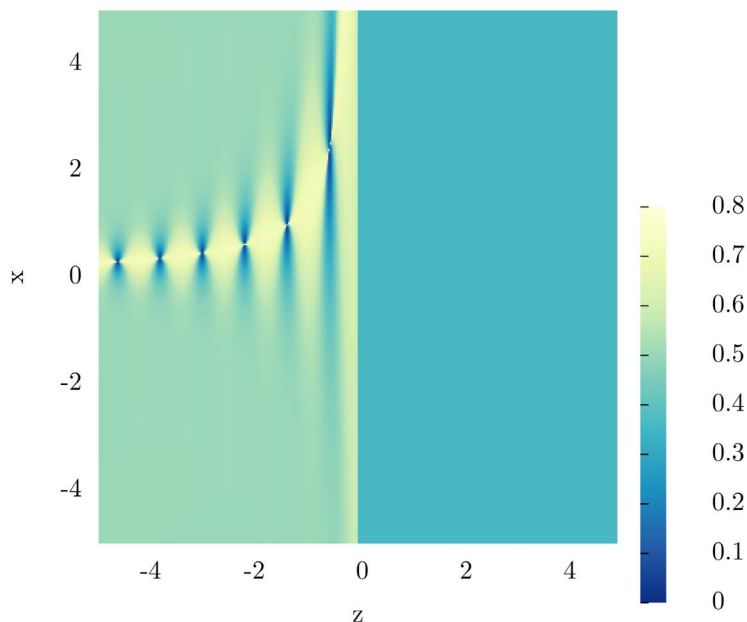


**Figure 7.** Proportion between  $|\tilde{\alpha}|^2$  and  $\|s_h\|$  for the SRR at 2 GHz and an incidence angle of  $\theta_i = 4\pi/16$ . This plot corresponds to the same parameters as **Figure 5**.

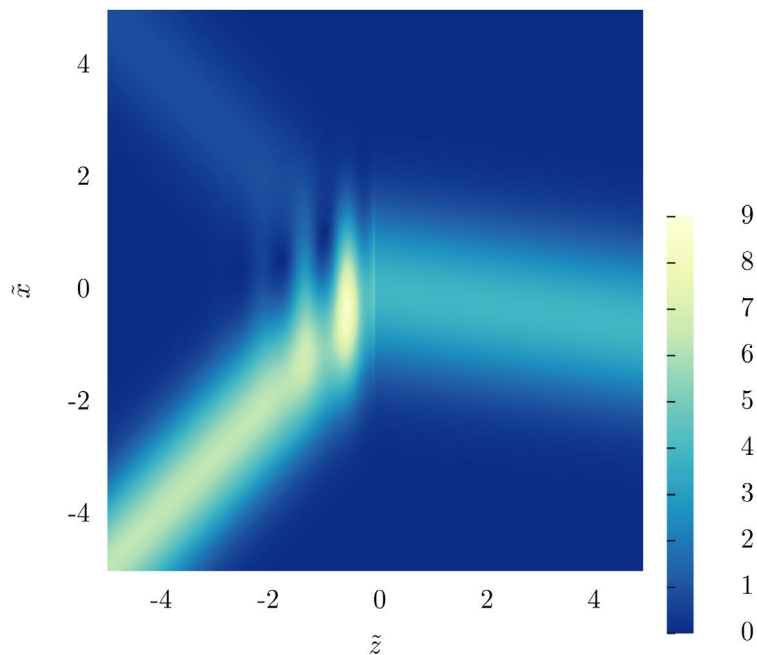


**Figure 8.** Magnitude of  $s_h$  for the same parameters of **Figure 2**.

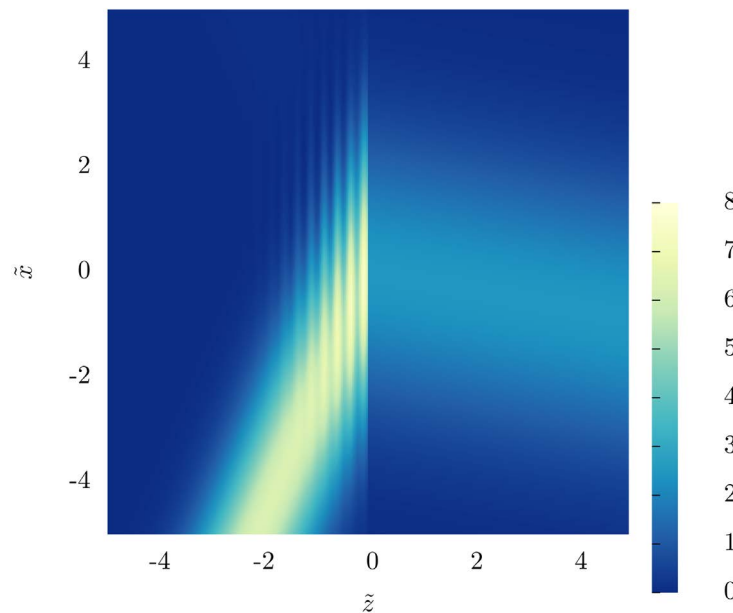


Figure 9. Magnitude of  $s_h$  for the same parameters of Figure 4.

The discussion of the intensity predictions of the two choices of the Poynting vector also leads to an interesting question: Since we define intensity as proportional to the energy density, one could ask if there exists a device capable of responding to this quantity. Consider an idealized “intensity detector” consisting of a small plane screen, whose detection result is the integration of the intensity over such surface. Center this detector in a point along the axis of the Gaussian beam. First, put the screen aligned with the axis and take a measure with this device. Afterwards, put the screen in the orthogonal position (remember this is a 2D beam) and take a second measure. Since in the first case the axis coincides with the line of maxima of intensity, the measure is necessarily greater than in the second. But our experience with detectors tells us this is not the case; in fact, it is exactly opposite. This is important because, since  $i_b$  and  $i_h$  produce the same intensity profiles, one could think that there is no practical difference if the flux comes from one or the other, because it is the profile what we measure. But if we accept that the detector in some way reacts to the energy flux (as a vector quantity) through the surface integral of its projection over the screen's normal, the maximum value would be obtained, with  $s_h$ , when the screen is orthogonal to the axis, while for  $s_b$  it would be obtained in different directions, as it can be seen in Figure 2, Figures 4-6. With this assumption, to measure the intensity at a given point one has to either *know* the direction of flow *a priori*, or rotate the detector (with normal  $\hat{n}$ ) in all possible directions, obtaining a measure of  $s \cdot \hat{n}$  for each direction; when this quantity is the greatest of all ( $s \cdot \hat{n}$ , with  $\hat{n}$  parallel to  $s$ ), one gets the intensity *and* the direction of the energy flow in that point.

It is also important to stress that the results we show here make evident that in general the ray directions in the formalism of geometrical optics and the notion of a ray as an idealized narrow beam (characterized by its intensity) are not equivalent.

## 6. Conclusions

We discussed the choice between two possible expressions for the Poynting vector: 1)  $\mathbf{S}_B = \mathbf{E} \times \mathbf{B} / \mu_0$  and 2)  $\mathbf{S}_H = \mathbf{E} \times \mathbf{H}$ , in order to discriminate which of them truly represents the direction of energy flow within anisotropic media. We construct a 2D monochromatic beam and calculate how this beam refracts at an interface between vacuum and an uniaxial anisotropic metamaterial, at frequency bands in which dissipation is negligible and with optical parameters unrestricted with respect to sign. The results obtained make us conclude that:

1) For *any* monochromatic 2D field and in *any* medium (even absorbing ones) there is a “ray” formalism which extends the eikonal formalism. The directions of those “rays” are given, in *s* polarization, by  $\mathbf{E} \times \mathbf{B} / \mu_0$ , and in *p* polarization by  $\mathbf{D} \times \mathbf{H} / \epsilon_0$ .

2) The directions of the rays, defined in this work as idealized narrow beams, coincide within the simulations presented here with the Poynting vector if we define it as  $\mathbf{E} \times \mathbf{H}$  rather than  $\mathbf{E} \times \mathbf{B}/\mu_0$ . Thus:

a) The “ray” formalism described in conclusion 1 (and therefore the eikonal formalism) is *not equivalent* to the “intuitive” notion of light ray given by idealized narrow beams.

b) Following the geometrical criterion proposed here, the field  $\mathbf{E} \times \mathbf{H}$  is more suitable as a definition of the energy flux compared to  $\mathbf{E} \times \mathbf{B}/\mu_0$ .

c) The definition of light ray as an idealized narrow beam and the results obtained here allow us to associate the light rays with the field lines of the  $\mathbf{E} \times \mathbf{H}$  vector.

## Acknowledgements

We would like to thank Vadim A. Markel for stimulating discussion at the early stages of this project; Augusto García-Valenzuela and Roberto Alexander-Katz for their comments and the full review of the paper; and to Víctor Romero-Rochín for very interesting discussions related to topics about energy conservation. One of us (CP-L) must acknowledge that the work presented here was supported by a graduate scholarship granted by Consejo Nacional de Ciencia y Tecnología (México).

## References

- [1] Brillouin, L. (1960) Wave Propagation and Group Velocity. Academic Press, New York.
- [2] Jackson, J.D. (1998) Classical Electrodynamics. 3rd Edition, John Wiley & Sons Inc., Hoboken.
- [3] Landau, L.D. and Lifshitz, E.M. (1984) Electrodynamics of Continuous Media. Pergamon Press, Oxford.
- [4] Slepian, J. (1942) *Journal of Applied Physics*, **13**, 512-518. <http://dx.doi.org/10.1063/1.1714903>
- [5] Lai, C.S. (1981) *American Journal of Physics*, **49**, 841-843. <http://dx.doi.org/10.1119/1.12719>
- [6] Peters, P.C. (1982) *American Journal of Physics*, **50**, 1165. <http://dx.doi.org/10.1119/1.13024>
- [7] Romer, R.H. (1982) *American Journal of Physics*, **50**, 1166-1168. <http://dx.doi.org/10.1119/1.12903>
- [8] Gough, W. (1982) *European Journal of Physics*, **3**, 83-87. <http://dx.doi.org/10.1088/0143-0807/3/2/005>
- [9] Henrotte, F. and Hameyer, K. (2006) *IEEE Transactions on Magnetics*, **42**, 903-906. <http://dx.doi.org/10.1109/TMAG.2006.871441>
- [10] Barrera, R.G., Mochán, W.L., García-Valenzuela, A. and Gutiérrez-Reyes, E. (2010) *Physica B Condensed Matter*, **405**, 2920-2924. <http://dx.doi.org/10.1016/j.physb.2010.01.004>
- [11] Feynman, R.P., Leighton, R.B. and Sands, M. (1964) The Feynman Lectures on Physics. Volume 2, Addison-Wesley, Upper Saddle River.
- [12] Mansuripur, M. and Zakharian, A.R. (2009) *Physical Review E*, **79**, Article ID: 026608. <http://dx.doi.org/10.1103/physreve.79.026608>
- [13] Furry, W.H. (1969) *American Journal of Physics*, **37**, 621-636. <http://dx.doi.org/10.1119/1.1975729>
- [14] Campos, I. and Jiménez, J.L. (1992) *European Journal of Physics*, **13**, 117-121. <http://dx.doi.org/10.1088/0143-0807/13/3/003>
- [15] Nelson, D.F. (1996) *Physical Review Letters*, **76**, 4713-4716. <http://dx.doi.org/10.1103/PhysRevLett.76.4713>
- [16] Roche, J.J. (2000) *American Journal of Physics*, **68**, 438-449. <http://dx.doi.org/10.1119/1.19459>
- [17] Ginzburg, V.L. (1973) *Soviet Physics Uspekhi*, **16**, 434. <http://dx.doi.org/10.1070/PU1973v016n03ABEH005193>
- [18] Abraham, M. (1909) *Annalen der Physik*, **322**, 891-921. <http://dx.doi.org/10.1007/bf03018208>
- [19] Minkowsky, H. (1910) *Mathematische Annalen*, **68**, 472-525. <http://dx.doi.org/10.1007/BF01455871>
- [20] Pfeifer, R.N.C. and Nieminen, N.R. (2007) *Reviews of Modern Physics*, **79**, 1197-1216. <http://dx.doi.org/10.1103/RevModPhys.79.1197>
- [21] Mischenko, M.I. (2014) *Journal of Quantitative Spectroscopy & Radiative Transfer*, **146**, 4-33. <http://dx.doi.org/10.1016/j.jqsrt.2014.02.033>
- [22] Markel, V.A. (2008) *Optics Express*, **16**, 19152-19168. <http://dx.doi.org/10.1364/OE.16.019152>
- [23] Marqués, R. (2009) *Optics Express*, **17**, 7322-7324. <http://dx.doi.org/10.1364/OE.17.007322>
- [24] Markel, V.A. (2009) *Optics Express*, **17**, 7325-7327. <http://dx.doi.org/10.1364/OE.17.007325>
- [25] Mansuripur, M. (2011) *Optics Communications*, **284**, 594-602. <http://dx.doi.org/10.1016/j.optcom.2010.08.079>

- [26] Silveirinha, M.G. (2009) *Physical Review B*, **80**, Article ID: 235120. <http://dx.doi.org/10.1103/physrevb.80.235120>
- [27] Silveirinha, M.G. (2010) *Physical Review B*, **82**, Article ID: 037104. <http://dx.doi.org/10.1103/physrevb.82.037104>
- [28] Richter, F., Florian, M. and Henneberger, K. (2008) *Europhysics Letters*, **81**, 67005-67009. <http://dx.doi.org/10.1209/0295-5075/81/67005>
- [29] Obukhov, Y.N. and Hehl, F.W. (2003) *Physics Letters A*, **311**, 277-284. [http://dx.doi.org/10.1016/S0375-9601\(03\)00503-6](http://dx.doi.org/10.1016/S0375-9601(03)00503-6)
- [30] Kinsler, P., Favaro, A. and McCall, M.W. (2009) *European Journal of Physics*, **30**, 983-993. <http://dx.doi.org/10.1088/0143-0807/30/5/007>
- [31] Richter, F., Henneberger, K. and Florian, M. (2010) *Physical Review B*, **82**, Article ID: 037103. <http://dx.doi.org/10.1103/physrevb.82.037103>
- [32] Simovski, C.R. and Tretyakov, S.A. (2007) *Physical Review B*, **75**, Article ID: 195111. <http://dx.doi.org/10.1103/physrevb.75.195111>
- [33] Tretyakov, S.A. (2005) *Physics Letters A*, **343**, 231-237. <http://dx.doi.org/10.1016/j.physleta.2005.06.023>
- [34] Ziolkowski, R.W. and Heyman, E. (2001) *Physical Review E*, **64**, Article ID: 056625.
- [35] Cui, T.J. and Kong, J.A. (2004) *Physical Review B*, **70**, Article ID: 205106. <http://dx.doi.org/10.1103/physrevb.70.205106>
- [36] Ruppin, R. (2002) *Physics Letters A*, **299**, 309-312. [http://dx.doi.org/10.1016/S0375-9601\(01\)00838-6](http://dx.doi.org/10.1016/S0375-9601(01)00838-6)
- [37] Boardman, A.D. and Marinov, K. (2006) *Physical Review B*, **73**, Article ID: 165110. <http://dx.doi.org/10.1103/physrevb.73.165110>
- [38] Costa, J.T., Silveirinha, M.G. and Alù, A. (2011) *Physical Review B*, **83**, Article ID: 165120. <http://dx.doi.org/10.1103/physrevb.83.165120>
- [39] Alonso, M.A. (2010) *Phase-Space Optics: Fundamentals and Applications*. McGraw-Hill Professional, New York.
- [40] Kline, M. and Kay, I.W. (1965) *Electromagnetic Theory and Geometrical Optics*. Interscience Publishers, Hoboken.
- [41] Malacara-Hernández, D. and Malacara-Hernández, Z. (2003) *Handbook of Optical Design*. 2nd Edition, CRC Press, Boca Raton. <http://dx.doi.org/10.1201/9780203912942>
- [42] Prieto-López, C. and Barrera, R.G. (2012) *Physica Status Solidi (b)*, **249**, 1110-1118. <http://dx.doi.org/10.1002/pssb.201100747>
- [43] Papadakis, G.T., Yeh, P. and Atwater, H.A. (2014) *Physical Review B*, **91**, Article ID: 155406.
- [44] Chen, H., Zhang, J., Bai, Y., Luo, Y., Ran, L. and Jiang, Q. (2006) *Optics Express*, **14**, 12944-12949. <http://dx.doi.org/10.1364/OE.14.012944>



**Submit or recommend next manuscript to SCIRP and we will provide best service for you:**

Accepting pre-submission inquiries through Email, Facebook, LinkedIn, Twitter, etc.

A wide selection of journals (inclusive of 9 subjects, more than 200 journals)

Providing 24-hour high-quality service

User-friendly online submission system

Fair and swift peer-review system

Efficient typesetting and proofreading procedure

Display of the result of downloads and visits, as well as the number of cited articles

Maximum dissemination of your research work

Submit your manuscript at: <http://papersubmission.scirp.org/>

# Complex Systems Are Not Black Boxes but Solvable Systematical Problems; Proven by Simulation and New Conception

**Deok-Soo Cha**

Research Center, Eho Technology Co., Busansi, Korea

Email: chdsoo@hotmail.com, ehoeng25@naver.com

Received 9 July 2016; accepted 27 August 2016; published 30 August 2016

Copyright © 2016 by author and Scientific Research Publishing Inc.

This work is licensed under the Creative Commons Attribution International License (CC BY).

<http://creativecommons.org/licenses/by/4.0/>



Open Access

---

## Abstract

**This paper presents an innovative solution regarding complex systems to scientists, and prepares a novel system simulator for complex systems. A complex system in nature is not a black box but a solvable systematic problem. The solution is not derived from conventional physics based on reductionism, but rather from engineering sciences such as the feedback systems analysis method and engineering principles. Furthermore, this paper presents the conception of the solution to scientists for solving the problem. Moreover, nobody can doubt this research based on simulator. Complex systems are not mysterious science and not black box.**

## Keywords

**Complex Systems, Feedback System, System Simulator, System Analysis Theory**

---

## 1. Introduction

This paper presents an incredible scientific solution for complex systems based on multidisciplinary physics and engineering to scientists engaged in those fields. Complex systems represent unsolvable problems in science, such as black holes, sun magnetism, nuclear fusion, nuclear theory, super conductor, plasma, turbulence, climate change, and the subconscious in human. Many scientists have said that these phenomena are mysterious science that can be solved by God alone and not by humans. Many geniuses in the field of physics have attempted to find answers to these questions over the last century, but nobody has succeeded yet.

In addition, famous research organizations, such as the Santa Fe Institute (SFI) in the United States, have worked to study the complexity originating from complex systems. The SFI was established by Dr. Murray Gell-Mann (1929) and other scientists based on their mission of statement (<http://www.santafe.edu/about/mission-and-vision/>).

However, they have not yet succeeded in spite of the money, time, and effort expended by many scientists. This leaves us to wonder: Does science have a solution to these problems?

The answer is here. If someone discovered a solution for the algorithm of complex systems in other sciences, the other approximately ten million physicists in the world might say that it is an unbelievable miracle in science, or a trick. However, the author would like to present a report on complex systems to these scientists for careful reading. The report was previously published in this journal in October 2015 [1]; it contains an incredible scientific result, which is as follows. Natural systems, such as the stock market system, ecological systems, or thermodynamic systems, are not black boxes; rather they are solvable systematic problems such as a closed-loop system with a negative feedback property based on energy conservation ([https://en.wikipedia.org/wiki/Conservation\\_of\\_energy](https://en.wikipedia.org/wiki/Conservation_of_energy)), as shown in **Figure 1**. This is the basic concept in the solution.

This can be analyzed by the feedback systems analysis method ([https://en.wikipedia.org/wiki/Control\\_theory](https://en.wikipedia.org/wiki/Control_theory)) based on the automatic control theory [2] in engineering. Nevertheless, this is a serious problem for physicists. Most physicists do not use the analysis method in conventional physics, based on reductionism. Accordingly, most physicists cannot read the report written by the method and they cannot accept the research result. Why do not they use the method? There is a hidden serious and important thing in physical science. It is involved with the principal rule of physics (<https://en.wikipedia.org/wiki/Physics>), according to which, most physical phenomena in nature must be “quantitative and qualitative”, and “measurable and reversible”; physicists deal it with the physical science. (It is a keyword in this paper.) The other hand, the external behavior of complex systems such as the stock market or ecosystems is not measurable and reversible within quantitative and qualitative. Instead, it must be solved by a time series function in real time, similar to the systems analysis method in engineering. Refer to Section 3 for more details. Despite of, no argument to physicists; because most physicists have good mathematical capabilities, they begin to study the principle immediately. This is a good idea for physicists and can be vital for the cooperation between physicists and engineers.

In addition, the author proudly provides a system simulator (shown in **Figure 2**), designed using an electrotype for scientists to prove the research. It is a novel design, which can simulate the behavior of dynamic systems for any type of system in nature; moreover, it can be demonstrated by anyone, at any time, and anywhere. If anyone has a doubt about this research, the author will support a simulator to him/her freely. Finally, complexity is not a mysterious science; this research provides a revolutionary scientific result in modern science. Therefore, if the solution is sufficient, it represents an incredible scientific success and a great discovery, similar to the Copernican theory. Maybe a human is the winner.

Nevertheless, there is another serious issue to consider. Most scientists will not welcome the new solution presented in this report. The following are the possible reasons for this response. Many scientists have a fixed idea, and so it is possible that they absolutely believe that complexity is an unsolvable problem, and they cannot visualize anything that contradicts this belief and is beyond their assertions. Indeed, the report may be shocking and unbelievable for them. Therefore, they may fall into a dilemma, because they cannot contradict against the experimental results. Apart from these concerns, the author would like to stress that the solution is not dangerous

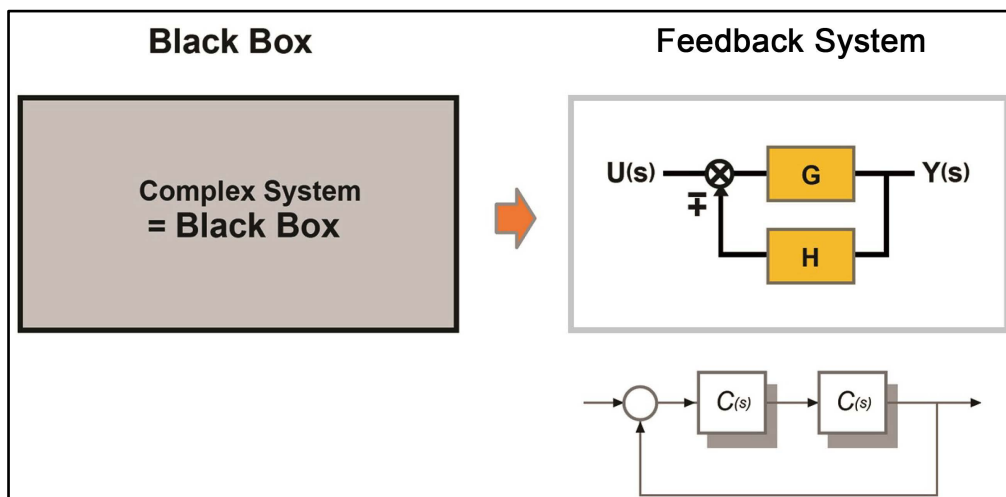


**Figure 1.** Mechanism of a complex system.

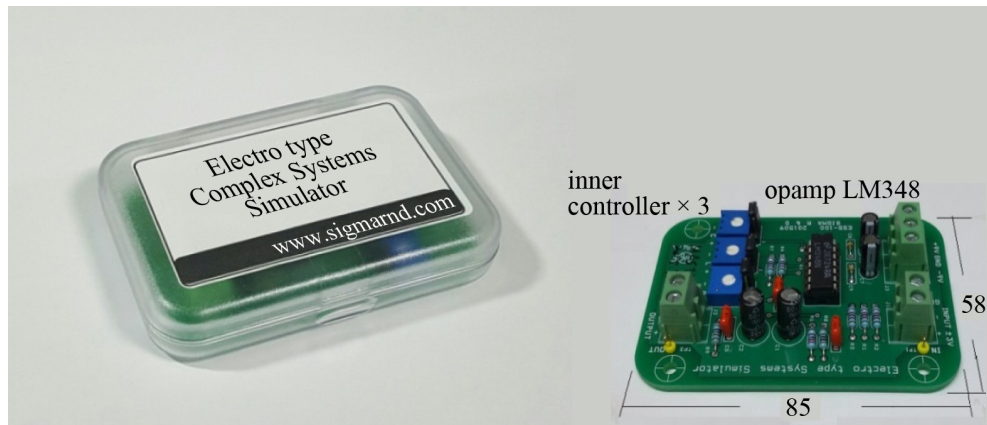


**Figure 2.** Electrotype complex systems simulator (50% size) and the system simulator prototype (available eBay).

to anyone, and that no damage can occur to anybody in case of failure.

## 2. Experiment and Result

### 2.1. Experiment

However, the author would like to explain the experiment again using the complex system simulator developed for this, because, many scientists do not believe this research yet. The author has additionally prepared a video to supplement this report (<https://youtu.be/-EnU4L5uH5o>), the experiment was performed in a sequence of two steps, as shown below.

In step one, the characteristics of all systems can be tested by their response to a unit step function  $u(t)$ . We add a constant value as a unit step function  $u(t)$  to the simulator using a function generator ([https://en.wikipedia.org/wiki/Function\\_generator](https://en.wikipedia.org/wiki/Function_generator)), and we can then observe the output  $y(t)$  as displayed on an oscilloscope (<https://en.wikipedia.org/wiki/Oscilloscope>) as shown in **Figure 3**, where the blue line represents the input  $U(s)$  and the yellow curve represents the output  $Y(s)$ . In addition, the original function  $y(t)$  is given by Equation (1)

$$y(t) = 1 - A \cdot e^{-Bt} \cdot \sin(W \cdot t + \varphi), \quad (1)$$

where  $A$ ,  $B$ ,  $W$ ,  $\varphi$  are constant, and  $t$  is time.

We can find that the output  $y(t)$  increases gradually by the input  $u(t)$  with a sine wave. This is a well-known characteristic of feedback systems, such as the mechanism as shown in **Figure 1**, and is similar to a transient phenomenon in electronics. (Further details are provided in [2].) Nevertheless, we can observe the characteristics of complexity though the yellow curve shown in **Figure 3**, which is described by Equation (1). For example, the curve displays an initial phenomenon in **Figure 3** that is similar to the butterfly effect, whereas the periodic decreasing curve in **Figure 3** is similar to the self-organization or fractal. Moreover, the output and input in **Figure 3** are not reversible because they have chaotic properties. This is a basic property in complex systems, as shown in Equation (1). For further details about complexity, refer to [4] and other reference books.

In step two, we consider many other cases, where the source of a complex system, such as stock market systems or thermodynamic systems, is not constantly static but is variably dynamic. We add an irregular value as a random function  $r(t)$  into  $U(S)$ . The response to the random function  $r(t)$  can be observed in **Figure 4**; the yellow curve in the figure displays a time-varying output  $y(t)$ , and we cannot determine anything. Nevertheless, we can make the following observations throughout this simulation, as shown in **Figure 3**: The four kinds of behavior as mentioned previously *overlap* as chaotic, fractal, self-organization, butterfly-effect ([https://en.wikipedia.org/wiki/Complex\\_systems](https://en.wikipedia.org/wiki/Complex_systems)), and other phenomena. Similar to the dynamic daily stock price, dynamic daily climate, or dynamic individuals in ecosystems; in addition, we have found important properties: The input and output are not measurable and reversible, or quantitative and qualitative; and if the input source of a complex system disappears, the output product converges to zero with time. Incidentally, we wonder why

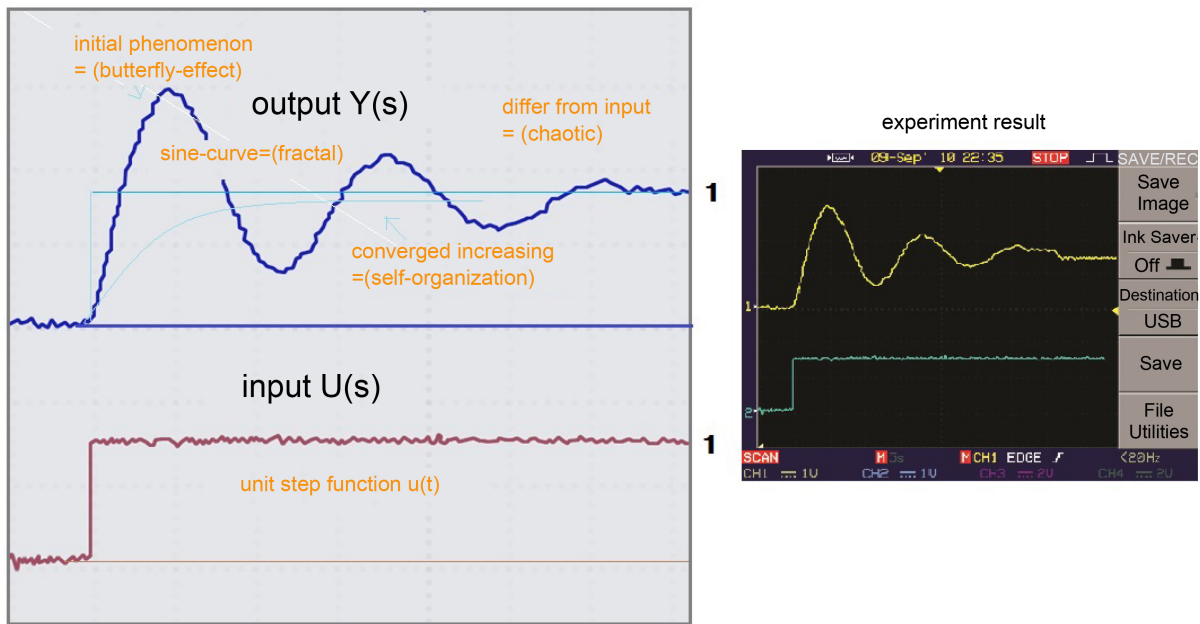


**Figure 3.** Response of a unit step function. The lower blue curve shows the unit step function, whereas the upper yellow curve shows the output of the complex system.

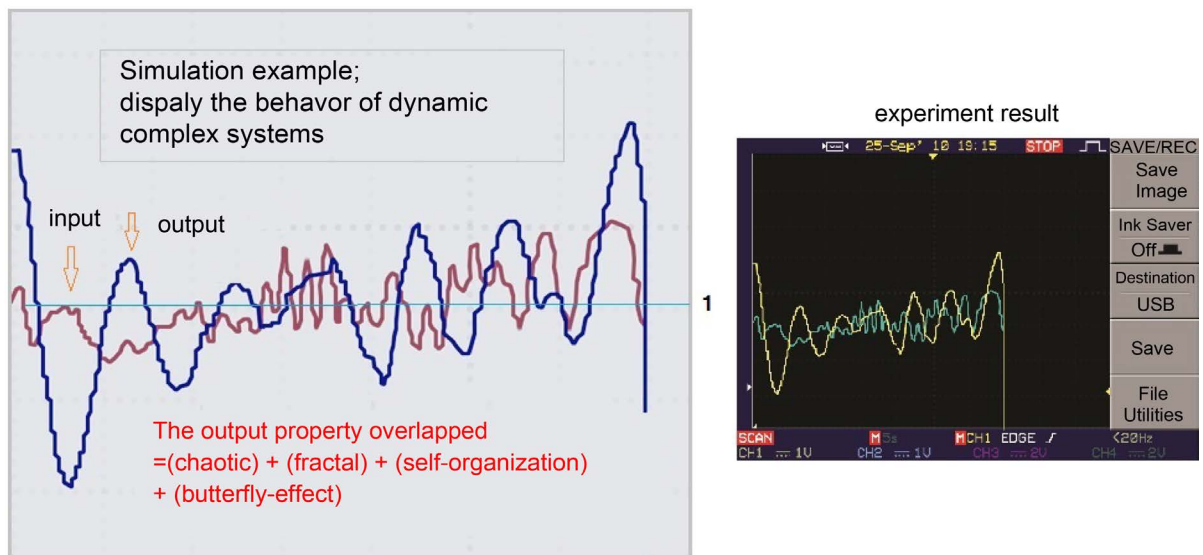


**Figure 4.** Response of a random function. The blue curve shows the random function, and the yellow curve shows the output of the complex system.

Equation (1) is not reversible between input and output, and further, stock prices cannot be forecast easily and completely.

## 2.2. Results

We can confirm many characteristics of complex systems through the experiment described above. For instance, complex systems never overflow, never run away to destruction, and are certainly not dangerous, but safe, because once the entropy of the input disappears, the output converges to zero based on the law of conservation of energy. Moreover, complex systems can be externally controlled by humans, but not completely as daily stock prices in the market. Therefore, complex systems are solvable systematic problems and are not black boxes. In

people cannot forecast stock prices; if we could, we would be rich. Why cannot we forecast the prices? Because addition, the most important aspects of this study are the dynamic characteristics of the input source and the output products of complex systems. These properties are non-quantitative, non-qualitative, non-measurable, and non-reversible, as illustrated by the many verified complex systems in nature, including economic systems, thermodynamic systems, or ecosystems.

### 3. Discussion

#### 3.1. Conception

This paper contains a revolutionary solution for complexity in the science of the complex. This solution is not dangerous and no damage to anyone. Moreover, it is easily applicable to science. Therefore, the author would like to share with scientists (including those of the SFI) the origin of the concept. The concept of the solution was discovered in 2008 when the author was cultivating an interest in another science, namely economics, and was surveying complexity in physics. Previously, the author had already studied a course in electrical power and control engineering.

One day, the author discovered strange properties from the stock market while analyzing the pricing of stocks. One of these properties was that the relationship between the transaction volume of a stock and the variations in the stock price are multiplied. Another property is that the equation describing the relationship between a seller and a buyer,  $\lim_{t \rightarrow \infty} \frac{d}{dt} \{P(t) + P^{-1}(t - D)\} = 0$ , [where  $P(t)$ ; stock price in real time,  $D$ ; time delay,  $t$ ; time], is

based on the law of conservation of energy. Therefore, the relationship between a seller and a buyer in the market is an inverse relationship, and they always counterbalance each other with negative feedback that is related to the “law of supply and demand” in economics. Indirectly, this provided the insight that that the stock market is a feedback system and not a black box, as shown in **Figure 1**. For more details, refer to [1].

Furthermore, the author observed a similar phenomenon in other sciences as well. For example, non-linear dynamic systems in a variety of fields exhibit this phenomenon, including representative social economics, nuclear reactor systems in engineering, thermodynamic systems, and ecological systems in nature. Thus, the author discovered that it is possible to solve complex systems using the systems analysis method. Therefore, the author started reporting this discovery to many physical journals. Unfortunately, the author is aware that most scientists in conventional physics do not use or understand systems analysis theory. Consequently, the author decided to design a system simulator that could be used to demonstrate the concept, as shown in **Figure 2**, based on the basic model system shown in **Figure 1**. The system simulator can be manufactured at a cost under U.S. \$100; further details on this topic are omitted for now.

#### 3.2. Simulator Designing

(Simulator) The design concept for the system simulator is as follows. The basic system feedback model and an equivalent electronic circuit are shown in **Figure 5**, and are published here for use by scientists. It cleverly comprises an operational amplifier that acts as a comparator, integrator, and differentiator.

The corresponding system transfer function  $F(s)$  is

$$F(s) = \frac{G(S)}{1 + G(s)H(s)} = \frac{B}{s^2 + As + B}. \quad (2)$$

Next, the electronic circuit transfer function  $F(s)$  is

$$F(s) = \frac{\left(\frac{1}{RC}\right)}{s^2 + \left(\frac{rc}{RC}\right)s + \left(\frac{1}{RC}\right)} = \frac{B}{s^2 + As + B}. \quad (3)$$

In Equation (3), the elements  $[R]$  and  $[r]$  are adjustable via the embedded controller in the simulator. This implies that anyone can experimentally test any system at any time.

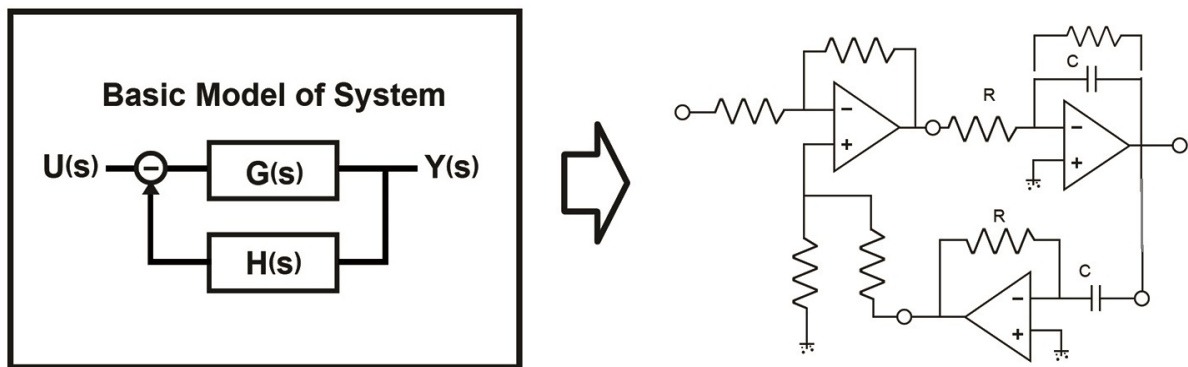


Figure 5. Basic feedback system and the equivalent electronic circuit [3].

#### 4. Conclusion

Complex systems in nature are not black boxes; rather they are solvable systematic problems. If anyone has a doubt about this research, the author is willing to provide a simulator for him/her. If this paper is acceptable, it provides a revolutionary scientific solution for science, similar to relativity. Furthermore, the scientists (or SFI) can review this report with honor. The author concludes that no more research for complexity and chaos will be disappeared in future.

#### References

- [1] Cha, D.-S. (2015) *Journal of Modern Physics*, **6**, 1927-1934.  
<http://www.scirp.org/Journal/PaperInformation.aspx?PaperID=60738>  
<http://dx.doi.org/10.4236/jmp.2015.613198>
- [2] Kuo, B. and Golnaraghi, F. (2003) *Automatic Control System*. John Wiley & Sons, Hoboken.  
<http://dl.acm.org/citation.cfm?id=535813>
- [3] Cha, D.-S. (2012) *KIEE in Korea*, 45-54. <http://www.kiee.or.kr/data/ebook/2012-03/EBook.htm>
- [4] Casti, J.L. (1995) *Complexification*. Harper Perennial.  
<http://www.goodreads.com/book/show/1888200.Complexification>



Scientific Research Publishing

**Submit or recommend next manuscript to SCIRP and we will provide best service for you:**

Accepting pre-submission inquiries through Email, Facebook, LinkedIn, Twitter, etc.

A wide selection of journals (inclusive of 9 subjects, more than 200 journals)

Providing 24-hour high-quality service

User-friendly online submission system

Fair and swift peer-review system

Efficient typesetting and proofreading procedure

Display of the result of downloads and visits, as well as the number of cited articles

Maximum dissemination of your research work

Submit your manuscript at: <http://papersubmission.scirp.org/>

# Quantum Statistical Theory of Superconductivity in MgB<sub>2</sub>

S. Fujita<sup>1</sup>, A. Suzuki<sup>2</sup>, Y. Takato<sup>3</sup>

<sup>1</sup>Department of Physics, University at Buffalo, State University of New York, Buffalo, NY, USA

<sup>2</sup>Department of Physics, Faculty of Science, Tokyo University of Science, Tokyo, Japan

<sup>3</sup>Okinawa Institute of Science and Technology Graduate University, Okinawa, Japan

Email: [fujita@buffalo.edu](mailto:fujita@buffalo.edu), [asuzuki@rs.kagu.tus.ac.jp](mailto:asuzuki@rs.kagu.tus.ac.jp), [yoichi.takato@oist.jp](mailto:yoichi.takato@oist.jp)

Received 30 June 2016; accepted 28 August 2016; published 31 August 2016

Copyright © 2016 by authors and Scientific Research Publishing Inc.

This work is licensed under the Creative Commons Attribution International License (CC BY).

<http://creativecommons.org/licenses/by/4.0/>



Open Access

---

## Abstract

A quantum statistical theory of the superconductivity in MgB<sub>2</sub> is developed regarding it as a member of the graphite intercalation compound. The superconducting temperature  $T_c$  for MgB<sub>2</sub>, C<sub>8</sub>K ≡ KC<sub>8</sub>, CaC<sub>6</sub>, are 39 K, 0.6 K, 11.5 K, respectively. The differences arise from the lattice structures. In the plane perpendicular to the c-axis, B's form a honeycomb lattice with the nearest neighbour distance  $a_0$  while Mg's form a base-hexagonal lattice with the nearest neighbour distance  $\sqrt{3}a_0$  above and below the B-plane distanced by  $c_0$ . The more compact B-plane becomes superconducting due to the electron-phonon attraction. Starting with the generalized Bardeen-Cooper-Schrieffer (BCS) Hamiltonian and solving the generalized Cooper equation, we obtain a linear dispersion relation  $\varepsilon = cp$  for moving Cooper pairs. The superconducting temperature  $T_c$  identified as the Bose-Einstein condensation temperature of the Cooper pairs in two dimensions is given by  $T_c = 1.954\hbar cn_0^{1/2} k_B^{-1}$ , where  $n_0$  is the Cooper pair density,  $k_B$  the Boltzmann constant. The lattices of KC<sub>8</sub> and CaC<sub>6</sub> are clearly specified.

## Keywords

Crystal Structure, BCS Hamiltonian, Electron-Phonon Interaction, Cooper Pairs, Bose-Einstein Condensation, Superconductivity

---

## 1. Introduction

Nagamatsu *et al.* [1] reported in 2001 superconductivity at 39 K in magnesium diboride MgB<sub>2</sub>. MgB<sub>2</sub> forms a lattice closely related to that of a graphite intercalation compound (GIC). It is similar to NaC<sub>2</sub> composition-wise, but the

lattice structures are distinct as shown below. The superconducting temperatures  $T_c$  of  $\text{MgB}_2$  and  $\text{NaC}_2$  are 39 K and 5 K, respectively. This difference arises from the lattice structures. Canfield and Crabtree [2] wrote a comprehensive review in *Physics Today* (2003). From the isotope effect study [2] [3] they concluded that the B-plane contains a honeycomb lattice which becomes superconducting at 0 K, while the Mg-plane is base-hexagonal and is metallic. Their conjectured lattice structure of  $\text{MgB}_2$  is shown in Ref. 2, **Figure 3**. The superconducting state occurs at 0 K, where the entropy of an electron-phonon system vanishes. The third law of the thermodynamics applies. The crystal must be specified with the location of all atoms. Ref. 2, **Figure 3** contains only the B-lattice and Mg-lattice with unspecified lattice constants. We must specify lattice systems with basic lattice units with the lattice constants. A currently presumed lattice for  $\text{MgB}_2$  [4] is a fully intercalated graphite compound similar to that in  $\text{NaC}_2$ . We propose a different lattice. The two lattices have the same first neighbour configurations but different second nearest neighbours. Our proposed lattice has a lower Coulomb energy and should be realized in practice.

We shall develop a quantum statistical theory of the superconductivity in  $\text{MgB}_2$ , starting with a generalized Bardeen-Cooper-Schrieffer (BCS) Hamiltonian [5] and calculating everything using the standard quantum statistical methods. Canfield-Crabtree's and our lattices have nearly the same energies if the first neighbour configurations are examined. The second neighbour configurations are different. Each  $\text{B}^+$  in our lattice is surrounded by six  $\text{Mg}^+$ 's while each  $\text{B}^+$  in Canfield-Crabtree's lattice is surrounded by three  $\text{Mg}^+$ . Hence our lattice is more stable. In the course of the development, we clearly specify the lattices of  $\text{C}_8\text{K} \equiv \text{KC}_8$  and  $\text{CaC}_6$ .

## 2. Electron Dynamics

Following Ashcroft and Mermin (AM) [6], we assume that “electrons” and “holes” in solids run as wave packets (not point-particles). We adopt the semiclassical model of electron dynamics in solids [6]. It is necessary to introduce a  $k$ -vector:

$$\mathbf{k} = k_x \hat{e}_x + k_y \hat{e}_y + k_z \hat{e}_z, \quad (1)$$

where  $\hat{e}_x$ ,  $\hat{e}_y$ ,  $\hat{e}_z$  are the orthonormal vectors, since the  $k$ -vectors are involved in the semiclassical equation of motion:

$$\hbar \dot{\mathbf{k}} \equiv \hbar \frac{d\mathbf{k}}{dt} = q(\mathbf{E} + \mathbf{v} \times \mathbf{B}), \quad (2)$$

where  $q = -e$  is the electron charge, and  $\mathbf{E}$  and  $\mathbf{B}$  are the electric and magnetic fields, respectively. The vector

$$\mathbf{v} \equiv \frac{1}{\hbar} \frac{\partial \varepsilon}{\partial \mathbf{k}} \quad (3)$$

is the electron velocity, where  $\varepsilon = \varepsilon(\mathbf{k})$  is the energy.

If the electron is in a continuous energy range (energy band), then it will be accelerated by the electric force  $q\mathbf{E}$ , and the material is a conductor. If the electron's energy is in a forbidden band (energy gap), it does not move under a small electric force, and the material is insulator. If the acceleration occurs only for a mean free time (inverse of scattering frequency)  $\tau$ , the conductivity  $\sigma$  for a simple metal is given by Drude's formula [6]:

$$\sigma = q^2 n \tau / m^*, \quad (4)$$

where  $n$  is the electron density and  $m^*$  the effective mass.

We consider a graphene which forms a 2D honeycomb lattice. The Wigner-Seitz (WS) unit cell, a rhombus, contains two C's. We showed in our earlier work [7] [8] that graphene has “electrons” and “holes” based on the rectangular unit cell. We briefly review our calculations below. We assume that the “electron” (“hole”) wave packet has the charge  $-e$  ( $+e$ ) and a size of the rectangular unit cell, generated above (below) the Fermi energy  $\varepsilon_F$ . We showed [7] earlier that a) the “electron” and “hole” have different charge distributions and different effective masses; b) that the “electrons” and “holes” move in different easy channels; c) that the “electrons” and “holes” are thermally excited with different activation energies  $(\varepsilon_1, \varepsilon_2)$ , and d) that the “electron” activation energy  $\varepsilon_1$  is smaller than the “hole” activation energy  $\varepsilon_2$ :

$$\varepsilon_1 < \varepsilon_2. \quad (5)$$

Hence, “electrons” are the majority carriers in graphene. The thermally activated electron densities are given by

$$n_j(T) = n_j e^{-\varepsilon_j/k_B T}, \quad n_j = \text{constant}, \quad (6)$$

where  $j = 1$  and  $2$  represent the “electron” and “hole”, respectively.

### 3. Lattice Structures in $C_8K = KC_8$ , $CaC_6$ and $MgB_2$

Graphite is composed of graphene layers stacked in the manner ABAB... along the  $c$ -axis. We may choose an orthogonal unit cell shown in **Figure 1**.

The carbons (circles) in the A (B) planes are shown in dark (light) gray circles.

The unit cell contains 16 C's. The two rectangles (white solid lines) are stacked vertically with the interlayer separation,  $c_0 = 3.35 \text{ \AA}$ , much greater than the nearest neighbour distance between two C's,  $a_0 = 1.42 \text{ \AA}$ :

$$c_0 \gg a_0. \quad (7)$$

The unit cell has three side-lengths:

$$b_1 = 3a_0, \quad b_2 = 2\sqrt{3}a_0, \quad b_3 = 2c_0. \quad (8)$$

Clearly, the system is periodic along the orthogonal directions with the three periods  $(b_1, b_2, b_3)$  given in Equation (8). Hence, the system can be considered as orthorhombic with the sides  $(b_1, b_2, b_3)$ ,  $b_1 \neq b_2$ ,  $b_1 \neq b_3$ ,  $b_2 \neq b_3$ .

The negatively charged “electron” (with the charge  $-e$ ) in graphite are welcomed by the positively charged  $C^+$  when moving vertically up or down in the plane. Then, the easy direction for the “electrons” is vertical. The easy direction for the “holes” is horizontal. There are no hindering hills for “holes” moving horizontally. Hence, the “electron” in graphite has the lower activation energy  $\varepsilon$  than the “hole”:  $\varepsilon_1 < \varepsilon_2$ . Then, “electrons” are the majority carriers in graphite. The thermoelectric power (Seebeck coefficient) measurements by Kang *et al.* [9] show that the majority carriers in graphite are “electrons” in agreement with our theory.

We now consider GIC. Let us first take  $C_8K$ . The  $K^+$  ions should enter as interstitials and occupy the sites away from the positive ions  $C^+$ . We see in **Figure 1** that the center of the unit cell is empty. Each  $K^+$  should occupy the midpoint between two graphene layers. The 3D unit cell contains 16 C's and 2 K's. Alkali metal GIC, including  $C_8Li$ ,  $C_8Rb$ , should form similar lattices. Next we consider  $C_6Ca$ . Carbons (C) in graphite form a honeycomb lattice in the A plane as shown in **Figure 1**. There are eight (8) C's and four (4) hexagon centers, (two full circles, two half-circles and four quarter-circles). If we fill the hexagon centers with C's, then we obtain twelve (12) C's in the 2D unit cell. Similarly the configuration of the B-plane and that one below is prescribed. There are  $2 \times 12$  C's in the planes A and B, and  $2 \times 2$  Ca's between the planes for  $C_6Ca$ . The composition ratio 6:1 is correct. After the C-filling, the C-plane becomes primitive (base)-hexagonal and has a  $60^\circ$  rotation symmetry. The primitive unit cell contains six (6) C's. Two Ca's are likely to occupy below the centers of the primitive cells located at the two-light gray circles in **Figure 1**. A real 3D  $C_6Ca$  is obtained by stacking the  $C_6Ca$  sheets in the manner ABAB... We note that the structure of  $C_6Ca$  is significantly more compact than that of  $C_8K$ .  $C_6Yb$  should have a similar lattice structure. GIC  $C_4Na$  ( $C_3K$ ,  $C_2Na$ ) should have the same 12 C-sheets and 3 Na (4 K, 6 Na) intersheets.

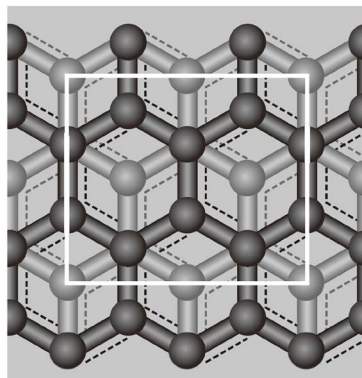


**Figure 1.** An orthogonal unit cell (white solid lines) viewed from the top for graphite. The carbons (circles) in the A (B) planes are shown in dark (light) gray circles.

Consider now  $\text{MgB}_2$ . It is only natural to start with the B-plane since this plane becomes superconducting at 0 K. Let us look at the top sheet in **Figure 1**. Within the white rectangle, there are eight (8) balls and four (4) vacant hexagons. If B's occupy the ball sites and Mg's occupy the hexagon-centers sites in the neighbour sheet above (or below), then we obtain the most likely lattice. The composition ratio 2:1 is correct. The B-plane contains a honeycomb lattice with a nearest neighbour distance  $a_0$  with a  $120^\circ$  rotation symmetry. The Mg-plane contains a base-hexagonal lattice with the nearest neighbour distance  $\sqrt{3}a_0$ . Crystals Mg and B are known divalent and trivalent hexagonal metals [6]. Since the B-plane in  $\text{MgB}_2$  is more compact with the smaller lattice constant, the B-plane is likely to become superconducting at the lowest temperatures. Note that all ions position are specified. Ions  $\text{Mg}^+$  and  $\text{B}^+$  are positively charged so that they tend to stay away among and between them.

Our lattice and Canfield-Crabtree's are different in the second nearest neighbour configuration. Each  $\text{B}^+$  in our lattice is surrounded by six  $\text{Mg}^+$  while each  $\text{B}^+$  in Canfield-Crabtree's lattice is surrounded by three  $\text{Mg}^+$ . Hence our lattice is more stable. The B-plane contains a honeycomb lattice of B's for both. Our Mg-plane contains a base-hexagonal lattice of the nearest neighbour distance  $\sqrt{3}a_0$ . In summary we found that a) the B-honeycomb lattice has smaller nearest neighbour distance  $a_0$  than the Mg hexagonal lattice with the nearest neighbour distance  $\sqrt{3}a_0$ . The more compact means the higher conduction electron density; b) The centers of mass (CM) of hexagons are displaced upward by a short distance  $a_0/2$  to take advantage of the smaller repulsive Coulomb energy. There is a mismatch between the B-plane and the Mg-plane centers, a unique feature for  $\text{MgB}_2$ .

#### 4. The Hamiltonian

The countability and statistics of the fluxons (magnetic flux quanta) are the fundamental particle properties. We postulate that the fluxon is a half-spin fermion with zero mass and zero charge.

We assume that the magnetic field  $\mathbf{B}$  is applied perpendicular to the graphene plane. The 2D Landau level energy,

$$\varepsilon = \hbar\omega_c \left( N_L + \frac{1}{2} \right), \quad \omega_c \equiv eB/m^*, \quad (9)$$

with the states  $(N_L, k_y)$ ,  $N_L = 0, 1, 2, \dots$ , have a great degeneracy (no  $k_y$ -dependence). The  $m^*$  is the effective mass of an "electron". Following Zhang, Hansson and Kivelson [10], we introduce composite (c-) particles. The Center-of-Mass (CM) of *any* c-particle moves as a fermion or a boson. That is, the eigenvalues of the CM momentum are limited to 0 or 1 (unlimited) if the composite contains an odd (even) number of elementary fermions. This rule is known as the *Ehrenfest-Oppenheimer-Bethe's* (EOB's) *rule* [11]. Hence the CM motion of the composite containing an electron and  $Q$  fluxons is bosonic (fermionic) if  $Q$  is odd (even). The system of the c-bosons condenses below some critical temperature  $T_c$  and exhibits a superconducting state while the system of c-fermions shows a Fermi liquid behavior.

A longitudinal phonon, acoustic or optical, generates a charge density wave, which affects the electron (fluxon) motion through the charge displacement (current). Let us first consider the case of superconductivity. The phonon exchange between two electrons shown in **Figure 2** generates a transition in the electron states with the effective interaction

$$\mathcal{V}_{\text{eff}} = |V_q|^2 \frac{\hbar\omega_q}{\left( \varepsilon_{|k+q} - \varepsilon_k \right)^2 - \left( \hbar\omega_q \right)^2}, \quad (10)$$

where  $\varepsilon_k$  is the electron energy,  $\hbar\omega_q$  the phonon energy, and  $V_q$  the electron-phonon interaction strength.

An electric current ( $\mathbf{J}$ ) loop generates a magnetic field (flux)  $\mathbf{B}$  while a magnetic flux  $\mathbf{B}$  is surrounded by diamagnetic currents  $\mathbf{J}$ . Thus the currents  $\mathbf{J}$  and the magnetic field  $\mathbf{B}$  are coupled. The exchange of a phonon between an *electron* and a *fluxon* also generates a transition in the electron states with the effective interaction:

$$|V_q V_q'| \frac{\hbar\omega_q}{\left( \varepsilon_{|k+q} - \varepsilon_k \right)^2 - \left( \hbar\omega_q \right)^2}, \quad (11)$$

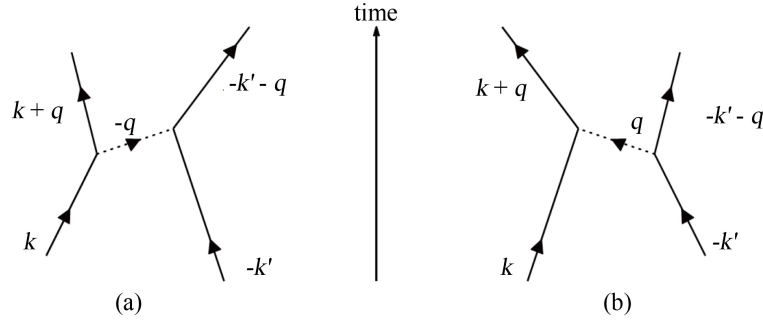


**Figure 2.** Electron’s (phonon’s) motions are represented by solid (dotted) lines, and the time is measured upwards. Two phonon exchange processes (a) and (b) generate the momenta change from the initial pair state  $(\mathbf{k}, -\mathbf{k}')$  to the final states  $(\mathbf{k} + \mathbf{q}, -\mathbf{k}' - \mathbf{q})$ .

where  $V'_q$  ( $V_q$ ) is the fluxon-phonon (electron-phonon) interaction constant. The Landau oscillator quantum number  $N_L$  is omitted; the bold  $\mathbf{k}$  denotes the momentum ( $k_y$ ) and the italic  $k$  ( $=|\mathbf{k}|$ ) the magnitude. There are two processes, one with the *absorption* of a phonon with momentum  $\mathbf{q}$  and the other with the *emission* of a phonon with momentum  $-\mathbf{q}$ , see **Figure 3(a)** and **Figure 3(b)**, which contribute to the effective interaction with the energy denominators  $(\varepsilon_{|\mathbf{k}+\mathbf{q}|} - \varepsilon_k - \hbar\omega_q)^{-1}$  and  $(\varepsilon_{|\mathbf{k}+\mathbf{q}|} - \varepsilon_k + \hbar\omega_q)^{-1}$ , generating Equation (11). The interaction is attractive (negative) and most effective when the states before and after the exchange have the same energy ( $\varepsilon_{|\mathbf{k}+\mathbf{q}|} - \varepsilon_k = 0$ ) as for the degenerate 2D LL.

BCS [5] assumed the existence of Cooper pairs [12] in a superconductor, and wrote down a Hamiltonian containing the “electron” and “hole” kinetic energies and the pairing interaction Hamiltonian with the phonon variables eliminated. We start with a BCS-like Hamiltonian  $\mathcal{H}$  for the QHE: [13]

$$\mathcal{H} = \sum'_k \sum_s \varepsilon_k^{(1)} n_{ks}^{(1)} + \sum'_k \sum_s \varepsilon_k^{(2)} n_{ks}^{(2)} + \sum'_k \sum_s \varepsilon_k^{(3)} n_{ks}^{(3)} - \sum'_q \sum'_k \sum'_k' \sum'_s v_0 \left[ B_{k'qs}^{(1)\dagger} B_{kqs}^{(1)} + B_{k'qs}^{(1)\dagger} B_{kqs}^{(2)\dagger} + B_{k'qs}^{(2)} B_{kqs}^{(1)} + B_{k'qs}^{(2)} B_{kqs}^{(2)\dagger} \right], \quad (12)$$

where  $n_{ks}^{(j)} \equiv c_{ks}^{(j)\dagger} c_{ks}^{(j)}$  is the number operator for the “electron” (1) (“hole” (2), fluxon (3)) at momentum  $\mathbf{k}$  and spin  $s$  with the energy  $\varepsilon_{ks}^{(j)}$ , with annihilation (creation) operators  $c$  ( $c^\dagger$ ) satisfying the Fermi anti-commutation rules:

$$\{c_{ks}^{(i)}, c_{k's'}^{(j)\dagger}\} \equiv c_{ks}^{(i)} c_{k's'}^{(j)\dagger} + c_{k's'}^{(j)\dagger} c_{ks}^{(i)} = \delta_{\mathbf{k}, \mathbf{k}'} \delta_{s, s'} \delta_{i, j}, \quad \{c_{ks}^{(i)}, c_{k's'}^{(j)}\} = 0. \quad (13)$$

The fluxon number operator  $n_{ks}^{(3)}$  is represented by  $a_{ks}^\dagger a_{ks}$  with  $a$  ( $a^\dagger$ ) satisfying the anti-commutation rules:

$$\{a_{ks}, a_{k's'}^\dagger\} = \delta_{\mathbf{k}, \mathbf{k}'} \delta_{s, s'}, \quad \{a_{ks}, a_{k's'}\} = 0. \quad (14)$$

The phonon exchange can create electron-fluxon composites, bosonic or fermionic, depending on the number of fluxons. The CM of any composite moves as a fermion (boson) if it contains an odd (even) numbers of elementary fermions. The electron (hole)-type c-particles carry negative (positive) charge. Electron (hole)-type Cooper-pair-like c-bosons are generated by the phonon-exchange attraction from a pair of electron (hole)-type c-fermions. The pair operators  $B$  are defined by

$$B_{kq,s}^{(1)\dagger} \equiv c_{k+q/2,-s}^{(1)\dagger} a_{-k+q/2,-s}^\dagger, \quad B_{kq,s}^{(2)} \equiv a_{-k+q/2,-s} c_{k+q/2,-s}^{(2)}. \quad (15)$$

The prime on the summation in Equation (12) means the restriction:

$$0 < \varepsilon_{ks}^{(j)} < \hbar\omega_D, \quad \omega_D = \text{Debye frequency}. \quad (16)$$

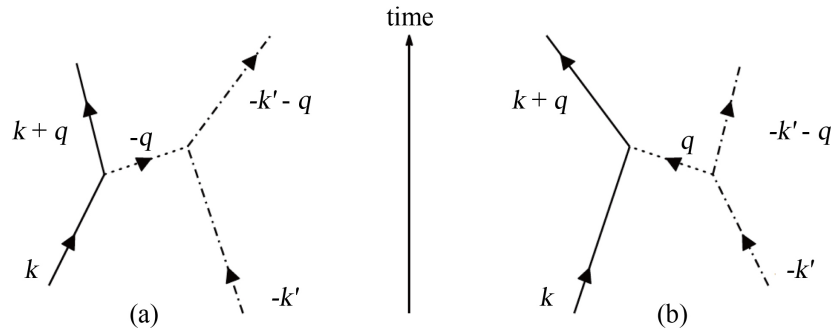


**Figure 3.** Fluxon's motion is represented by dot-dashed lines. The phonon exchange processes (a) and (b) generate the momenta change from the initial (electron, fluxon) state  $(k, -k')$  to the final states  $(k+q, -k'-q)$ .

The pairing interaction terms in Equation (12) conserve the charge. The term  $-v_0 B_{kq_s}^{(1)\dagger} B_{kq_s}^{(1)}$ , where  $v_0$  is the pairing strength, generates a transition in electron-type c-particle states. Similarly, the exchange of a phonon generates a transition between hole-type c-particle states, represented by  $-v_0 B_{kq_s}^{(2)\dagger} B_{kq_s}^{(2)}$ . The phonon exchange can also pair-create (pair-annihilate) electron (hole)-type c-boson pairs, and the effects of these processes are represented by  $-v_0 B_{kq_s}^{(1)\dagger} B_{kq_s}^{(2)\dagger}$  ( $-v_0 B_{kq_s}^{(1)} B_{kq_s}^{(2)}$ ).

The Cooper pair, also called the pairon, is formed from two “electrons” (or “holes”). The pairons move as bosons, which are shown in Appendix. Likewise the c-bosons may be formed by the phonon-exchange attraction from two like-charge c-fermions. If the density of the c-bosons is high enough, then the c-bosons will be Bose-condensed and exhibit a superconductivity.

The pairing interaction terms in Equation (12) are formally identical with those in the generalized BCS Hamiltonian [13]. Only we deal here with c-fermions instead of conduction electrons.

The c-bosons, having the linear dispersion relation, can move in all directions in the plane with the constant speed  $(2/\pi)v_F^{(j)}$  [13]. For completeness we show the linear dispersion relation in Appendix. The supercurrent is generated by  $\mp$  c-bosons monochromatically condensed, running along the sample length. The supercurrent density (magnitude)  $j$ , calculated by the rule:

$$j = (e^* : \text{carrier charge}) \times (n_0 : \text{carrier density}) \times (v_d : \text{carrier drift velocity}) \quad (17)$$

is given by

$$j \equiv e^* n_0 v_d = e^* n_0 \frac{2}{\pi} |v_F^{(1)} - v_F^{(2)}|, \quad (18)$$

where  $e^*$  is the *effective charge* of carriers. The induced Hall field (magnitude)  $E_H$  equals  $v_d B$ . The magnetic flux is quantized:

$$B = n_\phi \Phi_0, \quad n_\phi = N_\phi / A \quad (19)$$

where  $N_\phi$  is the fluxon number, and

$$\Phi_0 \equiv h/e. \quad (20)$$

Hence we obtain the Hall resistivity as

$$\rho_H \equiv \frac{E_H}{j} = \frac{v_d B}{e^* n_0 v_d} = \frac{1}{e^* n_0} n_\phi \Phi_0 = \frac{n_\phi}{e^* n_0} \left( \frac{h}{e} \right). \quad (21)$$

For the integer QHE at  $\nu = 1$ , we have  $e^* = e$ ,  $n_\phi = n_0$ . Hence, we obtain  $\rho_H = h/e^2$ , the plateau value observed.

The supercurrent generated by equal numbers of  $\pm$  c-bosons condensed monochromatically is neutral. This is reflected in our calculations in Equation (18). The supercondensate whose motion generates a supercurrent must

be neutral. If it has a charge, it would then be accelerated indefinitely by any external electric field because the impurities and phonons cannot stop the supercurrent to grow. That is, the circuit containing a superconducting sample and a battery must be burnt out if the supercondensate is not neutral. In the calculation of  $\rho_H$  in Equation (21), we used the *unaveraged* drift velocity  $v_d = (2/\pi) \left| v_F^{(1)} - v_F^{(2)} \right|$ , which is significant. *Only* the unaveraged drift velocity cancels out  $v_d$  exactly from numerator/denominator, leading to an exceedingly accurate plateau value.

We now extend our theory to include elementary fermions (electron, fluxon) as members of the c-fermion set. We can then treat the 2D superconductivity and the QHE in a unified manner. The c-boson containing one electron and one fluxon can be used to describe the principal QHE. Important pairings and effects are listed below: a) a pair of conduction electrons, superconductivity; b) c-fermions and fluxon, QHE; c) a pair of like-charge conduction electrons with two fluxons, QHE in graphene.

## 5. Superconductivity in $C_8K$ , $CaC_6$ and $MgB_2$

### 5.1. Preliminaries

#### 5.1.1. “Electrons”, “Holes” and “Phonons”

The conduction electrons (“electrons”, “holes”) are excited based on the orthogonal unit cells. As mentioned earlier the “electrons” are the majority carriers in both graphene and graphite. The excitation energy for the “electrons” is smaller than for the “holes”. Phonons are generated based on the same orthogonal unit cells. Phonons are bosons, and hence can be generated with no activation energies. The phonons are distributed, following the Planck distribution function:

$$f_p(\varepsilon) = \left[ \exp(\varepsilon/k_B T) - 1 \right]^{-1}, \quad (22)$$

which is a sole function of the Kelvin temperature  $T$ .

As an example consider acoustic phonons with a linear dispersion relation:

$$\varepsilon = sp, \quad (23)$$

where  $s$  is the sound speed. The phonon size may be characterized by the average wave length:

$$\lambda = s/k. \quad (24)$$

The average size of phonons at the room temperature is greater by a few orders of magnitudes than the electron size.

#### 5.1.2. The Ground-State Cooper Pair (Pairon) Energy

Cooper solved the Cooper equation [Ref. 12, Equation (1)] with a negative interaction energy constant,  $-v_0$ , and obtained the ground-state pairon energy:

$$w_0 = \frac{-2\hbar\omega_D}{\exp[2/v_0\mathcal{D}(0)] - 1}, \quad (25)$$

where  $\omega_D$  = Deby frequency,  $\mathcal{D}(0) = \mathcal{D}(\varepsilon_F = 0)$  = density of states at the Fermi energy. The energy  $w_0$  is singular at  $v_0 = 0$ . Hence, this bound-state energy  $w_0$  cannot be obtained by a perturbation theory. For illustration, consider a hydrogen atom levels problem with a negative Coulomb interaction  $\mathcal{V}$ . The bound states and energies are obtained by directly solving the Schrödinger equation with the full Hamiltonian containing the kinetic energy and the interaction energy  $\mathcal{V}$ . The Cooper pair is formed from two “electrons” (or “holes”). Likewise the c-bosons may be formed by the phonon-exchange attraction from c-fermions and fluxons. If the density of the c-bosons is high enough, then the c-bosons will be Bose-condensed and exhibit a superconductivity.

### 5.2. The Superconductivity in GIC and $MgB_2$

The superconductivity occurs only in regular crystals. That is, it occurs only in crystals *and not* in liquids.  $C_8K$  and graphene have a  $120^\circ$  rotation symmetry.  $C_6Ca$  has a base-hexagonal ( $60^\circ$  rotation) symmetry.

C<sub>8</sub>K has graphene sheets, and each sheet is likely to become superconducting below the critical temperatures  $T_c$ . The numbers of “electrons” and “holes” depend on the environments arising from the lattice structures. Since the lattice structures are very different in C<sub>8</sub>K and C<sub>6</sub>Ca, the critical temperatures should be different significantly.

BCS [5] used the fermionic pair operator equation.

$$B_{k_0}^2 \equiv B_{k_0} B_{k_0} = 0, \quad (26)$$

constructed a ground-state vector and obtained a ground-state energy of an electron-phonon system:

$$W_0 = 2Nw_0, \quad (27)$$

where  $N$  is the pairon number per spin and  $w_0$  the ground-state energy of the pairon, see Equation (17). The center-of-mass (CM) of the pairons move as bosons. That is, the eigenvalues of the pairon number operator  $n_q$  are unlimited:

$$n'_q = 0, 1, 2, \dots, \quad (28)$$

which is shown below.

The number operator in the  $k$ - $q$  representation

$$n_{kq} \equiv B_{kq}^\dagger B_{kq}, \quad (29)$$

has eigenvalues 0 or 1: [13]

$$n'_{kq} = 0 \text{ or } 1. \quad (30)$$

The total number of a system of pairons,  $N$ , is represented by

$$N \equiv \sum_k \sum_q n_{kq} = \sum_q n_q, \quad (31)$$

where

$$n_q \equiv \sum_k n_{kq} - \sum_k B_{kq}^\dagger B_{kq} \quad (32)$$

represents the number of pairons having net momentum  $q$ . From Equations (30)-(32) we can establish Equation (28). To explicitly see this property, we introduce

$$B_q \equiv \sum_k B_{kq}, \quad (33)$$

and obtain, after simple calculations,

$$[B_q, n_q] = \sum_k \left( 1 - n_{k+\frac{1}{2}q} - n_{-k+\frac{1}{2}q} \right) B_{kq} = B_q, \quad [n_q, B_q^\dagger] = B_q^\dagger. \quad (34)$$

Although the occupation number  $n_q$  is not connected with  $B_q$  as  $N_q \neq B_q^\dagger B_q$ , the eigenvalues  $n'_q$  of  $n_q$  satisfying Equation (34) can be shown straightforwardly to yield Equation (28) with the eigenstates  $|0\rangle$ ,  $|1\rangle = B_q^\dagger |0\rangle$ ,  $|2\rangle = B_q^\dagger |1\rangle = B_q^\dagger B_q^\dagger |0\rangle$ ,  $\dots$ .

The present author's group [7] [8] [13] regards the superconductivity as a result of the BEC of the c-bosons. The free c-bosons moving in 2D with the linear dispersion relation  $\varepsilon = cp$  undergoes a BEC at [13]

$$k_B T_c = 1.954 \hbar c n_0^{1/2}, \quad (35)$$

where  $n_0$  is the pairon number density. The derivation of the linear dispersion relation  $\varepsilon = cp$  and the BEC is outlined in [Appendix](#). The average interpairon distance

$$r_0 \equiv n_0^{-1/2} \quad (36)$$

is greater several times than the BCS coherence length (pairon size):

$$\zeta_0 \equiv \hbar v_F / \pi \Delta_0, \quad (37)$$

where  $\Delta_0$  is the zero temperature BCS energy gap. We have

$$r_0 = 6.89\zeta_0. \quad (38)$$

Thus 2D pairons do not overlap in space. Hence the  $T_c$  can be calculated based on the free moving pairons model. See Ref. 12 for more details.

Formula (25) is distinct from the BCS formula in the weak coupling limit:

$$2\Delta_0 = 3.53k_B T_c. \quad (39)$$

Our Formula (35) obtained after identifying superconducting temperature as the BEC condensation temperature contains familiar quantities, the Fermi speed  $v_F$  and the boson density  $n_0$  only.

For illustration let us take GaAs/AlGaAs. We assume  $m^* = 0.067m_e$  and  $v_F = 1.36 \times 10^8 \text{ m} \cdot \text{s}^{-1}$ , then we obtain  $n_0 = 10^{11} \text{ cm}^{-2}$ ,  $T_c = 1.29 \text{ K}$  (reasonable). Not all electrons are bound with fluxons since the simultaneous generation of  $\pm$  c-bosons is required. The plateau width vanishes at  $T_c$  since the energy gap vanishes there.

The neutral supercondensate is generated from the two ranges of energies of “electrons” and “holes”. Hence it is difficult to precisely determine the critical temperature from the theoretical consideration alone. The comparison between theory and experiment may be carried out as follows. First we find the Fermi speed  $v_F^{(j)}$  from the Hall effect measurements or others. We then find the supercondensate density  $n_0$  from the measured critical temperature  $T_c$  by using Equation (35). In the mean field approximation we obtain

$$-w_0 = 2\varepsilon_g(0) = k_B T_c, \quad (40)$$

which indicates a close connection between the zero temperature gap  $\varepsilon_g(0)$  and the critical temperature  $T_c$ . A rigorous treatment of the BEC of free pairons shows a phase transition of the third order [13]. The molar heat rises like  $T^2$ , reaches  $4.38 R$  ( $R = \text{gas constant}$ ) at  $T_c$ , and then decreases to  $2R$  in the high-temperature limit [14] as shown in **Figure 4**. We note that the molar heat does not vanish above  $T_c$ .

## 6. Summary and Discussion

We have developed a theory regarding  $\text{MgB}_2$  as a member of GIC. We start with the lattice configuration with all ions locations specified, and find that each B-plane contains B's forming a honeycomb lattice of the nearest neighbour distance (lattice constant)  $a_0$  while each Mg-plane contains a base-hexagonal lattice of the lattice constant  $\sqrt{3}a_0$ . Since the B-lattice is more compact, it becomes superconducting at the lowest temperatures.

We obtain a linear dispersion relation  $\varepsilon = cp$  for the moving pairons. The superconducting temperature  $T_c$ , identified as the BEC temperature of the pairons, is given by  $k_B T_c = 1.954 \hbar c n_0^{1/2}$ . The supercurrent density is

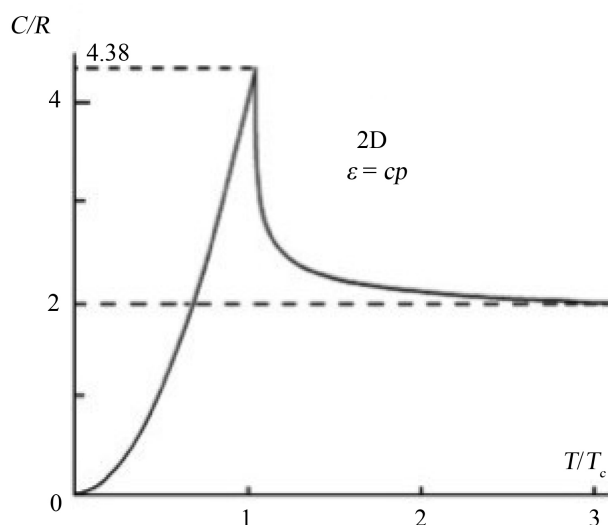


**Figure 4.** The molar heat capacity  $C$  for 2D free massless bosons (after Ref. 14, Figure 6.3).

calculated without introducing the averaging. The superconducting energy gap  $\varepsilon_g$  is identified as the gap in the pairon energy spectrum, distinct from the BCS energy gap  $\Delta$ .

Canfield and Crabtree have discussed two energy gaps, which is strange since there is one superconducting state at 0 K. We shall discuss this topic in a separate publication.

## References

- [1] Nagamatsu, J., Nakagawa, N., Muranaka, T., Zenitani, Y. and Akimitsu, J. (2001) *Nature*, **410**, 63. <http://dx.doi.org/10.1038/35065039>
- [2] Canfield, P.C. and Crabtree, G.W. (2003) *Physics Today*, **56**, 34. <http://dx.doi.org/10.1063/1.1570770>
- [3] Hinks, D.G., Claus, H. and Jorgenson, J.D. (2001) *Nature*, **411**, 457. <http://dx.doi.org/10.1038/35078037>  
Kortus, J., *et al.* (2001) *Physical Review Letters*, **86**, 4656. <http://dx.doi.org/10.1103/PhysRevLett.86.4656>
- [4] Uchida, S. (2015) *High Temperature Superconductivity*. Springer, Japan, 9.
- [5] Bardeen, J., Cooper, L.N. and Schrieffer, J.R. (1957) *Physical Review*, **108**, 1175. <http://dx.doi.org/10.1103/PhysRev.108.1175>
- [6] Ashcroft, N.W. and Mermin, N.D. (1976) *Solid State Physics*. Saunders, Philadelphia, 6-7, 216-217, 228-229.
- [7] Fujita, S., Takato, Y. and Suzuki, A. (2011) *Modern Physics Letters B*, **25**, 223. <http://dx.doi.org/10.1142/S021794911025675>
- [8] Fujita, S. and Suzuki, A. (2010) *Journal of Applied Physics*, **107**, 013711. <http://dx.doi.org/10.1063/1.3280035>
- [9] Kang, N., Lu, L., Kong, W.J., Hu, J.S., Yi, W., Wang, Y.P., Zhang, D.L., Pan, Z.W. and Xie, S.S. (2003) *Physical Review B*, **67**, 033404. <http://dx.doi.org/10.1103/PhysRevB.67.033404>
- [10] Zhang, S.C., Hansson, T.H. and Kivelson, S. (1989) *Physical Review Letters*, **62**, 82. <http://dx.doi.org/10.1103/PhysRevLett.62.82>
- [11] Ehrenfest, P. and Oppenheimer, J.R. (1931) *Physical Review*, **37**, 333. <http://dx.doi.org/10.1103/PhysRev.37.333>  
Bethe, H.A. and Jackiw, R.W. (1989) *Intermediate Quantum Mechanics*. 2nd Edition, Benjamin, New York, 23.  
Fujita, S. and Morabito, D.L. (1998) *Modern Physics Letters B*, **12**, 1061.
- [12] Cooper, L.N. (1956) *Physical Review*, **104**, 1189. <http://dx.doi.org/10.1103/PhysRev.104.1189>
- [13] Fujita, S. and Godoy, S. (2001) *Theory of High Temperature Superconductivity*. Kluwer, Dordrecht, 54-58, 96-98, 107-109, 164-167, 230-231. <http://dx.doi.org/10.1007/0-306-48216-9>
- [14] Fujita, S., Ito, K. and Godoy, S. (2009) *Quantum Theory of Conducting Matter—Superconductivity*. Springer, New York, 79-83. <http://dx.doi.org/10.1007/978-0-387-88211-6>

## Appendix: Linear Dispersion Relation and Bose-Einstein Condensation

We consider the case of a 2D superconductor. The phonon exchange attraction is in action for any pair of electrons near the Fermi surface. In general the bound pair has a net momentum, and hence, it moves. Such a pair is called a *moving pairon*. The energy  $w_q$  of a moving pairon can be obtained from

$$w_q a(\mathbf{k}, \mathbf{q}) = \left\{ \varepsilon(|\mathbf{k} + \mathbf{q}/2|) + \varepsilon(|-\mathbf{k} + \mathbf{q}/2|) \right\} a(\mathbf{k}, \mathbf{q}) - \frac{v_0}{(2\pi\hbar)^2} \int' d^2 k' a(\mathbf{k}', \mathbf{q}), \quad (41)$$

which is *Cooper's equation* in 2D, Equation (1) of his 1956 Physical Review paper [12]. The prime on the  $k'$ -integral means the restriction on the integration domain arising from the phonon exchange attraction, see below. The *pair wavefunctions*  $a(\mathbf{k}, \mathbf{q})$  are coupled with respect to the other variable  $\mathbf{k}$ , meaning that the exact (energy-eigenstate) pair wavefunctions are superpositions of  $a(\mathbf{k}, \mathbf{q})$ .

Equation (41) can be solved simply. We briefly review the calculations and results here. We assume that the energy  $w_q$  is negative:

$$w_q < 0. \quad (42)$$

Then,  $\varepsilon(|\mathbf{k} + \mathbf{q}/2|) + \varepsilon(|-\mathbf{k} + \mathbf{q}/2|) - w_q > 0$ . Rearranging the terms in Equation (41) and dividing by  $\varepsilon(|\mathbf{k} + \mathbf{q}/2|) + \varepsilon(|-\mathbf{k} + \mathbf{q}/2|) - w_q$ , we obtain from Equation (41)

$$a(\mathbf{k}, \mathbf{q}) = \frac{C(\mathbf{q})}{\varepsilon(|\mathbf{k} + \mathbf{q}/2|) + \varepsilon(|-\mathbf{k} + \mathbf{q}/2|) - w_q}, \quad (43)$$

where

$$C(\mathbf{q}) \equiv \frac{v_0}{(2\pi\hbar)^2} \int' d^2 k' a(\mathbf{k}', \mathbf{q}) \quad (44)$$

is  $k$ -independent. Introducing Equation (43) in Equation (44), and dropping the common factor  $C(\mathbf{q})$ , we obtain

$$1 = \frac{v_0}{(2\pi\hbar)^2} \int' \frac{d^2 k}{\varepsilon(|\mathbf{k} + \mathbf{q}/2|) + \varepsilon(|-\mathbf{k} + \mathbf{q}/2|) + |w_q|}. \quad (45)$$

We now assume a free-electron model in 2D. The Fermi surface is a circle of the radius (momentum)

$$k_F \equiv (2m_1 \varepsilon_F)^{1/2}, \quad (46)$$

where  $m_1$  represents the effective mass. The energy  $\varepsilon(|\mathbf{k}|)$  is given by

$$\varepsilon(|\mathbf{k}|) \equiv \varepsilon_k = \frac{|\mathbf{k}|^2 - |k_F|^2}{2m_1}. \quad (47)$$

The prime on the  $k$ -integral in Equation (45) means the restriction:

$$0 < \varepsilon(|\mathbf{k} + \mathbf{q}/2|), \varepsilon(|-\mathbf{k} + \mathbf{q}/2|) < \hbar\omega_D. \quad (48)$$

We may choose the  $z$ -axis along  $\mathbf{q}$  as shown in [Figure 5](#).

The  $k$ -integral in Equation (45) can then be expressed by

$$\frac{(2\pi\hbar)^2}{v_0} = 4\pi \int_0^{\pi/2} d\theta \sin\theta \int_{k_F + \frac{1}{2}q \cos\theta}^{k_F + k_D - \frac{1}{2}q \cos\theta} \frac{k^2 dk}{|w_q| + 2\varepsilon_k + (4m_1)^{-1} q^2}, \quad (49)$$

where  $k_D$  is

$$k_D \equiv m_1 \hbar \omega_D k_F^{-1}. \quad (50)$$

After performing the integration and taking the small- $q$  and small- $(k_D/k_F)$  limits, we obtain

$$w_q = w_0 + (2/\pi) v_F q, \quad (51)$$

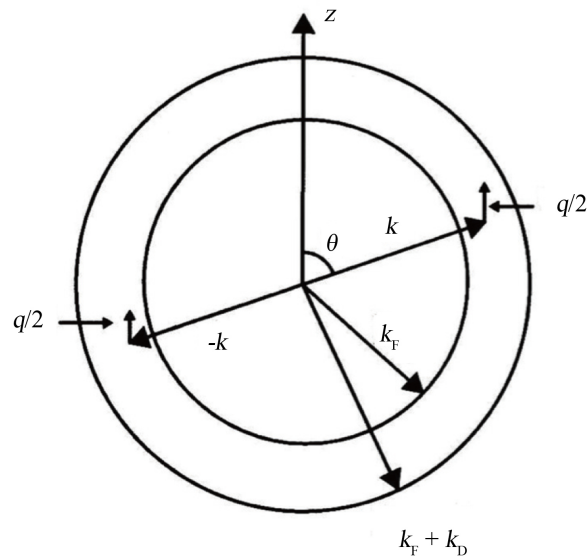


**Figure 5.** The range of the interaction variables  $(k, \theta)$  is limited to a circular shell of thickness  $k_D$ .

where

$$w_0 = \frac{-2\hbar\omega_D}{\exp\{2/v_0\mathcal{D}(0)\} - 1} \quad (52)$$

is the pairon ground state energy.

As expected, the zero-momentum pair has the lowest energy  $w_0$ . The excitation energy is continuous with *no* energy gap. The energy  $w_q$  increases *linearly* with momentum  $q$  for small  $q$ . Hence, the *Cooper pair moves like a massless particle with a common speed*  $(2/\pi)v_F$ .

Such a linear dispersion relation is valid for pairs moving in any dimensions (D). However the coefficients slightly depend on the dimension as follows:

$$w_q = w_0 + cq, \quad (53)$$

where  $c = (1/2)v_F$  and  $(2/\pi)v_F$  for 3 and 2 D, respectively.

The velocity  $\mathbf{v}$  of the particle having a linear dispersion relation  $\varepsilon = cp$  is defined and calculated as

$$v_x \equiv \frac{\partial \varepsilon}{\partial p_x} = c \frac{\partial}{\partial p_x} p = c \frac{p_x}{p}. \quad (54)$$

The velocity magnitude  $|\mathbf{v}|$  is  $c$ . Hence, the pair moves with the speed  $c$ .

We consider a system of free bosons having a linear dispersion relation:  $\varepsilon = cp = (2/\pi)v_F$  moving in 2 D. The system undergoes a Bose-Einstein condensation with the critical temperature  $T_c$ :

$$k_B T_c = 1.954 \hbar c n^{1/2} = 1.244 \hbar v_F n^{1/2}, \quad (55)$$

where  $n$  is the 2D boson density. The  $T_c$  is proportional to the square root density. The derivation of Equation (55) is given in Ref. 13. Briefly, the chemical potential  $\mu$  vanishes below  $T_c$  and decreases further above  $T_c$ . The difference between the boson density  $n$  and the zero momentum density  $n_0$  is given by

$$2\pi\hbar^2 c^2 \beta^2 (n - n_0) = \int_0^\infty dx \frac{x}{e^{-\beta\mu} e^x - 1}, \quad (56)$$

where  $x \equiv \beta\varepsilon$ ,  $\beta \equiv (k_B T)^{-1}$ . We put  $\mu = 0$  on the right-hand side and  $\beta_c = (k_B T_c)^{-1}$  and  $n_0 = 0$  on the left-hand side, and obtain Equation (55).

# Diffraction Line Width in Quasicrystals—Sharper than Crystals

**Antony J. Bourdillon**

UHRL, San Jose, CA, USA

Email: [bourdillona@xraylithography.us](mailto:bourdillona@xraylithography.us), [www.xraylithography.us](http://www.xraylithography.us)

Received 7 July 2016; accepted 28 August 2016; published 31 August 2016

Copyright © 2016 by author and Scientific Research Publishing Inc.

This work is licensed under the Creative Commons Attribution International License (CC BY).

<http://creativecommons.org/licenses/by/4.0/>



Open Access

---

## Abstract

A quasicrystal has a structure intermediate between crystals and compound glasses. The disorder in glass makes its diffraction diffuse, so it is surprising that quasicrystals diffract more sharply than crystals. The greater sharpness is computed to be due to the hierarchic structure with unit cell alignment in 3-dimensional space. Electron microscope phase contrast images map the comparatively heavy *Mn* atoms in icosahedral *Al<sub>6</sub>Mn*, where the transition metal locates the centers of unit cells inside clusters and superclusters. Because the solid is aperiodic, each diffracted beam is a product of multiple interplanar spacings combined, and this contrasts with the unique relationship between spacing and incident angle in Bragg diffraction from crystals. Simulated quasi-structure factors add the relative phase shifts that are in geometric series from cell to cluster to superclusters of increasing order. The scattering becomes coherent in best fit, angular configuration between the aperiodic solid and a longitudinally periodic X-ray or electron probe. The quasi-structure factors express angular divergence in each diffracted beam from its corresponding Bragg condition, and the divergence provides a special metric, essential for atomic measurement in the geometric solids. The fit is reinforced at all levels from the unit cell to cluster to high order superclusters. The optics operates under a new quasi-Bragg law in a new geometric space. In this paper, we proceed to examine the effect of specimen size on line resolution in diffraction, first analytically and secondly in simulation. The line resolution follows a power law on the supercluster order, matching its atomic population.

## Keywords

Quasicrystal, Line Width, Quasi-Structure Factor, Geometric Space, Hierarchic, Metric

---

## 1. Introduction

*Prima facie*, an aperiodic solid should scatter incoherently or diffusely, as from an amorphous material or a gas.

In these, bond length information can be obtained by measuring Bragg angles observed in coarse patterns with cylindrical symmetry about the incident probe. The quasicrystalline, icosahedral phase,  $i\text{-Al}_6\text{Mn}$ , was discovered thirty four years ago. It has a sharp diffraction pattern containing five-fold axial symmetries and an aperiodic atomic map. The quasicrystal does not belong to any member of the complete set of fourteen Bravais lattices that contain all crystals. These comprise unit cells that fill space with face sharing surfaces. Nine years ago, Se-nechal wrote for the American Mathematical Society the paper, “What is a quasicrystal?” It began, “The short answer is no one is sure [1]”. Since then, the structure has become clear by consistent interpretation of phase contrast micrographs [2]-[7] together with understanding of the 3-dimensional diffraction patterns [4] [8], and consistent measurement at the atomic scale.

Like fused silica, quasicrystals have unit cells, as imaging shows, and these are likewise edge sharing, but they differ from the glasses because the unit cells in the quasicrystal are uniformly oriented due to multiple edge sharing. The structure is hierarchic so that the diffraction and many other physical properties can be calculated easily. The diffraction does not follow Bragg’s law of diffraction for crystals for many reasons, the most obvious being that the diffraction series are not in linear order; they are in 3-dimensional geometric series [3] [4]. Moreover, because the solids are aperiodic, the diffraction of a single beam from a quasicrystal is due not to a single, specular, diffraction plane selected by precise crystal orientation, but is due to many planes of atoms, at various planar separations ( $d$  spacings) scattering simultaneously. Each scattered beam results from an *effective* interplanar spacing which is a compromise between many real interplanar spacings. Likewise the diffraction angle is a compromise that is not given by Bragg’s law. In quasicrystals, the diffraction follows a quasi-Bragg law that describes the geometric series that is observed [6] [9]. With both of these compromises in the aperiodic material, a special metric is needed to derive atomic measurements from the diffraction. This metric is calculated through simulated quasi structure factors. We have shown previously how quasi-structure factors are calculated for large quasicrystals [6] [10]; here we show why diffracted beams have to be sharper in ideal quasicrystals than diffraction from perfect crystals.

## 2. Structure

**Figure 1** shows, at left, a micrograph of  $\text{Al}_6\text{Mn}$  obtained at optimum defocus in phase contrast electron microscopy [2] [3]. Each circular spot maps a  $\text{Mn}$  atom. It is located at the centre of a unit cell and the atom is surrounded by 12 extremely tightly bound  $\text{Al}$  atoms. The tight binding depends on the precise ratio of atomic diameters in the metal alloy:

$$\frac{d_{\text{solute}}}{d_{\text{solvent}}} = \sqrt{1 + \tau^2} - 1 \quad (1)$$

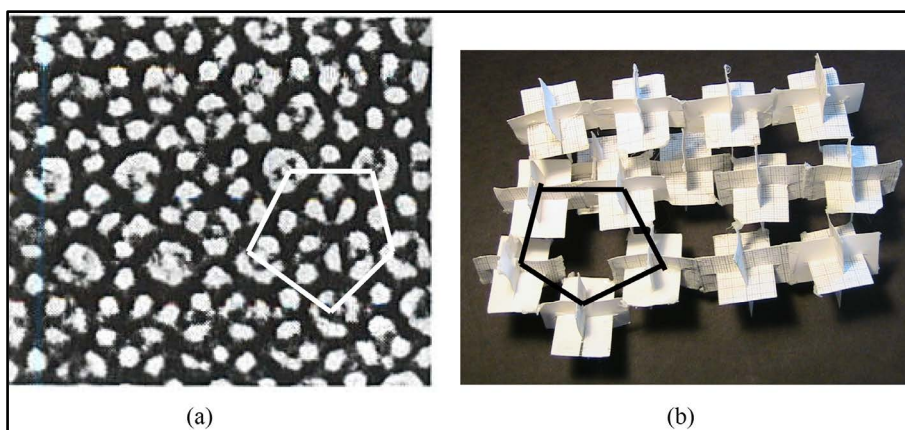


**Figure 1.** (a) Optimum defocus electron microscope image of  $\text{Al}_6\text{Mn}$  [2] [3] (reprinted with permissions from L. A. Bursill, J. L. Peng and from *Nature*). (b) In mirror image, skeletal structures, representing icosahedral clusters, match the micrograph. As a cluster, each corner of the golden rectangular triads locates an icosahedral unit cell of one central  $\text{Mn}$  surrounded by 12  $\text{Al}$  atoms. Note the sections of supercluster order 1 outlined in each image with pentagons that connect cluster centres. The unit cells are edge sharing and aligned.

where the golden section,  $\tau = (1 + \sqrt{5})/2$ . The ratio is found generally in diatomic quasicrystals. The micrograph maps cluster sections as circles of 10 unit cells. The white pentagon connects five clusters in a section of a supercluster. The clusters are represented, at right, by golden triads formed from golden rectangles, each with length to width ratio  $\tau$ . The golden triad is a skeleton for an icosahedron, having 12 corners that connect 20 triangular faces with 30 congruent edges. On scales that vary by the stretching factor  $\tau^2$ , the triads may also be used to represent unit cells or any order of supercluster in the hierarchic structure.

### 3. The Metric $c_s$ that Relates Structure to Diffraction Angle

Since the quasicrystal diffraction pattern does not follow Bragg's law, how are measurements to be made at the atomic scale? The logarithmically periodic solid (LPS) [6] has many advantages: measurement is its greatest. Calculations of structure factors for the LPS demonstrate that they are all approximately zero: there is no Bragg diffraction, and this is a consequence of aperiodicity. In each single quasi-Bragg reflection, multiple interplanar spacings operate—contrasting with crystals where the spacing is unique for each reflection. However by scanning over the scattering angle, a compromise scattering angle is found at best fit. A quasi-Bloch wave for this fit is illustrated in Figure 2 [6]. The quasi-Bloch wave peaks do not coincide with atomic planes<sup>1</sup>.

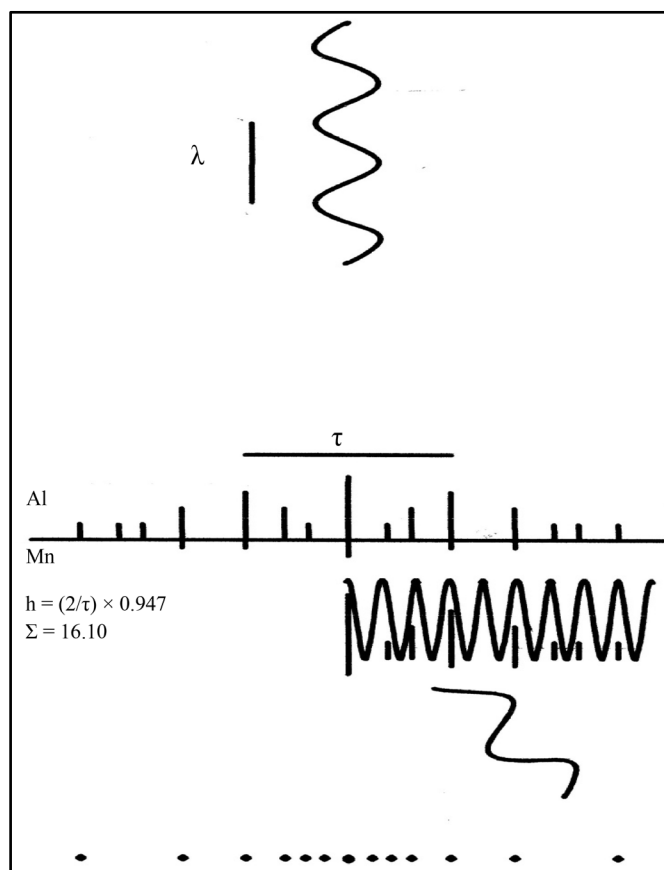


**Figure 2.** A periodic electron beam, moving downwards, scatters from atomic planes on an aperiodic quasicrystal cluster to form a diffraction pattern in geometric space. This is due to a quasi-Bloch wave having maximum overlap with the populations on the atomic planes ([6] reprinted with permission). *Al* atomic populations lie above the abscissa; *Mn* atoms below, as shown. The maximum overlap occurs at the quasi-Bragg angle  $c_s \theta_B$ , where  $\theta_B$  would be the crystalline Bragg angle for diffraction from a corresponding unique interplanar spacing such as  $1/\tau$ , or  $1$ ,  $\tau$ ,  $\tau^2$  etc.

<sup>1</sup>High resolution transmission electron microscopy does not image atoms; the Fourier transform method of analysis is misleading.

Moreover, this scattering angle maximizes only in second Bragg order,  $n = 2$ ; The linear Bragg orders, 1, 3, 4, 5... are forbidden owing to approximately half integral values in the geometric series  $1/\tau$ , or  $1, \tau, \tau^2$  [3] [4]<sup>2</sup>. Without this restriction the diffraction pattern would not be geometric, as observed. Dividing iteratively by the scaling stretching factor  $\tau^2$ , the half integrals repeat throughout the geometric series. The maximum in the quasi-scattering factor is found at a quasi Bragg angle  $\theta' = c_s \theta_B$ , where  $c_s$  is what we called the compromise spacing effect and  $\theta_B = \sin^{-1}(n\lambda/2d)$  the corresponding angle under Bragg's law for an interplanar spacing  $d$ . The wavelength of the X-ray or electron beam is  $\lambda$ . Computations show that  $c_s$  has the same value for all quasi-Bragg diffracted beams, and that value is about 0.947, so that  $\theta'$  is 5.3% less than  $\theta_B$ . The simulated compromise spacing effect has a value close to the intuitive value  $2.5/\tau^2$ , and is employed in the following section. The numerator is the nearest half integral to the denominator, which is the stretching factor between hierarchic orders. With these adjustments the quasi-Bragg law may be written:

$$\tau^m \lambda = d' \sin(c_s \theta) \quad (2)$$

with order  $-\infty < m < \infty$ . Computations show that  $c_s$  is the same for all  $m$  and all indexed reflections. Notice that every term in the quasi-Bragg law is different from every term in Bragg's law excepting only the wavelength. While aperiodicity requires a new law in physics, the geometric diffraction defines a new space.

## 4. Computations on Quasi-Scattering Factors

### 4.1. The Metric $c_s$ , That Relates Structure to Diffraction angle

Quasi-scattering factors  $F_{hkl}$  were calculated using the corresponding standard formula in crystallography [11] for a centrosymmetric crystal, adapted with the factor  $c_s$ :

$$F_{hkl} = \sum_{i=1}^N f_i \cos\left(2\pi \cdot c_s \left(\overline{h_{hkl}} \cdot \overline{r_i}\right)\right) \quad (3)$$

summed over all  $N$  atoms in a truncated hierarchic quasicrystal. The factor modifies the projections of the atoms onto a scattering plane normal  $\overline{h_{hkl}}$  having indices  $h, k, l$ . The atomic scattering factors  $f_i$  are appropriate for either  $Al$  or  $Mn$  and are found in tables [12] [13]. The LPS is centro-symmetric.

In large quasicrystals, computation of Equation 3 is restricted by truncation errors. However, the number of computations is reduced, without sacrifice of accuracy, by calculating quasi-structure factors iteratively from unit cell to cluster to superclusters of increasing order  $p$  [10]:

$$F_{hkl}^p = \sum_{cc=1}^{12} \cos\left(2\pi \cdot c_s \left(\overline{h_{hkl}} \cdot \tau^{2p} \overline{r_{cc}}\right)\right) F_{hkl}^{p-1} \quad (4)$$

where  $\overline{r_{cc}}$  describes the 12 vectors to cluster centers [10], and  $F_{hkl}^{cluster}$  may be written  $F_{hkl}^0$ :

$$F_{hkl}^{cluster} = \sum_{cc=1}^{12} \cos\left(2\pi \cdot c_s \left(\overline{h_{hkl}} \cdot \overline{r_{cc}}\right)\right) F_{hkl}^{cell} \quad (5)$$

while  $F_{hkl}^{cell}$  uses Equation (3) to sum over the 13 atoms in the unit cell. In these calculations care is taken to halve the scattering factors in atoms, in clusters or supercluster of whatever order, that are counted twice; or to divide by three times on atoms counted thrice (Appendix). These Equations (1) to (5) have been previously described in greater detail than is given here in summary. The chief purpose of this paper is to demonstrate how the sharpness of the diffraction pattern is represented by these structure factors. Now we proceed to a mathematical representation of resolution by an application of second derivatives in hierarchic arrangement. To prove it, we shall compute the dependence of  $c_s$  on specimen size, and then its dependence on both short range (unit cell) or long range (lattice) symmetries<sup>3</sup>. A differential formula is used to express resolution, or line width. The formula itself matches the computations made on larger quasicrystals, and provides confidence that the sharp diffraction is completely understood in these wonderful, but no longer so new materials. Clearly, since the diffraction does not follow Bragg's law, there are many aspects that we cannot take for granted; one is the sharpness of the diffraction. The theoretical understanding will make it possible to interpret, in various samples, the effect of defects, espe-

<sup>2</sup>In icosahedral units the unit cell has length,  $a = \tau$ ; and edge width unity. The conversion to SI units is given in [4].

<sup>3</sup>The terms in the geometric series tend to integral values at high order [3]. The overlap with the linear, Bragg series has no effect on  $c_s$ .

cially in rapidly quenched material. One of the defects is truncation of the ideal structure that can, in principle, be estimated from the results presented here. The simulations described in this paper take no account of thermal effects, normally represented in crystallography by the Debye-Waller factor, nor do the simulations account for absorption and lesser effects.

## 4.2. Hierarchic Computation of Resolution

We begin with two hypotheses. The first is that the profile that is given by scanning the value of  $c_s$  in Equation (4) is approximately Gaussian as in the normal distribution. This hypothesis is suggested by the requirements for the best fit illustrated in **Figure 2** and is indicated in the following simulations. The second hypothesis is that there exists a resolution function  $f(c_s)$ , that is approximately the same for all levels of unit cell, cluster and orders of supercluster. This hypothesis is supported by the repeating features of the geometric series (ratio  $\tau$ ) scaled between orders by the stretching factor  $\tau^2$ . To fix ideas, we suppose that the resolution function depends on the second derivative of the profile, at its peak (where the first derivative is zero), of the scan in  $c_s$ . A Gaussian profile,  $f = A \exp\left(-\frac{(c_s - c_p)^2}{2\sigma^2}\right)$ , will then yield the second derivative as follows:

$$\frac{\partial f}{\partial c_s} = -A \frac{2(c_s - c_p)}{2\sigma^2} \exp\left(-\frac{(c_s - c_p)^2}{2\sigma^2}\right)$$

$$f''|_{c_s=c_p} = -\frac{A}{\sigma^2} \quad (6)$$

The metric is the mean value of  $c_s$  in the peak profile: the value that is scanned in Equation (3), gives the metric that maximizes at  $c_p$ , since the profile is symmetric. The least squares linear fit, as illustrated in **Figure 2**, does not provide an analytical solution for  $A$  and  $\sigma$ , but they can be assessed in the computational scans recorded below. Suppose the resolution is some product  $B \cdot f''(c_s)$ . The iterative nature of Equation (5) will then give for the resolution  $R$  of a supercluster order  $p$ , a value  $(B \cdot f''(c_s))^p$ .

$$R_{hkl}^p = (B \cdot f''(c_s))^p$$

Since  $p = \log\left(R_{phkl} / (B f''(c_s))\right)$ , on a logarithmic scale this resolution dependence on  $p$  should plot onto a straight line.

This dependence would be consistent with a dependence on the number of scattering atoms which has approximately the same power law dependence on the order of supercluster. Where the unit cell has 13 atoms, some of them shared with neighboring atoms, the cluster contains 12 unit cells, again with some atoms shared. The number of scattering atoms increases by about an order of magnitude with each increase in order, the cluster being supercluster order 0, with about 100 atoms. Further details are given in **Appendix**.

## 4.3. Dependence of $c_s$ on Specimen Size and Range

The diffraction in quasicrystals is not Bragg diffraction and the structure factors demonstrate the fact. Quasi-structure factors provide the value for  $c_s$ , the metric which is necessary for atomic scale measurements in the solids. The following two figures have previously been discussed in detail [14] so we give here the conclusions in summary form. **Figure 3** is a log plot of quasi-structure factors calculated by scanning  $c_s$  in Equation (5) [6]. The reflection peak shown is typical and is here calculated for the  $(2/\tau, 0, 0)$  reflection [3] [4] from a supercluster order 6. The fractional divergence from the Bragg position ( $\theta_B = \sin^{-1}(n\lambda/2d)$ ) is  $c_s = 0.947$  (or  $1.0 - 534 \times 0.0001$ ). The quasi-Bragg angle  $\theta'$  is 5.3% smaller than the equivalent Bragg angle  $\theta_B$  for crystals on a corresponding interplanar spacing, such as  $d = \tau^{-1}$ ,  $1$ ,  $\tau$ ,  $\tau^2$  etc. In consequence, the measured quasi-spacing  $d'$  is 5.3% larger than would be given by using Bragg's formula,  $d = n\lambda/2\sin(\theta)$ . The difference is the compromise effect due to logarithmic periodicity and gives the value for the metric  $c_s$  at the peak of the computational scan. The simulated metric is found to have the same value in all quasi-Bragg reflected beams. It provides consistent values for atomic size, cell size, cluster size etc. The Bragg angle corresponds to channel 1 in the plot. All struc-

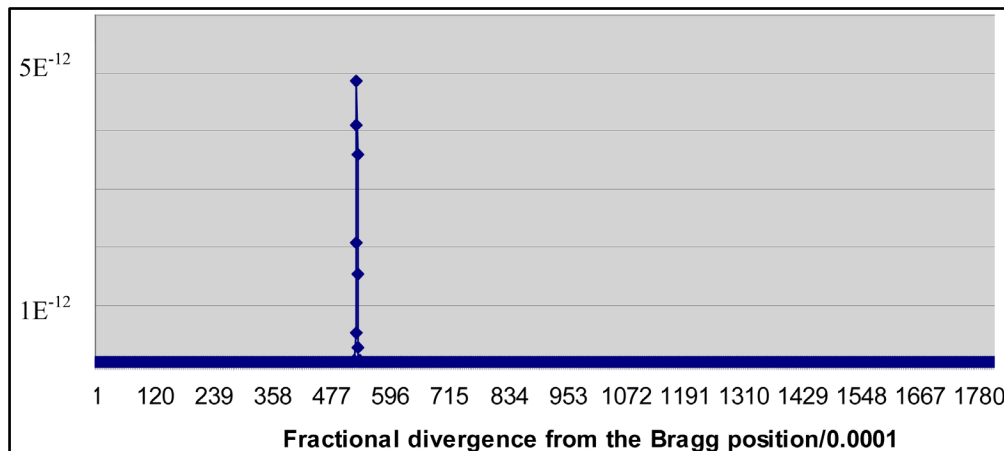


**Figure 3.** Simulated quasi-structure factors, scanned away from the Bragg angle for the reflection  $(2/\tau, 0, 0) < c_s < 0.8(2/\tau, 0, 0)$ . The calculation is for a supercluster order 6. Fractional divergence is zero at the nominal Bragg angle on channel 1 [6] (reprinted with permission from Nova Science Publishers).

ture factors (as for Bragg's law) are zero. The ordinate values compare with the square of the number of atoms in the supercluster, the atomic scattering factors  $f_i$  being of order 1 (see [Appendix](#)).

Does  $c_s$  change as the cluster size is increased or decreased? The computations shown in [Figure 4\(a\)](#) were performed on superclusters orders 0, 1, 2 and 3, using the method of Equations (3) - (5). The value of the metric  $c_s$  at the peak of the scan is constant; while there is a general decrease in line width as the order increases. The figure shows simulated profiles for diffracted beams from the hierarchic icosahedral structure. This is compared with three computational devices: in [Figure 4\(b\)](#) the structure factor profile is calculated for the face centered cubic (fcc) structure. Notice that the peak occurs at the Bragg angle (channel 1). Its width is more than double the width of the profile for the supercluster order 2 ([Figure 4\(a\)](#)), having an equivalent number of atoms. This fact implies stronger coherence in the logarithmic solid. [Figure 4\(c\)](#) and [Figure 4\(d\)](#) are computational devices on unrealistic structures: in the former case an fcc unit cell is placed in an icosahedral lattice; in the latter an icosahedral cell is placed in a cubic lattice. These cases have similar profiles with similar  $c_s$  offsets. They demonstrate that the offsets are due to the geometric series whether it occurs in the cell or in the lattice, and that the influence of the long range lattice is the same as the influence of the short range unit cell. Both filter-in the offset and filter-out Bragg diffraction. This computational fact is consistent with the repeated series of spacings, scaled between supercluster orders by the ratio  $\tau$  in the geometric series and by the stretching factor  $\tau^2$  in the hierarchic structure.

In [Figure 5](#), the logarithms of simulated line widths in [Figure 3](#) and [Figure 4\(a\)](#) are plotted against supercluster orders. The straight line fit is predicted by the power law in Equation (7). This least squares fit and these graphs confirm consistently the origin of both the compromise spacing effect and the line widths, *i.e.* the hierarchic structure and geometric series diffraction. The least squares, linear fit to the computation is  $\log(\text{half width}) = -0.96(3) - 0.42(7)p$  as illustrated in the figure.

Experimental measurement of line width is complicated by the restricted dynamic range of CCD (charge coupled device) detectors and of camera plate. Moreover, most diatomic quasicrystals are dual phase with fine structures, or metastable so that large crystals are grown with difficulty. We therefore leave for another time the various ways in which line width might be measured in specimens prepared under particular conditions. However measured, divergence of resolution, or line width, from the linear fit shown in the figure could be used to measure defects or defect concentrations, including truncations of the hierarchic structure.

## 5. Discussion

What new properties do these comparatively new materials have? While they share some properties in common with metallic glasses, such as corrosion resistance [15] they have special electronic, magnetic and mechanical properties associated with their geometric electronic band structures [5] [14]. Their most fundamental property is the one that is analyzed here because most of the other properties follow from it: how it comes about that an aperiodic material can diffract with a sharp pattern in geometric series? Besides the new quasi-Bragg law and new

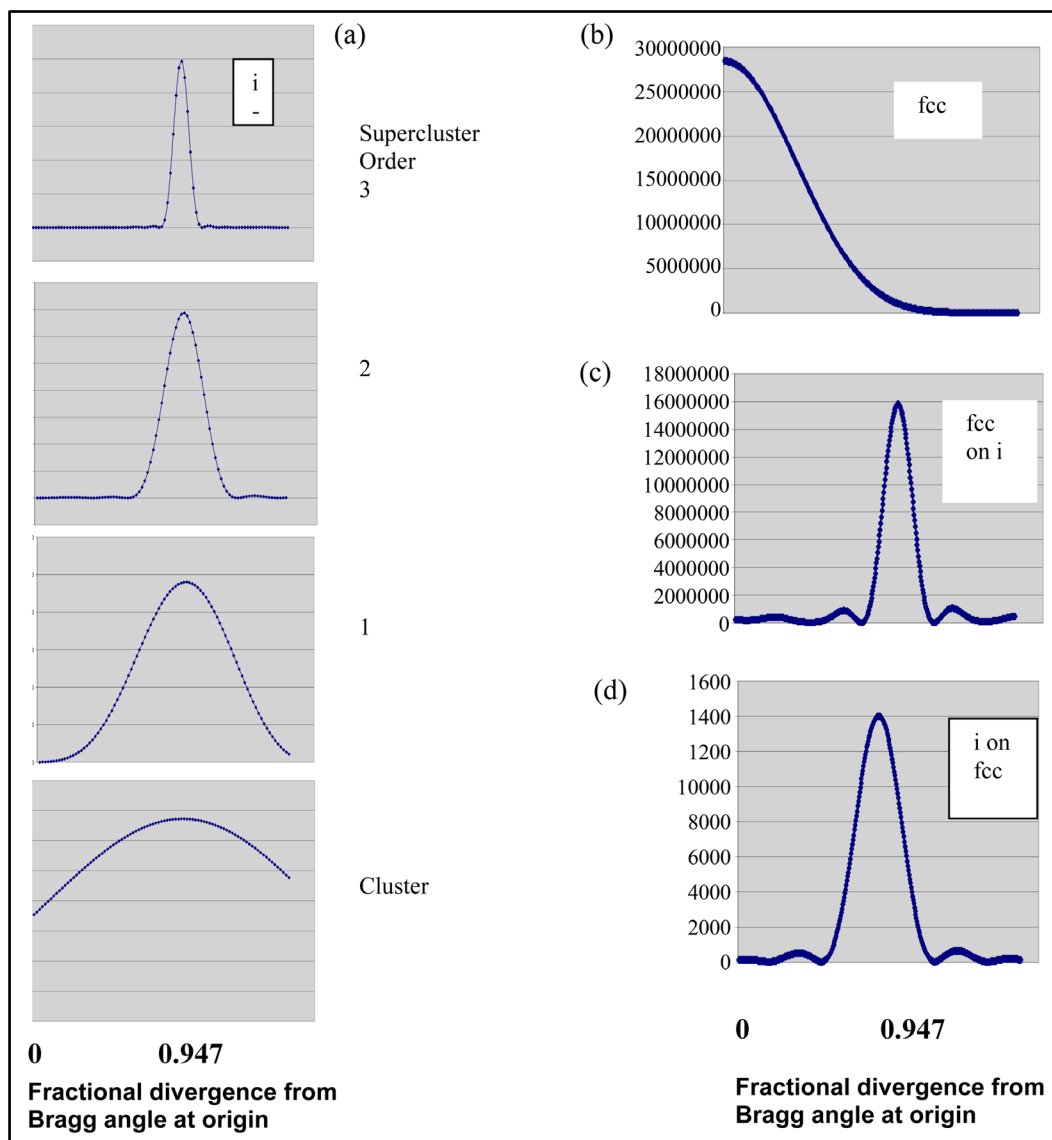


**Figure 4.** (a). Computed intensities, *i.e.* squared structure factors, for  $(2/\tau, 0, 0)$  diffraction in supercluster orders 3, 2, 1, and in an  $i\text{-Al}_6\text{Mn}$  cluster. The intensities are plotted against divergence from Bragg angle and span  $\sim 15\%$  of this angle. The Compromise Spacing Effect (CSE) shifts quasi-Bragg angle from the calculated Bragg angle by 5.3%. The lines from different supercluster orders show the same  $c_s$  displacement from the Bragg angle. (b) (111) structure factors, computed against angle as above, for a cubic cluster of fcc Al, having about 19,000 atom sites, similar to quasicrystal supercluster order 2. There is no CSE. At this size, the peaks are computed to be comparatively broad, typically 5% of the Bragg angle. (c) Computed structure factor for (111) diffraction by an imaginary cubic fcc cell in a logarithmically periodic icosahedral grid, as in supercluster order 2. The CSE occurs with a peak narrower than in **Figure 4(b)** for the crystalline structure. (d) Computed structure factor for  $(\tau \tau \tau)$   $i\text{-Al}_6\text{Mn}$  icosahedral cell in an imaginary cubic grid of side  $\tau$  and site population about 20,000 (like (b) and (c)).

geometric space, the hierarchy provides, theoretically, higher sharpness and coherence than does the periodicity of crystals.

The fact also suggests a possible extension of finite element analysis. On reflection, it is very surprising that the hierarchic structure produces greater coherence in geometric space than do crystals in linear space. It might prove possible to eliminate subsidiary minima or maxima by overlaying geometric analysis on conventional linear calculations. The stretching factor, that is strict in the present model, might be replaced by diffusion

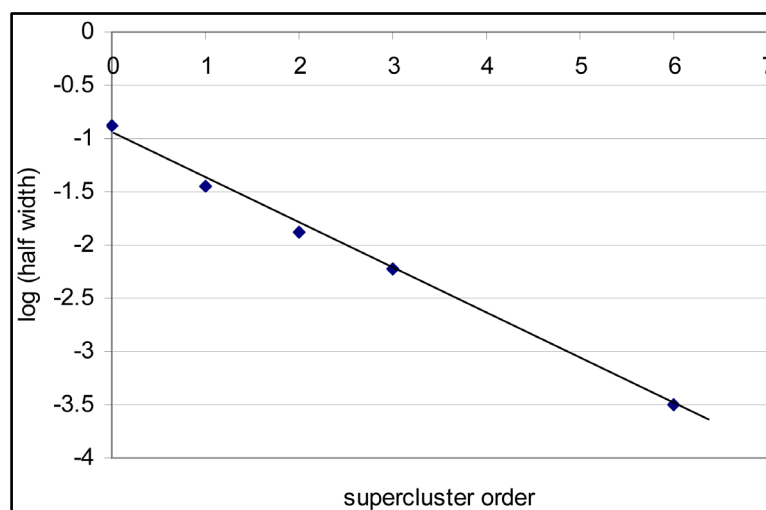


**Figure 5.** Logarithm of half widths shown in **Figure 3** and **Figure 4(a)** plotted against supercluster order, compared with least squares linear fit. The straight line was predicted in Equation (7).

coefficient, thermal conductivity, viscosity coefficient, or other physical parameter. These extensive influences expressed logarithmically in either initial conditions or by progressive computation, might be found to accelerate convergence and to eliminate subsidiary solutions.

## 6. Conclusion

A mathematical treatment of the geometric relationships inherent in the ideal hierarchic structure has been applied to examine sharpness in quasicrystal diffraction. It is not only sharp, but in principle, sharper than in perfect crystals. These calculations ignore the blurring effects of defects, which may be expected to depend on materials processing routes. However, they also suggest methods for characterizing the defects. More generally, the results, showing greater sharpness in geometric space than in linearly periodic crystals, suggest opportunities for both optics and for general computational methods in finite element analysis.

## References

- [1] Senechal, M. (2006) *Notices to the American Mathematical Society*, **3**, 886-887.
- [2] Bursill, L.A. and Peng, J.L. (1985) *Nature*, **316**, 50-51. <http://dx.doi.org/10.1038/316050a0>
- [3] Bourdillon, A.J. (2012) *Metric, Myth and Quasicrystals*. UHRL, ISBN 978-0-9789-8393-2. <https://www.youtube.com/watch?v=xD30KF93qio>
- [4] Bourdillon, A.J. (2009) *Quasicrystals and Quasi Drivers*. UHRL, USA, ISBN 978-1-4389-5589-6.
- [5] Bourdillon, A.J. (2009) *Solid State Communications*, **149**, 1221-1225. <http://dx.doi.org/10.1016/j.ssc.2009.04.032>
- [6] Bourdillon, A.J. (2011) *Logarithmically Periodic Solids*. Nova Science, USA, ISBN 978-1-61122-977-6.
- [7] Bourdillon, A.J. (2010) *Youtube/Quasicrystals, Logarithmically Periodic*. <https://www.youtube.com/watch?v=A6vpsWv9nsQ>
- [8] Bourdillon, A.J. (2014) *Journal of Modern Physics*, **5**, 488-496. <http://dx.doi.org/10.4236/jmp.2014.56060>
- [9] Bourdillon, A.J. (2013) *Micron*, **51**, 21-25. <http://dx.doi.org/10.1016/j.micron.2013.06.004>
- [10] Bourdillon, A.J. (2014) *Journal of Modern Physics*, **5**, 1079-1084.
- [11] Bourdillon, A.J. (2015) *Youtube/Log-Lin Metric in Quasicrystals*. <http://dx.doi.org/10.4236/jmp.2014.512109>
- [12] Bourdillon, A.J. (2016) *Journal of Modern Physics*, **7**, 43-50. <http://dx.doi.org/10.4236/jmp.2016.71005>
- [13] Cullity, B.D. (1978) *Elements of X-Ray Diffraction*. Addison-Wesley, Boston.
- [14] Hirsch, P., Howie, A., Nicholson, R.B., Pashley, D.W. and Whelan, M.J. (1977) *Electron Microscopy of Thin Crystals*. Krieger.

- [13] Doyle, P.A. and Turner, P.S. (1968) *Acta Crystallogr*, **24**, 39.
- [14] Bourdillon, A.J. (2010) *Quasicrystals' 2D Tiles in 3D Superclusters*. Author House, ISBN 978-1-4490-8395-3.
- [15] Puckerman, B.E. (2011) *Quasicrystals, Types, Systems and Techniques*. Nova, New York.
- [16] Pauling, L. (1985) *Letters to Nature*, **317**, 512-514. <http://dx.doi.org/10.1038/317512a0>
- [17] Bourdillon, A.J. (1987) *Philosophical Magazine Letters*, **55**, 21-26. <http://dx.doi.org/10.1080/09500838708210435>

## Appendix. How Many Atoms Are There in a Supercluster Order $p$ ?

The hierarchic model is an ideal that makes way for defects. Beyond accounting for optimum defocus phase contrast micrographs, such as **Figure 1**, the second greatest benefit is the facility that the model provides for making meaningful and striking calculations for atomic structure and diffraction. The principal result is the discovery of the generic compromise spacing effect, as a product term in the quasi structure factor calculations. On scanning this term, the peak in the profile yields the measured metric that enables atomic measurements through the new quasi-Bragg law. Atomic sites in the LPS are described in ref. [7].

The simplest way of estimating the number of atoms in a supercluster is to count the number of atomic sites: the unit cell has 13 atoms, each with a *Mn* atom at the center. A cluster is made from 12 cells with  $13 \times 12 = 156$  sites, but with fewer atoms as we shall see. Then, by hierarchic extension, the number of *sites* in a supercluster order  $p$  is  $156 \times 12^p$ . The number of *atoms* is less than this.

*Start with the cluster*: some sites are shared between neighboring cells; some sites a mobile, with neighbors so close that one is vacant; in particular, the central “hole”, averted to by Pauling [16], includes several vacancies. Take these three groups one at a time.

*Shared sites* lie on adjoining edges of neighboring cells. Each cell shares five edges out of 30. Each edge has two *Al* atoms shared three ways. In all, 60 sites are occupied by only 20 atoms.

*Mobile sites* contain two sites separated by a distance less than the diameter of metallic *Al*. Each edge, of the cluster contains 4 sites including one mobile site. There are 120 edge sites, but only 90 atomic sites.

*Hole sites* occur at the center of the cluster. There are 12 of them on an icosahedron with edge length  $1/\tau$ , *i.e.* smaller than the unit *Al* diameter. The sites are like mobile sites, except that they have space for only 3 atoms. Toting the deficits, the cluster has  $156 - 40 - 30 - 9 = 77$  atoms.

Proceed to the *supercluster*, first order. This has 12 clusters in the hierarchic order. The number of *sites* is  $12 \times 77 = 924$ . Dimensions are generally scaled up by  $\tau^2 \approx 2.6$ , so that *mobile sites* do not occur beyond the cluster.

As before, each cluster *shares* 5 edges. Each edge has 3 *Al* atoms. So 90 sites are occupied by 45 atoms.

The supercluster has a larger hole than the cluster and this is supposedly filled by interstitials. The space is an icosahedron with edge width  $\tau^3$ . We have previously suggested how the *hole* could be filled [4] but there is so far no dark field microscopic evidence for support. We estimate that, by contrast with vacancies in the cluster; there is at least a cell of interstitial atoms, *i.e.*  $>13$  atoms. Toting the discrepancies, the supercluster is estimated to contain  $924 - 45 + 13 \approx 892$  atoms.

By similar considerations, we can proceed to *superclusters orders* 2, 3, 4, 5, 6 etc. Estimates become increasingly significant with increasing order, and enter into approximations made in the calculations of quasi-structure factors [4] [6]. These take into account shared sites and mobile sites by corresponding computational adjustments on atomic scattering factors; but omit the central holes for fear of introducing errors due to structural misplacements. The numbers derived above lead to the conclusion that there is an increase in atomic populations of about an order of magnitude for each order of supercluster, starting with a population of  $\approx 900$  atoms in a first order supercluster. If, more precisely, the ratio  $892/77 = 11.6$  is maintained, then a nearer estimate for the atomic populations in a supercluster order  $p$  is approximately  $892 \times (11.6)^{p-1}$ . Remembering that the atomic scattering factor for *Al* is about 1.1 for 100 kV electrons, and for *Mn* about 2.1 [12], the atomic populations given are consistent with the values for the squared quasi-structure factors calculated in **Figure 3** for the supercluster order 6.

Notice also that the different atomic scattering factors in the two atoms give to the *Mn* atom an intensity increase that is four times greater than *Al*. This is evident in optimum defocus, phase contrast micrograph in **Figure 1**.

This treatment raises the issue of stoichiometry. The supercluster has a nominal ratio *Al:Mn* = 6:1. The deficits discussed were all on the part of the solute atoms on unit cell edges. However the metastable icosahedral phase grows inside a matrix *Al* alloy with reduced *Mn* concentration [17]. The depletion in *Al* in the hierarchic, icosahedral phase, compensates the residual concentration of *Mn* in the matrix.

# Towards the Unification of All Interactions (The First Part: The Spinor Wave)

Claude Daviau<sup>1</sup>, Jacques Bertrand<sup>2</sup>, Dominique Girardot<sup>3</sup>

<sup>1</sup>Le Moulin de la Lande, Pouillé-les-Coteaux, France

<sup>2</sup>15 Avenue Danielle Casanova, Saint-Gratien, France

<sup>3</sup>95 Rue Marceau, Palaiseau, France

Email: [claudedaviau@nordnet.fr](mailto:claudedaviau@nordnet.fr), [bertrandjacques-m@orange.fr](mailto:bertrandjacques-m@orange.fr), [dominique.girardot2@sfr.fr](mailto:dominique.girardot2@sfr.fr)

Received 22 July 2016; accepted 28 August 2016; published 31 August 2016

Copyright © 2016 by authors and Scientific Research Publishing Inc.

This work is licensed under the Creative Commons Attribution International License (CC BY).

<http://creativecommons.org/licenses/by/4.0/>



Open Access

---

## Abstract

For the unification of gravitation with electromagnetism, weak and strong interactions, we use a unique and very simple framework, the Clifford algebra of space  $Cl_3 = M_2(\mathbb{C})$ . We enlarge our previous wave equation to the general case, including all leptons, quarks and antiparticles of the first generation. The wave equation is a generalization of the Dirac equation with a compulsory non-linear mass term. This equation is form invariant under the  $Cl_3^*$  group of the invertible elements in the space algebra. The form invariance is fully compatible with the  $U(1) \times SU(2) \times SU(3)$  gauge invariance of the standard model. The wave equations of the different particles come by Lagrange equations from a Lagrangian density and this Lagrangian density is the sum of the real parts of the wave equations. Both form invariance and gauge invariance are exact symmetries, not only partial or broken symmetries. Inertia is already present in the  $U(1)$  part of the gauge group and the inertial chiral potential vector simplifies weak interactions. Relativistic quantum physics is then a naturally yet unified theory, including all interactions.

## Keywords

Electromagnetism, Weak Interactions, Strong Interactions, Gravitation, Clifford Algebra, Dirac Equation, Lagrangian Formalism, Gauge Groups, Relativistic Invariance, Electron, Magnetic Monopole, Quark, Photon, Gauge Boson, Unification

---

## 1. Introduction

The aim of this work is to construct with the same logic and mathematical rigour of General Relativity (GR), a

quantum wave of all fermions of one generation in a well-defined framework: the wave is a function of space and time into  $Cl_3^8$  where  $Cl_3$  is the Clifford algebra of space. We extend the relativistic constraints and replace the  $SL(2, \mathbb{C})$  group by the greater group  $Cl_3^* = GL(2, \mathbb{C})$  and we use only true representations and exact calculations. The Lagrangian density has a double link with the wave equations, both cause and consequence. This is new and gives both the limits and the physical reason of the existence of a Lagrangian formalism. We present here the fermionic part of the wave equations. The wave equations have mass terms, and they are invariant both under  $Cl_3^*$  and under precisely the  $U(1) \times SU(2) \times SU(3)$  gauge group of the Standard Model of Quantum Physics (SM). This gauge symmetry is a local and exact one. Complicated calculations of the second quantization are not used. Spontaneously broken symmetry is useless. Nevertheless we get many results of the SM, with less free parameters, which is better. Mass terms of our wave equations allow us to study inertia and gravitation directly from the wave equations. The inertial part of the gravitation generates eight potential space-time vectors. Only seven of these eight terms are present in the Christoffel symbols used in differential geometry. The eighth, the chiral one, is yet in the  $U(1)$  gauge and explains the complexity of weak interactions. Using this chiral inertial potential vector, we simplify the electro-weak gauge. We study here the fermionic part of the SM. This SM uses also twelve bosons whose components are built from the tensorial densities available from the spinor wave. They will be detailed in another article.

After Maxwell's electromagnetism, the discovery of electromagnetic wave and the understanding of the electromagnetic properties of light, electromagnetic laws became relativistic covariant laws [1]. The electromagnetic field became an anti-symmetric tensor and the Maxwell's laws were invariant under a greater group than the invariance group of mechanics. In 1915, Einstein was able to include the gravitation in the same frame. His theory of gravitation (GR) [2] [3] is extremely precise, and gravitational waves are now experimentally observed. Next Einstein tried to reunite electromagnetism and gravitation into a unique field theory [4].

From relativistic ideas de Broglie found the wave associated to the movement of any particle [5]. Only a few months after his dissertation, Schrödinger found a non-relativistic wave equation for his wave. This wave equation explained the quantization of energy levels and started quantum mechanics. At the same time, the spin 1/2 of the electron was discovered. Pauli gave a non-relativistic wave equation accounting for the spin 1/2. This equation was the starting point used by Dirac to get his wave equation [6]. The Dirac equation is such a success that now again it is an important item of the SM. Only the Dirac equation actually explained the true number of energy levels, the true energy levels and quantum numbers of the hydrogen atom [7]. Nevertheless if the Dirac equation was, a long time ago, explained in many books from Ref. [8] to [9], then quantum mechanics even forgot to teach this part of the quantum theory [10]. First the Dirac wave was the wave of only one electron while the Schrödinger equation accounted for systems of electrons. Next the problem of negative energies was not solved by the Dirac equation, the charge conjugation did not account for negative energies in the framework of the first quantization, only the second. With this second quantization the electromagnetic field became a field of operators creating and annihilating photons, with bras and kets in Hilbert linear spaces. This field followed a Hamiltonian dynamics with a Schrödinger equation and its unique time variable [11]. Therefore, even if quantum fields incorporated the electromagnetic field and should be compatible with GR, the methods of the second quantization, with path integrals and Feynman graphs, were not sufficient to incorporate GR. Several problems arose<sup>1</sup>, often not well exposed, either presenting the Dirac equation from a Hamiltonian dynamics<sup>2</sup>, either forgetting that the matrices of  $SL(2, \mathbb{C})$  replacing the Lorentz transformations were not unitary [11], either with wrong calculations.<sup>3</sup> The result was an unsolved problem: the union of GR and SM. Nowadays quantum mechanics is understood as a gauge theory using a  $U(1) \times SU(2) \times SU(3)$  gauge group [14]. The electron is a member of the "first generation" of fundamental fermions. This first generation is replicated into a second and a

<sup>1</sup>The non-relativistic wave of a system of n electrons is a function on the  $\mathbb{C}$  field of  $3n + 1$  variables, the  $3n$  coordinates of each particle, and a unique time. The number of particles is changing with creations and annihilations; therefore it is impossible to know precisely what a quantum state is. Nevertheless it is necessary to be able to compute integration on these indefinite linear spaces. The Dirac wave is a function on  $\mathbb{C}^4$  not on  $\mathbb{C}$ .

<sup>2</sup>In Ref. [12] the first part of the book presents canonical quantization, Green functions, path integrals and S-matrix from the non-relativistic quantum theory. The author writes (page 162) "the Dirac equation may be thought of as a relativistic generalization of the Schrödinger equation", which is false because the four  $\gamma_\mu$  cannot be all Hermitian matrices. So he even does not know that the unitary operators needed on page 147 cannot exist.

<sup>3</sup>The matrix  $\gamma^0$  written page 7 in Ref. [13] is different from the definition given in (A.13) page 390. This book had four editions, all with the same error.

third one with increasing mass. A Lagrangian density gives the wave equations, both for fermions and gauge bosons. Each generation has a separate Lagrangian density [12]. After the great success of the Weinberg-Salam theory [15] unifying electromagnetism and weak interactions with a  $U(1) \times SU(2)$  gauge group [16], great unified theories [17] tried to extend this unification to include strong interactions. These theories predicted the disintegration of the proton, but none disintegration was observed. Numerous and complicated attempts with quantum groups, strings, branes and many supplementary dimensions, supergravity, loop quantum gravity, were developed. All these attempts were based on the methods of the second quantization and consequently were finally based upon the non-relativistic Schrödinger equation. None of these attempts were able to incorporate GR in a renormalizable way.

We began our work with the Dirac equation of the electron [6]. All calculations are there made with mathematical rigour [7] and with very accurate experimental results. Another reason of this work is the study of the finite representations of the Lorentz proper group [18]: relativistic quantum mechanics uses not the Lorentz group but another one, in a way which is not a consequence of the principles of the theory.

## 2. Waves and Wave Equations

Since 1928 the relativistic invariance of the Dirac theory used the previous Pauli matrices for the spin of the electron: the space-time variable  $x = (x^0, x^1, x^2, x^3)$  was replaced by

$$x = x^0 + \bar{x} = \begin{pmatrix} x^0 + x^3 & x^1 - ix^2 \\ x^1 + ix^2 & x^0 - x^3 \end{pmatrix}, \quad x^0 = ct. \quad (2.1)$$

This is equivalent to say that the three Pauli matrices:

$$\sigma_1 = \begin{pmatrix} 0 & 1 \\ 1 & 0 \end{pmatrix}; \quad \sigma_2 = \begin{pmatrix} 0 & -i \\ i & 0 \end{pmatrix}; \quad \sigma_3 = \begin{pmatrix} 1 & 0 \\ 0 & -1 \end{pmatrix}, \quad (2.2)$$

form a orthogonal oriented basis in space. We shall put arrows on vectors in space, so any vector reads

$$\vec{v} = v^j \sigma_j = v^1 \sigma_1 + v^2 \sigma_2 + v^3 \sigma_3. \quad (2.3)$$

Contrary to the Clifford community [19]-[22] we use the matrix representation generated by the Pauli matrices. First the geometric algebra of space  $Cl_3$  and  $M_2(\mathbb{C})$  are isomorphic algebras on the real field, the sum and the product of matrices are familiar in quantum physics. This matrix representation identifies complex numbers and scalar matrices in the Pauli algebra. With this identification we write the  $x$  of (2.1) as  $x = x^\mu \sigma_\mu$ , we consider  $(\sigma_0, \sigma_1, \sigma_2, \sigma_3)$  as a basis in space-time and we use the Einstein's convention of summation on up and down indexes, with Latin indexes in space and Greek indexes in space-time. Any element  $z$  in the Clifford algebra of space  $Cl_3$  is a sum of a real part  $x$ , a vector part  $\vec{v}$ , an axial-vector part  $i\vec{w}$  and a pseudo-scalar part  $iy$  and we need (a detailed course on Clifford Algebra is available in the first chapter of [23]-[26]).

$$\begin{aligned} z &= x + \vec{v} + i\vec{w} + iy; \quad \hat{z} = x - \vec{v} + i\vec{w} - iy, \\ \tilde{z} &= z^\dagger = x + \vec{v} - i\vec{w} - iy; \quad \bar{z} = x - \vec{v} - i\vec{w} + iy. \end{aligned} \quad (2.4)$$

The application  $z \mapsto \hat{z}$  is the main automorphism of  $Cl_3$ . The reverse is also the adjoint (transposed conjugate matrix), so  $z \mapsto \tilde{z} = z^\dagger$  is the reversion. The third conjugation,  $z \mapsto \bar{z}$  is the product of the two previous ones and we shall need:

$$\bar{z} = \hat{z}^\dagger = \widehat{z^\dagger}; \quad \overline{AB} = \bar{B}\bar{A}; \quad M\bar{M} = \bar{M}M = \det(M). \quad (2.5)$$

Space-time is then made of the auto-adjoint part of the space algebra. We use:

$$\hat{x} = \bar{x} = x^0 - \vec{x}; \quad x^\dagger = x; \quad \det(x) = x\hat{x} = x \cdot x = (x^0)^2 - \vec{x}^2 = (x^0)^2 - (x^1)^2 - (x^2)^2 - (x^3)^2.$$

The main reason to the use of the geometric algebra  $Cl_3$  is the ability to read all relativistic quantum physics in this algebra: The fermion wave is a function of space and time into  $Cl_3^8$ :

$$x \mapsto \phi = (\phi^1, \phi^2, \dots, \phi^8); \quad \phi^n = \phi^n(x) \in Cl_3. \quad (2.6)$$

It is made of eight waves, functions of space-time with value in  $Cl_3$  which is a 8-dimensional linear space on the real field. The link between  $Cl_3$  and the complex formalism is simple only if we use the left and right Weyl spinors  $\eta^n$  and  $\xi^n, n=1,2,3,4$ , by letting:

$$\begin{aligned}\phi^n &= \sqrt{2}(\xi^n \hat{\eta}^n) = \sqrt{2} \begin{pmatrix} \xi_1^n & -\eta_2^{n*} \\ \xi_2^n & \eta_1^{n*} \end{pmatrix}; \quad \hat{\eta}^n = -i\sigma_2 \eta^{n*} = \begin{pmatrix} -\eta_2^{n*} \\ \eta_1^{n*} \end{pmatrix}, \\ \hat{\phi}^n &= \sqrt{2}(\eta^n \hat{\xi}^n) = \sqrt{2} \begin{pmatrix} \eta_1^n & -\xi_2^{n*} \\ \eta_2^n & \xi_1^{n*} \end{pmatrix}; \quad \hat{\xi}^n = -i\sigma_2 \xi^{n*} = \begin{pmatrix} -\xi_2^{n*} \\ \xi_1^{n*} \end{pmatrix}.\end{aligned}\quad (2.7)$$

For  $n=5,6,7,8$ , we let:

$$\begin{aligned}\tilde{\phi}^n &= \sqrt{2}(\xi^n \hat{\eta}^n) = \sqrt{2} \begin{pmatrix} \xi_1^n & -\eta_2^{n*} \\ \xi_2^n & \eta_1^{n*} \end{pmatrix}; \quad \hat{\eta}^n = -i\sigma_2 \eta^{n*} = \begin{pmatrix} -\eta_2^{n*} \\ \eta_1^{n*} \end{pmatrix}, \\ \bar{\phi}^n &= \sqrt{2}(\eta^n \hat{\xi}^n) = \sqrt{2} \begin{pmatrix} \eta_1^n & -\xi_2^{n*} \\ \eta_2^n & \xi_1^{n*} \end{pmatrix}; \quad \hat{\xi}^n = -i\sigma_2 \xi^{n*} = \begin{pmatrix} -\xi_2^{n*} \\ \xi_1^{n*} \end{pmatrix}.\end{aligned}\quad (2.8)$$

Our non-linear wave equation of the electron, which has the Dirac equation as linear approximation when the Yvon-Takabayasi angle is small or negligible, reads [23]-[35]:

$$\bar{\phi}^1(\nabla \hat{\phi}^1) \sigma_{21} + \bar{\phi}^1 q A \hat{\phi}^1 + m \rho = 0; \quad \nabla = \sigma^\mu \partial_\mu; \quad \sigma_{21} = \sigma_2 \sigma_1; \quad \rho = |\det(\phi^1)|. \quad (2.9)$$

where  $q = e/\hbar c, m = m_0 c/\hbar, 1 = \sigma^0 = \sigma_0, \sigma^j = -\sigma_j, j=1,2,3$ . This equation is invariant under any transformation  $D$  defined by an element  $M$  of the Lie group  $Cl_3^*$  (group of invertible elements of  $Cl_3$ ):

$$x' = D(x) = MxM^\dagger = x'^\mu \sigma_\mu; \quad \partial'_\mu = \frac{\partial}{\partial x'^\mu}; \quad x'^\nu = D^\nu_\mu x^\mu, \quad (2.10)$$

$$\phi'^n(x') = M \phi^n(x), \quad n=1,2,3,4; \quad \tilde{\phi}'^n(x') = M \tilde{\phi}^n(x), \quad n=5,6,7,8. \quad (2.11)$$

$$\nabla = \bar{M} \nabla' \hat{M}; \quad \nabla' = \sigma'^\mu \partial'_\mu; \quad qA = \bar{M} q' A' \hat{M}; \quad (2.12)$$

$$\xi'^n = M \xi^n; \quad \eta'^n = \hat{M} \eta^n, \quad n=1, \dots, 8. \quad (2.13)$$

Relations (2.13) are the reason of the existence and the definition of “left” and “right” waves in quantum physics. Right waves transform with a left multiplication by  $M$  while left waves transform by a multiplication by  $\hat{M}$ . Therefore  $\xi^n$  and  $\eta^n$  are right waves while  $\eta^n$  and  $\hat{\xi}^n$  are left waves. Only one  $M$  term is present in (2.11) when two  $M$  terms are present in (2.10) and (2.12): consequently the wave turns with the  $\theta$  angle when the space turns with the  $2\theta$  angle. The invariant form of the Dirac equation, which is the linear approximation of (2.9) reads:

$$\bar{\phi}^1(\nabla \hat{\phi}^1) \sigma_{21} + \bar{\phi}^1 q A \hat{\phi}^1 + m \rho e^{-i\beta} = 0; \quad \det(\phi^1) = \rho e^{i\beta}, \quad (2.14)$$

where  $\beta$  is the Yvon-Takabayasi angle. Our wave equation, in the invariant form, appears then as a simplification of the Dirac equation.

Equations (2.10)-(2.13) have no geometric reason to be restricted to  $\det(M)=1$ . The main change that we propose replaces this condition by the less restrictive condition  $\det(M) \neq 0$ . We then enlarge  $SL(2, \mathbb{C})$  to  $GL(2, \mathbb{C})$  which is also the multiplicative group  $Cl_3^*$  in the  $Cl_3$  geometric algebra. This is significant because geometry is linked to gravitation in GR. First reason: this change is possible and astonishing! For any invertible  $M$  Equations (2.10) - (2.13) are satisfied, so the restriction  $\det(M)=1$  is unnecessary. Next the representations used in the case of spin 1/2 particles are now correctly used. The quantum theory associated to each Lorentz transformation  $R$  an element  $M = M(R)$  but there are two  $M$  for one  $R$  and only for particular  $R$  (“bi-valued” representations). Now to any  $M$  we associate one  $R = R(M)$  and  $f: M \mapsto R$  is a true mathematical function. Moreover for the gravitation we shall need below the four kinds of representations of  $GL(2, \mathbb{C})$  while  $SL(2, \mathbb{C})$  has only two kinds of representations. Finally this important change is validated by all new results that we get from this hypothesis. Considering all  $M$  elements with  $r = \det(M) \neq 0$  and noting  $Cl_3^* = GL(2, \mathbb{C})$  the set of these elements, we let:

$$\det(M) = re^{i\theta}; M = \sqrt{r}e^{i\theta/2}\underline{M}; R: x \mapsto \underline{x} = \underline{M}x\underline{M}^\dagger. \quad (2.15)$$

and the  $R$  transformation satisfies:

$$x' = MxM^\dagger = \sqrt{r}e^{i\theta/2}\underline{M}x\sqrt{r}e^{-i\theta/2}\underline{M}^\dagger = r\underline{M}x\underline{M}^\dagger = r\underline{x}. \quad (2.16)$$

Then  $D(x) = rR(x)$  and  $D$  is a ‘‘Lorentz dilation’’ made of the Lorentz transformation  $R$  conserving space orientation and time orientation (this is not a trivial result, relations (2.12) like  $\det(D_\mu^\nu) = r^4$  and  $D_0^0 > 0$  are proved in Ref. [23] p. 115-118) and of the homothety  $h: x \mapsto rx$  with ratio  $r = |\det(M)|$ . We explained previously how these dilations constitute a 7-dimensional Lie group [32] and how all laws of electromagnetism, quantum wave of the electron included, are invariant not only under the  $SL(2, \mathbb{C})$  group found in 1928 from the Dirac theory, necessary to account for the spin 1/2, but under the  $GL(2, \mathbb{C}) = Cl_3^*$  group. Since the study of the Lie groups [36] used in quantum physics is based on the properties of the  $GL(n, \mathbb{C})$  groups, and since  $Cl_3^*$  is exactly one of them, we conserve the matrix representations of this group, Clebsh-Gordan or Racah coefficients and so on. The first difference is the four kinds of matrix representations that we use now with  $\hat{\phi}^n, \hat{\phi}^{\bar{n}}, \hat{\phi}^{\tilde{n}}, \hat{\phi}^{\bar{\tilde{n}}}$ . This has no incidence on spin representations because  $x = \tilde{x}$ . Main difference: we now know from where come the representations of  $SU(2)$  which is a subgroup of  $Cl_3^*$ . Wave Equations (2.9) and (2.14) are invariant under  $Cl_3^*$  because:

$$\begin{aligned} \bar{\phi}^1 \nabla \hat{\phi}^1 &= \bar{\phi}^1 \bar{M} \nabla' \hat{M} \hat{\phi}^1 = \bar{\phi}^1 \nabla' \hat{\phi}^1 \\ \bar{\phi}^1 q A \hat{\phi}^1 &= \bar{\phi}^1 \bar{M} q' A' \hat{M} \hat{\phi}^1 = \bar{\phi}^1 q' A' \hat{\phi}^1 \\ \rho' &= \det(\phi'^1) = \det(M \phi^1) = \det(M) \det(\phi^1) = r \rho. \end{aligned} \quad (2.17)$$

Then, if we suppose  $m = m'r$  we get:

$$\begin{aligned} m\rho &= m'r\rho = m'\rho'; \\ 0 &= \bar{\phi}^1 (\nabla \hat{\phi}^1) \sigma_{21} + \bar{\phi}^1 q A \hat{\phi}^1 + m\rho = \bar{\phi}^1 (\nabla' \hat{\phi}^1) \sigma_{21} + \bar{\phi}^1 q' A' \hat{\phi}^1 + m'\rho'. \end{aligned} \quad (2.18)$$

And we are allowed to say that this equation is ‘‘form invariant’’ since it has exactly the same form in the primed and non-primed basis. We explained how the variation of the mass term is linked to the  $E = h\nu$  relation, then to the existence of the Planck constant [26]. This enlarged invariance has another unexpected consequence: if we compute in the basis  $(1, \sigma_1, \sigma_2, \sigma_3, i\sigma_1, i\sigma_2, i\sigma_3, i)$  of  $Cl_3$  the eight numeric equations equivalent to (2.9) or (2.14) the real part (first term of the basis, 1) is  $\mathcal{L} = 0$ , where  $\mathcal{L}$  is the Lagrangian density allowing us to get the wave Equation (2.9) or (2.14) by means of variation calculus. Therefore a **double link** exists between wave equation and Lagrangian formalism. We prove below that this double link is conserved in the general case. Another one of the eight numeric equations is simple, the equation corresponding to the  $i\sigma_3$  term which reads:

$$\partial_\mu J^\mu = 0; J = J^\mu \sigma_\mu = \phi^1 \phi^{1\dagger}. \quad (2.19)$$

This  $J$  current is the conservative probability current,  $J^0$  being the probability density. We shall see in the next section how this is generalized for the whole wave.

### 3. Weak and Strong Interactions

We studied strong and weak interactions with Clifford algebras having two fictitious supplementary dimensions [25] [37]-[41] of space. Since space-time has one dimension more than space, we passed from three to six dimensions. This induces three doubling of the dimension of the algebra, and we get the same number of variables if we replace  $Cl_3$  by  $Cl_3^8$ . The general wave that we consider is a function of space and time into  $\phi = (\phi^1, \phi^2, \dots, \phi^8)$  with  $\phi^j = R^j + L^j$  where  $R$  is the right part and  $L$  is the left part of the wave. The states of color of the quark  $d$  that we named  $d_r, d_g, d_b$  are associated to  $\phi^2, \phi^3$  and  $\phi^4$ . The states of color of the quark  $u$  that we named  $u_r, u_g, u_b$  are associated to  $\tilde{\phi}^5, \tilde{\phi}^6, \tilde{\phi}^7$ . Similarly we let for the neutrino:  $\phi_n = \tilde{\phi}^8$ . We remark that this conserves the  $1 + 3 + 3 + 1$  structure of the algebra of space. Moreover we now consider these states of color like complete waves, with a left and a right part. This is then a generalization of our previous works. We use now:

$$\Psi = \begin{pmatrix} \Psi_l & \Psi_r \\ \Psi_g & \Psi_b \end{pmatrix} = \begin{pmatrix} \phi^1 & \tilde{\phi}^8 & \phi^2 & \tilde{\phi}^5 \\ \bar{\phi}^8 & \hat{\phi}^1 & \bar{\phi}^5 & \hat{\phi}^2 \\ \phi^3 & \tilde{\phi}^6 & \phi^4 & \tilde{\phi}^7 \\ \bar{\phi}^6 & \hat{\phi}^3 & \bar{\phi}^7 & \hat{\phi}^4 \end{pmatrix}, \quad (3.1)$$

with the Weyl representation:

$$\begin{aligned} \gamma_0 = \gamma^0 &= \begin{pmatrix} 0 & I_2 \\ I_2 & 0 \end{pmatrix}; \quad \gamma_j = -\gamma^j = \begin{pmatrix} 0 & \sigma_j \\ -\sigma_j & 0 \end{pmatrix}, \quad j=1,2,3; \quad I_2 = \begin{pmatrix} 1 & 0 \\ 0 & 1 \end{pmatrix}; \\ L_\mu &= \begin{pmatrix} 0 & \gamma_\mu \\ \gamma_\mu & 0 \end{pmatrix}; \quad L_4 = \begin{pmatrix} 0 & -I_4 \\ I_4 & 0 \end{pmatrix}; \quad L_5 = \begin{pmatrix} 0 & \mathbf{i} \\ \mathbf{i} & 0 \end{pmatrix}; \quad \mathbf{i} = \gamma_{0123} = \begin{pmatrix} \mathbf{i} I_2 & 0 \\ 0 & -\mathbf{i} I_2 \end{pmatrix}. \end{aligned} \quad (3.2)$$

Consequently the  $\Psi_c$  waves,  $c=l,r,g,b$  have value in the Clifford algebra of space-time  $Cl_{1,3}$  and the global wave  $\Psi$  has value in the Clifford algebra of an extended space-time  $Cl_{1,5}$ , with two more dimensions of space which are fictitious and not present in the dynamics of the wave. Main interest of this writing, this allows an equal treatment of the eight  $\phi^n$  that we need. The  $\Psi_l$  part of the wave is the lepton part, made of the  $\phi^1$  wave of the electron and the  $\tilde{\phi}^8$  wave of the neutrino which is also the wave of the Lochak's magnetic monopole [26] [42]-[44]. The wave equation reads:

$$\begin{aligned} 0 &= (\underline{D}\Psi)L_{012} + \underline{\mathbf{M}}; \\ \underline{\mathbf{M}} &= m\rho \begin{pmatrix} \chi_b & \chi_g \\ \chi_r & \chi_l \end{pmatrix}. \end{aligned} \quad (3.3)$$

The covariant derivative reads:

$$\underline{D}(\Psi) = \underline{\partial}(\Psi) + \frac{\underline{g}_1}{2} \underline{B} P_0(\Psi) + \frac{\underline{g}_2}{2} \underline{W}^j P_j(\Psi) + \frac{\underline{g}_3}{2} \underline{G}^k \underline{\Gamma}_k(\Psi), \quad (3.4)$$

with

$$\underline{W}^j = L^\mu W_\mu^j, \quad j=1,2,3; \quad \underline{D} = L^\mu D_\mu; \quad L^0 = L_0; \quad L^j = -L_j \quad (3.5)$$

for  $j=1,2,3$ . We use two projectors  $\underline{P}_\pm$  satisfying

$$\underline{P}_\pm(\Psi) = \frac{1}{2}(\Psi \pm \underline{\mathbf{i}}\Psi L_{21}); \quad \underline{\mathbf{i}} = L_{0123}. \quad (3.6)$$

Three operators act on the quark sector like on the lepton sector:

$$\underline{P}_1 = \underline{P}_+(\Psi)L_{35}; \quad \underline{P}_2 = \underline{P}_+(\Psi)L_{0125}; \quad \underline{P}_3 = \underline{P}_+(\Psi)L_{0132}. \quad (3.7)$$

The fourth operator acts differently on the lepton wave and on the quark sector:

$$\begin{aligned} \underline{P}_0(\Psi) &= \begin{pmatrix} P_0(\Psi_l) & P_0(\Psi_r) \\ P_0(\Psi_g) & P_0(\Psi_b) \end{pmatrix}; \\ P_0(\Psi_l) &= \Psi_l \gamma_{21} + P_-(\Psi_l) \mathbf{i} = \Psi_l \gamma_{21} + \frac{1}{2}(\Psi_l \mathbf{i} + \mathbf{i} \Psi_l \gamma_{30}); \\ P_0(\Psi_c) &= -\frac{1}{3} \Psi_c \gamma_{21} + P_-(\Psi_c) \mathbf{i} = -\frac{1}{3} \Psi_c \gamma_{21} + \frac{1}{2}(\Psi_c \mathbf{i} + \mathbf{i} \Psi_c \gamma_{30}), \quad c=r,g,b. \end{aligned} \quad (3.8)$$

The value  $-1/3$  is compulsory [45] [46] and gives the four correct values of the charges of quarks and anti-quarks [25] [47]. To simplify notations we use now  $l,r,g,b$  instead  $\Psi_l, \Psi_r, \Psi_g, \Psi_b$ . So we have  $\Psi = \begin{pmatrix} l & r \\ g & b \end{pmatrix}$

and

$$\begin{aligned}
\Gamma_1(\Psi) &= \frac{1}{2}(L_4\Psi L_4 + L_{01235}\Psi L_{01235}) = \begin{pmatrix} 0 & g \\ r & 0 \end{pmatrix}; \quad \Gamma_2(\Psi) = \frac{1}{2}(L_5\Psi L_4 - L_{01234}\Psi L_{01235}) = \begin{pmatrix} 0 & -ig \\ ir & 0 \end{pmatrix}; \\
\Gamma_3(\Psi) &= P^+\Psi P^- - P^-\Psi P^+ = \begin{pmatrix} 0 & r \\ -g & 0 \end{pmatrix}; \quad \Gamma_4(\Psi) = L_{01253}\Psi P^- = \begin{pmatrix} 0 & b \\ 0 & r \end{pmatrix}; \\
\Gamma_5(\Psi) &= L_{01234}\Psi P^- = \begin{pmatrix} 0 & -ib \\ 0 & ir \end{pmatrix}; \quad \Gamma_6(\Psi) = P^-\Psi L_{01253} = \begin{pmatrix} 0 & 0 \\ b & g \end{pmatrix}; \\
\Gamma_7(\Psi) &= -iP^-\Psi L_4 = \begin{pmatrix} 0 & 0 \\ -ib & ig \end{pmatrix}; \quad \Gamma_8(\Psi) = \frac{1}{\sqrt{3}}(P^-\Psi L_{012345} + L_{012345}\Psi P^-) = \frac{1}{\sqrt{3}}\begin{pmatrix} 0 & r \\ g & -2b \end{pmatrix}.
\end{aligned} \tag{3.9}$$

Since the left up term of each matrix  $\Gamma_j(\Psi)$  is zero, the wave equation splits into a lepton part and a quark part.

### 3.1. The Lepton Wave

Only the  $U(1) \times SU(2)$  part of the gauge group acts on electron + neutrino. The physical translation is: leptons do not strongly interact; they have only electromagnetic and weak interactions. This is fully satisfied in experiments. Since it is independent on the energy scale, two consequences result: strict conservation of the baryonic number, general failure of great unified theories. The wave equation acts separately in a lepton part and a quark part:

$$\begin{aligned}
0 &= (\underline{D}\Psi^l)L_{012} + m\rho \begin{pmatrix} 0 & 0 \\ 0 & \chi_l \end{pmatrix}; \quad \Psi^l = \begin{pmatrix} \Psi_l & 0 \\ 0 & 0 \end{pmatrix}; \\
0 &= (\underline{D}\Psi^c)L_{012} + m\rho\chi^c; \quad \chi^c = \begin{pmatrix} \chi_b & \chi_g \\ \chi_r & 0 \end{pmatrix}; \quad \Psi^c = \begin{pmatrix} 0 & \Psi_r \\ \Psi_g & \Psi_b \end{pmatrix}.
\end{aligned} \tag{3.10}$$

We study first the lepton part of the wave equation. The lepton sector of the standard model, for the first generation, accounts for the electron, the positron, the left neutrino and the right anti-neutrino. We note the wave  $\psi_e$  of the electron and the wave  $\psi_n$  of the neutrino as

$$\psi_e = \begin{pmatrix} \xi^1 \\ \eta^1 \end{pmatrix}; \quad \psi_n = \begin{pmatrix} \xi^8 \\ \eta^8 \end{pmatrix}; \quad \xi^j = \begin{pmatrix} \xi_1^j \\ \xi_2^j \end{pmatrix}; \quad \eta^j = \begin{pmatrix} \eta_1^j \\ \eta_2^j \end{pmatrix}; \quad j = 1, 8. \tag{3.11}$$

Like previously  $\xi^j$  are right waves and  $\eta^j$  are left waves. The SM uses a charge conjugation which, up an electric phase, lets for the positron wave  $\psi_p$  and for the anti-neutrino wave  $\psi_a$ :

$$\psi_p = i\gamma_2\psi_e^*; \quad \psi_a = i\gamma_2\psi_n^*, \tag{3.12}$$

where we use the matrix representation of Weyl matrices (3.2) which gives:

$$\partial = \gamma^\mu \partial_\mu = \begin{pmatrix} 0 & \nabla \\ \hat{\nabla} & 0 \end{pmatrix}. \tag{3.13}$$

We use (2.7),  $\phi_e = \phi^1$  and  $\phi_n = \tilde{\phi}^8$ . The link (3.12) of the SM between the wave of the particle and the wave of its anti-particle simply reads:

$$\hat{\phi}_p = \hat{\phi}_e\sigma_1 = \hat{\phi}^1\sigma_1; \quad \hat{\phi}_a = \hat{\phi}_n\sigma_1 = \tilde{\phi}^8\sigma_1. \tag{3.14}$$

The lepton wave reads:

$$\Psi_l = \begin{pmatrix} \phi_e & \phi_n \\ \hat{\phi}_a\sigma_1 & \hat{\phi}_p\sigma_1 \end{pmatrix} = \begin{pmatrix} \phi_e & \phi_n \\ \hat{\phi}_n & \hat{\phi}_e \end{pmatrix} = \begin{pmatrix} \phi^1 & \tilde{\phi}^8 \\ \tilde{\phi}^8 & \phi^1 \end{pmatrix}. \tag{3.15}$$

It is a well-defined function of space and time with value into the space-time algebra  $Cl_{1,3}$ . Separating  $\xi_e$ ,  $\eta_e$  and  $\eta_n$  the Weinberg-Salam model uses projectors  $\frac{1}{2}(1 \pm \gamma_5)$ , which read with our choice (3.2) of Dirac

matrices:

$$\frac{1}{2}(1-\gamma_5)\psi = \psi_L = \begin{pmatrix} 0 & 0 \\ 0 & I_2 \end{pmatrix} \begin{pmatrix} \xi \\ \eta \end{pmatrix} = \begin{pmatrix} 0 \\ \eta \end{pmatrix}; \quad \frac{1}{2}(1+\gamma_5)\psi = \psi_R = \begin{pmatrix} I_2 & 0 \\ 0 & 0 \end{pmatrix} \begin{pmatrix} \xi \\ \eta \end{pmatrix} = \begin{pmatrix} \xi \\ 0 \end{pmatrix}. \quad (3.16)$$

Then for particles left waves are  $\eta$  waves and right waves are  $\xi$  waves. This is  $CI_3^*$  invariant, consequently relativistic invariant. With space algebra the separation between left and right waves uses:

$$\begin{aligned} R^1 &= \sqrt{2} \begin{pmatrix} \xi^1 & 0 \\ 0 & 0 \end{pmatrix} = \phi_e \begin{pmatrix} 1 & 0 \\ 0 & 0 \end{pmatrix} = \phi_e \frac{1}{2}(1+\sigma_3); \quad \tilde{R}^8 = \sqrt{2} \begin{pmatrix} \xi^8 & 0 \\ 0 & 0 \end{pmatrix} = \phi_n \begin{pmatrix} 1 & 0 \\ 0 & 0 \end{pmatrix} = \phi_n \frac{1}{2}(1+\sigma_3); \\ L^1 &= \sqrt{2} \begin{pmatrix} 0 & -i\sigma_2\eta^{1*} \\ 0 & 0 \end{pmatrix} = \sqrt{2} \begin{pmatrix} 0 & \hat{\eta}^1 \\ 0 & 1 \end{pmatrix} = \phi_e \begin{pmatrix} 0 & 0 \\ 0 & 1 \end{pmatrix} = \phi_e \frac{1}{2}(1-\sigma_3); \\ \tilde{L}^8 &= \sqrt{2} \begin{pmatrix} 0 & -i\sigma_2\eta^{8*} \\ 0 & 0 \end{pmatrix} = \sqrt{2} \begin{pmatrix} 0 & \hat{\eta}^8 \\ 0 & 1 \end{pmatrix} = \phi_n \begin{pmatrix} 0 & 0 \\ 0 & 1 \end{pmatrix} = \phi_n \frac{1}{2}(1-\sigma_3). \end{aligned} \quad (3.17)$$

To get the gauge group of the Weinberg-Salam theory we let (see [26] 6.1):

$$\begin{aligned} P_{\pm}(\Psi) &= \frac{1}{2}(\Psi \pm i\Psi\gamma_{21}); \quad \mathbf{i} = \gamma_{0123} \\ P_0(\Psi) &= \Psi\gamma_{21} + \frac{1}{2}\Psi\mathbf{i} + \frac{1}{2}i\Psi\gamma_{30} = \Psi\gamma_{21} + P_-(\Psi)\mathbf{i}; \quad P_1(\Psi) = \frac{1}{2}(i\Psi\gamma_0 + \Psi\gamma_{012}) = P_+(\Psi)\gamma_3\mathbf{i}; \\ P_2(\Psi) &= \frac{1}{2}(\Psi\gamma_3 - i\Psi\gamma_{123}) = P_+(\Psi)\gamma_3; \quad P_3(\Psi) = \frac{1}{2}(-\Psi\mathbf{i} + i\Psi\gamma_{30}) = P_+(\Psi)(-\mathbf{i}). \end{aligned} \quad (3.18)$$

We explained there how the covariant derivative of the Weinberg-Salam model used:

$$D_{\mu} = \partial_{\mu} - ig_1 \frac{Y}{2} B_{\mu} - ig_2 T_j W_{\mu}^j, \quad (3.19)$$

with  $T_j = \frac{\tau_j}{2}$  for a doublet of left-handed particles and  $T_j = 0$  for a singlet of right-handed particle.  $Y$  was the weak hypercharge,  $Y_L = -1, Y_R = -2$  for the electron. The transposition into Clifford algebra used four space-time vectors named ‘‘potentials’’:

$$\begin{aligned} D &= \sigma^{\mu} D_{\mu}; \quad \mathbf{D} = \gamma^{\mu} D_{\mu} = \begin{pmatrix} 0 & D \\ \hat{D} & 0 \end{pmatrix}; \quad B = \sigma^{\mu} B_{\mu}; \quad \mathbf{B} = \gamma^{\mu} B_{\mu} = \begin{pmatrix} 0 & B \\ \hat{B} & 0 \end{pmatrix}; \\ W^j &= \sigma^{\mu} W_{\mu}^j; \quad \mathbf{W}^j = \gamma^{\mu} W_{\mu}^j = \begin{pmatrix} 0 & W^j \\ \hat{W}^j & 0 \end{pmatrix}, \end{aligned} \quad (3.20)$$

which express the covariant derivative in a unique term:

$$\mathbf{D} = \partial + \frac{\mathbf{g}_1}{2} \mathbf{B} P_0 + \frac{\mathbf{g}_2}{2} (\mathbf{W}^1 P_1 + \mathbf{W}^2 P_2 + \mathbf{W}^3 P_3). \quad (3.21)$$

For the calculation of the covariant derivative we use the Socroun’s method incorporating the  $g_j$  constants into the potentials [48]. The  $h_j^k$  potentials simplify the calculation of the  $SU(3)$  group by using three  $SU(2)$  subgroups. We let:

$$\begin{aligned} \mathbf{b} &= \frac{\mathbf{g}_1}{2} \mathbf{B}; \quad \mathbf{w}^j = \frac{\mathbf{g}_2}{2} \mathbf{W}^j, \quad j = 1, 2, 3; \quad h_1^1 = \frac{\mathbf{g}_3}{2} G^1; \quad h_1^2 = \frac{\mathbf{g}_3}{2} G^2; \quad h_1^3 - h_3^3 = \frac{\mathbf{g}_3}{2} \left( G^3 + \frac{G^8}{\sqrt{3}} \right), \\ h_2^1 &= \frac{\mathbf{g}_3}{2} G^6; \quad h_2^2 = \frac{\mathbf{g}_3}{2} G^7; \quad h_2^3 - h_1^3 = \frac{\mathbf{g}_3}{2} \left( -G^3 + \frac{G^8}{\sqrt{3}} \right); \\ h_3^1 &= \frac{\mathbf{g}_3}{2} G^4; \quad h_3^2 = -\frac{\mathbf{g}_3}{2} G^5; \quad h_3^3 - h_2^3 = \frac{\mathbf{g}_3}{2} \left( -2 \frac{G^8}{\sqrt{3}} \right). \end{aligned} \quad (3.22)$$

A detailed calculation was made in [26] 6.1. We have previously supposed that  $\phi^1$  and  $\phi^8$  have the same behaviour under the dilation  $R$  induced by  $M$ . We need here another behaviour:  $\phi^8 \mapsto \phi^8 \tilde{M}$ . We got, with the replacement of  $\phi^8$  by  $\tilde{\phi}^8$ , the replacement of  $\nabla$  by  $\tilde{\nabla} = \nabla$  and the replacement of  $D$  by  $\tilde{D} \neq D$ :

$$\begin{aligned} \tilde{D}\tilde{R}^8 &= \tilde{\nabla}\tilde{R}^8; \quad \hat{D}R^1 = \hat{\nabla}R^1 + 2i\hat{b}R^1; \quad \tilde{D}\tilde{L}^8 = \tilde{\nabla}\tilde{L}^8 + i(b - w^3)\tilde{L}^8 + i(-w^1 + iw^2)\hat{L}^1; \\ D\hat{L}^1 &= \nabla\hat{L}^1 + i(b + w^3)\hat{L}^1 - i(w^1 + iw^2)\tilde{L}^8. \end{aligned} \quad (3.23)$$

This system is equivalent to:

$$\begin{aligned} R^8\hat{D} &= R^8\hat{\nabla}; \quad \hat{D}R^1 = \hat{\nabla}R^1 + 2i\hat{b}R^1; \quad \hat{L}^8D = \hat{L}^8\nabla - i\hat{L}^8(b - w^3) + i\hat{L}^1(w^1 + iw^2); \\ D\hat{L}^1 &= \nabla\hat{L}^1 + i(b + w^3)\hat{L}^1 - i(w^1 + iw^2)\tilde{L}^8. \end{aligned} \quad (3.24)$$

These derivatives are exactly equivalent to those of the Weinberg-Salam model. Equation (3.10) reads

$$(D\Psi_l)\gamma_{012} + m\rho\chi_l = 0, \quad (3.25)$$

where  $\chi_l$  is a term (below) depending on  $\Psi_l$ . The Weinberg-Salam model does not use  $R^8$  and for electro-weak interactions we can cancel this right wave of the neutrino. But when some neutrinos are observed they are able to change into neutrinos of other generations. These changes are studied by using both right and left waves. It is the same if we study the Lochak's magnetic monopole. If the  $\phi^8$  wave is used we get many relativistic invariants, unknown in the Dirac theory where only  $a_1$  was used:

$$\begin{aligned} a_1 &= 2(\xi_1^1\eta_1^{1*} + \xi_2^1\eta_2^{1*}) = 2\eta^{1\dagger}\xi^1; \quad a_2 = 2(\eta_1^{8*}\eta_2^{8*} - \eta_2^{8*}\eta_1^{8*}) = 2\eta^{1\dagger}\hat{\eta}^8 = -2\eta^{8\dagger}\hat{\eta}^1; \\ a_3 &= 2(\xi_1^1\eta_1^{8*} + \xi_2^1\eta_2^{8*}) = 2\eta^{8\dagger}\xi^1; \quad a_4 = 2(\xi_1^8\eta_1^{1*} + \xi_2^8\eta_2^{1*}) = 2\eta^{1\dagger}\xi^8; \\ a_5 &= 2(\xi_1^1\xi_2^8 - \xi_2^1\xi_1^8) = 2\hat{\xi}^{1\dagger}\xi^8 = -2\hat{\xi}^{8\dagger}\xi^1; \quad a_6 = 2(\xi_1^8\eta_1^{8*} + \xi_2^8\eta_2^{8*}) = 2\eta^{8\dagger}\xi^8. \end{aligned} \quad (3.26)$$

When the wave of quarks is zero we also have:

$$\begin{aligned} \rho^2 &= \sum_{j=1}^{j=6} a_j a_j^*; \quad \chi_l = \frac{1}{\rho^2} \begin{pmatrix} M_1 & M_2 \\ \widehat{M}_2 & \widehat{M}_1 \end{pmatrix}, \quad M_1 = a_1^*(L^1 + R^1) + a_2^*\tilde{L}^8\sigma_1 + a_3^*\tilde{L}^8 + a_4^*\tilde{R}^8 + a_5^*\tilde{R}^8\sigma_1, \\ M_2 &= a_6^*(\tilde{L}^8 + \tilde{R}^8) - a_2^*L^1\sigma_1 + a_3^*R^1 + a_4^*L^1 - a_5^*R^1\sigma_1. \end{aligned} \quad (3.27)$$

The lepton wave Equation (3.25) is equivalent to the system:

$$\begin{aligned} 0 &= \hat{\nabla}R^1 + 2i\hat{b}R^1 + i\frac{m}{\rho}(a_1\hat{L}^1 + a_3\hat{L}^8 - a_5\tilde{R}^8\sigma_1). \\ 0 &= \tilde{\nabla}\tilde{R}^8 + i\frac{m}{\rho}(a_6\tilde{L}^8 + a_4\hat{L}^1 + a_5\hat{R}^1\sigma_1). \\ 0 &= \nabla\hat{L}^1 + i(b + w^3)\hat{L}^1 - i(w^1 + iw^2)\tilde{L}^8 + i\frac{m}{\rho}(a_1^*R^1 + a_2^*\tilde{L}^8\sigma_1 + a_4^*\tilde{R}^8). \\ 0 &= \tilde{\nabla}\tilde{L}^8 + i(b - w^3)\tilde{L}^8 - i(w^1 - iw^2)\hat{L}^1 + i\frac{m}{\rho}(a_6^*\tilde{R}^8 - a_2^*L^1\sigma_1 + a_3^*R^1). \end{aligned} \quad (3.28)$$

### 3.2. Double Link with the Lagrangian Density

For comparing the previous equations with the usual complex matrix formalism, we associate to  $R^1, \tilde{R}^8, \hat{L}^1$  and  $\tilde{L}^8$  the Weyl spinors  $\xi^j$  and  $\eta^j$  and we get:

$$\begin{aligned} R^1 &= \sqrt{2}(\xi^1 \quad 0); \quad \tilde{R}^1 = \sqrt{2}\begin{pmatrix} \xi^{1\dagger} \\ 0 \end{pmatrix}; \quad \hat{L}^1 = \sqrt{2}(\eta^1 \quad 0); \quad \tilde{L}^1 = \sqrt{2}\begin{pmatrix} \eta^{1\dagger} \\ 0 \end{pmatrix}; \\ \tilde{R}^8 &= \sqrt{2}(\xi^8 \quad 0); \quad R^8 = \sqrt{2}\begin{pmatrix} \xi^{8\dagger} \\ 0 \end{pmatrix}; \quad \tilde{L}^8 = \sqrt{2}(\eta^8 \quad 0); \quad \hat{L}^8 = \sqrt{2}\begin{pmatrix} \eta^{8\dagger} \\ 0 \end{pmatrix}. \end{aligned} \quad (3.29)$$

Equations (3.28) are equivalent to:

$$\begin{aligned}
0 &= \hat{\nabla} \xi^1 + 2i\hat{b}\xi^1 + i\frac{m}{\rho}(a_1\eta^1 + a_3\eta^8 - a_5\hat{\xi}^8), \\
0 &= \hat{\nabla} \xi^8 + i\frac{m}{\rho}(a_6\eta^8 + a_4\eta^1 + a_5\hat{\xi}^1), \\
0 &= \nabla \eta^1 + i(\mathbf{b} + \mathbf{w}^3)\eta^1 - i(\mathbf{w}^1 + i\mathbf{w}^2)\eta^8 + i\frac{m}{\rho}(a_1^*\xi^1 + a_2^*\hat{\eta}^8 + a_4^*\xi^8), \\
0 &= \nabla \eta^8 + i(\mathbf{b} - \mathbf{w}^3)\eta^8 - i(\mathbf{w}^1 - i\mathbf{w}^2)\eta^1 + i\frac{m}{\rho}(a_6^*\xi^8 - a_2^*\hat{\eta}^1 + a_3^*\xi^1).
\end{aligned} \tag{3.30}$$

Like with the linear Dirac mass term, the covariant derivatives of left spinors are linked by the mass term to right ones and the covariant derivatives of right spinors are linked by the mass term to left ones. But we now have  $a_j$  terms which also change with a gauge transformation [26], compensating exactly the difference between left and right spinors: these equations are both invariant under  $Cl_3^*$  (therefore relativistic invariant) and gauge invariant under the  $U(1) \times SU(2)$  gauge group generated by the four  $P_n$ . The form invariance under  $Cl_3^*$  is proved in [26] B.4.1 and gauge invariance is proved in B.4.2 to B.4.4.

Now we multiply on the left side the second relation (3.28) by  $-iR^8$ :

$$0 = -iR^8\bar{\nabla}\hat{R}^8 + \frac{m}{\rho}(a_6R^8\bar{L}^8 + a_4R^8\hat{L}^1 + a_5R^8\hat{R}^1\sigma_1). \tag{3.31}$$

With the left  $\eta$  and right  $\xi$  spinors this equation reads:

$$0 = \left[ -2i\xi^{8\dagger}(\hat{\nabla}\xi^8) + \frac{m}{\rho}(a_6a_6^* + a_4a_4^* + a_5a_5^*) \right] \frac{1 + \sigma_3}{2}. \tag{3.32}$$

We name  $\delta_R^j$  the real part of  $-2i\xi^{j\dagger}(\hat{\nabla}\xi^j)$ :

$$\delta_R^j = -i\xi^{j\dagger}\hat{\sigma}^\mu\partial_\mu\xi^j + i(\partial_\mu\xi^{j\dagger})\hat{\sigma}^\mu\xi^j. \tag{3.33}$$

This gives:

$$\begin{aligned}
-2i\xi^{j\dagger}(\hat{\nabla}\xi^j) &= \delta_R^j - i\partial_\mu D_R^{j\mu}; \quad D_R^1 = R^1\tilde{R}^1 = D_R^{1\mu}\hat{\sigma}_\mu; \quad D_R^{1\mu} = \xi^{1\dagger}\hat{\sigma}^\mu\xi^1; \\
D_R^8 &= \tilde{R}^8R^8 = D_R^{8\mu}\hat{\sigma}_\mu; \quad D_R^{8\mu} = \xi^{8\dagger}\hat{\sigma}^\mu\xi^8.
\end{aligned} \tag{3.34}$$

Then (3.32) is equivalent to:

$$0 = \delta_R^8 - i\partial_\mu D_R^{8\mu} + \frac{m}{\rho}(a_6a_6^* + a_4a_4^* + a_5a_5^*). \tag{3.35}$$

This complex equation is equivalent to the real system:

$$0 = \delta_R^8 + \frac{m}{\rho}(a_6a_6^* + a_4a_4^* + a_5a_5^*); \quad 0 = \partial_\mu (D_R^8)^\mu. \tag{3.36}$$

We remark that we get not four numeric equations but only two for the four variables of the  $R^8$  spinor wave. This will be the same for the other spinor waves. We see this first with  $R^1$ . We multiply on the left the first equation (3.28) by  $-iR^{1\dagger}$ :

$$0 = -i\tilde{R}^1\hat{\nabla}R^1 + 2\tilde{R}^1\hat{b}R^1 + \frac{m}{\rho}(a_1\tilde{R}^1\hat{L}^1 + a_3\tilde{R}^1\bar{L}^8 - a_5\tilde{R}^1\bar{R}^8\sigma_1). \tag{3.37}$$

With the left  $\eta$  and right  $\xi$  spinors this equation reads:

$$0 = \left[ -2i\xi^{1\dagger}(\hat{\nabla}\xi^1) + 4\xi^{1\dagger}\hat{b}\xi^1 + \frac{m}{\rho}(a_1a_1^* + a_3a_3^* + a_5a_5^*) \right] \frac{1 + \sigma_3}{2}. \tag{3.38}$$

This equation is equivalent to:

$$0 = \delta_R^1 - i\partial_\mu D_R^{1\mu} + 4\xi^{1\dagger} \hat{b} \xi^1 + \frac{m}{\rho} (a_1 a_1^* + a_3 a_3^* + a_5 a_5^*). \quad (3.39)$$

This complex equation is equivalent to the real system:

$$0 = \delta_R^1 + 4b_\mu (D_R^1)^\mu + \frac{m}{\rho} (a_1 a_1^* + a_3 a_3^* + a_5 a_5^*); \quad 0 = \partial_\mu (D_R^1)^\mu, \quad (3.40)$$

because  $(D_R^j)^\mu = \xi^{j\dagger} \hat{\sigma}^\mu \xi^j$ . Next we multiply on the left the third Equation (3.28) by  $-i\bar{L}^1$ :

$$-i\bar{L}^1 \nabla \hat{L}^1 + \bar{L}^1 (b + w^3) \hat{L}^1 - \bar{L}^1 (w^1 + iw^2) \bar{L}^8 + \frac{m}{\rho} \bar{L}^1 (a_1^* R^1 + a_2^* \bar{L}^8 \sigma_1 + a_4^* \bar{R}^8) = 0. \quad (3.41)$$

We let:

$$\begin{aligned} \delta_L^j &= -i\eta^{j\dagger} (\nabla \eta^j) + i(\eta^{j\dagger} \nabla) \eta^j; \quad D_L^1 = L^1 \bar{L}^1; \quad D_L^8 = \bar{L}^8 L^8; \quad L^{jk} = (L^{jk})^\mu \sigma_\mu; \\ (L^{jk})^\mu &= \eta^{j\dagger} \sigma^\mu \eta^k; \quad 2D_L^{jk} = L^{jk} + L^{kj}; \quad 2d_L^{jk} = iL^{jk} - iL^{kj}; \quad L^{jk} = D_L^{jk} - id_L^{jk}. \end{aligned} \quad (3.42)$$

We get:

$$\bar{L} b \hat{L}^1 = (D_L^1)^\mu b_\mu \frac{1+\sigma_3}{2}; \quad (D_L^j)^\mu = \eta^{j\dagger} \sigma^\mu \eta^j; \quad \hat{L}^8 b \bar{L}^8 = (D_L^8)^\mu b_\mu \frac{1+\sigma_3}{2}. \quad (3.43)$$

With the left  $\eta$  and right  $\xi$  spinors (3.41) reads:

$$0 = \left[ -2i\eta^{1\dagger} (\nabla \eta^1) + 2(b_\mu + w_\mu^3) (D_L^1)^\mu - 2(w_\mu^1 + iw_\mu^2) (L^{18})^\mu + \frac{m}{\rho} (a_1 a_1^* + a_2 a_2^* + a_4 a_4^*) \right] \frac{1+\sigma_3}{2}. \quad (3.44)$$

This equation is equivalent to:

$$0 = -2i\eta^{1\dagger} (\nabla \eta^1) + 2(b_\mu + w_\mu^3) (D_L^1)^\mu - 2(w_\mu^1 + iw_\mu^2) (L^{18})^\mu + \frac{m}{\rho} (a_1 a_1^* + a_2 a_2^* + a_4 a_4^*). \quad (3.45)$$

Separating the real and the imaginary part we get the equivalent system:

$$\begin{aligned} 0 &= \delta_L^1 + 2(b_\mu + w_\mu^3) (D_L^1)^\mu - \left[ w_\mu^1 (D_L^{18})^\mu + w_\mu^2 (d_L^{18})^\mu \right] + \frac{m}{\rho} (a_1 a_1^* + a_2 a_2^* + a_4 a_4^*); \\ 0 &= \partial_\mu (D_L^1)^\mu + \left[ w_\mu^2 (D_L^{18})^\mu - w_\mu^1 (d_L^{18})^\mu \right]. \end{aligned} \quad (3.46)$$

We multiply on the left the last Equation (3.28) by  $-i\hat{L}^8$ :

$$0 = -i\hat{L}^8 \left[ \tilde{\nabla} \bar{L}^8 + (b - w^3) \bar{L}^8 - (w^1 - iw^2) \hat{L}^1 + \frac{m}{\rho} (a_6^* R^8 - a_2^* L^1 \sigma_1 + a_3^* R^1) \right]. \quad (3.47)$$

With the left  $\eta$  and right  $\xi$  spinors (3.47) reads:

$$0 = \left[ -2i\eta^{8\dagger} (\nabla \eta^8) + 2(b_\mu - w_\mu^3) (D_L^8)^\mu - 2(w_\mu^1 - iw_\mu^2) (L^{81})^\mu + \frac{m}{\rho} (a_6 a_6^* + a_2 a_2^* + a_3 a_3^*) \right] \frac{1+\sigma_3}{2}. \quad (3.48)$$

This equation is equivalent to:

$$0 = -2i\eta^{8\dagger} (\nabla \eta^8) + 2(b_\mu - w_\mu^3) (D_L^8)^\mu - 2(w_\mu^1 - iw_\mu^2) (L^{81})^\mu + \frac{m}{\rho} (a_6 a_6^* + a_2 a_2^* + a_3 a_3^*). \quad (3.49)$$

Separating the real and the imaginary part we get the equivalent system:

$$\begin{aligned} 0 &= \delta_L^8 + 2(b_\mu - w_\mu^3) (D_L^8)^\mu - \left[ w_\mu^1 (D_L^{18})^\mu + w_\mu^2 (d_L^{18})^\mu \right] + \frac{m}{\rho} (a_6 a_6^* + a_2 a_2^* + a_3 a_3^*); \\ 0 &= \partial_\mu (D_L^8)^\mu - \left[ w_\mu^2 (D_L^{18})^\mu - w_\mu^1 (d_L^{18})^\mu \right]. \end{aligned} \quad (3.50)$$

Adding and subtracting the second Equations (3.46) and (3.50) we get:

$$\begin{aligned} 0 &= \partial_\mu (D_L^1 + D_L^8)^\mu; \\ 0 &= \partial_\mu (D_L^1 - D_L^8)^\mu + 2 \left[ w_\mu^2 (D_L^{18})^\mu - w_\mu^1 (d_L^{18})^\mu \right]. \end{aligned} \quad (3.51)$$

The lepton part of the Lagrangian density is the sum of the real parts in (3.36), (3.40), (3.46), (3.50):

$$\begin{aligned} 0 = \mathcal{L}_l &= \frac{1}{2} \left[ \delta_R^8 + \frac{m}{\rho} (a_6 a_6^* + a_4 a_4^* + a_5 a_5^*) \right] + \frac{1}{2} \left[ \delta_R^1 + 4b_\mu (D_R^1)^\mu + \frac{m}{\rho} (a_1 a_1^* + a_3 a_3^* + a_5 a_5^*) \right] \\ &+ \frac{1}{2} \left[ \delta_L^1 + 2(b_\mu + w_\mu^3) (D_L^1)^\mu - 2 \left[ w_\mu^1 (D_L^{18})^\mu + w_\mu^2 (d_L^{18})^\mu \right] + \frac{m}{\rho} (a_1 a_1^* + a_2 a_2^* + a_4 a_4^*) \right] \\ &+ \frac{1}{2} \left[ \delta_L^8 + 2(b_\mu - w_\mu^3) (D_L^8)^\mu - 2 \left[ w_\mu^1 (D_L^{18})^\mu + w_\mu^2 (d_L^{18})^\mu \right] + \frac{m}{\rho} (a_6 a_6^* + a_2 a_2^* + a_3 a_3^*) \right]. \end{aligned} \quad (3.52)$$

This gives:

$$\begin{aligned} 0 = \mathcal{L}_l &= \frac{1}{2} \left[ \delta_R^1 + \delta_R^8 + \delta_L^1 + \delta_L^8 \right] + b_\mu (2D_R^{1\mu} + D_L^{1\mu} + D_L^{8\mu}) \\ &- \left[ w_\mu^1 D_L^{18\mu} + w_\mu^2 d_L^{18\mu} + w_\mu^3 (D_L^{8\mu} - D_L^{1\mu}) \right] + \frac{m}{\rho} (a_1 a_1^* + a_2 a_2^* + a_3 a_3^* + a_4 a_4^* + a_5 a_5^* + a_6 a_6^*). \end{aligned} \quad (3.53)$$

Since  $a_1 a_1^* + a_2 a_2^* + a_3 a_3^* + a_4 a_4^* + a_5 a_5^* + a_6 a_6^* = \rho^2$  we get:

$$\begin{aligned} 0 = \mathcal{L}_l &= \frac{i}{2} \left( -\xi^{1\dagger} \hat{\sigma}^\mu \partial_\mu \xi^1 + (\partial_\mu \xi^1)^\dagger \hat{\sigma}^\mu \xi^1 - \xi^{8\dagger} \hat{\sigma}^\mu \partial_\mu \xi^8 + (\partial_\mu \xi^8)^\dagger \hat{\sigma}^\mu \xi^8 \right. \\ &- \eta^{1\dagger} \sigma^\mu \partial_\mu \eta^1 + (\partial_\mu \eta^1)^\dagger \sigma^\mu \eta^1 - \eta^{8\dagger} \sigma^\mu \partial_\mu \eta^8 + (\partial_\mu \eta^8)^\dagger \sigma^\mu \eta^8 \left. \right) \\ &+ m\rho + b_\mu (2\xi^{1\dagger} \hat{\sigma}^\mu \xi^1 + \eta^{1\dagger} \sigma^\mu \eta^1 + \eta^{8\dagger} \sigma^\mu \eta^8) \\ &- \left[ (w_\mu^1 + i w_\mu^2) \eta^{1\dagger} \sigma^\mu \eta^8 + (w_\mu^1 - i w_\mu^2) \eta^{8\dagger} \sigma^\mu \eta^1 + w_\mu^3 (-\eta^{1\dagger} \sigma^\mu \eta^1 + \eta^{8\dagger} \sigma^\mu \eta^8) \right]. \end{aligned} \quad (3.54)$$

Now we derive the wave equations resulting from the Lagrange equations. The Lagrange equation:

$$\frac{\partial \mathcal{L}}{\partial \xi^{1\dagger}} = \partial_\mu \left( \frac{\partial \mathcal{L}}{\partial (\partial_\mu \xi^{1\dagger})} \right) \quad (3.55)$$

gives

$$0 = -i\hat{\nabla} \xi^1 + 2\hat{b}\xi^1 + \frac{m}{\rho} (a_1 \eta^1 + a_3 \eta^8 - a_5 \hat{\xi}^8), \quad (3.56)$$

which is the first Equation (3.30), equivalent to the first Equation (3.28). Similarly deriving with  $\eta^{1\dagger}$  we get the third Equation (3.30), equivalent to the third Equation (3.28). Next the Lagrange equation

$$\frac{\partial \mathcal{L}}{\partial \xi^{8\dagger}} = \partial_\mu \left( \frac{\partial \mathcal{L}}{\partial (\partial_\mu \xi^{8\dagger})} \right) \quad (3.57)$$

gives

$$0 = -i\hat{\nabla} \xi^8 + \frac{m}{\rho} (a_4 \eta^1 + a_5 \hat{\xi}^1 + a_6 \eta^8), \quad (3.58)$$

which is equivalent to the second Equation (3.28). The Lagrange equation  $\frac{\partial \mathcal{L}}{\partial \eta^{8\dagger}} = \partial_\mu \left( \frac{\partial \mathcal{L}}{\partial (\partial_\mu \eta^{8\dagger})} \right)$  gives the

last Equation (3.28). This establishes the double link between wave equations and Lagrangian density. The link from Lagrangian density to wave equations was known from the beginning of quantum mechanics. The link from wave equations to Lagrangian density is the true reason of the existence of a Lagrangian mechanism. This link is much stronger than the first one on the physical point of view, because the old link supposes an integration by parts and a cancellation of terms. The possibility of this cancellation is dubious in the case of propagating waves (like gravitational waves).

### 3.3. Double Link with the Lagrangian Density (Quark Case)

Noting  $P_j \begin{pmatrix} \phi^n & \tilde{\phi}^{3+n} \\ \bar{\phi}^{3+n} & \hat{\phi}^n \end{pmatrix} = \begin{pmatrix} P_j(\phi^n) & P_j(\tilde{\phi}^{3+n}) \\ \hat{P}_j(\tilde{\phi}^{3+n}) & \hat{P}_j(\phi^n) \end{pmatrix}, j=0,1,2,3$  and  $n=2,3,4$  we have

$$\begin{aligned} P_0(\phi^n) &= \frac{2i}{3}R^n + \frac{i}{3}L^n; P_1(\phi^n) = i\tilde{L}^{3+n}; P_2(\phi^n) = \tilde{L}^{3+n}; P_3(\phi^n) = -iL^n; \\ P_0(\tilde{\phi}^{3+n}) &= -\frac{4i}{3}\tilde{R}^{3+n} + \frac{i}{3}\tilde{L}^{3+n}; P_1(\tilde{\phi}^{3+n}) = iL^n; P_2(\tilde{\phi}^{3+n}) = -L^n; P_3(\tilde{\phi}^{3+n}) = i\tilde{L}^{3+n}. \end{aligned} \tag{3.59}$$

We note  $\underline{n} = n \bmod 3: \underline{3} = 3, \underline{4} = 1$  and  $\underline{5} = 2$ . The covariant derivative reads, with  $n = 2, 3, 4$ :

$$\begin{aligned} \hat{D}R^n &= \hat{\nabla}R^n + \frac{2i}{3}\hat{\mathbf{b}}R^n + i(\hat{h}_{n-1}^1 + i\hat{h}_{n-1}^2)R^{n+1} + i(\hat{h}_{n+1}^1 - i\hat{h}_{n+1}^2)R^{n+2} + i(\hat{h}_{n-1}^3 - \hat{h}_{n+1}^3)R^n, \\ \bar{D}\tilde{R}^{3+n} &= \bar{\nabla}\tilde{R}^{3+n} - \frac{4i}{3}\hat{\mathbf{b}}\tilde{R}^{3+n} + i(\hat{h}_{n-1}^1 + i\hat{h}_{n-1}^2)\tilde{R}^{3+n+1} + i(\hat{h}_{n+1}^1 - i\hat{h}_{n+1}^2)\tilde{R}^{3+n+2} + i(\hat{h}_{n-1}^3 - \hat{h}_{n+1}^3)\tilde{R}^{3+n}, \\ D\hat{L}^n &= \nabla\hat{L}^n - \frac{i}{3}\mathbf{b}\hat{L}^n - i[(w^1 + iw^2)\bar{L}^{3+n} - w^3\hat{L}^n] - i(h_{n-1}^1 + ih_{n-1}^2)\hat{L}^{n+1} \\ &\quad - i(h_{n+1}^1 - ih_{n+1}^2)\hat{L}^{n+2} - i(h_{n-1}^3 - h_{n+1}^3)\hat{L}^n, \\ \tilde{D}\bar{L}^{3+n} &= \tilde{\nabla}\bar{L}^{3+n} - \frac{i}{3}\mathbf{b}\bar{L}^{3+n} - i[(w^1 - iw^2)\hat{L}^n + w^3\bar{L}^{3+n}] - i(h_{n-1}^1 + ih_{n-1}^2)\bar{L}^{3+n+1} \\ &\quad - i(h_{n+1}^1 - ih_{n+1}^2)\bar{L}^{3+n+2} - i(h_{n-1}^3 - h_{n+1}^3)\bar{L}^{3+n}. \end{aligned} \tag{3.60}$$

When  $\Psi_l$  is zero the  $\rho^2$  term is a sum of 66 terms (relativistic invariants):

$$\rho^2 = \sum_{n=2}^{n=7} d_n d_n^* + \sum_{n,p,q} s_n^{pq} (s_n^{pq})^*; d_n = R^n \bar{L}^n + L^n \bar{R}^n = 2\eta^{n\dagger} \xi^n, \tag{3.61}$$

where in  $s_n^{pq}, n=2,3,4,5$   $pq = 23, 34, 42, 56, 67, 75, 52, 53, 54, 62, 63, 64, 72, 73, 74$  and:

$$s_2^{pq} = 2\eta^{p\dagger} \hat{\eta}^q = -2\eta^{q\dagger} \hat{\eta}^p; s_3^{pq} = 2\eta^{q\dagger} \xi^p; s_4^{pq} = 2\eta^{p\dagger} \xi^q; s_5^{pq} = 2\xi^{p\dagger} \xi^q = -2\xi^{q\dagger} \xi^p. \tag{3.62}$$

And when the  $\Psi$  wave is complete, with both lepton and quarks terms we have:

$$\rho^2 = \sum_{n=1}^{n=6} a_n a_n^* + \sum_{n=2}^{n=7} d_n d_n^* + \sum_{n,p,q} s_n^{pq} (s_n^{pq})^*. \tag{3.63}$$

This is a sum of 72 terms, all positive.

### 3.4. The Quark Wave

Like in the lepton case the Lagrangian density is doubly linked to wave equations in the quark case. The Lagrangian density reads:

$$\begin{aligned} \mathcal{L}_q &= m\rho + \frac{i}{2} \sum_{n=2}^{n=7} [-\eta^{n\dagger} \sigma^\mu (\partial_\mu \eta^n) + (\partial_\mu \eta^{n\dagger}) \sigma^\mu \eta^n - \xi^{n\dagger} \hat{\sigma}^\mu (\partial_\mu \xi^n) + (\partial_\mu \xi^{n\dagger}) \hat{\sigma}^\mu \xi^n] \\ &\quad + \sum_{n=2,3,4} \left[ \frac{2}{3} \xi^{n\dagger} \hat{\mathbf{b}} \xi^n - \frac{4}{3} (\xi^{3+n})^\dagger \hat{\mathbf{b}} \xi^{3+n} \right] - \frac{1}{3} \sum_{n=2}^{n=7} \eta^{n\dagger} \mathbf{b} \eta^n + \sum_{n=2,3,4} [\mathcal{L}_1^n + \mathcal{L}_2^n + \mathcal{L}_3^n + \mathcal{L}_4^n + \mathcal{L}_5^n + \mathcal{L}_6^n + \mathcal{L}_7^n], \end{aligned} \tag{3.64}$$

$$\begin{aligned}
 \mathcal{L}_1^n &= -(\eta^{n\dagger} w^1 \eta^{3+n} + \eta^{3+n\dagger} w^1 \eta^n) - i(\eta^{n\dagger} w^2 \eta^{3+n} - \eta^{3+n\dagger} w^2 \eta^n) + (\eta^{n\dagger} w^3 \eta^n - \eta^{3+n\dagger} w^3 \eta^{3+n}); \\
 \mathcal{L}_2^n &= \left[ (\xi^{n\dagger} \hat{h}_{n-1}^1 \xi^{n+1}) + (\xi^{n\dagger} \hat{h}_{n-1}^1 \xi^{n+1})^\dagger - (\eta^{n\dagger} h_{n-1}^1 \eta^{n+1}) - (\eta^{n\dagger} h_{n-1}^1 \eta^{n+1})^\dagger \right]; \\
 \mathcal{L}_3^n &= i \left[ -(\xi^{n\dagger} \hat{h}_{n-1}^2 \xi^{n+1}) + (\xi^{n\dagger} \hat{h}_{n-1}^2 \xi^{n+1})^\dagger - (\eta^{n\dagger} h_{n-1}^2 \eta^{n+1}) + (\eta^{n\dagger} h_{n-1}^1 \eta^{n+1})^\dagger \right]; \\
 \mathcal{L}_4^n &= \left[ \xi^{n\dagger} \hat{h}_{n-1}^3 \xi^n - (\xi^{n+1})^\dagger \hat{h}_{n-1}^3 \xi^{n+1} - \eta^{n\dagger} h_{n-1}^3 \eta^n + (\eta^{n+1})^\dagger h_{n-1}^3 \eta^{n+1} \right]; \\
 \mathcal{L}_5^n &= \left[ (\xi^{(3+n)\dagger} \hat{h}_{n-1}^1 \xi^{3+n+1}) + (\xi^{(3+n)\dagger} \hat{h}_{n-1}^1 \xi^{3+n+1})^\dagger - (\eta^{(3+n)\dagger} h_{n-1}^1 \eta^{3+n+1}) - (\eta^{(3+n)\dagger} h_{n-1}^1 \eta^{3+n+1})^\dagger \right]; \\
 \mathcal{L}_6^n &= i \left[ -(\xi^{(3+n)\dagger} \hat{h}_{n-1}^2 \xi^{3+n+1}) + (\xi^{(3+n)\dagger} \hat{h}_{n-1}^2 \xi^{3+n+1})^\dagger - (\eta^{(3+n)\dagger} h_{n-1}^2 \eta^{3+n+1}) + (\eta^{(3+n)\dagger} h_{n-1}^1 \eta^{3+n+1})^\dagger \right]; \\
 \mathcal{L}_7^n &= \left[ \xi^{(3+n)\dagger} \hat{h}_{n-1}^3 \xi^{3+n} - (\xi^{3+n+1})^\dagger \hat{h}_{n-1}^3 \xi^{3+n+1} - \eta^{(3+n)\dagger} h_{n-1}^3 \eta^{3+n} + (\eta^{3+n+1})^\dagger h_{n-1}^3 \eta^{3+n+1} \right].
 \end{aligned} \tag{3.65}$$

We can derive from this Lagrangian density the wave equations:

$$\begin{aligned}
 -i\hat{D}R^n + m\rho\hat{\chi}_R^n &= 0, \quad n = 2, 3, 4. \\
 \rho^2 \hat{\chi}_R^n &= d_n \hat{L}^n - s_5^{n+1} \hat{R}^{n+1} \sigma_1 + s_3^{n+1} \hat{L}^{n+1} + s_5^{n+2} \hat{R}^{n+2} \sigma_1 + s_4^{n+2} \hat{L}^{n+2} \\
 &\quad + s_5^{5n} \bar{R}^5 \sigma_1 + s_5^{6n} \bar{R}^6 \sigma_1 + s_5^{7n} \bar{R}^7 \sigma_1 + s_4^{5n} \bar{L}^5 + s_4^{6n} \bar{L}^6 + s_4^{7n} \bar{L}^7.
 \end{aligned} \tag{3.66}$$

$$\begin{aligned}
 -i\bar{D}\bar{R}^{3+n} + m\rho\bar{\chi}_R^{3+n} &= 0, \quad n = 2, 3, 4. \\
 \rho^2 \bar{\chi}_R^{3+n} &= d_{3+n} \bar{L}^{3+n} - s_5^{3+n+1} \bar{R}^{3+n+1} \sigma_1 + s_3^{3+n+1} \bar{L}^{3+n+1} + s_5^{3+n+2} \bar{R}^{3+n+2} \sigma_1 + s_4^{3+n+2} \bar{L}^{3+n+2} \\
 &\quad - s_5^{3+n+2} \hat{R}^2 \sigma_1 - s_5^{3+n+3} \hat{R}^3 \sigma_1 - s_5^{3+n+4} \hat{R}^4 \sigma_1 + s_3^{3+n+2} \hat{L}^2 + s_3^{3+n+3} \hat{L}^3 + s_3^{3+n+4} \hat{L}^4.
 \end{aligned} \tag{3.67}$$

$$\begin{aligned}
 -iD\hat{L}^n + m\rho\chi_L^n &= 0, \quad n = 2, 3, 4. \\
 \rho^2 \chi_L^n &= d_n^* R^n + (s_2^{n+1})^* L^{n+1} \sigma_1 + (s_4^{n+1})^* R^{n+1} - (s_2^{n+2})^* L^{n+2} \sigma_1 + (s_3^{n+2})^* R^{n+2} \\
 &\quad - (s_2^{5n})^* \tilde{L}^5 \sigma_1 - (s_2^{6n})^* \tilde{L}^6 \sigma_1 - (s_2^{7n})^* \tilde{L}^7 \sigma_1 + (s_3^{5n})^* \tilde{R}^5 + (s_3^{6n})^* \tilde{R}^6 + (s_3^{7n})^* \tilde{R}^7.
 \end{aligned} \tag{3.68}$$

$$\begin{aligned}
 -i\bar{D}\bar{L}^{3+n} + m\rho\bar{\chi}_L^{3+n} &= 0, \quad n = 2, 3, 4. \\
 \rho^2 \bar{\chi}_L^{3+n} &= d_{3+n}^* \bar{R}^{3+n} + (s_2^{3+n+1})^* \bar{L}^{3+n+1} \sigma_1 + (s_4^{3+n+1})^* \bar{R}^{3+n+1} - (s_2^{3+n+2})^* \bar{L}^{3+n+2} \sigma_1 + (s_3^{3+n+2})^* \bar{R}^{3+n+2} \\
 &\quad + (s_2^{3+n+2})^* L^2 \sigma_1 + (s_2^{3+n+3})^* L^3 \sigma_1 + (s_2^{3+n+4})^* L^4 \sigma_1 + (s_4^{3+n+2})^* R^2 + (s_4^{3+n+3})^* R^3 + (s_4^{3+n+4})^* R^4.
 \end{aligned} \tag{3.69}$$

To get the Lagrangian density from these wave equations we multiply (3.66) on the left by  $\tilde{R}^n$ ,  $n = 2, 3, 4$  and (3.67) by  $\bar{R}^{3+n}$ ,  $n = 2, 3, 4$ . We let:

$$R^{jk\mu} = \xi^{k\dagger} \hat{\sigma}^\mu \xi^j; \quad D_R^{jk\mu} = R^{jk\mu} + R^{kj\mu}; \quad d_R^{jk\mu} = -iR^{jk\mu} + iR^{kj\mu}, \tag{3.70}$$

and we get:

$$\tilde{R}^n \hat{b}R^k = 2\xi^{n\dagger} \hat{\sigma}^\mu \xi^k b_\mu \frac{1+\sigma_3}{2}; \quad R^{3+n} \hat{b}\bar{R}^{3+k} = 2\xi^{3+n\dagger} \hat{\sigma}^\mu \xi^{3+k} b_\mu \frac{1+\sigma_3}{2}, \quad n, k = 2, 3, 4. \tag{3.71}$$

Then (3.66) gives:

$$\begin{aligned}
 0 &= \left[ \delta_R^n - i\partial_\mu D_R^{n\mu} + \frac{2}{3} b_\mu D_R^{n\mu} + (h_{n-1\mu}^1 + ih_{n-1\mu}^2) R^{n+1\ n\mu} + (h_{n+1\mu}^1 - ih_{n+1\mu}^2) R^{n+2\ n\mu} + (h_{n-1\mu}^3 - h_{n+1\mu}^2) D_R^{n\mu} \right. \\
 &\quad \left. + \frac{m}{\rho} \left( |d_n|^2 + |s_5^{n+1}|^2 + |s_3^{n+1}|^2 + |s_5^{n+2}|^2 + |s_4^{n+2}|^2 + |s_5^{5n}|^2 + |s_5^{6n}|^2 + |s_5^{7n}|^2 + |s_4^{5n}|^2 + |s_4^{6n}|^2 + |s_4^{7n}|^2 \right) \right] \frac{1+\sigma_3}{2}.
 \end{aligned} \tag{3.72}$$

Like in the lepton case, the particular form of this wave equation allows us to get an equivalent system with

only two numeric equations:

$$0 = \delta_R^n + \frac{2}{3} \mathbf{b}_\mu D_R^{n\mu} + (h_{n-1\mu}^3 - h_{n+1\mu}^2) D_R^{n\mu} + \frac{1}{2} (h_{n-1\mu}^1 D_R^{n+1\ n\mu} - h_{n-1\mu}^2 d_R^{n+1\ n\mu} + h_{n+1\mu}^1 D_R^{n+2\ n\mu} - h_{n+1\mu}^2 d_R^{n+2\ n\mu}) + \frac{m}{\rho} (|d_n|^2 + |s_5^{n\ n+1}|^2 + |s_3^{n\ n+1}|^2 + |s_5^{n+2\ n}|^2 + |s_4^{n+2\ n}|^2 + |s_5^{5n}|^2 + |s_5^{6n}|^2 + |s_5^{7n}|^2 + |s_4^{5n}|^2 + |s_4^{6n}|^2 + |s_4^{7n}|^2). \quad (3.73)$$

$$\partial_\mu D_R^{n\mu} = h_{n-1\mu}^1 d_R^{n+1\ n\mu} + h_{n-1\mu}^2 D_R^{n+1\ n\mu} + h_{n+1\mu}^1 d_R^{n+2\ n\mu} - h_{n+1\mu}^2 D_R^{n+2\ n\mu}. \quad (3.74)$$

By adding and using  $d^{qp} = -d^{pq}$  we get:

$$\partial_\mu (D_R^{2\mu} + D_R^{3\mu} + D_R^{4\mu}) = 0. \quad (3.75)$$

Only the sum of the three currents generated by the three colors of the  $d$  quark is a conservative space-time vector. Similarly for the  $u$  quark, with colour states  $\tilde{\phi}^{3+n}, n = 2, 3, 4$ , we get:

$$0 = \left[ \delta_R^{3+n} - i\partial_\mu D_R^{3+n\ \mu} - \frac{4}{3} \mathbf{b}_\mu D_R^{3+n\ \mu} + (h_{n-1\mu}^1 + ih_{n-1\mu}^2) R^{3+n+1\ 3+n\ \mu} + (h_{n+1\mu}^1 - ih_{n+1\mu}^2) R^{3+n+2\ 3+n\ \mu} + (h_{n-1\mu}^3 - h_{n+1\mu}^2) D_R^{3+n\ \mu} + \frac{m}{\rho} (|d_{3+n}|^2 + |s_5^{3+n\ 3+n+1}|^2 + |s_3^{3+n\ 3+n+1}|^2 + |s_5^{3+n+2\ 3+n}|^2 + |s_4^{3+n+2\ 3+n}|^2 + |s_5^{3+n\ 2}|^2 + |s_5^{3+n\ 3}|^2 + |s_5^{3+n\ 4}|^2 + |s_3^{3+n\ 2}|^2 + |s_3^{3+n\ 3}|^2 + |s_3^{3+n\ 4}|^2) \right] \frac{1 + \sigma_3}{2}. \quad (3.76)$$

Next the particular form of this wave equation allows us to get an equivalent system with only two numeric equations:

$$0 = \delta_R^{3+n} - \frac{4}{3} \mathbf{b}_\mu D_R^{3+n\ \mu} + (h_{n-1\mu}^3 - h_{n+1\mu}^2) D_R^{3+n\ \mu} + \frac{m}{\rho} (|d_{3+n}|^2 + |s_5^{3+n\ 3+n+1}|^2 + |s_3^{3+n\ 3+n+1}|^2 + |s_5^{3+n+2\ 3+n}|^2 + |s_4^{3+n+2\ 3+n}|^2 + |s_5^{3+n\ 2}|^2 + |s_5^{3+n\ 3}|^2 + |s_5^{3+n\ 4}|^2 + |s_3^{3+n\ 2}|^2 + |s_3^{3+n\ 3}|^2 + |s_3^{3+n\ 4}|^2) + \frac{1}{2} (h_{n-1\mu}^1 D_R^{3+n+1\ 3+n\ \mu} - h_{n-1\mu}^2 d_R^{n+1\ n\mu} + h_{n+1\mu}^1 D_R^{3+n+2\ 3+n\ \mu} - h_{n+1\mu}^2 d_R^{3+n+2\ 3+n\ \mu}). \quad (3.77)$$

$$\partial_\mu D_R^{3+n\ \mu} = h_{n-1\mu}^1 d_R^{3+n+1\ 3+n\ \mu} + h_{n-1\mu}^2 D_R^{3+n+1\ 3+n\ \mu} + h_{n+1\mu}^1 d_R^{3+n+2\ 3+n\ \mu} - h_{n+1\mu}^2 D_R^{3+n+2\ 3+n\ \mu}. \quad (3.78)$$

And we also get

$$\partial_\mu (D_R^{5\mu} + D_R^{6\mu} + D_R^{7\mu}) = 0. \quad (3.79)$$

For the left waves, we multiply (3.68) on the left by  $\bar{L}^n, n = 2, 3, 4$  or (3.69) by  $\tilde{L}^{3+n}, n = 2, 3, 4$  and we get, with:

$$D_L^n = L^n \tilde{L}^n; \quad D_L^{3+n} = \tilde{L}^{3+n} L^{3+n}; \quad L^{pq\mu} = \eta^{p\dot{q}} \sigma^\mu \eta^q, \quad (3.80)$$

$$0 = \left[ -2i\eta^{n\dot{q}} (\nabla \eta^q) + \left( -\frac{\mathbf{b}}{3} + \mathbf{w} \right)_\mu D_L^{n\mu} - 2(\mathbf{w}^1 + i\mathbf{w}^2)_\mu L^{3+n\ \mu} - 2(h_{n-1}^1 + ih_{n-1}^2)_\mu L^{n\ n+1\ \mu} - 2(h_{n+1}^1 - ih_{n+1}^2)_\mu L^{n\ n+2\ \mu} - (h_{n-1}^3 - h_{n+1}^3)_\mu D_L^{n\mu} + \frac{m}{\rho} (|d_n|^2 + |s_2^{n\ n+1}|^2 + |s_4^{n\ n+1}|^2 + |s_2^{n+2\ n}|^2 + |s_3^{n+2\ n}|^2 + |s_2^{5n}|^2 + |s_2^{6n}|^2 + |s_2^{7n}|^2 + |s_3^{5n}|^2 + |s_3^{6n}|^2 + |s_3^{7n}|^2) \right] \frac{1 + \sigma_3}{2}. \quad (3.81)$$

Here also this wave equation is equivalent to a system of only two numeric equations:

$$\begin{aligned}
 0 = & \delta_L^n + \left(-\frac{b}{3} + w\right) D_L^{n\mu} - (h_{n-1}^3 - h_{n+1}^3)_{\mu} D_L^{n\mu} - (w_{\mu}^1 D_L^{n\ 3+n\ \mu} + w_{\mu}^2 d_L^{n\ 3+n\ \mu}) \\
 & - (h_{n-1}^{1\mu} D_L^{n\ n+1\ \mu} + h_{n-1}^{2\mu} d_L^{n\ n+1\ \mu}) - h_{n+1}^{1\mu} D_L^{n\ n+2\ \mu} + h_{n+1}^{2\mu} d_L^{n\ n+2\ \mu} + \frac{m}{\rho} \left(|d_n|^2 + |s_2^{n\ n+1}|^2\right. \\
 & \left. + |s_4^{n\ n+1}|^2 + |s_2^{n+2\ n}|^2 + |s_3^{n+2\ n}|^2 + |s_2^{5n}|^2 + |s_2^{6n}|^2 + |s_2^{7n}|^2 + |s_3^{5n}|^2 + |s_3^{6n}|^2 + |s_3^{7n}|^2\right). \\
 \partial_{\mu} D_L^{n\mu} = & w_{\mu}^1 d_L^{n\ 3+n\ \mu} - w_{\mu}^2 D_L^{n\ 3+n\ \mu} + h_{n-1}^{1\mu} d_L^{n\ n+1\ \mu} - h_{n-1}^{2\mu} D_L^{n\ n+1\ \mu} + h_{n+1}^{1\mu} d_L^{n\ n+2\ \mu} + h_{n+1}^{2\mu} D_L^{n\ n+2\ \mu}.
 \end{aligned} \tag{3.82}$$

Finally for the left waves of the  $u$  quark we have:

$$\begin{aligned}
 0 = & \left[-2i\eta^{3+n\ \dagger} (\nabla \eta^{3+n}) - \left(\frac{b}{3} + w\right) D_L^{3+n\ \mu} - 2(w^1 - iw^2)_{\mu} L^{3+n\ n\ \mu}\right. \\
 & \left.- 2(h_{n-1}^1 + ih_{n-1}^2)_{\mu} L^{3+n\ 3+n+1\ \mu} - 2(h_{n+1}^1 - ih_{n+1}^2)_{\mu} L^{3+n\ 3+n+2\ \mu} - (h_{n-1}^3 - h_{n+1}^3)_{\mu} D_L^{3+n\ \mu}\right. \\
 & \left. + \frac{m_2}{\rho_2} \left(|d_{3+n}|^2 + |s_2^{3+n\ 3+n+1}|^2 + |s_4^{3+n\ 3+n+1}|^2 + |s_2^{3+n+2\ 3+n}|^2 + |s_3^{3+n+2\ 3+n}|^2\right.\right. \\
 & \left. \left. + |s_2^{3+n\ 2}|^2 + |s_2^{3+n\ 3}|^2 + |s_2^{3+n\ 4}|^2 + |s_4^{3+n\ 2}|^2 + |s_4^{3+n\ 3}|^2 + |s_4^{3+n\ 4}|^2\right)\right] \frac{1 + \sigma_3}{2}
 \end{aligned} \tag{3.83}$$

Here also this wave equation is equivalent to a system of only two numeric equations:

$$\begin{aligned}
 0 = & \delta_L^{3+n} - \left(\frac{b}{3} + w\right)_{\mu} D_L^{3+n\ \mu} - (h_{n-1}^3 - h_{n+1}^3)_{\mu} D_L^{3+n\ \mu} - (w_{\mu}^1 D_L^{3+n\ n\ \mu} - w_{\mu}^2 d_L^{3+n\ n\ \mu}) \\
 & - (h_{n-1}^{1\mu} D_L^{3+n\ 3+n+1\ \mu} + h_{n-1}^{2\mu} d_L^{3+n\ 3+n+1\ \mu}) - h_{n+1}^{1\mu} D_L^{3+n\ 3+n+2\ \mu} + h_{n+1}^{2\mu} d_L^{3+n\ 3+n+2\ \mu} \\
 & + \frac{m}{\rho} \left(|d_{3+n}|^2 + |s_2^{3+n\ 3+n+1}|^2 + |s_4^{3+n\ 3+n+1}|^2 + |s_2^{3+n+2\ 3+n}|^2 + |s_3^{3+n+2\ 3+n}|^2\right. \\
 & \left. + |s_2^{3+n\ 2}|^2 + |s_2^{3+n\ 3}|^2 + |s_2^{3+n\ 4}|^2 + |s_4^{3+n\ 2}|^2 + |s_4^{3+n\ 3}|^2 + |s_4^{3+n\ 4}|^2\right). \\
 \partial_{\mu} D_L^{3+n\ \mu} = & -w_{\mu}^1 d_L^{n\ 3+n\ \mu} - w_{\mu}^2 D_L^{n\ 3+n\ \mu} + h_{n-1}^{1\mu} d_L^{n\ n+1\ \mu} - h_{n-1}^{2\mu} D_L^{n\ n+1\ \mu} + h_{n+1}^{1\mu} d_L^{3+n\ 3+n+2\ \mu} + h_{n+1}^{2\mu} D_L^{3+n\ 3+n+2\ \mu}.
 \end{aligned} \tag{3.84}$$

For the left waves of quarks only one sum gives a conservative space-time vector, because the weak gauge links the waves of the  $u$  and  $d$  quarks:

$$\partial_{\mu} \left(\sum_{n=2}^{n=7} D_L^{n\mu}\right) = 0. \tag{3.85}$$

This means that a conservative probability current does not exist for an isolated coloured quark, and this is well known, since it is impossible to observe such isolated states.

The Lagrangian density  $2\mathcal{L}_q$  is the sum on 2,3,4 of the sum of Equations (3.73), (3.77), (3.82) and (3.84). All mass terms are gotten twice and the sum of all squares is exactly  $2\rho^2$ . The Lagrangian density for all objects of the first generation is the sum  $\mathcal{L} = \mathcal{L}_l + \mathcal{L}_q$ . Since  $\rho^2$  is the sum of the lepton part and the quark part, it is sufficient to add the 16 equations, 4 from the lepton case, 12 from the quark case, to get the simplification by  $\rho^2$  in the mass term. This achieves the general proof of the double link between wave equations and Lagrangian density.

### 3.5. Lessons of This Calculation

The previous calculation proves that the use of  $Cl_{1,3}$  and  $Cl_{1,5}$  algebras is unnecessary. The  $Cl_3$  algebra is then the unique framework allowing us to describe all interactions of quantum physics, if we use also this framework to describe gravitation. In this framework we are also able to establish the double link between wave equations and Lagrangian density. The existence of a Lagrangian principle is then compulsory; it is not the con-

sequence of a meta-physical prescription but a mere consequence of the physical laws of quantum physics. The necessity of a physical reason for the Lagrangian formalism was explored by L. de Broglie, his idea was the stationary action of the particle as a limit case of the growing entropy in thermodynamics [49]. We may now consider the quantum wave equations themselves as a necessary consequence of the geometry of the space-time: the form of the mass term results from the constraints of the invariance under  $Cl_3^*$  and from the gauge group which is the greatest possible group compatible with the  $Cl_3$  algebra.

The existence of the double link has other consequences that we shall develop in the second part of this work on the boson part of the SM: only the fermion wave is linked to a Lagrangian density which is made of the wave equations and is then necessary. The dynamics of the boson part must then be a consequence of the dynamics of the fermion wave. The SM considers the dynamics of boson waves as a consequence of the Lagrangian density, but the relations between potentials and fields are not deduced, they are postulated independently of the laws giving the dynamics of the fields.

We previously got this double link, first in the wave of the electron [33], next for electro-weak and strong interactions [25] [26], but we did not see the reduction of the number of the numeric equations. The reason was the rebuilding of the wave equation on the Dirac form from the Lagrangian density, the  $\phi^l$  wave of the electron incorporating both left and right waves, while the Lagrangian density separates the left and right parts of the wave. It is very easy, in this rebuilding, to use the main automorphism  $z \mapsto \hat{z}$  equivalent to the P transformation of quantum physics. But this transformation is not a symmetry of quantum physics, because it is not a symmetry of weak interactions. All our wave equations have a  $(1 + \sigma_3)/2$  factor which becomes  $(1 - \sigma_3)/2$  when we use the main automorphism, losing the possibility of factorization.

Moreover the 16 equations containing  $\partial_\mu D_R^\mu$  and  $\partial_\mu D_L^\mu$  are consequence of the Lagrangian formalism which is a consequence of the 16 other equations. This was first seen by Boudet [50] in the frame of the linear Dirac theory of the electron. Our study proves that it is general: the numeric equations equivalent to the wave equations of the “matter” (spinor waves) may be split into two parts: a dynamical part containing rotational-like terms, and a conservative part containing divergence-like terms, and the conservative part is a consequence of the dynamical equations.

The building of the wave equations from the Lagrangian density uses  $(1 + \sigma_3)/2$  but this process could also use  $(1 + \sigma_1)/2$  or  $(1 + \sigma_2)/2$ . This may be the origin of the existence of three and only three generations of fundamental fermions with same dynamics.

Finally the synthesis of all interactions in a unified frame is the simple question: how these dynamical quantum equations are linked to GR?

#### 4. Inertia and Gravitation

In [26] Ch.9 we considered an element  $M$  not restricted to be constant in space-time. In the vicinity of a point  $x$  where  $M(0) = 1$  we use:

$$\begin{aligned}
 M &= 1 + \frac{dx^\mu}{2} (p_\mu + f_\mu \sigma_1 + l_\mu \sigma_2 + a_\mu \sigma_3 + h_\mu i \sigma_1 + g_\mu i \sigma_2 + b_\mu i \sigma_3 + i b_\mu) \\
 \tilde{M} &= 1 + \frac{dx^\mu}{2} (p_\mu + f_\mu \sigma_1 + l_\mu \sigma_2 + a_\mu \sigma_3 - h_\mu i \sigma_1 - g_\mu i \sigma_2 - b_\mu i \sigma_3 - i b_\mu) \\
 \hat{M} &= 1 + \frac{dx^\mu}{2} (p_\mu - f_\mu \sigma_1 - l_\mu \sigma_2 - a_\mu \sigma_3 + h_\mu i \sigma_1 + g_\mu i \sigma_2 + b_\mu i \sigma_3 - i b_\mu) \\
 \bar{M} &= 1 + \frac{dx^\mu}{2} (p_\mu - f_\mu \sigma_1 - l_\mu \sigma_2 - a_\mu \sigma_3 - h_\mu i \sigma_1 - g_\mu i \sigma_2 - b_\mu i \sigma_3 + i b_\mu),
 \end{aligned} \tag{4.1}$$

where  $b$  is the chiral potential  $b = g_1 B/2$ . We get

$$\begin{aligned}
 M\bar{M} &= \det(M) = 1 + dx^\mu (p_\mu + i b_\mu); \quad \det(M^{-1}) = 1 - dx^\mu (p_\mu + i b_\mu); \\
 \bar{M}^{-1} &= M \det(M^{-1}) = 1 + \frac{dx^\mu}{2} (-p_\mu + f_\mu \sigma_1 + l_\mu \sigma_2 + a_\mu \sigma_3 + h_\mu i \sigma_1 + g_\mu i \sigma_2 + b_\mu i \sigma_3 - i b_\mu), \\
 \hat{M}^{-1} &= 1 + \frac{dx^\mu}{2} (-p_\mu + f_\mu \sigma_1 + l_\mu \sigma_2 + a_\mu \sigma_3 - h_\mu i \sigma_1 - g_\mu i \sigma_2 - b_\mu i \sigma_3 + i b_\mu).
 \end{aligned} \tag{4.2}$$

The dilation  $D$  defined from  $M$  in (2.10) gives:

$$\begin{aligned}x^0 &= x^0 + (p_\mu x^0 + f_\mu x^1 + l_\mu x^2 + a_\mu x^3) dx^\mu \\x^1 &= x^1 + (f_\mu x^0 + p_\mu x^1 + b_\mu x^2 - g_\mu x^3) dx^\mu \\x^2 &= x^2 + (l_\mu x^0 - b_\mu x^1 + p_\mu x^2 + h_\mu x^3) dx^\mu \\x^3 &= x^3 + (a_\mu x^0 + g_\mu x^1 - h_\mu x^2 + p_\mu x^3) dx^\mu\end{aligned}\quad (4.3)$$

Christoffel's symbols  $\Gamma_{\beta\gamma}^\alpha$  being defined as

$$x'^\alpha = x^\alpha + \Gamma_{\beta\gamma}^\alpha x^\beta dx^\gamma, \quad (4.4)$$

we then get

$$\begin{aligned}\Gamma_{0\mu}^0 &= \Gamma_{1\mu}^1 = \Gamma_{2\mu}^2 = \Gamma_{3\mu}^3 = p_\mu \\ \Gamma_{0\mu}^1 &= \Gamma_{1\mu}^0 = f_\mu; \quad \Gamma_{0\mu}^2 = \Gamma_{2\mu}^0 = l_\mu; \quad \Gamma_{0\mu}^3 = \Gamma_{3\mu}^0 = a_\mu \\ \Gamma_{3\mu}^2 &= -\Gamma_{2\mu}^3 = h_\mu; \quad \Gamma_{1\mu}^3 = -\Gamma_{3\mu}^1 = g_\mu; \quad \Gamma_{2\mu}^1 = -\Gamma_{1\mu}^2 = b_\mu\end{aligned}\quad (4.5)$$

Since  $D$  is a dilation, product in any order of a Lorentz transformation and an homothety, the Christoffel's symbols have this particular form and we get not 64 but only  $28 = 4 \times 7$  functions: the four  $b_\mu$  present in (4.1) are not in the geometry, because the kernel of the group homomorphism  $M \mapsto D$  is the  $U(1)$  group generated by  $i$  [23] [47]. Since the Christoffel's symbols are not symmetric, a torsion exists, like in any geometry able to account for spin 1/2. Vectors transforming as (4.4) are the contravariant ones. Now for covariant vectors we have

$$\nabla = \sigma^\mu \partial_\mu = \bar{M} \sigma^\mu \hat{M}' \partial'_\mu, \quad (4.6)$$

with the same  $\sigma^\mu$ . This is an important difference with all preceding attempts, using always variable  $\gamma_\mu$ . This gives

$$\nabla' = \sigma^\nu \partial'_\nu = \bar{M}^{-1} \sigma^\nu \hat{M}'^{-1} \partial_\nu = \sigma^\nu (\partial_\nu - dx^\mu \Gamma_{\nu\mu}^\rho \partial_\rho). \quad (4.7)$$

Therefore we get for covariant vectors the usual transformation:

$$\partial'_\nu = \partial_\nu - dx^\mu \Gamma_{\nu\mu}^\rho \partial_\rho. \quad (4.8)$$

This relation allows the covariant derivative to be commutative with contractions. It leads the covariant derivative back to partial derivative for scalars. The connection (4.5) is new, because all preceding attempts have used variable  $\gamma^\mu$ , while we use constant  $\sigma_\mu$ . The relativistic transformation of the Dirac  $\psi$  wave uses a

$4 \times 4$  matrix  $N = \begin{pmatrix} M & 0 \\ 0 & \hat{M} \end{pmatrix}$  and transforms  $\psi(x)$  into  $\psi'(x') = N\psi(x)$ , the Dirac equation satisfies, if

$\det(M) = 1: 0 = [\gamma^\mu (\partial_\mu + iqA_\mu) + im]\psi = N^{-1} [\gamma^\mu (\partial'_\mu + iqA'_\mu) + im]\psi'$ , and we may remark that the  $\gamma^\mu$  matrices are not changed in the frame of  $x'$ . Then why could they change as soon as the theory uses curvilinear coordinates? Actually the first Dirac theory used the transformation (2.10) and constant matrices, as soon as 1928.

A non vanishing torsion was used previously by A. Einstein [4] to unify gravitation and electromagnetism. Since his attempt was studied at the very early times of quantum mechanics he evidently did not start from the Dirac wave, which was invented 3 years later. We next get

$$\begin{aligned}\bar{\phi} \nabla' \hat{\phi}' &= (\bar{M}\hat{\phi}) \bar{M}^{-1} \sigma^\mu \hat{M}'^{-1} \partial_\mu (\hat{M}\hat{\phi}) = \bar{\phi} \bar{M} \bar{M}^{-1} \sigma^\mu \hat{M}'^{-1} \left[ (\partial_\mu \hat{M}) \hat{\phi} + \hat{M} (\partial_\mu \hat{\phi}) \right] \\ &= \bar{\phi} \sigma^\mu \hat{M}'^{-1} (\partial_\mu \hat{M}) \hat{\phi} + \bar{\phi} \sigma^\mu \partial_\mu \hat{\phi} = \bar{\phi} \sigma^\mu \left[ -(\partial_\mu \hat{M}'^{-1}) \hat{M} \right] \hat{\phi} + \bar{\phi} \nabla \hat{\phi} = \bar{\phi} \left[ \nabla - (\nabla \hat{M}'^{-1}) \hat{M} \right] \hat{\phi}. \\ \bar{\phi} \nabla' \hat{\phi}' &= \bar{\phi} D \hat{\phi},\end{aligned}\quad (4.9)$$

with

$$D = \nabla - (\nabla \hat{M}^{-1}) \hat{M} = \sigma^\mu \left[ \partial_\mu + \frac{1}{2} (p_\mu - f_\mu \sigma_1 - l_\mu \sigma_2 - a_\mu \sigma_3 + h_\mu i \sigma_1 + g_\mu i \sigma_2 + b_\mu i \sigma_3 - i b_\mu) \right]. \quad (4.10)$$

This introduces 8 space-time vectors that we name “potentials of inertia”:

$$\begin{aligned} p &= \sigma^\mu p_\mu = \sigma^\mu \Gamma_{0\mu}^0; & f &= \sigma^\mu f_\mu = \sigma^\mu \Gamma_{0\mu}^1; & l &= \sigma^\mu l_\mu = \sigma^\mu \Gamma_{0\mu}^2; & a &= \sigma^\mu a_\mu = \sigma^\mu \Gamma_{0\mu}^3; \\ h &= \sigma^\mu h_\mu = \sigma^\mu \Gamma_{3\mu}^2; & g &= \sigma^\mu g_\mu = \sigma^\mu \Gamma_{1\mu}^3; & b &= \sigma^\mu b_\mu = \sigma^\mu \Gamma_{2\mu}^1; & \mathbf{b} &= \sigma^\mu \mathbf{b}_\mu; \end{aligned} \quad (4.11)$$

$$D = \nabla + \frac{1}{2} (p - f \sigma_1 - l \sigma_2 - a \sigma_3 + h i \sigma_1 + g i \sigma_2 + b i \sigma_3 - i \mathbf{b}).$$

In space algebra we need also

$$\begin{aligned} \hat{\phi}' \tilde{\nabla}' \bar{\phi}' &= \hat{\phi} \tilde{D} \bar{\phi}, \\ \tilde{D} &= \tilde{\nabla} - (\tilde{\nabla} \bar{M}^{-1}) \bar{M} = \tilde{\nabla} + \frac{1}{2} (p - \sigma_1 f - \sigma_2 l - \sigma_3 a + i \sigma_1 h + i \sigma_2 g + i \sigma_3 b + i \mathbf{b}). \end{aligned} \quad (4.12)$$

Now we look at the simple case (negligible gravitation) where all terms  $p_\mu, f_\mu, l_\mu, a_\mu, h_\mu, g_\mu, b_\mu$  are zero, but not  $\mathbf{b}_\mu$ . We then get simply:

$$\Gamma_{\beta\gamma}^\alpha = 0; x'^\mu = x^\mu; D = \nabla - \frac{i}{2} \mathbf{b}; \tilde{D} = \tilde{\nabla} + \frac{i}{2} \mathbf{b}. \quad (4.13)$$

Without the neutrino and quarks wave, we have  $R^8 = L^8 = W^3 \hat{L}^1 = 0$  and  $a_1 = \rho e^{i\beta}$ , where  $\beta$  is the Yvon-Takabayasi angle. We then get

$$\begin{aligned} 0 &= \hat{\nabla} R^1 + 2i \hat{\mathbf{b}} R^1 + i \frac{m}{\rho} a_1 \hat{L}^1, \\ 0 &= \nabla \hat{L}^1 + i \mathbf{b} \hat{L}^1 + i \frac{m}{\rho} a_1^* R^1. \end{aligned} \quad (4.14)$$

Using the main automorphism on the first Equation (4.14) we get

$$\nabla \hat{R}^1 - 2i \mathbf{b} \hat{R}^1 - i \frac{m}{\rho} a_1^* L^1 = 0. \quad (4.15)$$

The wave equation of the electron alone is then equivalent to the system:

$$\begin{aligned} \nabla \hat{R}^1 &= 2i \mathbf{b} \hat{R}^1 + i m e^{-i\beta} L^1, \\ \nabla \hat{L}^1 &= -i \mathbf{b} \hat{L}^1 - i m e^{-i\beta} R^1. \end{aligned} \quad (4.16)$$

This system reads:

$$\begin{aligned} \nabla \hat{R}^1 &= \frac{i}{2} \mathbf{b} \hat{R}^1 + \frac{3i}{2} \mathbf{b} \hat{R}^1 + i m e^{-i\beta} L^1, \\ \nabla \hat{L}^1 &= \frac{i}{2} \mathbf{b} \hat{L}^1 - \frac{3i}{2} \mathbf{b} \hat{L}^1 - i m e^{-i\beta} R^1. \end{aligned} \quad (4.17)$$

If we have:

$$qA = \frac{3}{4} g_1 B = \frac{3}{2} \mathbf{b}, \quad (4.18)$$

using

$$\phi^1 \sigma_3 = R^1 - L^1; \hat{\phi}^1 \sigma_3 = \hat{L}^1 - \hat{R}^1; \sigma_{12} = i \sigma_3, \quad (4.19)$$

we get:

$$\begin{aligned} 0 &= \left( \nabla - \frac{i}{2} \mathbf{b} \right) \hat{\phi}^1 + qA \hat{\phi}^1 \sigma_{12} + m e^{-i\beta} \phi^1 \sigma_{12}, \\ 0 &= D \hat{\phi}^1 \sigma_{21} + qA \hat{\phi}^1 + m e^{-i\beta} \phi^1, \\ 0 &= \bar{\phi}^1 D \hat{\phi}^1 \sigma_{21} + \bar{\phi}^1 qA \hat{\phi}^1 + m \rho. \end{aligned} \quad (4.20)$$

which is our wave Equation (2.9) of the electron alone, with the only change of  $\nabla$  into  $D$ . The complication of the two parts of the electron wave with different eigenvalues of the weak hypercharge simply comes from the strange fact that the chiral potential  $\mathbf{b}$  is both a gauge potential and a potential of inertia. The introduction of the inertial potential  $\mathbf{b}$  into the Dirac equation gives the weak hypercharge. This means that the Dirac wave is yet a unitary electromagnetic-gravitational wave.

Now we consider the neutrino wave where  $\tilde{\phi}^8$  replaces  $\phi^8$ . This means that, when  $\phi^n, n=1,2,3,4$  sees the Clifford algebra of space with the basis  $(\sigma_1, \sigma_2, \sigma_3)$  as a direct oriented basis,  $\phi^n, n=5,6,7,8$  sees the same algebra reversed, or with the same basis  $(\sigma_1, \sigma_2, \sigma_3)$  as an inverse basis. These waves satisfy:

$$\phi^n = \phi^n \tilde{M}; (\bar{\phi}^n \nabla') \hat{\phi}^n = (\bar{\phi}^n D) \hat{\phi}^n; \nabla = \tilde{\nabla} = \tilde{D} - \frac{i}{2} \mathbf{b}. \quad (4.21)$$

Without quark and electron waves, we have  $R^1 = L^1 = W^3 \bar{L}^8 = 0$  and  $a_6 = \rho e^{i\beta}$ , we then get

$$\begin{aligned} 0 &= \tilde{\nabla} \bar{R}^8 + i m e^{i\beta} \bar{L}^8, \\ 0 &= \tilde{\nabla} \bar{L}^8 + i \mathbf{b} \bar{L}^8 + i m e^{-i\beta} \tilde{R}^8. \end{aligned} \quad (4.22)$$

Using the main automorphism on the first Equation (4.22) we get the system:

$$\begin{aligned} \tilde{\nabla} \bar{R}^8 &= i m e^{-i\beta} \tilde{L}^8, \\ \tilde{\nabla} \bar{L}^8 &= -i \mathbf{b} \bar{L}^8 - i m e^{-i\beta} \tilde{R}^8. \end{aligned} \quad (4.23)$$

This gives:

$$\begin{aligned} \left( \tilde{D} - \frac{i}{2} \mathbf{b} \right) \bar{R}^8 &= i m e^{-i\beta} \tilde{L}^8, \\ \left( \tilde{D} - \frac{i}{2} \mathbf{b} \right) \bar{L}^8 &= -i \mathbf{b} \bar{L}^8 - i m e^{-i\beta} \tilde{R}^8, \end{aligned} \quad (4.24)$$

Adding we get:

$$\begin{aligned} 0 &= \tilde{D} \bar{\phi}^8 + \frac{\mathbf{b}}{2} \bar{\phi}^8 i \sigma_3 + m e^{-i\beta} \tilde{\phi}^8 i \sigma_3, \\ 0 &= \sigma_{12} (\hat{\phi}^8 D) + \hat{\phi}^8 \frac{\mathbf{b}}{2} + m e^{i\beta} \phi^8, \end{aligned} \quad (4.25)$$

which is a Dirac-like wave equation in inverse order. Next if we consider the  $d_c$  wave alone we have  $\phi_{dc} = \phi^n$  while if we consider the  $u_c$  wave alone we have  $\phi_{uc} = \tilde{\phi}^{3+n}$  and we get:

$$\begin{aligned} 0 &= \hat{\nabla} R^n + \frac{2i}{3} \hat{\mathbf{b}} R^n + i m e^{i\beta} \hat{L}^n; \quad 0 = \nabla \hat{L}^n - \frac{i}{3} \hat{\mathbf{b}} \hat{L}^n + i m e^{-i\beta} R^n, \\ 0 &= \tilde{\nabla} \bar{R}^{3+n} - \frac{4i}{3} \hat{\mathbf{b}} \bar{R}^{3+n} + i m e^{i\beta} \bar{L}^{3+n}; \quad 0 = \tilde{\nabla} \bar{L}^{3+n} - \frac{i}{3} \hat{\mathbf{b}} \bar{L}^{3+n} + i m e^{-i\beta} \tilde{R}^{3+n}. \end{aligned} \quad (4.26)$$

This gives:

$$\begin{aligned} 0 &= \nabla \hat{R}^n - \frac{i}{2} \hat{\mathbf{b}} \hat{R}^n - \frac{i}{6} \hat{\mathbf{b}} \hat{R}^n - i m e^{-i\beta} L^n, \\ 0 &= \nabla \hat{L}^n - \frac{i}{2} \hat{\mathbf{b}} \hat{L}^n + \frac{i}{6} \hat{\mathbf{b}} \hat{L}^n + i m e^{-i\beta} R^n, \\ 0 &= \tilde{\nabla} \bar{R}^{3+n} + \frac{i}{2} \hat{\mathbf{b}} \bar{R}^{3+n} + \frac{5i}{6} \hat{\mathbf{b}} \bar{R}^{3+n} - i m e^{-i\beta} \tilde{L}^{3+n}, \\ 0 &= \tilde{\nabla} \bar{L}^{3+n} + \frac{i}{2} \hat{\mathbf{b}} \bar{L}^{3+n} - \frac{5i}{6} \hat{\mathbf{b}} \bar{L}^{3+n} + i m e^{-i\beta} \tilde{R}^{3+n}. \end{aligned} \quad (4.27)$$

And the wave equations become:

$$\begin{aligned} 0 &= \bar{\phi}^n (D \hat{\phi}^n) \sigma_{21} + \bar{\phi}^n \frac{\mathbf{b}}{6} \hat{\phi}^n + m \rho, \\ 0 &= \sigma_{12} (\hat{\phi}^{3+n} D) \bar{\phi}^{3+n} - \frac{5}{6} \hat{\phi}^{3+n} \mathbf{b} \bar{\phi}^{3+n} + m \rho. \end{aligned} \quad (4.28)$$

which also are Dirac-like wave equations.

Since a mass term is present in the wave equations we are able to study in an unified way quantum behaviour and inertia-gravitation. In a rotating frame [51] the limit speed is not equal to  $c$  but varies. The limit speed becomes  $v = c(1 + a/m)$ ,  $m = m_0 c/\hbar$ ,  $a = \pi/cT$  where  $T$  is the period of the rotation of the frame. We also have  $v/c = 1 + v/(2\nu_0)$  where  $\nu = 1/T$  is the frequency of rotation of the frame and  $\nu_0$  is the frequency of the wave. Therefore this effect is very small.

The inclusion of inertia necessitates the use of two forms of differential operator, acting on the right or on the left side. This unified behaviour links the complicated operators of the electro-weak gauge to the unique electric gauge. The SM is not only able to incorporate inertia and gravitation. This is already realized since 1928 in the Dirac theory. The gravitation is not a very little force, it has the same strength as electromagnetism, but this is usually not obvious, because the proper masses of quantum physics are very small in comparison with the Planck mass.

## 5. Conclusions

All waves of the fermion part of the SM may be described as functions of space-time in the Clifford algebra of space. Contrary to the common expectation, the algebra of space is the framework of the unification of all interactions, not the algebra of space-time. The global wave is a function of space-time in a 64-dimensional linear space isomorphic to  $Cl_3^8$ , or to the space of all linear applications (called operators in the SM) from  $Cl_3$  into  $Cl_3$ . In this space multiplications by the left and multiplication by the right place play the same role. Consequently, 32 parameters concern waves similar to the wave of the electron ruled by a Dirac equation. 32 parameters are those of waves similar to the wave of the neutrino, with a reverse Dirac equation. This global wave is obtained also as eight waves which are functions  $x \mapsto \phi^n(x)$ ,  $n = 1, \dots, 8$  of space-time into  $Cl_3$ .

The wave equations result from Lagrange equations calculated from a Lagrangian density and this Lagrangian density is exactly the sum of the real part of these wave equations. This gives both the reason and the limit of the Lagrangian physics. This limit comes from the fact that only the fermion part of the SM allows us to get a double link between wave equations and Lagrangian density.

The Lorentz group of the restricted relativity is extended to a greater group of invariance. This group has a geometric origin, since it is the  $Cl_3^*$  group of the invertible elements of the algebra constructed from the 3-dimensional space. The invariance under this greater group rules all waves of quantum physics. This group has not only two kinds of non-equivalent representations, but four, all necessary for the waves. We must consider not only  $\phi$  waves but also  $\tilde{\phi}$  waves. The use of the  $Cl_3$  algebra seems paradoxical for a relativistic unified model. Nevertheless  $Cl_3$  is the best framework since including both the space-time and the group of invariance of the quantum waves. The four kinds of representations of the  $Cl_3^*$  group are necessary used, and we must distinguish  $M, \tilde{M}, \hat{M}$  and  $\bar{M}$ . Since  $x = \tilde{x}$  only two kinds of representations are used in space-time algebra. Then it is very difficult to account there for chirality and to include both weak interactions and gravitation. Nonatural differential operator in space-time algebra includes the four  $D, \tilde{D}, \hat{D}$  and  $\bar{D}$  operators. In space-time algebra, the orientation of the global space-time is available, not the separate orientations of time and space needed in quantum physics.

We previously studied several particular cases and we obtained several important results: the gauge invariance is exact in the particular case where only the electron has a non-zero right wave [26]. In a second paper, we will study this gauge invariance in the general case. We explained in [46] how the additivity of the potential terms is equivalent to the Pauli principle. We have less free parameters in comparison with the SM using second quantification, because the study of the electron fixes the value of the Weinberg-Salam angle [45]. Consequently this fixes the values of the charges of quarks and antiquarks [46]. The proper masses are no more the fundamental quantities that the theory must account for. These fundamental quantities are actually the  $m\rho$  products and there is only one proper mass in each generation.

Old questions may also receive a very different answer: the density of probability is in the non-relativistic quantum theory a fundamental quantity; it is the square of the modulus of the wave. This has survived in the Dirac theory, because the density of probability becomes  $J^0$ , the time component of the  $J = \phi_e \tilde{\phi}_e$  conservative current, and because  $J \cdot J = \rho^2$ . This induces the confusion between  $J^0$  and  $\rho$ . The generalization of the wave breaks this confusion:  $J$  is generalized as the contravariant sum of the 16 currents of the Weyl spinors, while  $\rho^2$  is the sum of 72 relativistic invariant terms. The density of probability always exists (see [26] Chap-

ter 9) and the wave is normalized in the stationary case, but this density has none metaphysical property ruling all physical laws. The normalization of the wave is only a consequence of the principle of equivalence between the inertial mass-energy (sum over the whole space of the density of energy of the wave) and the gravitational mass-energy of the particle (linked to the frequency of the de Broglie's clock).

## References

- [1] Einstein, A. (1905) *Annalen der Physik*, **322**, 891-921. <http://dx.doi.org/10.1002/andp.19053221004>
- [2] Einstein, A. (1915) Preussische Akademie der Wissenschaften. Sitzungsberichte, Berlin, 778-786, 799-801.
- [3] Einstein, A. (1915) Preussische Akademie der Wissenschaften. Sitzungsberichte, Berlin, 831-839.
- [4] Einstein, A. (1925) Sitzungsberichte der Preussischen AKADEMIE der Wissenschaften. Physikalisch-matheatische Klasse, Berlin, 414-419.
- [5] De Broglie, L. (1924) *Annales de la Fondation Louis de Broglie*, **17**, 1-109.
- [6] Dirac, P.A.M. (1928) *Proceedings of the Royal Society of London*, **117**, 610-624. <http://dx.doi.org/10.1098/rspa.1928.0023>
- [7] Darwin, C.G. (1928) *Proceedings of the Royal Society of London*, **118**, 554.
- [8] DeBroglie, L. (1934) L'électron magnétique. Hermann, Paris.
- [9] Messiah, A. (1959) Mécanique quantique. tomes 1 et 2, Dunod, Paris.
- [10] Cohen-Tannoudji, C., Diu, B. and Laloë, F. (1973) Mécanique Quantique. tomes 1 et 2, Hermann, Paris.
- [11] Strange, P. (1998) Relativistic Quantum Mechanics. Cambridge University Press, Cambridge. <http://dx.doi.org/10.1017/CBO9780511622755>
- [12] Serman, G. (1993) An Introduction to Quantum Field Theory. Cambridge University Press, Cambridge. <http://dx.doi.org/10.1017/CBO9780511622618>
- [13] Greiner, W. and Müller, B. (2009) Gauge Theory of Weak Interactions. Springer-Verlag, Berlin. <http://dx.doi.org/10.1007/978-3-540-87843-8>
- [14] Scheck, F. (1996) Electroweak and Strong Interactions. Springer, Berlin. <http://dx.doi.org/10.1007/978-3-662-03245-9>
- [15] Weinberg, S. (1967) *Physical Review Letters*, **19**, 1264-1266. <http://dx.doi.org/10.1103/PhysRevLett.19.1264>
- [16] Taylor, J.C. (1976) Gauge Theories of Weak Interactions. Cambridge University Press, Cambridge.
- [17] Georgi, H. and Glashow, S.L. (1974) *Physical Review Letters*, **32**, 438-441. <http://dx.doi.org/10.1103/PhysRevLett.32.438>
- [18] Naïmark, M.A. (1962) Les représentations linéaires du groupe de Lorentz. Dunod, Paris.
- [19] Hestenes, D. (1973) *Journal of Mathematical Physics*, **14**, 893-905. <http://dx.doi.org/10.1063/1.1666413>
- [20] Hestenes, D. (1986) A Unified Language for Mathematics and Physics and Clifford Algebra and the Interpretation of Quantum Mechanics. In: Chisholm, J. and Common, A., Eds., *Clifford Algebras and Their Applications in Mathematics and Physics*, Reidel, Dordrecht, 1-23.
- [21] Boudet, R. (1995) The Takabayasi Moving Frame, from a Potential to the Z Boson. In: Jeffers, S. and Vigier, J., Eds., *The Present Status of the Quantum Theory of the Light*, Kluwer, Dordrecht, 471-481.
- [22] Boudet, R. (2011) Quantum Mechanics in the Geometry of Space-Time. Springer, Berlin. <http://dx.doi.org/10.1007/978-3-642-19199-2>
- [23] Daviau, C. (2011) L'espace-temps Double. Je Publie, Pouillé-les-coteaux.
- [24] Daviau, C. (2012) Nonlinear Dirac Equation, Magnetic Monopoles and Double Space-Time. CISP, Cambridge.
- [25] Daviau, C. and Bertrand, J. (2014) New Insights in the Standard Model of Quantum Physics in Clifford Algebra. Je Publie, Pouillé-les-coteaux. <http://hal.archives-ouvertes.fr/hal-00907848>
- [26] Daviau, C. and Bertrand, J. (2016) The Standard Model of Quantum Physics in Clifford Algebra. World Scientific, Singapore. [http://dx.doi.org/10.1142/9789814719872\\_fmatter](http://dx.doi.org/10.1142/9789814719872_fmatter)
- [27] Daviau, C. (1993) Equation de Dirac non linéaire. PhD Thesis, Université de Nantes, Nantes.
- [28] Daviau, C. (1997) *Advances in Applied Clifford Algebras*, **7**, 175-194.
- [29] Daviau, C. (1997) *Annales de la Fondation Louis de Broglie*, **22**, 87-103.
- [30] Daviau, C. (1998) *Annales de la Fondation Louis de Broglie*, **23**, 1.
- [31] Daviau, C. (2001) *Annales de la Fondation Louis de Broglie*, **26**, 149-171.

- [32] Daviau, C. (2005) *Annales de la Fondation Louis de Broglie*, **30**, 3-4.
- [33] Daviau, C. (2012) Double Space-Time and More. Je Publie, Pouillé-les-coteaux.
- [34] Daviau, C. (2012) *Advances in Applied Clifford Algebras*, **22**, 611-623.  
<http://dx.doi.org/10.1007/s00006-012-0351-7>
- [35] Daviau, C. (2015) *Advances in Applied Clifford Algebras*. <http://dx.doi.org/10.1007/s00006-015-0566-5>
- [36] LoebI, E. (Editor) (1968) Group Theory and Its Applications. Academic Press, New York.
- [37] Daviau, C. and Bertrand, J. (2014) *Journal of Modern Physics*, **5**, 1001-1022.  
<http://dx.doi.org/10.4236/jmp.2014.511102>
- [38] Daviau, C. and Bertrand, J. (2014) *Journal of Modern Physics*, **5**, 2149-2173.  
<http://dx.doi.org/10.4236/jmp.2014.518210>
- [39] Daviau, C. and Bertrand, J. (2015) *Journal of Modern Physics*, **6**, 1647-1656.  
<http://dx.doi.org/10.4236/jmp.2015.611166>
- [40] Daviau, C. and Bertrand, J. (2015) *Journal of Applied Mathematics and Physics*, **3**, 46-61.  
<http://dx.doi.org/10.4236/jamp.2015.31007>
- [41] Daviau, C. and Bertrand, J. (2016) *Journal of Modern Physics*, **7**, 936-951. <http://dx.doi.org/10.4236/jmp.2016.79086>
- [42] Lochak, G. (1983) *Annales de la Fondation Louis de Broglie*, **8**, 345.
- [43] Lochak, G. (1984) *Annales de la Fondation Louis de Broglie*, **9**, 5.
- [44] Lochak, G. (1985) *International Journal of Theoretical Physics*, **24**, 1019-1050. <http://dx.doi.org/10.1007/BF00670815>
- [45] Daviau, C. and Bertrand, J. (2015) *Journal of Modern Physics*, **6**, 2080-2092.  
<http://dx.doi.org/10.4236/jmp.2015.614215>
- [46] Daviau, C. and Bertrand, J. (2015) *Annales de la Fondation Louis de Broglie*, **40**, 181-209.
- [47] Daviau, C. (2013) *Advances in Imaging and Electron Physics*, **179**, 1-137.  
<http://dx.doi.org/10.1016/B978-0-12-407700-3.00001-6>
- [48] Socroun, T. (2015) *Advances in Applied Clifford Algebras*, **25**, 1-9.
- [49] de Broglie, L. (1964) La Thermodynamique de la particule isolée. Gauthier-Villars, Paris.
- [50] Boudet, R. (1985) *Journal of Mathematical Physics*, **26**, 718-724. <http://dx.doi.org/10.1063/1.526613>
- [51] Daviau, C. and Bertrand, J. (2012) *Annales de la Fondation Louis de Broglie*, **37**, 129-134.



**Submit or recommend next manuscript to SCIRP and we will provide best service for you:**

Accepting pre-submission inquiries through Email, Facebook, LinkedIn, Twitter, etc.

A wide selection of journals (inclusive of 9 subjects, more than 200 journals)

Providing 24-hour high-quality service

User-friendly online submission system

Fair and swift peer-review system

Efficient typesetting and proofreading procedure

Display of the result of downloads and visits, as well as the number of cited articles

Maximum dissemination of your research work

Submit your manuscript at: <http://papersubmission.scirp.org/>

# The Accurate Mass Formulas of Leptons, Quarks, Gauge Bosons, the Higgs Boson, and Cosmic Rays

**Ding-Yu Chung**

Utica, MI, USA

Email: [dy\\_chung@yahoo.com](mailto:dy_chung@yahoo.com)

Received 21 July 2016; accepted 28 August 2016; published 31 August 2016

Copyright © 2016 by author and Scientific Research Publishing Inc.  
This work is licensed under the Creative Commons Attribution International License (CC BY).  
<http://creativecommons.org/licenses/by/4.0/>



Open Access

---

## Abstract

One of the biggest unsolved problems in physics is the particle masses of all elementary particles which cannot be calculated accurately and predicted theoretically. In this paper, the unsolved problem of the particle masses is solved by the accurate mass formulas which calculate accurately and predict theoretically the particle masses of all leptons, quarks, gauge bosons, the Higgs boson, and cosmic rays (the knees-ankles-toe) by using only five known constants: the number (seven) of the extra spatial dimensions in the eleven-dimensional membrane, the mass of electron, the masses of Z and W bosons, and the fine structure constant. The calculated masses are in excellent agreements with the observed masses. For examples, the calculated masses of muon, top quark, pion, neutron, and the Higgs boson are 105.55 MeV, 175.4 GeV, 139.54 MeV, 939.43 MeV, and 126 GeV, respectively, in excellent agreements with the observed 105.65 MeV, 173.3 GeV, 139.57 MeV, 939.27 MeV, and 126 GeV, respectively. The mass formulas also calculate accurately the masses of the new particle at 750 GeV from the LHC and the new light boson at 17 MeV. The theoretical base of the accurate mass formulas is the periodic table of elementary particles. As the periodic table of elements is derived from atomic orbitals, the periodic table of elementary particles is derived from the seven principal mass dimensional orbitals and seven auxiliary mass dimensional orbitals. All elementary particles including leptons, quarks, gauge bosons, the Higgs boson, and cosmic rays can be placed in the periodic table of elementary particles. The periodic table of elementary particles is based on the theory of everything as the computer simulation model of physical reality consisting of the mathematical computation, digital representation and selective retention components. The computer simulation model of physical reality provides the seven principal mass dimensional orbitals and seven auxiliary mass dimensional orbitals for the periodic table of elementary particles.

## Keywords

Mass Formulas, Particle Masses, Leptons, Quarks, Gauge Bosons, Higgs Boson, Cosmic Rays,

---

## The Periodic Table of Elementary Particles, Computer Simulation, Knees-Ankles-Toe, The Theory of Everything

---

### 1. Introduction

According to Johan Hansson, one of the ten biggest unsolved problems in physics [1] is the incalculable particle masses of leptons, quarks, gauge bosons, and the Higgs boson. The Standard Model of particle physics contains the particles masses of leptons, quarks, and gauge bosons which cannot be calculated or predicted theoretically. From a theoretical point of view, the particle mass is a total unsolved problem and they might as well have been random numbers drawn from a hat. The repetition of leptons and quarks with increasing masses has also remained as unsolved problem. Max Jammer [2] concluded that nobody knows what particle masses really are. The mass parameters experimentally measured for elementary particles have no theoretical explanation whatsoever. From the vantage point of theory, the masses could just as well be a set of randomly generated numbers.

This paper provides a solution to the unsolved problem of particle masses. In this paper, all elementary particles and cosmic rays (the knees-ankles-toe) can be calculated accurately and predicted theoretically by the accurate mass formulas of leptons, quarks, gauge bosons, the Higgs boson, and cosmic rays by using only five known constants: the number (seven) of the extra spatial dimensions in the eleven-dimensional membrane, the mass of electron, the masses of Z and W bosons, and the fine structure constant. The calculated masses are in excellent agreements with the observed masses. For examples, the calculated masses of muon, top quark, pion, neutron, and the Higgs boson are 105.55 MeV, 175.4 GeV, 139.54 MeV, 939.43 MeV, and 126 GeV, respectively, in excellent agreements with the observed 105.65 MeV, 173.3 GeV, 139.57 MeV, 939.27 MeV, and 126 GeV, respectively. The theoretical base of the accurate mass formulas is the periodic table of elementary particles [3]-[6]. As the periodic table of elements is derived from atomic orbitals, the periodic table of elementary particles is derived from the seven principal mass dimensional orbitals and seven auxiliary mass dimensional orbitals. All elementary particles including leptons, quarks, gauge bosons, the Higgs boson, and cosmic rays can be placed in the periodic table of elementary particles.

The periodic table of elementary particles is derived from the computer simulation model of physical reality [7] which is the theory of everything [8]. We are living in a computer simulation to simulate physical reality which has the same computer simulation process as virtual reality (computer-simulated reality). The computer simulation process involves the digital representation of data, the mathematical computation of the digitized data in geometric formation and transformation in space-time, and the selective retention of events in a narrative. Conventional physics cannot explain physical reality clearly, while computer-simulated physics can explain physical reality clearly by using the computer simulation process consisting of the digital representation component, the mathematical computation component, and the selective retention component. The computer simulation model of physical reality provides the seven principal mass dimensional orbitals and seven auxiliary mass dimensional orbitals for the periodic table of elementary particles.

In Section 2, the periodic table of elementary particles is derived from the computer simulation of physical reality. Section 3 deals with the gauge boson mass formula and the cosmic ray mass formula. Section 4 explains the lepton mass formula and the quark mass formula. Section 5 describes the Higgs boson mass formula.

### 2. The Periodic Table of Elementary Particles

The periodic table of elementary particles is derived from the computer simulation model of physical reality consisting of the mathematical computation, digital representation, and selective retention components.

#### 2.1. The Mathematical Computation Component

The geometry in the mathematic computation component for the computer simulation process is oscillating M-theory. M-theory with eleven-dimensional membrane is an extension of string theory with ten-dimensional string, in contrast to the observed 4D. In conventional M-theory, space-time dimensional number (D) is fixed. As a result, the observed 4D results from the compactization of the extra space dimensions in 11D M-theory. However, there is no experimental proof for compactized extra space dimensions, and there are numerous ways for

the compactization of the extra space dimensions [9]. As described before [7], the geometry for the mathematical computation is oscillating M-theory derived from oscillating membrane-string-particle whose space-time dimension number oscillates between 11D and 10D and between 10D and 4D dimension by dimension reversibly. There is no compactization. Matters in oscillating M-theory include 11D membrane ( $2_{11}$ ) as membrane (denoted as 2 for 2 space dimensions) in 11D, 10D string ( $1_{10}$ ) as string (denoted as 1 for 1 space dimension) in 10D, and variable D particle ( $0_{4 \text{ to } 11}$ ) as particle (denoted as 0 for 0 space dimension) in 4D to 11D.

As described previously [10], the QVSL (quantum varying speed of light) transformation transforms both space-time dimension number (D) and mass dimension number (d). In the QVSL transformation, the decrease in the speed of light leads to the decrease in space-time dimension number and the increase of mass in terms of increasing mass dimension number from 4 to 10,

$$c_D = c/\alpha^{D-4}, \quad (1a)$$

$$E = M_0 \cdot \left( c^2/\alpha^{2(D-4)} \right) \quad (1b)$$

$$= \left( M_0/\alpha^{2(d-4)} \right) \cdot c^2. \quad (1c)$$

$$c_D = c_{D-n}/\alpha^{2n}, \quad (1d)$$

$$M_{0,D,d} = M_{0,D-n,d+n} \alpha^{2n}, \quad (1e)$$

$$D, d \xrightarrow{\text{QVSL}} (D \mp n), (d \pm n) \quad (1f)$$

$$E_{\text{vacuum},D} = E - M_{0,D} c^2, \quad (1g)$$

where  $c_D$  is the quantized varying speed of light in space-time dimension number, D, from 4 to 10;  $c$  is the observed speed of light in the 4D space-time;  $\alpha$  is the fine structure constant for electromagnetism,  $E$  is energy;  $M_0$  is rest mass; D is the space-time dimension number from 4 to 10; d is the mass dimension number from 4 to 10;  $n$  is an integer; and  $E_{\text{vacuum}}$  = vacuum energy. For example, in the QVSL transformation, a particle with 10D4d is transformed to a particle with 4D10d from Equation (1f). Calculated from Equation (1e), the rest mass of 4D10d is  $1/\alpha^{12} \approx 137^{12}$  times of the mass of 10D4d. In terms of rest mass, 10D space-time has 4d with the lowest rest mass, and 4D space-time has 10d with the highest rest mass. Rest mass decreases with increasing space-time dimension number. The decrease in rest mass means the increase in vacuum energy ( $E_{\text{vacuum},D}$ ), so vacuum energy increases with increasing space-time dimension number. The vacuum energy of 4D particle is zero from Equation (1g). The mass dimension number is limited from 4 to 10, because 4D is the minimum space-time, and 11D membrane and 10D string are equal in the speed of light, rest mass, and vacuum energy. Since the speed of light for >4D particle is greater than the speed of light for 4D particle, the observation of >4D superluminal particles by 4D particles violates casualty. Thus, >4D particles are hidden particles with respect to 4D particles. Particles with different space-time dimensions are transparent and oblivious to one another, and separate from one another if possible.

In the digital representation component for the computer simulation process, data in physical reality are represented by digital representations. Both data and digital representations exist. For the digital representation component of physical reality, the three intrinsic data (properties) are rest mass-kinetic energy, electric charge, and spin which are represented by the digital space structure, the digital spin, and the digital electric charge, respectively.

## 2.2. Digital Space Structure

The digital representations of rest mass and kinetic energy are 1 as attachment space for the space of matter and 0 as detachment space for the zero-space of matter, respectively [7] [11]. In the digital space structure, attachment space attaches to matter permanently or reversibly. Detachment space detaches from the object at the speed of light. Attachment space relates to rest mass and reversible movement, while detachment space relates to irreversible kinetic energy.

As shown previously [8], our universe is the dual asymmetrical positive-energy-negative-energy universe where the positive-energy universe on attachment space absorbed the interuniversal void on detachment space to result in the combination of attachment space and detachment space. The combination of  $n$  units of attachment space as 1 and  $n$

units of detachment space as 0 brings about three different digital space structures: binary partition space, miscible space, or binary lattice space as below.

$$(1)_n + (0)_n \xrightarrow{\text{combination}} (1)_n(0)_n, (1+0)_n, \text{ or } (1\ 0)_n \tag{2}$$

attachment space    detachment space    binary partition space, miscible space, binary lattice space

Binary partition space,  $(1)_n(0)_n$ , consists of two separated continuous phases of multiple quantized units of attachment space and detachment space. In miscible space,  $(1+0)_n$ , attachment space is miscible to detachment space, and there is no separation of attachment space and detachment space. Binary lattice space,  $(1\ 0)_n$ , consists of repetitive units of alternative attachment space and detachment space. Binary partition space, miscible space, and binary lattice space relate to quantum mechanics, special relativity, and force fields, respectively [7].

Bounias and Krasnoholovets [12] propose that the reduction of dimension can be done by slicing dimension, such as slicing 3 space dimension object (block) into infinite units of 2 space dimension objects (sheets). As shown previously [8], the positive-energy 10D4d particle universe as our observable universe with high vacuum energy was transformed into the 4D10d universe with zero vacuum energy at once, resulting in the inflation. During the Big Bang following the inflation, the 10d (mass dimension) particle in attachment space denoted as 1 was sliced by detachment space denoted as 0. For example, the slicing of 10d particle into 4d particle is as follows.

$$1_{10} \xrightarrow{\text{slicing}} 1_4 \sum_{d=5}^{10} (0_4\ 1_4)_{n,d} \tag{3}$$

10d particle    4d core particle    binary lattice space

where  $1_{10}$  is 10d particle;  $1_4$  is 4d particle;  $d$  is the mass dimension number of the dimension to be sliced;  $n$  as the number of slices for each dimension; and  $(0_4\ 1_4)_n$  is binary lattice space with repetitive units of alternative 4d attachment space and 4d detachment space. For 4d particle starting from 10d particle, the mass dimension number of the dimension to be sliced is from  $d = 5$  to  $d = 10$ . Each mass dimension is sliced into infinite quantized units ( $n = \infty$ ) of binary lattice space,  $(0_4\ 1_4)_\infty$ . For 4d particle, the 4d core particle is surrounded by 6 types (from  $d = 5$  to  $d = 10$ ) of infinite quantized units of binary lattice space. Such infinite quantized units of binary lattice space represent the infinite units ( $n = \infty$ ) of separate virtual orbitals in a gauge force field, while the dimension to be sliced is “mass dimensional orbital” (DO), representing a type of gauge force field. In addition to the six DO’s for gauge force fields from  $d = 5$  to  $d = 10$ , gravity appears as the seventh DO at  $d = 11$ . As a result, there are seven mass dimensional orbitals as in Figure 1.

### 2.3. The Digital Spin

The digital representations of the exclusive and the inclusive occupations of positions are 1/2 spin fermion and integer spin boson, respectively [7]. Fermions, such as electrons and protons, follow the Pauli exclusion principle which excludes fermions of the same quantum-mechanical state from being in the same position. Bosons, such as photons or helium atoms, follow the Bose-Einstein statistics which allows bosons of the same quantum-mechanical state being in the same position. As a result, the digital representations of the exclusive and the inclusive occupations of positions are 1/2 spin fermion and integer spin boson, respectively. The symmetry between fermion and boson is supersymmetry. Two supersymmetry transformations from boson to fermion and from fermion to boson yield a spatial translation. In physical reality, supersymmetry is varying supersymmetry [8]. In varying supersymmetry, the repetitive transformation between fermion and boson brings about a spatial translation and the transformation into the adjacent mass dimension number. Varying supersymmetry transformation is one of the two steps in transformation involving the oscillation between 10D particle and 4D particle. The transformation during the oscillation between 10D particle and 4D particle involves the stepwise two-step transformation consisting of the QVSL transformation and the varying supersymmetry transformation. The QVSL

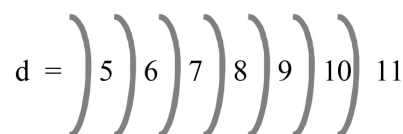


Figure 1. The seven mass dimensions as mass dimensional orbitals.

transformation involves the transformation of space-time dimension,  $D$  whose mass increases with decreasing  $D$  for the decrease in vacuum energy. The varying supersymmetry transformation involves the transformation of the mass dimension number,  $d$  whose mass decreases with decreasing  $d$  for the fractionalization of particle, as follows.

stepwise two-step varying transformation

$$(1) \quad D, d \xleftarrow{\text{QVSL}} (D \mp 1), (d \pm 1) \quad (4)$$

$$(2) \quad D, d \xleftarrow{\text{varying supersymmetry}} D, (d \pm 1)$$

The repetitive stepwise two-step transformation between 10D4d and 4D4d as follows.

$$10D4d \leftrightarrow 9D5d \leftrightarrow 9D4d \leftrightarrow 8D5d \leftrightarrow \dots \leftrightarrow 4D5d \leftrightarrow 4D4d \quad (5)$$

In this two-step transformation, the transformation from 10D4d to 9D5d involves the QVSL transformation as in Equation (1d). Calculated from Equation (1e), the mass of 9D5d is  $1/\alpha^2 \approx 137^2$  times of the mass of 10D4d. The transformation of 9D5d to 9D4d involves the varying supersymmetry transformation. In the normal supersymmetry transformation, the repeated application of the fermion-boson supersymmetry transformation carries over a boson (or fermion) from one point to the same boson (or fermion) at another point at the same mass. In the varying supersymmetry transformation, the repeated application of the fermion-boson supersymmetry transformation carries over a boson from one point to the boson at another point at different mass dimension number in the same space-time number. The repeated varying supersymmetry transformation carries over a boson  $B_d$  into a fermion  $F_d$  and a fermion  $F_d$  to a boson  $B_{d-1}$ , which can be expressed as follows

$$M_{d,F} = M_{d,B} \alpha_{d,B}, \quad (6a)$$

$$M_{d-1,B} = M_{d,F} \alpha_{d,F}, \quad (6b)$$

where  $M_{d,B}$  and  $M_{d,F}$  are the masses for a boson and a fermion, respectively;  $d$  is the mass dimension number; and  $\alpha_{d,B}$  or  $\alpha_{d,F}$  is the fine structure constant that is the ratio between the masses of a boson and its fermionic partner. Assuming  $\alpha$ 's are the same, it can be expressed as

$$M_{d,B} = M_{d+1,B} \alpha_{d+1}^2. \quad (6c)$$

## 2.4. The Digital Electric Charge

As described before [13], the digital representations of the allowance and the disallowance of irreversible kinetic energy are integral electric charges and fractional electric charges, respectively. Individual integral charge with irreversible kinetic energy to cause irreversible movement is allowed, while individual fractional charge with irreversible kinetic energy is disallowed. The disallowance of irreversible kinetic energy for individual fractional charge brings about the confinement of individual fractional charges to restrict the irreversible movement resulted from kinetic energy. Collective fractional charges are confined by the short-distance confinement force field where the sum of the collective fractional charges is integer. As a result, fractional charges are confined and collective. The confinement force field includes gluons in QCD (quantum chromodynamics) for collective fractional charge quarks in hadrons and the magnetic flux quanta for collective fractional charge quasiparticles in the fractional quantum Hall effect (FQHE) [14]-[16].

In the periodic table of elementary particles, fractional charge quarks have their own seven mass dimensional orbitals as the seven auxiliary mass dimensional orbitals in addition to the seven principal mass dimensional orbitals for leptons as in **Figure 2**.

## 2.5. The Selective Retention Component

The selective retention component retains selectively events in a narrative. The retained events are unified by the common narrative. The narrative of physical reality is the four-stage evolution of our cyclic dual universe. The four force fields are unified by the four-stage evolution.

Our dual universe is the globally reversible cyclic dual universe as shown in **Figure 3** [7] for the evolution of our universe as described previously [7].

The four reversible stages in the globally reversible cyclic dual universe are: 1) the formation of the 11D

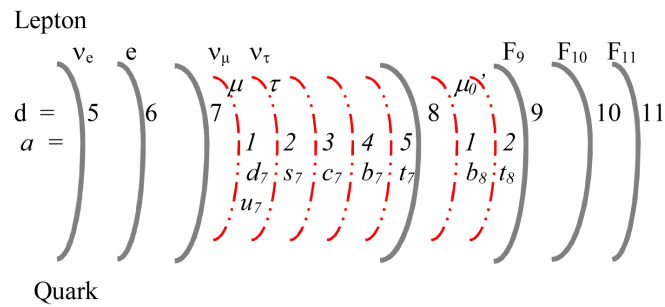


**Figure 2.** Leptons and quarks in the seven principal dimensional orbitals (solid lines) denoted by the principal dimensional orbital number  $d$  and the seven auxiliary dimensional orbitals (dash-dotted lines) denoted by the auxiliary dimensional number  $a$ .

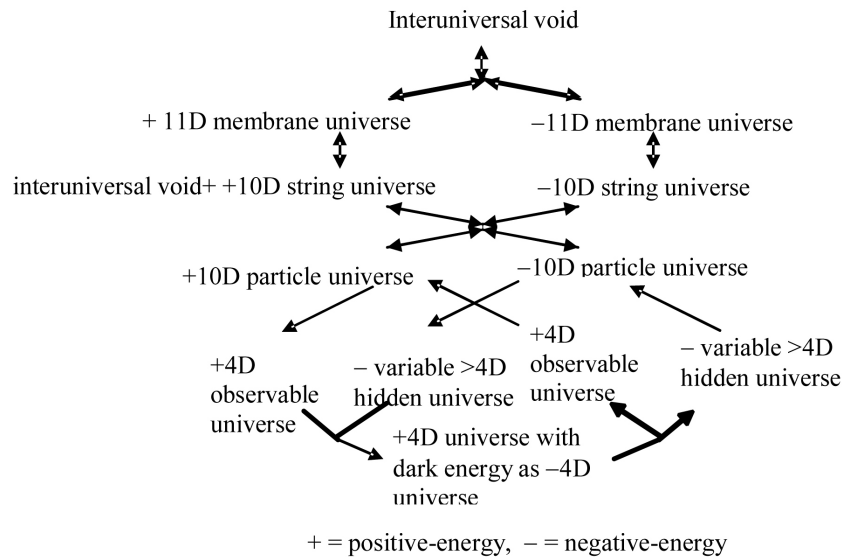


**Figure 3.** The globally reversible cyclic dual universe.

membrane dual universe; 2) the formation of the 10D string dual universe; 3) the formation of the 10D particle dual universe; and 4) the formation of the asymmetrical dual universe. The pre-strong force (the prototype of observed strong force) and pre-gravity emerged in the stage 2. The pre-electromagnetism emerged in the stage 3, while the weak force emerged in the stage 4. The selective retention of the four force fields provides the four force fields (gauge bosons) for the four of the seven principal mass dimensional orbitals ( $B_d$ ) as in **Table 1**. The other three of the seven principal mass dimensional orbitals are for the CP (right) nonconservation, the CP (left) nonconservation, and the weak (right) force.

The periodic table of elementary particles for leptons, quarks, and gauge boson is in **Table 2** with both the principal mass dimensional orbital numbers and the auxiliary mass dimensional orbital numbers.

### 3. The Gauge Boson Mass Formula and the Cosmic Ray Mass Formula

The gauge boson mass formula is Equation (7) derived from Equation (6c) based on the digital spin structure,

$$M_{d+1, \text{gauge boson}} = M_{d, \text{gauge boson}} / \alpha_{d+1}^2 \tag{7}$$

Each dimension has its own  $\alpha_d$ , and all  $\alpha_d$ 's except  $\alpha_7$  ( $\alpha_w$ ) of the seventh dimension (weak interaction) are equal to  $\alpha$ , the fine structure constant of electromagnetism. The lowest energy boson is the Coulombic field for electromagnetism based on Equation (6b) and the second lowest boson energy is  $\pi_{1/2}$  (a spin 1 boson as a half of the spin 0 pion) with the mass of 70 MeV for the strong interaction. As described in Section 4, this boson  $B_6$  is used to construct gluon.

**Table 1.** The masses of the principal mass dimensional orbitals (gauge bosons)  $\alpha = \alpha_e$ ,  $d =$  mass dimensional orbital number.

$B_d$	$M_d$	GeV (calculated)	Gauge boson	Interaction
$B_5$	$M_e \alpha$	$3.7 \times 10^{-6}$	A = photon	Electromagnetic
$B_6$	$M_e / \alpha$	$7 \times 10^{-2}$	$\pi_{1/2}$	Strong
$B_7$	$M_6 / \alpha_w^2$	91.1876 (given)	$Z_L^0$	weak (left)
$B_8$	$M_7 / \alpha^2$	$1.71 \times 10^6$	$X_R$	CP (right) nonconservation
$B_9$	$M_8 / \alpha^2$	$3.22 \times 10^{10}$	$X_L$	CP (left) nonconservation
$B_{10}$	$M_9 / \alpha^2$	$6.04 \times 10^{14}$	$Z_R^0$	weak (right)
$B_{11}$	$M_{10} / \alpha^2$	$1.13 \times 10^{19}$	G	Gravity

**Table 2.** The periodic table of elementary particles  $d =$  principal mass dimensional orbital number,  $a =$  auxiliary mass dimensional orbital number.

d	a=0	1	2	1	2	3	4	5	
	Lepton			Quark					Boson
5	$\nu_e$								$B_5 = A$
6	e								$B_6 = \pi_{1/2}$
7		$\nu_{\mu}, \mu$	$\nu_{\tau}, \tau$	$d_7/u_7$	$s_7$	$c_7$	$b_7$	$t_7$	$B_7 = Z_L^0$
8		$\mu'_0$ (hidden)		$b_8$ (hidden)	$t_8$				$B_8 = X_R$
9	$F_9$								$B_9 = X_L$
10	$F_{10}$								$B_{10} = Z_R^0$
11	$F_{11}$								$B_{11}$ gravity

$$M_{5,B} = \alpha M_{6,F} = \alpha M_e. \tag{8a}$$

$$M_{B_6} = M_{B_5} / \alpha^2 = M_e / \alpha = M_{\pi_{1/2}} \tag{8b}$$

In **Table 1**,  $\alpha_w$  is not same as  $\alpha$  because there is a mixing between electromagnetism and the weak interaction in the standard theory of the electroweak interaction, and  $\sin \theta_w$  is not equal to 1 where  $\theta_w$  is the weak mixing angle [17]. As a result,  $\alpha_w$  instead of  $\alpha$  is used to calculate  $M_{B_7}$  from  $M_{B_6}$  based on the gauge boson formula Equation (7).  $M_{B_7}$  is the mass of weak Z boson  $M_Z$  which is 91.1876 GeV.

$$\begin{aligned} M_{B_7} &= M_Z = M_{B_6} / \alpha_w^2 \\ \alpha_w &= \sqrt{M_{B_6} / M_Z} \end{aligned} \tag{9}$$

The calculated value for  $\alpha_w$  is 0.02771. As described in the following paragraphs and **Table 3**,  $B_8$ ,  $F_9$  and  $B_9$  in **Table 2** are observed in cosmic rays as the first knee, the second knee, and the toe, respectively, where the calculated masses are in good agreement with the observed masses [6]. The calculated energy for  $B_{11}$  is  $1.13 \times 10^{19}$  GeV in good agreement with the Planck mass,  $1.22 \times 10^{19}$  GeV for gravity.

High-energy cosmic rays which have much higher energies than the energy of particles accelerated by the Large Hadron Collider provide the study of elementary particles beyond the capacity of particle accelerators. The cosmic ray mass formula is to the energy spectrum for the knees-ankles-toe of cosmic rays [6]. The energy spectrum from  $10^9$  eV to  $10^{20}$  eV appears to follow a single power law except few breaks at the knees-ankles-toe [18]. The power index increases at the first knee and the second knee, and decreases at the ankle. Above  $4 \times 10^{19}$  eV, the power index increases as the ‘‘toe’’. The fine structure of the cosmic ray spectrum [19] shows that an ankle with decrease in power index is in between the first knee and the second knee, resulting in two knees, two ankles, and one toe. As explained previously [6], the knees-ankles-toe are explained by the very high-energy fermions and bosons in the periodic table of elementary particles. In the periodic table, some high-energy dimensional fermions ( $F_d$  where  $d =$  dimen-

**Table 3.** The calculated masses for dimensional bosons-fermions and the observed eV for the knees-ankles-toe.  $B_d$  = mass dimensional boson,  $F_d$  = mass dimensional fermion.

$B_d, F_d$	calculated eV	Calculation	cosmic rays	observed eV
$B_8$	$1.7 \times 10^{15}$		the first knee	$3 \times 10^{15}$
the midpoint between $B_8$ and $F_9$	$2 \times 10^{16}$	Equation (11)	the first ankle	$2 \times 10^{16}$
$F_9$	$2.4 \times 10^{17}$	$M_{B_8}/\alpha$	the second knee	$3 \times 10^{17}$
the midpoint between $F_9$ and $B_9$	$2.8 \times 10^{18}$	Equation (11)	the second ankle	$3 \times 10^{18}$
$B_9$	$3.2 \times 10^{19}$	$M_{F_9}/\alpha$	the toe	$4 \times 10^{19}$
$F_{10}$	$4.4 \times 10^{21}$	$M_{B_9}/\alpha$	beyond the GZK limit	not observed

sional orbital number from 5 to 11) and bosons ( $B_d$ ) are involved in the knees-ankles-toe. At the knees and the toe, some parts of the energies from the energy sources of cosmic rays are spent to generate  $F_d$  and  $B_d$ , resulting in the increase of power index. The ankles are the the middle points (midpoints) between the adjacent dimensional fermions and bosons. At a midpoint, the energy is too high to keep the thermally unstable high- energy dimensional particle, resulting in the decay and the decrease of power index.

The cosmic ray mass formula is derived from Equations (6a) and (6b)

$$M_{d,F} = M_{d,B} \alpha \tag{10a}$$

$$M_{d-1,B} = M_{d,F} \alpha \tag{10b}$$

where  $M_{d,B}$  and  $M_{d,F}$  are the masses for a boson and a fermion, respectively; d is the mass dimension number from 8 to 10; and  $\alpha_{d,B}$  or  $\alpha_{d,F}$  is the fine structure constant. The midpoint is expressed as follows.

$$M_{\text{midpoint}} = \exp\left(\left(\ln\left(M_{\text{adjacent dimensional ferion}}\right) + \ln\left(M_{\text{adjacent dimensional boson}}\right)\right)/2\right) \tag{11}$$

The calculated masses of  $B_8$ , the midpoint,  $F_9$ , the midpoint, and  $B_9$ , are  $1.7 \times 10^{15}$ ,  $2 \times 10^{16}$ ,  $2.4 \times 10^{17}$ ,  $2.8 \times 10^{18}$ , and  $3.2 \times 10^{19}$  eV, respectively, which are in good agreement with observed  $3 \times 10^{15}$ ,  $2 \times 10^{16}$ ,  $3 \times 10^{17}$ ,  $3 \times 10^{18}$ , and  $4 \times 10^{19}$  eV for the first knee, the first ankle, the second knee, the second ankle, and the toe, respectively as in **Table 3**.

The mass of  $F_{10}$  is  $4.4 \times 10^{21}$  eV beyond the GZK (Greisen-Zatsepin-Kuzmin) limit, which occurs at about  $5 \times 10^{19}$  eV, as the maximum energy of cosmic ray particles that have traveled long distances (about 160 million light years), due to the theoretical energy losses of higher-energy ray particles and to scattering from photons in the cosmic microwave background. Therefore,  $F_{10}$  and above are not observed.

#### 4. The Lepton Mass Formula and the Quark Mass Formula

The lepton mass formula and the quark mass formula are derived from the electric digital charge structure where the digital representations of the allowance and the disallowance of irreversible kinetic energy are integral electric charges and fractional electric charges, respectively [13]. The collectivity of fractional charges requires the attachment of energy as flux quanta to bind fractional charges. As a result, the integer-fraction transformation from integral charges to fractional charges involves the integer-fraction transformation to incorporate flux quanta similar to the composite fermion theory for the FQHE [20] [21]. In the composite fermion model, the formation of composite fermion is through the attachment of an even number of magnetic flux quanta to electron, while the formation of composite boson is through the attachment of an odd number of magnetic flux quanta to electron. In the same way, the integer-fraction transformation from integral charges to fractional charges for quarks consists of the three steps: 1) the attachment of an even number of flux quanta to individual integral charge fermions to form individual integral charge composite fermions ( $F_c$ ); 2) the attachment of an odd number of flux quanta to individual integral charge composite fermions to form transitional collective integral charge composite bosons ( $B_c$ ); and 3) the conversion of flux quanta into the confinement force field to confine collective fractional charge composite quarks ( $Q_c$ ) converted from composite bosons as follows.

$$\begin{array}{l}
\text{individual } e \bar{e} \xrightarrow{2 \text{ flux quanta}} \text{individual } F_c \bar{F}_c \xrightarrow{3 \text{ flux quanta}} \\
\text{transitional collective } B_c \bar{B}_c \xrightarrow{\text{QCD}} \\
\text{collective } 2 Q_c \bar{Q}_c \text{ of } \pm \frac{1}{3} \text{ and } \pm \frac{2}{3} \text{ charge with 3 gluons + individual } e \bar{e}
\end{array} \quad (12)$$

where  $F_c$ ,  $B_c$ , and  $Q_c$  are the composite fermion, the composite boson, and the composite quark, respectively. The first step of the integer-fraction transformation from electron to quark is the attachment of 2 flux quanta to individual integral charge electrons to form individual composite fermions ( $F_c$ 's). The flux quanta (70.0252 MeV) are the flux quanta as proposed by Peter Cameron to calculate accurately the masses of pion, muon, and proton [22]. The quantum of 70.0252 MeV is also the bosonic mass quantum proposed by Malcolm H. MacGregor for a basic building block to calculate accurately the masses of hadrons [23]. According to the periodic table of elementary particles, the flux quantum is  $B_6$  from Table 1. From Equation (6b), the relationship between  $B_6$  and electron ( $F_5$ ) is as follows.

$$M_{B_6} = M_{F_5} / \alpha = M_e / \alpha = 70.0252 \text{ MeV} \quad (13)$$

where  $\alpha$  is the fine structure constant for electromagnetism. The  $F_{pc}$  (the principal composite fermion) consists of two  $B_6$  as flux quanta.

$$M_{F_{pc}} = 2M_{B_6} = 140.0505 \text{ MeV} \quad (14)$$

The mass of pion (boson) is the mass of the principal composite fermion ( $F_{pc}$ ) minus the mass of electron (fermion) [22].

$$M_\pi = M_{F_{pc}} - M_e = 139.5395 \text{ MeV} \quad (15)$$

which is in excellent agreement with the observed 139.5702 MeV.

In the second step for the attachment of odd number of flux quanta, the odd number of flux quanta can be one flux quantum for one principal composite fermion or three flux quanta for three principal composite fermions, resulting in lepton or quark, respectively. For the formation of lepton, the second step is the attachment of one flux quantum to one individual integral charge principal composite fermion to form the transitional integral charge principal composite boson. In the second step, the principal composite boson for composite lepton is  $B_6 + F_{pc}$ . In the third step, the principal composite boson is converted into two composite leptons ( $L_c$ ) with the addition of electrons, resulting in muon as follows.

$$M_{B_{pc}} \text{ for } L_c = M_{F_{pc}} + M_{B_6} = 2M_{B_6} + M_{B_6} = 3M_{B_6} \quad (16a)$$

$$M_{L_c} = M_\mu = M_e + M_{B_{pc}} / 2 = M_e + 3M_{B_6} / 2 = M_e + \frac{3M_e}{2\alpha} = 105.5491 \text{ MeV} \quad (16b)$$

which is in excellent agreement with the observed 105.6584 MeV. The muon mass formula in Equation (16b) is identical to the Barut lepton mass formula for muon [24]. Equation (16b) explains the origin of 3/2 which cannot be explained easily by Cameron, MacGregor, and Barut. Without binding the composite leptons together by the flux quanta, leptons have integral electric charges instead of fractional electric charges.

The Barut lepton mass formula [24] is expressed as follows.

$$M_{\text{lepton}} = M_e + \frac{3M_e}{2\alpha} \sum_{a=0}^n a^4, \quad (17)$$

where  $n = 0, 1, \text{ and } 2$  are for  $e, \mu, \text{ and } \tau$ , respectively. The calculated mass of  $\tau$  is 1786.2 MeV in good agreement with the observed mass as 1776.82 MeV. According to Barut, the second term,  $\sum_{a=0}^n a^4$  of the mass formula is for the Bohr-

Sommerfeld quantization for a charge-dipole interaction in a circular orbit. The experimental proof of this dipole-interaction in a circular orbit is shown as the light boson at 17 MeV from the generation of pairs of electrons and positrons by firing protons at thin targets of lithium-7 [25] [26]. The light boson is the orbit  $e_0 \bar{e}_0$  in the circular orbit. The masses of the bosons from orbit  $e_0 \bar{e}_0$  are calculated as follows.

$$M_{\text{boson}} = M_{e_0\bar{e}_0} = 2M_{e_0} = 2M_e \sum_{a=1}^n a^4 \quad (18)$$

where the masses of the bosons for  $n = 1$  and  $2$  are  $2M_e$  for  $e\bar{e}$  (electron-positron pair) and  $34M_e$  for the light boson, respectively. The calculated mass of the light boson is 17.374 MeV in excellent agreement with the observed mass as 17 MeV [25]. As in **Figure 2** and **Table 2**,  $\nu_\mu$  and  $\nu_\tau$  share the same orbitals with  $\mu$  and  $\tau$ , respectively. All neutrinos ( $\nu_e$ ,  $\nu_\mu$  and  $\nu_\tau$ ) in the periodic table of elementary particles (**Table 2**) are nearly massless because of chiral symmetry (permanent left-handed).

For the formation of quark, the second step is the attachment of 3 flux quanta ( $B_6$ 's) to three individual integral charge principal composite fermions ( $F_{pc}$ 's) to form the transitional collective integral charge principal composite bosons ( $B_{pc}$ 's). The transitional principal composite bosons are derived from the combination of the three principal composite fermions (3  $F_{pc}$ 's) with the three flux quanta (3  $B_6$ 's) which are connected and located at the same position in the same 3- $F_{pc}$  energy level. One 3- $F_{pc}$  energy level consists of the three connected  $F_{pc}$  sites with the connected three flux quanta (3  $B_6$ 's). The mass of the transitional principal composite bosons  $B_{pc}$  is as follows.

$$M_{B_{pc}} = 3M_{F_{pc}} + 3M_{B_6} = 6M_{B_6} + 3M_{B_6} = 9M_{B_6} = 9M_e/\alpha = 630.227 \text{ MeV} \quad (19)$$

In the third step, 3 flux quanta ( $B_6$ 's) are converted to 3-color gluons (red, green, and blue) in QCD. Each of the three  $F_{pc}$  sites in the energy level has  $\pm 1/3$  charge. The fractional charges of quarks are the integer multiples of  $\pm 1/3e$ . One principal composite boson ( $B_{pc}$ ) is converted into two composite quarks (fermions) in the same way as the conversion of one photon (boson) into two fermions (electron-positron). As a result, the principal composite quark ( $Q_{pc}$ ) has 1/2 mass of the principal composite boson ( $B_{pc}$ ) in addition to the mass of 1/3 and 2/3 electrons for the three  $F_c$  sites for different electric charges as follows.

$$M_{Q_{pc}} = \frac{1 \text{ or } 2M_e}{3} + \frac{M_{B_{pc}}}{2} = \frac{1 \text{ or } 2M_e}{3} + \frac{9M_e}{2\alpha} = 315.28 \text{ or } 315.45 \text{ MeV} \quad (20)$$

From Equation (20), the principal composite quark with 1/3 electric charge is the principal composite d quark with 315.28 MeV, and the principal composite quark with 2/3 charge is the principal composite u quark with 315.45 MeV.

According to the periodic table of elementary particles (**Table 2**), quarks have the auxiliary mass dimensional orbital in addition to the principal mass dimensional orbital as in **Figure 2**. As a result, there are the auxiliary composite quarks ( $Q_{ac}$ ) in addition to the principal composite quarks ( $Q_{pc}$ ). The three-step transformation in the integer-fraction transformations from integral charge to fractional charge is applicable to the auxiliary composite quarks. The auxiliary flux quantum is  $B_{a7}$  which is in between  $d_7$  and  $d_8$  as shown in **Figure 2**. As a result,  $\alpha_w$  instead of  $\alpha$  is used for  $B_{a7}$ . Muon, a composite lepton, instead of electron is used for  $B_{a7}$  as follows.

$$M_B = M_\mu \alpha_w \quad (21)$$

where  $\alpha_w$  is the fine structure constant for weak force from Equation (9). In the first step, the  $F_{ac}$  (the auxiliary composite fermion) consists of two  $B_{a7}$  as auxiliary flux quanta.

$$M_{F_{ac}} = 2M_{B_{a7}} = 2M_\mu \alpha_w \quad (22)$$

The second step is the attachment of 3 auxiliary flux quanta ( $B_{a7}$ 's) to the individual integral charge auxiliary composite fermions ( $F_{ac}$ 's) to form the transitional collective integral charge auxiliary composite bosons ( $B_{ac}$ 's). The transitional auxiliary composite bosons are derived from the combination of the three auxiliary composite fermions (3  $F_{ac}$ 's) with the three flux quanta (3  $B_{a7}$ 's) which are connected and located at the same position in the same 3- $F_{ac}$  energy level. One 3- $F_{ac}$  energy level consists of the three connected  $F_{ac}$  sites with the connected three auxiliary flux quanta (3  $B_{a7}$ 's). The mass of the transitional auxiliary composite bosons  $B_{ac}$  is as follows.

$$M_{B_{ac}} = 3M_{F_{ac}} + 3M_{B_{a7}} = 6M_{B_{a7}} + 3M_{B_{a7}} = 9M_{B_{a7}} = 9M_\mu \alpha_w \quad (23)$$

In the third step, 3 auxiliary flux quanta ( $B_{a7}$ 's) are converted to 3-color gluons (red, green, and blue) in QCD to confine the collective fractional charge auxiliary composite quarks ( $Q_{ac}$ 's) converted from the transitional auxiliary composite bosons ( $B_{ac}$ 's). One composite boson ( $B_{ac}$ ) is converted into two composite quarks (fermions) in the same way as the conversion of one photon (boson) into two fermions (electron-positron). As a re-

sult, the auxiliary composite quark ( $Q_{ac}$ ) has 1/2 mass of the auxiliary composite boson ( $B_{ac}$ ).

$$M_{Q_{ac}} = M_{B_{ac}}/2 = 9M_{\mu}\alpha_w/2 = 13.16 \text{ MeV} \quad (24)$$

The composite quark mass formula is the combination of the principal composite quark and the auxiliary composite quark with the Bohr-Sommerfeld quantization for a charge-dipole interaction in a circular orbit as follows.

$$M_{Q_c} = M_{Q_{pc}} + M_{Q_{ac}} \sum_{a=1}^n a^4 = \frac{1 \text{ or } 2M_e}{3} + \frac{9M_e}{2\alpha} + \frac{9M_{\mu}\alpha_w}{2} \sum_{a=1}^n a^4 \quad (25)$$

where  $n = 1, 2, 3, 4,$  and  $5$  for  $u/d, s, c, b,$  and a part of  $t$ , respectively.

At  $n = 5$  for Equation (25), the mass (140.4 GeV) is greater than  $B_7$  (91.1876 GeV) as in **Table 1**, so the last two auxiliary mass dimensional orbitals of the seven auxiliary dimensional orbitals are in between  $d_8$  and  $d_9$ . The formation of the auxiliary mass dimensional orbitals between  $d_8$  and  $d_9$  requires the extra-principal flux quantum as  $B_7$  instead of  $B_6$ . For the first step in the three-step transformation from integer charge to fractional charge for the extra quarks is to form the extra composite fermion.  $B_7$  is  $Z$  boson. The  $F_{epc}$  (the extra principal composite fermion) consists of two  $B_7$  as flux quanta. The  $F_{epc}$  (the extra principal composite fermion) consists of two  $B_7$  as flux quanta.

$$M_{F_{epc}} = 2M_{B_7} = 2M_Z \quad (26)$$

For the second step to form the extra principal composite boson, only one extra-principal flux quantum is added to one extra-principal composite fermion, because the 3-color principal electric and 3-color auxiliary flux quanta already exist, and there is no need for three extra-principal flux quanta.

$$M_{B_{epc}} = M_{F_{epc}} + M_{B_7} = 2M_Z + M_Z = 3M_Z \quad (27)$$

The third step is the conversion of the extra-principal composite boson to two extra-principal quarks ( $Q_{epc}$ ). Only The neutral  $B_{epc}$  is used for  $Q_{epc}$ , so no electron is added.

$$M_{Q_{epc}} = M_{B_{epc}}/2 = 3M_Z/2 = 136.78 \text{ GeV} \quad (28)$$

Since  $Q_{epc}$  involves only one extra-principal flux quantum,  $Q_{epc}$  is identical to the extra-composite lepton  $L_{ec}$  which is neutral extra-muon  $\mu'_0$ .

$$M_{\mu'_0} = M_{Q_{epc}} = 3M_Z/2 = 136.78 \text{ GeV} \quad (29)$$

The extra-auxiliary flux quantum is  $B_{ea}$  is like Equation (21).

$$M_{B_{ea}} = M_{\mu'_0} \alpha \quad (30)$$

where the fine structure constant in between  $d_8$  and  $d_9$  is  $\alpha$ . For the first step in the three-step transformation from integer charge to fractional charge, the extra-auxiliary composite fermion ( $F_{eac}$ ) is the composite of two  $B_{8ea}$ 's.

$$M_{F_{eac}} = 2M_{B_{8ea}} = 2M_{\mu'_0} \alpha \quad (31)$$

For the second step to form the extra-auxiliary composite boson  $B_{eac}$ , only one extra-auxiliary flux quantum is needed in the same way for the formation of the extra-principal composite boson.

$$M_{B_{eac}} = M_{F_{eac}} + M_{B_{8ea}} = 2M_{B_{8ea}} + M_{B_{8ea}} = 3M_{B_{8ea}} = 3M_{\mu'_0} \alpha \quad (32)$$

For the third step to form quark from composite boson  $B_{eac}$ , extra-auxiliary composite boson is converted into two extra-auxiliary composite quarks ( $Q_{eac}$ ).

$$M_{Q_{eac}} = M_{B_{eac}}/2 = 3M_{\mu'_0} \alpha/2 = 3(3M_Z/2)\alpha/2 = 9M_Z \alpha/4 \quad (33)$$

The mass formula for the extra- composite quark ( $Q_{ec}$ ) with the Bohr-Sommerfeld quantization for a charge-dipole interaction in a circular orbit is as follows.

$$M_{Q_{ec}} = M_{Q_{epc}} + M_{Q_{eac}} \sum_{a'=1}^{n'} a'^4 = \frac{3M_Z}{2} + \frac{9M_Z \alpha}{4} \sum_{a'=1}^{n'} a'^4 \quad (34)$$

where  $n' = 1$  and  $2$  for  $b$  and  $t$ , respectively.

Quark is the combination of the composite quark from Equation (25) and the extra-composite quark from Equation (34). The quark mass formula is as follows.

$$M_{\text{quark}} = M_{Q_c} + M_{Q_{ec}} = \frac{1 \text{ or } 2M_e}{3} + \frac{9M_e}{2\alpha} + \frac{9M_\mu\alpha_w}{2} \sum_{a=1}^n a^4 + \frac{3M_Z}{2} + \frac{9M_Z\alpha}{4} \sum_{a'=1}^{n'} a'^4 \quad (35)$$

where  $n = 1, 2, 3, 4,$  and  $5$  for  $d/u, s, c, b,$  and  $t$ , respectively; and  $n' = 1$  and  $2$  for  $b$  and  $t$  respectively. The calculated masses for  $d, u, s, c, b,$  and  $t$  are  $328.4 \text{ MeV}, 328.6 \text{ MeV}, 539 \text{ MeV}, 1605.3 \text{ MeV}, 4974.6 \text{ MeV},$  and  $175.4 \text{ GeV},$  respectively. In the Standard Model, there are three generations of leptons. Extra-muon  $\mu'_0$  is outside of the three generations of leptons in the Standard Model, so  $\mu'_0$  is hidden as shown in **Table 2**. As shown in **Table 2**, to be symmetrical to the hidden  $\mu'_0$ , the extra composite quark, ( $Q_{epc}$ ) and the extra auxiliary composite quark ( $Q_{eac}$ ) for  $b$  quark are also hidden (absent).

The calculated mass of top quark is  $175.4 \text{ GeV}$  in good agreement with the observed  $173.3 \text{ GeV}$ . The calculated masses are the constituent masses which include all different types of the flux quanta ( $B_6, B_{7a}, B_8,$  and  $B_{8ea}$ ). The calculated constituent masses are comparable to the quark masses proposed by De Rujula, Georgi, and Glashow [27], Griffiths [28], and El Naschie [29]. The masses of hadrons are the combinations of the constituent quark masses minus the binding energy in the hadronic bond among quarks [30] [31]. The hadronic bond is the overlapping of the auxiliary dimensional orbitals, so it involves the auxiliary composite quarks, consisting of the primary auxiliary composite quark ( $Q_{ac}$ ) from Equation (24), the secondary auxiliary composite quark ( $Q'_{ac}$ ), and the tertiary auxiliary composite quark ( $Q''_{ac}$ ). The secondary auxiliary composite quark ( $Q'_{ac}$ ) is generated from the primary auxiliary composite quark in the same way as Equation (24).

$$M_{Q'_{ac}} = 9M_{Q_{ac}} \alpha_w / 2 = 1.64 \text{ MeV} \quad (36)$$

The tertiary auxiliary composite quark ( $Q''_{ac}$ ) is generated from the secondary auxiliary composite quark in the same way as Equation (36).

$$M_{Q''_{ac}} = 9M_{Q'_{ac}} \alpha_w / 2 = 0.20 \text{ MeV} \quad (37)$$

For neutron, the binding energy ( $E_{Q-Q}$ ) in the hadronic bond between quarks involves the primary auxiliary composite quark to become the binding energy and the secondary auxiliary composite quark to become the mass to replace the primary auxiliary composite quark as below.

$$E_{Q-Q} = 2(M_{Q_{ac}} - M_{Q'_{ac}}) = 23.04 \text{ MeV} \quad (38)$$

The mass of neutron which has two hadronic bonds is the sum of the constituent masses of  $u, d,$  and  $d$  quarks minus the binding energy from the two hadronic bonds.

$$M_N = M_u + 2M_d - 2E_{Q-Q} = 939.43 \text{ MeV} \quad (39)$$

The calculated mass of neutron is in good agreement with the observed value  $939.57 \text{ MeV}$ .

Proton is more stable than neutron, so it involves the additional binding energy from the tertiary auxiliary composite quark as below.

$$E_{Q-Q} = 2(M_{Q_{ac}} - M_{Q'_{ac}} + M_{Q''_{ac}}) = 23.45 \text{ MeV} \quad (40)$$

The mass of proton which has two hadronic bonds is the sum of the constituent masses of  $u, u,$  and  $d$  quarks minus the binding energy from the two hadronic bonds.

$$M_p = 2M_u + M_d - 2E_{Q-Q} = 938.78 \text{ MeV} \quad (41)$$

The calculated mass of proton is in good agreement with the observed value  $938.21 \text{ MeV}$ .

Another way to form hadrons is through the combinations of  $M_e/\alpha$  ( $= 70.03 \text{ MeV}$ ) and  $3M_e/2\alpha$  ( $= 105.04 \text{ MeV}$ ) as the mass quanta (mass building blocks) by the MacGregor's constituent quark model [23] [32]. Therefore, the masses of hadrons can be calculated by the combinations of the constituent quark masses from the quark mass formula as Equation (35) and by the combinations of the mass quanta from the MacGregor's constituent quark model [23] [30]-[32]. Another type of quark mass is the current mass which is much lower than the constituent mass, because it does not include some parts of principal composite quark ( $Q_{pc}$ ) and auxiliary com-

posite quark ( $Q_{ac}$ ) which become massless gluon [28] [33].

Another extra-muon is charge extra-muon,  $\mu'_{\pm}$ , derived from  $W^{\pm}$  boson. The formation of  $\mu'_{\pm}$  is same as  $\mu'_0$  based on Equations (28) and (29). (The observed mass of W boson is 80.385 GeV.)

$$M_{\mu'_{\pm}} = 3M_W/2 = 120.58 \text{ GeV} \quad (42)$$

Extra-muon  $\mu'$  includes neutral  $\mu'_0$  and charge  $\mu'_{\pm}$ .

## 5. The Higgs Boson Mass Formula

In the conventional model, under spontaneous symmetry breaking, zero-energy ground state space turns into the nonzero-energy scalar Higgs Field which exists permanently in the universe. The problem with such nonzero-energy field is the cosmological constant problem from the huge gravitational effect by the nonzero-energy Higgs field [34]. The coupling of massless particle to the Higgs field produces the transitional nonzero-energy Higgs field-particle composite which under spontaneous symmetry restoring produces the massive particle with the longitudinal component on zero-energy ground state space without the Higgs field as follows.

$$\begin{array}{l} \text{zero-energy ground state space} \xrightarrow{\text{spontaneous symmetry breaking}} \text{nonzero-energy scalar Higgs field} \\ \xrightarrow{\text{massless particle}} [\text{the transitional nonzero-energy Higgs field-particle composite}] \xrightarrow{\text{spontaneous symmetry restoring}} \\ \text{massive particle with the longitudinal component on zero-energy ground state space without the Higgs field} \end{array} \quad (43)$$

To avoid the cosmological problem from the huge gravitational effect by the nonzero-energy Higgs field is to make the Higgs field a transitional field which exists momentarily and to make zero-energy ground state space a permanent zero-energy ground state space which exists permanently in the universe [8]. For the digital space structure, such zero-energy ground state space is zero-energy attachment space which attaches particles to account for the longitudinal component, mass, and reversible movement. Unlike the conventional model, attachment space actively couples to massless particle. Under spontaneous symmetry breaking, the coupling of massless particle to zero-energy attachment space produces the transitional nonzero-energy Higgs field-particle composite which under spontaneous symmetry restoring produces massive particle on zero-energy attachment space with the longitudinal component without the Higgs field as follows.

$$\begin{array}{l} \text{massless particle} + \text{zero-energy attachment space} \xrightarrow{\text{spontaneous symmetry breaking}} \\ [\text{the transitional non-zero energy Higgs field-particle composite}] \xrightarrow{\text{spontaneous symmetry restoring}} \\ \text{massive particle with the longitudinal component on zero-energy attachment space without the Higgs field} \end{array} \quad (44)$$

The opposite of attachment space is zero-energy detachment space which detaches particles to account for irreversible kinetic energy. Unlike the conventional model, detachment space actively couples to massive particle. Under spontaneous symmetry breaking, the coupling of massive particle to zero-energy detachment space produces the transitional nonzero-energy reverse Higgs field-particle composite which under spontaneous symmetry restoring produces massless particle on zero-energy detachment space without the longitudinal component without the reverse Higgs field as follows.

$$\begin{array}{l} \text{massive particle} + \text{zero-energy detachment space} \xrightarrow{\text{spontaneous symmetry breaking}} \\ [\text{the transitional nonzero-energy reverse Higgs field-particle composite}] \\ \xrightarrow{\text{spontaneous symmetry restoring}} \text{massless particle without the longitudinal component} \\ \text{on zero-energy detachment space without the reverse Higgs field} \end{array} \quad (45)$$

For the electroweak interaction in the Standard model where the electromagnetic interaction and the weak interaction are combined into one symmetry group, under spontaneous symmetry breaking, the coupling of the massless weak W, weak Z, and electromagnetic A (photon) bosons to zero-energy attachment space produces the transitional nonzero-energy Higgs fields-bosons composites which under partial spontaneous symmetry restoring produce massive W and Z bosons on zero-energy attachment space with the longitudinal component without the Higgs field, massless A (photon), and massive Higgs boson as follows.

$$\begin{aligned}
& \text{massless WZ + zero-energy WZ attachment space + massless A + zero-energy A attachment space A} \\
& \xrightarrow{\text{spontaneous symmetry breaking}} [\text{the transitional nonzero-energy WZ Higgs field -WZ composite}] \\
& + [\text{nonzero-energy A Higgs field -A composite}] \xrightarrow{\text{partial spontaneous symmetry restoring}} \\
& \text{massive WZ with the longitudinal component on attachment space without the Higgs field} \\
& + \text{massless A + the nonzero energy massive Higgs boson}
\end{aligned} \tag{46}$$

Being outside of the three-generation lepton-quark in the Standard Model, the Higgs boson adopts the extra-muon condensate  $\mu'\bar{\mu}'$  which is outside of the three-generation lepton-quark. In other words, the extra-muon condensate becomes the Avatar Higgs boson [5]. The extra-muon condensate  $\mu'\bar{\mu}'$  includes  $\mu'_0\bar{\mu}'_0$  and  $\mu'_\pm\bar{\mu}'_\pm$ . The extra-muon condensate composite consists of  $\mu'_0\bar{\mu}'_0$ ,  $\mu'_+\bar{\mu}'_+$ , and  $\mu'_-\bar{\mu}'_-$ . From Equations (29) and (42), the mass of the  $\mu'\bar{\mu}'$  condensate composite as the Higgs boson composite is as follows.

$$\begin{aligned}
M_{\text{Higgs boson composite}} &= M_{\mu'_0\bar{\mu}'_0} + M_{\mu'_+\bar{\mu}'_+} + M_{\mu'_-\bar{\mu}'_-} \\
&= 2(136.78) \text{ GeV} + 2(120.58) \text{ GeV} + 2(120.58) \text{ GeV} \\
&= 756 \text{ GeV}
\end{aligned} \tag{47}$$

This extra-muon condensate composite as the Higgs boson composite at 750 GeV is in good agreement with the 756 GeV diphoton excess observed from the Large Hadron Collider (LHC) with zero charge and zero spin [35] [36]. The  $\mu'\bar{\mu}'$  condensate composite decays into three  $\mu'\bar{\mu}'$  condensates. Just as the observed top quark is a bare quark with the observed mass of about 173 GeV instead of about 346 GeV (two times 173 GeV) for top quark-antitop quark boson, the observed mass of  $\mu'\bar{\mu}'$  as the Higgs boson is the mass of bare  $\mu'$  as follows.

$$M_{\text{observed } \mu'\bar{\mu}' \text{ as the Higgs boson}} = M_{\mu'\bar{\mu}' \text{ composite}} / 6 = 756 \text{ GeV} / 6 = 126 \text{ GeV} \tag{48}$$

The calculated mass (126 GeV) is in excellent agreement with the observed 125 GeV [37] or 126 GeV [38].

## 6. Conclusions

One of the biggest unsolved problems in physics is the particle masses of all elementary particles which cannot be calculated accurately and predicted theoretically. In this paper, the unsolved problem of the particle masses is solved by the accurate mass formulas which calculate accurately and predict theoretically the particle masses of all leptons, quarks, gauge bosons, the Higgs boson, and cosmic rays (the knees-ankles-toe) by using only five known constants: the number (seven) of the extra spatial dimensions in the eleven-dimensional membrane, the mass of electron, the masses of Z and W bosons, and the fine structure constant. The calculated masses are in excellent agreements with the observed masses. For examples, the calculated masses of muon, top quark, pion, neutron, and the Higgs boson are 105.55 MeV, 175.4 GeV, 139.54 MeV, 939.43 MeV, and 126 GeV, respectively, in excellent agreements with the observed 105.65 MeV, 173.3 GeV, 139.57 MeV, 939.27 MeV, and 126 GeV, respectively. The mass formulas also calculate accurately the masses of the new particle at 750 GeV from the LHC and the new light boson at 17 MeV. The theoretical base of the accurate mass formulas is the periodic table of elementary particles. As the periodic table of elements is derived from atomic orbitals, the periodic table of elementary particles is derived from the seven principal mass dimensional orbitals and seven auxiliary mass dimensional orbitals. All elementary particles including leptons, quarks, gauge bosons, the Higgs boson, and cosmic rays can be placed in the periodic table of elementary particles.

The periodic table of elementary particles is derived from the theory of everything as the computer simulation model of physical reality consisting of the mathematical computation, digital representation and selective retention components. The mathematical computation involves oscillating M-theory as oscillating membrane-string-particle whose space-time dimension (D) oscillates between 11D and 10D and between 10D and 4D. For the digital representation component, the three intrinsic data (properties) are rest mass-kinetic energy, electric charge, and spin which are represented by the digital space structure, the digital spin, and the digital electric charge, respectively. The digital representations of rest mass and kinetic energy are 1 as attachment space for the space of matter and 0 as detachment space for the zero-space of matter. The digital representations of the exclusive and the inclusive occupations of positions are 1/2 spin fermion and integer spin boson, respectively. The digital representations of the allowance and the disallowance of irreversible kinetic energy are integral electric charges and fractional electric charges, respectively. For the selective retention component, gravity, the strong

**Table 4.** The mass formulas of gauge bosons, cosmic rays, leptons, quarks, and the Higgs boson.

mass formula of	Equation #	Table #	Particles involved
gauge bosons	7	1	gauge bosons for electromagnetism, strong force, weak force (left), CP non-conservation (right), CP non-conservation (left), weak force (right), and gravity
cosmic rays	10a, 10b, 11	3	knees, ankles, and toe
leptons	17	2	electron, muon, tau, and the light boson
quarks	35	2	d, u, s, c, b, and t
Higgs boson	47, 48		the Higgs boson and the Higgs boson composite

force, electromagnetism, and the weak force are the retained events during the reversible four-stage evolution of our universe, and are unified by the common narrative of the evolution. The computer simulation model of physical reality provides the seven principal mass dimensional orbitals and seven auxiliary mass dimensional orbitals to place leptons, quarks, gauge bosons, the Higgs boson, and cosmic rays in the periodic table of elementary particles.

The summary of the mass formulas is in **Table 4**.

## References

- [1] Hansson, J. (2015) *International Journal of Modern Physics and Applications*, **1**, 12-16.
- [2] Jammer, M. (2009) *Concepts of Mass in Contemporary Physics and Philosophy*. Princeton University Press, USA. <http://dx.doi.org/10.1515/9781400823789>
- [3] Chung, D. (1997) *Speculations in Science and Technology*, **20**, 259-268. <http://dx.doi.org/10.1023/A:1026433207862>
- [4] chung, D. (2014) *Journal of Modern Physics*, **5**, 1234-1243. <http://dx.doi.org/10.4236/jmp.2014.514123>
- [5] Chung, D. and Hefferlin, R. (2013) *Journal of Modern Physics*, **4**, 21-26. <http://dx.doi.org/10.4236/jmp.2013.44A004>
- [6] Chung, D. (2014) *Journal of Modern Physics*, **5**, 1467-1472. <http://dx.doi.org/10.4236/jmp.2014.515148>
- [7] Chung, D. (2016) *Journal of Modern Physics*, **7**, 1210-1227. <http://dx.doi.org/10.4236/jmp.2016.710110>
- [8] Chung, D. (2016) *Journal of Modern Physics*, **7**, 642-655. <http://dx.doi.org/10.4236/jmp.2016.77064>
- [9] Woit, P. (2006) *Not Even Wrong: The Failure of String Theory and the Search for Unity in Physical Law*. Basic Books, New York.
- [10] Chung, D. (2015) *Journal of Modern Physics*, **6**, 1820-1832. <http://dx.doi.org/10.4236/jmp.2015.613186>
- [11] Chung, D. and Krasnoholovets, V. (2013) *Journal of Modern Physics*, **4**, 27-31. <http://dx.doi.org/10.4236/jmp.2013.44A005>
- [12] Bounias, M. and Krasnoholovets, V. (2003) *The International. Journal of Systems and Cybernetics*, **32**, 1005-1020.
- [13] Chung, D. (2016) *Journal of Modern Physics*, **7**, 1150-1159. <http://dx.doi.org/10.4236/jmp.2016.710104>
- [14] Tsui, D., Stormer, H. and Gossard, A. (1982) *Physical Review Letters*, **48**, 1559. <http://dx.doi.org/10.1103/PhysRevLett.48.1559>
- [15] Stormer, H. (1999) *Reviews of Modern Physics*, **71**, 875. <http://dx.doi.org/10.1103/RevModPhys.71.875>
- [16] Laughlin, R. (1983) *Physical Review Letters*, **50**, 1395. <http://dx.doi.org/10.1103/PhysRevLett.50.1395>
- [17] Salam, A. (1968) *Weak and Electromagnetic Interactions*. In: Svartholm, W., Ed., *Elementary Particle Theory*, Almqvist and Wiksell, Stockholm, 367-387.
- [18] Drury, L. (2012) *Astroparticle Physics*, **39-40**, 52-60. <http://dx.doi.org/10.1016/j.astropartphys.2012.02.006>
- [19] Sveshnikova, L., Korosteleva, E., Kuzmichev, L., Prosin, V., Ptuskin, V. and Strelnikova, O. (2013) *Journal of Physics: Conference Series (JPCS)*, **409**, Article ID: 012062. <http://dx.doi.org/10.1088/1742-6596/409/1/012062>
- [20] Kamilla, R., Wu, X. and Jain, J. (1996) *Physical Review Letters*, **76**, 1332-1335. <http://dx.doi.org/10.1103/PhysRevLett.76.1332>
- [21] Jain, J. (2007) *Composite Fermions*. Cambridge University Press, New York. <http://dx.doi.org/10.1017/CBO9780511607561>
- [22] Cameron, P. (2011) *Apeiron*, **18**, 29-42.

- [23] MacGregor, M. (2007) *The Power of Alpha: The Electron Elementary Particle Generation with Alpha-Quantized Lifetimes and Masses*. World Scientific Publishing, Singapore.
- [24] Barut, A. (1979) *Physical Review Letters*, **42**, 1251-1253. <http://dx.doi.org/10.1103/PhysRevLett.42.1251>
- [25] Krasznahorkay, A., *et al.* (2016) *Physical Review Letters*, **116**, Article ID: 042501. <http://dx.doi.org/10.1103/PhysRevLett.116.042501>
- [26] Feng, J., *et al.* (2016) *Physical Review Letters*, **117**, Article ID: 071803.
- [27] De Rujula, A., Georgi, H. and Glashow, S. (1975) *Physics Review D*, **12**, 147. <http://dx.doi.org/10.1103/PhysRevD.12.147>
- [28] Griffiths, D. (2008) *Introduction to Elementary Particles*. Wiley-VCH, Weinheim, 135.
- [29] El Naschie, M. (2002) *Chaos, Solitons and Fractals*, **14**, 369-376. [http://dx.doi.org/10.1016/S0960-0779\(02\)00022-X](http://dx.doi.org/10.1016/S0960-0779(02)00022-X)
- [30] Chung, D. (1999) *Speculations in Science and Technology*, **21**, 277-289. <http://dx.doi.org/10.1023/A:1005513404873>  
<http://link.springer.com/article/10.1023/A:1005513404873>
- [31] Chung, D. (2001) arXiv:hep-th/0111147v5.
- [32] MacGregor, M. (1990) *Il Nuovo Cimento A*, **103**, 983-1052. <http://dx.doi.org/10.1007/BF02782738>
- [33] Watson, A. (2004) *The Quantum Quark*. Cambridge University Press, Cambridge, 285-286.
- [34] Weinberg, S. (1989) *Review Modern Physics*, **61**, 1-23. <http://dx.doi.org/10.1103/RevModPhys.61.1>
- [35] ATLAS and CMS (2015) CMS PAS EXO-15-004 and ATLAS-CONF-2015-081. <https://indico.cern.ch/event/442432/>
- [36] Nakai, Y., Sato, R. and Tobioka, K. (2016) *Physical Review Letters*, **116**, Article ID: 151802. <http://dx.doi.org/10.1103/PhysRevLett.116.151802>
- [37] The CMS Collaboration (2012) *Physics Letters B*, **716**, 30-61. <http://dx.doi.org/10.1016/j.physletb.2012.08.021>
- [38] The ATLAS Collaboration (2012) *Physics Letters B*, **716**, 1-29. <http://dx.doi.org/10.1016/j.physletb.2012.08.020>



Scientific Research Publishing

---

**Submit or recommend next manuscript to SCIRP and we will provide best service for you:**

Accepting pre-submission inquiries through Email, Facebook, LinkedIn, Twitter, etc.

A wide selection of journals (inclusive of 9 subjects, more than 200 journals)

Providing 24-hour high-quality service

User-friendly online submission system

Fair and swift peer-review system

Efficient typesetting and proofreading procedure

Display of the result of downloads and visits, as well as the number of cited articles

Maximum dissemination of your research work

Submit your manuscript at: <http://papersubmission.scirp.org/>

# The Hubble Field vs Dark Energy

Juan Lartigue

Department of Nuclear Chemistry, Faculty of Chemistry, National University of México, México City, México  
Email: jmlg5@hotmail.com

Received 28 June 2016; accepted 28 August 2016; published 31 August 2016

Copyright © 2016 by author and Scientific Research Publishing Inc.

This work is licensed under the Creative Commons Attribution International License (CC BY).

<http://creativecommons.org/licenses/by/4.0/>



Open Access

---

## Abstract

The Hubble equation was considered valid enough to calculate the recession velocity of galaxies, until further observations showed that there would be an accelerated recession in the Hubble flow, necessarily tied to an accelerated expansion of the Universe. So, this paper postulates the existence of a Hubble field as a possible cause for such an accelerated expansion, with some conditions: it must be a scalar field whose intensity should be a constant in respect to distance and whose Poisson equation should not be zero nor a function of mass; such field could rather be a property of the space-time. The obvious expression for acceleration should be the derivative of the Hubble equation respect to time, which gives two opposed-signs terms whose substitution by the De-Sitter equation drives to a permanent negative acceleration, similarly to that obtained by the 2<sup>nd</sup> Friedmann equation. Otherwise, the inclusion of the  $\Lambda$  term in the gravitational Einstein equation has led to a two opposed-signs terms expression, resembled to a non-published Newton equation. The negative term expresses the gravitational attraction and the positive one expresses the accelerated expansion as a  $\Lambda$  function, which usually is attributed to dark energy. In this paper it is shown that  $\Lambda$  is proportional to the squared Hubble parameter and that the uncertain dark energy may be substituted by the calculable Hubble field intensity to obtain an equation for the net Universe acceleration. Equations for the Hubble parameter as functions of time and radius are also deduced. A relation is shown between the various assumed masses of the Universe and its critical radius. Additional Universe parameters are estimated such as the deceleration factor and a solution for the Poisson equation in the Hubble field. A brief comment on high-standard candles is included.

## Keywords

Hubble Law, Hubble Field, Cosmological Constant, Friedmann Equations

---

## 1. Introduction

Since the A. Riess *et al.* [1] discovery of the acceleration of the Universe expansion, the cause of this phenomenon has been attributed to a mysterious dark energy whose nature and characteristics remain unknown. Dark

energy has been associated to the cosmological constant,  $\Lambda$ , which was previously discarded by Einstein and now is related to dark energy density,  $\rho_\Lambda$ , as

$$\Lambda = 4\pi G\rho_\Lambda. \tag{1.1}$$

The dark energy presents two problems. The first one is that such alleged energy has not been detected or measured experimentally. The second one is that its density is usually expressed as an equivalent mass density ( $\text{kg}\cdot\text{m}^{-3}$ ) though a so-crucial relationship such as

$$E_\Lambda = m_\Lambda c^2 \tag{1.2}$$

has not been proved yet. Its present numerical value has been estimated from the WMAP experiments [2] to a figure that allows the Universe to reach its critical condition at the present time. Its hypothetical value is expressed by reference [3] as: “Dark energy is necessary to balance the books”.

Besides, there is a problematic complement of dark energy theory: it is assumed that it generates a negative pressure or vacuum energy that pulls the Universe to expand itself. Though the equation of state is feasible

$$\rho_\Lambda = -p, \tag{1.3}$$

where  $-p$  is the negative pressure generate d) the implied numerical values would not be big enough to pull the entire Universe back. Reference [4] expresses on both topics: “The relevant fact about dark energy is not its pressure: it is that it is persistent; it doesn’t dilute away as the Universe expands”. And adds: “Banning negative pressure from popular expositions of Cosmology would be a great step forward”.

In explaining the Universe acceleration, several alternative theories have been published based on extensions of the relativistic theory of gravity and MOND theory [5], as well as on variations of gravitation as a function of scales [6]. This later reference mentions the possible substitution of the constant  $\Lambda$  by a scalar field. Such is the proposal of this paper, assuming a constant intensity of a scalar field. It follows a review of previous concepts.

The Hubble parameter,  $H(t)$  is defined as:

$$H(t) = \frac{\dot{a}}{a} \tag{1.4}$$

where  $a$  is the radial Universe function, related to the distance  $r$  by the co-moving equation

$$r = x \cdot a \tag{1.5}$$

$x$  is the constant commoving coordinate and  $\dot{a}$  is the time derivative of a substitution of the co-moving equation in (1.1) to give the Hubble equation:

$$\dot{r} = H(t) \cdot r \tag{1.6}$$

The time derivative of this equation would represent the accelerated radial expansion:

$$\ddot{r} = H^2 r - \dot{H}r. \tag{1.6.a}$$

The problem here is that  $\dot{H}$ , usually obtained by the De-Sitter expression, drives to an Universe acceleration,  $\ddot{r} < 0$ , as opposed to the present accepted criteria [7]:.

Bergstron and Goobar [8] had included the cosmological constant,  $\Lambda$ , in the Einstein gravitation equation as follows:

$$R_{\mu\nu} - \frac{1}{2} g_{\mu\nu} R - \Lambda g_{\mu\nu} = 8\pi G T_{\mu\nu} \tag{1.7}$$

the two first terms form the Einstein tensor,  $G_{\mu\nu}$ ;  $g_{\mu\nu}$  stands for the fundamental covariant tensor;  $G$  is the gravitational constant, while  $T_{\mu\nu}$  represents the energy-momentum tensor. This expression assumes a unitary value for light velocity. Einstein added  $\Lambda$  to his equations in 1917 in order to match a static Universe concept. However, A. Friedmann did not take  $\Lambda$  into account in obtaining two basic solutions, five years later [9]

$$\frac{\dot{a}^2}{a^2} = \frac{8\pi G\rho_b}{3} - \frac{kc^2}{a^2} \tag{1.8a}$$

$$\frac{\ddot{a}}{a} = -\frac{4\pi G}{3} \left( \rho_b + \frac{3p}{c^2} \right) \tag{1.9}$$

$\ddot{a}$  is the acceleration of matter at the Universe radial function,  $a$ ;  $\rho_b$  is the Universe baryonic density;  $p$  is the total pressure;  $k$  is a curvature parameter of the Universe, and  $c$  is the light velocity in a vacuum. Accordingly to R. Tolman [10], the Einstein Universe is filled by incoherent matter and, in a first Friedmann model, the total pressure is assumed to be zero, yet both energy and matter get conserved. An adequate way to fulfill Einstein and Friedmann conditions would be assuming the Universe as a powder cloud with a tiny matter density and  $p = 0$ , which implies that the energy momentum tensor [11] is

$$T^{\mu\nu} = \rho u^\mu u^\nu \tag{1.9}$$

$u^\mu$  and  $u^\nu$  are the 4-velocity vectors that, in a co-moving frame, are  $\mathbf{u} = (1, 0, 0, 0)$ . Therefore,  $T^{00} = \rho_s$

(When the value for  $\Lambda$  is substituted).

By applying to (1.7) the conservation criteria for matter in the Universe, plus the co-moving equation and the baryonic density concept as well, the present Universe acceleration would be:

$$r = -\frac{GM_b}{r^2} \tag{1.8},$$

where  $M_b$  is the baryonic (or if preferred, gravitational mass) contained in a sphere of radius  $r$ . Equation (1.8) is the same of Newton for gravitational acceleration, so implying that it remains negative as  $r$  increases, a conclusion that would result opposed to recent works [1] [12]. The first solution for Equation (1.3) was that of De-Sitter in 1917, though he did assume an empty Universe, *i.e.*  $T^{\mu\nu} = 0$ . In what follows, a  $\Lambda$  value and its relationship to the Hubble parameter are calculated. Thereafter, an equation for the Hubble field is deduced, and two equations for  $H$  as functions of time and distance are also proposed. The criticality and deceleration parameters are calculated as well as a Poisson equation for the scalar Hubble field. A brief comment on high- $z$  standard candles is included at the end of the paper.

## 2. The $\Lambda$ and $H$ Values

By applying the FLRW metric to the Einstein equation, reference [13] gives way to a very useful form of the second Friedmann equation:

$$\frac{\ddot{a}}{a} = -\frac{4\pi G \rho_b}{3} + \frac{\Lambda}{3} \tag{2.1}$$

This equation has been also deduced by L. Calder and O. Lahav in a landmark paper [14]. It can be expressed by means of the commoving equation and the density definition, as:

$$\ddot{r} = -\frac{GM_b}{r^2} + \frac{\Lambda r}{3} \tag{2.2}$$

Since  $\Lambda$  had not been considered a function of time, reference [15] did assume a constant value for  $\Lambda = 1.0$  (supposed it is dark energy), which should intersect the  $\Omega_U$  curve at the present time. Such a constant unitary value (assumed as vacuum energy) intersecting the  $\Omega_U$  curve at the present time is also mentioned by reference [16].  $\Omega_U$  is the ratio between the Universe total density and its own critical density. These and other authors [2] conclude that the present time is the critical one, an assumption that would imply now that  $\ddot{r} = 0$ , as opposed to the discovery of reference [1].

Calder and Lahav [17] have referred an original Newton equation for the Universe acceleration (not published by Newton in his *Principia*) which may be written as:

$$\ddot{r} = -\frac{GM_b}{r^2} + CM_b r \tag{2.3}$$

where  $C$  is an arbitrary constant. By comparing Equations ((2.2) and (2.3)), they conclude that  $\Lambda$  must be proportional to the entire mass of the Universe,  $M_b$  (a constant) as:

$$\Lambda = CM_b \tag{2.4}$$

However, the constancy of  $\Lambda$  would require  $C$  to be a true constant. It may be calculated at the equilibrium point ( $\ddot{\mathbf{r}} = 0$ ) in Equation (2.3) as follows:

$$C = G/(r_c)^3 \tag{2.5}$$

Equating the expressions for  $C$  from (2.4) and (2.5) it gives:

$$\Lambda = \frac{3GM_b}{r_c^3} \tag{2.6}$$

So showing that  $\Lambda$  is a constant being related to the critical radius. Otherwise, the equation presented by reference [8] and anywhere ( $\Lambda = 8\pi G\rho_\Lambda$ ) would require knowing the dark energy density, an uncertain parameter at the present time.

The proposition of M. Carmeli and T. Kuzmenko [18] for the  $\Lambda$  constant value could be a real solution:

$$\Lambda = 3/\tau \tag{2.7}$$

$\tau_o$  is the age of the Universe; if it is  $\tau_o = 14.0 \times 10^9$  (y) [19], then  $\Lambda = 1.53 \times 10^{-35}$  (s<sup>-2</sup>) [19].

Accordingly to Equation (1.1) the Hubble parameter is a function of time. Its present (constant) value,  $H_o$  is defined as:

$$H_o = \frac{1}{\tau_o} = 2.25 \times 10^{-18} \text{ (s}^{-1}\text{)} \tag{2.8}$$

Therefore, from (2.7) and (2.8):

$$\Lambda = 3H_o^2 \tag{2.9}$$

Multiplying Equation (2.9) by  $r_o$  gives:

$$\frac{\Lambda r_o}{3} = H_o^2 \cdot r_o = \text{constant} \tag{2.10}$$

If this equation is valid at the present time, it is postulated in this work to be valid also at the critical time, *i.e.*

$$H_c^2 r_c = \text{constant} \tag{2.11}$$

and therefore, at any time:

$$H^2(t)r(t) = \text{constant} \tag{2.12}$$

Equation (2.10) shows that the second term of Equation (2.2) does imply a positive acceleration expansion, with a constant value as proposed by reference [4], and opposed to the gravitational attraction in the Universe. So, if Equation (2.12) is valid, the Equation (2.2) may be written as:

$$\ddot{\mathbf{r}}(r) = H^2 \mathbf{r} - 12 \frac{GM_b}{r^2} \tag{2.13}$$

Equation (2.13) represents the net acceleration of the Universe expansion, *i.e.*, the difference between the attractive gravitational field and the expansive Hubble field. It seems clear that, when the Universe radius was small, the gravitational field intensity was dominant, but nowadays, at a bigger Universe radius, the Hubble field intensity should be overbearing, as shown in **Figure 1**.

### 3. The Hubble Field

In what follows, the variable intensity of the gravitational field is represented by  $G$  and the constant intensity of the Hubble field is written as  $\Gamma_H$ , *i.e.*

$$\Gamma_G = -\frac{GM_b}{r^2} \text{ (m} \cdot \text{s}^{-2}\text{)} \tag{3.1}$$

$$\Gamma_H = H^2 \mathbf{r} \text{ (m} \cdot \text{s}^{-2}\text{)} \tag{3.2}$$

Therefore, the net Universe acceleration may be expressed, from Equation (2.13), as the difference:

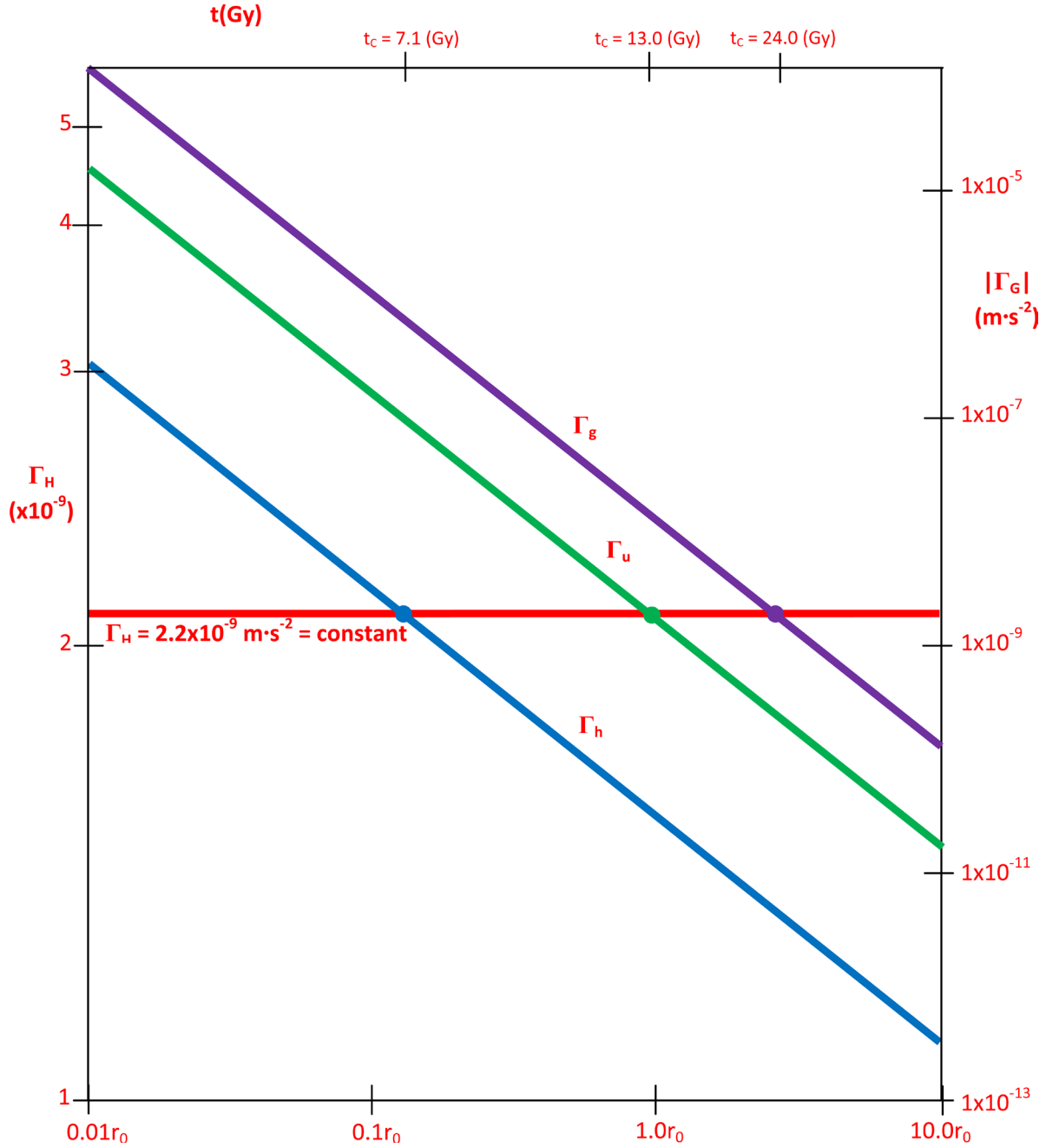


**Figure 1.** The constant Hubble field intensity  $\Gamma_H$  ( $\text{m}\cdot\text{s}^{-2}$ , red line) vs 3 cases of gravitational acceleration  $\Gamma_G$  ( $\text{m}\cdot\text{s}^{-2}$ , blue, green, purple lines, see text) as functions of the Universe ratio,  $r/r_0$ . The intersection points correspond to the 3 possible critical Universe radii. The critical times are marked in the upper abscissa. The difference between the  $\Gamma_G$  lines and the  $\Gamma_H$  line represents the net acceleration,  $\ddot{r}$  ( $\text{m}\cdot\text{s}^{-2}$ ), Equation (2.13).

$$\ddot{r} = [\Gamma_H] - [\Gamma_G] \quad (\text{m}\cdot\text{s}^{-2}) \tag{3.3}$$

Since the potential energy in the gravitational field is always negative ( $U < 0$ ), the gravitational potential (energy per unit mass) is negative too; it is expressed as:

$$V_G = -\frac{GM_G}{r} \quad (\text{J}\cdot\text{kg}^{-1}) \tag{3.4}$$

By definition [20], the intensity of the gravitational field is the negative of the gradient of the gravitational potential:

$$\Gamma_G = -\nabla V_G \quad (3.5)$$

it is therefore negative, as expressed in Equation (3.1).

Similarly, the Hubble field intensity could be defined as the gradient of a positive scalar Hubble field potential:

$$\Gamma_H = \nabla V_H \quad (3.6)$$

The substitution of Equation (3.2) in (3.6) gives a definition of the Hubble field intensity

$$\Gamma_H = H^2 \mathbf{r} = \nabla V_H \quad (3.7)$$

By assuming from Equation (2.12) that  $\Gamma_H = \text{constant}$  in Equation (3.7), the radial integration of this equation gives an expression for the Hubble potential:

$$V_H = \Gamma_H \cdot \mathbf{r} = H^2 r^2 \left( \text{m}^2 \cdot \text{s}^{-2} \right) \quad (3.8)$$

(alternative units applied in Equation (3.8) point out that there is no mass involved in the Hubble potential).

Assuming that Equation (2.12) is valid, it is possible to estimate the constant Hubble field intensity by using the present values of  $H_o$  and the Universe radius,  $r_o$  [21]:

$$\Gamma_H = H_o^2 r_o = 2.2 \times 10^{-9} \left( \text{m} \cdot \text{s}^{-2} \right) \quad (3.9)$$

This would be the value of the Hubble field intensity, *i.e.* the Hubble acceleration of the Universe at any time, if there was not a gravitational field. Since it is not feasible to assign to the Hubblefield any known physical entity, it may be assumed that it corresponds, rather, to a property of the space-time. The present net acceleration results, from Equation (2.13),  $\ddot{r}(r_o) = 1.7 \times 10^{-9} \left( \text{m} \cdot \text{s}^{-2} \right)$  and the velocity  $\dot{r}(r_o) = 7.5 \times 10^8 \left( \text{m} \cdot \text{s}^{-1} \right)$ . This value, higher than  $c$ , could be feasible in a particular non-inertial frame, such as it would be outside the Hubble sphere, where  $\dot{r} > c$ .

The assumption for  $\Gamma_H$  to be constant allows obtain a general expression for  $H$  as a function of distance, from Equations ((2.12) and (3.9)):

$$H(r) = \frac{4.7 \times 10^{-5}}{r^{1/2}} \left( \text{s}^{-1} \right) \quad (3.10)$$

The present  $H_o$  value has been defined as the reciprocal of the Universe age (Equation (2.8)) but there is not a general expression to determine  $H(t)$ . The same Equations ((2.12) and (3.9)) could allow calculate the Hubble parameter at any time if the distance is expressed as a function of time in a continuously accelerated movement:

$$H(t) = \frac{1.8 \times 10^{-12}}{t^{1/3}} \left( \text{s}^{-1} \right) \quad (3.11)$$

Therefore, Equations ((3.10) and (3.11)) are proposed as general functions for  $H(r)$  and  $H(t)$ .

## 4. Additional Relevant Parameters

### 4.1. Critical Parameters Corresponding to the Assumed Values of Mass in the Universe

From R. Johnson [22], the values assigned to the baryonic mass of the Universe vary according to several criteria: one is based on the total number of stars and it yields  $1.0 \times 10^{52}$  kg; even figure, as modified by the intergalactic and interstellar media, is  $1.7 \times 10^{53}$  kg; another one, based in the Hoyle-Carvalho equation [23], assigns  $M_h = 1.84 \times 10^{53}$  (kg) as the value covering the Hubble length ( $1.37 \times 10^{26}$  m). All these figures have been obtained by research inside the observable Universe, *i.e.* into the Hubble sphere. So, accordingly to the cosmological principle, trying to determine the total mass contained in the total volume of the Universe is a valid problem. From the above given data, the density of the observable Universe is  $\rho_h = 1.8 \times 10^{-26}$  ( $\text{kg} \cdot \text{m}^{-3}$ ) a value here assumed for the entire Universe whose radius is estimated to be  $r_o = 4.4 \times 10^{26}$  (m) [2] giving, for the total baryonic mass in the Universe,  $M_u = 6.5 \times 10^{54}$  (kg). Besides, dark mass could eventually be included as a gravitational mass, giving a total of  $M_g = 3.25 \times 10^{55}$  (kg).

The critical point of the Universe may be defined as the time when the Universe becomes flat, *i.e.* when it may change from positive to a negative curvature. That implies  $\ddot{r} = 0$  in Equation (2.13), which gives:

$$(H_c)^2 r_c = \frac{GM}{r_c^2} \tag{4.1}$$

In Equation (4.1) it has not been specified the kind of mass to apply, which must be selected in any case. Since the l.h.s. is a constant ( $\Gamma_H$ ), it is possible to directly obtain the value of the critical radius from:

$$(r_c)^2 = \frac{GM}{\Gamma_H} \tag{4.2}$$

Since  $G$  and  $\Gamma_H$  are constants, this equation gives

$$r_c = 0.173 \times (M)^{1/2} \tag{4.3}$$

In **Table 1** they are shown the corresponding critical radius and times for the three above assumed masses.

### 4.2. The Deceleration Parameter

The deceleration parameter,  $q$ , is defined as:

$$q = \frac{r\ddot{r}}{\dot{r}^2} \tag{4.1} [32]$$

Its present value results  $q = -1.3$ , which confirms the possibility of an accelerated Universe.

### 4.3. The Poisson Equation

The spatial derivative of Equation (3.7) is a solution of the Poisson equation in the Hubble field:

$$\nabla^2 V_H = H^2 (s^{-2}) \tag{4.4}.$$

It means that there exists a force-flow in the Hubble field.

## 5. A Brief Comment

As assumed above, the constancy of  $\Gamma_H$  would require some kind of justification. Subsequent studies to that of Riess *et al.* [1], which was limited to  $z \leq 1$ , refer also to the present accelerated expansion of the Universe, *i.e.* whose velocity is continuously increasing but there is no mention about the acceleration's magnitude, even less about any variation; so, by now, it may be assumed that the expansive acceleration value obtained by Equation (3.9) in this work is a constant, as expressed by the product  $H^2 r$  in Equation (2.12).

Reference [24] analyses the Universe evolution for redshifts  $z \leq 3.0$  and concludes, in his Figure 4, that there were two epochs: an slowing down expansion and, after that, the present accelerated expansive period; it would mean that after the enormous velocity reached in the inflationary period, it followed a slowing down expansion period that, just before the present time, with  $z = 0$ , has changed to a positively accelerated expansive process; in this way, the present time would almost correspond to the critical time with its implicit critical radius and density as well as a flat geometry ( $k = 0$ ). These results do not coincide at all with those of A. Riess [25] who proposes a value of  $z = 0.46$  for the curvature change, a value that would imply a critical time of 10.5 Gy. It was an event considered by the same author [26] as "a cosmic jerk: the transition from deceleration in the past to acceleration in the future". A possible partial matching of **Figure 1** of this work with Figure 4 of reference [24] could be that: if  $H$  is a constant respect to time and distance, the slowing down expansion period would correspond to the

**Table 1.** Critical radius and critical time for three cases of universe' mass.

Mass of the Universe (kg)	Critical radius $r_c$ (m)	Critical time $t_c$ (Gy)
$M_b = 1.84 \times 10^{53}$ (in the Hubble sphere)	$7.0 \times 10^{25}$	7.1
$M_u = 6.54 \times 10^{54}$ (in the Universe)	$4.3 \times 10^{26}$	13.6
$M_g = 3.25 \times 10^{55}$ (including dark matter)	$1.0 \times 10^{27}$	24.0

$[\Gamma_G] > \Gamma_H$  epoch (in the total Universe case, curve sphere case, curve  $\Gamma_h$ ). Consequently, the  $\Gamma_H = [\Gamma_G]$  step would have defined the critical time in two possible cases. If dark matter would have been added, the critical point would still have to wait for another  $t_o$  period. The validity of the model here proposed could only be proven if future SN observations detect additional increases in the expected distances, at several ( $z > 1$ ) values, and if they match with the net acceleration given by Equation (3.3). Some important experiments at higher  $z$  values (8.6 and 11.0) have been performed in two recent projects [27] [28] that mention mag variations but say nothing about older acceleration values.

Anyway, there is a limit to distance measurements by present methods: it comes from the estimation of reference [29] about the first star formation, that he assumes to have occurred at a Universe age of  $\sim 50$  (My), or  $z \sim 50$ , a fact that puts a limit to the use of SN as standard candles. The same restriction could apply to the efforts to use quasars [30] and  $\gamma$ -ray bursts [31] as standard candles. However, spectroscopic methods could always been applied if higher redshifts ( $z > 50$ ) could be identified; for example, the CMB defines the maximum observable cosmological value at  $z \sim 10^3$  [29]; it implies e.g., if  $\lambda_o$  is today about 1 (mm), the emitted  $\lambda_e$  should have been about 1 ( $\mu\text{m}$ ) *i.e.* infrared photons traveling till now, in a co-moving coordinate, since the decoupling time.

## 6. Conclusions

1) The value of the cosmological constant,  $\Lambda$  is proportional to the reciprocal of the squared Universe age (Equation (2.9)). So, it results proportional to the present value of the squared Hubble parameter.

2) Since  $\Lambda$  cannot be directly associated to any known field, the present work substitutes the  $\Lambda$  term by a constant Hubble field intensity term (Equation (2.10)), to obtain the Equation (2.13), expressed in **Figure 1**. The form of this equation could have been foreseen from the time derivative of the Hubble Equation (1.2) which shows that the net acceleration of the Universe would depend on two opposed-signs terms.

3) The Hubble field intensity is defined as the gradient of a positive Hubble potential (Equation (3.6)). Its constant value is  $2.2 \times 10^{-9}$  ( $\text{m}\cdot\text{s}^{-2}$ ). However, the present net acceleration is  $1.7 \times 10^{-9}$  ( $\text{m}\cdot\text{s}^{-2}$ ). The expansion velocity at the astronomical radius results today  $\dot{r}(r_o) = 2.5c$ , a feasible value in a co-moving coordinate that, if Equation (3.6) is valid, it would imply a new physical theory after that of  $c$  (max).

4) The assumption of the constancy of the Hubble field intensity drives to obtain two general functions of time and distance for the Hubble parameter (Equation (3.10), Equation (3.11)).

5) Equation (2.13) gives the net acceleration of the Universe, as well as its critical radius when  $\ddot{r} = 0$ . So, it is not necessary to appeal to  $a\Omega_U$  balance. The critical conditions of the Universe are found to depend of the Universe's mass chosen; here they were considered 3 cases: baryonic into the Hubble sphere, baryonic in the assumed total volume of the Universe and baryonic plus dark matter in the total volume. They are shown in **Figure 1**, which presents both the Hubble and Newton accelerations ( $\Gamma_H, \Gamma_G$ ) as functions of the  $r/r_o$  ratio and points out both the critical radius and critical time for the 3 cases above mentioned.

6) The deceleration parameter gave a negative value, so showing that the Universe is self-expanding. The Poisson equation for the Hubble field is  $\nabla^2 V_H = H^2$ , since matter is not a component of the Hubble field.

7) The validity of the model here proposed could only be proven if future SN observations detect additional increases, such as it is being assumed in a recent academic project.

## Acknowledgements

Author thanks to Sc. M. M. A. Zúñiga, C.P. V.M. Torres Tovar, D. Camargo, B. M. Cota and R. Cervantes, by their kind collaboration in the final version of this paper.

## References

- [1] Riess, A., *et al.* (1998) *The Astronomical Journal*, **116**, 1009-1038. <http://dx.doi.org/10.1086/300499>
- [2] NASA/WMAP Science Team (2014) [http://map.gsfc.nasa.gov/universe/uni\\_matter](http://map.gsfc.nasa.gov/universe/uni_matter)
- [3] Freedman, W.L. and Turner, M.S. (2003) *Reviews of Modern Physics*, **75**, 1446. <http://dx.doi.org/10.1103/RevModPhys.75.1433>
- [4] Carroll, S. (2013) Why Does Dark Energy Make the Universe Accelerate? [www.preposterousuniverse.com/blog](http://www.preposterousuniverse.com/blog)
- [5] Mendoza, S. (2015) *Canadian Journal of Physics*, **93**, 217-231. <http://dx.doi.org/10.1139/cjp-2014-0208>
- [6] Capotziello, S., *et al.* (2009) A Bird's Eye of f(R) Gravity. arXiv: 0909.4672v2.

- [7] Lidsey, J.E. (2014) Cosmology Course ASTM108/PHY7010U, eq. (2.7), School of Physics and Astronomy, Queen Mary, University of London.
- [8] Bergström, L. and Goobar, A. (2004) Cosmology and Particle Astrophysics. 2nd Edition, Springer, Berlin.
- [9] Lidsey, J.E. (2014) Cosmology Course ASTM108/PHY7010U, eq. (2.27) and (2.29).
- [10] Tolman, R. (1958) Relativity, Thermodynamics and Cosmology. Oxford-Clarendon Press, p. 344,
- [11] Terzic, B. (2008) Astrophysics Course Phys. 652, eq.(50), NICADD, Northern Illinois University.
- [12] Sartori, L. (1996) Understanding Relativity, Fig. 9.1. University of California Press, Oakland.
- [13] Bergström, L. and Goobar, A. (2004) Cosmology and Particle Astrophysics eq. (4.97). 2nd Edition, Springer, Berlin.
- [14] Calder, L. and Lahav, O. (2008) Dark Energy: Back to Newton? invited conference in Reference [11].
- [15] Terzic, B. (2008) Astrophysics Course Phys. 652, Appendix to Lecture 6, Fig. 17.
- [16] Taylor, E.F., Wheeler, J.A. and Bertschinger, E. (2009) Exploring Black Holes: Introduction to General Relativity. Chapter 19, Figure 1, Draft of the 2nd Edition, Pearson Addison Wesley, San Francisco.
- [17] Calder, L. and Lahav, O. (2008) Dark Energy: Back to Newton? Invited Conference in Reference [11]
- [18] Carmeli, M. and Kuzmenko, T. (2001) Value of the Cosmological Constant: Theory versus Experiment. Arxiv: astro-ph0102033, eq. (5).
- [19] Lidsey, J.E. (2014) Cosmology Course ASTM108/PHY7010U. Figure 6.5.
- [20] Lindsey, R.B. and Margenau, H. (1957) Foundations of Physics. Dover Publications, 284.
- [21] Sartori, L. (1996) Understanding Relativity. University of California Press, Berkeley, eq. 9.29.
- [22] Johnson, J.R. (2013) Comprehending the Cosmos: A Macro View of the Universe. 2nd Edition, CreateSpace Independent Publishing Platform, 264-294.
- [23] Valev, D. (2012) Estimation of the Total Mass and Energy in the Universe. 2010arXiv1004-1035.
- [24] Perlmutter, S. (2003) *Physics Today*, 53-60. <http://dx.doi.org/10.1063/1.1580050>
- [25] Riess, A., *et al.* (2004) *Astrophysical Journal*, **607**, 665-687. <http://dx.doi.org/10.1086/383612>
- [26] Riess, A., *et al.* (2007) *Astrophysical Journal*, **659**, 98-121. <http://dx.doi.org/10.1086/510378>
- [27] Lehnert, M.D., *et al.* (2010) *Nature*, **467**, 940-942. <http://dx.doi.org/10.1038/nature09462>
- [28] Coe, D., *et al.* (2012) *Astrophysical Journal*, **762**, 1-23. arxiv 1211.3663.
- [29] Goodstein, D. (2011) Adventures in Cosmology. Figure 3.2, World Scientific, Singapore.
- [30] Dai, D.-C., *et al.* (2012) *Physical Review Letters*, **108**, Article ID: 231302. <http://dx.doi.org/10.1103/PhysRevLett.108.231302>
- [31] Sartori, L. (1996) Understanding Relativity. Figure 9.1, University of California Press, Berkeley.
- [32] Schaefer, B.E. (2007) *Astrophysics Journal*, **660**, 16-46. <http://dx.doi.org/10.1086/511742>



**Submit or recommend next manuscript to SCIRP and we will provide best service for you:**

Accepting pre-submission inquiries through Email, Facebook, LinkedIn, Twitter, etc.

A wide selection of journals (inclusive of 9 subjects, more than 200 journals)

Providing 24-hour high-quality service

User-friendly online submission system

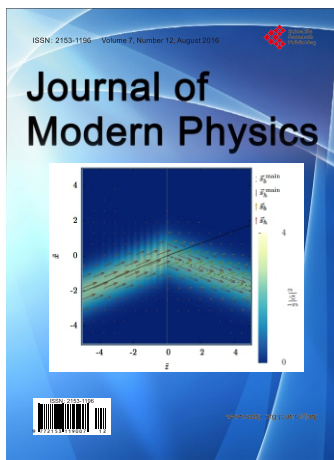
Fair and swift peer-review system

Efficient typesetting and proofreading procedure

Display of the result of downloads and visits, as well as the number of cited articles

Maximum dissemination of your research work

Submit your manuscript at: <http://papersubmission.scirp.org/>



Call for Papers

# Journal of Modern Physics

ISSN: 2153-1196 (Print)    ISSN: 2153-120X (Online)  
<http://www.scirp.org/journal/jmp>

**Journal of Modern Physics (JMP)** is an international journal dedicated to the latest advancement of modern physics. The goal of this journal is to provide a platform for scientists and academicians all over the world to promote, share, and discuss various new issues and developments in different areas of modern physics.

## Editor-in-Chief

**Prof. Yang-Hui He**

City University, UK

## Executive Editor-in-Chief

**Prof. Marko Markov**

Research International, Buffalo Office, USA

## Subject Coverage

Journal of Modern Physics publishes original papers including but not limited to the following fields:

Biophysics and Medical Physics  
Complex Systems Physics  
Computational Physics  
Condensed Matter Physics  
Cosmology and Early Universe  
Earth and Planetary Sciences  
General Relativity  
High Energy Astrophysics  
High Energy/Accelerator Physics  
Instrumentation and Measurement  
Interdisciplinary Physics  
Materials Sciences and Technology  
Mathematical Physics  
Mechanical Response of Solids and Structures

New Materials: Micro and Nano-Mechanics and Homogeneization  
Non-Equilibrium Thermodynamics and Statistical Mechanics  
Nuclear Science and Engineering  
Optics  
Physics of Nanostructures  
Plasma Physics  
Quantum Mechanical Developments  
Quantum Theory  
Relativistic Astrophysics  
String Theory  
Superconducting Physics  
Theoretical High Energy Physics  
Thermology

We are also interested in: 1) Short Reports—2-5 page papers where an author can either present an idea with theoretical background but has not yet completed the research needed for a complete paper or preliminary data; 2) Book Reviews—Comments and critiques.

## Notes for Intending Authors

Submitted papers should not have been previously published nor be currently under consideration for publication elsewhere. Paper submission will be handled electronically through the website. All papers are refereed through a peer review process. For more details about the submissions, please access the website.

## Website and E-Mail

<http://www.scirp.org/journal/jmp>

E-mail: [jmp@scirp.org](mailto:jmp@scirp.org)

